U.PORTO

DOUTORAMENTO

CIÊNCIAS BIOMÉDICAS

Association of 3D Printing and Cellular Therapies for Regenerative Medicine

Ana Catarina Sousa

D

2024

Ana Catarina Sousa. Association of 3D Printing and Cellular Therapies for Regenerative Medicine

U.PORTO

Association of 3D Printing and Cellular Therapies for Regenerative Medicine

Ana Catarina Soares de Sousa

D.ICBAS **2024**

SEDE ADMIISTRATIVA

INSTITUTO DE CIÊNCIAS BIOMÉDICAS ABEL SALAZAR

ANA CATARINA SOARES DE SOUSA

ASSOCIATION OF 3D PRINTING AND CELLULAR THERAPIES FOR REGENERATIVE MEDICINE

Tese de Candidatura ao grau de Doutor em Ciências Biomédicas;

Programa Doutoral da Universidade do Porto (Instituto de Ciências Biomédicas de Abel Salazar)

Orientadora – Professora Doutora Ana Colette Pereira de Castro Osório Maurício

Categoria – Professora Catedrática

Afiliação – Instituto de Ciências Biomédicas Abel Salazar da Universidade do Porto.

Coorientador – Professor Doutor Nuno Manuel Fernandes Alves

Categoria – Professor Coordenador

Afiliação – Instituto Politécnico de Leiria Escola Superior de Tecnologia e Gestão, Portugal.

Coorientador – Professor Doutor José Domingos da Silva Santos

Categoria – Professor Associado com Agregação

Afiliação – Faculdade de Engenharia da Universidade do Porto.

Coorientador – Professor Doutor Luís Miguel Paiva Benites Da Silva Atayde

Categoria – Professor Auxiliar

Afiliação – Instituto de Ciências Biomédicas Abel Salazar da Universidade do Porto

[This page is intentionally left blank.]

I dedicate this thesis to my family,

[This page is intentionally left blank.]

Science knows no country, because knowledge belongs to humanity, and is the torch which illuminates the world.

(Louis Pasteur, chemist and microbiologist)

[This page is intentionally left blank.]

FINANCIAMENTO/ FUNDING

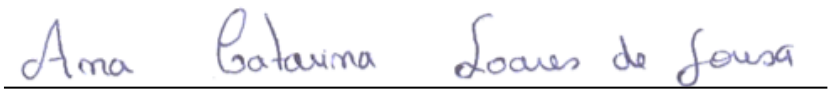
Ana Catarina Soares de Sousa reconhece a **Fundação para a Ciência e a Tecnologia** pelo apoio financeiro ao projeto de doutoramento ora apresentado, sob a Bolsa de Doutoramento com a referência **SFRH/BD/146689/2019**.

Este doutoramento contou ainda com o contributo do Centro de Estudos de Ciência Animal - Instituto de Ciências e Tecnologias Agrárias e Agro-Alimentares da Universidade do Porto (CECA-ICETA) e da Universidade do Porto pelo financiamento e acessibilidade de todos os recursos técnicos, estruturais e humanos necessários ao desenvolvimento do presente trabalho.

[This page is intentionally left blank.]

DECLARATION OF HONOUR

"Declaro que a presente tese é de minha autoria e não foi utilizada previamente noutro curso ou unidade curricular, desta ou de outra instituição. As referências a outros autores (afirmações, ideias, pensamentos) respeitam escrupulosamente as regras da atribuição, e encontram-se devidamente indicadas no texto e nas referências bibliográficas, de acordo com as normas de referenciação. Tenho consciência de que a prática de plágio e auto-plágio constitui um ilícito académico".



LIST OF PUBLICATIONS

The author of this thesis declares that, in accordance with "nº 2, alínea a, do Art.º 31º do Decreto-Lei nº 230/2009" she has made a substantial contribution to the design and technical execution of the work, the interpretation of the results, and the preparation of the manuscript, as evidenced by the following articles:

Articles in International Peer-Reviewed Scientific Journals:

Sousa AC, Veiga A, Maurício AC, Lopes MA, Santos JD, Neto B (2020). Assessment of the environmental impacts of medical devices: a review, in *Environment, Development and Sustainability*. DOI: 10.1007/s10668-020-01086-1.

Sousa AC, Biscaia S, Alvites R, Branquinho MV, Lopes B, Sousa P, Valente J, Franco M, Santos JD, Mendonça C, Atayde L, Alves N, Maurício AC (2022). Assessment of 3D-Printed Polycaprolactone, Hydroxyapatite Nanoparticles and Diacrylate Poly (ethylene glycol) Scaffolds for Bone Regeneration. In *Pharmaceutics*, 2022, 14, 2643. DOI: 10.3390/pharmaceutics14122643.

Sousa AC, Alvites R, Lopes B, Sousa P, Moreira A, Coelho A, Rêma A, Biscaia S, Cordeiro C, Faria F, Silva GF, Amorim I, Santos JD, Atayde L, Alves N, Domingos M, Maurício AC (2024). Hybrid Scaffolds for Bone Tissue Engineering: Integration of Composites and Bioactive Hydrogels Loaded with hDPSCs. in *Biomaterials Advances,* 2025, 166, 214042. DOI: 10.1016/j.bioadv.2024.214042.

Sousa AC, Mcdermott G, Shields F, Alvites R, Lopes B, Sousa P, Moreira A, Coelho A, Santos JD, Atayde L, Alves N, Richardson S, Domingos M, Maurício AC (2024). Innovative Ink-Based 3D Hydrogel Bioprinted Formulations for Tissue Engineering Applications. In *Gels.* 2024, 10, 83. DOI: 10.3390/ gels10120831.

Sousa AC, Alvites R, Lopes B, Sousa P, Moreira A, Coelho A, Santos JD, Atayde L, Alves N, Domingos M, Maurício AC (2025). Three-Dimensional Printing/Bioprinting and Cellular Therapies for Regenerative Medicine: Current Advances. In *Journal of Functional Biomaterials*. 16;16(1):28. DOI: 10.3390/jfb16010028.

AGRADECIMENTOS/ ACKNOWLEDGEMENTS

Em primeiro lugar, gostaria de realçar que esta tese só foi possível graças ao trabalho conjunto de uma equipa interdisciplinar ao longo destes quatro anos. Esta tese não é apenas minha, mas de todos nós.

Agradeço ao Instituto de Ciências Biomédicas Abel Salazar da Universidade do Porto (ICBAS-UP) e ao Centro de Estudos de Ciência Animal – Instituto de Ciências, Tecnologias e Agroambiente da Universidade do Porto (CECA-ICETA), por terem aceitado ser as minhas instituições de acolhimento e por disponibilizarem todos os recursos necessários para a realização do meu trabalho ao longo dos anos.

Ao Centro para o Desenvolvimento Rápido e Sustentado de Produto (CDRSP) do Politécnico de Leiria e ao Henry Royce Institute da Universidade de Manchester, pela oportunidade que me deram ao acolherem-me como estudante de doutoramento visitante e por proporcionarem as condições necessárias para expandir o meu trabalho e fomentar novas colaborações.

À Fundação para a Ciência e Tecnologia (FCT) pelo bolsa de doutoramento concedida, que viabilizou o desenvolvimento desta tese.

Sinto-me privilegiada por ter tido a oportunidade de colaborar com diversas pessoas brilhantes e inspiradoras ao longo do meu percurso doutoral. Gostaria, portanto, de expressar gratidão:

À minha orientadora, Professora Doutora Ana Colette Maurício, o meu sincero agradecimento por acreditar em mim, pelo apoio em todos os desafios que enfrentei durante o doutoramento, pela sua força inabalável e por me proporcionar a liberdade de explorar as minhas ideias. Admiro-a profundamente, tanto como pessoa quanto como cientista, sendo para mim um verdadeiro exemplo a seguir.

Ao meu coorientador Professor Doutor Nuno Alves, pela forma como me acolheu no CDRSP e pelos ensinamentos que partilhou comigo ao longo do tempo e que foram fundamentais para a evolução do meu trabalho e para o meu crescimento como investigadora.

Ao meu coorientado Professor Doutor José Domingos Santos, por me ter recebido como recém-mestre e por compartilhar a sua *expertise* na área dos

biomateriais. Obrigada por me ajudar a transformar ideias em resultados concretos e relevantes para a área dos biomateriais.

Ao meu coorientador Professor Doutor Luís Atayde, pelo apoio incansável e pela dedicação ao longo de todo o meu percurso. A sua orientação e o compromisso constante foram essenciais, especialmente na condução dos testes *in vivo*, que representaram uma etapa crucial para o desenvolvimento deste trabalho.

Agradeço também às Professoras Doutoras Carla Mendonça, Irina Amorim e Ana Lúcia Luís pelo constante apoio, ajuda e atenção demonstrada durante o meu doutoramento.

Um agradecimento especial ao Professor Doutor Marco Domingos, pela orientação, incentivo e acolhimento no seu laboratório, onde me senti integrada e onde tive aprendizagens fundamentais para o desenvolvimento do meu doutoramento. Foi uma fonte constante de motivação e orientação, sempre disponível para discutir estratégias e desafios, o que muito contribuiu para o sucesso deste trabalho.

A todos os meus colegas e amigos do **Laboratório de Terapias Celulares Veterinárias** (Rui Alvites, Mariana Branquinho, Bruna Lopes, Patrícia Sousa, Alícia Moreira, André Coelho, Alexandra Rêma, Maria João Maia e Sofia Meireles), do **Laboratório de Patologia Veterinária** (Diana Araújo, Fátima Faria e Gabriela Silva), do **CDRSP** (Sara Biscaia, Rachel Cordeiro, Carolina Ferreira e Sara Guerreiro) e do **Henry Royce Institute** (Sophia Read, Beatriz Alves, Adrian Barreto, Gianni Pecorini e Grace Mcdermott).

Um agradecimento especial ao Rui Alvites, pelo constante companheirismo e apoio desde os primeiros passos da minha carreira científica. Também agradeço à Bruna Lopes, que, mais do que uma colega, tornou-se uma amiga para a vida. Obrigada por estarem sempre dispostos a ajudar-me.

À Sara Biscaia, expresso a minha gratidão pelo papel de mentora durante o meu tempo no CDRSP, pela paciência e pelo conhecimento transmitido.

To Sophia Read, Beatriz Alves, Adrian Barreto and Gianni Pecorini, thank you for making my stay in Manchester an unforgettable experience. Your support, both within the institute and beyond, was invaluable - whether through professional

collaboration or the memorable walks through Manchester's beautiful parks. A special thanks to my housemate, Sophia, who made my stay even more delightful.

Quero estender os meus sinceros agradecimentos a outros amigos que estiveram presentes com o seu apoio incondicional e que tornaram esta jornada mais leve e repleta de momentos de alegria:

A todos os meus grandes amigos, agradeço de coração: Ana Luísa Castro, João Cabaço, Maria João Rino, Paula Silva, Ricardo Santos, Rodolfo Ferreira, Sara Silva e Vânia Araújo.

A todas as minhas amigas da mágica Tuna Feminina da Universidade Católica Portuguesa do Porto (TFUCP), com um especial obrigada a: 2-pac, Béne, Curita, Dama, Estalinhos, Hemelin, Hobby, Induh, Nani, Samequi, San__nie, Upi e Xutai. À minha querida madrinha Mi, por estar sempre presente e a apoiar-me nos bons e nos maus momentos e a dar-me forças para continuar este caminho.

Ao Raimundo Teixeira, por toda a motivação, mesmo nos momentos mais difíceis. Obrigada pela ajuda, paciência, força e por tudo o que contribuíste para esta tese. A tua presença foi fundamental e sou eternamente grata por isso.

À Anabela Veiga, à Cláudia Sousa e à Vânia Correia, que são as melhores amigas que podia ter! Obrigada por me ouvirem incansavelmente e por sempre me motivarem a seguir em frente. Sinto-me verdadeiramente sortuda por vos ter na minha vida, e estou muito orgulhosa de ver como todas nós estamos a "crescer".

Por último, mas não menos importante, quero exprimir a minha mais profunda gratidão à minha família. Mãe, Pai, Avó e Avô, nenhum dos meus feitos seria possível sem o vosso apoio incondicional, educação, amor infinito e dedicação ao longo desta jornada. Vocês são a minha maior força. Esta conquista é tanto minha quanto vossa.

[This page is intentionally left blank.]

RESUMO

Nas últimas décadas, a Medicina Regenerativa tem procurado desenvolver novas terapias capazes de substituir ou restaurar tecidos e órgãos danificados, destruídos ou envelhecidos no corpo humano, com o objetivo de recuperar a sua função original. Um dos maiores desafios clínicos atuais, particularmente nas áreas da cirurgia ortopédica e maxilofacial, é a perda de tecido ósseo. Os defeitos ósseos, resultantes de traumatismos, tumores, doenças infeciosas, distúrbios metabólicos, doenças congénitas ou desenvolvimento esquelético anormal, são as principais causas de incapacidades funcionais, além de terem impactos estéticos e psicológicos significativos para os pacientes. O tratamento eficaz de um defeito ósseo visa restaurar tanto a morfologia quanto a função normal da estrutura afetada. Nos últimos anos, foram desenvolvidas técnicas cirúrgicas avançadas, como a implantação de biomateriais (substitutos ósseos) e o uso de enxertos ósseos, com o objetivo de promover a regeneração óssea.

A procura por enxertos ósseos é elevada, sendo a realização destes o segundo procedimento mais comum após as transfusões de sangue, com mais de 2,2 milhões de enxertos efetuados anualmente em todo o mundo. No entanto, embora o enxerto ósseo autólogo seja considerado o "padrão de ouro" no tratamento de defeitos ósseos, apresenta várias limitações, como as morbilidades inerentes, os elevados custos, o desconforto do paciente e as complicações associadas. Além disso, a quantidade de tecido autólogo disponível muitas vezes não é suficiente, e a sua qualidade pode ser influenciada por fatores como a idade e a condição metabólica do paciente. Para superar estas limitações, foram introduzidos vários substitutos ósseos sintéticos na prática clínica nas últimas décadas. Apesar de promissores, muitos desses produtos não atendem plenamente aos requisitos necessários, especialmente no que diz respeito à arquitetura tridimensional e às propriedades osteogénicas e osteoindutoras, o que limita o seu sucesso na regeneração óssea. Diante desses desafios, a engenharia de tecidos surgiu como uma disciplina fundamental, proporcionando as ferramentas necessárias para alcançar a regeneração e restauração óssea eficazes.

A combinação de técnicas da impressão 3D e de terapias baseadas em células estaminais mesenquimatosas/estromais (MSCs) apresenta um enorme potencial na regeneração óssea, permitindo a criação de estruturas personalizadas com propriedades biológicas e mecânicas que imitam o tecido ósseo natural.

Neste contexto, esta tese explora a sinergia entre técnicas de bioimpressão 3D e terapias celulares baseadas em MSCs para desenvolver *scaffolds* tecidulares funcionais, com o objetivo de promover a regeneração e cicatrização ósseas. A investigação foca-se no design e otimização de *scaffolds* de biomateriais, utilizando tecnologias avançadas de impressão 3D, para a criação de implantes personalizáveis e específicos para cada paciente. Este trabalho proporciona uma abordagem detalhada dos testes pré-clínicos, englobando as etapas de produção, caracterização e avaliação dos *scaffolds* utilizando métodos *in vitro* e *in vivo*, com o objetivo de validar as suas propriedades funcionais e biocompatibilidade em contextos biológicos. Além disso, o estudo avalia o impacto de terapias celulares, incluindo o uso de células estaminais mesenquimatosas/estromais da polpa dentária humana (hDPSCs) e células estaminais mesenquimatosas/estromais da medula óssea (hBMSCs), na melhoria da capacidade regenerativa desses *scaffolds*. Este trabalho aborda questões críticas, como a biocompatibilidade, a arquitetura dos *scaffolds* e a viabilidade celular, contribuindo para o avanço de abordagens terapêuticas personalizadas em Medicina Regenerativa.

A combinação de tecnologias de impressão 3D e terapias celulares representa uma abordagem promissora para o avanço da Medicina Regenerativa. Esta tese explora o potencial de integração destas duas estratégias para desenvolver soluções inovadoras para a regeneração de tecido ósseo.

O trabalho está dividido em sete capítulos, começando com uma revisão abrangente da literatura atual sobre impressão 3D, bioimpressão e terapias baseadas em células. A revisão analisa sistematicamente as aplicações destas tecnologias em vários campos da engenharia de tecidos, incluindo as áreas cardiovascular, óssea, hepática, cutânea e neural, abordando ainda os desafios e limitações da sua integração na prática clínica.

Os capítulos experimentais subsequentes apresentam a caracterização das hDPSCs como uma fonte celular viável para a regeneração de tecidos; a essa caracterização segue-se a produção de enxertos ósseos sintéticos usando uma combinação de policaprolactona (PCL), nanopartículas de hidroxiapatite (nHA) e polietilenoglicol diacrilato (PEGDA), através da impressão 3D baseada em extrusão. Estes *scaffolds* foram extensivamente caracterizados em termos das suas propriedades mecânicas, químicas e biológicas, demonstrando citocompatibilidade favorável e resistência mecânica adequada para suportar

defeitos ósseos. Em seguida, o estudo envolveu a bioimpressão de uma matriz composta por alginato, nHA, colagénio (Col) e hBMSCs, com o objetivo de desenvolver um modelo 3D capaz de replicar a composição da matriz extracelular (ECM) do osso nativo. Este modelo visa facilitar o estudo da osteogénese e das fases iniciais de maturação tecidular *in vitro*. Após uma extensa caracterização e avaliação *in vitro*, os resultados indicam que a incorporação de nHA e Col no alginato melhoraram as propriedades físicas e biológicas da biotinta, apresentando um modelo promissor para a bioimpressão 3D de tecidos ósseos.

A tese investiga ainda a fabricação de *scaffolds* híbridos, resultantes da combinação de estruturas 3D impressas à base de PCL e nHA, com hidrogéis bioativos contendo alginato, nHA, Col e hDPSCs, ambos mencionados separadamente nos capítulos anteriores. A caracterização *in vitro* e *in vivo* destes *scaffolds* híbridos confirmou a sua capacidade de melhorar a viabilidade celular, promover a diferenciação osteogénica e garantir a biocompatibilidade geral, sugerindo o seu potencial para aplicações de engenharia de tecido ósseo. Adicionalmente, foram avaliados *scaffolds* compostos por PCL combinado com Bonelike® (BL), com uma posterior injeção de meio condicionado derivado de hDPSCs (hDPSCs-CM). Estes *scaffolds* foram testados no modelo ovino, e os resultados mostraram melhorias significativas na regeneração óssea e no potencial osteogénico, quando comparado com os grupos controlo, reforçando seu potencial para futuras aplicações em terapias de regeneração óssea.

Os resultados demonstram que a combinação de bioimpressão 3D e terapias celulares tem um elevado potencial no desenvolvimento de soluções inovadoras para o tratamento de lesões ósseas complexas, com implicações promissoras para futuras aplicações clínicas. Esta tese demonstra, assim, que esta integração da impressão 3D com terapias celulares tem um grande potencial para o desenvolvimento de construções avançadas em engenharia de tecidos. Os resultados contribuem para o crescente conhecimento em Medicina Regenerativa, indicando que estas tecnologias possam ser ainda mais otimizadas para enfrentar desafios clínicos e melhorar terapias personalizadas para a regeneração de tecido ósseo.

Este trabalho destaca-se pela sua abordagem multidisciplinar e inovadora, integrando tecnologias avançadas e conhecimento biomédico para fazer face aos

desafios que surgem no âmbito da regeneração óssea, com o objetivo de proporcionar soluções terapêuticas mais eficazes e individualizadas.

Palavras-chave: biomateriais; bioimpressão; células estaminais mesenquimatosas/estromais; impressão 3D; medicina regenerativa; substitutos ósseos.

ABSTRACT

Over the past decades, Regenerative Medicine has sought to develop new therapies capable of replacing or restoring damaged, destroyed, or aging tissues and organs within the human body, with the purpose of recovering their original function. One of the greatest current clinical challenges, particularly in orthopedic and maxillofacial surgery, is bone tissue loss. Bone defects, resulting from trauma, tumors, infectious diseases, metabolic disorders, congenital diseases, or abnormal skeletal development, are major causes of functional disabilities, in addition to having significant aesthetic and psychological impacts on patients. Effective treatment of a bone defect aims to restore both the morphology and the normal function of the affected structure. In recent years, advanced surgical techniques have been developed, such as the implantation of biomaterials (bone substitutes) and the use of bone grafts, with the goal of promoting bone regeneration. The demand for bone grafts is high, making this the second most common procedure after blood transfusions, with over 2.2 million grafts performed annually worldwide. However, while autologous bone grafting is considered the "gold standard" for treating bone defects, it presents several limitations, such as inherent morbidities, high costs, patient discomfort, and associated complications. Furthermore, the available quantity of autologous tissue is often insufficient, and its quality may be influenced by factors such as the patient's age and metabolic condition. To overcome these limitations, several synthetic bone substitutes have been introduced into clinical practice over the past decades. Despite their promise, many of these products do not fully meet the necessary requirements, particularly in terms of three-dimensional architecture and osteogenic and osteoinductive properties, which limits their success in bone regeneration. Faced with these challenges, tissue engineering has emerged as a key discipline, providing the necessary tools to achieve effective bone regeneration and restoration.

The combination of 3D printing techniques and mesenchymal stem/stromal cell (MSC)-based therapies shows tremendous potential in bone regeneration, allowing the creation of customized structures with biological and mechanical properties that mimic natural bone tissue.

In this context, this thesis explores the synergy between 3D bioprinting techniques and MSC-based cellular therapies to develop functional tissue constructs aimed at promoting bone regeneration and healing. The research

focuses on the design and optimization of biomaterial scaffolds, using advanced 3D printing technologies, to create customizable, patient-specific implants.

This work provides a detailed approach to preclinical testing, encompassing the stages of production, characterization, and evaluation of the scaffolds using *in vitro* and *in vivo* methods, with the aim of validating their functional properties and biocompatibility in biological contexts. Additionally, the study evaluates the impact of cell therapies, including the use of human dental pulp mesenchymal stem/stromal cells (hDPSCs) and human bone marrow mesenchymal stem/stromal cells (hBMSCs), on improving the regenerative capacity of these scaffolds. This work addresses critical issues such as biocompatibility, scaffold architecture, and cell viability, contributing to the advancement of personalized therapeutic approaches in Regenerative Medicine.

The combination of 3D printing technologies and cellular therapies represents a promising approach for advancing Regenerative Medicine. This thesis explores the potential integration of these two strategies to develop innovative solutions for bone tissue regeneration.

The work is divided into seven chapters, beginning with a comprehensive literature review on 3D printing, bioprinting, and cell-based therapies. The review systematically analyzes the applications of these technologies in various fields of tissue engineering, including cardiovascular, bone, hepatic, skin, and neural areas, while also addressing the challenges and limitations of their integration into clinical practice.

The subsequent experimental chapters present the characterization of hDPSCs as a viable cell source for tissue regeneration, followed by the production of synthetic bone grafts using a combination of polycaprolactone (PCL), nano-hydroxyapatite (nHA) and polyethylene glycol diacrylate (PEGDA) through extrusion-based 3D printing. These scaffolds were extensively characterized in terms of their mechanical, chemical and biological properties, demonstrating favorable cytocompatibility and adequate mechanical strength to support bone defects. The study then involved bioprinting a matrix composed of alginate, nHA, collagen (Col) and hBMSCs, with the purpose of developing a 3D model capable of replicating the extracellular matrix (ECM) composition of native bone. This model aims to facilitate the study of osteogenesis and early stages of tissue maturation

in vitro. Following extensive characterization and *in vitro* evaluation, the results indicate that the incorporation of nHA and Col into alginate improved the physical and biological properties of the bioink, presenting a promising model for 3D bioprinting of bone tissue.

The thesis also investigates the fabrication of hybrid scaffolds, resulting from the combination of 3D-printed structures based on PCL and nHA, with bioactive hydrogels containing alginate, nHA, Col and hDPSCs, both mentioned separately in the previous chapters. The *in vitro* and *in vivo* characterization of these hybrid scaffolds confirmed their ability to enhance cell viability, promote osteogenic differentiation, and ensure overall biocompatibility, suggesting their potential for bone tissue engineering applications. Additionally, scaffolds composed of PCL combined with Bonelike® (BL), with subsequent injection of conditioned medium derived from hDPSCs (hDPSCs-CM), were evaluated. These scaffolds were tested in an ovine model, and the results showed significant improvements in bone regeneration and osteogenic potential compared to control groups, reinforcing their potential for future applications in bone regeneration therapies.

The results demonstrate that the combination of 3D bioprinting and cellular therapies holds great potential in developing innovative solutions for the treatment of complex bone injuries, with promising implications for future clinical applications. This thesis thus demonstrates that the integration of 3D printing with cellular therapies has significant potential for the development of advanced tissue constructs in tissue engineering. The results contribute to the growing knowledge in Regenerative Medicine, indicating that these technologies can be further optimized to address clinical challenges and improve personalized therapies for bone tissue regeneration.

This work stands out for its multidisciplinary and innovative approach, integrating cutting-edge technology and biomedical knowledge to tackle the challenges of bone regeneration, with the aim of providing more effective and individualized therapeutic solutions.

Keywords: 3D printing; biomaterials; bioprinting; bone substitutes; mesenchymal/stromal stem cells; regenerative medicine.

[This page is intentionally left blank.]

TABLE OF CONTENTS

FINANCIAMENTO/ FUNDING ____ **VII**

DECLARATION OF HONOUR ____ **IX**

LIST OF PUBLICATIONS ____ **IX**

AGRADECIMENTOS/ ACKNOWLEDGEMENTS ____ **XI**

RESUMO ____ **XV**

ABSTRACT ____ **XIX**

TABLE OF CONTENTS ____ **XXIII**

LIST OF FIGURES ____ **XXIX**

LIST OF TABLES ____ **XXXIX**

LIST OF ABBREVIATIONS ____ **XLV**

SCOPE AND OUTLINE ____ **LV**

CHAPTER I – STATE OF ART ____ 1

INTRODUCTORY NOTE ____ **3**

Three-Dimensional Printing/Bioprinting and Cellular Therapies for Regenerative Medicine: Current Advances *7*

1. Introduction ____ 10
2. Three-Dimensional Printing ____ 11
   - 2.1. Vat Photopolymerization ____ 12
   - 2.2. Material Extrusion ____ 13
   - 2.3. Powder Bed Fusion ____ 13
   - 2.4. Material Jetting ____ 14
   - 2.5. Binder Jetting ____ 14
   - 2.6. Directed Energy Deposition ____ 14
   - 2.7. Sheet Lamination ____ 15
3. Bioprinting ____ 1
   - 3.1. Techniques ____ 2
   - 3.2. Materials used in 3D bioprinting ____ 4
4. Cellular Therapies ____ 5
   - 4.1. Stem Cell-based Therapies ____ 6
   - 4.2. Non-Stem Cell-based Therapies ____ 7

4.3. Multicellular Therapies _____ 8
5. Advancements in 3D printed/ bioprinting and cellular therapies for Regenerative Medicine _____ 8
5.1. Cardiovascular tissue engineering _____ 10
5.2. Bone tissue engineering _____ 18
5.3. Liver tissue engineering _____ 27
5.4. Skin tissue engineering _____ 38
5.5. Neural tissue engineering _____ 48
6. Limitations and challenges _____ 58
7. Current state and future outlook _____ 61
8. Conclusion _____ 63
Abbreviations _____ 65
References _____ 70

REFERENCES _____ 105

CHAPTER II – CHARACTERIZATION OF MESENCHYMAL STEM/STROMAL CELLS __ 111

INTRODUCTORY NOTE _____ 113

Human Dental Pulp Stem/Stromal Cells 117
1. Introduction _____ 119
2. Materials and Methods _____ 120
2.1 Isolation, processing and cryopreservation of hDPSCs _____ 120
2.2 Cell behaviour in culture _____ 122
2.2.1. Growth Curve and Population Doubling Time (PDT) ___ 122
2.2.2. Colony Forming Unit (CFU) Assays _____ 123
2.3 Multilineage Differentiation _____ 123
2.3.1. Adipogenic Differentiation _____ 123
2.3.2. Chondrogenic Differentiation _____ 124
2.3.3. Osteogenic Differentiation _____ 124
2.4 Gene expression _____ 125
2.5 Statistical analysis _____ 129
3. Results _____ 129
3.1 Isolation, processing and cryopreservation of hDPSCs _____ 129
3.2 Cell behaviour in culture _____ 130
3.2.1. Growth Curve and Population Doubling Time (PDT) ___ 130
3.2.2. Colony Forming Unit (CFU) Assays _____ 132
3.3 Multilineage Differentiation _____ 132

3.4 Gene expression_____ 134
4. Discussion_____ 136
5. Conclusions _____ 139

REFERENCES_____ 141

CHAPTER III – FABRICATION AND CHARACTERIZATION OF A 3D SCAFFOLD FOR REGENERATIVE MEDICINE_____ 157

INTRODUCTORY NOTE _____ 159

Assessment of 3D-Printed Polycaprolactone, Hydroxyapatite Nanoparticles and Diacrylate Poly(ethylene glycol) Scaffolds for Bone Regeneration..... 163

1. Introduction _____ 166
2. Materials and Methods _____ 168
2.1. Materials _____ 168
2.2. Sample Design_____ 168
2.3 Material Characterisation _____ 170
2.3.1. Fourier-transform infrared spectroscopy _____ 170
2.3.2. Contact Angle Measurement_____ 170
2.3.3. X-ray micro-computed Tomography_____ 171
2.3.4. Scanning Electron Microscopy and Energy Dispersive X-ray analysis _____ 171
2.3.5. Mechanical Analysis_____ 171
2.4 In Vitro Tests_____ 172
2.4.1. Cell culture and maintenance _____ 172
2.4.2 Cytocompatibility assessment _____ 172
2.5 Statistical analysis _____ 173
3. Results _____ 173
3.1 Scaffolds production_____ 173
3.2 Material Characterisation _____ 174
3.3 In vitro cytocompatibility test _____ 180
4. Discussion_____ 183
5. Conclusions _____ 187
6. References _____ 189

REFERENCES_____ 203

CHAPTER IV – BIOINKS FOR OSTEOGENIC DIFFERENTIATION _____ 205

INTRODUCTORY NOTE ____ **207**

Innovative Ink-Based 3D Hydrogel Bioprinted Formulations for Tissue Engineering Applications ____ *211*

1. Introduction ____ 214
2. Results and Discussion ____ 217
   2.1. Rheological Characterization ____ 219
   2.2. Mechanical Analysis ____ 221
   2.3. Hydrogel Swelling Behavior ____ 222
   2.4. Bioprinting of Cell-Laden Hydrogels ____ 224
   2.5. Live/Dead Staining ____ 225
   2.6. Cell Viability Assay ____ 227
   2.7. Gene Expression ____ 228
3. Conclusions ____ 230
4. Materials and Methods ____ 231
   4.1. Materials ____ 231
   4.2. Preparation of Alginate-Based Solutions ____ 231
   4.3. Cell Culture and Maintenance ____ 232
   4.4. Oscillatory Rheological Measurements ____ 232
   4.5. Hydrogel Swelling Behavior ____ 234
   4.6. Mechanical Analysis ____ 234
   4.7. Bioprinting of Cell-Laden Hydrogels ____ 235
   4.8. Live/Dead Staining ____ 236
   4.9. Cell Viability Assay ____ 236
   4.10. Gene Expression ____ 237
   4.11. Statistical Analysis ____ 237

References ____ 240

5. REFERENCES ____ **249**

CHAPTER V – HYBRID SCAFFOLD FOR BONE TISSUE ENGINEERING ____ 253

INTRODUCTORY NOTE ____ **255**

Hybrid Scaffolds for Bone Tissue Engineering: Integration of Composites and Bioactive Hydrogels Loaded with hDPSCs ____ *257*

1. Introduction ____ 261
2. Materials and Methods ____ 264
   2.1. Materials ____ 264

2.2. Preparation of Scaffolds _____ 264
2.3. Encapsulation of the Cells in Hydrogel and Injection Into the Scaffolds _____ 264
2.4. In Vitro Assays _____ 265
2.4.1. Cell Culture and Maintenance _____ 265
2.4.2. Cytocompatibility Assessment _____ 265
2.4.3. Osteogenic Differentiation Assay _____ 266
2.4.4. Scanning Electronic Microscopy (SEM) _____ 267
2.5. *In Vivo* Biocompatibility Assessment of Hydrogel/ Hybrid Scaffolds in Subcutaneous Tissue _____ 268
2.6. Statistical Analysis _____ 270
3. Results _____ 270
3.1. Cytocompatibility Assessment _____ 270
3.2. Osteogenic Differentiation Assay _____ 272
3.3. Scanning Electronic Microscopy (SEM) _____ 274
3.4. In Vivo Biocompatibility Assessment of Hydrogel/ Hybrid Scaffolds in Subcutaneous Tissue _____ 276
4. Discussion _____ 280
5. Conclusions _____ 283
6. Abbreviations _____ 285
7. References _____ 287
8. Supporting Material _____ 295

REFERENCES _____ 297

CHAPTER VI – APPLICATION OF BIOMATERIALS AND CELLULAR THERAPIES FOR THE IN VIVO TREATMENT OF CRITICAL-SIZED BONE DEFECTS _____ 301

INTRODUCTORY NOTE _____ 303

The Application of Bonelike® and hDPSCs Conditioned Medium for the Management of Critical-Sized Bone Defects 305

1. Introduction _____ 307
2. Materials and Methods _____ 310
2.1. Biomaterials _____ 310
2.1.1. Materials _____ 310
2.1.2. Sample Design _____ 310
2.2 Scanning electron microscopy (SEM) and energy-dispersive X-ray spectroscopy (EDX) _____ 311

2.3. Conditioned Medium (CM) _____ 312
2.3.1. Cell culture and maintenance _____ 312
2.3.2. Conditioned medium (CM) preparation _____ 312
2.4. Cytocompatibility Assessment _____ 312
2.5. Osteogenic Differentiation Assay _____ 313
2.6. In vivo bone regeneration assessment _____ 314
2.6.1. Animals and Ethical Issues _____ 314
2.6.2. Surgical Procedure _____ 315
2.7. Statistical Analysis _____ 318
3. Results _____ 319
3.1. Scanning electron microscopy (SEM) and energy-dispersive X-ray spectroscopy (EDX) _____ 319
3.2. Cytocompatibility Assessment _____ 320
3.3. Osteogenic Differentiation Assay _____ 323
3.4. In vivo bone regeneration assessment _____ 324
3.4.1 Macroscopic Analysis _____ 324
3.4.2 Radiographic Analysis _____ 324
4. Discussion _____ 327
5. Conclusions _____ 331
REFERENCES _____ 333
CHAPTER VII – GENERAL DISCUSSION, CONCLUSIONS AND FUTURE PERSPECTIVES _____ 347
General Discussion and Conclusions 349
Future Perspectives 369
REFERENCES _____ 375

LIST OF FIGURES

Figure 1. Overview of the chapters conducted during the present doctoral thesis. _____ LIX

Chapter I – State of Art

Figure 1. Schematic representation of the various AM processes._____ 12
Figure 2. Major milestones in the history of 3D bioprinting._____ 2
Figure 3. Advances in cell therapies, 3D printing, and bioprinting are addressing the challenges in engineering cardiovascular, bone, liver, skin, and neural tissues. _____ 9
Figure 5. Advances 3D printing/ bioprinting and cell therapies in engineering cardiovascular: A: Bioprinted cellularized construct incorporating human Umbilical Vein Endothelial Cells (hUVECs) and induced pluripotent stem cell-derived cardiomyocytes (iPSC-CMs), embedded in alginate and PEG-Fibrinogen (PF) (adapted from [173]); B: Printed patches composed of decellularized cardiac extracellular (cECM) matrix hydrogel and GelMA, for delivery of pediatric human cardiac progenitor cell (hCPC) (adapted from [174]); C: MSC-loaded gel patches with microchannels of controlled diameters. Three models tested: one without microchannels and two with nine evenly spaced microchannels, maintained at diameters of 500 μm and 1000 μm (adapted from [175] Copyright 2024, American Chemical Society); D: A 3D-printed cellularized human heart is shown. (Left: CAD model of the human heart; Middle and right: The printed cardiac structure immersed in a supportive bath) (adapted from [176]); E: Printed fibrin scaffold using modified thermal inkjet printer (adapted from [177], Copyright (5839410409139) with permission from Elsevier)._____ 13
Figure 6. Advances 3D printing/ bioprinting and cell therapies in bone tissue engineering: A: Ti6Al4V-based porous tantalum (Ta) scaffolds and scanning electron microscopy images (adapted from [197]); B: Newly formed bone within the scaffold was assesses through ex vivo micro-computed tomography(micro-CT) scans at 6 and 12 weeks (adapted from [198]); C: Visual representations of 3D-printed samples at different alginate concentrations, alginate alone or alginate with beta-tricalcium phosphate (β-TCP) (adapted from [199], Copyright (5841970729622) with permission from Elsevier); D: Bone scaffolds based on magnesium (Mg^{2+}), strontium (Sr^{2+}) and zinc (Zn^{2+})-substituted hydroxyapatite, as represented in the CAD model [200])._____ 20

Figure 7. Advances 3D printing/bioprinting and cell therapies in liver tissue engineering: (A): Human liver functions of 3D bioprinted hepatorganoids in mice. First column: Macroscopic observation of transplanted 3D bioprinted hepatorganoids. The vascular system is illustrated following the infu-sion of dextran. Second and third column: The figure shows the dextran infusion with the for-mation of functional vessels and the red fluorescence showing the expression of human ALB at 4 weeks (adapted from [226]); (B): The study details the production of patient-derived 3D bioprinted hepatocellular carcinoma models. Initially, HCC samples were obtained following post-surgical resection and subsequently processed into cell suspensions. These suspensions were then combined with sodium alginate and gelatin to create the bioink used for bioprinting. The images provided in the second line include the following: (1) the general appearance of the 3D bioprinted hepatocellu-lar carcinoma model, (2) a light microscopy image showing the distribution of cells within the model and (3) an in vitro view of the model, where live cells are marked in green and dead cells are marked in red (adapted from [227], Copyright (5842091348696) with permission from Elsevier); (C): First line: schematic representation of the 3D printed scaffold, including strut spacing, nozzle diameter and angle between adjacent layers (90 or 60 degrees). Second line: large-scale 3D printed gelatin structure. Third line: cross-linked scaffolds and biopsy-punched samples (adapted from [228], Copyright (5842111318276) with permission from Elsevier); (D): Construction of 3D-printed mCherry-HepG2 hepatic structures: (D-A) 3D bioprinting machine; (D-B) extrusion of alginate combined with mCherry-HepG2 cells through nozzle pressure; (D-C) layer-by-layer dep-osition of cross-linked structures in square arrays; (D-D) phase contrast microscopy showing a confluent monolayer of HepG2 cells; (D-E) fluorescence microscopy image of mCherry-HepG2 cells within the alginate scaffold; (D-F) multilayered mCherry-HepG2 cells solidified and stacked repet-itively (adapted from [229]); (E): Schematic representation of the liver lobule-mimetic honeycomb structure, including top and side views of the embedded-printed scaffolds (adapted from [230]). _____ 30
Figure 8. Advances 3D printing/bioprinting and cell therapies in skin tissue engineering: (A): The image shows the printed epidermal layer (red) composed of alginate-gelatin hydrogel, and the dermal layer (green) made of phosphosilicate calcium bioglass (PSC)-alginate-GelMA hydrogel embedded with hUVECs and hUCMSCs (adapted from [241], Copyright (5842131198782) with permission from Elsevier); (B): Diagram overview of the produced structure design: diagram

illustration of the CAD model; illustration of human skin anatomy, with the dermis and epidermis; approach for designing the dual-layered 3D printed structure; dimensions of the layers: the dermal layer consists of 10 layers, while the epidermal layer has eight filaments, oriented perpendicularly with an interfilament spacing of 0.75 mm and a Z-axis increment of 0.08 mm per layer; microscopic view of the printed structure; dual-layered 10 × 10 mm 3D printed structure in culture; and the mechanically printed structure is noted for its optimal handling properties, which facilitate thorough characterization and assessment (adapted from [247], Copyright (5842131492259) with permission from Elsevier); (C): Assessment of the printability of acellular dermal matrix and GelMA hydrogels by fabricating identical structural patterns using these materials (adapted from [248], Copyright (5842140280407) with permission from Elsevier); (D): Macrographs and scanning electron microscopy (SEM) images of PCL-AMX, SG-rhEGF, and PCL-AMX-SG-rhEGF structures (adapted from [249], Copyright (5842140587126) with permission from Elsevier). _____ 40
Figure 9. Advances 3D printing/ bioprinting and cell therapies in neural tissue engineering: A: Evaluation of bioink printability was conducted for various compositions of methacrylated silk fibroin and methacrylated silk fibroin/pectin hydrogels. Optical microscopy images were captured to examine the morphology, while a live/dead assay was performed on L929 cells embedded within 3D bioprinted constructs using bioinks composed of 10% methacrylated silk fibroin/0.5% pectin and 15% methacrylated silk fibroin/0.5% pectin (adapted from [259], Copyright (5842151229827) with permission from Elsevier); B: Characterization of the scaffolds was conducted as follows: (A) Normal spinal cord tissue; (B) Decellularized spinal cord scaffold; (C) Polycaprolactone (PCL) microfiber structure; (D) Overall morphology of the 3D-bioprinted composite scaffold; (E–H) Microstructure of scaffolds visualized through scanning electron microscopy (SEM). The SEM images of both the scaffold alone and the scaffold combined with OMT reveal parallel microfibers of consistent thickness, with hydrogels adhering to the fibers. The interior of the scaffold exhibited uniform and densely packed pores, which are conducive to neural stem cell (NSC) growth and efficient nutrient exchange (adapted from [260]); C: Schematic representation of the experimental procedure for spinal cord injury repair utilizing stereolithography apparatus (SLA) to create neural scaffolds. (a) Computer-aided design (CAD) to develop the scaffold model corresponding to the injured region for bioprinting; (b) Construction of neural scaffolds employing the SLA technique; (c) Utilization of the fabricated

scaffolds for in vitro cell culture; (d) Assessment of the functionality of scaffolds following a period of in vitro cultivation (adapted from [261], Copyright (5842160814781) with permission from Elsevier). _____ 50

Chapter II – Characterization of Mesenchymal Stem/Stromal Cells

Figure 1. Schematic representation of the process for the isolation, preservation and cryopreservation of hDPSCs. _____ 122

Figure 2. (a) hDPSCs after 1 day in culture (50% confluence); (b) hDPSCs after 5 days in culture (80-90% confluence) (magnification 40x). _____ 130

Figure 3. Growth curve of hDPSCs at passage 5 (P5), for up to 10 days of culture. _____ 131

Figure 4. Population Doubling Times (PDTs) of the different passages of hDPSCs. The significance of the results is denoted by symbols corresponding to p values: two symbols (**) for $0.001 \leq p < 0.01$, three symbols (***) for $0.0001 \leq p < 0.001$, and four symbols (****) for $p < 0.0001$. _____ 131

Figure 5. CFU assay: observation of individualized colonies in a 6-well tissue culture treated plate, stained with crystal violet solution (magnification 100x). _____ 132

Figure 6. CFU assay: observation of individualized colonies in a 6-well tissue culture treated plate, stained with crystal violet solution (magnification: 100x). _____ 132

Figure 7. Multilineage differentiation of isolated cells following culture in (A) Oil Red O staining reveals large, round-shaped cells with red-stained lipid vacuoles in the cytoplasm; (B) Alcian blue staining highlights chondrogenic aggregates and blue-stained extracellular matrix; (C) Alizarin Red staining reveals calcium-containing osteocytes and extracellular calcium deposits in red, and (D) Von Kossa staining indicates mineral matrix deposition through dark pigmentation on the cellular surface. (magnification: 100x). _____ 134

Figure 8. ΔCq values for the different genes under study in hDPSCs for P6 and P9. Higher ΔCq values indicate lower gene expression levels (mean ± SEM). The significance of the results is denoted by symbols corresponding to p values: three symbols (***) for $0.0001 \leq p < 0.001$, and four symbols (****) for $p < 0.0001$. 136

Chapter III – Fabrication and Characterization of a 3D Scaffold for Regenerative Medicine

Figure 1. The bone fracture healing process. It can be categorized into three primary stages: hematoma formation, primary callus formation, and callus repair and remodeling (adapted from [1], Copyright (5851501384882) with permission from Elsevier). _____ 160

Figure 1. Schematic representation of the process for the manufacture of scaffolds. _____ 170
Figure 2. Observation of the 3D printed scaffolds for each group: (a) PCL scaffolds; (b) PCL scaffolds with the addition of hydroxyapatite nanoparticles; (c) PCL/HANp scaffolds submerged in PEGDA solution. _____ 174
Figure 3. FTIR spectra of each group (PCL, PCL/HANp, PCL/HANp/PEGDA and PEGDA). _____ 175
Figure 4. Contact angle measurements mean ± standard deviation of PCL, PCL/HANp and PCL/HANp/PEGDA scaffolds. Differences were considered statistically significant at $p \leq 0.05$. The results' significance is presented through the symbol (*), according to the p-value, with three symbols, corresponding to $0.0001 < p \leq 0.001$. _____ 175
Figure 5. 3D micro-CT images of (a) PCL scaffolds; (b) PCL scaffolds with the addition of hydroxyapatite nanoparticles; (c) PCL/HANp scaffolds submerged in PEGDA solution. _____ 176
Figure 6. SEM images of PCL, PCL/HANp and PCL/HANp/PEGDA scaffolds. The red arrows show the presence of hydroxyapatite nanoparticles in the sample. Magnification: A.1, B.1 and C.1: 50x and, A.2, B.2 and C.2: 1000x. _____ 177
Figure 7. EDX Si-mapping micrographs. _____ 179
Figure 8. Compressive modulus (MPa) of the produced scaffolds. _____ 180
Figure 9. Corrected absorbance evaluated by PrestoBlue® viability assay for hDPSCs after 24, 72, 120 and 168 hours. _____ 181
Figure 10. % Viability inhibition evaluated by PrestoBlue® viability assay for hDPSCs after 24, 72, 120 and 168 hours. Results are normalized to the PCL as 0%. The 30% threshold shown in the graph (dashed line) represents the inhibition above which the effect is considered cytotoxic (in accordance with ISO 10993-5:2009 guidelines). _____ 182

Chapter IV –Bioinks for Osteogenic Differentiation

Figure 1. Rheological experiments with the storage moduli (G') (shown in black) and loss moduli (G") (shown in red) of crosslinked alginate and alginate-nHA-Col under a range of conditions. (a) Amplitude sweeps performed at a frequency of 1 Hz. (b) Frequency sweeps performed at an oscillation strain of 0.1%. The evaluations were performed in triplicate. _____ 220
Figure 2. Stress–strain curves resulting from compression tests of alginate hydrogel (red) and alginate-nHA-Col hydrogel (black) (n = 3). _____ 222

Figure 3. Hydrogel swelling rate from 1 to 72h. Alg: alginate (red); Alg-nHA-Col (black) (n = 3). _____ 223
Figure 4. (A) CAD model designed in BioCAM™ software (version 2.0); (B) 3D generated model; (C) 3D generated model in a 12-well plate; (D) Cell-laden print in the agarose support bath. _____ 225
Figure 5. (A) Live/dead staining images of printed hBMSCs in alginate and alginate-nHA-Col after 1, 3, and 7 days in culture. Live cells are stained green and dead cells are stained red. (B) The percentage of cell viability of bioprinted hBMSCs cultured in 2% alginate and 2% alginate-0.5% nHA-0.5% Col for 1, 3, and 7 days (n = 3). 226
Figure 6. (A) Corrected absorbance evaluated by Presto Blue® viability assay for hBMSCs (n = 3). Result significances are presented through the symbol (*), according to the p value, with * $p < 0.05$. (B) Percent viability inhibition assay. The results were normalized in relation to the control. The 30% threshold shown (dashed line) represents the inhibition above which the effect is considered cytotoxic (under ISO 10993-5:2009 guidelines). _____ 228
Figure 7. Gene expression levels of printed hBMSCs in alginate and alginate-nHA-Col bioinks after 7 and 14 days under osteogenic differentiation: runt-related transcription factor 2 (RUNX2) (A), alkaline phosphatase (ALPL) (B), integrin-binding sialoprotein (IBSP) (C), secreted phosphoprotein-1 (SPP1) (D), and collagen type 1 alpha 2 chain (COL1A2) (E).____ 230
Figure 8. Graphical representation of the preparation of alginate and alginate-nHA-Col-based solutions. _____ 232
Figure 9. (A) 3D Discovery Evolution bioprinter; (B) Schematic representation of the pressure-assisted extrusion process, in which pressurized air drives the bioink from the bioprinter cartridge through a needle into a well plate containing a suspension bath. _____ 235

Chapter V – Hybrid Scaffold for Bone Tissue Engineering

Figure 1. Schematic representation of the experimental set-up for the in vitro cytocompatibility evaluation. _____ 266
Figure 2. A: Trichotomy of the region to be intervened; B: After aseptic skin preparation, four linear incisions are made, paired along the dorsum; C: Biomaterials are implanted subcutaneously; D: The skin and subcutaneous tissues are sutured. _____ 269
Figure 3. Cytocompatibility tested by PrestoBlue™ viability assay for hDPSCs. Results presented in mean ± SE (standard error of the mean). _____ 270

Figure 4. % of viability inhibition assessed by PrestoBlue® viability assay after 24, 72, 120 and 168 h. The results were normalized to the control group as 0%. The 30 per cent threshold presented in the graph (dashed line) indicates the inhibition above which the effect is considered cytotoxic (in conformity with ISO 10993-5:2009 guidelines). _____ 272
Figure 5. ARS Semi-Quantification in mM between groups. Results presented in Mean ± SE. Differences were considered statistically significant at $p \leq 0.05$. Results significance are presented through the symbol (*), according to the p value, with one, two, three or four symbols, corresponding to $0.01 < p \leq 0.05$; $0.001 < p \leq 0.01$; $0.0001 < p \leq 0.001$ and $p \leq 0.0001$, respectively. _____ 273
Figure 6. ARS Semi-Quantification in mM between groups. Results of % mineral deposition enhancement are presented in mean ± SE, normalized to the control group as 100%. _____ 273
Figure 7. SEM images for the control, hybrid scaffold with alginate hydrogel plus hDPSCs, and hybrid scaffold with alginate-nHA-Col plus hDPSCs groups. Upper panel 100x magnification, middle panel 500x magnification and lower panel 1000x magnification. First column: control; middle column: hybrid scaffold with alginate plus hDPSCs; third column: hybrid scaffold with alginate-nHA-Col plus hDPSCs. _____ 275
Figure 8. SEM images for the hybrid scaffold with alginate-nHA-Col plus hDPSCs (2500x magnification). _____ 276
Figure 9. Global histological score, according to ISO-10993-6 guidelines for the sham, hydrogel, hydrogel plus hDPSCs, hybrid scaffold, and hybrid scaffold plus hDPSCs groups, at 3, 7, 15 and 30 days after implantation. Results presented in mean ± SEM. Differences were considered statistically significant at $p \leq 0.05$. Results significance are presented through the symbol (*), according to the p value, with one, two, three or four symbols, corresponding to $0.01 < p \leq 0.05$; $0.001 < p \leq 0.01$; $0.0001 < p \leq 0.001$ and $p \leq 0.0001$, respectively._____ 277
Figure 10. Calculated score, according to ISO-10993-6 guidelines, for the hydrogel, hydrogel plus hDPSCs, hybrid scaffold, and hybrid scaffold plus hDPSCs groups, at 3, 7, 15 and 30 days after implantation. _____ 278
Figure 11. Histological evaluation following H&E staining for hydrogel, hydrogel plus hDPSCs, hybrid scaffold, and hybrid scaffold plus hDPSCs groups. The sections were assessed using a Nikon microscope (Nikon Eclipse E600) coupled to a photo camera (Nikon Digital Sight DS-5M). For each panel, the main image corresponds to a magnification of 20x and the inset image to a magnification of 200x. ___ 279

Figure S1. SEM image (1000x magnification) and corresponding EDX analysis of the control group. _____ 295
Figure S2. SEM image (100x magnification) and corresponding EDX analysis of the hybrid scaffold with alginate plus hDPSCs group. _____ 295
Figure S3. SEM image (100x magnification) and corresponding EDX analysis of the hybrid scaffold with alginate-nHA-Col plus hDPSCs group. _____ 296

Chapter VI – Application of Biomaterials and Cellular Therapies for the *In Vivo* Treatment of Critical-Sized Bone Defects

Figure 1. Merino sheep (Ovis aries). _____ 315
Figure 2. Experimental design of 10 Merino sheep, with bone defects divided into four groups (control, PCL plus hDPSCs-CM, PCL/nHA plus hDPSCs-CM, and PCL/BL plus hDPSCs-CM). The image of the surgical field represents the scaffolds PCL/BL plus hDPSCs-CM after application in the critical defect created in the iliac ala. 317
Figure 3. SEM images of Bonelike® granules (total magnification: (A) 250x, (B) 2000x and (C) 10000x). Figure C illustrates the measurement of microporosity, highlighted in red. _____ 319
Figure 4. SEM image (2000x magnification) and corresponding EDX analysis of the Bonelike®(BL). _____ 320
Figure 5. Cytocompatibility tested by PrestoBlue™-based viability assay for hDPSCs. Results presented in Mean ± SEM (standard error of the mean). _____ 321
Figure 6. % of viability inhibition assessed by PrestoBlue® viability assay after 24, 72, 120 and 168 h. The results were normalized to the control group as 0%. The 30 % threshold presented in the graph (dashed line) indicates the inhibition above which the effect is considered cytotoxic (in conformity with ISO 10993-5:2009 guidelines). _____ 322
Figure 7. ARS Semi-Quantification in mM between groups. Results presented in mean ± SEM. Differences were considered statistically significant at $p \leq 0.05$. Results significances are presented through the symbol (*), according to the p value, with two or three (*) corresponding to $0.001 < p \leq 0.01$ and $0.0001 < p \leq 0.001$, respectively. _____ 323
Figure 8. Post-mortem ex vivo representative X-Ray images for control, PCL plus hDPSCs-CM, PCL/nHA plus hDPSCs-CM, and PCL/BL plus hDPSCs-CM groups after 90 and 150 days. _____ 326

Figure 9. Representative ex vivo post-mortem X-ray images with and without membrane for the PCL plus hDPSCs-CM, PCL/nHA plus hDPSCs-CM, and PCL/BL plus hDPSCs-CM groups after 150 days._____ 327

Chapter VII – General Discussion, Conclusions and Future perspectives

Figure 1. Stages of preclinical trials in scaffold development for bone regeneration. _____ 355

[This page is intentionally left blank.]

LIST OF TABLES

Chapter I – State of Art

Table 1. Advantages and drawbacks of each AM technique [22-24, 33, 42-44]. 16
Table 2. Comparison of the bioprinting techniques [60, 72-75]. _____ 4
Table 3. Recent advances in 3D printing/bioprinting and cellular therapies for cardiovascular tissue engineering. Abbreviations: human microvascular endothelial cells (hMVECs); mouse embryonic fibroblasts (mEFs); human cardiac-derived cardiomyocyte progenitor cells (hCMPCs); human umbilical vein endothelial cells (hUVECs); cardiomyocytes (H9c2 cells); induced pluripotent stem cell-derived cardiomyocytes (iCMs); human cardiac fibroblasts (CFs); human coronary artery endothelial cells (hCAECs); gelatin methacrylate (GelMA); decellularized cardiac extracellular matrix hydrogel (cECM); human cardiac progenitor cells (hCPCs); heart tissue-derived extracellular matrix (hdECM); neonatal rat cardiomyocytes (NRCMs); poly(ethylene glycol)-fibrinogen (PF); induced pluripotent stem cell-derived cardiomyocytes (iPSC-CMs); digital light processing (DLP); poly (glycerol sebacate) (PGS); poly (ε-caprolactone) (PCL); fused deposition modeling (FDM); not applicable (n/a); stereolithographic assembly (SLA); poly(ethylene glycol) dimethacrylate (PEGDMA); bone marrow-derived mesenchymal stem cells (BMSCs); mesenchymal stem/stromal cell (MSC); hyaluronic acid (HA); human embryonic stem cells (hESCs); early vascular cells (EVCs); hyaluronic acid glycidyl methacrylate (HAGM); neonatal rat cardiomyocytes (NRCMs). _____ 14
Table 4. Recent developments in 3D printing/bioprinting and cellular therapies for bone tissue engineering. Abbreviations: selective laser melting (SLM); bone marrow-derived mesenchymal stem cells (BMSCs); beta-tricalcium phosphate (β-TCP); gelatin methacrylate (GelMA); Xonotlite (Sr-CSH); poly(lactic-co-glycolic acid) (PLGA); bone morphogenetic protein 2 (BMP-2); human umbilical cord mesenchymal stem cells (hUCMSCs); alkaline phosphatase (ALP); hydroxyapatite (nHA); Magnesium (Mg2+); Strontium (Sr2+); Zinc (Zn2+); not applicable (n/a); polycaprolactone (PLC); amorphous calcium phosphate (ACP); dental pulp stem cells (DPSCs); Polyethylene glycol diacrylate) (PEGDA); digital light processing (DLP); tantalum (Ta); rat bone marrow mesenchymal stem cells (r-BMSCs); diamond (DO); rhombic dodecahedron (RD); iron (Fe) ; manganese (Mn); calcium (Ca); magnesium (Mg); titanium (Ti); niobium (Nb); zirconium (Zr); stromal cells from apical papilla (SCAPs); human umbilical vein endothelial cells (hUVECs). _____ 21

Table 5. Recent advances in 3D printing/bioprinting and cellular therapies for liver tissue engineering. Abbreviations: digital light processing (DLP); methacrylated gelatin (GelMA); decellularized extracellular matrix (dECM); human-induced hepatocyte (hiHep cells); hyaluronic acid (HA); primary mouse hepatocytes (PMHs); human induced pluripotent stem cells (hiPSCs); human embryonic stem cells (hESCs); human pluripotent stem cells (hPSCs); induced pluripotent stem cells (iPSC); 3D bioprinted hepatorganoids (3DP-HOs); hepatocellular carcinoma (HCC); poly (ε-caprolactone) (PCL); human bone marrow-derived mesenchymal stem cells (BMMSCs); human hepatocellular carcinoma (hepG2); cellulose nanocrystals (CNCs); bioink with alginate (1%), cellulose nanocrystal (3%), and gelatin methacryloyl (5%) (135ACG); undifferentiated hepatocyte cell line (HUH7); primary rat hepatocytes cells (PrHCs); human umbilical vein endothelial cells (hUVECs); human lung fibroblasts (hLFs); human extracellular matrix (hECM); human hepatic stellate cell line (L × 2); primary fetal activated hepatic stellate cells (aHSC). ___ 32
Table 6. Recent advances in 3D printing/bioprinting and cellular therapies for skin tissue engineering. Abbreviations: strontium silicate (SS); matrix hydrogel with 2.8% of gellan gum, 1.6% of alginate, and 2.8% of methyl cellulose (GAM); human dermal fibroblasts (hDFs); human umbilical vascular endothelial cells (hUVECs); murine umbilical vein endothelial cells (MUVECs); dextran (Dex); vascular endothelial (VEGF); gelatin (Gel); keratin (Kr); not applicable (n/a); bi-layer (BL); poly (ε-caprolactone) (PCL); amoxicillin (AMX); external human epidermal growth factor (rhEGF); Digital light processing (DLP); gelatin methacrylate (GelMA), hyaluronic acid (HA); N-(2-aminoethyl)-4-(4-(hydroxymethyl)-2-methoxy-5-nitrosophenoxy) butanamide (NB); lithium phenyl-2,4,6-trimethylbenzoylphosphinate (LAP); human skin fibroblasts (hSFs); silk fibroin (SF); 4-arm polyethylene glycol acrylate (PEG4A); platelet-rich plasma (PRP); dermal fibroblasts (DFs); epidermal stem cells (ESCs); acellular dermal matrix (ADM); polyurethane (PU); endothelial progenitor cells (EPCs); human keratinocytes (hKCs); pectin methacrylate (PecMA); human neonatal dermal fibroblasts (hNDFs); extracellular matrix (ECM); human endothelial cells (hECs); human placental pericytes (hPCs); phosphosilicate calcium bioglasses (PSCs); human umbilical cord mesenchymal stem cells (hUCMSCs); poly-(lactic-co-glycolic acid) (PLGA).__ 42
Table 7. Recent advances in 3D printing/bioprinting and cellular therapies for neural tissue engineering. Abbreviations: methacrylated silk fibroin (SilMA); pectin methacryloyl (PecMA); silk fibroin (SF); neural stem/progenitor cells (NSPCs); polyurethane (PU); neural stem cells (NSCs); hyaluronic acid (HA); neural progenitor

cells (NPCs); poly(lactic-co-glycolic acid) (PLGA); primary human dermal fibroblasts (phDFs); vascular endothelial growth factor (VEGF); murine neural stem cells (C17.2); interferon-gamma (IFN-γ); poly (ε-caprolactone) (PCL); oxymatrine (OMT); polyethylene glycol diacrylate (PEGDA); digital light processing (DLP); gelatin methacrylate (GelMA); Poly(3,4-ethylenedioxythiophene) (PEDOT); not applicable (n/a); chondroitin sulphate methacrylate (CSMA); bone marrow-derived mesenchymal stem cells (BMSCs); stereolithography (SLA); rat adrenal medullary pheochromocytoma (pc-12); reduced graphene oxide (rGO). _____ 52

Chapter II – Characterization of Mesenchymal Stem/Stromal Cells

Table 1. The source and potential applications of some MSCs. Abbreviations: ADMSCs – adipose-derived mesenchymal stem cells; AFMSCs - amniotic fluid mesenchymal stem cells; BMMSCs - bone marrow mesenchymal stem cells; DPSCs - dental pulp stem cells; SHEDs - Human Exfoliated Deciduous Teeth Stem Cells; GMSCs - gingival mesenchymal stem cells; PDLSCs - periodontal ligament stem cells; PMSCs - placental mesenchymal stem cells; UCMSCs - umbilical cord mesenchymal stem cells. _____ 115

Table 2. Primer name, ensembl gene id, amplicon context sequences, and marker type. A- housekeeping gene; B- pluripotency markers; C- specific MSCs markers; D- hematopoietic markers; E- cell proliferation, adhesion, and compatibility markers; F- genes specific for osteogenic differentiation; G- genes specific for adipogenic differentiation; H- genes specific for chondrogenic differentiation. _____ 126

Table 3. Quantitative PCR of hDPSCs cultured. Avg Cq ± SEM: average quantification cycle ± standard error of the mean; Avg ΔCq: average quantification cycle (differential expression of target and housekeeping genes); ΔΔCq: differential expression of hDPSCs P6 and hDPSCs P9 genes; RQ: relative quantification; Regulation: ↑: up-regulated over 2-fold; ↓: down-regulated under 0.5 fold; nd: not detected; na: not applicable. _____ 135

Chapter III – Fabrication and Characterization of a 3D Scaffold for Regenerative Medicine

Table 1. Porosity of PCL, PCL/HANp and PCL/HANp/PEGDA scaffolds (mean ± standard deviation). Differences were considered statistically significant at $p \leq 0.05$. _____ 176

Table 2. EDX analysis of the scaffolds produced and CA/P molar ratio results. 178

Table 3. Compressive mechanical properties of the formulations produced (mean ± sd values). _____ 180
Table 4. Statistical significance of viability assay for hDPSCs after 24, 72, 120 and 168 hours (CT – control; ns - not significant). Results significances are presented through the symbol (*), according to the P value, with one, two, three or four symbols, corresponding to 0,01 < P ≤ 0,05; 0,001 < P 0,01; 0,0001 < P ≤ 0,001 and P ≤ 0,0001, respectively. _____ 181
Table 5. Corrected absorbance evaluated by PrestoBlue® viability assay for hDPSCs after 24, 72, 120 and 168 hours. Results presented in Mean ± SE._____ 182
Table 6. % Viability inhibition evaluated by PrestoBlue® viability assay for hDPSCs after 24, 72, 120 and 168 hours. Results presented in Mean ± SE._____ 183

Chapter IV –Bioinks for Osteogenic Differentiation

Table 1. Young's modulus measurement of alginate and alginate-nHA-Col hydrogels produced (mean ± sd values) (n = 3). _____ 222
Table 2. Parameters used in the RegenHU 3D Discovery Evolution system. The values are shown in the respective units._____ 224
Table 3. Composition of alginate-based solutions._____ 232
Table 4. Name, accession number, forward/reverse sequences, and concentrations of the primers used to assess osteogenic differentation._____ 233

Chapter V – Hybrid Scaffold for Bone Tissue Engineering

Table 1. Differences were considered statistically significant at p ≤ 0.05. Results significances are presented through the symbol (*), according to the p-value, with one, two, three or four symbols, corresponding to 0.01 < p ≤ 0.05; 0.001 < p ≤ 0.01; 0.0001 < p ≤ 0.001 and p ≤ 0.0001, respectively. A – Control; B - Alginate; C - Alginate-nHA-Col; D – Hybrid scaffold with alginate; E – Hybrid scaffold with alginate-nHA-Col. _____ 271
Table 2. Global histological scores presented as mean ± SE following ISO-10993-6 guidelines for the sham, hydrogel, hydrogel plus hDPSCs, hybrid scaffold, and hybrid scaffold plus hDPSCs groups, at 3, 7, 15 and 30 days after implantation. ISO SCORE: "minimal or no reaction" (score 0.0 to 2.9), "slight reaction" (score 3.0 to 8.9), "moderate reaction" (score 9.0 to 15.0), or "severe reaction" (score > 15).277

Chapter VI – Application of Biomaterials and Cellular Therapies for the *In Vivo* Treatment of Critical-Sized Bone Defects

Table 1. Corrected absorbance evaluated by PrestoBlue®-based viability assay for hDPSCs after 24, 72, 120 and 168 hours. Results presented in Mean ± SE.____ 321
Table 2. % Viability inhibition evaluated by PrestoBlue®-based viability assay for hDPSCs after 24, 72, 120 and 168 hours. Results presented in Mean ± SE.____ 323
Table 3. ARS Semi-Quantification in mM between groups. Results presented in mean ± SEM._____ 324

Chapter VII – General Discussion, Conclusions and Future Perspectives

Table 1. Bone-tissue engineering applications of the different scaffolds studied in this thesis. _____ 367

[This page is intentionally left blank.]

LIST OF ABBREVIATIONS

132ACG	Bioink with alginate (1%), cellulose nanocrystal (3%), and gelatin methacryloyl (5%)
2D	Two-dimensional
2PP	Two-photon polymerization
3D	Three-dimensional
3DP-HOs	Three-dimensional bioprinted hepatorganoids
4D	Four-dimensional
ACP	Amorphous calcium phosphate
AD	Additive manufacturing
ADM	Acellular dermal matrix
ADMSCs	Adipose-derived mesenchymal stem cells
AFMSCs	Amniotic fluid mesenchymal stem cells
aHSC	Primary fetal activated hepatic stellate cells
ALP	Alkaline phosphatase
ALPL	Alkaline phosphatase
AMX	Amoxicillin
ARS	Alizarin Red S
ASTM	American Society for Testing and Materials
Au	Gold
BFGF	Basic fibroblast growth factor
BJ	Binder jetting

BL	Bonelike®
BMP-2	Bone morphogenetic protein 2
BMSCs	Bone marrow-derived mesenchymal stem/stromal cells
BTE	Bone tissue engineering
C	Carbon
C17.2	Murine neural stem cells
Ca	Calcium
$Ca(OH)_2$	Calcium hydroxide
$CaCl_2$	Calcium chloride
CAD	Computer-aided design
CBER	Center for Biologics Evaluation and Research
CDRSP	Centre for Rapid and Sustainable Product Development
CECA	Centro de Estudos de Ciência Animal
CECA-ICETA	Centro de Estudos de Ciência Animal - Instituto de Ciências e Tecnologias Agrárias e Agro-Alimentares da Universidade do Porto
cECM	decellularized cardiac extracellular
CFs	Human cardiac fibroblasts
CFU	Colony Forming Unit
CLIP	Continuous light interface production
CM	Conditioned medium
CNC	Cellulose nanocrystal
Col	Collagen

COL1A2	Collagen type 1 alpha 2 chain
CSMA	Chondroitin sulfate methacrylate
CT	Computed tomography
dECM	Decellularized extracellular matrix
DEP	Directed energy deposition
Dex	Dextran
DFPCs	Dental follicle precursor cells
DFs	Dermal fibroblasts
DGAV	Veterinary Authorities of Portugal
DLP	Digital light processing
DMF	N,N-Dimethylformamide
DMLS	Direct metal laser sintering
DO	Diamond
DPBS	Dulbecco's phosphate-buffered saline
DPSCs	Dental Pulp stem/stromal cells
EBM	Electron beam melting
ECM	Extracellular matrix
EDX	Energy Dispersive X-ray Spectroscopy
EMA	European medicines agency
EPCs	Endothelial progenitor cells
ESCs	Embryonic stem cells
ESCs	Epidermal stem cells

EVCs	Early vascular cells
FBS	Fetal Bovine Serum
FDA	Food and Drug Administration
FDM	Fused deposition modeling
Fe	Iron
FFF	Fused filament fabrication
FTIR	Fourier Transform Infrared Spectroscopy
G'	Storage modulus
G''	Loss modulus
GAM	Matrix hydrogel with 2.8% of gellan gum, 1.6% of alginate, and 2.8% of methyl cellulose
Gel	Gelatin
GelMA	Gelatin methacrylate
GMSCs	Gingival mesenchymal stem cells
H&E	Hematoxylin-Eosin
H_3PO_4	Orthophosphoric acid
H9c2	Cardiomyocytes
HA	Hyaluronic acid
HAGM	Hyaluronic acid-gelatin methacrylate
HAp	Hydroxyapatite nanoparticles
Hap/β-TCP	Biphasic calcium phosphate system
hBMSCs	Human bone marrow stem/stromal cells

hCAECs	Human coronary artery endothelial cells
HCC	Hepatocellular carcinoma
hCMPCs	Human cardiac-derived cardiomyocyte progenitor cells
hCPCs	Human cardiac progenitor cells
hdECM	Heart tissue-derived extracellular matrix
hDFs	Human dermal fibroblasts
hDPSCs-CM	Conditioned medium derived from human dental pulp stem cells
hECM	Human extracellular matrix
hECs	Human endothelial cells
hepG2	Human hepatocellular carcinoma
hESCs	Human embryonic stem cells
hiHep	Human-induced hepatocyte
hiPSCs	Human induced pluripotent stem cells
hKCs	Human keratinocytes
hLFs	Human lung fibroblasts
hMVECs	Human microvascular endothelial cells
hnDFs	Human neonatal dermal fibroblasts
hPCs	Human placental pericytes
hPSCs	Human pluripotent stem cells
hSFs	Human skin fibroblasts
hUCMSCs	Human umbilical cord mesenchymal stem cells

HUH7	Undifferentiated hepatocyte cell line
hUVECs	Human umbilical vein/vascular endothelial cells
i3S	Institute for Research and Innovation in Health
IBSP	Integrin-binding sialoprotein
ICBAS - UP	School of Medicine and Biomedical Sciences - University of Porto
iCMs	Induced pluripotent stem cell-derived cardiomyocytes
IFN-γ	Interferon-gamma
IPATIMUP	Institute of Molecular Pathology and Immunology, University of Porto
iPSC-CMs	Induced pluripotent stem cell-derived cardiomyocytes
iPSCs	Induced pluripotent stem cells
ISCT	International Society for Cellular Therapy
ISO	International Standard Organization
Kr	Keratin
L x 2	Human hepatic stellate cell line
LAP	Lithium phenyl-2,4,6-trimethylbenzoylphosphinate
LOM	Laminated object manufacturing
LVR	Linear viscoelastic region
mEFs	Mouse embryonic fibroblasts
MFDS	Ministry of Food and Drug Safety
Mg	Magnesium
Micro-CT	X-ray Micro-computed Tomography

MJ	Material jetting
Mn	Manganese
MSCs	Mesenchymal stem/stromal cells
MUVECs	Murine umbilical vein endothelial cells
n/a	Not applicable
Nb	Niobium
NB	N-(2-aminoethyl)-4-(4-(hydroxymethyl)-2-methoxy-5-nitrosophenoxy) butanamide
NPCs	Neural progenitor cells
NRCMs	Neonatal rat cardiomyocytes
NSCs	Neural stem cells
NSPCs	Neural stem/progenitor cells
O	Oxygen
OMT	Oxymatrine
ORBEA	Animal Welfare Organism of the Ethics Committee
P	Phosphorus
PBF	Powder bed fusion
pc-12	Rat adrenal medullary pheochromocytoma
PCL	Poly (ε-caprolactone)
Pd	Palladium
PDLSCs	Periodontal ligament stem cells
PDT	Population Doubling Time

PecMA	Pectin methacrylate
PEDOT	Poly(3,4-ethylenedioxythiophene)
PEEK	Polyether ether ketone
PEG	Polyethylene glycol
PEG4A	4-arm polyethylene glycol acrylate
PEGDA	Polyethylene glycol diacrylate
PEGDMA	Poly (ethylene glycol) dimethacrylate
PEGMA	Poly (ethylene glycol) methacrylate
PF	PEG-Fibrinogen
PF	Poly (ethylene glycol)-fibrinogen
PGA	Poly (glycolic acid)
PGS	Poly (glycerol sebacate)
phDFs	Primary human dermal fibroblasts
PLA	Poly(l-lactic) acid
PLGA	Poly (lactic-co-glycolic) acid
PMDA	Pharmaceuticals and Medical Devices Agency
PMHs	Primary mouse hepatocytes
PMN	Polymorphonuclear
PMSCs	Placental mesenchymal stem cells
PrHCs	Primary rat hepatocytes cells
PRP	Platelet-rich plasma
PSC	Phosphosilicate calcium bioglass

PSCs	Phosphosilicate calcium bioglasses
PU	Polyurethane
PVP	Polyvinylpyrrolidone
qPCR	Quantitative real-time polymerase chain reaction
r-BMSCs	Rat bone marrow mesenchymal stem cells
RD	Rhombic dodecahedron
rGO	Reduced graphene oxide
rhEGF	External human epidermal growth factor
RUNX2	Runt-related transcription factor 2
SCAPs	Stem cells from the apical papilla
SCAPs	Stromal cells from apical papilla
SE	Standard deviation of the mean
SEM	Scanning Electron Microscopy
SF	Silk fibroin
SHEDS	Human Exfoliated Deciduous Teeth Stem Cells
SilMA	Methacrylated silk fibroin
SLA	Stereolithography
SLM	Selective laser melting
SLS	Selective laser sintering
SPP1	Secreted phosphoprotein-1
Sr-CSH	Xonotlite

SR^{2+}	Strontium
SS	Strontium silicate
Ta	Tantalum
Ti	Titanium
Ti6AI4V	Titanium alloy
UAM	Ultrasonic additive manufacturing
UCMSCs	Umbilical cord mesenchymal stem cells.
UV	Ultraviolet
VEGF	Vascular endothelial
XG	Xanthan gum
Zn^{2+}	Zinc
Zr	Zirconium
β-TCP	Beta-tricalcium phosphate

SCOPE AND OUTLINE

The overarching goal of this doctoral thesis is to develop an innovative medical device designed to promote tissue regeneration, leveraging advanced 3D printing and cell therapies. The research is driven by the need to overcome the limitations inherent in traditional autografts and allografts, which, despite their widespread use, present significant drawbacks such as donor site morbidity, limited availability and the potential for immune rejection. By integrating these manufacturing techniques with cell-based therapies, particularly those using human dental pulp stem cells (hDPSCs), this work seeks to create more effective, versatile and biocompatible alternatives for tissue repair and regeneration. The thesis is structured into seven chapters, each addressing a critical aspect of this multifaceted research endeavor (**Figure 1**).

Chapter I: State of the Art

The thesis begins with an extensive literature review, presented in **Chapter I**, which presents a detailed analysis of the current state of research in 3D printing and bioprinting, especially within the context of Regenerative Medicine (article "**Three-Dimensional Printing/Bioprinting and Cellular Therapies for Regenerative Medicine: Current Advances**"). This chapter not only provides a historical perspective on the evolution of these technologies, but also delves into the latest advancements, highlighting how these cutting-edge techniques are being employed to create complex, tissue-like structures that closely mimic natural biological tissues. The chapter also explores the integration of these technologies with cell-based therapies, emphasizing the potential of mesenchymal stem/stromal cells (MSCs) as a versatile and potent cell source for regenerative applications. By providing a thorough analysis of existing research, this chapter sets the stage for the innovative approaches developed and tested in the subsequent chapters.

Chapter II: Characterization of Mesenchymal Stem/Stromal Cells

Chapter II focuses on the isolation and characterization of hDPSCs, which are central to the cell therapy strategies explored in this thesis. This chapter outlines the protocols used for the extraction and purification of hDPSCs from human dental pulp, followed by a comprehensive characterization of their biological properties. The analysis covers the cell behavior in culture, multilineage differentiation and gene expression. This chapter examines the cells' capacity as

MSCs, offering valuable insights into their suitability for bone and other tissue regeneration applications. This foundational work is essential for understanding the potential of hDPSCs to enhance the performance of the 3D-printed scaffolds developed in later chapters.

Chapter III: Fabrication and Characterization of a 3D Scaffold for Regenerative Medicine

In **Chapter III**, the focus shifts to the fabrication and characterization of a 3D scaffold designed specifically for Regenerative Medicine applications (article "**Assessment of 3D-Printed Polycaprolactone, Hydroxyapatite Nanoparticles and Diacrylate Poly(ethylene glycol) Scaffolds for Bone Regeneration**"). Utilizing extrusion-based 3D printing, a method chosen for its precision, reproducibility, and versatility, this chapter details the development of scaffolds that can serve as supportive matrices for tissue regeneration. The material selection process is thoroughly explained, with an emphasis on choosing biocompatible and biodegradable polymers that provide the necessary mechanical support while promoting cell attachment and proliferation. The chapter also covers the optimization of printing parameters, post-processing techniques, and the characterization of the scaffold's mechanical properties. Additionally, *in vitro* tests are conducted to evaluate the scaffold's ability to support cell growth and differentiation, laying the groundwork for the *in vivo* studies.

Chapter IV: Bioinks for Osteogenic Differentiation

Chapter IV addresses the development of a bioink formulation specifically designed to promote osteogenic differentiation in the context of extrusion-based bioprinting (article "**3D Bioprinting of Alginate-Based Hydrogels to Investigate Osteogenic Differentiation of hBMSCS *in vitro***"). The formulation process is discussed in detail, including the selection of bioactive components that support the differentiation of hDPSCs into osteoblasts, the bone-forming cells. The chapter also examines the rheological properties of the bioink, ensuring it possesses the appropriate viscosity and flow characteristics for successful bioprinting. The printability of the bioink is tested through the fabrication of cell-laden structures, and subsequent biological assays are performed to assess the osteogenic potential of the printed constructs. This chapter is pivotal in demonstrating how bioinks can

be tailored to enhance the functionality of bioprinted tissues, specifically in the context of bone regeneration.

Chapter V: Hybrid Scaffold for Bone Tissue Engineering

The research progresses in **Chapter V** with the development of hybrid scaffolds that combine 3D-printed constructs with cell-laden hydrogels (article "**Hybrid Scaffolds for Bone Tissue Engineering: Integration of Composites and Bioactive Hydrogels Loaded with hDPSCs**"). These hybrid scaffolds are designed to merge the mechanical strength of the printed scaffold in **Chapter III: Fabrication and Characterization of a 3D Scaffold for Regenerative Medicine** with the biological activity of the hydrogel developed in **Chapter IV: Bioinks for Osteogenic Differentiation**, which is infused with hDPSCs. The current chapter details the fabrication process of these hybrid constructs, including the integration of bioinks with the 3D-printed framework. *In vitro* studies are conducted to evaluate the hybrid scaffold's ability to support cell viability, proliferation, and differentiation. Following these studies, *in vivo* analyses are performed using a rat model to assess the scaffold's biocompatibility in a living organism. The results from these studies provide crucial data on the scaffold's potential for clinical application, highlighting its capacity to facilitate the repair of bone defects in a controlled and predictable manner.

Chapter VI: Application of Biomaterials and Cellular Therapies for the *In Vivo* Treatment of Critical-Sized Bone Defect

Chapter VI represents a critical transition from *in vitro* to *in vivo* applications, focusing on the real-world efficacy of the developed scaffolds in treating critical-sized bone defects. This chapter explores the combination of polycaprolactone (PCL) and Bonelike® (BL) scaffolds with conditioned medium derived from hDPSCs (hDPSCs-CM) to enhance bone regeneration. The research is conducted using an ovine model, chosen for its anatomical and physiological similarities to humans, particularly in bone structure and healing processes. The chapter describes the surgical creation of bone defects in the ovine model, the application of the developed scaffolds and cell therapies, and the subsequent evaluation of bone regeneration. Imaging techniques, such as X-rays, are employed alongside histological analyses to assess the extent of bone repair and integration. This comprehensive study provides critical insights into the potential clinical

application of these scaffolds for treating large bone defects, offering a promising alternative to traditional grafting techniques.

Chapter VII: General Discussion, Conclusions, and Future Perspectives

The final chapter, **Chapter VII**, provides a synthesis of the research findings, drawing connections between the various studies presented throughout the thesis. This chapter presents a critical evaluation of the methodologies used, the results obtained, and the implications for the field of tissue engineering and Regenerative Medicine. It discusses the successes achieved, such as the effective integration of 3D printing and cell therapy for bone regeneration, as well as the limitations encountered, including the challenges of translating *in vitro* success to *in vivo* models. The chapter concludes with a discussion of future research directions, outlining the remaining challenges and proposing new avenues for exploration. Key future prospects include completing the ongoing *in vivo* analyses in larger animal models, such as sheep, to better replicate human clinical conditions, and further refining the scaffold and bioink formulations to enhance their clinical efficacy and applicability. The thesis ends by emphasizing the potential impact of this research on developing new, more effective treatments for bone and tissue regeneration, ultimately contributing to the advancement of Regenerative Medicine and improving patient outcomes.

This thesis represents a significant contribution to the field of tissue engineering and Regenerative Medicine, laying the groundwork for future advancements in the development of effective, biocompatible, and customizable solutions for bone regeneration.

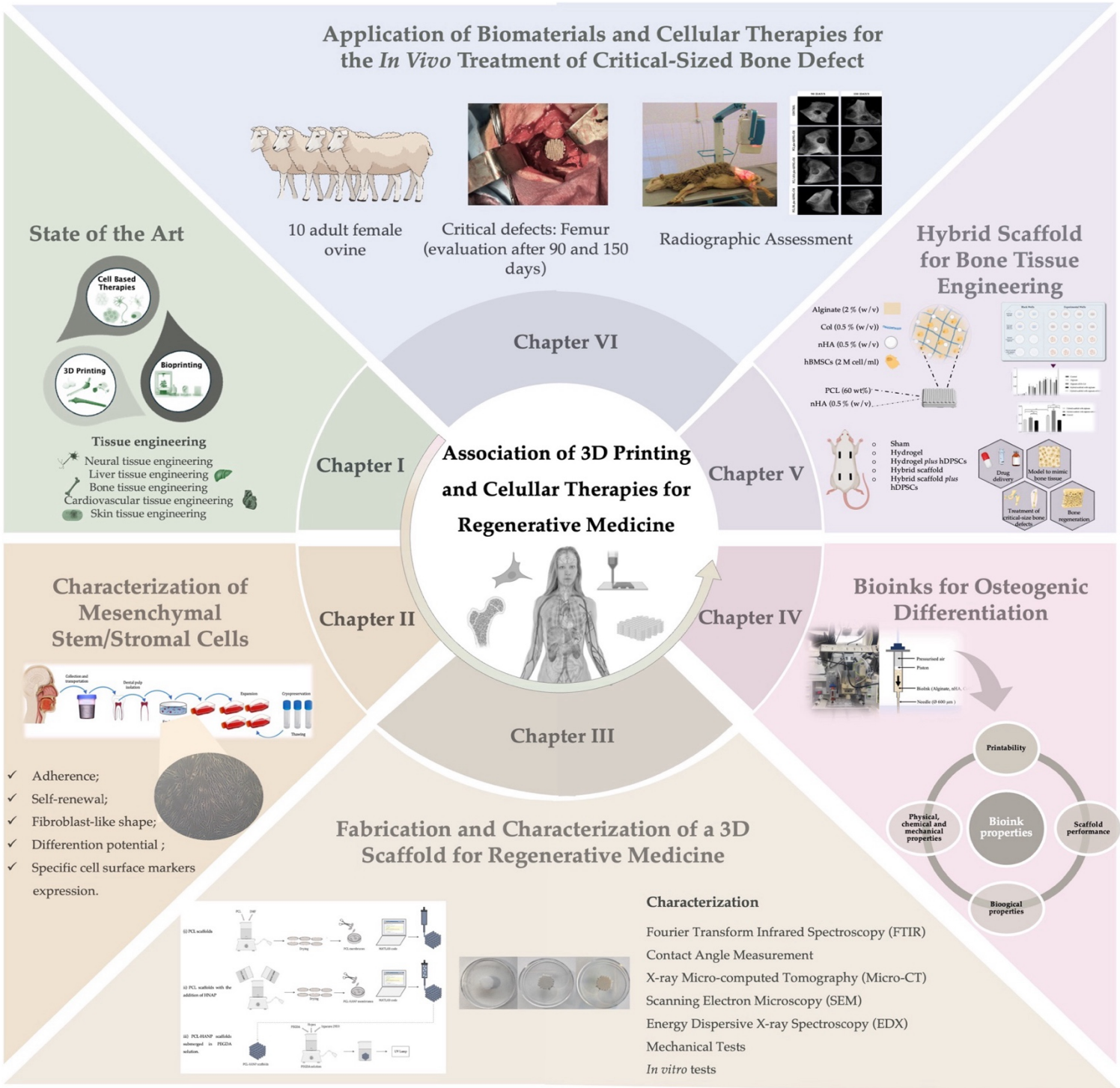


Figure 1. Overview of the chapters conducted during the present doctoral thesis.

[This page is intentionally left blank.]

CHAPTER I

STATE OF ART

[This page is intentionally left blank.]

Introductory Note

Regenerative Medicine is an advancing field focused on the restoration and regeneration of functional tissue components that have been compromised by disease or injury [1]. This field offers a compelling alternative to organ transplantation, mitigating challenges such as donor organ shortages and immune rejection. Its applications are broad, encompassing areas such as osteogenic repair, cardiac therapy, and skeletal muscle regeneration [2-4]. Over the past decades, Regenerative Medicine has evolved into a major industry, supported by the commercialization of various therapeutic products [5-7].

A key area of Regenerative Medicine is the development of biomaterials for tissue restoration and therapeutic intervention. These materials function as tissue scaffolds, delivery systems, decellularized tissue matrices, among others, fulfilling essential roles in aiding tissue repair and regeneration [8-18]. The design and engineering of biomaterials with precise structural and physicochemical properties, along with optimal biocompatibility, are fundamental for enhancing regenerative outcomes [19-25].

The concept of "living materials" has recently emerged as a significant innovation in the field. These are materials that incorporate biologically active components and medicines and biologics, particularly living cells, which interact dynamically with their environment to promote tissue regeneration [26-28]. A variety of advanced engineering techniques have been employed in the development of “living materials”, including genetic modification of cells, encapsulation of cells within polymeric or nanoparticle matrices, fabrication of scaffolds or films with embedded cells, and the creation of microfluidic-based three-dimensional (3D) tissue and organ models [29-32]. These living materials combine the biological activity of cellular components with the structural and

functional benefits of natural/synthetic materials, closely mimicking the properties of native tissues. Their enhanced bioactivity and tunable microstructures offer precise control over cellular behaviour, making them highly effective in targeted regenerative applications [33].

The integration of 3D printing technologies into Regenerative Medicine has further advanced the field, enabling the fabrication of complex tissue constructs that closely replicate the architecture and functionality of native tissues. Recent developments in 3D bioprinting have led to the creation of specialized tissue models that surpass traditional tissue engineering methods in complexity and precision. This technological advancement represents a significant leap forward in the development of more effective and personalized regenerative therapies [34].

Regenerative Medicine is centered on supporting the body's intrinsic self-healing abilities to promote cell and tissue growth *in vivo* [35]. This is accomplished using tissue engineering methods in combination with other *in vivo* therapies such as cellular therapies [9,10,36].

Cellular therapies are increasingly recognized as an essential component in the future of medical interventions aimed at repairing damaged or destroyed tissues. These therapies encompass a range of approaches, including the use of autologous (derived from the same individual) or allogeneic (derived from a different individual of the same species) stem cell progenitors, sourced from either adult or embryonic tissues. Additionally, these strategies often involve the application of various trophic factors or cellular secretome that are produced by these stem cells, with the goal of mobilizing the host's own resident stem cells and stimulating their proliferation and differentiation [37].

This chapter presents a comprehensive review of the current literature on the potential applications of 3D printing, bioprinting, and cell therapies in the field

of Regenerative Medicine. It systematically analyses the unique aspects of 3D printing and bioprinting technologies, alongside the principles and methodologies underlying cell-based therapies. The chapter further explores the diverse applications of these innovative approaches across various domains of tissue engineering, including cardiovascular, bone, liver, skin, and neural tissues. Moreover, the chapter addresses the existing limitations and challenges associated with the integration of 3D printing and cell therapies in Regenerative Medicine. It also provides a forward-looking perspective on the future developments and potential advancements in these fields.

[This page is intentionally left blank.]

Three-Dimensional Printing/Bioprinting and Cellular Therapies for Regenerative Medicine: Current Advances

Ana Catarina Sousa, Rui Alvites, Bruna Lopes, Patrícia Sousa, Alícia Moreira, André Coelho, José Domingos Santos, Luís Atayde, Nuno Alves and Ana Colette Maurício

In *Journal of Functional Biomaterials*

DOI: 10.3390/jfb16010028.

[This page is intentionally left blank.]

Review

Three-Dimensional Printing/Bioprinting and Cellular Therapies for Regenerative Medicine: Current Advances

Ana Catarina Sousa [1,2,3], Rui Alvites [1,2,3,4], Bruna Lopes [1,2,3], Patrícia Sousa [1,2,3], Alícia Moreira [1,2,3], André Coelho [1,2,3], José Domingos Santos [5], Luís Atayde [1,2,3], Nuno Alves [6] and Ana Colette Maurício[1,2,3,*]

[1] Departamento de Clínicas Veterinárias, Instituto de Ciências Biomédicas de Abel Salazar (ICBAS), Universidade do Porto (UP), Rua de Jorge Viterbo Ferreira, nº 228, 4050-313 Porto, Portugal; anacatarinasoaressousa@hotmail.com (A.C.S.); ruialvites@hotmail.com (R.A.); brunisabel95@gmail.com (B.L.); pfrfs_10@hotmail.com (P.S.); alicia.moreira.1998@gmail.com (A.M.); andrefmc17@gmail.com (A.C.); ataydelm@gmail.com (L.A); ana.colette@hotmail.com or acmauricio@icbas.up.pt (A.C.M.).

[2] Centro de Estudos de Ciência Animal (CECA), Instituto de Ciências, Tecnologias e Agroambiente da Universidade do Porto (ICETA), Rua D. Manuel II, Apartado 55142, 4051-401, Porto, Portugal.

[3] Associate Laboratory for Animal and Veterinary Science (AL4AnimalS), Av. Universidade Técnica, 1300-477, Lisboa, Portugal.

[4] Instituto Universitário de Ciências da Saúde (CESPU), Instituto Universitário de Ciências da Saúde (IUCS), Avenida Central de Gandra 1317, Gandra, 4585-116 Paredes, Portugal.

[5] REQUIMTE-LAQV, Departamento de Engenharia Metalúrgica e Materiais, Faculdade de Engenharia, UP, Rua Dr. Roberto Frias, 4200-465, Porto, Portugal; jdsantos@fe.up.pt (J.D.S.).

[6] Centre for Rapid and Sustainable Product Development (CDRSP), Polytechnic Institute of Leiria, Rua de Portugal – Zona Industrial, 2430-028 – Marinha Grande, Portugal; nuno.alves@ipleiria.pt.

* Correspondence: ana.colette@hotmail.com or acmauricio@icbas.up.pt (A.C.M.)

Abstract: The application of three-dimensional (3D) printing/bioprinting technologies and cell therapies has garnered significant attention due to their potential in the field of Regenerative Medicine. This paper aims to provide a comprehensive overview of 3D printing/bioprinting technology and cell therapies, highlighting their results in diverse medical applications, while also discussing the capabilities and limitations of their combined use. The synergistic combination of 3D printing and cellular therapies has been recognised as a promising and innovative approach, and it is expected that these technologies will progressively assume a crucial role in the treatment of various diseases and conditions in the foreseeable future. This review concludes with a forward-looking perspective on the future impact of these technologies, highlighting their potential to revolutionize Regenerative Medicine through enhanced tissue repair and organ replacement strategies.

Keywords: 3D printing; Additive manufacturing; Biomaterials; Biomedical applications, Bioprinting; Cellular therapies; Tissue regeneration.

---

1. Introduction

Nowadays, regenerative medicine is considered an emerging field of research worldwide with the potential to revolutionise healthcare (improving patient outcomes and quality of life) in the 21st century [1]. This field is focused on the replacement, engineering and regeneration of human cells, tissues and organs. Its aim is to repair, restore, supplement or replace the normal function of a biological system following treatment with autologous, allogeneic stem and stromal cells [2-4].

In recent years, two promising approaches that have gained attention, namely three-dimensional (3D) printing and cellular therapies. 3D printing has revolutionized tissue engineering through the manufacture of complex, patient-specific, whilst providing precise control over the spatial distribution of cells and biomaterials. On the other hand, cellular therapies encompass the use of living cells to replace, repair, or regenerate injured tissues. The integration of 3D printing

with cell therapies provides personalised, cell-laden constructs that mimic the complex architecture and function of native tissues. This approach stimulates cell-cell interactions, cell-matrix interactions and the creation of functional tissue-like constructs [5, 6].

This review presented an overview of current advances in the combination of 3D printing/ bioprinting and cell therapies in the field of regenerative medicine. Firstly, the principles and applications of 3D printing/bioprinting and cell therapies were addressed individually. Subsequently, we explored recent advances in the integration of these technologies to create 3D-printed cellular structures. The limitations and challenges associated with these approaches were also mentioned, and the current state was analysed. Finally, we presented a future perspective on the potential impact of these technologies in the field of regenerative medicine and concluded with a summary of the main findings.

By providing a detailed understanding of the current state and future directions, this review seeks to contribute to the growing body of knowledge in this challenging and rapidly evolving field.

2. Three-Dimensional Printing

Three-dimensional (3D) printing (alternatively termed as additive manufacturing (AM)) is a burgeoning technique for rapid prototyping of structures in diverse fields, encompassing regenerative medicine [7-11]. In the past two decades, 3D printing has been widely researched due to its simplicity and its highly flexible manufacture provides unlimited possibilities for creating complex structures [12, 13]. Several examples of 3D printed medical devices include instrumentation, guides to facilitate the correct surgical placement of devices; implants, such as hip joints; and external prostheses, such as bionic hands [14].

This advanced manufacturing technology, pioneered by Charles Hull in the early 1980s, enables the creation of customized and intricate structures with high precision and accuracy [15]. The technology operates by using computer-aided design (CAD) software to create a virtual model of the structure, which is subsequently converted into a physical object through the use of various 3D printing techniques [16]. The International Standard Organization (ISO) and the American Society for Testing and Materials (ASTM) [17] have established a classification system comprising seven overarching categories to categorize AM

methods based on part manufacturing approaches, as outlined in Figure 1. The subsequent sections provide a succinct overview of AM processes.

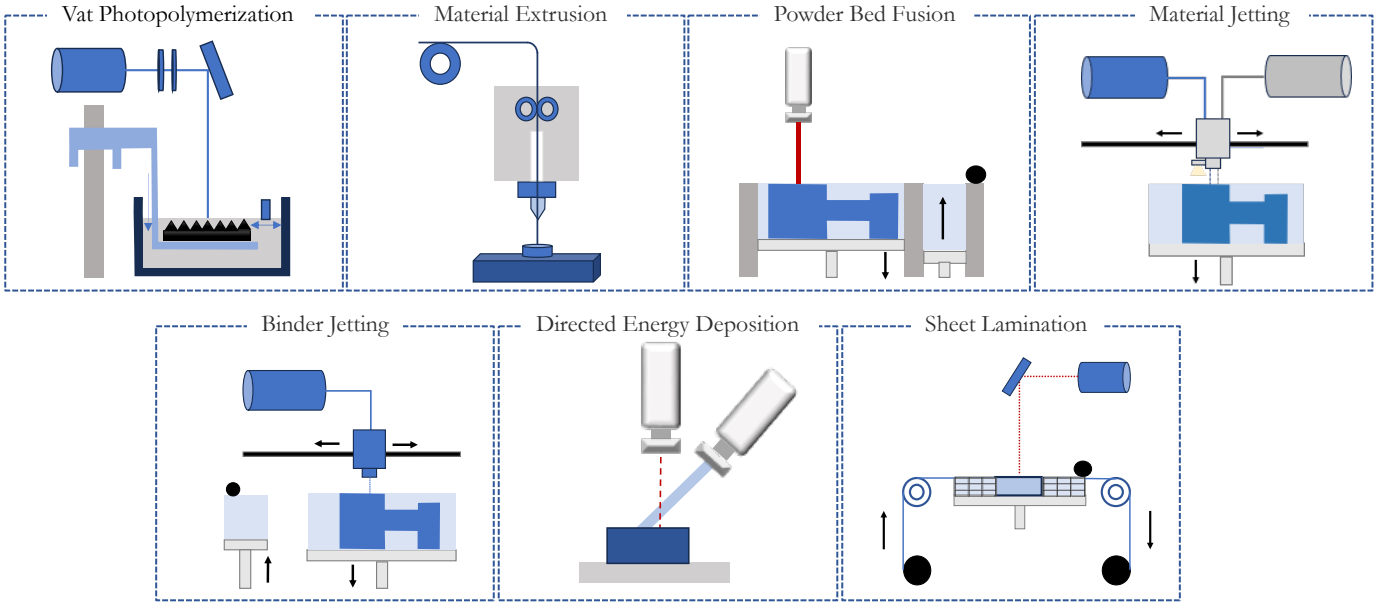


Figure 1. Schematic representation of the various AM processes.

2.1. Vat Photopolymerization

This method is characterized by principle of selectively solidifying a liquid photopolymer resin by exposing it to specific light sources or patterns. In the procedure, a vat contains the liquid resin, which is selectively cured layer by layer in the desired regions, gradually constructing the intended object. The laser, guided by predetermined digital coordinates, provides the necessary information to cure the resin at precise locations within each layer. To facilitate this curing process, a photoinitiator is introduced into the resin material. The photoinitiator absorbs the incident ultraviolet (UV) radiation and generates active species that initiate the photopolymerization reaction [18, 19].

The vat photopolymerization technique includes various commonly utilized processes, such as stereolithography (SLA), continuous light interface production (CLIP), digital light processing (DLP) and two-photon polymerization (2PP) [20]. These methods involve SLA, which uses a laser or digital light projector to cure the resin layer by layer, whereas DLP employs a digital light projector to cure an entire layer at once. CLIP employs a continuous liquid interface production approach, where a continuous liquid interface is established between the resin and a transparent window, enabling continuous printing. Lastly, 2PP utilizes a focused

laser beam and a photosensitive resin to achieve high-resolution printing via a nonlinear optical process [21]. These vat photopolymerization techniques offer versatile and AM capabilities for fabricating complex and detailed structures.

2.2. Material Extrusion

Materials extrusion is a widely adopted AM technique due to its fast manufacturing, cost efficiency, simplicity, user-friendly nature and the potential to produce complex components [22-24]. This technique involves extruding the material through an orifice and depositing it on a construction platform [25-27].

The most common technique is the fused filament fabrication (FFF), which is also referred to as fused deposition modelling (FDM) [28]. In this method, the filament is heated to a temperature typically between 150–250°C until it melts, and the molten material is extruded through a nozzle [25]. The extruded material is then placed onto a build plate, which can be adjusted in the z direction. This technique usually uses more polymers, although it is also used to print metal and ceramic components. FFF uses a support to create overhang features, which can be removed either mechanically by detaching it from the printed part or chemically by dissolving it in a solvent [29]. In contrast to FFF, which employs thermoplastics, direct ink writing (DIW) is a 3D printing technique that utilizes viscoelastic inks. In the DIW process, these inks are extruded through a nozzle mounted on a 3D translation platform, with the flow regulated by the application of pressure [30].

2.3. Powder Bed Fusion

The powder bed fusion (PBF) technique uses a laser or an electron beam to melt and fuse the material into powder [31]. The principle used in this technique is to produce the product layer by layer and melt it. A heat source concentrates its heat on a powdered base material and heats the cross-sectional area [32].

PBF is mainly used due to the low cost of producing the object and the powder can be recycled to produce another piece from it [33]. This method encompasses several commonly utilized processes, including direct metal laser sintering (DMLS), selective laser sintering (SLS), electron beam melting (EBM), and selective laser melting (SLM). PBF utilizes a laser source or an electron beam (EBM) to selectively melt or sinter layers of material, thereby fabricating a solid

component. This technique is applicable to a range of powder-based materials, with metals and polymers being the most commonly processed [29].

2.4. Material Jetting

The material jetting (MJ) deposits the liquid in droplets to bind powder material [34]. In the MJ, the material is injected into the surface/building platform, where it solidifies, and the model is assembled layer by layer. The layers are subsequently cured or toughened with ultraviolet light. In this method, the material must be deposited in droplets, and therefore the materials used are limited. Generally, polymers and waxes are used, considering their viscous nature and ability to produce droplets [35]. This is a fast and proficient method and offers greater freedom when designing and printing complex models [24].

2.5. Binder Jetting

In the binder jetting (BJ), a liquid bonding compound is applied selectively to bind powder materials. A relevant feature of this technique today is the possibility of using color inkjet technology to create colored objects in the binders [36].

Binders are used to ensure adhesion between the powdered material particles. These binders contribute to obtaining the strength of the part and the desired form of the final product [32, 37]. The materials commonly used in this method are metals (e.g., stainless steel), ceramics (e.g., glass) and polymers (e.g., acrylonitrile butadiene styrene, polyamide and polycarbonate) [33].

2.6. Directed Energy Deposition

The directed energy deposition (DEP) is an AM technique that utilizes focused thermal energy to melt materials, which are fused as they are deposited. In this method, an energy source - such as an electron beam, a laser and a plasma - is used to melt the materials which are then deposited [36].

The DED involves a nozzle assembled on a multi-hub arm that deposits the dissolved material at a surface layer where it solidifies A significant advantage of this method is its ability to precisely control the grain structure of the deposited material [33, 38, 39].

This process is analogous to material extrusion; however, the nozzle in DED has the capacity to transverse multiple directions rather than being restricted to a single axis. While the process is applicable to polymers and ceramics, it is predominantly utilized for metals, which are provided in either powder or wire form [40].

2.7. Sheet Lamination

Sheet lamination involves the sequential bonding of thin sheets of material, normally fed through a set roller [41]. This technique can employ various materials, including paper, polymer and metal [28]. Although this is a less precise method, it offers advantages in terms of speed and cost-effectiveness [41].

The predominant sheet lamination techniques are laminated object manufacturing (LOM) and ultrasonic additive manufacturing (UAM). LOM employs a layer-by-layer method similar to other additive manufacturing processes, utilizing paper as the primary material and adhesive for bonding, rather than welding. Conversely, UAM involves metals such as aluminum, stainless steel, and titanium, and operates at relatively low temperatures, enabling the production of complex internal geometries [42].

To highlight the advantages and drawbacks of each of the previously discussed AM techniques, a summary is provided in Table 1.

Table 1. Advantages and drawbacks of each AM technique [22-24, 33, 42-44].

Printing Technology	Vat Photopolymerization	Material Extrusion	Power Bed Fusion	Material Jetting	Binder jetting	Directed Energy Deposition	Sheet Lamination
Advantages	• High precision and good surface finish • Capability to use transparent materials • Relatively fast processing time • Typically large build volumes	•Widely adopted and cost-effective •Exhibits favorable material properties •Minimal material waste •Relatively high fabrication speed •User-friendly nature •Capability to produce complex components	•Relatively cost-effective •Capable of integration into small-scale applications •Broad compatibility with a wide range of materials •Extensive material versatility	• High precision • High processing speed • Minimal material waste • Capability to produce multi-material and multi-color components within a single process	• Diverse color options • Wide range of material choices • Rapid processing time • Capability to process two materials simultaneously	• High-quality components • Speed is frequently compromised to achieve higher accuracy	• High processing speed • Cost-efficient fabrication • Simplified material handling
Drawbacks	• Relatively high cost • Extended post-processing time • Limited range of compatible materials • Necessity for support structures during fabrication	• Limited by nozzle radius • Low precision and fabrication speed • Requires consistent material pressure during operation • Prone to delamination issues	• Relatively low fabrication speed • Materials often lack robust structural properties • Size constraints limit the scalability of produced componentes • High energy consumption during processing • Surface finish quality is influenced by powder grain size • Thermal stress and material degradation are common challenges	• Support structures are frequently necessary • Limited material options • Frequent nozzle blockages • Low viscosity and mechanical strength	• Not always suitable for structural components due to the use of binder materials • Extended post-processing time required • High porosity and low surface quality	• Post-processing may be required to achieve the desired effect • Limited material availability • Thermal stresses and the need for controlled atmospheric conditions	• Low precision • Prone to shrinkage during processing • Generates a significant amount of material waste • Delamination is a frequent issue

3. Bioprinting

According to Moroni et al., in the context of tissue engineering and regenerative medicine, the term "bioprinting" refers to the use of computer-assisted transfer techniques for the modelling and assembly of living and non-living materials in a predefined 2D or 3D configuration to create bioengineered structures [45]. By incorporating active sub-stances, such as biomaterials, living cells and bioactive molecules, bioprinting imparts biological functions to the manufactured structures [12].

Bioprinting technology allows for the manufacture of complex, functional structures that promote cell growth and tissue formation. The prospect of manufacturing complete tissues or organs using 3D printing is very promising and has the potential to revolutionise regenerative medicine [46].

In recent decades, significant advancements have been made in the field of 3D bioprinting (Figure 2) [47-50]. The evolution of this technology began with the invention of SLA by Charles Hull in 1984, which marked the beginning of 3D bioprinting [48]. Subsequently, in 2002, Landers et al. introduced extrusion-based bioprinting technology, which was later commercialized under the name "3D-Bioplotter" [51, 52]. In 2003, Thomas and Boland's research team adapted a conventional inkjet printer to develop the first inkjet bioprinter capable of printing living cells [51, 52]. Later, the engineering of scaffold-free vascular tissue via bioprinting was achieved by Norotte et al. [53]. The subsequent years witnessed the development and introduction of various bioprinted constructs, including an artificial liver in 2012, full human skin in 2014, a heart valve in 2016, and a lung-mimicking air sac with surrounding blood vessels in 2019, among other innovations [47-50].

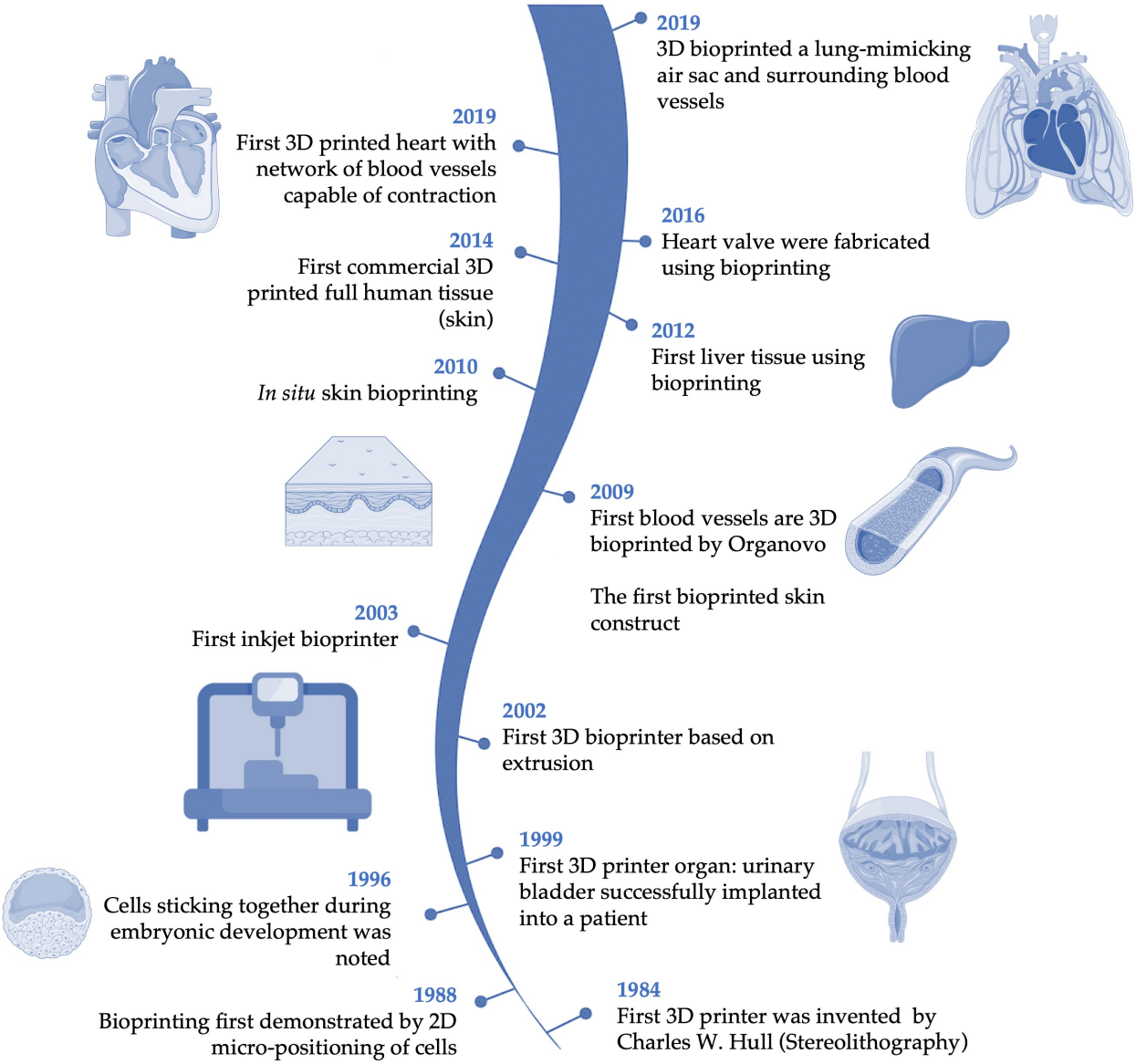


Figure 2. Major milestones in the history of 3D bioprinting.

3.1. Techniques

Among the diverse AM techniques, the most employed in bioprinting are laser-based printing (SLA and SLS), extrusion printing and inkjet printing [54-56].

SLA is a vat photopolymerization process that consists of photocurable bioinks that are subjected to UV, infrared or visible light to produce 3D pieces using the layer-by-layer procedure [57, 58]. Among the advantages of SLA is its capacity to rapidly cure at physiological temperatures, which facilitates the production of constructs suitable for regenerative medicine applications. This technique has been widely employed to fabricate micro-needles designed for transdermal drug

delivery, hearing aids, surgical guides for placing dental implants, temporary crowns and bridges and supports for tissue engineering with/ without encapsulated cells [57, 59].

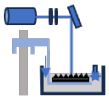
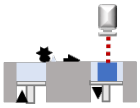
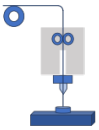
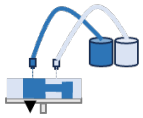
During SLS printing, fine particles of the entire substance are fused by the heat of a high-powered laser to fabricate a 3D structure [60, 61]. In this technique, several categories of powders, including polymers, ceramics and metals, must be processed into powder. SLS is a PBF process that is used in numerous applications in the medical field, namely the fabrication of prototypes for medical devices, physical models used in surgery and scaffolds for tissue engineering. The popularity of SLS printers is attributed to their affordability, high productivity and material versatility [61, 62].

Extrusion printing is considered the most popular bioprinting technology [63]. In this method, material is melted and extruded through a nozzle, orifice or needle using a screw, piston or high-pressure pneumatic force to form successive layers of the part [64-68]. This technique has been used extensively in the medical field, enabling the biofabrication of tissues, organs, implants and personalised drug delivery systems. Extrusion is also highly applicable in the field of disease modelling. Models made by extrusion can pro-vide a baseline for the comprehension of the underlying biological mechanisms behind disease progression, thus contributing to the identification of effective treatments [69].

Inkjet bioprinting is considered the pioneering technology in the field of bioprinting. The printing process utilizing this technique comprises two phases: first, the generation of discrete droplets that are precisely directed to specific locations on a substrate, and second, the subsequent interaction between these droplets and the substrate [48, 70]. It is employed in various medical applications, including the creation of patient-specific or project-specific implants for static load-bearing purposes (such as dental crowns and prosthetic structures), joint applications (such as osteochondral cartilage implants) and for facilitating in vivo blood vessel formation and tissue regeneration [71].

Table 2 presents the aforementioned techniques, as well as the advantages and drawbacks of each.

Table 2. Comparison of the bioprinting techniques [60, 72-75].

Printing Technology	Laser-based Printing		Extrusion Printing	Inkjet Printing
	Stereolithography 	Selective Laser Sintering 		
Advantages	✓ High accuracy/resolution ✓ Printing time independent of complex geometries ✓ Fast fabrication speed ✓ Good vertical printability ✓ Smooth surface finish	✓ No need for support structures ✓ Suitable for a wide range of materials ✓ High mechanical strength of printed constructs ✓ High productivity ✓ Ability to print complex structures	✓ Relatively simple and cost-effective setup ✓ Vesrsatile material choices ✓ Ability to print with high cell densities and high viscosity biomaterials ✓ No need for support materials	✓ Low cost and scalable ✓ High printable resolution/precision ✓ Fast fabrication speed ✓ Wide availability ✓ Ability to print low viscosity biomaterials ✓ Low material wastage ✓ Capable of depositing multiple cell types simultaneously
Drawbacks	▪ Limited to photocurable biomaterials ▪ Potential cytotoxicity of photoinitiators ▪ Lack of printing multi-cells ▪ Need for support materials ▪ Expensive equipment and materials	▪ Rough surface ▪ High equipment cost ▪ High energy consumption ▪ Difficulty in printing cell-laden constructs ▪ Slow fabrication speed ▪ Post-processing required to remove excess powder	▪ Slow fabrication speed ▪ Low printable resolution/precision ▪ Possible nozzle clogging ▪ Potential shear stress-induced cell damage during extrusion	▪ Lower mechanical strength of printed constructs ▪ Limited printable materials/requires low viscosity materials and low cell densities ▪ Need for support materials ▪ Potential clogging of print nozzles

3.2. Materials used in 3D bioprinting

Nowadays, a diverse range of biomaterials are being used in 3D bioprinting [76]. The interaction between biomaterials and cells is fundamental for cell viability, proliferation, and differentiation. Hence, it is fundamental to consider the characteristics of biomaterials, such as non-toxicity, biocompatibility, and the absence of immune reactions and foreign body responses [77].

Bioprinting materials are categorized into two types: natural and synthetic bio-materials. Natural biomaterials are particularly attractive due to their bioactivity, being both similar to the extracellular matrix (ECM) and biocompatible. The following are some examples of natural materials used in this field: collagen, xanthan gum (XG), silk fibroin (SF), gelatin, pectin, gellan gum, albumin, chitosan, sodium alginate, agarose, fibrin, keratin and hyaluronic acid (HA). However, these types of materials generally exhibit poor mechanical properties [78-99]. Conversely, synthetic materials provide distinct advantages compared to natural materials, including the ability to be customized with specific physical properties and greater uniformity. The following are some examples of synthetic materials used in this field: poly (ε-caprolactone) (PCL), poly(lactic-co-glycolic) acid (PLGA),

poly(l-lactic) acid (PLA), poly (glycolic acid) (PGA), polyurethane (PU), polyethylene glycol (PEG), polyether ether ketone (PEEK), polyvinylpyrrolidone (PVP) and pluronic. Nevertheless, synthetic materials for 3D bioprinting have some disadvantages, such as poor biocompatibility, the potential release of toxic degradation by-products and the absence of bioactive ligands [100-113].

To address these drawbacks, a more comprehensive knowledge of the physiological characteristics of the ECM and a higher ability to replicate the complex 3D structures mimetic of the ECM would represent a significant advance in 3D bioprinting. Advances in composite and hybrid bioprinting materials, as well as multimaterial bioprinting technologies, have emerged in the field of tissue regeneration [114, 115]. Nonetheless, human tissues and organs operate within a highly dynamic biochemical environment, and conventional bioprinted materials often fail to adapt to the evolving spatial and temporal requirements of tissue and organ development. Consequently, there is in-creasing interest in developing sophisticated stimuli-responsive biomaterials for 3D bioprinting, which would facilitate the adaptation of artificial constructs to intricate and dynamic physiological conditions [115-117].

4. Cellular Therapies

Cellular therapies, also known as cell therapy, cell transplantation or cytotherapy, involve the injection, grafting or implantation of cells into a patient (autologous or allogeneic) to achieve a medicinal effect [118, 119]. Cell therapies are frequently applied in combination with biomaterial supports, which are designed to support and guide the cells both during and after transplantation [120].

Advances in 3D printing technology allow for the precise spatial arrangement of multiple cells and biomaterials, thereby enhancing the efficiency of cell delivery and integration onto scaffolds. There are two primary methods to deliver cells via 3D printed scaffolds: post-printing cell seeding and embedding cells within bioinks during the 3D bioprinting process [121-124]. The approach of seeding the cells after printing provides more flexible requirements for both the conditions and 3D printing process, though it is hindered by low cell adhesion rates on the scaffolds. To address this challenge, one approach involves encapsulating cells in hydrogels prior to combining them with 3D printed scaffolds. Alternatively,

the bioprinting method enhances cell loading efficiency and allows for precise control over the spatial distribution of various cell types. However, this method demands stringent conditions and precise parameters during printing, as cells are sensitive to suboptimal environmental conditions. This necessitates detailed knowledge of the parameters of the bioinks and printing conditions beforehand [74, 125-128].

The selection of a specific type of cell therapy is highly important, since it affects the function and design of the tissue engineering model [129, 130]. There are three categories of cell therapies that can be applied to printed scaffolds, namely, stem cell-based, non-stem cell-based and multicellular therapies [118].

4.1. Stem Cell-based Therapies

Stem cells are among the most frequently utilised cell types due to their unspecialized nature, which allows them to self-renew and differentiate into various cell lineages. [11, 129, 131, 132]. Their ability to differentiate into specific cell types while continuously dividing and self-renewing makes their prospects interesting for regenerative medicine. They have successfully been used to create functional tissues that replicate the properties of natural organs. These stem cells can be sourced from several origins [133]. In the field of bioengineering, the three most frequently employed types are mesenchymal stem/stromal cells (MSCs), embryonic stem cells (ESCs) and induced pluripotent stem cells (iPSCs) [134].

Also known as multipotent cells, MSCs can be sourced from various tissues, including bone marrow, muscle, lung, teeth, adipose tissue, liver and perinatal/extra-embryonic tissues. They exhibit the capacity to proliferate and differentiate into a broad range of cell types, such as osteoblasts, chondrocytes and adipocytes [135]. Additionally, MSCs can differentiate into other mesenchymal and non-mesenchymal cells, including myocytes, tendocytes, neural cells, ligament cells, smooth muscle cells, endothelial cells, cardio-myocytes and hepatocytes [135, 136]. In regenerative medicine, these cells offer numerous advantages, including ease of expansion in culture and the capacity to differentiate into desired cell lines. They also possess specific immunological properties, such as being immunoprivileged and immunomodulatory, and have tropisms for injury sites. Additionally, they can stimulate trophic responses and modulate tissue functions and inflammation through the secretion of essential bioactive molecules [137].

However, MSCs present some possible challenges, such as poor-quality control and inconsistencies regarding their heterogeneity, stability, differentiation, immunocompatibility, and migratory capacity [138, 139].

In turn, ESCs are pluripotent cells originating from the inner cell mass of blastocytes (an early embryo). They possess the capability to differentiate into nearly all cell types originating from the three germ layers, with the exception of trophoblastic cells [140]. However, ESCs raise ethical concerns, exhibit challenges in controlling differentiation, and have the potential to form teratomas and provoke immune responses [134, 141-144].

Finally, iPSCs are pluripotent stem cells generated by reprogramming adult somatic cells through the introduction of specific genes and factors, thereby mimicking the plu-ripotent state of ESCs [145]. While iPSCs share many characteristics with ESCs, they do not carry the same ethical issues or immunogenicity concerns. Nonetheless, iPSCs, such as ESCs, are also associated with the risk of teratoma formation in vivo [134].

4.2. Non-Stem Cell-based Therapies

Non-stem cell therapies commonly use somatic cells that are isolated from humans, subsequently cultured and expanded in vitro and then applied to patients for therapeutic, preventive or diagnostic treatment [146]. These can be categorized into immune cells and non-immune cells. Immune cells, including natural killer cells, dendritic cells and macrophages, can be engineered to target specific antigens. This approach is used in therapeutic strategies, including for cancer, infections, autoimmune diseases and allogeneic transplantation. On the other hand, non-immune cells, such as chondrocytes, fibroblasts, hepatocytes, keratinocytes and pancreatic islet cells, normally are involved in the host's defence response as structural architectures, regulators and effectors of its protective immune reaction [118, 146-150].

These somatic cell-based therapies serve as in vivo resource of cytokines, enzymes and growth factors. Additionally, they are frequently used in adoptive cell therapy for cancer treatment and as transplanted cells (e.g., hepatocytes or pancreatic islet cells) to address genetic metabolic disorders. They also find applications as cell-based or scaffold-free systems in the treatment of burns, ulcers and cartilage injuries [118, 147, 151].

4.3. Multicellular Therapies

Multicellular therapies comprise at least two types of cultured stem and/or non-stem cells. This emerging approach holds that using a combination of cell types is more effective for promoting long-term tissue repair compared to single-cell therapy. This effectiveness is attributed to cell–cell interactions that extend beyond embryogenesis and play a crucial role in regenerative procedures [118, 149, 152].

Multicellular therapies include scaffold-supported and scaffold-free cell products, bone marrow aspirate-derived therapies, adoptive cell therapy products, stem cell transplantation and stromal vascular fraction [118, 147, 153-155].

5. Advancements in 3D printed/ bioprinting and cellular therapies for Regenerative Medicine

Advancements in combining 3D printing/bioprinting and cellular therapies hold considerable promise for advancing regenerative medicine. This synergy has the potential to enhance tissue engineering capabilities and introduce novel therapeutic approaches for a range of diseases and conditions. Such advancements could substantially improve patient outcomes and have the potential to significantly impact survival rates [13, 156, 157].

This approach has been successful in printing the structures of different tissues, including cardiovascular, bone, liver, skin and neural tissues (Figure 3). The following sections analyse the advancements in the integration of 3D printing/bioprinting and cellular therapies in several regenerative medicine applications.

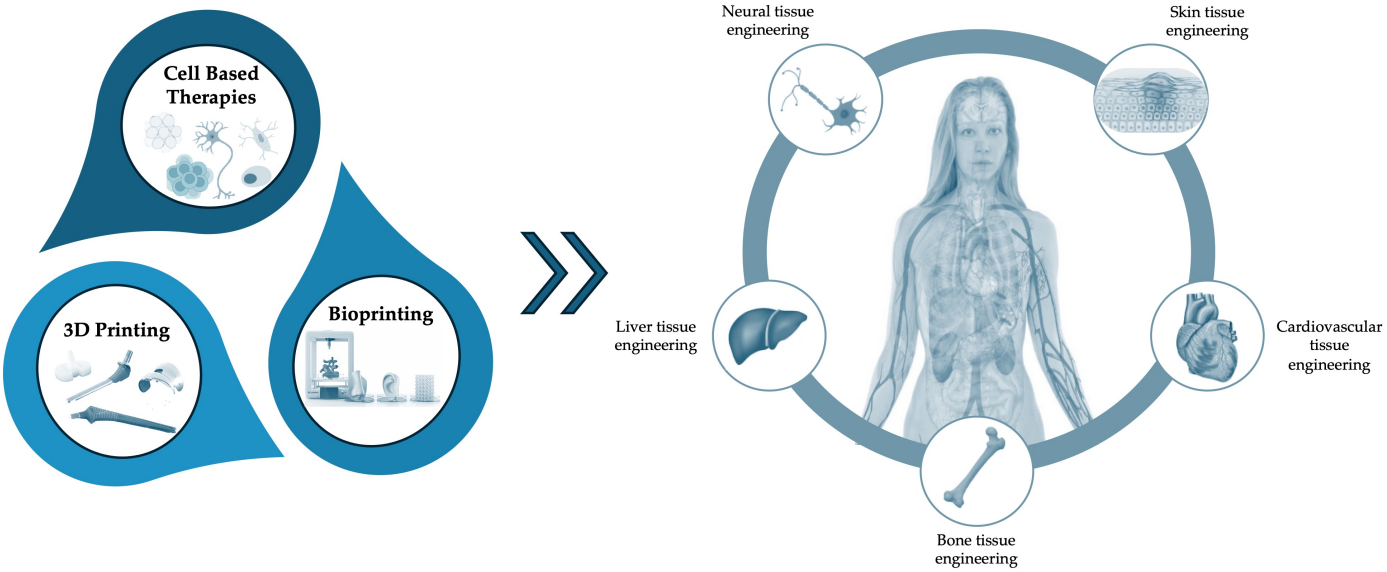


Figure 3. Advances in cell therapies, 3D printing, and bioprinting are addressing the challenges in engineering cardiovascular, bone, liver, skin, and neural tissues.

Over recent years, research concerning 3D printing and bioprinting technologies in regenerative medicine has grown significantly. As indicated in Figure 4, the number of publications related to bone regeneration is noticeably higher than the other fields. This prominence can be attributed to the compatibility of bone with 3D printing technologies, which allow precise control of scaffold porosity and the development of patient-specific implants. Furthermore, the high clinical demand for bone regeneration solutions, the limitations of traditional grafting techniques, and advancements in clinical translation, including regulatory approvals of 3D-printed bone supports, have significantly contributed to the extensive research focus in this area [158-160].

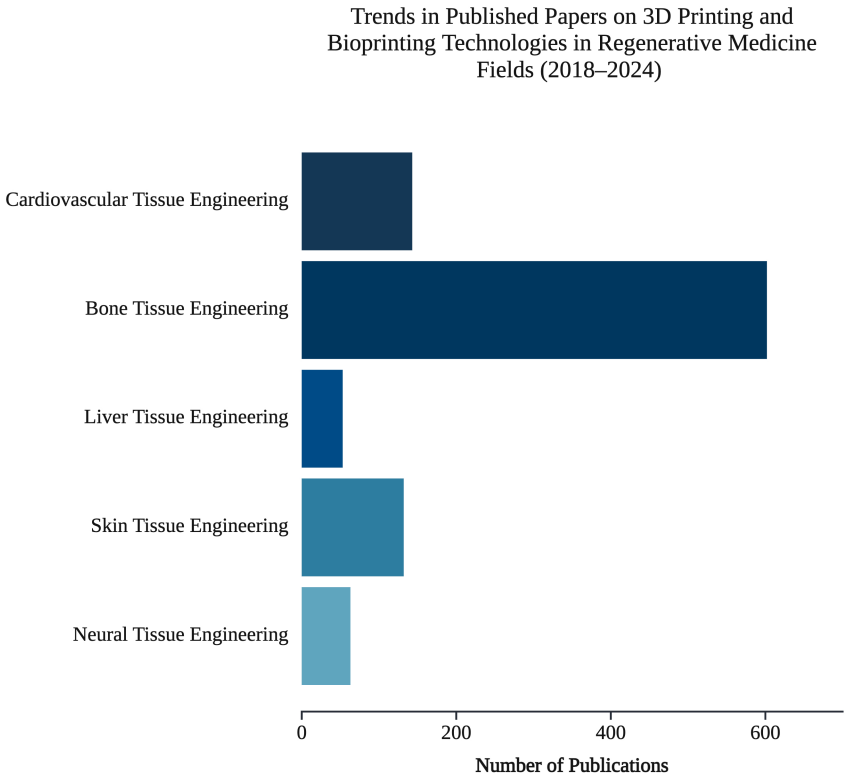


Figure 4. Trends in published papers on 3D printing and bioprinting technologies across regenerative medicine fields: cardiovascular, bone, liver, skin and neural tissue engineering. The number of publications was analysed using the PubMed database from 2018 to 2024, employing the search terms: (“Cardiovascular”)/(“Bone”)/(“Liver”)/(“Skin”)/(“Neural”) AND ((“3D Printing”) OR (“Bioprinting”)).

5.1. Cardiovascular tissue engineering

Cardiovascular diseases, which include pathologies affecting the myocardium, heart valves and body’s vasculature, are highly prevalent worldwide. These diseases are a leading cause of morbidity and mortality, especially in developed countries [161-164]. Current therapeutic approaches include cellular therapies, bypass grafting, the im-plantation of medical devices, cardiac tissue patches, and organ transplantation [161, 165-168]. Organ transplantation is often not the optimal solution due to the imbalance between the availability of donor organs and the high demand. Additionally, the success of organ transplants is frequently compromised by complications related to immune rejection [162, 169]. Among the various therapeutic approaches, cell therapy has demonstrated success in regenerating cardiovascular tissue. Nevertheless, the absence of ECM limits cell survival following injection, resulting in reduced long-term viability [169].

To address these concerns, 3D printing and bioprinting have emerged as effective approaches for developing scaffolds that incorporate ECM components and enhance cell viability [170]. These structures can more accurately mimic the spatial and mechanical properties of native tissues, which is relevant for their functionality and integration in vivo [164]. Currently, scaffolds for cardiovascular tissue engineering have been fabricated using various 3D printing technologies, such as inkjet printing, SLA and extrusion-based techniques.

These scaffolds commonly incorporate biocompatible materials of natural origin, including fibrin, alginate, gelatin, collagen, HA and fibrinogen [171]. However, to achieve complex structures with optimal physical, chemical and mechanical properties, synthetic materials, including poly (glycerol sebacate) (PGS), PCL and poly (ethylene glycol) methacrylate (PEGMA), are also employed. Additionally, some studies utilise a combination of natural and synthetic materials or semi-synthetic derivatives, such as gelatin methacrylate (GelMA) and hyaluronic acid-gelatin methacrylate (HAGM), to optimize scaffold properties while maintaining cell viability [13]. Furthermore, decellularized matrices are extensively utilised due to their provision of a porous, interconnected polymeric network that facilitates cell migration, proliferation and the delivery of essential nutrients for cell survival [172].

Maiullari et al. developed a technique for fabricating 3D cardiac tissue models that include a vascular network (Figure 5A). They created multi-cellular constructs using human umbilical vein endothelial cells (hUVECs) and induced pluripotent stem cell-derived cardiomyocytes (iPSC-CMs), encapsulated in alginate and PEG-Fibrinogen (PF). The constructs were fabricated using a custom-designed microfluidic printhead operating at an extrusion speed of 180 mm/min. Their research demonstrated that bioprinted endothelial cells are capable of forming functional vascular structures within the transplanted tissues and interacting with the host's existing vascular network [173].

To address damaged myocardium, Beijleri et al., produced a 3D-printed cardiac patch consisting of a decellularized cardiac extracellular matrix (cECM) hydrogel combined with GelMA. This patch was designed for the delivery of paediatric human cardiac progenitor cells (hCPC) (Figure 5B). The GelMA-cECM bioinks ensure uniform distribution of cECM and hCPCs, with the hCPCs

maintaining over 75% viability. Addition-ally, conditioned media from GelMA-cECM patches demonstrate more than a 2-fold in-crease in angiogenic potential. The patches also remain adhered to rat hearts and show vascularization over a 14-day period in vivo [174]. Also, in the development of tissue patches, Melhem et al. proposed a hydrogel patch embedded with multiple micro-channels to enhance cell retention and factor delivery at the target tissue (Figure 5C). They integrated bone marrow-derived MSCs (BMSCs) into a hydrogel by cross-linking a poly (ethylene glycol) dimethacrylate (PEGDMA) solution containing the cells. Microchannels with precise diameters were created within the cell-loaded hydrogel using an SLA unit for in situ cross-linking. This 3D-printed, microchanneled hydrogel was designed as an advanced therapeutic tool for sustained delivery of multiple therapeutics, aiming to improve outcomes in ischemic heart injury [175].

Noor et al. established a technique to 3D print thick, vascularized cardiac patches tailored to a patient's specific properties. They used patient-derived cells, reprogrammed into cardiomyocytes and endothelial cells, and a personalized hydrogel made from the patient's extracellular matrix. These components were combined to create bioinks for printing cardiac tissue and blood vessels. The patches, optimized for oxygen transfer, demonstrated proper structure and function in vitro, and the approach was further validated by successfully printing cellularised human hearts presenting a natural architecture (Figure 5D) [176].

In turn, to mimic human microvasculature, Cui et al. developed a bioink combining human microvascular endothelial cells (hMVECs) and fibrin, used to fabricate micron-sized fibrin channels via drop-on-demand polymerization (Figure 5E). This aqueous-based printing method reduces cellular damage. The hMVECs printed with fibrin aligned within the channels and proliferated to form continuous linings, resulting in a three-dimensional tubular structure. The study concluded that the concurrent printing of cells and scaffolds enhances the proliferation of hMVECs and supports the formation of microvascular networks [177].

Several researchers have employed 3D printing or bioprinting, with or without cell therapies, to advance cardiovascular tissue engineering. Table 3 provides a summary of these studies.

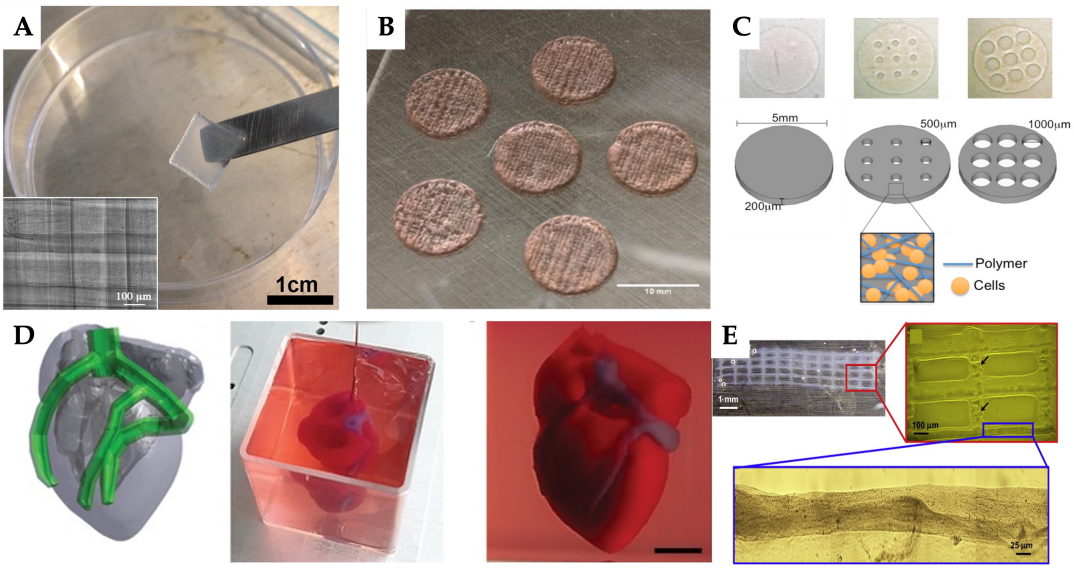


Figure 5. Advances 3D printing/ bioprinting and cell therapies in engineering cardiovascular: A: Bioprinted cellularized construct incorporating human Umbilical Vein Endothelial Cells (hUVECs) and induced pluripotent stem cell-derived cardiomyocytes (iPSC-CMs), embedded in alginate and PEG-Fibrinogen (PF) (adapted from [173]); B: Printed patches composed of decellularized cardiac extracellular (cECM) matrix hydrogel and GelMA, for delivery of pediatric human cardiac progenitor cell (hCPC) (adapted from [174]); C: MSC-loaded gel patches with microchannels of controlled diameters. Three models tested: one without microchannels and two with nine evenly spaced microchannels, maintained at diameters of 500 µm and 1000 µm (adapted from [175] Copyright 2024, American Chemical Society); D: A 3D-printed cellularized human heart is shown. (Left: CAD model of the human heart; Middle and right: The printed cardiac structure immersed in a supportive bath) (adapted from [176]); E: Printed fibrin scaffold using modified thermal inkjet printer (adapted from [177], Copyright (5839410409139) with permission from Elsevier).

Table 3. Recent advances in 3D printing/bioprinting and cellular therapies for cardiovascular tissue engineering. Abbreviations: human microvascular endothelial cells (hMVECs); mouse embryonic fibroblasts (mEFs); human cardiac-derived cardiomyocyte progenitor cells (hCMPCs); human umbilical vein endothelial cells (hUVECs); cardiomyocytes (H9c2 cells); induced pluripotent stem cell-derived cardiomyocytes (iCMs); human cardiac fibroblasts (CFs); human coronary artery endothelial cells (hCAECs); gelatin methacrylate (GelMA); decellularized cardiac extracellular matrix hydrogel (cECM); human cardiac progenitor cells (hCPCs); heart tissue-derived extracellular matrix (hdECM); neonatal rat cardiomyocytes (NRCMs); poly(ethylene glycol)-fibrinogen (PF); induced pluripotent stem cell-derived cardiomyocytes (iPSC-CMs); digital light processing (DLP); poly (glycerol sebacate) (PGS); poly (ε-caprolactone) (PCL); fused deposition modeling (FDM); not applicable (n/a); stereolithographic assembly (SLA); poly(ethylene glycol) dimethacrylate (PEGDMA); bone marrow-derived mesenchymal stem cells (BMSCs); mesenchymal stem/stromal cell (MSC); hyaluronic acid (HA); human embryonic stem cells (hESCs); early vascular cells (EVCs); hyaluronic acid glycidyl methacrylate (HAGM); neonatal rat cardiomyocytes (NRCMs).

3D printing technology	Biomaterials	Cellular Therapies	Application	Outcomes	Reference
Inkjet Printing	Fibrin gel	hMVECs	Microvasculature construction	The construction promoted hMVEC proliferation and microvasculature formation.	[177]
Extrusion 3D Bioprinting	NovoGel	mEFs	Aortic tissue construct	Support structure and mEF were successfully printed with the self-supporting approach.	[178]
	Alginate	hCMPCs	Construction with cardiogenic potential for use *in vitro* and *in vivo*	The printed hCMPCs were able to migrate in the alginate matrix while maintaining their functional properties.	[179]

	Alginate/ Gelatin	hUVECs, H9c2 cells	Cardiac tissue engineering	A new angular structure that replicates the alignment of cardiac fibers demonstrates excellent cell viability for both hUVECs and H9c2 cells, substantial mechanical strength, and appropriate characteristics for dilation and degradation.	[180]
	Alginate/Gelatin	iCMs, CFs, hCAECs	Cardiac tissue patches	Epicardial transplantation using 3D bioprinted patches based on AlgGel resulted in improved cardiac function.	[181]
	GelMA, Alginate	hUVECs	Endothelialized myocardial tissues	New method for generating endothelialised fabricated organoids.	[182]
	GelMA	cECM, hCPCs	Cardiac tissue patches	Cardiac patches printed with cECM and GelMA demonstrated significantly higher viability of hCPCs and exhibited a 30-fold increase in the gene expression of cardiogenic genes related to patches made exclusively of GelMA.	[174]

				In vivo studies on rats revealed vascularization over a period of 14 days.	
	Collagen	hdECM, NRCMs	Cardiac tissue model	It promoted early differentiation and improved the maturation of cardiomyocytes in hdECM.	[183]
3D bioprinting with microfluidic printing head	Alginate, PF	iPSC-CMs, hUVECs	Vascularized cardiac tissue	The 3D cardiac tissue composed of iPSC-CMs presents a high orientation index due to the distinct geometries and vascular-like formations generated by hUVECs.	[173]
DLP-based 3D printing	PGS/PCL/Gelatin	hUVECs	Heart valve substitute	A crosslinked 3D valve analog with elastomeric characteristics.	[184]
FDM 3D printing	PGS/PCL	n/a	Myocardial remodeling	It improved and preserved heart function.	[185]
SLA	PEGDMA	BMSCs	Gel patch to damaged cardiac tissue	Application of the MSC-laden microchanneled gel patch resulted in enhanced ejection fraction, fractional shortening, and stroke volume.	[175]

Pneumatic-extrusion	Fibrinogen, gelatin, aprotinin, HA	hESCs-derived EVCs	Cardiac tissues	Spheroids derived from hESC-derived endothelial and EVCs offer greater potential for engineering complex vascular structures compared to single cells.	[186]
Micro-continuous optical printing	GelMA, HAGM	hiPSC-CMs	Cardiac micro-tissue (for drug testing)	The micro-tissue exhibited a well-organized sarcomere structure and a marked upregulation in the expression of maturity markers.	[187]
Pneumatic 3D printing	Fibrinogen, gelatin, aprotinin, glycerol, HA	NRCMs	Functional and contractile cardiac tissue constructs	They fabricated a structured construct exhibiting physiological and biomechanical properties comparable to those of native cardiac tissue.	[188]

5.2. Bone tissue engineering

Severe bone defects resulting from aging, trauma, osteoporosis, degenerative dis-eases, autoimmune diseases (such as rheumatoid arthritis) or tumour removal are a leading cause of disability globally, affecting an estimated 1.71 billion people [189, 190]. Current therapeutic strategies for addressing these defects include autografting, allografting, xenografting and bone transplantation. Despite their application, these methods present significant risks, including the potential for infectious disease transmission and immune rejection [191, 192]. To address the limitations of traditional bone defect treatments, 3D printing and bioprinting techniques, with or without cellular therapies, have been developed for bone tissue engineering. These methods enable the large-scale fabrication of custom-tailored bone tissues, meeting the growing demand for functionalized bone implants [193]. The 3D-printed scaffolds serve as a support for cell growth and differentiation, forming a hierarchical bone microvascular architecture [194]. For optimal performance, a scaffold should possess several critical attributes: biocompatibility, sterility, osteoconductivity, biodegradability and a porous, interconnected structure that supports cellular infiltration and nutrient transport. Additionally, it should effectively repair bone defects while closely mimicking the characteristics of native bone tissue [16, 195, 196].

The most commonly employed printing techniques in bone tissue engineering are laser powder bed fusion, vat photopolymerization and extrusion-based methods.

Various biomaterials are utilised for printing scaffolds: ceramics (e.g., beta-tricalcium phosphate (β-TCP), hydroxyapatite (HAp) and amorphous calcium phosphate (ACP)); natural polymers (e.g., matrigel, alginate, HA and dextran emulsion); synthetic polymers (e.g., GelMA, PLGA, PCL and polyethylene glycol diacrylate (PEGDA); metals (e.g., titanium alloy (Ti6Al4V), tantalum (Ta) and titanium (Ti)), as well as the combinations of these materials.

Lei et al. developed Ti6Al4V-based porous tantalum (Ta) scaffolds with high interfacial strength using laser powder bed fusion. In this process, porous Ta was directly deposited onto a solid Ti6Al4V substrate (Figure 6A). The manufacturing process was carried out in an argon atmosphere, using a 300 W laser at 250 mm/s for Ta and a 250 W laser at 300 mm/s for Ti6Al4V. In vitro biocompatibility

assessments conducted with rat bone marrow mesenchymal stem cells (r-BMSCs) confirmed the scaffolds' biocompatibility. The findings demonstrated the strong mechanical compatibility and osteointegration properties of the Ti6Al4V-based porous Ta scaffold, underscoring its considerable potential for orthopaedic applications [197].

For mandibular bone defect reconstruction, Yu et al. encapsulated BMSCs in matrigel and infiltrated this mixture into porous Ti6Al4V scaffolds. The study demonstrated that rats with critical full-thickness mandibular defects treated with Matrigel-infused Ti6Al4V scaffolds exhibited significantly greater new bone formation compared to those treated with either local BMSC injections or Matrigel alone (Figure 6B). These results indicate that Matrigel enhances the 3D microenvironment for BMSCs, positioning Matrigel-infused scaffolds as a promising method for improving bone regeneration in 3D-printed Ti6Al4V scaffolds [198].

Wu et al. produced a 3D-bioprintable scaffold combining alginate and β-TCP for the treatment of bone defects (Figure 6C). The scaffolds were fabricated at a printing speed of 2 mm/s, with an extrusion pressure ranging from 60 to 200 kPa. MG-63 cells were seeded onto these scaffolds. The 3D-printed scaffolds using a 10% alginate/β-TCP bioink exhibited enhanced physical characteristics and significantly improved cell viability and alkaline phosphatase activity. These findings suggest that the scaffolds have considerable potential for application in personalized bone regeneration therapies [199].

To produce a scaffold that replicates bone microstructure, Ressler et al. developed trabecular-like porous scaffolds using ceramic vat photopolymerization with HAp powders doped with magnesium (Mg^{2+}), strontium (Sr^{2+}) and zinc (Zn^{2+}). Scaffolds sintered at 1100–1300 °C exhibited mechanical properties similar to trabecular bone, with optimal performance at 1300 °C. The microstructure resembled cancellous bone and the incorporation of trace elements resulted in a biphasic calcium phosphate system (HAp/β-TCP), potentially enhancing bioactivity [200].

Numerous studies have utilised 3D printing or bioprinting, either with or without cellular therapies, to advance bone tissue engineering. An overview of these studies is provided in Table 4.

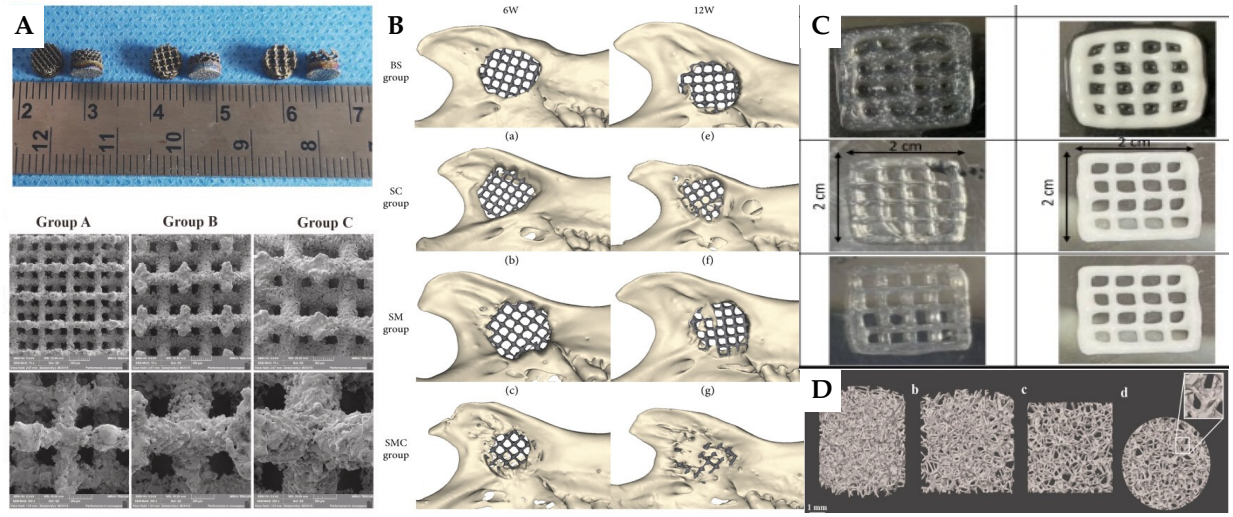


Figure 6. Advances 3D printing/ bioprinting and cell therapies in bone tissue engineering: A: Ti6Al4V-based porous tantalum (Ta) scaffolds and scanning electron microscopy images (adapted from [197]); B: Newly formed bone within the scaffold was assesses through ex vivo micro-computed tomography(micro-CT) scans at 6 and 12 weeks (adapted from [198]); C: Visual representations of 3D-printed samples at different alginate concentrations, alginate alone or alginate with beta-tricalcium phosphate (β-TCP) (adapted from [199], Copyright (5841970729622) with permission from Elsevier); D: Bone scaffolds based on magnesium (Mg^{2+}), strontium (Sr^{2+}) and zinc (Zn^{2+})-substituted hydroxyapatite, as represented in the CAD model [200]).

Table 4. Recent developments in 3D printing/bioprinting and cellular therapies for bone tissue engineering. Abbreviations: selective laser melting (SLM); bone marrow-derived mesenchymal stem cells (BMSCs); beta-tricalcium phosphate (β-TCP); gelatin methacrylate (GelMA); Xonotlite (Sr-CSH); poly(lactic-co-glycolic acid) (PLGA); bone morphogenetic protein 2 (BMP-2); human umbilical cord mesenchymal stem cells (hUCMSCs); alkaline phosphatase (ALP); hydroxyapatite (nHA); Magnesium (Mg2+); Strontium (Sr2+); Zinc (Zn2+); not applicable (n/a); polycaprolactone (PLC); amorphous calcium phosphate (ACP); dental pulp stem cells (DPSCs); Polyethylene glycol diacrylate) (PEGDA); digital light processing (DLP); tantalum (Ta); rat bone marrow mesenchymal stem cells (r-BMSCs); diamond (DO); rhombic dodecahedron (RD); iron (Fe) ; manganese (Mn); calcium (Ca); magnesium (Mg); titanium (Ti); niobium (Nb); zirconium (Zr); stromal cells from apical papilla (SCAPs); human umbilical vein endothelial cells (hUVECs).

3D printing technology	Biomaterials	Cellular Therapies	Application	Outcomes	Reference
SLM	Ti6Al4V, Matrigel	BMSCs	Mandibular bone defect reconstruction	Scaffold-Matrigel-BMSCs with enhanced bioactivity and mechanical properties for bone repair.	[198]
3D Bioprinting	Alginate, β-TCP	MG-63 fibroblasts	Bone defects	10 % alginate/β-TCP improved cells proliferation and alkaline phosphatase activity	[199]
	GelMA, Sr-CSH	BMSCs	Critical-size bone defects	GelMA-Sr-CSH scaffolds indicated complete regeneration of critical-size bone defects.	[201]

	Alginate, PLGA	BMP-2, hUCMSCs	Bone tissue engineering	hUCMSCs printing with Alginate/ BMP-2 loaded into PLGA improved osteogenesis of the printed cells as demonstrated by higher rates of ALP activity, calcium deposition, expression of genes associated with osteogenesis, and mineralization when compared with controls.	[202]
	Alginate, collagen I, nHA	hBMSCs	In vitro model for investigating osteogenesis and the initial stages of tissue maturation	The integration of nHA and Col into the alginate allowed the formation of a bioink with ideal physical and biological characteristics, providing a promising 3D bioprinting platform for replicating bone tissue.	[203]
3D Bioprinting and Fused Depositon Modeling	PCL and PLA	n/a	Periodontal defects	Using CBCT data from patients and employing fused deposition modelling, the	[204]

				printing process was straightforward and effectively produced personalized 3D models of periodontal defects.	
3D Bioprinting and Extrusion	PCL, nHA, alginate, collagen I	DPSCS	Treatment of critical-size bone defects, targeted drug administration, and 3D models for bone tissue engineering	The alginate-nHA-Col hybrid scaffold demonstrated superior cell attachment, proliferation, and osteogenic differentiation in vitro compared to controls, while in vivo studies in a rat model confirmed its biocompatibility with minimal inflammatory responses.	[205]
Vat photopolymerization	HAp multi-substituted with Mg^{2+}, Sr^{2+}, and Zn^{2+} ions	n/a	Cancellous bone defects	It is a suitable technique for manufacturing highly complex trabecular structures for bone regeneration.	[200]
Extrusion 3D Bioprinting	PCL, ACP	n/a	Bone defects	It presented suitable properties, such as compressive strength, pore size, rigidity and repeatability	[54]

				(related to the interconnectivity between the pores).	
	GelMA	DPSCs	Bone regeneration	DPSCs in GelMA bioprinted presented better osteogenic differentiation potential	[206]
	PCL, nHA, PEGDA	DPSCs	Bone regeneration	PCL/nHA/PEGDA revealed hydrophilic properties, suitable mechanical performance and significantly higher cell viability than the other groups.	[195]
DLP-based bioprinting	GelMA, dextran emulsion	BMSCs	Bone regeneration	It promoted the proliferation, migration, dissemination and differentiation of encapsulated BMSCs.	[207]
Laser Powder Bed Fusion	Ti6Al4V, Ta	r-BMSCs	Orthopedic clinical applications	It works well with the mechanics, supports the adhesion, growth, and development of r-BMSCs into osteoblasts.	[197]
	PCL, nHA	BMSCs	Human mandibular trabecular bone regeneration	The biodegradable structures (with DO and RD elementary unit cell geometry)	[208]

				demonstrated their suitability as supports for bone regeneration.	
Binder-jetting	Fe-Mn-Ca, Mg	n/a	Cranio-maxillofacial bone defects	The Fe-Mn and Fe-Mn-1Ca structures confirmed higher degradation from the addition of Ca to the 3D printed structures and good cytocompatibility.	[209]
Laser Directed Energy Deposition	Commercially pure Ti	n/a	Dental restoration	Commercially pure grade 4 titanium produced by Laser Directed Energy Deposition has a higher mechanical response than other techniques, which can be attributed to the modification of the microstructure inherent in the process.	[210]
	Ti-Nb, Ti-Zr-Nb	n/a	Orthopedic and dental applications	Ti-35Zr-25Nb presented a lower modulus of elasticity, higher hardness, good	[211]

				corrosion resistance and *in vitro* biocompatibility.	
Sheet lamination	AISI 302	n/a	Bone regeneration	The scaffold prototype was designed and fabricated with the parameters selected through experimental tests and using the mathematical model.	[212]
Laser-assisted bioprinting	BioRoot RCS®	SCAPs, hUVECs	Bone regeneration	The application of laser-assisted bioprinting techniques with this ink failed to provide complete bone repair, whether the SCAPs were printed in direct proximity or not.	[213]

5.3. Liver tissue engineering

The liver plays a vital role in blood protein synthesis, glucose metabolism and the detoxification of metabolites [214]. It is also the only organ in the human body capable of efficient regeneration. However, this regenerative capacity can be compromised by excessive drug use or viral infections, which can cause irreversible damage to hepatocytes and lead to liver failure [215, 216]. Chronic liver diseases, including fibrosis, cirrhosis, chronic viral hepatitis and fatty liver disease, significantly contribute to global morbidity and mortality. Unfortunately, advancements in treatment options for these conditions remain limited [217, 218].

The primary medical intervention for liver failure is partial or total liver transplantation. Nevertheless, this approach faces challenges, including limited donor availability, immune rejection and variable graft success rates. Alternative approaches in tissue engineering encompass bioartificial liver systems, which involve the in vitro creation of liver tissue to repair or replace damaged liver segments, as well as hepatocyte transplantation and cellular therapy methods [215]. There has been a continuous search for a reliable and reproducible source of hepatocytes, whether for liver regeneration therapy, seeding liver support devices or in vitro screening applications [216].

Numerous studies have investigated the 3D bioprinting of liver tissue utilizing either stem cells or immortalized hepatic cell lines [219, 220]. Stem cells are particularly promising due to their ability to express hepatocyte-like phenotypes. In contrast, adult hepatocytes are scarce, challenging to isolate, exhibit poor propagation and experience rapid functional deterioration in vitro [221].

In liver tissue engineering, a variety of biomaterials are employed, categorized into natural and synthetic polymers [222]. Natural polymers, such as alginate, HA, collagen, cellulose nanocrystal (CNC) and gelatin, present the advantages of enhanced cell compatibility and ease of manipulation. Nevertheless, they are constrained by relatively weaker mechanical properties, limited availability and variable degradation rates. Consequently, synthetic polymers, such as PCL, have been developed to provide superior mechanical strength, flexibility, processability and adjustable degradability. Despite these advantages, synthetic polymers generally lack cell recognition and adhesion sites, resulting in reduced biocompatibility compared to natural polymers [128]. To mitigate these issues, a

strategy of combining natural and synthetic polymers is employed to create effective bioinks for 3D bioprinting. Additionally, the liver decellularized extracellular matrix (dECM), sourced from animals, is frequently used to establish micro-environments for liver cells, offering cross-species tolerance and minimising the risk of immune rejection [223-225].

Yang et al. developed a liver tissue model through 3D bioprinting using HepaRG cells, a widely utilised hepatic progenitor cell line. Each 3D bioprinted hepatorganoid was produced through forced extrusion at a rate of 150 mm^3/min, using a layer-by-layer approach. This 3D bioprinted model, referred to as hepatorganoids, exhibited essential liver functions, including albumin production, drug metabolism and glycogen accumulation, after a 7-day differentiation period (Figure 7A). In vivo studies showed that the 3D bioprinted hepatorganoids further matured, exhibiting enhanced synthesis of liv-er-specific proteins and more human-like drug metabolism. Notably, transplantation of 3D bioprinted hepatorganoids significantly increased survival rates in recipient mice. These findings suggest that 3D bioprinted hepatorganoids can effectively undergo hepatic differentiation and ameliorate liver failure in vivo [226].

In the study conducted by Xie et al., a 3D bioprinted model of hepatocellular carcinoma, derived from patient cells, was created using isolated primary hepatocellular carcinoma cells mixed with gelatin and sodium alginate to form a bioink (Figure 7B). The resulting models were successfully generated and exhibited substantial growth over prolonged culture durations. They preserved key characteristics of the original hepato-cellular carcinoma tumours, including consistent biomarker expression and stable genetic alterations and expression profiles. Thus, 3D bioprinted hepatocellular carcinoma models prove to be reliable in in vitro systems, suitable for long-term culture and capable of predicting patient-specific drug responses for tailored therapeutic approaches [227].

Lewis et al. studied a technique for 3D printing gelatin into precisely defined geometries, which exhibit distinct biological effects on seeded hepatocytes (Figure 7C). Their research reveals that the structural configuration of gelatin can markedly impact biological processes. An undifferentiated hepatocyte cell line demonstrated high viability and proliferation on 3D-printed scaffolds with two distinct geometries. Notably, hepatocyte-specific functions—such as albumin secretion,

cytochrome P450 activity and bile transport—were enhanced in more interconnected 3D-printed gelatin structures compared to those with less interconnectivity and traditional two-dimensional (2D) cultures. This study underscores the gap between gene expression and protein functionality in simplistic 2D cultures, highlighting the importance of a physiologically relevant 3D environment for optimizing hepatocyte expression and functionality [228].

Jeon et al. employed 3D bioprinting technology to reconstruct liver tissues and organs using human hepatocellular carcinoma (HepG2) cells, a liver cancer-derived cell line. They created multi-layered 3D structures by integrating alginate with HepG2 cells (Figure 7D). The study demonstrated that replicating the 3D hepatic architecture using this technology enhances the stability and gene expression profiles of HepG2 cells. Cells cultured on these 3D alginate scaffolds for three weeks were analysed via fluorescence microscopy, histology and immunohistochemistry. Results indicated that HepG2 cells exhibited improved growth and liver-specific gene expression in 3D cultures compared to 2D cultures, highlighting the effectiveness of 3D bioprinting in mimicking liver architecture and enhancing cellular function [229].

Using the same 3D bioprinting technique, Wu et al. produced a novel bioink containing alginate, CNC and GelMA (namely, 135ACG hybrid ink), aimed at fabricating both cell-laden and acellular structures (Figure 7E). The structures were printed using a 32-gauge nozzle at a printing speed of 20 mm/s and an air pressure of 20 psi. The bioink presented good shear-thinning behaviour and solid-like characteristics, ensuring high printability and minimal cell damage. Following crosslinking, it formed a rigid ECM conducive to stromal cell growth. The team engineered a GelMA bioink with suitable mechanical properties to mimic human liver tissue, enabling the printing of liver lob-ule-mimetic constructs with precise cell placement (fibroblasts and hepG2) in different ECMs (135ACG and GelMA). These constructs were used to study the impact of mechanical stimuli and cellular interactions on cell behaviour. These findings demonstrated that fibroblasts proliferated effectively within the rigid 135ACG matrix, whereas HepG2 cells developed into spheroid structures in the more compliant GelMA matrix. Co-cultures of hepG2 and fibroblasts cells showed increased albumin production, highlighting the role of soluble factors in enhancing hepatic function. The study demonstrated that the developed bioinks and printing methods are effective for

creating complex, multi-cellular constructs with varied ECMs, advancing both fundamental research and tissue engineering applications [230].

Several studies have employed 3D printing/bioprinting with or without the incorporation of cellular therapies to advance liver tissue engineering. A summary of these studies is presented in Table 5.

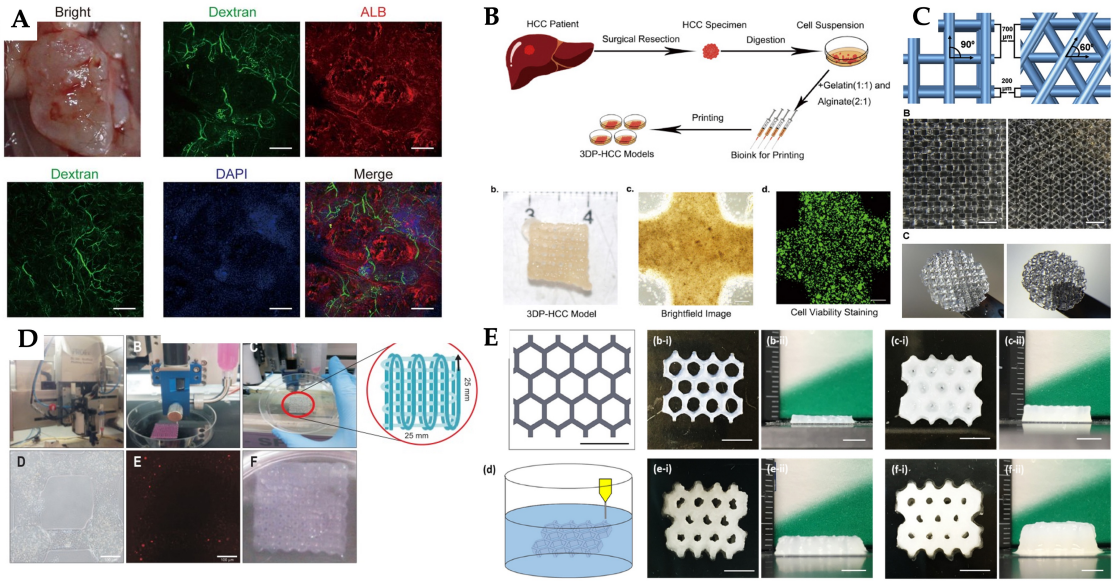


Figure 7. Advances 3D printing/bioprinting and cell therapies in liver tissue engineering: (A): Human liver functions of 3D bioprinted hepatorganoids in mice. First column: Macroscopic observation of transplanted 3D bioprinted hepatorganoids. The vascular system is illustrated following the infu-sion of dextran. Second and third column: The figure shows the dextran infusion with the for-mation of functional vessels and the red fluorescence showing the expression of human ALB at 4 weeks (adapted from [226]); (B): The study details the production of patient-derived 3D bioprinted hepatocellular carcinoma models. Initially, HCC samples were obtained following post-surgical resection and subsequently processed into cell suspensions. These suspensions were then combined with sodium alginate and gelatin to create the bioink used for bioprinting. The images provided in the second line include the following: (1) the general appearance of the 3D bioprinted hepatocellu-lar carcinoma model, (2) a light microscopy image showing the distribution of cells within the model and (3) an in vitro view of the model, where live cells are marked in green and dead cells are marked in red (adapted from [227], Copyright (5842091348696) with permission from Elsevier); (C): First line: schematic representation of the 3D printed scaffold, including strut spacing, nozzle diameter and angle between

adjacent layers (90 or 60 degrees). Second line: large-scale 3D printed gelatin structure. Third line: cross-linked scaffolds and biopsy-punched samples (adapted from [228], Copyright (5842111318276) with permission from Elsevier); (D): Construction of 3D-printed mCherry-HepG2 hepatic structures: (D-A) 3D bioprinting machine; (D-B) extrusion of alginate combined with mCherry-HepG2 cells through nozzle pressure; (D-C) layer-by-layer dep-osition of cross-linked structures in square arrays; (D-D) phase contrast microscopy showing a confluent monolayer of HepG2 cells; (D-E) fluorescence microscopy image of mCherry-HepG2 cells within the alginate scaffold; (D-F) multilayered mCherry-HepG2 cells solidified and stacked repet-itively (adapted from [229]); (E): Schematic representation of the liver lobule-mimetic honeycomb structure, including top and side views of the embedded-printed scaffolds (adapted from [230]).

Table 5. Recent advances in 3D printing/bioprinting and cellular therapies for liver tissue engineering. Abbreviations: digital light processing (DLP); methacrylated gelatin (GelMA); decellularized extracellular matrix (dECM); human-induced hepatocyte (hiHep cells); hyaluronic acid (HA); primary mouse hepatocytes (PMHs); human induced pluripotent stem cells (hiPSCs); human embryonic stem cells (hESCs); human pluripotent stem cells (hPSCs); induced pluripotent stem cells (iPSC); 3D bioprinted hepatorganoids (3DP-HOs); hepatocellular carcinoma (HCC); poly (ε-caprolactone) (PCL); human bone marrow-derived mesenchymal stem cells (BMMSCs); human hepatocellular carcinoma (hepG2); cellulose nanocrystals (CNCs); bioink with alginate (1%), cellulose nanocrystal (3%), and gelatin methacryloyl (5%) (135ACG); undifferentiated hepatocyte cell line (HUH7); primary rat hepatocytes cells (PrHCs); human umbilical vein endothelial cells (hUVECs); human lung fibroblasts (hLFs); human extracellular matrix (hECM); human hepatic stellate cell line (L × 2); primary fetal activated hepatic stellate cells (aHSC).

3D printing technology	Biomaterials	Cellular Therapies	Application	Outcomes	Reference
DLP bioprinting	GelMA	dECM, hiHep cells	Hepatic functional restoration	It was found that the addition of hepatic dECM to the biotints improved printing capacity and cell viability. Furthermore, hiHep cells exhibited increased spreading and enhanced functional performance within the liver microtissue.	[231]
3D bioprinting	HA, alginate, gelatin	dECM, PMHs	Functional *in vitro* liver tissue models	The inclusion of dECM enhanced the hepatic function of hepatocyte spheroids.	[232]

	Alginate	hiPSCs, hESCs	Mini-liver tissue structures	Using this approach, researchers have been successfully bioprinting hPSCs whilst preserving their pluripotency or directing their differentiation towards specific cell types.	[233]
	NovoGel 2.0	iPSC-derived hepatocyte	Functional *in vitro* liver tissue models	It demonstrated a method for rapidly fabricating multicellular 3D liver constructs in a multi-well format, displaying critical liver functions including albumin synthesis, cholesterol biosynthesis, production of fibrinogen and transferrin, and inducible activities of CYP 1A2 and CYP 3A4.	[219]
	Alginate	HepaRG cells	Hepatorganoids: Liver tissue model	The implantation of 3DP-HOs markedly enhanced the survival rates of mice experiencing liver failure.	[226]

Gelatin, Alginate	Primary HCC cell lines	*In vitro* models for patient-specific drug screening for HCC	The generated models preserved the key characteristics of the original HCCs, including consistent biomarker expression, stable genetic alterations, and maintained expression profiles.	[227]
PCL	dECM, BMMSCs, HepG2	3D cell printing-based liver tissue engineering	The liver dECM bioink proved to have excellent printing capacity without significant cell death during the process. It also improved stem cell differentiation and HepG2 cell function.	[234]
Alginate	HepG2	Reconstruction of liver tissues or organs	The cells proliferated well in the scaffold and the expression of liver-specific genes increased.	[229]
GelMA, alginate, CNC	NIH/3T3 fibroblasts, hepG2	Bicellular liver lobule-mimetic structures	NIH/3T3 cells proliferated effectively within the rigid 135ACG matrix and aligned along the boundary between 135ACG and GelMA,	[230]

				demonstrating durotaxis. In contrast, HepG2 cells formed spheroids exclusively within the softer GelMA matrix. The 3D co-culture of HepG2 and NIH/3T3 cells exhibited increased albumin secretion, indicating that the enhancement in liver cell functionality may be due to soluble factors in the environment.	
Pneumatic extrusion	Gelatin	HUH7	Model hepatocyte system	It has been proved that the scaffold geometry, using well-defined gelatine constructs, modulates hepatocyte function.	[228]
	PCL, collagen	PrHCs, hUVECs, hLFs	Liver tissue engineering	The 3D cell printed construct comprising a capillary-like network enhanced the protein secretion and metabolism of PrHCs. It demonstrated a great potential for functional liver tissue regeneration.	[235]

	Alginate, gelatin	hECM, human HepaRG liver cells	3D liver model for infection and transduction studies	It was demonstrated that supplementing an alginate/gelatin bioink with hECM enhanced cell viability and hepatic metabolic function in a 3D-printed humanized liver model.	[236]
Extrusion bioprinting	Alginate	HepG2/C3A, EA.hy926	Hepatic lobules within a highly vascularized construct	The successful bioprinting of hepatic lobules with a complex, highly vascularized architecture resulted in enhanced albumin secretion, urea production, and elevated levels of albumin, MRP2, and CD31 proteins. Additionally, cytochrome P450 enzyme activity was significantly greater in these constructs compared to other groups.	[237]
	HA, Collagen I	L × 2, aHSC	3D bioprinted liver model	The formulations seemed to facilitate cell viability, in line with the biomatrices used. The bioinks incorporating primary	[238]

			human hepatocytes were evaluated over two weeks, demonstrating sustained production of urea and albumin while showing a responsive reaction to acetaminophen.	
Alginate, CNCs	Fibroblasts, Human hepatoma cells	Liver-mimetic structures	This bioink showed excellent shear-thinning property, extrudability, and shape fidelity after the deposition. The bioprinting caused minimal cell damage.	[239]

5.4. Skin tissue engineering

The skin, regarded as the largest organ in the human body, plays essential roles in various functions, including serving as a protective barrier, regulating body temperature and preventing dehydration [240]. Extensive full-thickness skin wounds, which damage underlying blood vessels, pose serious risks due to induced cellular hypoxia and nutrient deprivation [241]. While autografts are considered the "gold standard" for treating severe skin injuries, their use is limited by issues such as donor site availability and associated morbidity [242]. Furthermore, existing commercial skin substitutes lack the sufficient vascular networks necessary for effective nutrient delivery in full-thickness wounds. Consequently, skin substitutes are seen as promising alternatives, offering the potential for vascularized skin reconstruction with customized cell compositions and controlled geometrical structures [241, 243].

3D printing/bioprinting has arisen as an innovative technological approach in skin tissue engineering, creating structures by depositing cell-embedded bioinks layer by layer [244, 245]. This approach includes several techniques, including DLP, extrusion bioprinting, inkjet printing and electrospinning. The materials commonly used in this field are natural polymers (e.g., collagen, alginate, HA, gelatin and fibroin) and synthetic polymers (e.g., PCL, PLGA, polyglycolic acid, polyurethanes, polycarbonates and PEGDA). These materials, often referred to as biopolymers, are biocompatible and biodegradable. In applications related to wound healing, bioinks can be integrated with antibiotic agents or antimicrobial peptides, as well as growth factors such as epidermal growth factor (EGF), fibroblast growth factor (FGF) or vascular endothelial growth factor (VEGF), to enhance cell stimulation, growth, proliferation and migration throughout the healing process [244, 246]. The latest developments in wound care and skin regeneration involve embedding various cell types, including fibroblasts, hUVECs, keratinocytes and human umbilical cord mesenchymal stem cells (hUCMSCs), directly into bioinks. Liu et al. fabricated vascularized full-thickness skin substitute by printing an alginate-gelatin hydrogel to simulate the epidermis, and a phosphosilicate calcium bioglass (PSC)-alginate-GelMA hydrogel containing hUVECs and hUCMSCs to replicate the dermis (Figure 8A). For the bioprinting process, the printing speed was 10 mm/s with a filament orientation of 60°. They showed a marked enhancement in blood vessel formation and collagen deposition, demonstrating the effectiveness of these skin substitutes

in reconstructing full-thickness skin injuries in rat models [241]. Also, with a view to developing a full-thickness skin substitute, Admane et al. employed extrusion-based 3D bioprinting to create a silk fibroin-gelatin construct containing fibroblasts to mimic the dermis, and a silk fibroin-gelatin layer with keratinocytes to replicate the epidermis (Figure 8B). The 3D bioprinted full-thickness skin model showed extensive keratinocyte migration and differentiation, mimicking reepithelization. Analysis revealed similarities to native human skin, involving pathways related to skin development, extra-cellular matrix organization and keratinization [247]. Also, Jin et al. developed an advanced 3D bioprinted structure designed to mimic natural full-thickness skin, incorporating the epidermis, dermis and a vascular network. For the 3D bioprinting of the full-thickness functional skin model, the printing speed was set at 5 mm/s, with the air compressor pressure maintained at 0.2 MPa. This model utilised GelMA with HaCaTs for the epidermal layer, an acellular dermal matrix (ADM) with fibroblasts for the dermis and a GelMA mesh with hUVECs for the vascular network (Figure 8C). They demonstrated that this functional skin model not only enhanced cell viability and proliferation but also supported epidermal reconstruction in vitro. In vivo, the functional skin model-maintained cell viability for at least one week and promoted wound healing, reepithelization, dermal ECM secretion and angiogenesis, thereby improving wound healing quality [248].

Song et al. developed a bilayer skin scaffold incorporating drug delivery for the repair of full-thickness skin defects. The scaffold features an outer layer of amoxicillin (AMX)-loaded PCL nanofibers fabricated through electrospinning which functions as an antibacterial membrane mimicking the epidermis (Figure 8D). The inner layer, designed to replicate the dermis, is a hydrogel composed of sodium alginate and gelatin, infused with recombinant human epidermal growth factor (rhEGF) to maintain wound moisture and promote healing. The successful incorporation of AMX and rhEGF into the scaffold was demonstrated, with the scaffold exhibiting excellent physicochemical properties, effective drug release, and antibacterial activity. Both in vitro and in vivo evaluations revealed enhanced cell adhesion, proliferation and accelerated skin wound healing, alongside favourable biocompatibility. These results suggest that the scaffold holds considerable potential for skin regeneration applications [249].

Numerous studies have utilised 3D printing and bioprinting techniques, both with and without the integration of cellular therapies, to advance skin tissue engineering. A comprehensive overview of these studies is provided in Table 6.

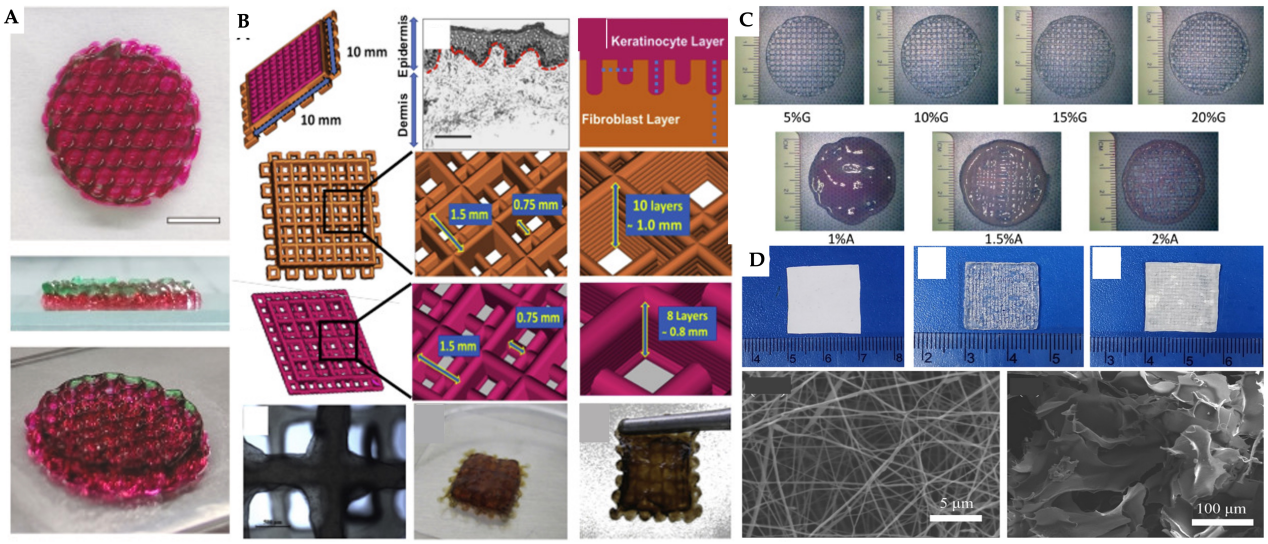


Figure 8. Advances 3D printing/bioprinting and cell therapies in skin tissue engineering: (A): The image shows the printed epidermal layer (red) composed of alginate-gelatin hydrogel, and the dermal layer (green) made of phosphosilicate calcium bioglass (PSC)-alginate-GelMA hydrogel embedded with hUVECs and hUCMSCs (adapted from [241], Copyright (5842131198782) with permission from Elsevier); (B): Diagram overview of the produced structure design: diagram illustration of the CAD model; illustration of human skin anatomy, with the dermis and epidermis; approach for designing the dual-layered 3D printed structure; dimensions of the layers: the dermal layer consists of 10 layers, while the epidermal layer has eight filaments, oriented perpendicularly with an interfilament spacing of 0.75 mm and a Z-axis increment of 0.08 mm per layer; microscopic view of the printed structure; dual-layered 10 × 10 mm 3D printed structure in culture; and the mechanically printed structure is noted for its optimal handling properties, which facilitate thorough characterization and assessment (adapted from [247], Copyright (5842131492259) with permission from Elsevier); (C): Assessment of the printability of acellular dermal matrix and GelMA hydrogels by fabricating identical structural patterns using these materials (adapted from [248], Copyright (5842140280407) with permission from Elsevier); (D): Macrographs and scanning electron microscopy (SEM) images of PCL-AMX, SG-rhEGF, and PCL-

AMX-SG-rhEGF structures (adapted from [249], Copyright (5842140587126) with permission from Elsevier).

Table 6. Recent advances in 3D printing/bioprinting and cellular therapies for skin tissue engineering. Abbreviations: strontium silicate (SS); matrix hydrogel with 2.8% of gellan gum, 1.6% of alginate, and 2.8% of methyl cellulose (GAM); human dermal fibroblasts (hDFs); human umbilical vascular endothelial cells (hUVECs); murine umbilical vein endothelial cells (MUVECs); dextran (Dex); vascular endothelial (VEGF); gelatin (Gel); keratin (Kr); not applicable (n/a); bi-layer (BL); poly (ε-caprolactone) (PCL); amoxicillin (AMX); external human epidermal growth factor (rhEGF); Digital light processing (DLP); gelatin methacrylate (GelMA), hyaluronic acid (HA); N-(2-aminoethyl)-4-(4-(hydroxymethyl)-2-methoxy-5-nitrosophenoxy) butanamide (NB); lithium phenyl-2,4,6-trimethylbenzoylphosphinate (LAP); human skin fibroblasts (hSFs); silk fibroin (SF); 4-arm polyethylene glycol acrylate (PEG4A); platelet-rich plasma (PRP); dermal fibroblasts (DFs); epidermal stem cells (ESCs); acellular dermal matrix (ADM); polyurethane (PU); endothelial progenitor cells (EPCs); human keratinocytes (hKCs); pectin methacrylate (PecMA); human neonatal dermal fibroblasts (hNDFs); extracellular matrix (ECM); human endothelial cells (hECs); human placental pericytes (hPCs); phosphosilicate calcium bioglasses (PSCs); human umbilical cord mesenchymal stem cells (hUCMSCs); poly-(lactic-co-glycolic acid) (PLGA).

3D printing technology	Biomaterials	Cellular Therapies	Application	Outcomes	Reference
3D bioprinting	Collagen, SS, GAM	hDFs, hUVECs, MUVECs, BALB/3T3 fibroblast	Vascularized Skin substitute	Collagen-2SS-GAM demonstrated significant capabilities in promoting angiogenesis, integrating with host tissue and facilitating wound repair *in vivo*.	[250]
Extrusion-based 3D printer and electrospinning	Dex-VEGF, Gel-Kr	n/a	Construct to accelerate wound healing	The BL-VEGF construct is identified as an optimal candidate for enhancing the healing process of full-thickness skin wounds.	[251]

	PCL, AMX, alginate, gelatin	rhEGF	Repair defective skin tissue and wound healing	The PCL-AMX@SG-rhEGF scaffold demonstrated superior drug release capabilities and significant antibacterial properties. Both *in vitro* and *in vivo* analyses indicated that the scaffold facilitates cell adhesion and proliferation, accelerates skin wound healing, and exhibits favorable biocompatibility.	[249]
DLP-based 3D printing	GelMA/HA, NB/LAP	hSFs, hUVECs	Functional living skin	The bioink exhibited rapid gelation, customizable mechanical properties, high biocompatibility, and effective tissue adhesion. *In vivo* studies in large animal models showed that the bioink elicited an immediate defense response and was particularly effective in enhancing dermal regeneration, including the development of skin appendages.	[252]
	SF, PEG4A	NIH 3T3 fibroblas, keratinocytes	Artificial skin model	SF-polyethylene glycol hydrogels presented higher cell proliferation, and the thickest keratin layer was produced	[253]

				with SF-PEG4A hydrogels when compared to PEG4A alone.	
Extrusion-based bioprinting (*in situ*)	Alginate, gelatin, PRP	DFs, ESCs	Wound repair	The addition of PRP enhanced the cellular behaviour of the cells, regulated vascular endothelial cell tube formation and macrophage polarisation in a paracrine manner. In *in-situ* bioprinting, incorporating PRP accelerated high-quality wound closure, regulated inflammation, and stareted angiogenesis more effectively than using alginate-gelatin bioink.	[254]
Extrusion-based bioprinting	GelMA	ADM, HaCaTs, hUVECs, fibroblasts	Functional skin model	The *in vivo* results showed that the functional skin model stimulated wound healing and re-epithelialisation, enhanced the production of dermal extracellular matrix, stimulated angiogenesis, and overall improved the quality of wound repair.	[248]
	PU, gelatin	Fibroblasts, keratinocytes, EPCs	Skin tissue engineering.	Curvilinear-bioprinted hydrogel showed superior structural integrity over planar-bioprinted hydrogel. In the treatment of	[255]

				large and irregular rat skin wounds, the curvilinear-bioprinted tri-cell-laden hydrogel achieved complete repair within 28 days.	
	Alginate, honey	3T3 fibroblast	Skin tissue engineering	The incorporation of honey resulted in bioprinted scaffolds with enhanced cell proliferation, without any visible decrease in printability.	[256]
	SF, gelatin	hDFs, hKCs	Full-thickness skin constructs	A silk and gelatine bioink have been printed that can be used to recapitulate a series of biological and design parameters comparable to human skin.	[247]
3D Bioprinting	PecMA	hNDFs	Biomimetic skin constructs	The hydrogels exhibited significant versatility, enabling precise adjustment of their rheological and viscoelastic properties. Additionally, they created an optimal microenvironment that supported the deposition of endogenous ECM by the entrapped hNDFs, which is rich in collagen and fibronectin.	[257]
	Rat tail type I collagen	hDFs, hKCs, hECs, hPCs,	Multilayered vascularized	In *in vitro* studies, hKCs grow and develop into a multi-layered barrier,	[258]

			human skin grafts	while hECs and hPCs form interconnected microvascular networks. *In vivo*, the presence of hPCs in the printed dermal tissue increased the integration of the graft with the host's microvessels and supports the generation of an epidermal network.	
	PSCs, alginate, gelMA, gelatin	hUVECS, hUCMSCs	Skin tissue grafts	The incorporation of PSCs revealed enhanced cell proliferation and elevated expression of angiogenesis-related genes *in vitro*. *In vivo* experiments showed an improved wound healing effect, characterized by an increase in angiogenesis and collagen deposition.	[241]
Pneumatic-assisted extrusion freeforming	Alginate, gelatin	hSFs	Bioactive dermal substitute scaffold	The three-phase crosslinking technique can produce dermal substitute supports with physicochemical and biological properties suitable to be used in skin tissue engineering.	[259]
Inkjet printing	PLGA, prednisolone	n/a	Personalized dermal patches for treatment	The first steps have been made towards the concept of manufacturing personalized patches by inkjet printing	[260]

	of skin diseases	that can be made for poorly soluble pharmaceuticals. The model drug prednisolone was successfully processed and printed in the format of a nanosuspension. The PLGA nanoparticles and the patches produced demonstrated a prolonged release of the pharmaceutical.

5.5. Neural tissue engineering

The nervous system represents one of the most intricate and complex biological systems formed during development [261]. The human nervous system is divided into two primary components: the central nervous system, consisting of the brain and spinal cord, and the peripheral nervous system, which includes cranial and spinal nerves along with associated ganglia [262]. Traumatic injuries, including traumatic brain injury and spinal cord injury, as well as neurodegenerative diseases such as Alzheimer's, Parkin-son's, Huntington's and multiple sclerosis, pose major public health challenges, with limited treatment options available that mainly offer symptomatic relief. Autologous nerve graft transplantation is widely regarded as the optimal approach for addressing severe nerve injuries. Nonetheless, its clinical utility is constrained by several substantial issues, such as the restricted availability of suitable donor nerves and the risk of in-compatibilities between the donor and recipient nerves [263-265]. Despite ongoing clinical advancements, fully effective therapies for neural regeneration are still in early stages, driving interest in neural tissue engineering [266]. Neural tissue engineering focuses on developing biological substitutes that integrate biomimetic 3D scaffolds with cells to improve neural tissue functionality. Advances in 3D printing technology have significantly impacted neural autograft engineering, enabling precise fabrication of tis-sue-engineered neural implants. Various 3D printing methods, such as extrusion-based printing, laser-assisted bioprinting, SLA and 4D printing, are increasingly employed to create accurately structured implants for nerve injury repair and to develop models and devices for in vitro neural tissue engineering.

The materials chosen for the printing of neural structures encompass biocompatible polymers (e.g., PCL and PU), composites (e.g., reduced graphene oxide (rGO)), and hydrogels (e.g., GelMa, HA, collagen and fibrin). These materials must meet specific requirements for printability and biocompatibility, as well as possess suitable physico-chemical properties and mechanical strength [265].

Researchers have combined 3D printing/bioprinting with cellular therapies for neural tissue engineering. Lee et al. created photocrosslinkable methacrylated silk fibroin-pectin bioinks (Figure 9A). The structures were printed with an extrusion pressure ranging from 50 to 100 mm/min and a printing speed between 1 and 30 mm/s, and they exhibited tunable mechanical properties, favourable

biocompatibility and an environment highly supportive of neural induction in 3D bioprinted constructs containing neural stem/progenitor cell spheroids [267].

For spinal cord injury treatment, Song et al. engineered scaffolds composed of PCL microfiber-reinforced spinal cord ECM hydrogels incorporating oxymatrine (OMT) using electrospinning techniques (Figure 9B). These scaffolds promoted neuronal differentiation of neural stem cells (NSCs) and suppressed astrocyte proliferation in vitro. In vivo, they promoted the recruitment of NSCs, stimulated neuronal growth, diminished glial scar formation and enhanced motor function recovery in rats with spinal cord injuries [268].

In turn, Lin et al. developed a model designed to forecast cell growth and distribution, aimed at reducing the need for empirical adjustments. They established a multiphysics model that integrates oxygen diffusion and substrate consumption dynamics within a rat adrenal medullary pheochromocytoma (pc-12) cell-laden nerve scaffold (Figure 9C). This model was used to simulate and forecast oxygen levels and cellular growth patterns. The scaffold was produced using SLA, and the distribution of cells was assessed through fluorescence staining to confirm the model. The findings demonstrated that the model effectively forecast cellular growth patterns [269].

Numerous studies have utilised 3D printing and bioprinting technologies, both with and without the integration of cellular therapies, to develop the area of neural tissue engineering. Table 7 provides a comprehensive overview of these investigations.

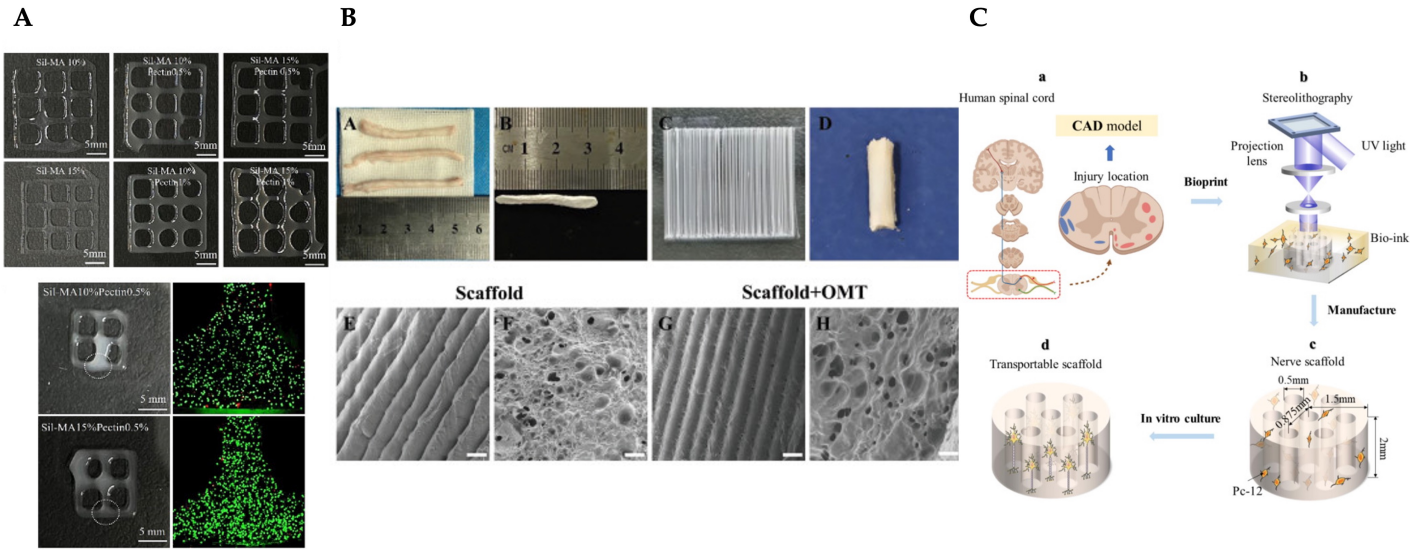


Figure 9. Advances 3D printing/ bioprinting and cell therapies in neural tissue engineering: A: Evaluation of bioink printability was conducted for various compositions of methacrylated silk fibroin and methacrylated silk fibroin/pectin hydrogels. Optical microscopy images were captured to examine the morphology, while a live/dead assay was performed on L929 cells embedded within 3D bioprinted constructs using bioinks composed of 10% methacrylated silk fibroin/0.5% pectin and 15% methacrylated silk fibroin/0.5% pectin (adapted from [259], Copyright (5842151229827) with permission from Elsevier); B: Characterization of the scaffolds was conducted as follows: (A) Normal spinal cord tissue; (B) Decellularized spinal cord scaffold; (C) Polycaprolactone (PCL) microfiber structure; (D) Overall morphology of the 3D-bioprinted composite scaffold; (E–H) Microstructure of scaffolds visualized through scanning electron microscopy (SEM). The SEM images of both the scaffold alone and the scaffold combined with OMT reveal parallel microfibers of consistent thickness, with hydrogels adhering to the fibers. The interior of the scaffold exhibited uniform and densely packed pores, which are conducive to neural stem cell (NSC) growth and efficient nutrient exchange (adapted from [260]); C: Schematic representation of the experimental procedure for spinal cord injury repair utilizing stereolithography apparatus (SLA) to create neural scaffolds. (a) Computer-aided design (CAD) to develop the scaffold model corresponding to the injured region for bioprinting; (b) Construction of neural scaffolds employing the SLA technique; (c) Utilization of the fabricated scaffolds for *in vitro* cell culture; (d) Assessment of the functionality of scaffolds following a

period of *in vitro* cultivation (adapted from [261], Copyright (5842160814781) with permission from Elsevier).

Table 7. Recent advances in 3D printing/bioprinting and cellular therapies for neural tissue engineering. Abbreviations: methacrylated silk fibroin (SilMA); pectin methacryloyl (PecMA); silk fibroin (SF); neural stem/progenitor cells (NSPCs); polyurethane (PU); neural stem cells (NSCs); hyaluronic acid (HA); neural progenitor cells (NPCs); poly(lactic-co-glycolic acid) (PLGA); primary human dermal fibroblasts (phDFs); vascular endothelial growth factor (VEGF); murine neural stem cells (C17.2); interferon-gamma (IFN-γ); poly (ε-caprolactone) (PCL); oxymatrine (OMT); polyethylene glycol diacrylate (PEGDA); digital light processing (DLP); gelatin methacrylate (GelMA); Poly(3,4-ethylenedioxythiophene) (PEDOT); not applicable (n/a); chondroitin sulphate methacrylate (CSMA); bone marrow-derived mesenchymal stem cells (BMSCs); stereolithography (SLA); rat adrenal medullary pheochromocytoma (pc-12); reduced graphene oxide (rGO).

3D printing technology	Biomaterials	Cellular Therapies	Application	Outcomes	Reference
Extrusion-based 3D Bioprinting	SilMA, Pectin, PecMA, SF	NSPCs	Neural tissue engineering applications or *in vitro* brain models	The SilMA/pectin biotints showed adjustable mechanical properties, biocompatibility and a highly propitious environment for neural induction.	[267]
	PU	NSCs	Neural tissue engineering	NSCs proliferated and differentiated favourably in PU2 bioprinted hydrogels. In the *in vivo* model of neural injury in the zebrafish embryo, the injection of hydrogels loaded with NSCs facilitated the repair of the damaged central nervous system.	[270]

				Additionally, the functionality of adult zebrafish with traumatic brain injury was recovered following the injection of constructs with NSCs.	
	Gelatin, alginate, fibrinogen, nanofibrillate cellulose, matrigel, HA	NPCs, astrocytes	Study the connection between human neuronal networks, model pathological processes and provide a platform for drug testing.	Imprinted neuronal progenitors differentiate into neurons and form functional neuronal circuits within and among tissue layers with specificity within weeks.	[271]
Laser Assisted Bioprinting	PLGA	NE-4C	Artificial neural tissue constructs	The findings of the work showed that the topological clue presents a relevant role in the development of clusters on the support, but the bioprinted laminin dots appeared to regulate the strength of the bond between them, paving the way for controlling the functional morphology of artificial neural tissue constructions.	[272]

3D Bioprinting	PU	FoxD3 plasmids, phDFs	Personalized drug screening or neuroregeneration.	The phDFs embedded with FoxD3 in the thermo-responsive PU hydrogel exhibited the capacity to undergo reprogramming and develop into a neural tissue-like structure within 14 days post-induction.	[273]
	Collagen, fibrin gel	VEGF, C17.2	Neural tissue regeneration	The bioprinting of fibrin gel containing VEGF facilitated the prolonged release of growth factors on the collagen scaffold.	[274]
3D printing technology based on low-temperature extrusion	Collagen, chitosan	IFN-γ, NSC-derived exosomes	Neurological recovery after traumatic brain injury	The 3D printed collagen/chitosan structure exhibited favorable biological and mechanical characteristics, creating an optimal microenvironment for NSC differentiation and exosome secretion. Additionally, this scaffold played a role in various pathological processes following traumatic brain injury in rats,	[275]

				significantly improving neurofunctional recovery.	
Electrospinning	PCL, OMT, gelatin, PEGDA, β-cyclodextrin	Spinal cord extracellular matrix	Treatment of spinal cord injuries	The manufactured scaffolds led to the differentiation of NSCs into neurons while suppressing their conversion into astrocytes. They established an optimal microenvironment for spinal cord tissue regeneration *in vivo* and directed axonal growth. Additionally, the transplantation of these scaffolds, combined with OMT, improved motor function recovery in rats with spinal cord injuries.	[268]
DLP printing	GelMA, chitosan, PEDOT	n/a	Neural tissue repair	The GelMA/Chitosan-PEDOT hydrogel showed good and stable electrical conductivity, enhanced mechanical strength and noticeable biocompatibility. *In vivo* tests showed that the hydrogels promoted nerve	[276]

				regeneration and helped muscle recovery in the repair of sciatic nerve defects.	
Microextrusion-based 3D bioprinting	GelMA, PEGDA, PEDOT, CSMA	NSCs	Nerve injury repair	3D bioprinted electroconductive hydrogel showed biocompatibility, suitable mechanical strength and good conductivity, thus promoting the adhesion, growth and proliferation of NSCs.	[277]
Additive-lathe 3D bioprinting	GelMA, PEGDA	BMSCs	Peripheral nerve injury repair	An integrated two-layer nerve conduit was developed, in which the BSMCs within the printed nerve conduits demonstrated excellent cell viability and extended cellular morphology. *In vitro* studies with PC12 cells revealed that the growth of neurons is significantly enhanced in nerve conduits embedded with BMSCs.	[278]

SLA	GelMA, PEGDA	Pc-12	Multi-physical model for cell-laden nerve scaffolds	This model enables the prediction of key regions for cell growth within neural scaffolds during *in vitro* culture experiments. By identifying these primary growth areas, the model allows for targeted increases in oxygen concentration in these regions, thereby enhancing cell density and distribution.	[269]
Electrohydrodynamic jet	PCL, rGO	PC-12	Peripheral nerve injury repair	The addition of rGO to scaffolds results in softer materials that enhance neural differentiation. *In vitro* studies with PC12 cells show increased cell proliferation and improved support for neural differentiation in PCL/rGO scaffolds compared to PCL-only scaffolds, as confirmed by RT-PCR and immunocytochemistry analyses.	[279]

6. Limitations and challenges

Despite the benefits of 3D printing/bioprinting and cellular therapies for regenerative medicine, there are several challenges that need to be addressed. Despite extensive research efforts in recent years, the clinical application of these technologies has been constrained. The lack of sufficient animal studies and the absence of viable 3D models in clinical trials underscore the need for further focus and development in these critical areas [280-282].

One of the current challenges is the advancement of functional vascular networks within bioprinted tissues and organs. Specifically, creating a vascular system that can seamlessly connect with the host's native blood vessels is complicated by the complex structural architecture and the variability of tissue components [283-285]. Vascularization is crucial for providing nutrients and oxygen, which are vital for maintaining cell viability and ensuring tissue functionality. A robust, multi-level vascular network is necessary to support the long-term survival and growth of bioprinted organs, incorporating smooth muscle cells and hUVECs into the blood vessels [286]. To overcome challenges related to nutrient and oxygen transport, researchers have utilised proangiogenic factors, such as vascular endothelial growth factor (VEGF) and basic fibroblast growth factor (BFGF), to promote the development of microvessels. Additionally, incorporating endothelial cells into the culture medium has been shown to promote microvessel formation and the development of angiogenic sprouts in engineered constructs [287]. However, endothelial cells and angiogenic factors generally do not produce perfusable constructs in a fast way [288]. Bioreactors offer a solution by continuously supplying media to porous constructs, reducing the reliance on arterial scaffolds and large tissue samples. Despite this, these constructs often lack microvessels and are stored outside of bioreactors, which can com-promise cell survival. Microfluidic systems represent a potential alternative for vascular network fabrication, though scaling these systems to larger physiological sizes remains a significant challenge [283].

The selection and sourcing of cells is another challenge in regenerative medicine. Cells used in bioinks must possess some key characteristics: high proliferative capacity, printability, functionality, safety and economic viability [286]. The choice of cells encapsulated in bioinks critically influences their differentiation potential and ability to develop into various lineages. Although live

cells, such as stem cells, are very promising, their practical application is limited by issues related to availability and ethical concerns. Researchers have reported the successful integration of stem cells with bioprinting technologies [280]. An additional challenge is the mass production of cells, which needs substantial quantities of cells and increases the demand on in vitro expansion cultures. Addressing the cost-effectiveness of large-scale cell production is a crucial challenge [286]. Extended processing times and mechanical forces experienced during 3D printing can adversely affect cell viability by altering cell geometry and disrupting signalling pathways [289]. To address these issues, it is essential to enhance existing bioprinting techniques to minimise processing duration and to develop specialized buffers that can protect cells throughout the printing process.

In 3D bioprinting, choosing the most appropriate biomaterials is critical for the effective fabrication of tissues with clinical relevance [289, 290]. Biomaterials are essential for providing structural support, maintaining cellular viability and ensuring long-term tissue integration. While numerous polymers traditionally utilised in 3D printing and tissue engineering have been explored for bioprinting due to their availability and previous applications, they may not always provide the optimal biological compatibility required for successful bioprinting outcomes [291]. These materials might display excessive biological reactivity, which can result in undesirable cellular interactions and premature or inappropriate differentiation of stem cells. For a bioink to be suitable for clinical applications, it must have specific characteristics, such as structural stability, the ability to support cell proliferation, and a degradation rate that matches the needs of tissue regeneration. Additionally, bioinks must be compatible with bioprinting technologies to facilitate rapid prototyping [13]. A major challenge is ensuring that printed structures are biocompatible and provide an appropriate environment for cell growth. Current research is focused on developing novel biopolymers and hydrogels that more accurately replicate the nanoscale features and responsive characteristics of the ECM and native tissue microenvironment [292]. However, these advanced materials often encounter compatibility issues with traditional bioprinting techniques. Many of these materials may lack the necessary structural integrity, leading to collapse if they are too soft [293]. One potential solution is to combine various materials to harness their individual strengths, such as merging the mechanical properties of more rigid materials with the cell-supportive and biocompatible features of softer ones [134, 294].

Furthermore, the development and implementation of 3D printing and cell therapies in regenerative medicine pose significant financial challenges, which could prevent the widespread adoption of these technologies. The costs associated with research, development and clinical trials are substantial, and securing funding for these endeavours can be difficult. Moreover, the cost-efficiency of these technologies needs careful consideration, particularly in relation to the high expenses of 3D printers, cellular materials and associated computer software [295]. Generally, the costs of maintaining and scaling bioprinting technologies limit the rapid integration of 3D printing capabilities into clinical settings [292]. Another challenge is the size of bioprinted tissues. Currently, bioprinted constructs are typically small and consist of a limited number of cell types, which restricts their functionality and scalability [292, 295-297]. Moreover, 3D printers are often constrained by their build volume, which limits the maximum size of bioprinted tissues and complicates the creation of entire 3D-printed organs [292].

Ethical considerations are increasingly influencing the development of 3D bioprinting technologies. The transition of 3D printing/bioprinting research from the laboratory to clinical applications raises both established ethical concerns, as discussed in the bioethics literature, and emerging issues specific to the unique features of these new treatments [298-300]. Several ethical concerns arise with the advancement of 3D printing/bioprinting technologies, including issues related to the sourcing of cells and tissues, as previously mentioned. Furthermore, the development of these technologies requires careful ethical consideration, particularly in research involving animal welfare and the design of human clinical trials. It is crucial to find a balance between the necessity of animal testing and the ethical treatment of research subjects, while thoroughly assessing the risks and benefits for human trials [301]. As bioprinting technologies evolve, ensuring equitable access becomes an ethical obligation. Addressing potential healthcare disparities and balancing the advantages of personalized medicine with fair healthcare delivery are significant challenges that must be addressed [302]. The rapid rate of the development of bioprinting has outpaced existing regulatory frameworks, resulting in gaps that need to be closed. Despite their complexity and time demands, valuable guidelines for these processes can be obtained from regulatory agencies such as the Food and Drug Ad-ministration (FDA) in the United States and the European Medicines Agency (EMA) in the European Union, especially regarding 3D-printed medical devices. For tissue bioprinting to achieve clinical

translation, it is essential to establish a clear and defined regulatory pathway [303]. Additionally, challenges and concerns related to biosafety and liability arise when fabricating internal tissues and organs. The clinical translation of bioprinting techniques will depend on regulatory bodies' thorough the evaluation of safety, efficacy and risk. Globally, regulatory authorities face challenges in addressing the potential and uncertain risks associated with 3D bioprinting, such as immune responses to bioinks or materials [292]. In the absence of specific regulations, the FDA is currently relying on the guidelines of the Center for Biologics Evaluation and Research (CBER) for 3D bioprinting products. These products require FDA approval, and adherence to regulatory guidelines is mandatory from the initial stages of product development. As the field advances, more 3D bioprinting products are likely to emerge, highlighting the need for more specific regulatory guidelines. Currently, only South Korea's Ministry of Food and Drug Safety (MFDS) and Japan's Pharmaceuticals and Medical Devices Agency (PMDA) have developed specific guidelines for 3D bioprinting. Thus, the global development of com-prehensive regulations for 3D bioprinting techniques, bioinks and printers is of in-creasing importance [13].

These limitations and challenges highlight the complexity of integrating 3D printing with cellular therapies in regenerative medicine, emphasizing the need for continuous research and development in this field. Overcoming these obstacles requires transdisciplinary collaboration among cell biologists, engineers, physiologists and pharmaceutical industry partners to advance and expand the potential of this technology [304]. Despite the existing challenges, advancements persist, and it is anticipated that these technologies will increasingly impact the treatment of various diseases and conditions in the future. Ongoing research is progressively making the goal of creating safe and fully functional bioprinted tissues more achievable [286].

7. Current state and future outlook

The current state of clinical trials combining 3D printing/bioprinting and cellular therapies is promising, though they are still in their early stages. Numerous research groups are actively developing and testing new treatments utilizing these technologies, and several clinical trials have been initiated in recent years to assess their safety and efficacy.

Tissue engineering currently has broad applications, including the development of various tissues, cardiac, vascular, bone, skin, neural, cartilage and retinal tissues, among others. Conventionally, this method entails seeding cells onto a porous scaffold to promote their growth and, subsequently, promote tissue development [305]. The approach presents several advantages, including providing strong structural support with suitable degradation timing, regulating the cellular environment and allowing for effective nutrient and waste exchange between the scaffold and cells [306, 307].

Bioprinting has opened up a whole new era in tissue regeneration, allowing the production of patient-specific autologous organs and tissues [18, 308-311]. This rapid prototyping technique allows for the fabrication of intricate tissue and organ structures by precisely depositing living cells and biomaterials layer by layer, based on a CAD model. Using this approach, 3D constructs can be produced with high accuracy in terms of positioning and architecture, including shape, pore geometry and interconnectivity. This allows for the development of tissue and organ models that closely resemble the human body, with high reproducibility [312-314]. By simultaneously printing multiple cell types and biomaterials, bioprinting can replicate the structural and biochemical complexity of living tissues, creating a heterogeneous microenvironment at specified locations [128, 315, 316].

Although in vitro models have advanced significantly for developing new therapies, their application in surgical settings is still not fully realized. However, significant progress is being made in hydrogel design and the development of advanced technological tools. These advancements are bringing us closer to meeting the fidelity and safety standards required for bioprinted constructs to be used consistently and in a personalized way in patients in the near future [317].

Additionally, artificial intelligence (AI) is leveraging significant advances in AM for regenerative medicine, particularly in the production of personalized medical devices, implants and tissue engineering. AI algorithms optimize 3D printing parameters such as speed, temperature and layer thickness, increasing the precision and quality of printed structures [318]. This optimization is crucial for the creation of patient-specific implants and prostheses, as well as for the development of 3D-printed tissues and organs, advancing the field of regenerative medicine [319]. In addition, AI-assisted 3D printing enables the manufacture of

detailed models for surgical planning and testing, improving surgical results and precision [320]. Moving forward, researchers predict that AI will continue to revolutionize AM, enabling a more seamless use of the technology for complex designs in artificial organs, flexible electronics and wearable biosensors [321]. The synergy between AI and AM promises to unlock new possibilities for design, production and innovation in regenerative medicine [322].

The future of tissue biomaterials is expected to replicate not only the structural design and characteristics of organs and tissues but also their dynamic, functional behaviours [159,160]. The concept of time as the fourth dimension (4D) has gained prominence, in the context of bioprinting, introducing two key aspects: materials capable of deformation and structures that mature after printing [323, 324]. This new approach to bioprinting ad-dresses the complexity of the system, which is very important for fully understanding the behaviour of functional living materials during the post-processing stage [317].

8. Conclusion

The combination of 3D printing/bioprinting technologies with cellular therapies represents a significant advancement in regenerative medicine. Advances in this area are leading to the development of new functional tissues that closely resemble native tissues. This review has detailed the fundamental principles and applications of each technology individually and has elucidated how their convergence is pushing the boundaries of tissue engineering

This study underlines that the latest developments have markedly enhanced the capacity to produce complex 3D cellular structures presenting high precision. Innovations in bioprinting techniques, coupled with improvements in biomaterials and cellular engineering, have enabled more sophisticated control over tissue architecture and cellular organization. These advancements facilitate the creation of more accurate and functional tissue models, which hold promise for personalized regenerative therapies.

Nevertheless, there are still several critical barriers that need to be addressed, such as the development of functional vascular networks, regulatory and ethical issues and the advancement of suitable biomaterials.

The potential impact of these integrated technologies in regenerative medicine is expected to be high in the future. As the field progresses, solving these

issues will be essential to realizing the full potential of 3D printing/bioprinting and cell therapies. Ongoing research and innovation in these areas is therefore expected to produce transformative advances in personalized medicine and tissue regeneration, ultimately improving outcomes for patients and advancing therapeutic options.

Author Contributions: Conceptualization, A.C.S., J.D.S., L.A., N.A. and A.C.M.; methodology, A.C.S., R.A., B.L., P.S., A.M. and A.C.; investigation, A.C.S.; writing—original draft preparation, A.C.S.; writing—review and editing, A.C.S., R.A., B.L., P.S., A.M. and A.C.; software, J.D.S. and L.A.; visu-alization, A.C.S.; supervision, J.D.S., L.A., N.A. and A.C.M.; project administration, A.C.M.; funding acquisition, J.D.S., L.A., N.A. and A.C.M. All authors have read and agreed to the published version of the manuscript.

Funding: Ana Catarina Sousa (SFRH/BD/146689/2019), Bruna Lopes (2021.05265.BD), Patrícia Sousa (2023.00246.BD), André Coelho (2023.00428.BD) and Alícia Moreira (2023.00544.BD) acknowledge the Fundação para a Ciência e Tecnologia (FCT) for financial support. Rui Alvites acknowledges the CECA, UP and FCT for the funding and accessibility of all technical, structural and human resources necessary for the development of this study. The research was supported through the project UIDB/00211/2020, funded by the FCT/MCTES national funds. This research was funded by Projects PEst-OE/AGR/UI0211/2011 from FCT, and COM-PETE 2020, from ANI–Projetos ID&T Empresas em Copromoção; by the project "InnovaBIOMAS—Optimized Additive Biofabrication System for the Production of Hierarchical Multi-Tissue Scaffolds Applied in the Treatment of Joint Diseases" with the reference 2022.10564; PTDC, by the project "Bone2Move- Development of "in vivo" experimental techniques and modelling methodologies for the evalua-tion of 4D scaffolds for bone defect in sheep model: an integrative research approach" with the reference POCI-01-0145-FEDER-031146.

Data Availability Statement: The data that support the findings of this study are available from the corresponding author on request.

Acknowledgments: The authors acknowledge BioRender for providing the platform used to create the illustrations included in this manuscript.

Conflicts of Interest: The authors declare no conflicts of interest.

Abbreviations

2D	Two-dimensional
132ACG	Bioink with alginate (1%), cellulose nanocrystal (3%), and gelatin methacryloyl (5%)
2PP	Two-photon polymerization
3D	Three-dimensional
3DP-HOs	Three-dimensional bioprinted hepatorganoids
4D	Four-dimensional
ACP	Amorphous calcium phosphate
AD	Additive manufacturing
ADM	Acellular dermal matrix
aHSC	Primary foetal activated hepatic stellate cells
ALP	Alkaline phosphatase
AMX	Amoxicillin
ASTM	American Society for Testing and Materials
BFGF	Basic fibroblast growth factor
BJ	Binder jetting
BL	Bi-layer
BMP-2	Bone morphogenetic protein 2
BMSCs	bone marrow-derived mesenchymal stem/stromal cells
C17.2	Murine neural stem cells
Ca	Calcium
CAD	Computer-aided design
CBER	Centre for Biologics Evaluation and Research
cECM	decellularized cardiac extracellular
CFs	Human cardiac fibroblasts
CLIP	Continuous light interface production
CNC	Cellulose nanocrystal

CSMA	Chondroitin sulphate methacrylate
dECM	Decellularized extracellular matrix
DEP	Directed energy deposition
Dex	Dextran
DFs	Dermal fibroblasts
DIW	Direct ink writing
DLP	Digital light processing
DMLS	Direct metal laser sintering
DO	Diamond
DPSCs	Dental Pulp stem/stromal cells
EBM	Electron beam melting
ECM	Extracellular matrix
EMA	European medicines agency
EPCs	Endothelial progenitor cells
ESCs	Embryonic stem cells
ESCs	Epidermal stem cells
EVCs	Early vascular cells
FDA	Food and Drug Administration
FDM	Fused deposition modelling
Fe	Iron
FFF	Fused filament fabrication
GAM	Matrix hydrogel with 2.8% of gellan gum, 1.6% of alginate, and 2.8% of methyl cellulose
Gel	Gelatin
GelMA	Gelatin methacrylate
H9c2	Cardiomyocytes
HA	Hyaluronic acid
HAGM	Hyaluronic acid-gelatine methacrylate

HAp	Hydroxyapatite
Hap/β-TCP	Biphasic calcium phosphate system
hCAECs	Human coronary artery endothelial cells
HCC	Hepatocellular carcinoma
hCMPCs	Human cardiac-derived cardiomyocyte progenitor cells
hCPCs	Human cardiac progenitor cells
hdECM	Heart tissue-derived extracellular matrix
hDFs	Human dermal fibroblasts
hECM	Human extracellular matrix
hECs	Human endothelial cells
hepG2	Human hepatocellular carcinoma
hESCs	Human embryonic stem cells
hiHep	Human-induced hepatocyte
hiPSCs	Human induced pluripotent stem cells
hKCs	Human keratinocytes
hLFs	Human lung fibroblasts
hMVECs	Human microvascular endothelial cells
hnDFs	Human neonatal dermal fibroblasts
hPCs	Human placental pericytes
hPSCs	Human pluripotent stem cells
hSFs	Human skin fibroblasts
hUCMSCs	Human umbilical cord mesenchymal stem cells
HUH7	Undifferentiated hepatocyte cell line
hUVECs	Human umbilical vein/vascular endothelial cells
iCMs	Induced pluripotent stem cell-derived cardiomyocytes
IFN-γ	Interferon-gamma

iPSC-CMs	Induced pluripotent stem cell-derived cardiomyocytes
iPSCs	Induced pluripotent stem cells
ISO	International Standard Organization
Kr	Keratin
L x 2	Human hepatic stellate cell line
LAP	Lithium phenyl-2,4,6-trimethylbenzoylphosphinate
LOM	Laminated object manufacturing
mEFs	Mouse embryonic fibroblasts
MFDS	Ministry of Food and Drug Safety
Mg	Magnesium
MJ	Material jetting
Mn	Manganese
MSCs	Mesenchymal stem/stromal cells
MUVECs	Murine umbilical vein endothelial cells
n/a	Not applicable
Nb	Niobium
NB	N-(2-aminoethyl)-4-(4-(hydroxymethyl)-2-methoxy-5-nitrosophenoxy) butanamide
NPCs	Neural progenitor cells
NRCMs	Neonatal rat cardiomyocytes
NSCs	Neural stem cells
NSPCs	Neural stem/progenitor cells
OMT	Oxymatrine
PBF	Powder bed fusion
pc-12	Rat adrenal medullary pheochromocytoma
PCL	Poly (ε-caprolactone)
PecMA	Pectin methacrylate
PEDOT	Poly(3,4-ethylenedioxythiophene)

PEEK	Polyether ether ketone
PEG	Polyethylene glycol
PEG4A	4-arm polyethylene glycol acrylate
PEGDA	Diacrylate poly (ethylene glycol)
PEGDMA	Poly (ethylene glycol) dimethacrylate
PEGMA	Poly (ethylene glycol) methacrylate
PF	PEG-Fibrinogen
PF	Poly (ethylene glycol)-fibrinogen
PGA	Poly (glycolic acid)
PGS	Poly (glycerol sebacate)
phDFs	Primary human dermal fibroblasts
PLA	Poly(l-lactic) acid
PLGA	Poly (lactic-co-glycolic) acid
PMDA	Pharmaceuticals and Medical Devices Agency
PMHs	Primary mouse hepatocytes
PrHCs	Primary rat hepatocytes cells
PRP	Platelet-rich plasma
PSC	Phosphosilicate calcium bioglass
PSCs	Phosphosilicate calcium bioglasses
PU	Polyurethane
PVP	Polyvinylpyrrolidone
r-BMSCs	Rat bone marrow mesenchymal stem cells
RD	Rhombic dodecahedron
rGO	Reduced graphene oxide
rhEGF	External human epidermal growth factor
SCAPs	Stromal cells from apical papilla
SF	Silk fibroin
SilMA	Methacrylated silk fibroin

SLA	Stereolithography
SLM	Selective laser melting
SLS	Selective laser sintering
Sr-CSH	Xonotlite
SR^{2+}	Strontium
SS	Strontium silicate
Ta	Tantalum
Ti	Titanium
Ti6AI4V	Titanium alloy
UAM	Ultrasonic additive manufacturing
UV	Ultraviolet
VEGF	Vascular endothelial
XG	Xanthan gum
Zn^{2+}	Zinc
Zr	Zirconium
β-TCP	Beta-tricalcium phosphate

References

1. Jessop, Z.M., et al., *Transforming healthcare through regenerative medicine.* BMC Medicine, 2016. **14**(1): p. 115.10.1186/s12916-016-0669-4.

2. Damaser, M.S. and K.D. Sievert, *Tissue engineering and regenerative medicine: bench to bedside in urology. Preface.* Adv Drug Deliv Rev, 2015. **82-83**: p. v-vii.10.1016/j.addr.2015.01.006.

3. Jacques, E. and E.J. Suuronen, *The Progression of Regenerative Medicine and its Impact on Therapy Translation.* Clinical and Translational Science, 2020. **13**(3): p. 440-450.https://doi.org/10.1111/cts.12736.

4. Edwards, J., R. Thomas, and R. Guilliatt, *Regenerative medicine: from the laboratory looking out.* Palgrave Communications, 2017. **3**(1): p. 27.10.1057/s41599-017-0036-x.

5. Pathak, K., et al., *3D printing in biomedicine: advancing personalized care through additive manufacturing.* Exploration of Medicine, 2023. **4**(6): p. 1135-1167.10.37349/emed.2023.00200.

6. Huang, G., et al., *Applications, advancements, and challenges of 3D bioprinting in organ transplantation.* Biomaterials science, 2024. **12**.10.1039/d3bm01934a.

7. Bakhtiar, S.M., et al., *Chapter 10 - 3D Printing Technologies and Their Applications in Biomedical Science*, in *Omics Technologies and Bio-Engineering*, D. Barh and V. Azevedo, Editors. 2018, Academic Press: Cambridge, MA, USA, 2018; p. 167-189. https://doi.org/10.1016/B978-0-12-804659-3.00010-5.

8. dos Santos, J., et al., *3D Printing and Nanotechnology: A Multiscale Alliance in Personalized Medicine.* Advanced Functional Materials, 2021.ARTN 200969110.1002/adfm.202009691.

9. Li, J., et al., *3D printing for regenerative medicine: From bench to bedside.* Mrs Bulletin, 2015. **40**(2): p. 145-153.10.1557/mrs.2015.5.

10. Amoyav, B., et al., *3D Printed Microfluidic Devices for Drug Release Assays.* Pharmaceutics, 2021. **13**(1).ARTN 1310.3390/pharmaceutics13010013.

11. Ong, C.S., et al., *3D bioprinting using stem cells.* Pediatric Research, 2018. **83**(1): p. 223-231.10.1038/pr.2017.252.

12. Liu, K., et al., *3D printing and bioprinting in urology.* IJB, 2023. **9**(6).10.36922/ijb.0969.

13. Jain, P., H. Kathuria, and N. Dubey, *Advances in 3D bioprinting of tissues/organs for regenerative medicine and in-vitro models.* Biomaterials, 2022. **287**: p. 121639.https://doi.org/10.1016/j.biomaterials.2022.121639.

14. Administration, U.S.F.D. *Medical Applications of 3D Printing*; Available from: https://www.fda.gov/medical-devices/3d-printing-medical-devices/medical-applications-3d-printing(accessed on 23 July 2024).

15. Martins, J.P., et al., *Chapter 4 - 3D printing: prospects and challenges*, in *Nanotechnologies in Preventive and Regenerative Medicine*, V. Uskoković and D.P. Uskoković, Editors. Elsevier: Amsterdam, The Netherlands, 2018 p. 299-379. https://doi.org/10.1016/B978-0-323-48063-5.00004-6.

16. Chung, J.J., et al., *Toward biomimetic scaffolds for tissue engineering: 3D printing techniques in regenerative medicine.* Frontiers in Bioengineering and Biotechnology, 2020. **8**: p. 586406

17. ASTM, *ASTM International Committee F42 on Additive Manufacturing Technologies ASTM F2792–10*, in *Standard Terminology for Additive Manufacturing Technologies* ; ASTM: West Conshohocken, PA, USA,2009.

18. Ng, W.L., et al., *Vat polymerization-based bioprinting-process, materials, applications and regulatory challenges.* Biofabrication, 2020. **12**(2): p. 022001.10.1088/1758-5090/ab6034.

19. Robles Martinez, P., A.W. Basit, and S. Gaisford, *The History, Developments and Opportunities of Stereolithography*, in *3D Printing of Pharmaceuticals*, A.W. Basit and S. Gaisford, Editors. 2018, Springer International Publishing: Cham. p. 55-79. 10.1007/978-3-319-90755-0_4.

20. Xu, X., et al., *Vat photopolymerization 3D printing for advanced drug delivery and medical device applications.* Journal of Controlled Release, 2021. **329**: p. 743-757.https://doi.org/10.1016/j.jconrel.2020.10.008.

21. Al Rashid, A., et al., *Vat photopolymerization of polymers and polymer composites: Processes and applications.* Additive Manufacturing, 2021. **47**: p. 102279.https://doi.org/10.1016/j.addma.2021.102279.

22. Rajan, K., et al., *Fused deposition modeling: process, materials, parameters, properties, and applications.* The International Journal of Advanced Manufacturing Technology, 2022. **120**(3): p. 1531-1570.10.1007/s00170-022-08860-7.

23. Marwah, O.M.F., et al., *Direct Investment Casting For Pattern Developed By Desktop 3D Printer.* MATEC Web of Conferences, 2017. **135**: p. 00036.10.1051/matecconf/201713500036.

24. Siddique, S.H., et al., *Lessons from nature: 3D printed bio-inspired porous structures for impact energy absorption – A review.* Additive Manufacturing, 2022. **58**: p. 103051.https://doi.org/10.1016/j.addma.2022.103051.

25. Chartrain, N.A., et al., *3D bioprinting for the repair of articular cartilage and osteochondral tissue.* Bioprinting, 2022. **28**: p. e00239.https://doi.org/10.1016/j.bprint.2022.e00239.

26. Gibson, I., et al., *Additive manufacturing technologies*. Vol. 17. 2021: Springer: Berlin/Heidelberg, Germany, 2021; Volume 17.

27. Ligon, S.C., et al., *Polymers for 3D Printing and Customized Additive Manufacturing.* Chemical Reviews, 2017. **117**(15): p. 10212-10290.10.1021/acs.chemrev.7b00074.

28. Alami, A.H., et al., *Additive manufacturing in the aerospace and automotive industries: Recent trends and role in achieving sustainable development goals.* Ain Shams Engineering Journal, 2023. **14**(11): p. 102516.https://doi.org/10.1016/j.asej.2023.102516.

29. Zhang, X. and F. Liou, *Chapter 1 - Introduction to additive manufacturing*, in *Additive Manufacturing*, J. Pou, A. Riveiro, and J.P. Davim, Editors. Elsevier: : Amsterdam, The Netherlands, 2021; p. 1-31. https://doi.org/10.1016/B978-0-12-818411-0.00009-4.

30. Gao, H., et al., *3D printed optics and photonics: Processes, materials and applications.* Materials Today, 2023. **69**: p. 107-132.https://doi.org/10.1016/j.mattod.2023.06.019.

31. University, L. *About Additive Manufacturing: Powder Bed Fusion*. 2024; Available from: https://www.lboro.ac.uk/research/amrg/about/the7categoriesofadditivemanufacturing/powderbedfusion/ (accessed on 20 July 2024).

32. Singh, R., et al., *Powder bed fusion process in additive manufacturing: An overview.* Materials Today: Proceedings, 2020. **26**: p. 3058-3070.https://doi.org/10.1016/j.matpr.2020.02.635.

33. Thakur, V., R. Singh, and R. Kumar, *Chapter Two - Materials for additive manufacturing in clinical podiatry*, in *3D Printing in Podiatric Medicine*, K. Sandhu, et al., Editors. Academic Press: Cambridge, MA, USA, 2023; p. 35-50. https://doi.org/10.1016/B978-0-323-91911-1.00006-7.

34. Bourell, D., et al., *Materials for additive manufacturing.* CIRP Annals, 2017. **66**(2): p. 659-681.https://doi.org/10.1016/j.cirp.2017.05.009.

35. University, L. *About Additive Manufacturing: Material Jetting* 2024; Available from: https://www.lboro.ac.uk/research/amrg/about/the7categoriesofadditivemanufacturing/materialjetting/

36. Bourell, D.L., *Perspectives on Additive Manufacturing.* Annual Review of Materials Research, 2016. **46**(Volume 46, 2016): p. 1-18.https://doi.org/10.1146/annurev-matsci-070115-031606.

37. Mostafaei, A., et al., *Binder jet 3D printing—Process parameters, materials, properties, modeling, and challenges.* Progress in Materials Science, 2021. **119**: p. 100707.https://doi.org/10.1016/j.pmatsci.2020.100707.

38. Naghieh, S. and X. Chen, *Printability–A key issue in extrusion-based bioprinting.* Journal of Pharmaceutical Analysis, 2021. **11**(5): p. 564-579.https://doi.org/10.1016/j.jpha.2021.02.001.

39. Tuominen, J. *Directed energy deposition–Review of materials, properties and applications*. In *3D Boosti ja Invest*; Tampere University of Technology: Tampere, Finland, 2017.

40. University, L. *About Additive Manufacturing: Directed Energy Deposition*. 2024; Available from: https://www.lboro.ac.uk/research/amrg/about/the7categoriesofadditivemanufacturing/directedenergydeposition/ (accessed on 10 July 2024).

41. Gibson, I., et al., *Sheet lamination.* Additive manufacturing technologies; Springer: Cham, Switzerland, 2021: p. 253-283

42. University, L. *About Additive Manufacturing: Sheet Lamination*. 2024; Available from:

https://www.lboro.ac.uk/research/amrg/about/the7categoriesofadditivemanufacturing/sheetlamination/(accessed on 25 July 2024).

43. Gail Kim, R., et al., *A Survey of Image-Based Fault Monitoring in Additive Manufacturing: Recent Developments and Future Directions.* Sensors, 2023. **23**: p. 6821.10.3390/s23156821.

44. Bermudo Gamboa, C., et al., *Fatigue behaviour analysis of AISI 316-L parts obtained by machining process and additive manufacturing.* IOP Conference Series: Materials Science and Engineering, 2021. **1193**: p. 012101.10.1088/1757-899X/1193/1/012101.

45. Moroni, L., et al., *Biofabrication: A Guide to Technology and Terminology.* Trends in Biotechnology, 2018. **36**(4): p. 384-402.10.1016/j.tibtech.2017.10.015.

46. Pantermehl, S., et al., *3D Printing for Soft Tissue Regeneration and Applications in Medicine.* Biomedicines, 2021. **9**(4).10.3390/biomedicines9040336.

47. Xing, F., et al., *Recent advances in biofabrication strategies based on bioprinting for vascularized tissue repair and regeneration.* Materials & Design, 2023. **229**: p. 111885.https://doi.org/10.1016/j.matdes.2023.111885.

48. Gu, Z., et al., *Development of 3D bioprinting: From printing methods to biomedical applications.* Asian Journal of Pharmaceutical Sciences, 2020. **15**(5): p. 529-557.https://doi.org/10.1016/j.ajps.2019.11.003.

49. Sufaru, I.-G., et al., *3D Printed and Bioprinted Membranes and Scaffolds for the Periodontal Tissue Regeneration: A Narrative Review.* Membranes, 2022. **12**(9): p. 902

50. Ayran, M., B. Bulut, and S. Ulag, *Bioprinting*, in *Biomaterials and Tissue Engineering*, O. Gunduz, et al., Editors. 2023, Springer International Publishing: Cham. p. 357-384. 10.1007/978-3-031-35832-6_13.

51. Mironov, V., et al., *Organ printing: computer-aided jet-based 3D tissue engineering.* TRENDS in Biotechnology, 2003. **21**(4): p. 157-161

52. Roth, E.A., et al., *Inkjet printing for high-throughput cell patterning.* Biomaterials, 2004. **25**(17): p. 3707-3715

53. Norotte, C., et al., *Scaffold-free vascular tissue engineering using bioprinting.* Biomaterials, 2009. **30**(30): p. 5910-5917

54. Roque, R., G.F. Barbosa, and A.C. Guastaldi, *Design and 3D bioprinting of interconnected porous scaffolds for bone regeneration. An additive manufacturing approach.* Journal of Manufacturing Processes, 2021. **64**: p. 655-663.https://doi.org/10.1016/j.jmapro.2021.01.057.

55. Dababneh, A.B. and I.T. Ozbolat, *Bioprinting technology: a current state-of-the-art review.* Journal of Manufacturing Science and Engineering, 2014. **136**(6): p. 061016

56. Rider, P., et al., *Additive Manufacturing for Guided Bone Regeneration: A Perspective for Alveolar Ridge Augmentation.* International Journal of Molecular Sciences, 2018. **19**(11): p. 3308

57. Bartolo, P., et al., *Biomedical production of implants by additive electro-chemical and physical processes.* CIRP Annals, 2012. **61**(2): p. 635-655.https://doi.org/10.1016/j.cirp.2012.05.005.

58. Yi, H.-G., et al., *Application of 3D bioprinting in the prevention and the therapy for human diseases.* Signal Transduction and Targeted Therapy, 2021. **6**(1): p. 177.10.1038/s41392-021-00566-8.

59. Ovsianikov, A., M. Farsari, and B.N. Chichkov, *Photonic and Biomedical Applications of the Two-Photon Polymerization Technique*, in *Stereolithography: Materials, Processes and Applications*, P.J. Bártolo, Editor. 2011, Springer US: Boston, MA. p. 257-297. 10.1007/978-0-387-92904-0_11.

60. Gu, B.K., et al., *3-dimensional bioprinting for tissue engineering applications.* Biomater Res, 2016. **20**: p. 12.10.1186/s40824-016-0058-2.

61. Song, Y., et al., *An overview of selective laser sintering 3D printing technology for biomedical and sports device applications: Processes,*

materials, and applications. Optics & Laser Technology, 2024. **171**: p. 110459.https://doi.org/10.1016/j.optlastec.2023.110459.

62. Xie, Z., et al., *3D Bioprinting in Tissue Engineering for Medical Applications: The Classic and the Hybrid.* Polymers, 2020. **12**(8): p. 1717

63. Ramesh, S., et al., *Extrusion bioprinting: Recent progress, challenges, and future opportunities.* Bioprinting, 2021. **21**: p. e00116.https://doi.org/10.1016/j.bprint.2020.e00116.

64. Arefin, A.M.E., et al., *Polymer 3D Printing Review: Materials, Process, and Design Strategies for Medical Applications.* Polymers, 2021. **13**(9): p. 1499

65. Dong, G., et al., *Optimizing process parameters of fused deposition modeling by Taguchi method for the fabrication of lattice structures.* Additive Manufacturing, 2018. **19**: p. 62-72.https://doi.org/10.1016/j.addma.2017.11.004.

66. Carneiro, O.S., A.F. Silva, and R. Gomes, *Fused deposition modeling with polypropylene.* Materials & Design, 2015. **83**: p. 768-776.https://doi.org/10.1016/j.matdes.2015.06.053.

67. Dong, C., M. Petrovic, and I.J. Davies, *Applications of 3D printing in medicine: A review.* Annals of 3D Printed Medicine, 2024. **14**: p. 100149.https://doi.org/10.1016/j.stlm.2024.100149.

68. Barbeck, M., et al., *Biomaterial-Supported Tissue Reconstruction or Regeneration*. BoD–Books on Demand: Norderstedt, Germany, 2019.

69. Rossi, A., et al., *Biomaterials for extrusion-based bioprinting and biomedical applications.* Frontiers in Bioengineering and Biotechnology, 2024. **12**.10.3389/fbioe.2024.1393641.

70. Saunders, R.E. and B. Derby, *Inkjet printing biomaterials for tissue engineering: bioprinting.* International Materials Reviews, 2014. **59**(8): p. 430-448.10.1179/1743280414Y.0000000040.

71. Barui, S., *3D inkjet printing of biomaterials: Principles and applications.* MEDICAL DEVICES & SENSORS, 2021. **4**(1): p. e10143.https://doi.org/10.1002/mds3.10143.

72. Saygili, E., et al., *3D bioprinting: A powerful tool to leverage tissue engineering and microbial systems.* Bioprinting, 2020. **18**: p. e00071.https://doi.org/10.1016/j.bprint.2019.e00071.

73. Derakhshanfar, S., et al., *3D bioprinting for biomedical devices and tissue engineering: A review of recent trends and advances.* Bioactive Materials, 2018. **3**(2): p. 144-156.https://doi.org/10.1016/j.bioactmat.2017.11.008.

74. Li, J., et al., *Recent advances in bioprinting techniques: approaches, applications and future prospects.* Journal of Translational Medicine, 2016. **14**(1): p. 271.10.1186/s12967-016-1028-0.

75. Ng, W.L., et al., *Microvalve-based bioprinting – process, bio-inks and applications.* Biomater. Sci., 2017. **5**.10.1039/C6BM00861E.

76. Vanaei, S., et al., *An Overview on Materials and Techniques in 3D Bioprinting Toward Biomedical Application.* Engineered Regeneration, 2021. **2**: p. 1-18.https://doi.org/10.1016/j.engreg.2020.12.001.

77. Ouyang, L., et al., *Effect of bioink properties on printability and cell viability for 3D bioplotting of embryonic stem cells.* Biofabrication, 2016. **8**(3): p. 035020.10.1088/1758-5090/8/3/035020.

78. Lozano, R., et al., *3D printing of layered brain-like structures using peptide modified gellan gum substrates.* Biomaterials, 2015. **67**: p. 264-73.10.1016/j.biomaterials.2015.07.022.

79. Su, C., et al., *Natural Materials for 3D Printing and Their Applications.* Gels, 2022. **8**(11).10.3390/gels8110748.

80. Marques, C.F., et al., *Collagen-based bioinks for hard tissue engineering applications: a comprehensive review.* J Mater Sci Mater Med, 2019. **30**(3): p. 32.10.1007/s10856-019-6234-x.

81. Suo, H., et al., *Low-temperature 3D printing of collagen and chitosan composite for tissue engineering.* Mater Sci Eng C Mater Biol Appl, 2021. **123**: p. 111963.10.1016/j.msec.2021.111963.

82. Dai, M., et al., *Elastin-like Polypeptide-Based Bioink: A Promising Alternative for 3D Bioprinting.* Biomacromolecules, 2021. **22**(12): p. 4956-4966.10.1021/acs.biomac.1c00861.

83. Aiyelabegan, H.T., et al., *Albumin-based biomaterial for lung tissue engineering applications.* International Journal of Polymeric Materials and Polymeric Biomaterials, 2016. **65**(16): p. 853-861.10.1080/00914037.2016.1180610.

84. Placone, J.K., et al., *Development and Characterization of a 3D Printed, Keratin-Based Hydrogel.* Ann Biomed Eng, 2017. **45**(1): p. 237-248.10.1007/s10439-016-1621-7.

85. Srinivasan, B., et al., *Porous keratin scaffold-promising biomaterial for tissue engineering and drug delivery.* J Biomed Mater Res B Appl Biomater, 2010. **92**(1): p. 5-12.10.1002/jbm.b.31483.

86. Khanarian, N.T., et al., *A functional agarose-hydroxyapatite scaffold for osteochondral interface regeneration.* Biomaterials, 2012. **33**(21): p. 5247-58.10.1016/j.biomaterials.2012.03.076.

87. Axpe, E. and M.L. Oyen, *Applications of Alginate-Based Bioinks in 3D Bioprinting.* Int J Mol Sci, 2016. **17**(12).10.3390/ijms17121976.

88. Petta, D., et al., *Hyaluronic acid as a bioink for extrusion-based 3D printing.* Biofabrication, 2020. **12**(3): p. 032001.10.1088/1758-5090/ab8752.

89. Dutta, P., K. Rinki, and J. Dutta, *Chitosan: A promising biomaterial for tissue engineering scaffolds.* Chitosan for biomaterials II, Springer: Berlin/Heidelberg, Germany, 2011; pp. 45–79.

90. Kumar, A., K.M. Rao, and S.S. Han, *Application of xanthan gum as polysaccharide in tissue engineering: A review.* Carbohydr Polym, 2018. **180**: p. 128-144.10.1016/j.carbpol.2017.10.009.

91. Jena, S.R., et al., *Harnessing the potential of dialdehyde alginate-xanthan gum hydrogels as niche bioscaffolds for tissue engineering.* Int J Biol Macromol, 2022. **207**: p. 493-506.10.1016/j.ijbiomac.2022.03.024.

92. Kumar, P.T., et al., *Drug delivery and tissue engineering applications of biocompatible pectin-chitin/nano CaCO3 composite scaffolds.* Colloids Surf B Biointerfaces, 2013. **106**: p. 109-16.10.1016/j.colsurfb.2013.01.048.

93. Akkineni, A.R., et al., *Addition of High Acyl Gellan Gum to Low Acyl Gellan Gum Enables the Blends 3D Bioprintable.* Gels, 2022. **8**(4).10.3390/gels8040199.

94. Li, S., et al., *Chitosans for tissue repair and organ three-dimensional (3D) bioprinting.* Micromachines, 2019. **10**(11): p. 765

95. Wu, Q., D. Therriault, and M.-C. Heuzey, *Processing and properties of chitosan inks for 3D printing of hydrogel microstructures.* ACS Biomaterials Science & Engineering, 2018. **4**(7): p. 2643-2652

96. Rastogi, P. and B. Kandasubramanian, *Review of alginate-based hydrogel bioprinting for application in tissue engineering.* Biofabrication, 2019. **11**(4): p. 042001

97. Gaetani, R., et al., *Epicardial application of cardiac progenitor cells in a 3D-printed gelatin/hyaluronic acid patch preserves cardiac function after myocardial infarction.* Biomaterials, 2015. **61**: p. 339-348

98. Negrini, N.C., et al., *Three-dimensional printing of chemically crosslinked gelatin hydrogels for adipose tissue engineering.* Biofabrication, 2020. **12**(2): p. 025001

99. Abelseth, E., et al., *3D printing of neural tissues derived from human induced pluripotent stem cells using a fibrin-based bioink.* ACS Biomaterials Science & Engineering, 2018. **5**(1): p. 234-243

100. Khoeini, R., et al., *Natural and Synthetic Bioinks for 3D Bioprinting.* Advanced NanoBiomed Research, 2021. **1**(8): p. 2000097.https://doi.org/10.1002/anbr.202000097.

101. Xin, S., et al., *Clickable PEG hydrogel microspheres as building blocks for 3D bioprinting.* Biomater Sci, 2019. **7**(3): p. 1179-1187.10.1039/c8bm01286e.

102. Izgordu, M.S., et al., *Investigation of 3D-printed polycaprolactone-/polyvinylpyrrolidone-based constructs.* Cartilage, 2021. **13**(2_suppl): p. 626S-635S

103. Hospodiuk, M., et al., *The bioink: A comprehensive review on bioprintable materials.* Biotechnology advances, 2017. **35**(2): p. 217-239

104. Diomede, F., et al., *Three-dimensional printed PLA scaffold and human gingival stem cell-derived extracellular vesicles: a new tool for bone defect repair.* Stem Cell Research & Therapy, 2018. **9**: p. 1-21

105. Wang, P., et al., *Effects of printing parameters of fused deposition modeling on mechanical properties, surface quality, and microstructure of PEEK.* Journal of Materials Processing Technology, 2019. **271**: p. 62-74

106. Lee, J., et al., *A 3D printing strategy for fabricating in situ topographical scaffolds using pluronic F-127.* Additive Manufacturing, 2020. **32**: p. 101023

107. Liu, F. and X. Wang, *Synthetic Polymers for Organ 3D Printing.* Polymers (Basel), 2020. **12**(8).10.3390/polym12081765.

108. Clapper, J.D., et al., *Development and characterization of photopolymerizable biodegradable materials from PEG–PLA–PEG block macromonomers.* Polymer, 2007. **48**(22): p. 6554-6564

109. Shan Wong, Y., et al., *Engineered polymeric biomaterials for tissue engineering.* Current Tissue Engineering (Discontinued), 2012. **1**(1): p. 41-53

110. S, S., et al., *A review on the recent applications of synthetic biopolymers in 3D printing for biomedical applications.* Journal of Materials Science: Materials in Medicine, 2023. **34**(12): p. 62.10.1007/s10856-023-06765-9.

111. Im, S.H., et al., *Stereocomplex Polylactide for Drug Delivery and Biomedical Applications: A Review.* Molecules, 2021. **26**(10): p. 2846

112. Alqurashi, H., et al., *Polyetherketoneketone (PEKK): An emerging biomaterial for oral implants and dental prostheses.* Journal of Advanced Research, 2021. **28**: p. 87-95.https://doi.org/10.1016/j.jare.2020.09.004.

113. Elmowafy, E.M., M. Tiboni, and M.E. Soliman, *Biocompatibility, biodegradation and biomedical applications of poly(lactic acid)/poly(lactic-co-glycolic acid) micro and nanoparticles.* Journal of Pharmaceutical Investigation, 2019. **49**(4): p. 347-380.10.1007/s40005-019-00439-x.

114. Rutz, A.L., et al., *A multi-material bioink method for 3D printing tunable, cell-compatible hydrogels.* Advanced materials (Deerfield Beach, Fla.), 2015. **27**(9): p. 1607

115. Mao, H., et al., *Recent advances and challenges in materials for 3D bioprinting.* Progress in Natural Science: Materials International, 2020. **30**(5): p. 618-634

116. Lui, Y.S., et al., *4D printing and stimuli-responsive materials in biomedical aspects.* Acta biomaterialia, 2019. **92**: p. 19-36

117. Li, Y.-C., et al., *4D bioprinting: the next-generation technology for biofabrication enabled by stimuli-responsive materials.* Biofabrication, 2016. **9**(1): p. 012001

118. El-Kadiry, A.E., M. Rafei, and R. Shammaa, *Cell Therapy: Types, Regulation, and Clinical Benefits.* Front Med (Lausanne), 2021. **8**: p. 756029.10.3389/fmed.2021.756029.

119. Kim, I., *A brief overview of cell therapy and its product.* J Korean Assoc Oral Maxillofac Surg, 2013. **39**(5): p. 201-2.10.5125/jkaoms.2013.39.5.201.

120. Facklam, A.L., L.R. Volpatti, and D.G. Anderson, *Biomaterials for Personalized Cell Therapy.* Advanced Materials, 2020. **32**(13): p. 1902005.https://doi.org/10.1002/adma.201902005.

121. Xue, J., C. Qin, and C. Wu, *3D printing of cell-delivery scaffolds for tissue regeneration.* Regenerative Biomaterials, 2023. **10**: p. rbad032.10.1093/rb/rbad032.

122. Urciuolo, A., et al., *Intravital three-dimensional bioprinting.* Nat Biomed Eng, 2020. **4**(9): p. 901-915.10.1038/s41551-020-0568-z.

123. Matai, I., et al., *Progress in 3D bioprinting technology for tissue/organ regenerative engineering.* Biomaterials, 2020. **226**: p. 119536.10.1016/j.biomaterials.2019.119536.

124. Mandrycky, C., et al., *3D bioprinting for engineering complex tissues.* Biotechnol Adv, 2016. **34**(4): p. 422-434.10.1016/j.biotechadv.2015.12.011.

125. Ventura, R.D., *An Overview of Laser-assisted Bioprinting (LAB) in Tissue Engineering Applications.* Medical Lasers, 2021. **10**(2): p. 76-81.10.25289/ML.2021.10.2.76.

126. Fahimipour, F., et al., *Enhancing cell seeding and osteogenesis of MSCs on 3D printed scaffolds through injectable BMP2 immobilized ECM-Mimetic gel.* Dent Mater, 2019. **35**(7): p. 990-1006.10.1016/j.dental.2019.04.004.

127. Jang, C.H., Y. Koo, and G. Kim, *ASC/chondrocyte-laden alginate hydrogel/PCL hybrid scaffold fabricated using 3D printing for auricle regeneration.* Carbohydr Polym, 2020. **248**: p. 116776.10.1016/j.carbpol.2020.116776.

128. Gungor-Ozkerim, P.S., et al., *Bioinks for 3D bioprinting: an overview.* Biomaterials science, 2018. **6**(5): p. 915-946

129. Polak, J.M. and S. Mantalaris, *Stem cells bioprocessing: an important milestone to move regenerative medicine research into the clinical arena.* Pediatr Res, 2008. **63**(5): p. 461-6.10.1203/pdr.0b013e31816a8c1c.

130. Saini, G., et al., *Applications of 3D Bioprinting in Tissue Engineering and Regenerative Medicine.* J Clin Med, 2021. **10**(21).10.3390/jcm10214966.

131. Jaenisch, R. and R. Young, *Stem cells, the molecular circuitry of pluripotency and nuclear reprogramming.* Cell, 2008. **132**(4): p. 567-582

132. Poliwoda, S., et al., *Stem cells: a comprehensive review of origins and emerging clinical roles in medical practice.* Orthop Rev (Pavia), 2022. **14**(3): p. 37498.10.52965/001c.37498.

133. Caddeo, S., M. Boffito, and S. Sartori, *Tissue Engineering Approaches in the Design of Healthy and Pathological In Vitro Tissue Models.* Front Bioeng Biotechnol, 2017. **5**: p. 40.10.3389/fbioe.2017.00040.

134. Irvine, S.A. and S.S. Venkatraman, *Bioprinting and Differentiation of Stem Cells.* Molecules, 2016. **21**(9): p. 1188

135. Kariminekoo, S., et al., *Implications of mesenchymal stem cells in regenerative medicine.* Artif Cells Nanomed Biotechnol, 2016. **44**(3): p. 749-57.10.3109/21691401.2015.1129620.

136. Huang, N.F. and S. Li, *Mesenchymal stem cells for vascular regeneration.* Regen Med, 2008. **3**(6): p. 877-92.10.2217/17460751.3.6.877.

137. Alvites, R.D., et al., *Rat Olfactory Mucosa Mesenchymal Stem/Stromal Cells (OM-MSCs): A Characterization Study.* International Journal of Cell Biology, 2020. **2020**(1): p. 2938258.https://doi.org/10.1155/2020/2938258.

138. Zhou, T., et al., *Challenges and advances in clinical applications of mesenchymal stromal cells.* Journal of Hematology & Oncology, 2021. **14**(1): p. 24.10.1186/s13045-021-01037-x.

139. Conrad, C., et al., *Multipotent mesenchymal stem cells acquire a lymphendothelial phenotype and enhance lymphatic regeneration in vivo.* Circulation, 2009. **119**(2): p. 281-9.10.1161/circulationaha.108.793208.

140. Paulo Zambon, J., A. Atala, and J.J. Yoo, *Methods to generate tissue-derived constructs for regenerative medicine applications.* Methods, 2020. **171**: p. 3-10.https://doi.org/10.1016/j.ymeth.2019.09.016.

141. Kaebisch, C., et al., *The role of purinergic receptors in stem cell differentiation.* Computational and Structural Biotechnology Journal, 2015. **13**: p. 75-84.https://doi.org/10.1016/j.csbj.2014.11.003.

142. Ntege, E.H., H. Sunami, and Y. Shimizu, *Advances in regenerative therapy: A review of the literature and future directions.* Regenerative Therapy, 2020. **14**: p. 136-153.https://doi.org/10.1016/j.reth.2020.01.004.

143. Feyen, D.A.M., et al., *Stem cell-based therapy: Improving myocardial cell delivery.* Advanced Drug Delivery Reviews, 2016. **106**: p. 104-115.https://doi.org/10.1016/j.addr.2016.04.023.

144. Cui, H., et al., *3D bioprinting for cardiovascular regeneration and pharmacology.* Advanced Drug Delivery Reviews, 2018. **132**: p. 252-269.https://doi.org/10.1016/j.addr.2018.07.014.

145. Ye, L., C. Swingen, and J. Zhang, *Induced pluripotent stem cells and their potential for basic and clinical sciences.* Curr Cardiol Rev, 2013. **9**(1): p. 63-72.10.2174/157340313805076278.

146. Golchin, A. and T.Z. Farahany, *Biological Products: Cellular Therapy and FDA Approved Products.* Stem Cell Rev Rep, 2019. **15**(2): p. 166-175.10.1007/s12015-018-9866-1.

147. De Pieri, A., Y. Rochev, and D.I. Zeugolis, *Scaffold-free cell-based tissue engineering therapies: advances, shortfalls and forecast.* NPJ Regen Med, 2021. **6**(1): p. 18.10.1038/s41536-021-00133-3.

148. Sánchez, A., T. Schimmang, and J. García-Sancho, *Cell and tissue therapy in regenerative medicine.* Adv Exp Med Biol, 2012. **741**: p. 89-102.10.1007/978-1-4614-2098-9_7.

149. Gyorgypal, A. *An Introduction to Cell Therapy*. 2023 [cited 2024 28-07-2024]; Available from: https://www.technologynetworks.com/biopharma/webinars/strategies-for-error-free-chromatographic-analyses-388826

150. Dainichi, T., et al., *Editorial: Regulation of Immunity by Non-Immune Cells.* Frontiers in Immunology, 2021. **12**.10.3389/fimmu.2021.770847.

151. *Guidance for human somatic cell therapy and gene therapy.* Hum Gene Ther, 2001. **12**(3): p. 303-14.10.1089/10430340150218431.

152. Bartel, R.L., et al., *The Aastrom experience.* Stem Cell Research & Therapy, 2012. **3**(4): p. 26.10.1186/scrt117.

153. Wolff, M., et al., *Injections of concentrated bone marrow aspirate as treatment for Discogenic pain: a retrospective analysis.* BMC Musculoskelet Disord, 2020. **21**(1): p. 135.10.1186/s12891-020-3126-7.

154. Buisseret, L., et al., *Tumor-infiltrating lymphocyte composition, organization and PD-1/ PD-L1 expression are linked in breast cancer.* Oncoimmunology, 2017. **6**(1): p. e1257452.10.1080/2162402x.2016.1257452.

155. Guo, J., et al., *Stromal vascular fraction: A regenerative reality? Part 2: Mechanisms of regenerative action.* J Plast Reconstr Aesthet Surg, 2016. **69**(2): p. 180-8.10.1016/j.bjps.2015.10.014.

156. Heo, D.N., et al., *3D bioprinting of carbohydrazide-modified gelatin into microparticle-suspended oxidized alginate for the fabrication of complex-shaped tissue constructs.* ACS applied materials & interfaces, 2020. **12**(18): p. 20295-20306

157. Dey, M. and I.T. Ozbolat, *3D bioprinting of cells, tissues and organs.* Scientific Reports, 2020. **10**(1): p. 14023.10.1038/s41598-020-70086-y.

158. Ivanovski, S., et al., *3D printing for bone regeneration: challenges and opportunities for achieving predictability.* Periodontology 2000, 2023. **93**(1): p. 358-384.https://doi.org/10.1111/prd.12525.

159. Yang, Z., et al., *Research landscape of 3D printing in bone regeneration and bone repair: A bibliometric and visualized analysis from 2012 to 2022.* IJB, 2023. **9**(4).10.18063/ijb.737.

160. Khan, A.R., et al., *Raising the Bar: Progress in 3D-Printed Hybrid Bone Scaffolds for Clinical Applications: A Review.* Cell Transplant, 2024. **33**: p. 9636897241273562.10.1177/09636897241273562.

161. Alonzo, M., et al., *3D Bioprinting of cardiac tissue and cardiac stem cell therapy.* Transl Res, 2019. **211**: p. 64-83.10.1016/j.trsl.2019.04.004.

162. Qasim, M., et al., *3D printing approaches for cardiac tissue engineering and role of immune modulation in tissue regeneration.* Int J Nanomedicine, 2019. **14**: p. 1311-1333.10.2147/ijn.S189587.

163. Roth, G.A., et al., *Global, Regional, and National Burden of Cardiovascular Diseases for 10 Causes, 1990 to 2015.* J Am Coll Cardiol, 2017. **70**(1): p. 1-25.10.1016/j.jacc.2017.04.052.

164. Bhandari, S., et al., *Trends and Challenges in the Development of 3D-Printed Heart Valves and Other Cardiac Implants: A Review of Current Advances.* Cureus, 2023. **15**(8): p. e43204.10.7759/cureus.43204.

165. Itier, R. and J. Roncalli, *New therapies for acute myocardial infarction: current state of research and future promise.* Future Cardiology, 2018. **14**(4): p. 329-342

166. Shi, W.Y., et al., *Role of coronary artery bypass surgery in acute myocardial infarction.* Primary Angioplasty: A Practical Guide; Springer: Singapore, 2018: p. 211-221

167. Kwon, Y.-W., H.-M. Yang, and H.-J. Cho, *Cell therapy for myocardial infarction.* International journal of stem cells, 2010. **3**(1): p. 8-15

168. Das, S., H. Nam, and J. Jang, *3D bioprinting of stem cell-laden cardiac patch: A promising alternative for myocardial repair.* APL bioengineering, 2021. **5**(3)

169. Fernandes, S., et al., *Synthetic matrices to serve as niches for muscle cell transplantation.* Cells Tissues Organs, 2011. **195**(1-2): p. 48-59

170. Vukicevic, M., et al., *Cardiac 3D printing and its future directions.* JACC: Cardiovascular Imaging, 2017. **10**(2): p. 171-184

171. Hinderer, S., E. Brauchle, and K. Schenke-Layland, *Generation and assessment of functional biomaterial scaffolds for applications in cardiovascular tissue engineering and regenerative medicine.* Advanced healthcare materials, 2015. **4**(16): p. 2326-2341

172. Zhu, J. and R.E. Marchant, *Design properties of hydrogel tissue-engineering scaffolds.* Expert review of medical devices, 2011. **8**(5): p. 607-626

173. Maiullari, F., et al., *A multi-cellular 3D bioprinting approach for vascularized heart tissue engineering based on HUVECs and iPSC-derived cardiomyocytes.* Scientific Reports, 2018. **8**(1): p. 13532.10.1038/s41598-018-31848-x.

174. Bejleri, D., et al., *A Bioprinted Cardiac Patch Composed of Cardiac-Specific Extracellular Matrix and Progenitor Cells for Heart Repair.* Advanced Healthcare Materials, 2018. **7**(23): p. 1800672.https://doi.org/10.1002/adhm.201800672.

175. Melhem, M.R., et al., *3D Printed Stem-Cell-Laden, Microchanneled Hydrogel Patch for the Enhanced Release of Cell-Secreting Factors and Treatment of Myocardial Infarctions.* ACS Biomaterials Science & Engineering, 2017. **3**(9): p. 1980-1987.10.1021/acsbiomaterials.6b00176.

176. Noor, N., et al., *3D Printing of Personalized Thick and Perfusable Cardiac Patches and Hearts.* Advanced Science, 2019. **6**(11): p. 1900344.https://doi.org/10.1002/advs.201900344.

177. Cui, X. and T. Boland, *Human microvasculature fabrication using thermal inkjet printing technology.* Biomaterials, 2009. **30**(31): p. 6221-7.10.1016/j.biomaterials.2009.07.056.

178. Kucukgul, C., et al., *3D bioprinting of biomimetic aortic vascular constructs with self-supporting cells.* Biotechnology and Bioengineering, 2015. **112**(4): p. 811-821.https://doi.org/10.1002/bit.25493.

179. Gaetani, R., et al., *Cardiac tissue engineering using tissue printing technology and human cardiac progenitor cells.* Biomaterials, 2012. **33**(6): p. 1782-1790.https://doi.org/10.1016/j.biomaterials.2011.11.003.

180. Ketabat, F., et al., *Optimization of 3D printing and in vitro characterization of alginate/gelatin lattice and angular scaffolds for potential cardiac tissue engineering.* Frontiers in Bioengineering and Biotechnology, 2023. **11**.10.3389/fbioe.2023.1161804.

181. Roche, C.D., et al., *3D bioprinted alginate-gelatin hydrogel patches containing cardiac spheroids recover heart function in a mouse model of myocardial infarction.* Bioprinting, 2023. **30**: p. e00263.https://doi.org/10.1016/j.bprint.2023.e00263.

182. Zhang, Y.S., et al., *Bioprinting 3D microfibrous scaffolds for engineering endothelialized myocardium and heart-on-a-chip.* Biomaterials, 2016. **110**: p. 45-59.https://doi.org/10.1016/j.biomaterials.2016.09.003.

183. Das, S., et al., *Decellularized extracellular matrix bioinks and the external stimuli to enhance cardiac tissue development in vitro.* Acta Biomaterialia, 2019. **95**: p. 188-200.https://doi.org/10.1016/j.actbio.2019.04.026.

184. Atari, M., S. Labbaf, and S.H. Javanmard, *Fabrication and characterization of a 3D scaffold based on elastomeric poly-glycerol Sebacate polymer for heart valve applications.* Journal of Manufacturing Processes, 2023. **102**: p. 350-364.https://doi.org/10.1016/j.jmapro.2023.07.011.

185. Yang, Y., et al., *Elastic 3D-Printed Hybrid Polymeric Scaffold Improves Cardiac Remodeling after Myocardial Infarction.* Advanced Healthcare Materials, 2019. **8**(10): p. 1900065.https://doi.org/10.1002/adhm.201900065.

186. Liu, Y., et al., *hESCs-Derived Early Vascular Cell Spheroids for Cardiac Tissue Vascular Engineering and Myocardial Infarction Treatment.* Adv Sci (Weinh), 2022. **9**(9): p. e2104299.10.1002/advs.202104299.

187. Miller, K.L., et al., *Rapid 3D BioPrinting of a human iPSC-derived cardiac micro-tissue for high-throughput drug testing.* Organs-on-a-Chip, 2021. **3**: p. 100007.https://doi.org/10.1016/j.ooc.2021.100007.

188. Wang, Z., et al., *3D bioprinted functional and contractile cardiac tissue constructs.* Acta Biomaterialia, 2018. **70**: p. 48-56.https://doi.org/10.1016/j.actbio.2018.02.007.

189. Cieza, A., et al., *Global estimates of the need for rehabilitation based on the Global Burden of Disease study 2019: a systematic analysis for the Global Burden of Disease Study 2019.* The Lancet, 2020. **396**(10267): p. 2006-2017

190. Bauso, L.V., et al., *Bone Tissue Engineering and Nanotechnology: A Promising Combination for Bone Regeneration.* Biology, 2024. **13**(4): p. 237

191. Smrke, D., et al., *Treatment of bone defects—allogenic platelet gel and autologous bone technique*, in *Regenerative medicine and tissue engineering*. 2013, IntechOpen: London, UK.

192. Schlickewei, C.W., et al., *Current and future concepts for the treatment of impaired fracture healing.* International journal of molecular sciences, 2019. **20**(22): p. 5805

193. Zhang, Y., et al., *3D printing of chemical-empowered tendon stem/progenitor cells for functional tissue repair.* Biomaterials, 2021. **271**: p. 120722

194. Aytac, Z., et al., *Innovations in craniofacial bone and periodontal tissue engineering–from electrospinning to converged biofabrication.* International materials reviews, 2022. **67**(4): p. 347-384

195. Sousa, A.C., et al., *Assessment of 3D-Printed Polycaprolactone, Hydroxyapatite Nanoparticles and Diacrylate Poly(ethylene glycol) Scaffolds for Bone Regeneration.* Pharmaceutics, 2022. **14**(12).10.3390/pharmaceutics14122643.

196. Dubey, N., et al., *Highly tunable bioactive fiber-reinforced hydrogel for guided bone regeneration.* Acta biomaterialia, 2020. **113**: p. 164-176

197. Lei, P., et al., *Porous tantalum structure integrated on Ti6Al4V base by Laser Powder Bed Fusion for enhanced bony-ingrowth implants: In vitro and in vivo validation.* Bioactive Materials, 2022. **7**: p. 3-13.https://doi.org/10.1016/j.bioactmat.2021.05.025.

198. Yu, L., et al., *3D Culture of Bone Marrow-Derived Mesenchymal Stem Cells (BMSCs) Could Improve Bone Regeneration in 3D-Printed Porous Ti6Al4V Scaffolds.* Stem Cells International, 2018. **2018**: p. 2074021.10.1155/2018/2074021.

199. Wu, Y.-F., et al., *3D-bioprinted alginate-based bioink scaffolds with β-tricalcium phosphate for bone regeneration applications.* Journal of Dental Sciences, 2024. **19**(2): p. 1116-1125.https://doi.org/10.1016/j.jds.2023.12.023.

200. Ressler, A., et al., *Vat photopolymerization of biomimetic bone scaffolds based on Mg, Sr, Zn-substituted hydroxyapatite: Effect of sintering temperature.* Ceramics International, 2024. **50**(15): p. 27403-27415.https://doi.org/10.1016/j.ceramint.2024.05.038.

201. Yu, X., et al., *Osteoimmunomodulatory bioinks for 3D bioprinting achieve complete regeneration of critical-sized bone defects.* Composites Part B: Engineering, 2024. **273**: p. 111256.https://doi.org/10.1016/j.compositesb.2024.111256.

202. Choe, G., et al., *Three-dimensional bioprinting of mesenchymal stem cells using an osteoinductive bioink containing alginate and BMP-2-loaded PLGA nanoparticles for bone tissue engineering.* Biomaterials Advances, 2022. **136**: p. 212789.https://doi.org/10.1016/j.bioadv.2022.212789.

203. Sousa, A.C., et al., *Innovative Ink-Based 3D Hydrogel Bioprinted Formulations for Tissue Engineering Applications.* Gels, 2024. **10**(12): p. 831

204. Verykokou, S., et al., *The Role of Cone Beam Computed Tomography in Periodontology: From 3D Models of Periodontal Defects to 3D-Printed Scaffolds.* Journal of Personalized Medicine, 2024. **14**(2): p. 207

205. Sousa, A.C., et al., *Hybrid scaffolds for bone tissue engineering: Integration of composites and bioactive hydrogels loaded with hDPSCs.* Biomaterials Advances, 2025. **166**: p. 214042.https://doi.org/10.1016/j.bioadv.2024.214042.

206. Wang, W., et al., *3D bioprinting of DPSCs with GelMA hydrogel of various concentrations for bone regeneration.* Tissue and Cell, 2024. **88**: p. 102418.https://doi.org/10.1016/j.tice.2024.102418.

207. Tao, J., et al., *DLP-based bioprinting of void-forming hydrogels for enhanced stem-cell-mediated bone regeneration.* Materials Today Bio, 2022. **17**: p. 100487.https://doi.org/10.1016/j.mtbio.2022.100487.

208. Gatto, M.L., et al., *Biomechanical performances of PCL/HA micro- and macro-porous lattice scaffolds fabricated via laser powder bed fusion for bone tissue engineering.* Materials Science and Engineering: C, 2021. **128**: p. 112300.https://doi.org/10.1016/j.msec.2021.112300.

209. Hong, D., et al., *Binder-jetting 3D printing and alloy development of new biodegradable Fe-Mn-Ca/Mg alloys.* Acta Biomaterialia, 2016. **45**: p. 375-386.https://doi.org/10.1016/j.actbio.2016.08.032.

210. Barro, Ó., et al. *Improved Commercially Pure Titanium Obtained by Laser Directed Energy Deposition for Dental Prosthetic Applications*. Metals, 2021. **11**, DOI: 10.3390/met11010070.10.3390/met11010070.

211. Arias-González, F., et al. *In-Situ Laser Directed Energy Deposition of Biomedical Ti-Nb and Ti-Zr-Nb Alloys from Elemental Powders*. Metals, 2021. **11**, DOI: 10.3390/met11081205.10.3390/met11081205.

212. Cedeño-Viveros, L.D., et al., *Influence of process parameters for sheet lamination based on laser micro-spot welding of austenitic stainless steel sheets for bone tissue applications.* The International Journal of Advanced Manufacturing Technology, 2021. **115**(1): p. 247-262.10.1007/s00170-021-07113-3.

213. Touya, N., et al., *In vitro and in vivo characterization of a novel tricalcium silicate-based ink for bone regeneration using laser-assisted bioprinting.* Biofabrication, 2022. **14**(2): p. 024104.10.1088/1758-5090/ac584b.

214. Li, W., et al., *Application of 3D Bioprinting in Liver Diseases.* Micromachines (Basel), 2023. **14**(8).10.3390/mi14081648.

215. Kasturi, M., et al., *Three Dimensional Bioprinting for Hepatic Tissue Engineering: From In Vitro Models to Clinical Applications.* Tissue Eng Regen Med, 2024. **21**(1): p. 21-52.10.1007/s13770-023-00576-3.

216. Palakkan, A.A., et al., *Liver tissue engineering and cell sources: issues and challenges.* Liver Int, 2013. **33**(5): p. 666-76.10.1111/liv.12134.

217. Asrani, S.K., et al., *Burden of liver diseases in the world.* Journal of hepatology, 2019. **70**(1): p. 151-171

218. Singh, S., N.A. Osna, and K.K. Kharbanda, *Treatment options for alcoholic and non-alcoholic fatty liver disease: A review.* World journal of gastroenterology, 2017. **23**(36): p. 6549

219. Robbins, J.B., et al., *A novel in vitro three-dimensional bioprinted liver tissue system for drug development.* The FASEB Journal, 2013. **27**(S1): p. 872.12-872.12.https://doi.org/10.1096/fasebj.27.1_supplement.872.12.

220. Chang, R., et al., *Biofabrication of a three-dimensional liver micro-organ as an in vitro drug metabolism model.* Biofabrication, 2010. **2**(4): p. 045004

221. Lee, S.Y., H.J. Kim, and D. Choi, *Cell sources, liver support systems and liver tissue engineering: alternatives to liver transplantation.* International journal of stem cells, 2015. **8**(1): p. 36-47

222. Iqbal, S., et al., *Biomaterials evolution: from inert to instructive.* Biomaterials Science, 2023. **11**(18): p. 6109-6115

223. Allu, I., et al., *Decellularization techniques for tissue engineering: towards replicating native extracellular matrix architecture in liver regeneration.* Journal of Functional Biomaterials, 2023. **14**(10): p. 518

224. Khati, V., et al., *Indirect 3D bioprinting of a robust trilobular hepatic construct with decellularized liver matrix hydrogel.* Bioengineering, 2022. **9**(11): p. 603

225. Wang, Q., et al., *Innovations in 3D bioprinting and biomaterials for liver tissue engineering: Paving the way for tissue-engineered liver.* iLIVER, 2024. **3**(1): p. 100080.https://doi.org/10.1016/j.iliver.2024.100080.

226. Yang, H., et al., *Three-dimensional bioprinted hepatorganoids prolong survival of mice with liver failure.* Gut, 2021. **70**(3): p. 567.10.1136/gutjnl-2019-319960.

227. Xie, F., et al., *Three-dimensional bio-printing of primary human hepatocellular carcinoma for personalized medicine.* Biomaterials, 2021. **265**: p. 120416.https://doi.org/10.1016/j.biomaterials.2020.120416.

228. Lewis, P.L., R.M. Green, and R.N. Shah, *3D-printed gelatin scaffolds of differing pore geometry modulate hepatocyte function and gene expression.* Acta Biomaterialia, 2018. **69**: p. 63-70.https://doi.org/10.1016/j.actbio.2017.12.042.

229. Jeon, H., et al., *Generation of Multilayered 3D Structures of HepG2 Cells Using a Bio-printing Technique.* Gut Liver, 2017. **11**(1): p. 121-128.10.5009/gnl16010.

230. Wu, Y., et al., *3D bioprinting of bicellular liver lobule-mimetic structures via microextrusion of cellulose nanocrystal-incorporated shear-thinning bioink.* Sci Rep, 2020. **10**(1): p. 20648.10.1038/s41598-020-77146-3.

231. Mao, Q., et al., *Fabrication of liver microtissue with liver decellularized extracellular matrix (dECM) bioink by digital light processing (DLP) bioprinting.* Mater Sci Eng C Mater Biol Appl, 2020. **109**: p. 110625.10.1016/j.msec.2020.110625.

232. Kim, M.K., et al., *3D bioprinting of dECM-incorporated hepatocyte spheroid for simultaneous promotion of cell-cell and -ECM interactions.* Frontiers in Bioengineering and Biotechnology, 2023. **11**.10.3389/fbioe.2023.1305023.

233. Faulkner-Jones, A., et al., *Bioprinting of human pluripotent stem cells and their directed differentiation into hepatocyte-like cells for the generation of mini-livers in 3D.* Biofabrication, 2015. **7**(4): p. 044102.10.1088/1758-5090/7/4/044102.

234. Lee, H., et al., *Development of Liver Decellularized Extracellular Matrix Bioink for Three-Dimensional Cell Printing-Based Liver Tissue Engineering.* Biomacromolecules, 2017. **18**(4): p. 1229-1237.10.1021/acs.biomac.6b01908.

235. Lee, J.W., et al., *Development of a 3D cell printed construct considering angiogenesis for liver tissue engineering.* Biofabrication, 2016. **8**(1): p. 015007.10.1088/1758-5090/8/1/015007.

236. Hiller, T., et al., *Generation of a 3D Liver Model Comprising Human Extracellular Matrix in an Alginate/Gelatin-Based Bioink by Extrusion Bioprinting for Infection and Transduction Studies.* International Journal of Molecular Sciences, 2018. **19**(10): p. 3129

237. Kang, D., et al., *Bioprinting of Multiscaled Hepatic Lobules within a Highly Vascularized Construct.* Small, 2020. **16**(13): p. 1905505.https://doi.org/10.1002/smll.201905505.

238. Mazzocchi, A., et al., *Optimization of collagen type I-hyaluronan hybrid bioink for 3D bioprinted liver microenvironments.* Biofabrication, 2018. **11**(1): p. 015003.10.1088/1758-5090/aae543.

239. Wu, Y., et al., *3D bioprinting of liver-mimetic construct with alginate/cellulose nanocrystal hybrid bioink.* Bioprinting, 2018. **9**: p. 1-6.https://doi.org/10.1016/j.bprint.2017.12.001.

240. Calonje, J.E., et al., *McKee's Pathology of the Skin, 2 Volume Set E-Book*. 2018: Elsevier Health Sciences: Amsterdam, The Netherlands.

241. Liu, Y., et al., *3D bioprinting bioglass to construct vascularized full-thickness skin substitutes for wound healing.* Materials Today Bio, 2024. **24**: p. 100899.https://doi.org/10.1016/j.mtbio.2023.100899.

242. Zöller, N., et al., *Clinical application of a tissue-cultured skin autograft: an alternative for the treatment of non-healing or slowly healing wounds?* Dermatology, 2014. **229**(3): p. 190-198

243. Murphy, S.V. and A. Atala, *3D bioprinting of tissues and organs.* Nature biotechnology, 2014. **32**(8): p. 773-785

244. Tabriz, A.G. and D. Douroumis, *Recent advances in 3D printing for wound healing: A systematic review.* Journal of Drug Delivery Science and Technology, 2022. **74**: p. 103564.https://doi.org/10.1016/j.jddst.2022.103564.

245. Hong, N., et al., *3D bioprinting and its in vivo applications.* Journal of Biomedical Materials Research Part B: Applied Biomaterials, 2018. **106**(1): p. 444-459

246. Vijayavenkataraman, S., W. Lu, and J. Fuh, *3D bioprinting of skin: a state-of-the-art review on modelling, materials, and processes.* Biofabrication, 2016. **8**(3): p. 032001

247. Admane, P., et al., *Direct 3D bioprinted full-thickness skin constructs recapitulate regulatory signaling pathways and physiology of human skin.* Bioprinting, 2019. **15**: p. e00051.https://doi.org/10.1016/j.bprint.2019.e00051.

248. Jin, R., et al., *Three-dimensional bioprinting of a full-thickness functional skin model using acellular dermal matrix and gelatin methacrylamide*

bioink. Acta Biomaterialia, 2021. **131**: p. 248-261.https://doi.org/10.1016/j.actbio.2021.07.012.

249. Song, Y., et al., *Electrospinning/3D printing drug-loaded antibacterial polycaprolactone nanofiber/sodium alginate-gelatin hydrogel bilayer scaffold for skin wound repair.* International Journal of Biological Macromolecules, 2024: p. 129705.https://doi.org/10.1016/j.ijbiomac.2024.129705.

250. Ma, J., et al., *3D Printing of Strontium Silicate Microcylinder-Containing Multicellular Biomaterial Inks for Vascularized Skin Regeneration.* Advanced Healthcare Materials, 2021. **10**(16): p. 2100523.https://doi.org/10.1002/adhm.202100523.

251. Pajooh, A.M.D., et al., *Biomimetic VEGF-loaded bilayer scaffold fabricated by 3D printing and electrospinning techniques for skin regeneration.* Materials & Design, 2024. **238**: p. 112714.https://doi.org/10.1016/j.matdes.2024.112714.

252. Zhou, F., et al., *Rapid printing of bio-inspired 3D tissue constructs for skin regeneration.* Biomaterials, 2020. **258**: p. 120287.https://doi.org/10.1016/j.biomaterials.2020.120287.

253. Kwak, H., et al., *Formation of a keratin layer with silk fibroin-polyethylene glycol composite hydrogel fabricated by digital light processing 3D printing.* Journal of Industrial and Engineering Chemistry, 2019. **72**: p. 232-240.https://doi.org/10.1016/j.jiec.2018.12.023.

254. Zhao, M., et al., *Functionalizing multi-component bioink with platelet-rich plasma for customized in-situ bilayer bioprinting for wound healing.* Materials Today Bio, 2022. **16**: p. 100334.https://doi.org/10.1016/j.mtbio.2022.100334.

255. Wu, S.-D., et al., *Planar-/Curvilinear-Bioprinted Tri-Cell-Laden Hydrogel for Healing Irregular Chronic Wounds.* Advanced Healthcare Materials, 2022. **11**(16): p. 2201021.https://doi.org/10.1002/adhm.202201021.

256. Datta, S., et al., *Alginate-honey bioinks with improved cell responses for applications as bioprinted tissue engineered constructs.* Journal of Materials Research, 2018. **33**(14): p. 2029-2039.10.1557/jmr.2018.202.

257. Pereira, R.F., et al., *A single-component hydrogel bioink for bioprinting of bioengineered 3D constructs for dermal tissue engineering.* Materials Horizons, 2018. **5**(6): p. 1100-1111.10.1039/C8MH00525G.

258. Baltazar, T., et al., *Three Dimensional Bioprinting of a Vascularized and Perfusable Skin Graft Using Human Keratinocytes, Fibroblasts, Pericytes, and Endothelial Cells.* Tissue Eng Part A, 2020. **26**(5-6): p. 227-238.10.1089/ten.TEA.2019.0201.

259. Shi, L., et al., *Three-dimensional printing alginate/gelatin scaffolds as dermal substitutes for skin tissue engineering.* Polymer Engineering & Science, 2018. **58**(10): p. 1782-1790.https://doi.org/10.1002/pen.24779.

260. Fligge, M., et al., *Personalized dermal patches – Inkjet printing of prednisolone nanosuspensions for individualized treatment of skin diseases.* International Journal of Pharmaceutics, 2023. **630**: p. 122382.https://doi.org/10.1016/j.ijpharm.2022.122382.

261. Cadena, M., et al., *3D Bioprinting of Neural Tissues.* Adv Healthc Mater, 2021. **10**(15): p. e2001600.10.1002/adhm.202001600.

262. Joung, D., et al., *3D Printed Neural Regeneration Devices.* Adv Funct Mater, 2020. **30**(1).10.1002/adfm.201906237.

263. Yi, S., et al., *Application of stem cells in peripheral nerve regeneration.* Burns & trauma, 2020. **8**: p. tkaa002

264. Han, Y. and J. Yin, *Industry news: the additive manufacturing of nerve conduits for the treatment of peripheral nerve injury*. 2022, Springer: Berlin/Heidelberg, Germany. p. 1-3.

265. Zhu, H., et al., *3D printing of functional bioengineered constructs for neural regeneration: a review.* International Journal of Extreme Manufacturing, 2023. **5**(4): p. 042004.10.1088/2631-7990/ace56c.

266. Hsieh, F.-Y. and S.-h. Hsu, *3D bioprinting: A new insight into the therapeutic strategy of neural tissue regeneration.* Organogenesis, 2015. **11**(4): p. 153-158.10.1080/15476278.2015.1123360.

267. Lee, H.-W., et al., *Dual crosslinking silk fibroin/pectin-based bioink development and the application on neural stem/progenitor cells spheroid laden 3D bioprinting.* International Journal of Biological Macromolecules, 2024. **269**: p. 131720.https://doi.org/10.1016/j.ijbiomac.2024.131720.

268. Song, S., et al., *Three-dimensional printing of microfiber- reinforced hydrogel loaded with oxymatrine for treating spinal cord injury.* Int J Bioprint, 2023. **9**(3): p. 692.10.18063/ijb.692.

269. Li, J., et al., *The development of the multi-physical model for cell-laden nerve scaffolds and its bioprinting by stereolithography.* Materials Today: Proceedings, 2022. **70**: p. 388-394.https://doi.org/10.1016/j.matpr.2022.09.274.

270. Hsieh, F.-Y., H.-H. Lin, and S.-h. Hsu, *3D bioprinting of neural stem cell-laden thermoresponsive biodegradable polyurethane hydrogel and potential in central nervous system repair.* Biomaterials, 2015. **71**: p. 48-57.https://doi.org/10.1016/j.biomaterials.2015.08.028.

271. Yan, Y., et al., *3D bioprinting of human neural tissues with functional connectivity.* Cell Stem Cell, 2024. **31**(2): p. 260-274.e7.https://doi.org/10.1016/j.stem.2023.12.009.

272. Tortorella, S., et al., *Laser Assisted Bioprinting of laminin on biodegradable PLGA substrates: Effect on neural stem cell adhesion and differentiation.* Bioprinting, 2022. **26**: p. e00194.https://doi.org/10.1016/j.bprint.2022.e00194.

273. Ho, L. and S.-h. Hsu, *Cell reprogramming by 3D bioprinting of human fibroblasts in polyurethane hydrogel for fabrication of neural-like constructs.* Acta Biomaterialia, 2018. **70**: p. 57-70.https://doi.org/10.1016/j.actbio.2018.01.044.

274. Lee, Y.-B., et al., *Bio-printing of collagen and VEGF-releasing fibrin gel scaffolds for neural stem cell culture.* Experimental Neurology, 2010. **223**(2): p. 645-652.https://doi.org/10.1016/j.expneurol.2010.02.014.

275. Chen, C., et al., *3D printing of interferon γ-preconditioned NSC-derived exosomes/collagen/chitosan biological scaffolds for neurological recovery after TBI.* Bioactive Materials, 2024. **39**: p. 375-391.https://doi.org/10.1016/j.bioactmat.2024.05.026.

276. Han, Y., et al., *A 3D printable gelatin methacryloyl/chitosan hydrogel assembled with conductive PEDOT for neural tissue engineering.* Composites Part B: Engineering, 2024. **273**: p. 111241.https://doi.org/10.1016/j.compositesb.2024.111241.

277. Song, S., et al., *Neural stem cell-laden 3D bioprinting of polyphenol-doped electroconductive hydrogel scaffolds for enhanced neuronal differentiation.* Biomaterials Advances, 2022. **133**: p. 112639.https://doi.org/10.1016/j.msec.2021.112639.

278. Liu, J., et al., *Additive-lathe 3D bioprinting of bilayered nerve conduits incorporated with supportive cells.* Bioactive Materials, 2021. **6**(1): p. 219-229.https://doi.org/10.1016/j.bioactmat.2020.08.010.

279. Vijayavenkataraman, S., et al., *3D-Printed PCL/rGO Conductive Scaffolds for Peripheral Nerve Injury Repair.* Artificial Organs, 2019. **43**(5): p. 515-523.https://doi.org/10.1111/aor.13360.

280. Heinrich, M.A., et al., *3D bioprinting: from benches to translational applications.* Small, 2019. **15**(23): p. 1805510

281. Stanco, D., et al., *3D bioprinting for orthopaedic applications: Current advances, challenges and regulatory considerations.* Bioprinting, 2020. **20**: p. e00103

282. Agarwal, K., et al., *Insights of 3D bioprinting and focusing the paradigm shift towards 4D printing for biomedical applications.* Journal of Materials Research, 2023. **38**(1): p. 112-141.10.1557/s43578-022-00524-2.

283. Jafarkhani, M., et al., *Bioprinting in Vascularization Strategies.* Iran Biomed J, 2019. **23**(1): p. 9-20.10.29252/.23.1.9.

284. Jain, R.K., et al., *Engineering vascularized tissue.* Nat Biotechnol, 2005. **23**(7): p. 821-3.10.1038/nbt0705-821.

285. Zheng, K., et al., *Recent progress of 3D printed vascularized tissues and organs.* Smart Materials in Medicine, 2024. **5**(2): p. 183-195.https://doi.org/10.1016/j.smaim.2024.01.001.

286. Ma, Y., et al., *Advancements of 3D bioprinting in regenerative medicine: Exploring cell sources for organ fabrication.* Heliyon, 2024. **10**(3): p. e24593.https://doi.org/10.1016/j.heliyon.2024.e24593.

287. Inglis, S., et al., *Human endothelial and foetal femur-derived stem cell co-cultures modulate osteogenesis and angiogenesis.* Stem cell research & therapy, 2016. **7**: p. 1-16

288. Lovett, M., et al., *Vascularization strategies for tissue engineering.* Tissue Eng Part B Rev, 2009. **15**(3): p. 353-70.10.1089/ten.TEB.2009.0085.

289. Bishop, E.S., et al., *3-D bioprinting technologies in tissue engineering and regenerative medicine: Current and future trends.* Genes & Diseases, 2017. **4**(4): p. 185-195.https://doi.org/10.1016/j.gendis.2017.10.002.

290. Persaud, A., et al., *3D Bioprinting with Live Cells.* Engineered Regeneration, 2022. **3**(3): p. 292-309.https://doi.org/10.1016/j.engreg.2022.07.002.

291. Martin, I., P.J. Simmons, and D.F. Williams, *Manufacturing challenges in regenerative medicine.* Science translational medicine, 2014. **6**(232): p. 232fs16-232fs16

292. Jin, Z., et al., *3D Printing of Physical Organ Models: Recent Developments and Challenges.* Advanced Science, 2021. **8**(17): p. 2101394.https://doi.org/10.1002/advs.202101394.

293. Hinton, T.J., et al., *Three-dimensional printing of complex biological structures by freeform reversible embedding of suspended hydrogels.* Science advances, 2015. **1**(9): p. e1500758

294. Kang, H.-W., et al., *A 3D bioprinting system to produce human-scale tissue constructs with structural integrity.* Nature biotechnology, 2016. **34**(3): p. 312-319

295. Murphy, S.V., P. De Coppi, and A. Atala, *Opportunities and challenges of translational 3D bioprinting.* Nature Biomedical Engineering, 2020. **4**(4): p. 370-380.10.1038/s41551-019-0471-7.

296. Zhang, Y.S., et al., *Three-Dimensional Bioprinting Strategies for Tissue Engineering.* Cold Spring Harb Perspect Med, 2018. **8**(2).10.1101/cshperspect.a025718.

297. Jones, N., *Science in three dimensions: The print revolution.* Nature, 2012. **487**(7405): p. 22-23.10.1038/487022a.

298. Gilbert, F., et al., *Print Me an Organ? Ethical and Regulatory Issues Emerging from 3D Bioprinting in Medicine.* Sci Eng Ethics, 2018. **24**(1): p. 73-91.10.1007/s11948-017-9874-6.

299. Rizzo, M., et al., *3D printing and 3D bioprinting technology in medicine: ethical and legal issues.* La Clinica Terapeutica, 2023. **174**(1): p. 80-84.10.7417/CT.2023.2501.

300. Sekar, M.P., et al., *Current standards and ethical landscape of engineered tissues—3D bioprinting perspective.* Journal of Tissue Engineering, 2021. **12**: p. 20417314211027677.10.1177/20417314211027677.

301. Goddard, E. and S. Dodds, *Ethics and Policy for Bioprinting.* Methods Mol Biol, 2020. **2140**: p. 43-64.10.1007/978-1-0716-0520-2_4.

302. Lategan, L.O. and A.F. van der Merwe, *Ethical guidelines for using bioprinting for humans.* MATEC Web of Conferences, 2023. **388**: p. 10005.10.1051/matecconf/202338810005.

303. Liang, K., *Tissue Bioprinting: Promise and Challenges.* Bioengineering (Basel), 2023. **10**(12).10.3390/bioengineering10121400.

304. Ramadan, Q. and M. Zourob, *3D Bioprinting at the Frontier of Regenerative Medicine, Pharmaceutical, and Food Industries.* Frontiers in Medical Technology, 2021. **2**.10.3389/fmedt.2020.607648.

305. Muskan, D. Gupta, and N.P. Negi, *3D bioprinting: Printing the future and recent advances.* Bioprinting, 2022. **27**: p. e00211.https://doi.org/10.1016/j.bprint.2022.e00211.

306. Cui, H., et al., *3D bioprinting for organ regeneration.* Advanced healthcare materials, 2017. **6**(1): p. 1601118

307. Ghosh, R., et al., *Micro/nanofiber-based noninvasive devices for health monitoring diagnosis and rehabilitation.* Applied Physics Reviews, 2020. **7**(4)

308. Yilmaz, B., et al., *Bioprinting: A review of processes, materials and applications.* Bioprinting, 2021. **23**: p. e00148.https://doi.org/10.1016/j.bprint.2021.e00148.

309. Koons, G.L. and A.G. Mikos, *Progress in three-dimensional printing with growth factors.* J Control Release, 2019. **295**: p. 50-59.10.1016/j.jconrel.2018.12.035.

310. Zhang, Y.S., et al., *3D extrusion bioprinting.* Nature Reviews Methods Primers, 2021. **1**(1): p. 75.10.1038/s43586-021-00073-8.

311. Abbadessa, A., A. Ronca, and A. Salerno, *Integrating bioprinting, cell therapies and drug delivery towards in vivo regeneration of cartilage, bone and osteochondral tissue.* Drug Deliv Transl Res, 2024. **14**(4): p. 858-894.10.1007/s13346-023-01437-1.

312. Reddy, V.S., et al., *A review on electrospun nanofibers based advanced applications: From health care to energy devices.* Polymers, 2021. **13**(21): p. 3746

313. Bejoy, A.M., et al., *An insight on advances and applications of 3d bioprinting: A review.* Bioprinting, 2021. **24**: p. e00176

314. Ozbolat, I.T., W. Peng, and V. Ozbolat, *Application areas of 3D bioprinting.* Drug discovery today, 2016. **21**(8): p. 1257-1271

315. De Santis, M.M., et al., *Extracellular-matrix-reinforced bioinks for 3D bioprinting human tissue.* Advanced materials, 2021. **33**(3): p. 2005476

316. Reddy, V.S., et al., *Contemporary standpoint and future of 3D bioprinting in tissue/organs printing.* Current Opinion in Biomedical Engineering, 2023. **27**: p. 100461.https://doi.org/10.1016/j.cobme.2023.100461.

317. Veiga, A., et al., *Current Trends on Protein Driven Bioinks for 3D Printing.* Pharmaceutics, 2021. **13**(9): p. 1444

318. Hassan, M., et al., *A review of AI for optimization of 3D printing of sustainable polymers and composites.* Composites Part C: Open Access, 2024. **15**: p. 100513.https://doi.org/10.1016/j.jcomc.2024.100513.

319. Nosrati, H. and M. Nosrati, *Artificial Intelligence in Regenerative Medicine: Applications and Implications.* Biomimetics (Basel), 2023. **8**(5).10.3390/biomimetics8050442.

320. Ramesh, S., et al., *Advancing 3D bioprinting through machine learning and artificial intelligence.* Bioprinting, 2024. **38**: p. e00331.https://doi.org/10.1016/j.bprint.2024.e00331.

321. Liang, Z., et al., *Pioneering the future of dentistry: AI-Driven 3D bioprinting for next-generation clinical applications.* Translational Dental Research, 2024: p. 100005.https://doi.org/10.1016/j.tdr.2024.100005.

322. Ma, L., et al., *Application of artificial intelligence in 3D printing physical organ models.* Materials Today Bio, 2023. **23**: p. 100792.https://doi.org/10.1016/j.mtbio.2023.100792.

323. Gao, B., et al., *4D Bioprinting for Biomedical Applications.* Trends in Biotechnology, 2016. **34**(9): p. 746-756.https://doi.org/10.1016/j.tibtech.2016.03.004.

324. An, J., C.K. Chua, and V. Mironov, *A perspective on 4D bioprinting.* IJB. **2**(1).10.18063/ijb.2016.01.003.

Disclaimer/Publisher's Note: The statements, opinions and data contained in all publications are solely those of the individual author(s) and contributor(s) and not of MDPI and/or the editor(s). MDPI and/or the editor(s) disclaim responsibility for any injury to people or property resulting from any ideas, methods, instructions or products referred to in the content.

[This page is intentionally left blank.]

References

1. Leberfinger, A.N.; Moncal, K.K.; Ravnic, D.J.; Ozbolat, I.T. 3D Printing for Cell Therapy Applications. In *Cell Therapy: Current Status and Future Directions*, Emerich, D.F., Orive, G., Eds.; Springer International Publishing: Cham, 2017; pp. 227-248.

2. Mao, A.S.; Mooney, D.J. Regenerative medicine: Current therapies and future directions. *Proc Natl Acad Sci U S A* **2015**, *112*, 14452-14459, doi:10.1073/pnas.1508520112.

3. Pina, S.; Oliveira, J.M.; Reis, R.L. Natural-based nanocomposites for bone tissue engineering and regenerative medicine: A review. *Advanced Materials* **2015**, *27*, 1143-1169.

4. Cossu, G.; Birchall, M.; Brown, T.; De Coppi, P.; Culme-Seymour, E.; Gibbon, S.; Hitchcock, J.; Mason, C.; Montgomery, J.; Morris, S. Lancet Commission: Stem cells and regenerative medicine. *The Lancet* **2018**, *391*, 883-910.

5. Catoira, M.C.; Fusaro, L.; Di Francesco, D.; Ramella, M.; Boccafoschi, F. Overview of natural hydrogels for regenerative medicine applications. *Journal of Materials Science: Materials in Medicine* **2019**, *30*, doi:10.1007/s10856-019-6318-7.

6. Spiller, K.L.; Koh, T.J. Macrophage-based therapeutic strategies in regenerative medicine. *Advanced Drug Delivery Reviews* **2017**, *122*, 74-83, doi:10.1016/j.addr.2017.05.010.

7. Zhang, J.; Zhao, X.; Liang, L.; Li, J.; Demirci, U.; Wang, S. A decade of progress in liver regenerative medicine. *Biomaterials* **2018**, *157*, 161-176.

8. Caddeo, S.; Boffito, M.; Sartori, S. Tissue Engineering Approaches in the Design of Healthy and Pathological In Vitro Tissue Models. *Frontiers in Bioengineering and Biotechnology* **2017**, *5*, doi:10.3389/fbioe.2017.00040.

9. Han, F.; Wang, J.; Ding, L.; Hu, Y.; Li, W.; Yuan, Z.; Guo, Q.; Zhu, C.; Yu, L.; Wang, H.; et al. Tissue Engineering and Regenerative Medicine: Achievements, Future, and Sustainability in Asia. *Front Bioeng Biotechnol* **2020**, *8*, 83, doi:10.3389/fbioe.2020.00083.

10. Abdulghani, S.; Mitchell, G.R. Biomaterials for In Situ Tissue Regeneration: A Review. *Biomolecules* **2019**, *9*, doi:10.3390/biom9110750.

11. Derby, B. Printing and prototyping of tissues and scaffolds. *science* **2012**, *338*, 921-926.

12. Dong, R.; Ma, P.X.; Guo, B. Conductive biomaterials for muscle tissue engineering. *Biomaterials* **2020**, *229*, doi:10.1016/j.biomaterials.2019.119584.

13. Puetzer, J.L.; Ma, T.; Sallent, I.; Gelmi, A.; Stevens, M.M. Driving Hierarchical Collagen Fiber Formation for Functional Tendon, Ligament, and Meniscus Replacement. *Biomaterials* **2021**, *269*, doi:10.1016/j.biomaterials.2020.120527.

14. Wu, L.; Gu, Y.; Liu, L.; Tang, J.; Mao, J.; Xi, K.; Jiang, Z.; Zhou, Y.; Xu, Y.; Deng, L.; et al. Hierarchical micro/nanofibrous membranes of sustained releasing VEGF for periosteal regeneration. *Biomaterials* **2020**, *227*, doi:10.1016/j.biomaterials.2019.119555.

15. Saldin, L.T.; Cramer, M.C.; Velankar, S.S.; White, L.J.; Badylak, S.F. Extracellular matrix hydrogels from decellularized tissues: Structure and function. *Acta Biomaterialia* **2017**, *49*, 1-15, doi:10.1016/j.actbio.2016.11.068.

16. Zaokari, Y.; Persaud, A.; Ibrahim, A. Biomaterials for Adhesion in Orthopedic Applications: A Review. *Engineered Regeneration* **2020**, *1*, 51-63, doi:10.1016/j.engreg.2020.07.002.

17. Fiakos, G.; Kuang, Z.; Lo, E. Improved skin regeneration with acellular fish skin grafts. *Engineered Regeneration* **2020**, *1*, 95-101, doi:10.1016/j.engreg.2020.09.002.

18. Liu, X.; Liu, Y.; Du, J.; Li, X.; Yu, J.; Ding, B. Breathable, stretchable and adhesive nanofibrous hydrogels as wound dressing materials. *Engineered Regeneration* **2021**, *2*, 63-69.

19. Chaudhuri, O.; Cooper-White, J.; Janmey, P.A.; Mooney, D.J.; Shenoy, V.B. Effects of extracellular matrix viscoelasticity on cellular behaviour. *Nature* **2020**, *584*, 535-546, doi:10.1038/s41586-020-2612-2.

20. Annabi, N.; Tamayol, A.; Uquillas, J.A.; Akbari, M.; Bertassoni, L.E.; Cha, C.; Camci-Unal, G.; Dokmeci, M.R.; Peppas, N.A.; Khademhosseini, A. 25th anniversary article: Rational design and applications of hydrogels in regenerative medicine. *Advanced Materials* **2014**, *26*, 85-124, doi:10.1002/adma.201303233.

21. Yao, X.; Peng, R.; Ding, J. Cell-material interactions revealed via material techniques of surface patterning. *Advanced Materials* **2013**, *25*, 5257-5286, doi:10.1002/adma.201301762.

22. Zhang, Y.S.; Khademhosseini, A. Advances in engineering hydrogels. *Science* **2017**, *356*, doi:10.1126/science.aaf3627.

23. Sheng, L.; Zhang, Z.; Zhang, Y.; Wang, E.; Ma, B.; Xu, Q.; Ma, L.; Zhang, M.; Pei, G.; Chang, J. A novel “hot spring”-mimetic hydrogel with excellent angiogenic properties for chronic wound healing. *Biomaterials* **2021**, *264*, doi:10.1016/j.biomaterials.2020.120414.

24. Brown, T.E.; Anseth, K.S. Spatiotemporal hydrogel biomaterials for regenerative medicine. *Chemical Society Reviews* **2017**, *46*, 6532-6552, doi:10.1039/c7cs00445a.

25. Liu, Z.; Meyers, M.A.; Zhang, Z.; Ritchie, R.O. Functional gradients and heterogeneities in biological materials: Design principles, functions, and bioinspired applications. *Progress in Materials Science* **2017**, *88*, 467-498, doi:10.1016/j.pmatsci.2017.04.013.

26. Yao, Q.; Cosme, J.G.L.; Xu, T.; Miszuk, J.M.; Picciani, P.H.S.; Fong, H.; Sun, H. Three dimensional electrospun PCL/PLA blend nanofibrous scaffolds with significantly improved stem cells osteogenic differentiation and cranial bone formation. *Biomaterials* **2017**, *115*, 115-127, doi:10.1016/j.biomaterials.2016.11.018.

27. Fu, F.; Shang, L.; Chen, Z.; Yu, Y.; Zhao, Y. Bioinspired living structural color hydrogels. *Science Robotics* **2018**, *3*, doi:10.1126/SCIROBOTICS.AAR8580.

28. Wang, F.; Zhang, X.; Chen, G.; Zhao, Y. Living bacterial microneedles for fungal infection treatment. *Research* **2020**, *2020*, doi:10.34133/2020/2760594.

29. Madl, C.M.; Heilshorn, S.C.; Blau, H.M. Bioengineering strategies to accelerate stem cell therapeutics. *Nature* **2018**, *557*, 335-342, doi:10.1038/s41586-018-0089-z.

30. Matai, I.; Kaur, G.; Seyedsalehi, A.; McClinton, A.; Laurencin, C.T. Progress in 3D bioprinting technology for tissue/organ regenerative engineering. *Biomaterials* **2020**, *226*, doi:10.1016/j.biomaterials.2019.119536.

31. Dehaini, D.; Wei, X.; Fang, R.H.; Masson, S.; Angsantikul, P.; Luk, B.T.; Zhang, Y.; Ying, M.; Jiang, Y.; Kroll, A.V.; et al. Erythrocyte–Platelet Hybrid Membrane Coating for Enhanced Nanoparticle Functionalization. *Advanced Materials* **2017**, *29*, doi:10.1002/adma.201606209.

32. McCarty, N.S.; Graham, A.E.; Studená, L.; Ledesma-Amaro, R. Multiplexed CRISPR technologies for gene editing and transcriptional regulation. *Nature Communications* **2020**, *11*, doi:10.1038/s41467-020-15053-x.

33. Yu, Y.; Wang, Q.; Wang, C.; Shang, L. Living Materials for Regenerative Medicine. *Engineered Regeneration* **2021**, *2*, 96-104, doi:https://doi.org/10.1016/j.engreg.2021.08.003.

34. Saini, G.; Segaran, N.; Mayer, J.L.; Saini, A.; Albadawi, H.; Oklu, R. Applications of 3D Bioprinting in Tissue Engineering and Regenerative Medicine. *J Clin Med* **2021**, *10*, doi:10.3390/jcm10214966.

35. Ali, M.; P, R.A.; Lee, S.J.; Jackson, J.D. Three-dimensional bioprinting for organ bioengineering: promise and pitfalls. *Curr Opin Organ Transplant* **2018**, *23*, 649-656, doi:10.1097/mot.0000000000000581.

36. Salgado, A.J.; Oliveira, J.M.; Martins, A.; Teixeira, F.G.; Silva, N.A.; Neves, N.M.; Sousa, N.; Reis, R.L. Tissue engineering and regenerative medicine: past, present, and future. *Int Rev Neurobiol* **2013**, *108*, 1-33, doi:10.1016/b978-0-12-410499-0.00001-0.

37. Sánchez, A.; Schimmang, T.; García-Sancho, J. Cell and Tissue Therapy in Regenerative Medicine. In *Stem Cell Transplantation*, López-Larrea, C., López-Vázquez, A., Suárez-Álvarez, B., Eds.; Springer US: New York, NY, 2012; pp. 89-102.

[This page is intentionally left blank.]

CHAPTER II

CHARACTERIZATION OF MESENCHYMAL STEM/STROMAL CELLS

[This page is intentionally left blank.]

Introductory Note

As discussed in the previous chapter, mesenchymal stem/stromal cells (MSCs) are very promising as cell-based therapies for the treatment of various diseases. However, their clinical application is hindered by inherent cellular heterogeneity and by their vulnerability to cell death during injection [1]. To address these limitations, researchers have begun investigating the synergistic potential of MSC-biomaterial combination therapies. In these approaches, biomaterials act as protective scaffolds for MSCs, shielding them from environmental stressors while providing physiologically relevant physicochemical cues that guide their immunomodulatory behavior. This combination allows the proliferative and differentiation capabilities of MSCs to operate in concert with the structural and functional properties of the biomaterials, potentially enhancing therapeutic outcomes in Regenerative Medicine [2-4].

MSCs are among the most responsive cell populations to inflammatory processes within tissues [5]. Initially identified within the bone marrow stroma by Friedenstein in the late 1960s, MSCs were further characterized and redefined by Arnold Caplan [6,7]. These cells are recognized for their "stemness", a property that allows them to differentiate into multiple cell types, including osteoblasts, adipocytes and chondrocytes [8]. These cells are ubiquitously distributed across various types of tissues and present a high degree of mobility in response to signals indicative of tissue damage [9]. This responsiveness establishes MSCs as crucial players in tissue repair and regeneration processes, making them a significant focus of research in Regenerative Medicine and studies of inflammation.

Initially, MSCs were primarily regarded as "stromal" cells rather than stem cells [10]. However, with growing research, some investigators proposed renaming MSCs as "medicinal signaling cells" to better reflect their role in secreting bioactive molecules at sites of disease, injury and inflammation [11,12]. Subsequent studies provided evidence that MSCs secrete prostaglandin E2 (PGE2), a molecule that significantly contributes to their self-renewal capacity and immunomodulatory functions. The release of PGE2 initiates a cascade of events that underscores the inherent stemness of MSCs, reinforcing their classification as stem cells [13]. Consequently, the term "mesenchymal stem cells" is considered appropriate, as it accurately reflects the functional properties of these cells [14].

The most significant characteristics of MSCs include their clonogenic and proliferative abilities, their genetic stability, their undifferentiated state, and their capacity to differentiate into multiple cell lineages [15]. Although MSCs are most often derived from bone marrow, they can also be isolated from a wide variety of other tissues, such as adipose tissue, amniotic fluid, dental-related tissue, placenta, and umbilical cord tissue [3,16-23]. The accessibility of these tissues and the relative ease of the process of expanding MSCs in culture have positioned these cells as attractive candidates for use in cellular therapy. However, the increasing interest in MSC-based therapies has sparked debate regarding the equivalence of MSCs obtained from different sources and expanded using various protocols, raising questions about their functional consistency and therapeutic potential across different isolation methods.

According to the International Society for Cellular Therapy (ISCT), MSCs must meet specific criteria to be accurately identified as such. Firstly, MSCs must exhibit plastic adherence when cultured under standard conditions. Secondly, they should express surface markers such as CD105, CD73, and CD90, while lacking the expression of hematopoietic and endothelial markers, including CD45, CD34, CD14 or CD11b, CD79α or CD19 and HLA-DR. Thirdly, MSCs must possess the ability to differentiate into at least osteoblasts, adipocytes and chondroblasts *in vitro* [4]. These three markers are commonly employed as minimal criteria for characterizing *in vitro*-expanded MSCs. However, several considerations should be addressed. For instance, the absence of CD34 has traditionally been used to identify MSCs; however, this criterion is not universally definitive [24]. Variability in CD34 expression has been observed among adipose-derived stem cells, with some cells exhibiting CD34 positivity depending on the donor and passage number [25,26]. Furthermore, MSCs are generally characterized by the lack of HLA-DR expression, yet this marker can be up-regulated in response to interferon-gamma exposure [27], both in murine and human MSCs, and this up-regulation is influenced by the cell culture conditions [28]. These observations underscore the plasticity of cell surface markers and suggest that the definition of MSC identity based on initial cell surface markers is subject to ongoing refinement as our understanding of these cells evolves [8].

MSCs have gained widespread application in Regenerative Medicine, primarily due to their ability to secrete a variety of bioactive molecules. These

secreted factors play crucial roles in modulating the tissue microenvironment, promoting repair and regeneration, and reducing inflammation. As a result, MSC-based therapies have been developed to address a broad spectrum of human diseases. These include not only musculoskeletal disorders affecting bones, muscles and joints, but also conditions related to cardiac, hepatic and dermal tissues, among others [29-31]. **Table 1** provides an overview of several MSCs and their respective potential applications in Regenerative Medicine.

Table 1. The source and potential applications of some MSCs. Abbreviations: ADMSCs – adipose-derived mesenchymal stem cells; AFMSCs - amniotic fluid mesenchymal stem cells; BMMSCs - bone marrow mesenchymal stem cells; DPSCs - dental pulp stem cells; SHEDs - Human Exfoliated Deciduous Teeth Stem Cells; GMSCs - gingival mesenchymal stem cells; PDLSCs - periodontal ligament stem cells; PMSCs - placental mesenchymal stem cells; UCMSCs - umbilical cord mesenchymal stem cells.

Source	Mesenchymal stem cells	Potential applications	References
Adipose tissue	ADMSCs	Wound healing, nerve regeneration and soft tissue reconstruction/craniofacial surgery.	[18,32,33]
Amniotic fluid	AFMSCs	Fetal tissue reconstruction, lung epithelial regeneration, tissue engineering of congenital malformations, and central/peripheral nervous diseases	[34-38]
Bone marrow	BMMSCs	Bone diseases, cardiovascular diseases and autoimmune disorders.	[39-42]
Dental-related tissue	DPSCs	Dental diseases, neurological diseases, oral diseases, orthopedic disorders, eye diseases and skeletal muscle regeneration.	[43-46]
	SHEDs	Liver disease, Alzheimer's disease, kidney injury, nerve regeneration, and treatment of diabetic nephropathy.	[47-54]
	GMSCs	Skin wound repair, tendon regeneration, bone defect	[55-58]

		regeneration, periodontal regeneration, oral mucositis and collagen-induced arthritis	
	PDLSCs	Periodontium regeneration, bone diseases and tendon tissue regeneration	[59-62]
Placental tissue	PMSCs	Cardiovascular diseases (such as myocardial infarction, critical limb ischemia, stroke), cancer, neurological diseases (such as Parkinson 's disease, Alzheimer 's disease, multiple sclerosis) and liver diseases	[63-65]
Umbilical cord tissue	UCMSCs	Diabetes mellitus, liver disease, myocardial infarction, stroke, spinal cord injury and brain injuries	[66,67]

MSC-like populations have been identified in several dental tissues. The pioneering work by Gronthos *et al.* led to the identification of dental pulp stem cells (DPSCs) from human pulp tissue [44]. Following this, other MSC-like populations were discovered and characterized within dental tissues, including stem cells from human exfoliated deciduous teeth (SHEDs), periodontal ligament stem cells (PDLSCs), dental follicle precursor cells (DFPCs), and stem cells from the apical papilla (SCAPs) [60,68-70]. Among these, DPSCs and SHEDs are particularly promising as sources for Regenerative Medicine due to their accessibility and robust regenerative potential. DPSCs, which are isolated from adult human pulp tissue of impacted third molars, orthodontically extracted teeth and supernumerary teeth, have demonstrated significant clonogenicity, high proliferative capacity, and the ability to form mineralized nodules [71].

The following chapter is a complete characterization of the MSCs collected from the human dental pulp (hDPSCs). For this, the protocols for all procedures related to cell culture are described, as are the different biological characterization techniques performed, namely cell behavior in culture, confirmation of the capacity for trilineage differentiation, and identification of cell markers through cell gene expression.

Human Dental Pulp Stem/Stromal Cells

[This page is intentionally left blank.]

1. Introduction

Dental pulp, a connective tissue within the dental crown, has been highlighted as a good source of adult stem cells [44,72-75]. This tissue, which is soft, highly vascularized and situated beneath the protective enamel and dentin layers, harbors a unique population of stem-like cells first identified by Gronthos and colleagues [44]. These cells, known as Dental Pulp Stem/Stromal Cells (hDPSCs), present several notable characteristics, including accessibility, lifelong availability and significant potential for proliferation. They also exhibit multipotency, being capable of differentiating into various cell types and tissues [76]. The application of hDPSCs takes leverage of these properties, offering advantages such as the modulation of immune and inflammatory responses, intrinsic mobilization of progenitor cells to injury sites through various paracrine mechanisms, and a substantial presence of growth factors that facilitate tissue regeneration [77-80].

The DPSCs have been isolated from a range of species, including humans (hDPSCs), mouse, sheep, chimpanzee and pig [76,81-84]. The two most widely techniques used for the isolation of hDPSCs are the explant and the enzymatic methods. The explant method involves the placement of small fragments of dental pulp tissue onto a plastic culture surface. This technique relies on the outgrowth of cells from the tissue fragments, which then adhere to the plastic surface over time. This method is advantageous for its simplicity and its ability to maintain a relatively undisturbed tissue microenvironment [85,86]. On the other hand, the enzymatic digestion involves several steps: sterile surgical removal of dental pulp, enzymatic digestion using collagenase/dispase, characterization and screening using specific markers [87].

The hDPSCs are emerging as a significant source of stem cells for future applications in Regenerative Medicine [88]. These MSCs have shown promise in several regenerative therapies, including dental pulp regeneration [89], bone tissue engineering [3], angiogenesis/vasculogenesis [90], neurology [91], endocrinology [92], and wound healing [93]. Notably, dental stem cells are considered a potential source for bone tissue engineering, with the osteogenic differentiation capacity of hDPSCs being demonstrated in both *in vitro* and *in vivo* studies [3,94-96]. Leveraging their osteogenic potential, hDPSCs have been successfully combined with 3D polymeric scaffolds to generate bone-like hard tissues, highlighting their

utility in tissue engineering and Regenerative Medicine [97-99]. When compared to bone marrow stem cells (BMSCs), hDPSCs demonstrate superior proliferation rates [100].

In this study, hDPSCs were isolated and subsequently cultured. The cells were then characterized according to the minimal criteria for MSC acceptance, as recommended by the ISCT [4,79]. To achieve a comprehensive understanding of the cells, several parameters were assessed. Cell behavior in culture was evaluated through the analysis of growth curves, determination of population doubling time (PDT) in different passages, and colony-forming unit (CFU) assays, providing insights into the cells' proliferation rates and self-renewal capacities. Additionally, the trilineage differentiation potential of the cells was tested, focusing on their ability to differentiate into osteogenic, chondrogenic and adipogenic lineages, thereby confirming their multipotency. Further, gene expression analysis was conducted to examine the expression profiles of genes associated with MSC characteristics and differentiation potential. This analysis aimed to validate the identity and functional properties of the isolated cells. Overall, these extensive characterizations ensured that the cells met the necessary criteria for MSC classification, and offered a detailed understanding of their growth, differentiation capacities and molecular characteristics.

2. Materials and Methods

2.1 Isolation, processing and cryopreservation of hDPSCs

Protocols for the isolation, processing and cryopreservation of dental pulp tissue from permanent teeth extracted from adult individuals enable the establishment of a well-characterized system of hDPSCs. To study the development of this cell system, foundational protocols were reviewed from the literature [94,101-106]. To summarize, the procedures were as follows:

1. Sample collection and transportation: After an exodontia procedure, performed by dental professional, teeth were collected individually in a sterile container with DMEM culture medium, GlutaMAX™ (Gibco®, 21885-025), supplemented with 300 IU/mL penicillin, 0,3 mg/mL streptomycin (Gibco®, 15140122), and 5 μg/mL amphotericin B (Gibco®, 15290026), and stored at 4 ˚C for up to 24 hours;

2. Decontamination: Each tooth was placed in a Petri dish with 10 mL Dulbecco's phosphate-buffered saline (DPBS) (Gibco®, 14190-086) for initial washing. Debris and periodontal ligament were removed with a scaler, and the tooth was then rinsed with DPBS and wiped with 70% ethanol.
3. Dental pulp isolation from fresh teeth: Teeth were processed in a laminar flow hood. To access the pulp tissue, perforations were made in the teeth, and the pulp was subsequently placed onto a sterile Petri dish;
4. Explant culture: The isolated pulp tissue was cut into small fragments (1-2 mm^2) and transferred to a tissue culture-treated plate. After the fragments adhered, they were covered with α MEM culture medium, GlutaMAX™ supplement, no nucleosides (Gibco®, 32561029), supplemented with 10% (v/v) fetal bovine serum (FBS) (Gibco®, A3160802), 100 IU/mL penicillin, 0.1 mg/mL streptomycin, 2.05 μg/mL amphotericin B, and 10 mM HEPES solution, and incubated at 37°C in a 5% CO_2 atmosphere. The explants were observed regularly to identify possible contamination, the need for medium change and the identification of cells radiating from the tissue;
5. Cell passaging: Cells were allowed to proliferate until reaching 70-80% confluence. The culture medium was then removed, and the cells were washed three times with DPBS. After removing DPBS, trypsin (Trypsin-EDTA 0.25%, 25200-072, Gibco®) was added and incubated at 37°C for 3 minutes. Following incubation, culture medium was added to neutralize trypsin, and the detached cells were collected into a centrifuge tube. The cellular suspension was centrifuged at 1600 rpm, and the supernatant was discarded. The cell pellet was resuspended in fresh culture medium. The hDPSCs could then be cryopreserved or replanted;
6. Cryopreservation: To cryopreserve hDPSCs, the culture medium, cell suspension and 10% (v/v) dimethyl sulfoxide (DMSO, D2650, Sigma®) were added to each cryovial. Vials were placed in a freezing container (Mr. Frosty, Thermo Fisher Scientific, Waltham, USA) and stored at -80°C for 2-3 days. For long-term storage, vials were transferred to liquid nitrogen storage (-195.79°C);
7. Thawing: To thaw, the vial was removed from the nitrogen container and placed in a 37°C water bath until only a small ice crystal is visible. The contents are transferred to a centrifuge tube, and culture medium is

added. The cellular suspension is centrifuged at 1600 rpm for 10 minutes, and the supernatant is discarded. The cells are then resuspended, counted, and plated onto a new culture vessel.

A summary of the hDPSCs procedure is showed in **Figure 1**.

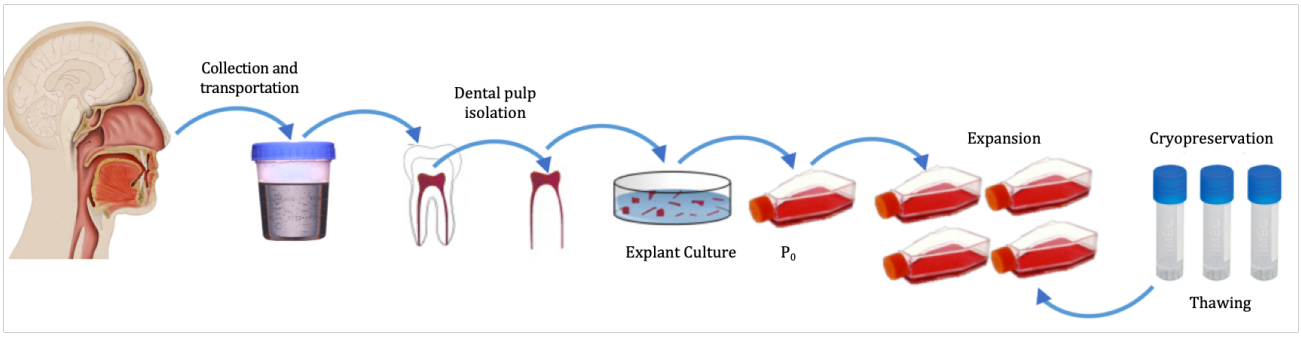


Figure 1. Schematic representation of the process for the isolation, preservation and cryopreservation of hDPSCs.

2.2 Cell behaviour in culture

2.2.1. Growth Curve and Population Doubling Time (PDT)

Cells were thawed and culture under standard conditions until reaching 70-80% confluence, at which point they were harvested for the assay. They were then seeded in a 24-well plate at a density of 6,000 cells per well. For daily recovery, triplicate wells were washed with DPBS and incubated with trypsin for 3 minutes. Following trypsin treatment, culture medium was added, and the cell suspension was transferred to 2 mL tubes. The final volume was recorded, and cells were counted using the Trypan Blue exclusion dye assay (T10282, Invitrogen®) (10µL Trypan Blue: 10µL cell suspension). Cell counting was performed for 10 consecutive days using the Countess II FL Automated Cell Counter (Thermo Fisher Scientific, Waltham, USA).

The PDT, also known as generation time, is defined as the average time required for a cellular population to double in number. This metric is typically assessed during the exponential growth phase, using the formula:

$$PDT = \frac{t \ln 2}{ln \frac{nf}{ni}}$$

where “t” is the incubation time; “nf” is the number of cells at the end of the incubation time, and “ni” is the number of cells at the beginning of the incubation time.

2.2.2. Colony Forming Unit (CFU) Assays

The CFU assay was performed by seeding cells in passage 6 (P6) until 70-80% confluency. Cells were trypsinized, quantified, and diluted to achieve densities of 60, 80, 100 and 150 cells per well in a 6-well plate. After 14 days of incubation, colonies were stained with 0.5% crystal violet, and only colonies larger than 1 mm in diameter, and non-overlapping, were counted. Clonogenicity was calculated using the formula:

$$Clonogenicity\ (\%) = \frac{Mean\ number\ of\ colonies\ counted}{Total\ number\ of\ cells\ seeded} \times 100$$

To determine clonogenicity, three replicates (n=3) were assessed for each cell density.

2.3 Multilineage Differentiation

2.3.1. Adipogenic Differentiation

Cells were harvested and subsequently re-seeded onto 24-well plates at a density of 8,000 viable cells/cm². The cells were cultured in standard growth medium until reaching 70-80% confluence. At this point, the expansion medium was substituted with adipogenic differentiation medium (StemPro™ Adipogenesis Differentiation Kit, Gibco A1007001, Thermo Fisher Scientific, Waltham, USA). Both the differentiation medium and the control medium were refreshed every 3 days.

Following 14 days of culture under adipogenic conditions, the cells were fixed with 4% paraformaldehyde (3.7-4% buffered to pH 7, Panreac AppliChem®, 252931.1315) and subsequently stained with Oil Red O (ORO) working solution (O0625, Sigma-Aldrich®) for 10-20 minutes. The wells were thoroughly rinsed to remove any excess stain. The formation of lipid droplets in the differentiated cells was then observed using an inverted light microscope.

2.3.2. Chondrogenic Differentiation

Chondrogenic differentiation was initiated in micromass cultures by seeding 2×10^4 viable cells per well, at the center of each well, in a 96-well plate. The cells were allowed to adhere and proliferate for 48 hours before replacing the expansion medium with a chondrogenic-specific culture medium (StemPro® Chondrogenesis Differentiation Kit, Gibco A1007101, Thermo Fisher Scientific, Waltham, USA). Both differentiation and control media were refreshed every other day. After 14 days, chondrogenic matrix deposition was evaluated using alcian blue staining to assess proteoglycan synthesis. Cells were fixed and stained with alcian blue (A9186, Sigma®) solution. The dye was subsequently removed, and the wells were repeatedly rinsed with 3% (v/v) acetic acid (A6289, Sigma-Aldrich®). Distilled water was added to neutralize the acidity, and the stained matrix was then observed under an inverted microscope.

2.3.3. Osteogenic Differentiation

Cells were harvested and re-seeded onto 24-well plates at a density of 31,500 viable cells/cm². The cells were cultured in standard growth medium until reaching 70-80% confluence, after which they were transitioned to osteogenic differentiation medium (StemPro™ Osteogenesis Differentiation Kit, Gibco A1007201, Thermo Fisher Scientific, Waltham, USA). Control wells were maintained in expansion medium. The culture medium was refreshed every 3 days.

Osteogenic differentiation and mineral matrix deposition were assessed after 21 days, using staining solutions. Regarding Von Kossa staining, cells were fixed in 4% formaldehyde (Merck KGaA, Darmstadt, Germany, 100496), dehydrated through a graded ethanol series, and air-dried. After rehydration, wells were incubated with 2% silver nitrate solution (85193, Sigma-Aldrich®) and under ultraviolet light exposure. Subsequently, the wells were incubated for 3 minutes in 5% sodium thiosulfate (72049, Sigma-Aldrich®). Concerning Alizarin-Red Staining (ARS) (TMS-008-C, Merck KGaA, Darmstadt, Germany), cells were fixed in 4% formaldehyde, stained with a 40 mM ARS solution and incubated under agitation for 30 minutes. For both stains, after removing the supernatant, wells were rinsed. The wells were thoroughly rinsed, and images were captured to document the results.

2.4 Gene expression

Reverse Transcriptase Polymerase Chain Reaction (RT-PCR) and quantitative Polymerase Chain Reaction (qPCR) were conducted targeting housekeeping genes, specifically glyceraldehyde-3-phosphate dehydrogenase (GAPDH), and mesenchymal stem cell (MSC)-related gene sequences, as listed in **Table 2**. These analyses were performed at P6 and P9.

For the specific characterization of MSCs, genes were selected as pluripotency markers (SOX2), MSC-specific markers (CD105/ENG, CD90/THY, CD73 (NT5E) and CD44), hematopoietic markers (CD14, CD19, CD45/PTPRC and CD34), and markers associated with cell proliferation, adhesion and compatibility (B2M, ITGB1, MCAM, NCAM1 and VCAM1). Additionally, genes specific to osteogenic (RUNX2 and IBSP), adipogenic (ADIPOQ and AAK1) and chondrogenic (COL2A1 and ACAN) differentiation were included.

For RNA extraction, cells were harvested from culture using Trypsin-EDTA, and pellets containing 2×10^6 cells per group were processed with the Aurum™ Total RNA Mini Kit (Catalog No. 732-6820, Bio-Rad Laboratories®). Cell pellets were lysed, and DNA was removed using DNase I enzyme. The resulting RNA was then eluted. Total RNA concentration and purity were assessed using a NanoPhotometer™ Pearl (Implen GmbH) with absorbance measurements at 260 and 280 nm, and 260 and 230 nm. After normalizing RNA concentrations across samples, complementary DNA (cDNA) was synthesized from the purified RNA using the iScript™ Reverse Transcription Kit (170-8891, Bio-Rad Laboratories®) and a T100™ Thermal Cycler (Bio-Rad Laboratories®), following the manufacturer's protocol.

The qPCR analysis was performed using the CFX96 Touch™ Real-Time PCR Detection System (Bio-Rad Laboratories®) with iTaq™ Universal SYBR Green Supermix (Bio-Rad Laboratories®), following the manufacturer's protocol. The Prime PCR Custom Plate 96 Well (Bio-Rad Laboratories®) contained a total of 21 genes, distributed and replicated multiple times. The genes were subjected to the thermal cycling conditions specified by the manufacturer, with each gene-primer pair selected to assess expression in isolated cells.

Quantification cycle (Cq) values lower than 29 (< 29) were interpreted as highly positive, indicating abundant nucleic acid expression in the sample; Cq

values between 30 and 39 (30 < Cq < 39) were considered positive, reflecting moderate nucleic acid expression; and Cq values higher than 40 (> 40) were considered indicative of weak reactions, suggestive of low nucleic acid expression or potential external contamination.

The ΔCq (differential expression between the Cqs) was calculated using the following formula:

$$\Delta Cq = Cq_{\ target\ gene} - Cq_{\ housekeeping\ gene}$$

The difference between cell passages (hDPSCs P6 / hDPSCs P9) was calculated using the following formula:

$$\Delta\Delta Cq = \Delta Cq_{hDPSCsP9} - \Delta Cq_{hDPSCsP6}$$

The relative quantification (RQ) was determined using the formula:

$$RQ = 2^{-(\Delta\Delta Ct)}$$

Gene expression levels were classified as down-regulated when RQ values were less than 0.5, and up-regulated when RQ values exceeded 2.

Table 2. Primer name, ensembl gene id, amplicon context sequences, and marker type. A- housekeeping gene; B- pluripotency markers; C- specific MSCs markers; D- hematopoietic markers; E- cell proliferation, adhesion, and compatibility markers; F- genes specific for osteogenic differentiation; G- genes specific for adipogenic differentiation; H- genes specific for chondrogenic differentiation.

Primer	Ensembl Gene ID	Amplicon Context Sequence	Marker type
Glyceraldehyde-3-phosphate dehydrogenase (GAPDH)	ENSG00000111640	GTATGACAACGAATTTGGCTACAGCAACA GGGTGGTGGACCTCATGGCCCACATGGCC TCCAAGGAGTAAGACCCCTGGACCACCAG CCCCAGCAAGAGCACAAGAGGAAGAGAGA GACCCTCACTGCTGGGGAGTCCCTGCCAC AC	**A**
Sex determining region Y-box 2 (SOX2)	ENSG00000181449	AGACTAGGACTGAGAGAAAGAAGAGGAGA GAGAAAGAAAGGGAGAGAAGTTTGAGCCC CAGGCTTAAGCCTTTCCAAAAAATAATAAT AACAATCATCGGCGGCGGCAGGATCGGCC AGAGGAGGAGG	**B**

CD44	ENSG00000026508	GTATGGGTTCATAGAAGGGCACGTGGTGA TTCCCCGGATCCACCCCAACTCCATCTGTG CAGCAAACAACACAGGGGTGTACATCCTC ACATCCAACACCTCCCAGTATGACACATAT TGCTTCAATGCTTCAGCTCCACCTGAAGAA GATTGTACATCAGTCACAGACCTGCCCAAT GCCTTTGA	C
Endoglin (CD105)	ENSG00000106991	CTGCCCCGGCTCGATGGTGTTGGAGGCCT GGAGGAAGTGTGGGCTGAGGTAGAGGCCC AGCTGGAAAGAGAGGCTGTCCATGTTGAG GCAGTGCACCTTTTTCCGCTGTGGTGATGA GCTCGACAGGATATTGACCACCGCCTCATT GCTGATC	
5'-nucleotidase ecto (CD73)	ENSG00000135318	GGATGGCTCCTCTCAATCATGCCGCTTTAG AGAATGCAACATGGGCAACCTGATTTGTGA TGCAATGATTAACAACAACCTGAGACACAC GGATGAAATGTTCTGGAACCACGTATCCAT GTGCATTTTAAATGGAGGTGGTATCCG	
Thy-1 cell surface antigen (CD90)	ENSG00000154096	ATGTTGTATTTGCTGGTGAAGTTGGTTCGG GAGCGGTATGTGTGCTCAGGCACCCCCAC AGTGCCAAAGAGCACGTGCTTCTTTGTCTC ACGGGTCAGGCTGAACTCGTACTGGATGG GTGAACTGCTGGTATTCTCATGGCGGCAGT CC	
CD14	ENSG00000170458	GATAAGTCTTCCGAACCTCTGAGCTCCGGA CAGGCTCTGGAAGTGCTTTAGCTTCTTTCC TACACAGCGGCACCCGCCGGCTTCCAGGC TTCACACTTGTGAACTCTTCGGCTGCCTCT GACAGTTTATGTAATCCTGGGATG	D
CD19	ENSG00000177455	TCACCGTGGCAACCTGACCATGTCATTCCA CCTGGAGATCACTGCTCGGCCAGTACTAT GGCACTGGCTGCTGAGGACTGGTGGCTGG AAGGTCTCAGCTGTGACTTTGGCTTATCTG ATCTTCTGCCTGTGTTCCCTTGTGGGCATT CT	
CD34	ENSG00000174059	AGATGCCCTGAGTCAATTTCACTTCTCTGA TGCCTGAACATTTGATTTCTGCCTTGATGT CACTTAGGATAGGAGAAGATGATGTATAG GGTTTAGTGGGAGATGTTGCAAGGCTAGT GCTAGTGGTTG	
Protein tyrosine phosphatase	ENSG00000081237	AAGGACGCATGCTGTTTCTTAGGGACACG GCTGACTTCCAGATATGACCATGTATTTGT	

receptor type C (CD45)		GGCTTAAACTCTTGGCATTTGGCTTTGCCT TTCTGGACAC	
Beta-2-microglobulin (B2M)	ENSG00000166710	TCCGTGGCCTTAGCTGTGCTCGCGCTACTC TCTCTTTCTGGCCTGGAGGCTATCCAGCGT ACTCCAAAGATTCAGGTTTACTCACGTCAT CCAGCAGAGAATGGAAAGTCAAATTTCCT GAATTGCTATGTGTCTGGGTTTCATCCATC CGAC	
Integrin subunit beta 1 (ITGB1)	ENSG00000150093	TTTACACCAGCAACTCTCAACATACTTGTC TTTCAGATATGTCATCAGTCATGTCTAACA GGCAAATAGCAAAATAACAGATTTAAAACA ATCCTTAACTAGCTAGCAGGACATTTACTT TGGATTCTGCATAA	
Melanoma cell adhesion molecule (MCAM)	ENSG00000076706	GGAGCTTATCTGACTTAACTTCAACTACAA GTTCGCTCTTACGAGACGGGGGTAGCGTG ATCTCCTGCTTCCCTGAGCGCCTGCACGGC AGCTTGCCCTTCTTATAGAGGAAATAGAGG ACAGCGCCCAGCACCGCCAGGACCAGGAT GCACACAATCACAGCCACGATGACCACG	**E**
Neural cell adhesion molecule 1 (NCAM1)	ENSG00000149294	AAGCTCACCCCAAACCAGCAGCGGATCTC AGTGGTGTGGAATGATGATTCCTCCTCCAC CCTCACCATCTATAACGCCAACATCGACGA CGCCGGCATTTACAAGTGTGTGGTTACAG GCGAGGATGGCAGTGAGTCAGA	
Vascular cell adhesion molecule 1 (VCAM1)	ENSG00000162692	GGAATTAACCAGGCTGGAAGAAGCAGAAA GGAAGTGGAATTAATTATCCAAGTTA CTCCAAAAGACATAAAACTTACAGCTTTTC CTTCTGAGAGTGTCAAAGAAGGAGA CACTGTCATCATCTCTTGTACATGTGGAAA TGTTCCAGAAACATGGATAATCCTG AA	
Runt-related transcription factor 2 (RUNX2)	ENSG00000124813	TTCCTCATCCCAGTATGAGAGTAGGTGTCC CGCCTCAGAACCCACGGCCCTCCCTGAAC TCTGCACCAAGTCCTTTTAATCCACAAGGA CAGAGTCAGATTACAGACCCCAGG	**F**
integrin-binding sialoprotein (IBSP)	ENSG00000029559	GTGAGAACGGGGAACCTCGTGGGGACAAT TACCGAGCCTATGAAGATGAGTACAGCTA CTTTAAAGGACAAGGCTACGATGGCTATGA TGGTCAGAATTACTACCACCACCAGTGAAG	
AP2 associated kinase 1 (AAK1)	ENSG00000115977	ATCCAAGAGCCCAAATGTCTGCCTTCGTAG TGATGATTTTGCCACTGTACAGGTTGACCA	**G**

		TTTCTGGTGCTCGATAGGACAGCGTTGTGT ATTTCTTAATCTCA	
Adiponectin (ADIPOQ)	ENSG00000181092	TGATTTTCTCTAAAATTTCAACAAGTAGCT AAAGTCTGGCTATGCTCACAGTCTCACATC TGGTTGGGGTGGGCTCCTTACAGAACACG CTTTCACAGTTACCCTAAACTCTCTGGGGC AGGGTTATTCCTTTGTGGAACCAGAGGCA	
Aggrecan (ACAN)	ENSG00000157766	AGGCTGCTATGGAGACAAGGATGAGTTTC CTGGTGTGAGGACGTATGGCATCCGAGAC ACCAACGAGACCTATGATGTGTACTGCTTC GCCGAGGAGATGGAGGGTGAGGTCTTTTA TGCAACATCTCCAGAGAAGTTCACCTTCCA GGAAGCAGCCAATGA	**H**
Collagen type 1 alpha 2 chain (COL1A2)	ENSG00000164692	CTAGACAGAGATGAACTGAGGTCCTTGTTT TGTTTTGTTCATAATACAAAGGTGCTAATT AATAGTATTTCAGATACTTGAAGAATGTTG ATGGTGCTAGAAGAATTTGAGAAGAAATAC TCCTGTATTGAGTTGTATCGTGTGGTGTAT TTTTTAAAAAATTTGATTT	

2.5 Statistical analysis

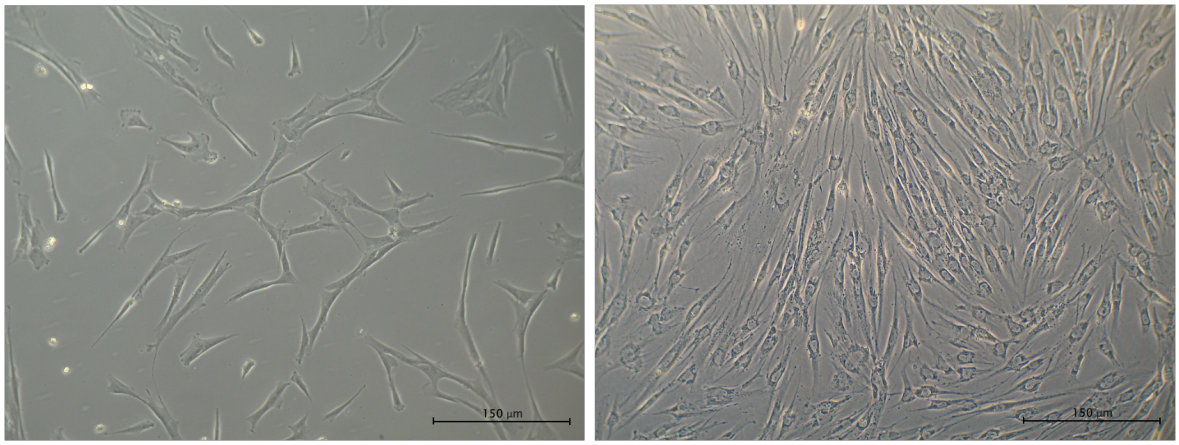
Statistical analysis was conducted using GraphPad Prism version 9.00 for Mac OS X (GraphPad Software, La Jolla, California, USA). All experiments were performed in triplicate, and results are expressed as the mean ± standard error of the mean (SEM). Group comparisons were conducted using one-way ANOVA followed, by Tukey´s multiple comparisons test. Statistical significance was set at $p < 0.05$, and results were considered statistically significant at this threshold. The significance of the results is denoted by symbols corresponding to p values: one symbol (*) for $0.01 \leq p < 0.05$, two symbols (**) for $0.001 \leq p < 0.01$, three symbols (***) for $0.0001 \leq p < 0.001$, and four symbols (****) for $p < 0.0001$.

3. Results

3.1 Isolation, processing and cryopreservation of hDPSCs

The explant method used for isolating MSCs from dental pulp was effective, yielding the desired cell quantity within two weeks of culture. This approach successfully facilitated the isolation of the target cell lines. At the first passage, two samples were randomly selected from those with negative microbiological

control and were subsequently expanded for further characterization. **Figure 2** illustrates the cultured cells after 1 and 5 days, highlighting their adherence to the plastic surface and their characteristic "fibroblast-like" morphology when maintained in tissue culture flasks.



(a) (b)

Figure 2. (a) hDPSCs after 1 day in culture (50% confluence); (b) hDPSCs after 5 days in culture (80-90% confluence) (magnification 40x).

3.2 Cell behaviour in culture

3.2.1. Growth Curve and Population Doubling Time (PDT)

Cells at passage 5 (P5) were counted, plated, and subsequently monitored for 10 days. Daily cell counts were used to generate growth curves (**Figure 3**). Isolated cells exhibited a slow growth rate during the first day (lag phase), followed by a period of rapid proliferation from the second to sixth day (log of exponential phase). After the seventh day, the proliferation rate decreased (stationary phase), resulting in a S-shaped growth curve. Observations indicated that the cultures reached complete confluence after 6 days, although a slight increase in cell numbers continued until the eighth day.

Furthermore, the population doubling time (PDT) was assessed across multiple passages, specifically from P0 to P1, P1 to P2, P2 to P3, and P3 to P4. The PDT values recorded for these passages were 70.5 ± 2.3 hours, 57.4 ± 0.7 hours, 46.7 ± 1.1 hours, and 43.4 ± 1.0 hours, respectively (**Figure 4**). Significant differences were noticed between passages. These results indicate a progressive

decrease in PDT in each subsequent passage, that is, a higher proliferation rate and less time required to double the cell population in culture.

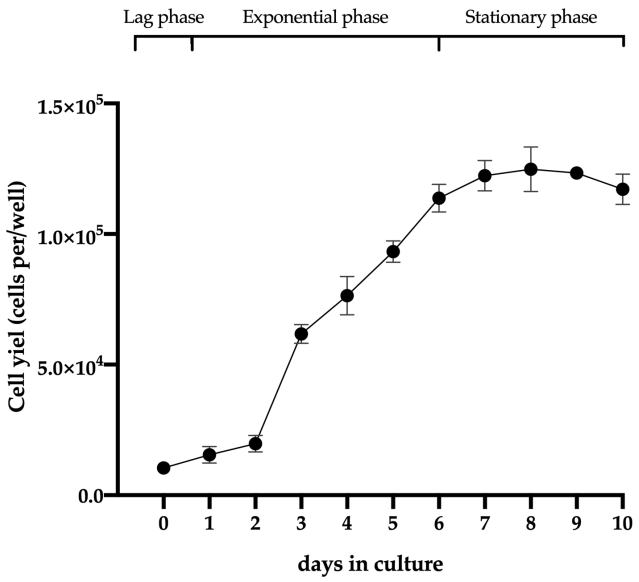


Figure 3. Growth curve of hDPSCs at passage 5 (P5), for up to 10 days of culture.

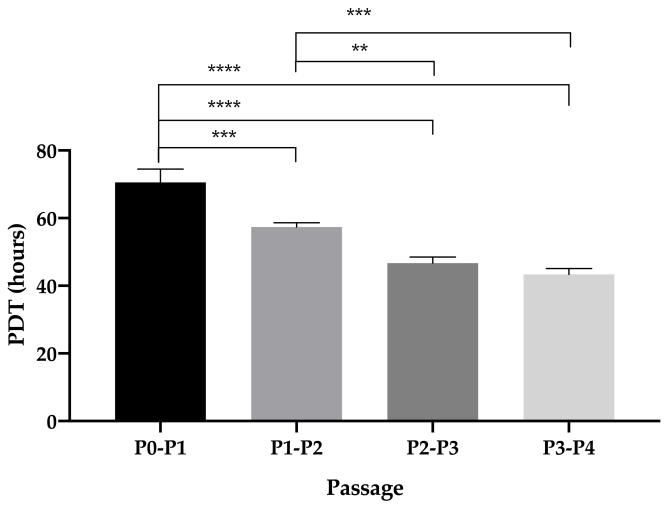


Figure 4. Population Doubling Times (PDTs) of the different passages of hDPSCs. The significance of the results is denoted by symbols corresponding to p values: two symbols (**) for $0.001 \leq p < 0.01$, three symbols (***) for $0.0001 \leq p < 0.001$, and four symbols (****) for $p < 0.0001$.

3.2.2. Colony Forming Unit (CFU) Assays

The CFU assay confirmed the ability of MSCs to form colonies from single cells seeded at low densities. After 14 days of incubation, colonies were identified (**Figure 5**). On average, 15.3 ± 3.3 colonies were observed for 60 seeded cells, 15.7 ± 2.1 for 80 seeded cells, 19.7 ± 3.9 for 100 seeded cells, and 29.0 ± 2.9 colonies for 150 seeded cells. These correspond to clonogenicity percentages of 25.6 ± 3.9%, 19.6 ± 1.8%, 19.7 ± 2.7%, and 19.3 ± 1.4% for 60, 80, 100, and 150 seeded cells, respectively (**Figure 6**). No statistically significant differences in clonogenicity percentages were observed among the different seeding densities.

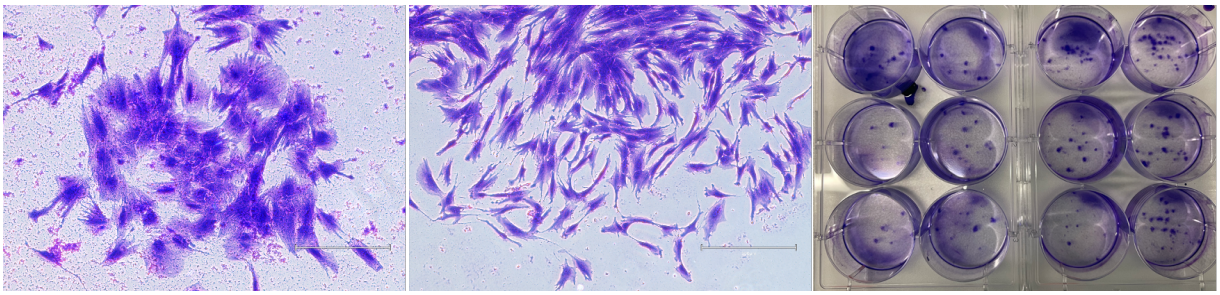


Figure 5. CFU assay: observation of individualized colonies in a 6-well tissue culture treated plate, stained with crystal violet solution (magnification 100x).

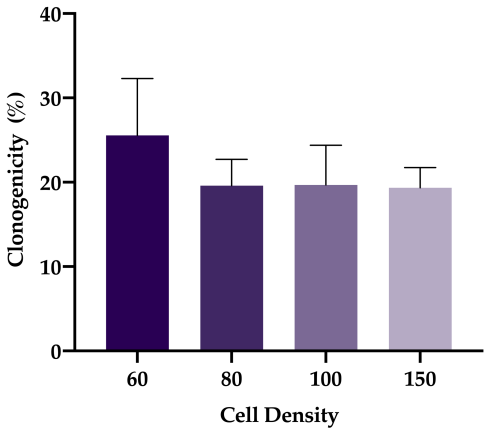


Figure 6. CFU assay: observation of individualized colonies in a 6-well tissue culture treated plate, stained with crystal violet solution (magnification: 100x).

3.3 Multilineage Differentiation

The differentiation potential of the isolated cells was assessed toward the three mesodermal lineages (**Figure 7**).

After 14 days of culture in adipogenic medium, the isolated cells showed intracytoplasmic lipid vacuoles, which were visualized by staining with ORO solution (**Figure 7-A**). This morphological change is characteristic of adipogenic differentiation, indicating that the cells successfully underwent lineage-specific differentiation into adipocytes. The presence of intracytoplasmic vacuoles confirms the accumulation of lipids, a characteristic of adipogenic commitment, thus verifying the adipogenic potential of the isolated cells under the specified culture conditions.

During the adipogenic differentiation process, micromass cultures in the center of the wells presented progressive aggregation over the 14-day culture period (**Figure 7-B**). The edges of these micromasses retracted, leading to the formation of "mountain-like" cellular structures that remained firmly attached to the well surface. Microscopic analysis of the wells stained with alcian blue revealed intense staining, indicating successful differentiation. The presence of extracellular chondrogenic aggregates, as evidenced by the characteristic morphology and positive alcian blue staining, confirmed the chondrogenic differentiation potential of the isolated cells and the production, secretion and deposition of sulfated proteoglycans deposits. This observation underscores the cells' capacity to undergo lineage-specific differentiation into chondrocytes.

The osteogenic differentiation capacity of the isolated cells was confirmed by the presence of extracellular calcium deposits, which were detected through staining with ARS, a characteristic morphological indicator of osteogenesis (**Figure 7-C**). Additionally, mineral matrix deposition was observed in wells stained with silver nitrate solution, as evidenced by the dark pigmentation on the cellular surface following the Von Kossa protocol (**Figure 7-D**). Microscopic analysis further validated the presence of mineralized matrix in the differentiated wells, supporting the successful osteogenic differentiation of the isolated cell populations.

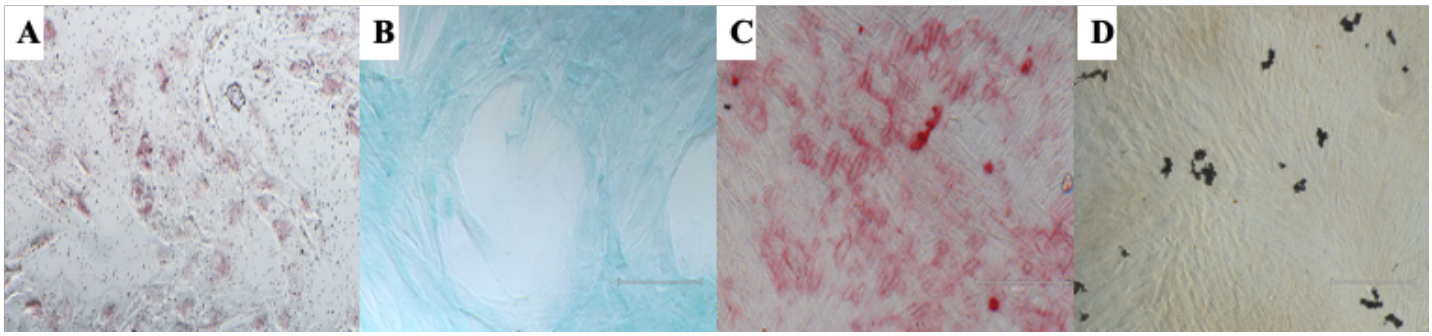


Figure 7. Multilineage differentiation of isolated cells following culture in (A) Oil Red O staining reveals large, round-shaped cells with red-stained lipid vacuoles in the cytoplasm; (B) Alcian blue staining highlights chondrogenic aggregates and blue-stained extracellular matrix; (C) Alizarin Red staining reveals calcium-containing osteocytes and extracellular calcium deposits in red, and (D) Von Kossa staining indicates mineral matrix deposition through dark pigmentation on the cellular surface. (magnification: 100x).

3.4 Gene expression

Total RNA was successfully extracted from the cultured isolated cells, enabling subsequent gene expression analysis. The expression levels of target genes were assessed using RT-qPCR, and the results are summarized in **Table 3** and **Figure 8**. The data are presented as the average quantification cycle ± standard error of the mean for each gene (Avg Cq ± SEM). Additionally, the average differential expression between the target and housekeeping genes (Avg ΔCq) is provided, along with the differential expression between hDPSCs at Passage 6 (P6) and Passage 9 (P9) (ΔΔCq). The relative quantification (RQ) values, which indicate the fold change in gene expression, and the corresponding gene regulation (up-regulation or down-regulation) from passage P9 compared to passage P6, are also reported.

SOX2, a pluripotency marker, was undetected in any of the hDPSC cultured cells across both passages.

Regarding MSC markers CD44, CD105, CD73, and CD90, all demonstrated strong expression levels (Cq < 29) in both passages, except for CD105, which showed moderate expression (Cq 30-35) in P9. In P9, CD105 and CD90 showed down-regulation compared to P6. Hematopoietic markers, including CD14, CD19, CD45, and CD34, were not expressed in either passage, except for CD14, which showed weak expression (Cq > 35) and down-regulation in P9 compared to P6.

Markers related to cell proliferation, adhesion and compatibility (B2M, ITGB1, MCAM, NCAM1, and VCAM1) were expressed in both passages. MCAM were down-regulated, showing moderate expression. B2M presented strong expression. Conversely, VCAM1 was up-regulated, presenting moderate expression in P6 and strong expression in P9. Statistically significant differences were observed in the ΔCq values for the VCAM1 gene.

Concerning osteogenic differentiation markers (RUNX2, IBSP), both were expressed throughout the passages. RUNX2 showed moderate expression, in both passages, and down-regulation in P9 compared to P6. IBSP, on the other hand, showed weak expression in P6 and strong expression in P9, accompanied by up-regulation. Statistically significant differences were noted in the ΔCq values for the IBSP gene. The AAK1 gene, an adipogenic differentiation marker, was strongly expressed and up-regulated. Contrastingly, ADIPOQ, another adipogenic marker, was not expressed in P6 but showed strong expression in P9. Regarding chondrogenic differentiation markers (ACAN and COL2A1), both were strongly expressed in P6. However, in P9, ACAN was not expressed, while COL2A1 was down-regulated with significant differences in ΔCq values between the passages.

Table 3. Quantitative PCR of hDPSCs cultured. Avg Cq ± SEM: average quantification cycle ± standard error of the mean; Avg ΔCq: average quantification cycle (differential expression of target and housekeeping genes); ΔΔCq: differential expression of hDPSCs P6 and hDPSCs P9 genes; RQ: relative quantification; Regulation: ↑: up-regulated over 2-fold; ↓: down-regulated under 0.5 fold; nd: not detected; na: not applicable.

	hDPSCs P6		**hDPSCs P9**				
Target gene	**Avg Cq ± SEM**	**Avg ΔCq ± SEM**	**Avg Cq ± sd**	**Avg ΔCq± SEM**	**ΔΔCq**	**RQ**	**Regulation**
SOX2	nd	nd	nd	nd	na	na	na
CD44	24.8 ± 0.5	2.9 ± 0.5	26.0 ± 0.2	3.4 ± 0.2	0.6	0.7	
CD105	28.3 ± 0.3	6.3 ± 0.3	30.5 ± 0.2	8.0 ± 0.2	1.6	0.3	↓
CD73	26.5 ± 0.4	4.6 ± 0.4	27.9 ± 0.6	5.4 ± 0.6	0.7	0.6	
CD90	26.4 ± 0.6	4.5 ± 0.6	29.3 ± 1.0	6.8 ± 1.0	2.3	0.2	↓
CD14	36.2 ± 1.2	14.3 ± 1.2	38.9 ± 1.6	16.3 ± 1.6	2.0	0.2	↓
CD19	nd	nd	nd	nd	na	na	na
CD34	nd	nd	nd	nd	na	na	na
CD45	nd	nd	nd	nd	na	na	na
B2M	23.9 ± 0.3	1.9 ± 0.3	25.5 ± 0.8	3.0 ± 0.8	1.1	0.5	

ITGB1	23.3 ± 0.5	1.4 ± 0.5	23.4 ± 0.7	0.9 ± 0.7	-0.5	1.4	
MCAM	31.9 ± 0.5	9.9 ± 0.5	34.2 ± 1.1	11.6 ± 1.1	1.7	0.3	↓
NCAM1	32.5 ± 0.6	10.6 ± 0.6	32.9 ± 1.1	10.3 ± 0.5	-0.3	1.2	
VCAM1	34.9 ± 0.6	13.0 ± 0.6	13.1 ± 0.0	-9.5 ± 1.1	-22.4	5693300.9	↑
RUNX2	31.1 ± 0.5	9.2 ± 0.5	33.4 ± 1.0	10.9 ± 0.0	1.7	0.3	↓
IBSP	36.1 ± 0.6	14.2 ± 0.6	5.2 ± 0.0	-17.4 ± 0.0	-31.6	3217879494,7	↑
AAK1	32.6 ± 2.9	10.7 ± 2.9	31.3 ± 0.6	8.7 ± 0.0	-2.0	4.0	↑
ADIPOQ	nd	nd	5.6 ± 0.0	-16.9 ± 0.0	na	na	
ACAN	2.4 ± 0.0	-19.6 ± 0.0	nd	nd	na	na	
COL1A2	6.6 ± 0.0	-15.4 ± 0.0	19.7 ± 0.0	-2.8 ± 0.0	12.5	0.0	↓

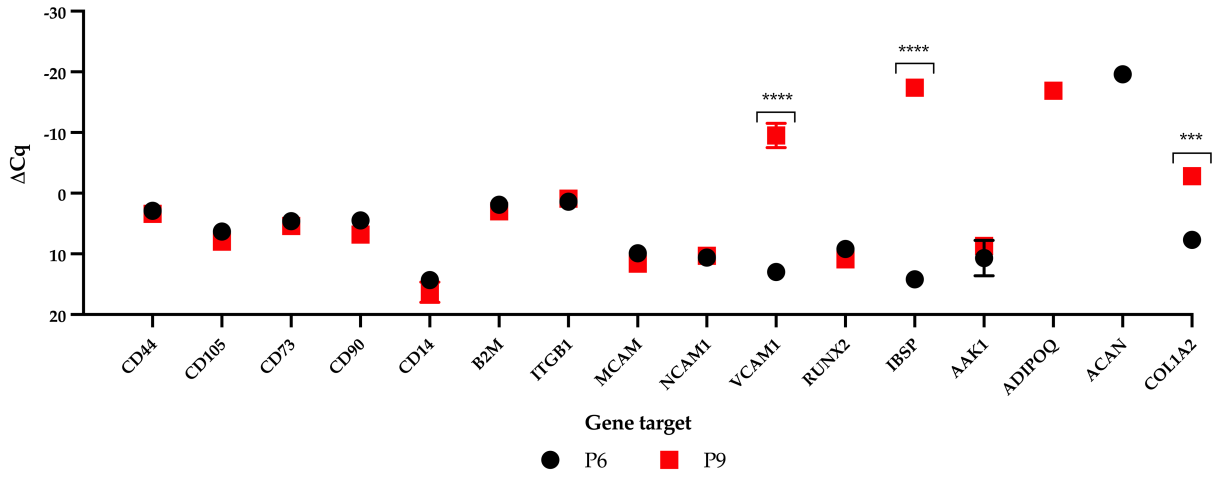


Figure 8. ΔCq values for the different genes under study in hDPSCs for P6 and P9. Higher ΔCq values indicate lower gene expression levels (mean ± SEM). The significance of the results is denoted by symbols corresponding to p values: three symbols (***) for 0.0001 ≤ p < 0.001, and four symbols (****) for p < 0.0001.

4. Discussion

This chapter provided a comprehensive overview of the isolation, culture and characterization of DPSCs derived from human tissue. It detailed the protocols used for the storage and proliferation of these cells, as well as the methods employed to assess their *in vitro* differentiation potential into osteoblasts, adipocytes and chondrocytes. Additionally, the chapter included an analysis of gene expression profiles associated with these differentiation processes, therefore offering insights into the molecular mechanisms underlying DPSC functionality and their potential applications in Regenerative Medicine.

The protocols were developed based on a thorough review of existing literature [94,101-106], which encompasses significant research on various aspects of hDPSC handling, including isolation techniques, expansion media, supplementation, and cryopreservation methods.

The MSCs were isolated from human dental pulp using the explant method. This approach proved to be highly effective, yielding the desired quantity of cells within two weeks of dental pulp culture. The method facilitated the successful isolation of targeted cell lines, which were subsequently utilized for further characterization and analysis.

The isolated cells were confirmed to be MSCs according to the criteria established by the ISCT [4]. These cells demonstrated adherence to plastic surfaces and maintained strong attachment to the culture substrate, even when subjected to mechanical stress from DPBS washing and trypsin-induced detachment. Additionally, the cells showed a characteristic "fibroblast-like" morphology when cultured in tissue culture flasks, further supporting their identification as MSCs.

The cells also displayed the expected proliferative dynamics, as evidenced by the growth curve under 10 days at P5. The growth curve observed is consistent with the growth patterns reported for hDPSCs in other studies [107-109]. The PDT results demonstrate a progressive reduction in each subsequent passage, indicating an enhanced proliferative capacity of the cells as they adapt to the culture conditions over time. A lower PDT signifies a faster doubling rate, reflecting increased cell proliferation efficiency. This reduction in doubling time is closely associated with *in vitro* aging, suggesting that cells exhibit accelerated growth as they approach later passages. This observation aligns with findings from previous studies [110,111], which reported successful scale-up of stem cell production at

these passages with minimal risk of stemness loss. The CFU assay further validated the clonogenic potential of MSCs, demonstrating their capacity to proliferate and form colonies when cultured at low cell densities. This capacity to generate colonies from single cells underscores the self-renewal and proliferative characteristics inherent to MSCs, which are critical for their application in Regenerative Medicine [112].

According to the criteria established by the ISCT, the ability to undergo trilineage differentiation - into adipogenic, osteogenic, and chondrogenic lineages - is a fundamental condition for the identification and characterization of MSCs [4]. In this study, hDPSCs demonstrated this trilineage differentiation capacity following the implementation of specific differentiation protocols. The observed potential of hDPSCs to differentiate into adipocytes, osteocytes and chondrocytes *in vitro* not only confirms their multipotency, but also aligns with findings from previous research on hDPSCs, further validating their characterization as MSCs [3,20,113-115].

Furthermore, the RT-PCR technique allowed the analysis and expression of specific markers for cellular characterization. SOX2, a pluripotency marker, was unexpectedly undetected in any of the hDPSC cultured cells across both passages. According to the study by Sei-Myoung Han *et al.* [116], SOX2 expression is initially present at low levels in early passages of MSCs, but its expression gradually diminishes with increasing passage numbers, indicating a tendency for these cells to lose some of their pluripotency and tend towards specific differentiation pathways. The absence of SOX2 in the present study may therefore be explained by the fact that the cells analyzed were from later passages (P6 and P9), where SOX2 levels may have decreased below detectable thresholds.

According to the criteria established by Dominici *et al.* [4], a MSC population should demonstrate that 95% of the cells expressed CD105, CD73 and CD90, while showing minimal expression (< 5% positivity) of hematopoietic and endothelial markers such as CD14, CD45, CD34 or CD11b, CD79α or CD19 and MHC class II. Therefore, in this study, the expression of CD105, CD73 and CD90, along with the absence of CD19, CD45 and CD34 markers, were considered essential for the characterization of the isolated cells as MSCs. Additionally, the frequent identification of other markers, such as CD44 (with Cq values < 29), within hMSC populations, further corroborates their mesenchymal lineage, supporting the

classification and functional properties of these cells [117]. The marker CD14, representative of a myeloid origin [118], is also among the hematopoietic genetic markers that should be negative in MSCs. However, at both P6 and P9 passages, it was present with low to moderate expression. Although this result seems to be contradictory, in the literature it is described that the presence of CD14 can occur depending on the specificity of the analysis in question, having already been detected in other works, and not invalidating the rest of the results and their consequent characterization [119].

Markers related to cell proliferation, adhesion and compatibility (B2M, ITGB1, MCAM, NCAM1 and VCAM1) were expressed in both passages. VCAM1 was up-regulated, presenting moderate expression in P6 and strong expression in P9, and statistically significant differences were observed in the ΔCq values for this gene. In the study by Nishihira *et al.* [120], it was demonstrated that the expression of VCAM1 in MSCs is significantly up-regulated under high cell density conditions. This observation suggests that VCAM1 expression is modulated by the density of cell populations. Consequently, this regulatory mechanism may contribute to the observed up-regulation of this gene in hDPSCs during higher passages.

Concerning differentiation markers, cells expressed markers associated with osteogenic differentiation (RUNX2 and IBSP), adipogenic differentiation (AAK1 and ADIPOQ) and chondrogenic differentiation (ACAN and COL2A1). These findings align with the results from *in vitro* trilineage differentiation assays (subsection 3.3), which confirmed the cells' ability to differentiate into adipogenic, osteogenic and chondrogenic lineages - a crucial criterion for the identification and characterization of MSCs [4]. However, ADIPOQ was not expressed at P6, and ACAN was not expressed at P9. Previous studies have reported that the expression of adipogenic markers tends to increase with passage number, while the expression of chondrogenic markers tends to decrease with higher passage numbers, which is consistent with our results [121-123]. The significant down-regulation of COL2A1, reflected in the differences in ΔCq values between passages, is indicative of this tendency, as it tends to decrease in expression with successive passages. This reduction in chondrogenic potential aligns with the well-documented decrease in differentiation capacity observed in MSCs as they undergo multiple passages [121].

5. Conclusions

Dental pulp presents a significant and promising source of MSCs for Regenerative Medicine due to their peripheral location, which facilitates their collection, isolation, and expansion in culture. In contrast to conventional sources, the collection of dental pulp for stem cell isolation is non-invasive, which enhances its application as a valuable alternative. HDPSCs are distinguished by their well-established biological characteristics, making them particularly suitable for therapeutic applications.

In this study, methodologies were successfully employed to isolate, culture, cryopreserve and thaw hDPSCs without compromising their morphological or functional properties. Subsequent biological characterization revealed that these cells present normal proliferative activity and the ability to form colonies, which is a key indicator of their self-renewal capacity. Furthermore, hDPSCs exhibited the potential for trilineage differentiation, differentiating into adipogenic, chondrogenic and osteogenic lineages. The expression of several genes' characteristic of MSCs further confirmed their stemness properties. These findings strongly support the potential therapeutic application of hDPSCs in Regenerative Medicine, highlighting their suitability for future clinical interventions.

In conclusion, hDPSCs demonstrate promise as candidates for cell-based therapies in several clinical approaches, underlining their potential for advancing Regenerative Medicine.

References

1. Keshavarz, R.; Olsen, S.; Almeida, B. Using biomaterials to improve mesenchymal stem cell therapies for chronic, nonhealing wounds. *Bioeng Transl Med* **2024**, *9*, e10598, doi:10.1002/btm2.10598.

2. Langer, R.; Vacanti, J.P. Tissue engineering. *Science* **1993**, *260*, 920, doi:10.1126/science.8493529.

3. Campos, J.M.; Sousa, A.C.; Caseiro, A.R.; Pedrosa, S.S.; Pinto, P.O.; Branquinho, M.V.; Amorim, I.; Santos, J.D.; Pereira, T.; Mendonça, C.M.; et al. Dental pulp stem cells and Bonelike(®) for bone regeneration in ovine model. *Regen Biomater* **2019**, *6*, 49-59, doi:10.1093/rb/rby025.

4. Dominici, M.; Le Blanc, K.; Mueller, I.; Slaper-Cortenbach, I.; Marini, F.C.; Krause, D.S.; Deans, R.J.; Keating, A.; Prockop, D.J.; Horwitz, E.M. Minimal criteria for defining multipotent mesenchymal stromal cells. The International Society for Cellular Therapy position statement. *Cytotherapy* **2006**, *8*, 315-317, doi:https://doi.org/10.1080/14653240600855905.

5. Zhou, J.; Shi, Y. Mesenchymal stem/stromal cells (MSCs): origin, immune regulation, and clinical applications. *Cellular & Molecular Immunology* **2023**, *20*, 555-557, doi:10.1038/s41423-023-01034-9.

6. Friedenstein, A.J.; Chailakhjan, R.K.; Lalykina, K.S. The development of fibroblast colonies in monolayer cultures of guinea-pig bone marrow and spleen cells. *Cell Tissue Kinet* **1970**, *3*, 393-403, doi:10.1111/j.1365-2184.1970.tb00347.x.

7. Caplan, A.I. Mesenchymal stem cells. *J Orthop Res* **1991**, *9*, 641-650, doi:10.1002/jor.1100090504.

8. Viswanathan, S.; Shi, Y.; Galipeau, J.; Krampera, M.; Leblanc, K.; Martin, I.; Nolta, J.; Phinney, D.G.; Sensebe, L. Mesenchymal stem versus stromal cells: International Society for Cell & Gene Therapy (ISCT®) Mesenchymal Stromal Cell committee position statement on nomenclature. *Cytotherapy* **2019**, *21*, 1019-1024, doi:10.1016/j.jcyt.2019.08.002.

9. Wang, Y.; Fang, J.; Liu, B.; Shao, C.; Shi, Y. Reciprocal regulation of mesenchymal stem cells and immune responses. *Cell Stem Cell* **2022**, *29*, 1515-1530, doi:10.1016/j.stem.2022.10.001.

10. Horwitz, E.M.; Le Blanc, K.; Dominici, M.; Mueller, I.; Slaper-Cortenbach, I.; Marini, F.C.; Deans, R.J.; Krause, D.S.; Keating, A. Clarification of the nomenclature for MSC: The International Society for Cellular Therapy position statement. *Cytotherapy* **2005**, *7*, 393-395, doi:10.1080/14653240500319234.

11. Caplan, A.I. What's in a name? *Tissue Eng Part A* **2010**, *16*, 2415-2417, doi:10.1089/ten.TEA.2010.0216.

12. Caplan, A.I. Mesenchymal Stem Cells: Time to Change the Name! *Stem Cells Transl Med* **2017**, *6*, 1445-1451, doi:10.1002/sctm.17-0051.

13. Lee, B.C.; Kim, H.S.; Shin, T.H.; Kang, I.; Lee, J.Y.; Kim, J.J.; Kang, H.K.; Seo, Y.; Lee, S.; Yu, K.R.; et al. PGE2 maintains self-renewal of human adult stem cells via EP2-mediated autocrine signaling and its production is regulated by cell-to-cell contact. *Sci Rep* **2016**, *6*, 26298, doi:10.1038/srep26298.

14. Margiana, R.; Markov, A.; Zekiy, A.O.; Hamza, M.U.; Al-Dabbagh, K.A.; Al-Zubaidi, S.H.; Hameed, N.M.; Ahmad, I.; Sivaraman, R.; Kzar, H.H.; et al. Clinical application of mesenchymal stem cell in regenerative medicine: a narrative review. *Stem Cell Research & Therapy* **2022**, *13*, 366, doi:10.1186/s13287-022-03054-0.

15. Chamberlain, G.; Fox, J.; Ashton, B.; Middleton, J. Concise review: mesenchymal stem cells: their phenotype, differentiation capacity, immunological features, and potential for homing. *Stem cells* **2007**, *25*, 2739-2749.

16. Pittenger, M.F.; Mackay, A.M.; Beck, S.C.; Jaiswal, R.K.; Douglas, R.; Mosca, J.D.; Moorman, M.A.; Simonetti, D.W.; Craig, S.; Marshak, D.R. Multilineage potential of adult human mesenchymal stem cells. *science* **1999**, *284*, 143-147.

17. Izadpanah, R.; Trygg, C.; Patel, B.; Kriedt, C.; Dufour, J.; Gimble, J.M.; Bunnell, B.A. Biologic properties of mesenchymal stem cells derived from

bone marrow and adipose tissue. *J Cell Biochem* **2006**, *99*, 1285-1297, doi:10.1002/jcb.20904.

18. Zuk, P.A.; Zhu, M.; Mizuno, H.; Huang, J.; Futrell, J.W.; Katz, A.J.; Benhaim, P.; Lorenz, H.P.; Hedrick, M.H. Multilineage cells from human adipose tissue: implications for cell-based therapies. *Tissue Eng* **2001**, *7*, 211-228, doi:10.1089/107632701300062859.

19. Roubelakis, M.G.; Pappa, K.I.; Bitsika, V.; Zagoura, D.; Vlahou, A.; Papadaki, H.A.; Antsaklis, A.; Anagnou, N.P. Molecular and proteomic characterization of human mesenchymal stem cells derived from amniotic fluid: comparison to bone marrow mesenchymal stem cells. *Stem Cells Dev* **2007**, *16*, 931-952, doi:10.1089/scd.2007.0036.

20. Caseiro, A.R. Cell-based therapies in Regenerative Medicine: The therapeutic potential of umbilical cord and dental pulp derived stem/stromal cells. Institute for the Biomedical Sciences Abel Salazar - Porto University, 2019.

21. Zhang, Y.; Li, C.; Jiang, X.; Zhang, S.; Wu, Y.; Liu, B.; Tang, P.; Mao, N. Human placenta-derived mesenchymal progenitor cells support culture expansion of long-term culture-initiating cells from cord blood CD34+ cells. *Exp Hematol* **2004**, *32*, 657-664, doi:10.1016/j.exphem.2004.04.001.

22. Bieback, K.; Kern, S.; Klüter, H.; Eichler, H. Critical parameters for the isolation of mesenchymal stem cells from umbilical cord blood. *Stem Cells* **2004**, *22*, 625-634, doi:10.1634/stemcells.22-4-625.

23. Erices, A.; Conget, P.; Minguell, J.J. Mesenchymal progenitor cells in human umbilical cord blood. *Br J Haematol* **2000**, *109*, 235-242, doi:10.1046/j.1365-2141.2000.01986.x.

24. Bellagamba, B.C.; Grudzinski, P.B.; Ely, P.B.; Nader, P.d.J.H.; Nardi, N.B.; da Silva Meirelles, L. Induction of Expression of CD271 and CD34 in Mesenchymal Stromal Cells Cultured as Spheroids. *Stem Cells International* **2018**, *2018*, 7357213, doi:https://doi.org/10.1155/2018/7357213.

25. Simmons, P.J.; Torok-Storb, B. CD34 Expression by Stromal Precursors in Normal Human Adult Bone Marrow. *Blood* **1991**, *78*, 2848-2853, doi:https://doi.org/10.1182/blood.V78.11.2848.2848.

26. Lin, C.S.; Ning, H.; Lin, G.; Lue, T.F. Is CD34 truly a negative marker for mesenchymal stromal cells? *Cytotherapy* **2012**, *14*, 1159-1163, doi:10.3109/14653249.2012.729817.

27. Stagg, J.; Pommey, S.; Eliopoulos, N.; Galipeau, J. Interferon-γ-stimulated marrow stromal cells: a new type of nonhematopoietic antigen-presenting cell. *Blood* **2006**, *107*, 2570-2577, doi:10.1182/blood-2005-07-2793.

28. Romieu-Mourez, R.l.; Françoıs, M.r.; Boivin, M.-N.l.; Stagg, J.; Galipeau, J. Regulation of MHC Class II Expression and Antigen Processing in Murine and Human Mesenchymal Stromal Cells by IFN-γ, TGF-β, and Cell Density1. *The Journal of Immunology* **2007**, *179*, 1549-1558, doi:10.4049/jimmunol.179.3.1549.

29. Saeedi, P.; Halabian, R.; Imani Fooladi, A.A. A revealing review of mesenchymal stem cells therapy, clinical perspectives and Modification strategies. *Stem Cell Investig* **2019**, *6*, 34, doi:10.21037/sci.2019.08.11.

30. Patel, D.M.; Shah, J.; Srivastava, A.S. Therapeutic potential of mesenchymal stem cells in regenerative medicine. *Stem Cells Int* **2013**, *2013*, 496218, doi:10.1155/2013/496218.

31. Vasanthan, J.; Gurusamy, N.; Rajasingh, S.; Sigamani, V.; Kirankumar, S.; Thomas, E.L.; Rajasingh, J. Role of Human Mesenchymal Stem Cells in Regenerative Therapy. *Cells* **2020**, *10*, doi:10.3390/cells10010054.

32. Alonso-Goulart, V.; Ferreira, L.B.; Duarte, C.A.; Lima, I.L.d.; Ferreira, E.R.; Oliveira, B.C.d.; Vargas, L.N.; Moraes, D.D.d.; Silva, I.B.B.; Faria, R.d.O.; et al. Mesenchymal stem cells from human adipose tissue and bone repair: a literature review. *Biotechnology Research and Innovation* **2018**, *2*, 74-80, doi:https://doi.org/10.1016/j.biori.2017.10.005.

33. Semenova, E.; Chroscinska-Krawczyk, M.; Grudniak, M.P.; Oldak, T.; Machaj, E.K. Clinical application of AD-MSCs–A review. *Journal of Pre-Clinical and Clinical Research* **2018**, *12*.

34. int Anker, P.S.; Scherjon, S.A.; Kleijburg-Van der Keur, C.; Noort, W.A.; Claas, F.H.; Willemze, R.; Fibbe, W.E.; Kanhai, H.H. Amniotic fluid as a novel source

of mesenchymal stem cells for therapeutic transplantation. *Blood* **2003**, *102*, 1548-1549.

35. Srivastava, M.; Ahlawat, N.; Srivastava, A. Amniotic Fluid Stem Cells: A New Era in Regenerative Medicine. *J Obstet Gynaecol India* **2018**, *68*, 15-19, doi:10.1007/s13224-017-1034-z.

36. Baghaban Eslaminejad, M.; Jahangir, S. Amniotic fluid stem cells and their application in cell-based tissue regeneration. *Int J Fertil Steril* **2012**, *6*, 147-156.

37. Kaviani, A.; Perry, T.E.; Dzakovic, A.; Jennings, R.W.; Ziegler, M.M.; Fauza, D.O. The amniotic fluid as a source of cells for fetal tissue engineering. *J Pediatr Surg* **2001**, *36*, 1662-1665, doi:10.1053/jpsu.2001.27945.

38. Cananzi, M.; Atala, A.; de Coppi, P. Chapter 11 - Stem Cells Derived from Amniotic Fluid. In *Essentials of Stem Cell Biology (Third Edition)*, Lanza, R., Atala, A., Eds.; Academic Press: Boston, 2014; pp. 141-156.

39. Chanda, D.; Kumar, S.; Ponnazhagan, S. Therapeutic potential of adult bone marrow-derived mesenchymal stem cells in diseases of the skeleton. *J Cell Biochem* **2010**, *111*, 249-257, doi:10.1002/jcb.22701.

40. Friedenstein, A.; Chailakhyan, R.; Gerasimov, U. Bone marrow osteogenic stem cells: in vitro cultivation and transplantation in diffusion chambers. *Cell proliferation* **1987**, *20*, 263-272.

41. Costa-Pinto, A.R.; Correlo, V.M.; Sol, P.C.; Bhattacharya, M.; Charbord, P.; Delorme, B.; Reis, R.L.; Neves, N.M. Osteogenic Differentiation of Human Bone Marrow Mesenchymal Stem Cells Seeded on Melt Based Chitosan Scaffolds for Bone Tissue Engineering Applications. *Biomacromolecules* **2009**, *10*, 2067-2073, doi:10.1021/bm9000102.

42. Hassan, H.T.; El-Sheemy, M. Adult bone-marrow stem cells and their potential in medicine. *J R Soc Med* **2004**, *97*, 465-471, doi:10.1258/jrsm.97.10.465.

43. Yamada, Y.; Nakamura-Yamada, S.; Kusano, K.; Baba, S. Clinical Potential and Current Progress of Dental Pulp Stem Cells for Various Systemic Diseases in

Regenerative Medicine: A Concise Review. *Int J Mol Sci* **2019**, *20*, 1132, doi:10.3390/ijms20051132.

44. Gronthos, S.; Mankani, M.; Brahim, J.; Robey, P.G.; Shi, S. Postnatal human dental pulp stem cells (DPSCs) in vitro and in vivo. *Proceedings of the National Academy of Sciences* **2000**, *97*, 13625-13630.

45. Kerkis, I.; Ambrosio, C.E.; Kerkis, A.; Martins, D.S.; Zucconi, E.; Fonseca, S.A.; Cabral, R.M.; Maranduba, C.M.; Gaiad, T.P.; Morini, A.C.; et al. Early transplantation of human immature dental pulp stem cells from baby teeth to golden retriever muscular dystrophy (GRMD) dogs: Local or systemic? *J Transl Med* **2008**, *6*, 35, doi:10.1186/1479-5876-6-35.

46. Karbanová, J.; Soukup, T.; Suchánek, J.; Pytlík, R.; Corbeil, D.; Mokrý, J. Characterization of dental pulp stem cells from impacted third molars cultured in low serum-containing medium. *Cells Tissues Organs* **2011**, *193*, 344-365, doi:10.1159/000321160.

47. Rao, N.; Wang, X.; Xie, J.; Li, J.; Zhai, Y.; Li, X.; Fang, T.; Wang, Y.; Zhao, Y.; Ge, L. Stem Cells from Human Exfoliated Deciduous Teeth Ameliorate Diabetic Nephropathy In Vivo and In Vitro by Inhibiting Advanced Glycation End Product-Activated Epithelial-Mesenchymal Transition. *Stem Cells Int* **2019**, *2019*, 2751475, doi:10.1155/2019/2751475.

48. Mita, T.; Furukawa-Hibi, Y.; Takeuchi, H.; Hattori, H.; Yamada, K.; Hibi, H.; Ueda, M.; Yamamoto, A. Conditioned medium from the stem cells of human dental pulp improves cognitive function in a mouse model of Alzheimer's disease. *Behav Brain Res* **2015**, *293*, 189-197, doi:10.1016/j.bbr.2015.07.043.

49. Ito, T.; Ishigami, M.; Matsushita, Y.; Hirata, M.; Matsubara, K.; Ishikawa, T.; Hibi, H.; Ueda, M.; Hirooka, Y.; Goto, H.; et al. Secreted Ectodomain of SIGLEC-9 and MCP-1 Synergistically Improve Acute Liver Failure in Rats by Altering Macrophage Polarity. *Sci Rep* **2017**, *7*, 44043, doi:10.1038/srep44043.

50. Matsushita, Y.; Ishigami, M.; Matsubara, K.; Kondo, M.; Wakayama, H.; Goto, H.; Ueda, M.; Yamamoto, A. Multifaceted therapeutic benefits of factors derived from stem cells from human exfoliated deciduous teeth for acute

liver failure in rats. *J Tissue Eng Regen Med* **2017**, *11*, 1888-1896, doi:10.1002/term.2086.

51. Yamaza, T.; Alatas, F.S.; Yuniartha, R.; Yamaza, H.; Fujiyoshi, J.K.; Yanagi, Y.; Yoshimaru, K.; Hayashida, M.; Matsuura, T.; Aijima, R.; et al. In vivo hepatogenic capacity and therapeutic potential of stem cells from human exfoliated deciduous teeth in liver fibrosis in mice. *Stem Cell Res Ther* **2015**, *6*, 171, doi:10.1186/s13287-015-0154-6.

52. Hirata, M.; Ishigami, M.; Matsushita, Y.; Ito, T.; Hattori, H.; Hibi, H.; Goto, H.; Ueda, M.; Yamamoto, A. Multifaceted Therapeutic Benefits of Factors Derived From Dental Pulp Stem Cells for Mouse Liver Fibrosis. *Stem Cells Transl Med* **2016**, *5*, 1416-1424, doi:10.5966/sctm.2015-0353.

53. Hattori, Y.; Kim, H.; Tsuboi, N.; Yamamoto, A.; Akiyama, S.; Shi, Y.; Katsuno, T.; Kosugi, T.; Ueda, M.; Matsuo, S.; et al. Correction: Therapeutic Potential of Stem Cells from Human Exfoliated Deciduous Teeth in Models of Acute Kidney Injury. *PLoS One* **2015**, *10*, e0143561, doi:10.1371/journal.pone.0143561.

54. Sugimura-Wakayama, Y.; Katagiri, W.; Osugi, M.; Kawai, T.; Ogata, K.; Sakaguchi, K.; Hibi, H. Peripheral Nerve Regeneration by Secretomes of Stem Cells from Human Exfoliated Deciduous Teeth. *Stem Cells Dev* **2015**, *24*, 2687-2699, doi:10.1089/scd.2015.0104.

55. Zhang, Q.; Shi, S.; Liu, Y.; Uyanne, J.; Shi, Y.; Shi, S.; Le, A.D. Mesenchymal stem cells derived from human gingiva are capable of immunomodulatory functions and ameliorate inflammation-related tissue destruction in experimental colitis. *The Journal of Immunology* **2009**, *183*, 7787-7798.

56. Xu, X.; Chen, C.; Akiyama, K.; Chai, Y.; Le, A.; Wang, Z.; Shi, S. Gingivae contain neural-crest-and mesoderm-derived mesenchymal stem cells. *Journal of dental research* **2013**, *92*, 825-832.

57. Zhang, Q.Z.; Su, W.R.; Shi, S.H.; Wilder-Smith, P.; Xiang, A.P.; Wong, A.; Nguyen, A.L.; Kwon, C.W.; Le, A.D. Human gingiva-derived mesenchymal stem cells elicit polarization of m2 macrophages and enhance cutaneous wound healing. *Stem cells* **2010**, *28*, 1856-1868.

58. Venkatesh, D.; Kumar, K.P.M.; Alur, J.B. Gingival mesenchymal stem cells. *J Oral Maxillofac Pathol* **2017**, *21*, 296-298, doi:10.4103/jomfp.JOMFP_162_17.

59. Wada, N.; Menicanin, D.; Shi, S.; Bartold, P.M.; Gronthos, S. Immunomodulatory properties of human periodontal ligament stem cells. *Journal of cellular physiology* **2009**, *219*, 667-676.

60. Seo, B.-M.; Miura, M.; Gronthos, S.; Bartold, P.M.; Batouli, S.; Brahim, J.; Young, M.; Robey, P.G.; Wang, C.Y.; Shi, S. Investigation of multipotent postnatal stem cells from human periodontal ligament. *The Lancet* **2004**, *364*, 149-155.

61. Tomokiyo, A.; Yoshida, S.; Hamano, S.; Hasegawa, D.; Sugii, H.; Maeda, H. Detection, Characterization, and Clinical Application of Mesenchymal Stem Cells in Periodontal Ligament Tissue. *Stem Cells International* **2018**, *2018*, 5450768, doi:10.1155/2018/5450768.

62. Moshaverinia, A.; Xu, X.; Chen, C.; Ansari, S.; Zadeh, H.H.; Snead, M.L.; Shi, S. Application of stem cells derived from the periodontal ligament or gingival tissue sources for tendon tissue regeneration. *Biomaterials* **2014**, *35*, 2642-2650, doi:10.1016/j.biomaterials.2013.12.053.

63. Fukuchi, Y.; Nakajima, H.; Sugiyama, D.; Hirose, I.; Kitamura, T.; Tsuji, K. Human Placenta-Derived Cells Have Mesenchymal Stem/Progenitor Cell Potential. *STEM CELLS* **2004**, *22*, 649-658, doi:https://doi.org/10.1634/stemcells.22-5-649.

64. Fazekasova, H.; Lechler, R.; Langford, K.; Lombardi, G. Placenta-derived MSCs are partially immunogenic and less immunomodulatory than bone marrow-derived MSCs. *Journal of Tissue Engineering and Regenerative Medicine* **2011**, *5*, 684-694, doi:https://doi.org/10.1002/term.362.

65. de la Torre, P.; Pérez-Lorenzo, M.J.; Flores, A.I. Human placenta-derived mesenchymal stromal cells: a review from basic research to clinical applications. In *Stromal Cells-Structure, Function, and Therapeutic Implications*; IntechOpen: 2018.

66. Guan, L.X.; Guan, H.; Li, H.B.; Ren, C.A.; Liu, L.; Chu, J.J.; Dai, L.J. Therapeutic efficacy of umbilical cord-derived mesenchymal stem cells in patients with type 2 diabetes. *Exp Ther Med* **2015**, *9*, 1623-1630, doi:10.3892/etm.2015.2339.

67. Wang, H.S.; Hung, S.C.; Peng, S.T.; Huang, C.C.; Wei, H.M.; Guo, Y.J.; Fu, Y.S.; Lai, M.C.; Chen, C.C. Mesenchymal stem cells in the Wharton's jelly of the human umbilical cord. *Stem cells* **2004**, *22*, 1330-1337.

68. Miura, M.; Gronthos, S.; Zhao, M.; Lu, B.; Fisher, L.W.; Robey, P.G.; Shi, S. SHED: Stem cells from human exfoliated deciduous teeth. *Proceedings of the National Academy of Sciences* **2003**, *100*, 5807-5812, doi:doi:10.1073/pnas.0937635100.

69. Morsczeck, C.; Schmalz, G.; Reichert, T.E.; Völlner, F.; Galler, K.; Driemel, O. Somatic stem cells for regenerative dentistry. *Clinical Oral Investigations* **2008**, *12*, 113-118, doi:10.1007/s00784-007-0170-8.

70. Sonoyama, W.; Liu, Y.; Fang, D.; Yamaza, T.; Seo, B.M.; Zhang, C.; Liu, H.; Gronthos, S.; Wang, C.Y.; Wang, S.; et al. Mesenchymal stem cell-mediated functional tooth regeneration in swine. *PLoS One* **2006**, *1*, e79, doi:10.1371/journal.pone.0000079.

71. Yoshida, S.; Tomokiyo, A.; Hasegawa, D.; Hamano, S.; Sugii, H.; Maeda, H. Insight into the Role of Dental Pulp Stem Cells in Regenerative Therapy. *Biology* **2020**, *9*, 160.

72. Papaccio, G.; Graziano, A.; d'Aquino, R.; Graziano, M.F.; Pirozzi, G.; Menditti, D.; De Rosa, A.; Carinci, F.; Laino, G. Long-term cryopreservation of dental pulp stem cells (SBP-DPSCs) and their differentiated osteoblasts: a cell source for tissue repair. *J Cell Physiol* **2006**, *208*, 319-325, doi:10.1002/jcp.20667.

73. Kawashima, N. Characterisation of dental pulp stem cells: a new horizon for tissue regeneration? *Archives of oral biology* **2012**, *57*, 1439-1458.

74. Ledesma-Martínez, E.; Mendoza-Núñez, V.M.; Santiago-Osorio, E. Mesenchymal Stem Cells Derived from Dental Pulp: A Review. *Stem Cells Int* **2016**, *2016*, 4709572, doi:10.1155/2016/4709572.

75. Masuda, K.; Han, X.; Kato, H.; Sato, H.; Zhang, Y.; Sun, X.; Hirofuji, Y.; Yamaza, H.; Yamada, A.; Fukumoto, S. Dental Pulp-Derived Mesenchymal Stem Cells for Modeling Genetic Disorders. *Int J Mol Sci* **2021**, *22*, 2269.

76. La Noce, M.; Paino, F.; Spina, A.; Naddeo, P.; Montella, R.; Desiderio, V.; De Rosa, A.; Papaccio, G.; Tirino, V.; Laino, L. Dental pulp stem cells: State of the art and suggestions for a true translation of research into therapy. *Journal of Dentistry* **2014**, *42*, 761-768, doi:https://doi.org/10.1016/j.jdent.2014.02.018.

77. Gronthos, S.; Brahim, J.; Li, W.; Fisher, L.W.; Cherman, N.; Boyde, A.; DenBesten, P.; Robey, P.G.; Shi, S. Stem cell properties of human dental pulp stem cells. *J Dent Res* **2002**, *81*, 531-535, doi:10.1177/154405910208100806.

78. Caseiro, A.; Pereira, T.; Bártolo, P.; Santos, J.; Luís, A.; Maurício, A. Mesenchymal stem cells and biomaterials systems–perspectives for skeletal muscle tissue repair and regeneration. *Procedia engineering* **2015**, *110*, 90-97.

79. Gärtner, A.; Pereira, T.; Armada-da-Silva, P.; Amado, S.; Veloso, A.; Amorim, I.; Ribeiro, J.; Santos, J.; Bárcia, R.; Cruz, P. Effects of umbilical cord tissue mesenchymal stem cells (UCX®) on rat sciatic nerve regeneration after neurotmesis injuries. *Journal of stem cells & regenerative medicine* **2014**, *10*, 14.

80. Pereira, T.; Ivanova, G.; Caseiro, A.R.; Barbosa, P.; Bártolo, P.J.; Santos, J.D.; Luís, A.L.; Maurício, A.C. MSCs Conditioned Media and Umbilical Cord Blood Plasma Metabolomics and Composition. *PLOS ONE* **2014**, *9*, e113769, doi:10.1371/journal.pone.0113769.

81. Nakatsuka, R.; Nozaki, T.; Uemura, Y.; Matsuoka, Y.; Sasaki, Y.; Shinohara, M.; Ohura, K.; Sonoda, Y. 5-Aza-2′-deoxycytidine treatment induces skeletal myogenic differentiation of mouse dental pulp stem cells. *Archives of Oral Biology* **2010**, *55*, 350-357.

82. Mrozik, K.M.; Zilm, P.S.; Bagley, C.J.; Hack, S.; Hoffmann, P.; Gronthos, S.; Bartold, P.M. Proteomic Characterization of Mesenchymal Stem Cell-Like Populations Derived from Ovine Periodontal Ligament, Dental Pulp, and Bone

Marrow: Analysis of Differentially Expressed Proteins. *Stem Cells and Development* **2010**, *19*, 1485-1499, doi:10.1089/scd.2009.0446.

83. Cheng, P.-H.; Snyder, B.; Fillos, D.; Ibegbu, C.C.; Huang, A.H.-C.; Chan, A.W. Postnatal stem/progenitor cells derived from the dental pulp of adult chimpanzee. *BMC cell biology* **2008**, *9*, 1-11.

84. Iohara, K.; Zheng, L.; Ito, M.; Tomokiyo, A.; Matsushita, K.; Nakashima, M. Side Population Cells Isolated from Porcine Dental Pulp Tissue with Self-Renewal and Multipotency for Dentinogenesis, Chondrogenesis, Adipogenesis, and Neurogenesis. *Stem Cells* **2006**, *24*, 2493-2503, doi:10.1634/stemcells.2006-0161.

85. Spath, L.; Rotilio, V.; Alessandrini, M.; Gambara, G.; De Angelis, L.; Mancini, M.; Mitsiadis, T.A.; Vivarelli, E.; Naro, F.; Filippini, A.; et al. Explant-derived human dental pulp stem cells enhance differentiation and proliferation potentials. *Journal of Cellular and Molecular Medicine* **2010**, *14*, 1635-1644, doi:https://doi.org/10.1111/j.1582-4934.2009.00848.x.

86. Hilkens, P.; Gervois, P.; Fanton, Y.; Vanormelingen, J.; Martens, W.; Struys, T.; Politis, C.; Lambrichts, I.; Bronckaers, A. Effect of isolation methodology on stem cell properties and multilineage differentiation potential of human dental pulp stem cells. *Cell and Tissue Research* **2013**, *353*, 65-78, doi:10.1007/s00441-013-1630-x.

87. Laino, G.; D'Aquino, R.; Graziano, A.; Lanza, V.; Carinci, F.; Naro, F.; Pirozzi, G.; Papaccio, G. A new population of human adult dental pulp stem cells: A useful source of living autologous fibrous bone tissue (LAB). *Journal of Bone and Mineral Research* **2005**, *20*, 1394-1402, doi:10.1359/JBMR.050325.

88. Anil, S.; Ramya, R.; Thomas, N.; George, J.; Sweety, V. Dental pulp stem cells and banking of teeth as a lifesaving therapeutic vista. *BIOCELL* **2022**, *47*, 71-80, doi:10.32604/biocell.2023.024334.

89. Iohara, K.; Murakami, M.; Takeuchi, N.; Osako, Y.; Ito, M.; Ishizaka, R.; Utunomiya, S.; Nakamura, H.; Matsushita, K.; Nakashima, M. A novel combinatorial therapy with pulp stem cells and granulocyte colony-stimulating factor for total pulp regeneration. *Stem Cells Transl Med* **2013**, *2*, 521-533, doi:10.5966/sctm.2012-0132.

90. Gandia, C.; Armiñan, A.; García-Verdugo, J.M.; Lledó, E.; Ruiz, A.; Miñana, M.D.; Sanchez-Torrijos, J.; Payá, R.; Mirabet, V.; Carbonell-Uberos, F.; et al. Human dental pulp stem cells improve left ventricular function, induce angiogenesis, and reduce infarct size in rats with acute myocardial infarction. *Stem Cells* **2008**, *26*, 638-645, doi:10.1634/stemcells.2007-0484.

91. Ahmed, N.E.-M.B.; Murakami, M.; Hirose, Y.; Nakashima, M. Therapeutic Potential of Dental Pulp Stem Cell Secretome for Alzheimer's Disease Treatment: An In Vitro Study. *Stem Cells International* **2016**, *2016*, 8102478, doi:https://doi.org/10.1155/2016/8102478.

92. Carnevale, G.; Riccio, M.; Pisciotta, A.; Beretti, F.; Maraldi, T.; Zavatti, M.; Cavallini, G.M.; La Sala, G.B.; Ferrari, A.; De Pol, A. In vitro differentiation into insulin-producing β-cells of stem cells isolated from human amniotic fluid and dental pulp. *Digestive and Liver Disease* **2013**, *45*, 669-676, doi:https://doi.org/10.1016/j.dld.2013.02.007.

93. Hirose, Y.; Yamamoto, T.; Nakashima, M.; Funahashi, Y.; Matsukawa, Y.; Yamaguchi, M.; Kawabata, S.; Gotoh, M. Injection of Dental Pulp Stem Cells Promotes Healing of Damaged Bladder Tissue in a Rat Model of Chemically Induced Cystitis. *Cell Transplant* **2016**, *25*, 425-436, doi:10.3727/096368915x689523.

94. Yasui, T.; Mabuchi, Y.; Morikawa, S.; Onizawa, K.; Akazawa, C.; Nakagawa, T.; Okano, H.; Matsuzaki, Y. Isolation of dental pulp stem cells with high osteogenic potential. *Inflammation and Regeneration* **2017**, *37*, 8, doi:10.1186/s41232-017-0039-4.

95. Fujii, Y.; Hatori, A.; Chikazu, D.; Ogasawara, T. Application of Dental Pulp Stem Cells for Bone and Neural Tissue Regeneration in Oral and Maxillofacial Region. *Stem Cells Int* **2023**, *2023*, 2026572, doi:10.1155/2023/2026572.

96. Bai, X.; Cao, R.; Wu, D.; Zhang, H.; Yang, F.; Wang, L. Dental Pulp Stem Cells for Bone Tissue Engineering: A Literature Review. *Stem Cells International* **2023**, *2023*, 7357179, doi:https://doi.org/10.1155/2023/7357179.

97. Hao, X.; Li, D.; Zhang, D.; Jia, L. Microarray analysis of long non-coding RNAs related to osteogenic differentiation of human dental pulp stem cells. *Journal of Dental Sciences* **2022**, *17*, 733-743, doi:https://doi.org/10.1016/j.jds.2021.10.014.

98. Xie, H.; Lin, Y.; Fang, F. Glycogen synthase kinase-3β inhibitor promotes the migration and osteogenic differentiation of rat dental pulp stem cells via the β-catenin/PI3K/Akt signaling pathway. *Journal of Dental Sciences* **2022**, *17*, 802-810, doi:https://doi.org/10.1016/j.jds.2021.09.035.

99. Pinto, P.O.; Branquinho, M.V.; Caseiro, A.R.; Sousa, A.C.; Brandão, A.; Pedrosa, S.S.; Alvites, R.D.; Campos, J.M.; Santos, F.L.; Santos, J.D.; et al. The application of Bonelike® Poro as a synthetic bone substitute for the management of critical-sized bone defects - A comparative approach to the autograft technique - A preliminary study. *Bone Reports* **2021**, *14*, 101064, doi:https://doi.org/10.1016/j.bonr.2021.101064.

100. Alge, D.L.; Zhou, D.; Adams, L.L.; Wyss, B.K.; Shadday, M.D.; Woods, E.J.; Gabriel Chu, T.; Goebel, W.S. Donor-matched comparison of dental pulp stem cells and bone marrow-derived mesenchymal stem cells in a rat model. *Journal of tissue engineering and regenerative medicine* **2010**, *4*, 73-81.

101. Suchánek, J.; Soukup, T.; Ivancaková, R.; Karbanová, J.; Hubková, V.; Pytlík, R.; Kucerová, L. Human dental pulp stem cells--isolation and long term cultivation. *Acta Medica (Hradec Kralove)* **2007**, *50*, 195-201.

102. Naz, S.; Khan, F.R.; Zohra, R.R.; Lakhundi, S.S.; Khan, M.S.; Mohammed, N.; Ahmad, T. Isolation and culture of dental pulp stem cells from permanent and deciduous teeth. *Pak J Med Sci* **2019**, *35*, 997-1002, doi:10.12669/pjms.35.4.540.

103. Pisciotta, A.; Carnevale, G.; Meloni, S.; Riccio, M.; Biasi, S.; Gibellini, L.; Ferrari, A.; Bruzzesi, G.; Pol, A. Human Dental pulp stem cells (hDPSCs): Isolation, enrichment and comparative differentiation of two sub-populations Integrative control of development. *BMC Developmental Biology* **2015**, *15*, doi:10.1186/s12861-015-0065-x.

104. Rodas-Junco, B.A.; Villicaña, C. Dental Pulp Stem Cells: Current Advances in Isolation, Expansion and Preservation. *Tissue Engineering and Regenerative Medicine* **2017**, *14*, 333-347, doi:10.1007/s13770-017-0036-3.

105. Ferro, F.; Spelat, R.; Baheney, C.S. Dental pulp stem cell (DPSC) isolation, characterization, and differentiation. In *Stem Cells and Tissue Repair*; Springer: 2014; pp. 91-115.

106. Machado, C.d.V.; Carvalho, C.M.; Campos, T.M.C.; Passos, S.T.; Telles, P.D.d.S. Isolation and culture of stem cells derived from dental pulp of permanent teeth: a successful method. *RFO UPF* **2015**, *20*, 159-163.

107. Mehrabani, D.; Mahdiyar, P.; Torabi, K.; Robati, R.; Zare, S.; Dianatpour, M.; Tamadon, A. Growth kinetics and characterization of human dental pulp stem cells: Comparison between third molar and first premolar teeth. *Journal of Clinical and Experimental Dentistry* **2017**, *9*, doi:10.4317/jced.52824.

108. Yu, J.; He, H.; Tang, C.; Zhang, G.; Li, Y.; wang, r.; Shi, J.; Jin, Y. Differentiation potential of STRO-1+ dental pulp stem cells changes during cell passaging. *BMC cell biology* **2010**, *11*, 32, doi:10.1186/1471-2121-11-32.

109. Anil, S.; Thomas, N.G.; Chalisserry, E.P.; Dalvi, Y.B.; Ramadoss, R.; Vellappally, S. Isolation, Culture, and Characterization of Dental Pulp Stem Cells from Human Deciduous and Permanent Teeth. *JoVE* **2024**, e65767, doi:doi:10.3791/65767.

110. Bressan, E.; Ferroni, L.; Gardin, C.; Pinton, P.; Stellini, E.; Botticelli, D.; Sivolella, S.; Zavan, B. Donor Age-Related Biological Properties of Human Dental Pulp Stem Cells Change in Nanostructured Scaffolds. *PloS one* **2012**, *7*, e49146, doi:10.1371/journal.pone.0049146.

111. Lizier, N.F.; Kerkis, A.; Gomes, C.M.; Hebling, J.; Oliveira, C.F.; Caplan, A.I.; Kerkis, I. Scaling-up of dental pulp stem cells isolated from multiple niches. *PLoS One* **2012**, *7*, e39885, doi:10.1371/journal.pone.0039885.

112. O'Connor, K. A cautionary tale about the use of colony-forming efficiency as a proxy for the survival of mesenchymal stem cells. *Stem Cell Res Ther* **2020**, *11*, 292, doi:10.1186/s13287-020-01805-5.

113. Chan, Y.-H.; Ho, K.N.; Lee, J.; Chou, M.-J.; Lew, W.-Z.; Huang, H.-M.; Lai, P.-C.; Feng, S.-W. Melatonin enhances osteogenic differentiation of dental pulp mesenchymal stem cells by regulating MAPK pathways and promotes the efficiency of bone regeneration in calvarial bone defects. *Stem Cell Research & Therapy* **2022**, *13*, doi:10.1186/s13287-022-02744-z.

114. Labedz-Maslowska, A.; Bryniarska, N.; Kubiak, A.; Kaczmarzyk, T.; Sekula-Stryjewska, M.; Noga, S.; Boruczkowski, D.; Madeja, Z.; Zuba-Surma, E. Multilineage Differentiation Potential of Human Dental Pulp Stem Cells-Impact of 3D and Hypoxic Environment on Osteogenesis In Vitro. *Int J Mol Sci* **2020**, *21*, doi:10.3390/ijms21176172.

115. Qu, G.; Li, Y.; Chen, L.; Chen, Q.; Zou, D.; Yang, C.; Zhou, Q. Comparison of Osteogenic Differentiation Potential of Human Dental-Derived Stem Cells Isolated from Dental Pulp, Periodontal Ligament, Dental Follicle, and Alveolar Bone. *Stem Cells International* **2021**, *2021*, 6631905, doi:https://doi.org/10.1155/2021/6631905.

116. Han, S.-M.; Han, S.-H.; Coh, Y.-R.; Jang, G.; Chan Ra, J.; Kang, S.-K.; Lee, H.-W.; Youn, H.-Y. Enhanced proliferation and differentiation of Oct4- and Sox2-overexpressing human adipose tissue mesenchymal stem cells. *Experimental & Molecular Medicine* **2014**, *46*, e101-e101, doi:10.1038/emm.2014.28.

117. Okolicsanyi, R.; Camilleri, E.; Oikari, L.; Yu, C.; Cool, S.; Wijnen, A.; Griffiths, L.; Haupt, L. Human Mesenchymal Stem Cells Retain Multilineage Differentiation Capacity Including Neural Marker Expression after Extended In Vitro Expansion. *PloS one* **2015**, *10*, e0137255, doi:10.1371/journal.pone.0137255.

118. Wu, Z.; Zhang, Z.; Lei, Z.; Lei, P. CD14: Biology and role in the pathogenesis of disease. *Cytokine & Growth Factor Reviews* **2019**, *48*, 24-31, doi:https://doi.org/10.1016/j.cytogfr.2019.06.003.

119. Pilz, G.A.; Braun, J.; Ulrich, C.; Felka, T.; Warstat, K.; Ruh, M.; Schewe, B.; Abele, H.; Larbi, A.; Aicher, W.K. Human mesenchymal stromal cells express CD14 cross-reactive epitopes. *Cytometry A* **2011**, *79*, 635-645, doi:10.1002/cyto.a.21073.

120. Nishihira, S.; Okubo, N.; Takahashi, N.; Ishisaki, A.; Sugiyama, Y.; Chosa, N. High-cell density-induced VCAM1 expression inhibits the migratory ability of mesenchymal stem cells. *Cell Biol Int* **2011**, *35*, 475-481, doi:10.1042/cbi20100372.

121. Zhao, A.G.; Shah, K.; Freitag, J.; Cromer, B.; Sumer, H. Differentiation Potential of Early- and Late-Passage Adipose-Derived Mesenchymal Stem Cells Cultured under Hypoxia and Normoxia. *Stem Cells Int* **2020**, *2020*, 8898221, doi:10.1155/2020/8898221.

122. Kwist, K.; Bridges, W.; Burg, K. The effect of cell passage number on osteogenic and adipogenic characteristics of D1 cells. *Cytotechnology* **2015**, *68*, doi:10.1007/s10616-015-9883-8.

123. Yang, Y.-H.K.; Ogando, C.R.; Wang See, C.; Chang, T.-Y.; Barabino, G.A. Changes in phenotype and differentiation potential of human mesenchymal stem cells aging in vitro. *Stem Cell Research & Therapy* **2018**, *9*, 131, doi:10.1186/s13287-018-0876-3.

CHAPTER III

FABRICATION AND CHARACTERIZATION OF A 3D SCAFFOLD FOR REGENERATIVE MEDICINE

[This page is intentionally left blank.]

Introductory Note

As mentioned in the last chapter, Regenerative Medicine comprises a wide range of techniques aimed at repairing and restoring damaged tissues and organs. Within this field, bone regeneration has emerged as an important area of study, addressing the need for more effective treatments for fractures, bone defects, and degenerative conditions.

Bone tissue plays a crucial role in homeostasis and in functionality of vital organs through continuous, lifelong remodeling [1]. This dynamic process allows bone to repair and regenerate minor defects with considerable efficiency. However, when it comes to the regeneration of large bone segment defects, known as critical-sized defects—typically defined as defects larger than approximately 3 cm—the body's natural healing capacity is often insufficient [2]. These defects, which can arise from various causes such as trauma, tumor resection, reconstructive surgery, congenital abnormalities, infections, or other surgical interventions, may exhibit slow, partial, or even complete failure to heal. This lack of adequate recovery poses significant threats to the overall health and well-being of affected individuals [3].

Bone regeneration is a highly complex and multifaceted process that can be delineated into three stages (**Figure 1**) [4]. After fracture, the first stage involves the hematoma formation, which serves to bridge the defect site. Following a severe injury, the rupture of blood vessels leads to ischemia at the fracture ends, resulting in necrosis of soft and bone tissues. This necrotic environment triggers an aseptic inflammatory response, wherein neutrophils, macrophages, lymphocytes, and monocytes infiltrate the hematoma, progressively clearing it of necrotic tissue and dead bone. As the hematoma transitions into granulation tissue, fibroblasts within the granulation tissue synthesize and secrete substantial amounts of collagen fibers. These collagen fibers subsequently transform into fibrous connective tissue, forming fibrous junctions that contribute to initial stabilization. The second stage is characterized by the formation of a primary callus, indicating the beginning of clinical healing. During this phase, new bone begins to form, gradually bridging the fracture site. Finally, the third stage involves the remodeling of the callus. Once the fracture has fully healed, the newly formed bone undergoes a remodeling process, where the stress-bearing regions of the fracture are progressively strengthened in response to weight-bearing activities, while the stress-free

portions of the callus are resorbed [5]. Hematoma formation, as the initial natural scaffold in the bone healing process, plays a crucial role in cellular growth and development [6]. It has long been recognized as a key factor in stimulating the chemotaxis of inflammatory immune cells and promoting the recruitment of bone mesenchymal progenitor cells [7]. This early phase of hematoma formation also provides the first hemostatic and immune microenvironment, which is essential for guiding subsequent bone regeneration processes. A particularly critical aspect of successful bone regeneration is the integration of hematomas formed at both ends of the fracture. As the size of the bone defect increases, the likelihood of successful healing diminishes, largely because the separate hematomas at the defect ends may fail to merge and bridge the gap [8]. Therefore, early intervention in bone repair is paramount in the treatment of bone defects, as it can significantly influence the overall healing outcome.

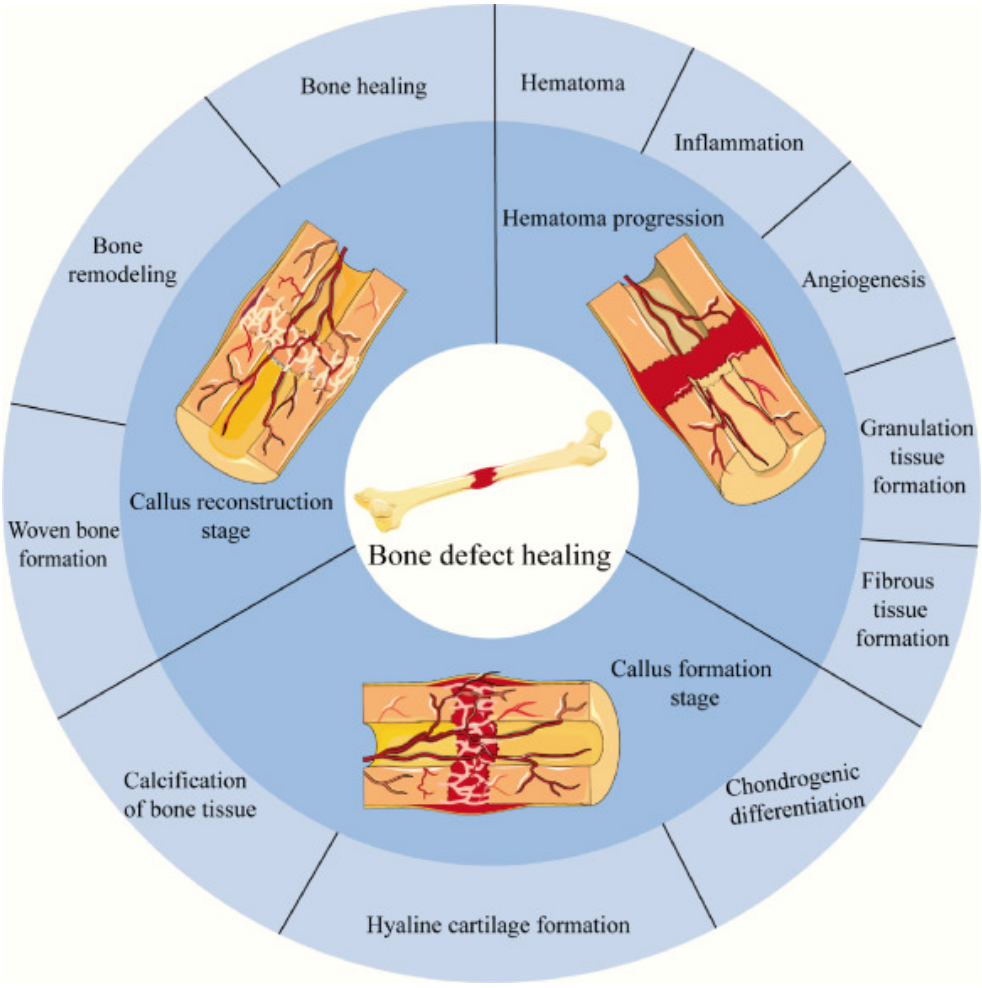


Figure 1. The bone fracture healing process. It can be categorized into three primary stages: hematoma formation, primary callus formation, and callus

repair and remodeling (adapted from [1], Copyright (5851501384882) with permission from Elsevier).

The current gold standard for clinical bone repair and reconstruction is the use of autografts. Nonetheless, autografts present several significant limitations, including persistent pain, limited availability of graft material, high morbidity at the donor site, potential infections, and secondary injuries, all of which can lead to suboptimal postoperative outcomes [9]. While allografts offer reduced donor-site morbidity compared to autografts, they are more prone to immune rejection and the transmission of infectious diseases [10].

As advancements in bone defect treatment continue, biomaterials have emerged as a promising therapeutic approach. Despite their availability and reproducibility, these materials often do not fully integrate with the host bone after implantation and may become encapsulated in fibrous tissue, which can hinder the bone's regenerative capacity. Therefore, it is crucial to investigate different techniques and biomaterials to enhance early bone healing to overcome the limitations of current clinical treatments and accelerate the bone regeneration process [11].

The following chapter presents the manufacture of synthetic bone grafts that closely replicate the complex architecture of natural bone, specifically aimed at the healing of critical-sized defects. In this innovative study, scaffolds were developed for the first time using a combination of polycaprolactone (PCL), hydroxyapatite nanoparticles (nHA), and polyethylene glycol diacrylate (PEGDA) via an extrusion-based additive manufacturing technique. Following the fabrication process, the surface chemistry of the 3D-printed scaffolds was extensively characterized. Additionally, the morphological properties were assessed, and compression tests were conducted to evaluate the mechanical strength of the scaffolds. Further *in vitro* characterization was performed to assess the cytocompatibility of these scaffolds.

[This page is intentionally left blank.]

Assessment of 3D-Printed Polycaprolactone, Hydroxyapatite Nanoparticles and Diacrylate Poly(ethylene glycol) Scaffolds for Bone Regeneration

Ana Catarina Sousa, Sara Biscaia, Rui Alvites, Mariana Branquinho, Bruna Lopes, Patrícia Sousa, Joana Valente, Margarida Franco, José Domingos Santos, Carla Mendonça, Luís Atayde, Nuno Alves and Ana Colette Maurício

In *Pharmaceutics*

DOI: 10.3390/pharmaceutics14122643

[This page is intentionally left blank.]

Article

Assessment of 3D printed polycaprolactone, hydroxyapatite nanoparticles and polyethylene glycol diacrylate scaffolds for bone regeneration

Ana Catarina Sousa [1,2,3], Sara Biscaia [4], Rui Alvites [1,2,3], Mariana Branquinho [1,2,3], Bruna Lopes [1,2,3], Patrícia Sousa [1,2,3], Joana Valente [4], Margarida Franco [4], José Domingos Santos [5,6], Luís Atayde [1,2,3], Nuno Alves [4,†] and Ana Colette Maurício [1,2,3,†,*]

[1] Veterinary Clinics Department, Abel Salazar Biomedical Sciences Institute (ICBAS), Porto, Portugal; anacatarinasoaressousa@hotmail.com (A.C.S.); ruialvites@hotmail.com (R.A.); m.esteves.vieira@gmail.com (M.B.); brunisabel95@gmail.com (B.L); pfrfs_10@hotmail.com (P.S.)

[2] Animal Science Studies Centre (CECA), Agroenvironment, Technologies and Sciences Institute (ICETA), University of Porto (UP), Rua D. Manuel II, Apartado 55142, 4051-401 Porto, Portugal

[3] Associate Laboratory for Animal and Veterinary Sciences (AL4AnimalS), Lisbon, Portugal

[4] Centre for Rapid and Sustainable Product Development (CDRSP), Polytechnic of Leiria, 2411-901 Leiria, Portugal; sara.biscaia@ipleiria.pt (S.B.); joana.valente@ipleiria.pt (J.F.A.V.); margarida.franco@ipleiria.pt (M.F.); nuno.alves@ipleiria.pt (N.A.)

[5] REQUIMTE-LAQV, Departamento de Engenharia Metalúrgica e Materiais, Faculdade de Engenharia, Universidade do Porto, Rua Dr. Roberto Frias, 4200-465, Porto, Portugal; jdsantos@fe.up.pt (J.D.S.)

† These authors contributed equally to this work.

* Correspondence: ana.colette@hotmail.com/acmauricio@icbas.up.pt (A.C.M)

Abstract: Notwithstanding the advances achieved in the last decades in the field of synthetic bone substitutes, the development of biodegradable 3D scaffolds with ideal mechanical and biological properties remains an unattained challenge. In this work, a novel approach is explored to produce synthetic bone grafts mimicking the complex bone structure using additive manufacturing. For the first time, scaffolds were produced, using an extrusion technique, composed of a thermoplastic polymer, polycaprolactone (PCL), hydroxyapatite nanoparticles (HANp), and polyethylene glycol diacrylate (PEGDA). These scaffolds were further compared with two groups of scaffolds: one composed of PCL and another of PCL and HANp. After production, optimisation and characterisation of these scaffolds, an *in vitro* evaluation was performed using human dental pulp stem/stromal cells (hDPSCs). Through the findings it was possible to conclude that PEGDA scaffolds were successfully produced presenting networks of interconnected channels, presenting hydrophilic properties (15.15 ± 4.06º), adequate mechanical performance (10.41MPa ± 0.934), and allowing a cell viability significantly superior to the other groups analysed. To conclude, findings in this study demonstrated that PCL, HANp and PEGDA scaffolds may have promising effects on bone regeneration and might open new insights for 3D tissue substitutes.

Keywords: Additive manufacturing; Biomaterials; Bone; Bone regeneration, Critical Bone Defects; Hydroxyapatite nanoparticles; Polycaprolactone; Polyethylene glycol diacrylate; Scaffolds.

---

1. Introduction

The population aging leads to a remarkable increase in the number of degenerative diseases, osteogenic disorders, fractures, and bone infections [1,2]. Although bone tissue can heal itself to a certain extent following bone pathology, when it concerns critical-sized defects (above about 3 cm), it may not be fully restored [3-5]. Particularly in such cases, the reconstruction of bone defects, with mechanical integrity to the original surrounding bone tissues is essential for a patient's rehabilitation [6]. Therefore, the search for new solutions has focused on tissue engineering through the development of three-dimensional (3D) structures, namely scaffolds for the regeneration of bone tissues [7-10]. Some properties must be considered when producing scaffolds for bone regeneration: (a) biocompatibility

devoid of unchained negative biological response in the body; (b) osteoconduction to promote cell adhesion and bone growth; (c) biodegradability to ensure controlled replacement of the biomaterial by the neoformed bone; (d) mechanical properties to ensure support during bone bridging; (e) sterility of the material ; and (f) appropriate design in terms of porosity, interconnectivity and pore size to provide the cell proliferation and angiogenesis [11-15]. In addition to the development of biomaterial support, cells and growth factors have an important role in the formation of biological substitute, so it is necessary to resort to Regenerative Medicine and tissue engineering [16]. The use of biomaterials with mesenchymal stem cells (MSCs) allows the proliferative and differentiation capacities of the latter to work in synergy with scaffolding properties [1,17].

According to the literature, synthetic rigid porous scaffolds have usually been made based on hydroxyapatite nanoparticles (HANp), biphasic calcium phosphate (BCP), beta-tricalcium phosphate (β-TCP), and polycaprolactone (PCL) [18-21]. Several studies combined PCL and HANp in scaffolds due to their properties and achieved good results inherent to bone regeneration both *in vitro* and *in vivo* [22-31]. PCL has been widely used due to its good biocompatibility, biodegradability, ease of processing (melting point between 55 and 60°C) and the fact that its blends well with other materials such as ceramics [32-34]. Furthermore, HANp, as a biomaterial, presents good stability, biocompatibility, degradability, promotes adhesion/proliferation of osteoblasts and has the potential to form chemical bonds with the bone itself [35-38]. Previous studies, consider PEGDA hydrogel as an effective biomaterial in bone regeneration due to its properties such as strength, gelation process, hydrophilicity, and cell adhesion [39-44].

Today, several additive manufacturing techniques are used to produce complex bone implants, namely, selective laser sintering, selective laser melting, stereolithography, electron beam melting, electrospinning, and fused deposition modelling [45]. Fused deposition modelling, commonly known as extrusion-based processes, is a promising 3D printing and manufacturing technique in the production of interconnected porous scaffolds [46]. This technique is easy to operate, safe, reliable, has controllable, and the produced structures normally have good mechanical properties [4].

For the present study, combined scaffolds of PCL, HANp, and PEGDA were produced by an extrusion additive manufacturing system. Subsequently, the surface chemistry of 3D printed scaffolds was characterised using Fourier Transform Infrared Spectroscopy (FTIR) and Contact Angle Measurement. The morphological properties were evaluated by X-ray Micro-computed Tomography (Micro-CT), Scanning Electron Microscopy (SEM) and Energy Dispersive X-ray Spectroscopy (EDX). Moreover, compression tests were performed to assess the mechanical response of the scaffolds. Scaffolds were further characterised *in vitro*, assessing their cytocompatibility properties. This study lays the groundwork for future research into the use of these three materials for more accelerated and effective bone regeneration.

2. Materials and Methods

2.1. Materials

PCL (CAPA® 6500) from Perstorp Caprolactones (Cheshire, United Kingdom) (Mw: 50 kDa) and HANp (particle size < 200 nm) from Sigma-Aldrich (Saint Louis, USA), were used. Formulations were produced using N,N-Dimethylformamide (DMF) from CHEM-LAB (Belgium) and by the solvent casting technique. For the hydrogel formulation, PEGDA, from Sigma-Aldrich (Saint Louis, USA), Mn= 750 (mol) and HEPES solution (Gibco, 15140122) were used. Photopolymerization was induced using 0.1% w/V 2-Hydroxy-4′-(2-hydroxyethoxy)-2-methylpropiophenone 98% (Irgacure 2959, Sigma-Aldrich) photoinitiator at UV light (365 nm) exposure.

2.2. Sample Design

To develop the scaffolds, protocols were designed, relying on available literature revised [47-50]. In the present work, a biomanufacturing system (Biomate Project from ANI), developed by the CDRSP-IPLeiria, was used [47,50-58]. This equipment integrates three biomanufacturing techniques: micro-extrusion system, multi-head dispensing system and electrospinning [48] . Three different matrices were produced in this system: i) PCL scaffolds; ii) PCL scaffolds with the addition of HANp; and iii) PCL/HANp scaffolds submerged in PEGDA solution.

For the production of the scaffolds, a nozzle with a diameter of 400 μm was used. The parameters employed were 240 mm/s of deposition velocity, 9 rpm of screw rotation velocity and 85◦C of liquefier temperature. The methodologies used

in the production of the scaffolds (diameter: 10 mm, height: 3 mm, and pore size: 380 μm) were as follows:

i) PCL scaffolds;

The PCL was dissolved in DMF at 80◦C and dried in a controlled environment for 96 hours. The membranes were cut into pieces to be subsequently placed in the bioextrusion equipment deposit.

ii) PCL scaffolds with the addition of hydroxyapatite nanoparticles (HANp);

PCL (60 wt%) and HANp (40 wt%) were dissolved in DMF and dried in a controlled environment. The completely dried membranes were cut into pieces to be subsequently placed in the bioextrusion equipment deposit.

iii) PCL/HANp scaffolds submerged in PEGDA solution.

For PCL/HANp scaffolds, the same procedure previously mentioned in point ii, was employed. The PEGDA (6 wv% in deionized water), Hepes and Irgacure 2959 solution was made by melt blending at 50◦C, using a heating plate with stirrer. Afterwards, the PCL/HANp scaffolds were submerged in the previously made solution. The scaffolds were carefully removed from the solution and were crosslinked using UV light exposure (365 nm). The schematic representation of the procedure is summarized in **Figure 1**.

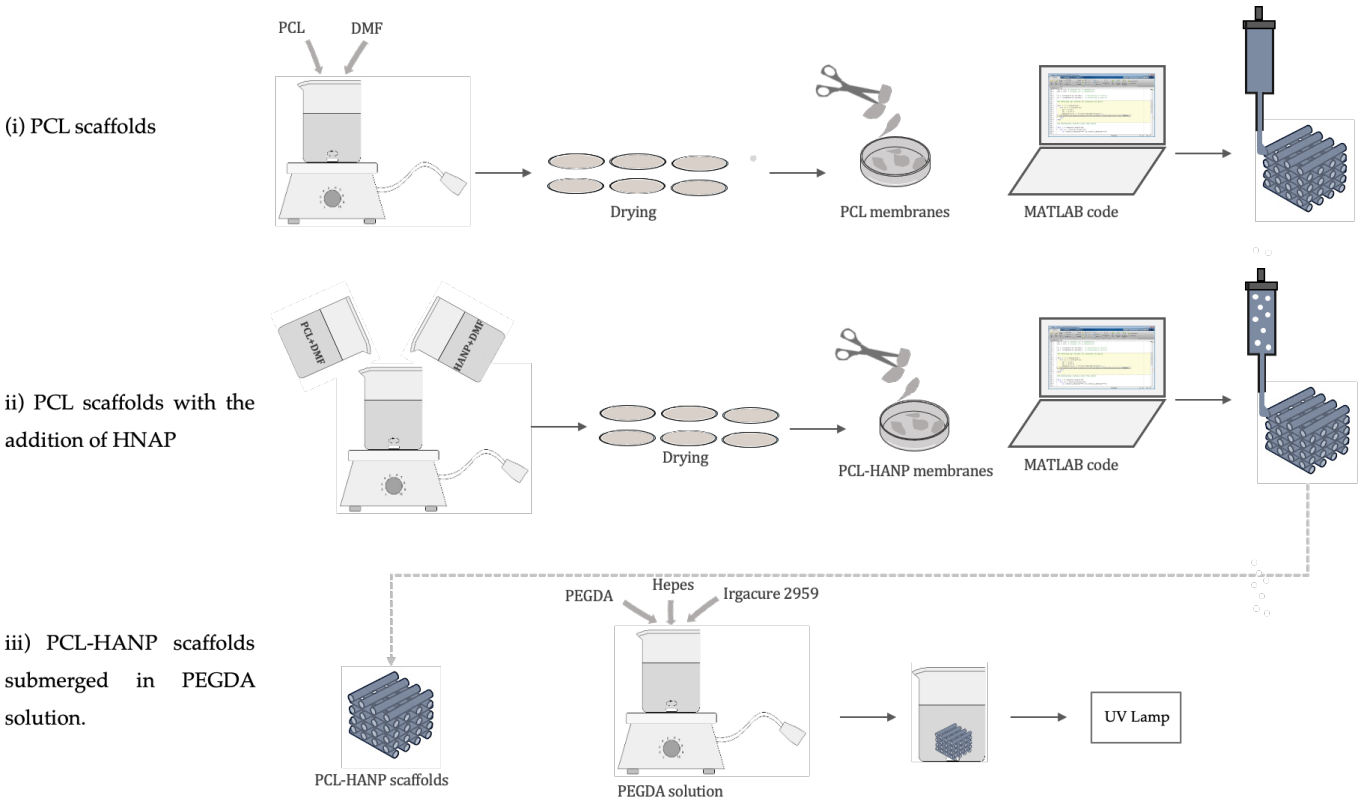


Figure 1. Schematic representation of the process for the manufacture of scaffolds.

2.3 Material Characterisation

The physical, chemical, and mechanical characterisation of the produced scaffolds was performed: Fourier-Transform Infrared Spectroscopy (FTIR), contact angle measurement, Micro-Computed Tomography (Micro-CT), Scanning Electron Microscopy (SEM), Energy Dispersive X-ray analysis (EDX), and compression tests.

2.3.1. Fourier-transform infrared spectroscopy

To extract qualitative chemical information, samples were analysed using the Bruker Alpha-P ATR FTIR spectrometer. The tests were carried out at room temperature, in a spectral range of 400–4000 cm^{-1}, with a resolution of 4 cm^{-1} in a total of 64 scans.

2.3.2. Contact Angle Measurement

The wettability of the formulations was evaluated by static contact angle measurement at 10s on a Theta Lite optical tensiometer (Attension, Finland). A

water droplet was dispensed on the surface of solid samples and the contact angle was measured by OneAttension 2.1 software (Attension).

2.3.3. X-ray micro-computed Tomography

Micro-CT scans of the scaffolds were performed using a SkyScan microtomograph model 1174 by Brucker Company (Brussels, Belgium). The scaffolds were scanned using the following parameters:

(i) For PCL (formulation and scaffolds scans): 50 Kv; 800 μA; 19.6 image pixel size; 4500 ms; averaging frames 3; 0.9 rotation degree; no filter;

(ii) For PCL/HANp and PCL/HANp scaffolds submerged in PEGDA solution (formulation and scaffolds scans): 50 Kv; 800 μA; 19.6 image pixel size; 6500 ms; averaging frames 3; 0.9 rotation degree; 0.25; Al filter.

Reconstructions, 3D images and porosity assessment were carried out through NRecon (v 1.7.0.4), CTVox (v 3.2.0) and CTAn (v 1.20) softwares, respectively.

2.3.4. Scanning Electron Microscopy and Energy Dispersive X-ray analysis

To analyze the filament and pore morphology, scaffolds from each experimental group were analysed by SEM using a Vega3 Tescan equipment (Tescan, Brno, Czechia), operating at an accelerating voltage of 20 kV, at variable magnifications. The samples were fixed on a brass stub using double-sided tape and then made electrically conductive by coating with gold/palladium (Au/Pd) thin film, by sputtering, using the sputter coater equipment (Quorum Technologies). The samples were also analysed using EDX (Xflash 6|30 from Brucker).

2.3.5. Mechanical Analysis

Compression tests were performed to evaluate the mechanical properties of each scaffold. The tests were conducted according to ASTM STP 1173 standards, using a TA.XTplusC, with using an extension rate of 0.6 mm/min. Mechanical testing was carried out using six scaffolds samples, with a diameter of 10 mm and a height of 3 mm. Stress (MPa) data was computed from load-displacement measurements.

2.4 In Vitro Tests

2.4.1. Cell culture and maintenance

The human dental pulp stem/stromal cells (hDPSCs) used in this study were sourced from AllCells, LLC (Cat. DP0037F, Lot No. DPSC090411-01). These were maintained in MEM α, GlutaMAX™ Supplement, nucleoside-free (Gibco, 32561029). This medium was supplemented with 10% (v/v) fetal bovine serum (FBS) (Gibco, A3160802), 100 IU/ml penicillin, 0.1 mg/ml streptomycin (Gibco, 15140122), 2.05 µm/ml amphotericin B (Gibco, 15290026) and 10 mM HEPES buffer solution (Gibco, 15630122). DPSCs were maintained in standard conditions, namely at 37˚C, 80% humidified atmosphere and 5% CO_2.

2.4.2 Cytocompatibility assessment

Prior to cytocompatibility tests, all scaffolds in this study were sterilised by gamma radiation (25 kGy) in a Red Perspex Dosimeter. Then, the samples were tested with hDPSCs using the PrestoBlue™ viability to assess the impact of the scaffolds on cell adhesion and viability. This reagent is a commercially available, ready-to-use, water-soluble, resazurin-based solution (7-hydroxy-3H-phenoxazin-3-one-10-oxide). The active cells reduce this compound into resazurin, a process that is accompanied by a change in the colour and fluorescence of the solution. Consequently, absorbance measurements of the solution indicate viability, thus allowing quantitative measurement of cell proliferation. Due to the reduction of the compound by the viable cells, the solution colour changes from blue to a reddish tone. Thus, changes in cell viability/proliferation were assessed by corresponding changes in absorbance measurements [59].

In brief, scaffolds were seeded using dynamic seeding, i.e., these were incubated in cell suspension (density of $2.5x10^5$ per scaffold) on a roller bench all overnight at 37˚C, 80% humidified atmosphere and 5% CO_2 environment. Later, the seeded scaffolds were moved to a 24-well non-adherent plate and submerged in fresh complete medium. Presto Blue™ evaluation was performed at different time-points: 24, 72, 120 and 168 hours. Thus, for each time point, culture media was removed from each well and replaced with fresh complete medium with 10% (v/v) of the PrestoBlue™ reagent (Invitrogen, A13262). Cells were incubated for 1 hour at 37˚C, 80% humidified atmosphere and 5% CO_2. Supernatant media were

transferred to a 96-well plate and absorbance was read at 570 and 595 nm. Changes in cell viability were detected by absorbance spectroscopy in a spectrophotometer, Multiskan™ FC Microplate Photometer (Thermo Scientific™, 51119000). For each well, the absorbance at 595 nm (normalization wavelength) was subtracted from the absorbance at 570nm (experimental result). The corrected absorbance is obtained by subtracting the mean of the control wells for each experimental well. The cells were then washed in Dulbecco's phosphate buffered saline (DPBS, Sigma®, D8537) to remove any residual PrestoBlue™ and then fresh culture medium is replenished to each well. The data were analysed and subsequently normalised to the mean of the gold standard (PCL group), presented as % viability inhibition.

2.5 Statistical analysis

In this study, statistical analysis was accomplished using GraphPad Prism® (version 8.40 for Mac OS X, GraphPad Software, La Jolla California USA). Results were reported as mean ± standard error of the mean (SE). The comparisons between groups were achieved by one-way ANOVA followed by Tukey's multiple comparisons test. Differences were considered statistically significant only when $P \leq 0.05$. Significant results are denoted according to P values with one, two, three or four of the symbols (*) corresponding to $0.01 < P \leq 0.05$, $0.001 < P \leq 0.01$, $0.0001 < P \leq 0.001$ and $P \leq 0.0001$, respectively.

3. Results

3.1 Scaffolds production

In this study, three scaffolds with different composition, namely, PCL, PCL/HANp and PCL/HANp/PEGDA were manufactured by extrusion. The samples were produced by filament deposition with 10 mm diameter, 3 mm height and 380 µm pore size. **Figure 2** shows 3D scaffolds representative of each group.

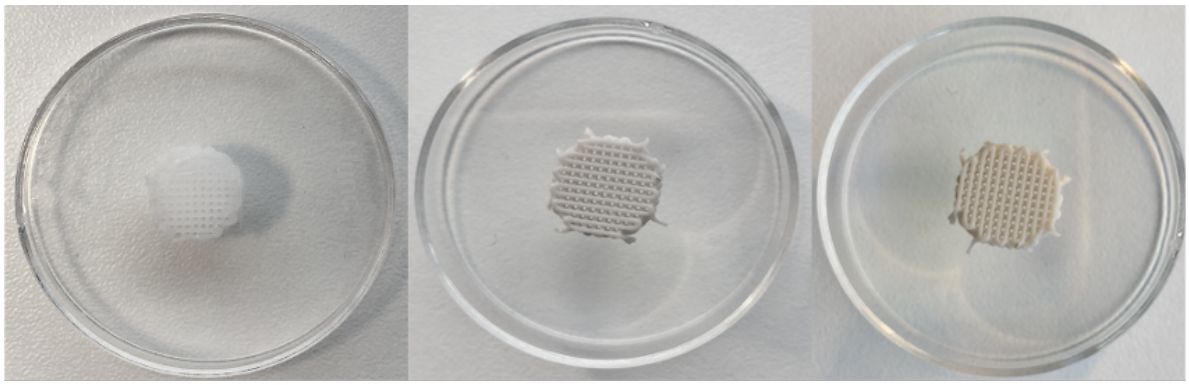


Figure 2. Observation of the 3D printed scaffolds for each group: (a) PCL scaffolds; (b) PCL scaffolds with the addition of hydroxyapatite nanoparticles; (c) PCL/HANp scaffolds submerged in PEGDA solution.

According to the results (**Figure 2 a**, **b** and **c**), the 3D scaffolds were successfully produced. The filaments, in all groups, seem to be well coordinated and positioned.

3.2 Material Characterisation

For the assessment of the functional groups, the samples were analysed by FTIR spectroscopy. Therefore, segments from each group (PCL, PCL/HANp, PCL/HANp/PEGDA and PEGDA) were analysed (**Figure 3**). In the PCL, PCL/HANp and PCL/HANp/PEGDA groups are represented the characteristic absorption bands of PCL which are asymmetric CH_2 at 2943 cm^{-1}, symmetric CH_2 at 2865 cm^{-1} and, C=O at around 1720 cm^{-1} [60,61]. Regarding HANp, in the PCL/HANp and PCL/HANp/PEGDA sample the peaks corresponding to phosphates (v1 and v3) around 1300 cm^{-1} and carbonates between 850 and 890 cm^{-1} are represented [60,62]. Finally, in the PCL/HANp/PEGDA sample, characteristic peaks of PEGDA are represented at 1638 cm^{-1}(double peak due to elongation of the vinyl groups), and 910 cm^{-1} and 1720 cm^{-1} [63].

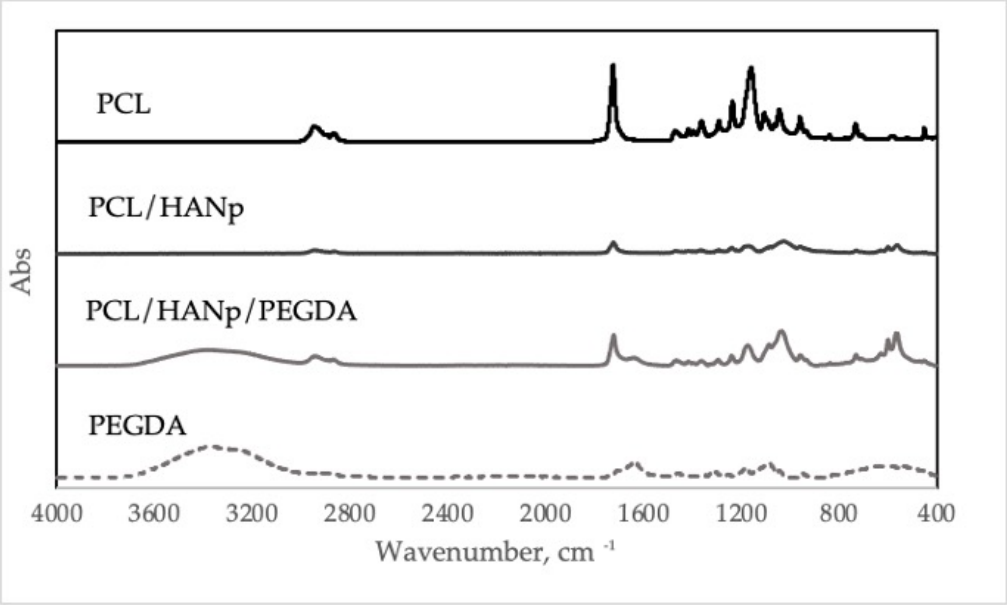


Figure 3. FTIR spectra of each group (PCL, PCL/HANp, PCL/HANp/PEGDA and PEGDA).

The wetting tendency of the samples was assessed by measuring the contact angle and shown in **Figure 4**.

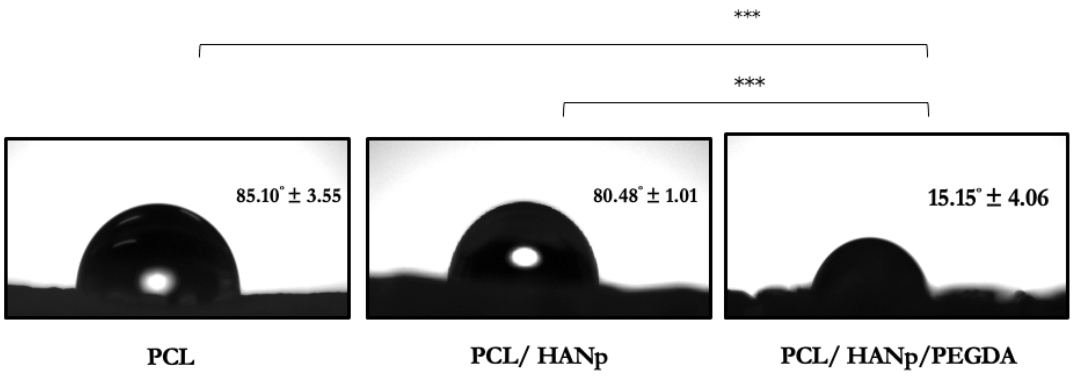


Figure 4. Contact angle measurements mean ± standard deviation of PCL, PCL/HANp and PCL/HANp/PEGDA scaffolds. Differences were considered statistically significant at $p \leq 0.05$. The results' significance is presented through the symbol (*), according to the p-value, with three symbols, corresponding to $0.0001 < p \leq 0.001$.

This characterisation test revealed that the PCL scaffolds (85.10 ± 3.54º) presented a slightly higher contact angle than the PCL/HANp scaffolds (80.48 ± 1.01º). Nevertheless, the PCL/HANp/PEGDA group showed a significantly lower contact angle (15.15 ± 4.06º) than the other groups. Considering the results, the addition of HANp and PEGDA seems to have decreased the contact angle of the samples.

The internal and external morphologies (**Figure 5**) and the porosity (**Table 1**) of the scaffolds were studied by using X-ray micro-computed tomography.

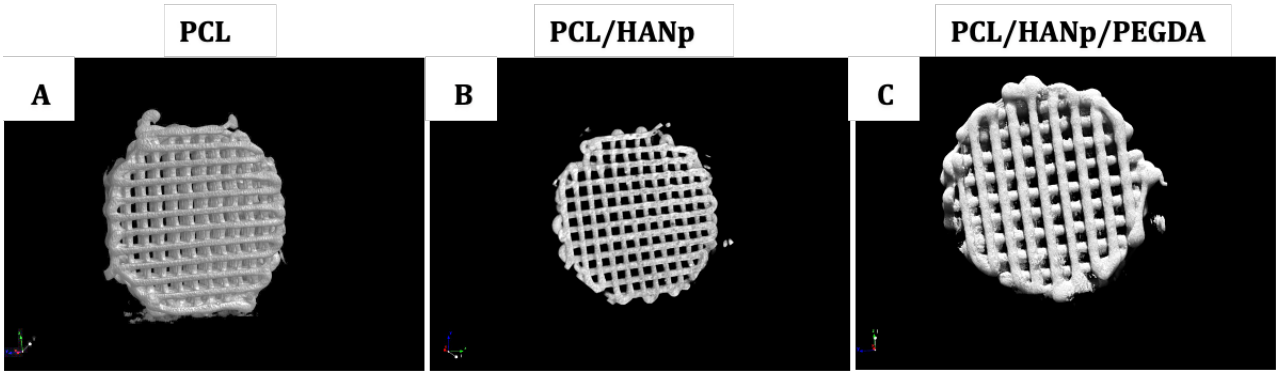


Figure 5. 3D micro-CT images of (a) PCL scaffolds; (b) PCL scaffolds with the addition of hydroxyapatite nanoparticles; (c) PCL/HANp scaffolds submerged in PEGDA solution.

Table 1. Porosity of PCL, PCL/HANp and PCL/HANp/PEGDA scaffolds (mean ± standard deviation). Differences were considered statistically significant at $p \leq 0.05$.

	PCL (1)	**PCL/HANp (2)**	**PCL/HANp /PEGDA (3)**	***p***
Porosity of scaffolds (%)	47.80 ± 0.90	52.20 ± 1.67	51.53 ± 2.00	(1) and (2) – 0.051 (1) and (3) – 0.065 (2) and (3) – 0.052

All scaffold groups were produced presenting interconnected channel networks and good geometric accuracy (**Figure 5**). Based on the results of porosity (%) of the scaffolds (**Table 1**), there is no evidence of significant statistical differences between the different scaffolds.

Concerning SEM analysis, it was used to visualise the filaments and pores of the prepared scaffolds, and details about their morphology and topography, as represented in **Figure 6**.

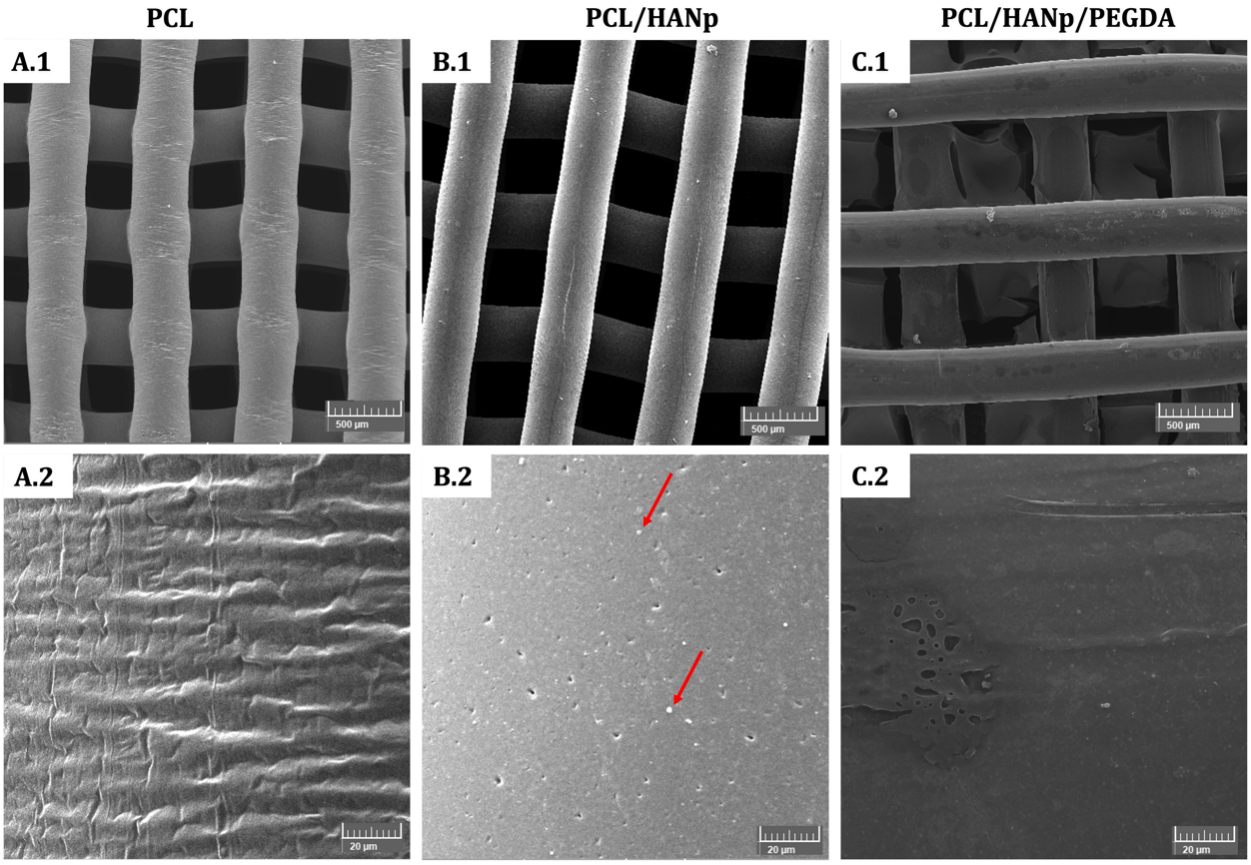


Figure 6. SEM images of PCL, PCL/HANp and PCL/HANp/PEGDA scaffolds. The red arrows show the presence of hydroxyapatite nanoparticles in the sample. Magnification: A.1, B.1 and C.1: 50x and, A.2, B.2 and C.2: 1000x.

According to the results, the scaffolds seem to have been successfully produced revealing interconnected porosity and well-accurate filaments (**Figure 6 A.1, B.1 and C.1**). The structural characteristics of the scaffolds were also analysed by measuring the filaments and pore size for each experimental group. No statistical differences were found between the filaments of the three experimental groups. These measured approximately 400 µm in diameter, which corroborates with the conception parameters of the scaffolds. Furthermore, all scaffolds presented interconnected and square pores with diameters of 380 µm (with no statistical differences between the groups). At high magnifications, the PCL

scaffolds revealed a filament surface with a small roughness (**Figure 6 A.2**). Already the PCL/HANp scaffold shows a flat filament surface with microporosities with a homogeneous dispersion in the matrix. It is also possible to distinguish small particles that suggest being hydroxyapatite nanoparticles (red arrows in **Figure 6 B.2**). **Figure 6 C.2** displays a filament surface with a plasticised appearance and some roughness which is in line with the production of this scaffold as it was submerged in PEGDA. The hydrogel appears to be a well-distributed and uniform layer, although it appears to have small irregularities.

Additionally, EDX analysis was performed to determine the presence of individual elements and the calcium/phosphate molar ratio (**Table 2**).

Table 2. EDX analysis of the scaffolds produced and CA/P molar ratio results.

Scaffold	Oxygen (O)		Calcium (Ca)		Carbon (C)		Phosphorus (P)		Ca/P Molar Ratio
	Mass (%)	Atomic (%)	Mass (%)	Atomic (%)	Mass (%)	Atomic (%)	Mass (%)	Atomic (%)	
PCL	32.94	26.94	0.00	0.00	67.06	73.06	0.00	0.00	-
PCL/HANp	2.30	16.69	3.02	8.76	7.00	67.72	1.82	6.83	1.66
PCL/HANp/PEGDA	5.55	30.18	2.76	6.00	8.11	58.75	1.81	5.08	1.52

To demonstrate the homogeneous dispersion of HANp (composed of calcium and phosphate as previously mentioned) in the matrix, the PCL/HANp and PCL/HANp/PEGDA groups were observed by EDX Si mapping analyse, and the result is shown in **Figure 7**.

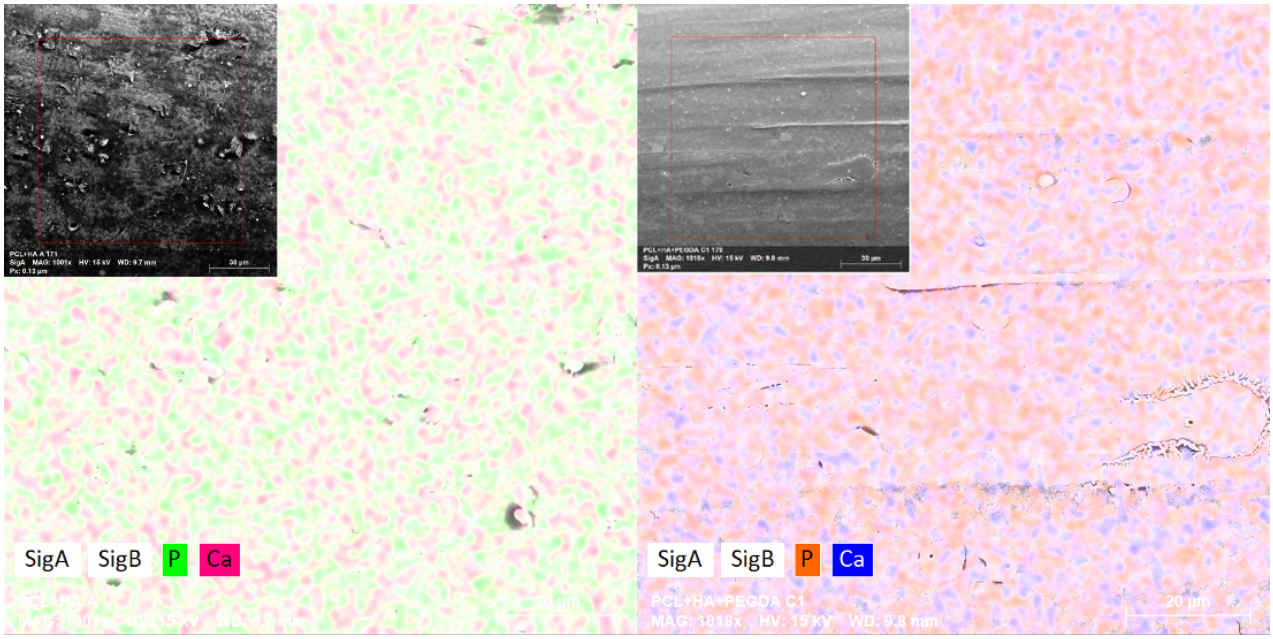


Figure 7. EDX Si-mapping micrographs.

Regarding mechanical behavior, compressive modulus (MPa) is reported in **Figure 8** and **Table 3**. The mechanical behavior is mainly conditioned by the structural characteristics, such as pore size, pore wall and connection between pores. Although with no statistical differences, the PCL/HANp group presented a higher compression modulus compared to the PCL group. In contrast, the scaffolds with PEGDA showed a slight decrease in compression behaviour compared to the same group. Despite these results, the mechanical response of the three groups presented no statistically significant differences.

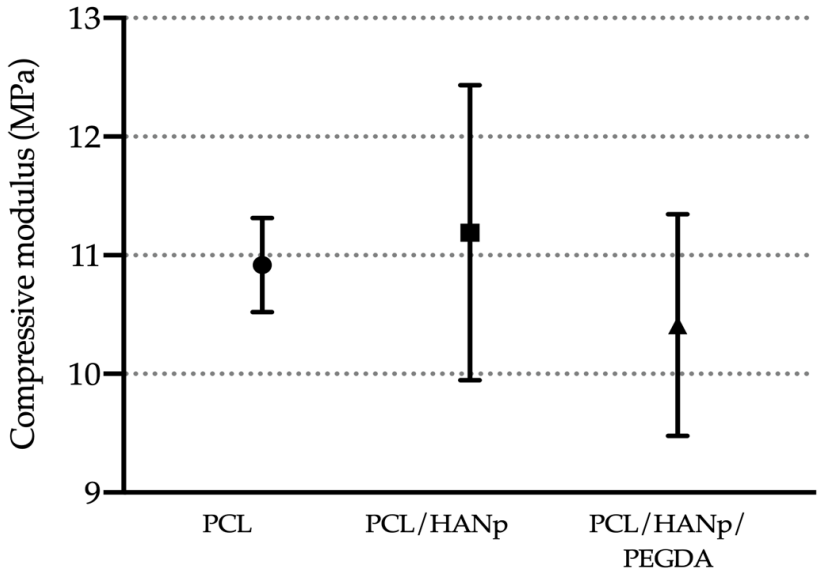


Figure 8. Compressive modulus (MPa) of the produced scaffolds.

Table 3. Compressive mechanical properties of the formulations produced (mean ± sd values).

Parameter (MPa)	PCL	PCL/HANp	PCL/HANp/PEGDA
Compressive modulus E	10.92 ± 0.3965	11.19 ± 1.244	10.41 ± 0.9344

3.3 In vitro cytocompatibility test

According to ISO 10993-5:2009 guidelines, the viability was determined using PrestoBlue™ on PCL (gold standard), PCL/HANP and PCL/HANP/PEGDA scaffolds in the presence of hDPSCs. **Figure 9** and **Table 4** represent the corrected absorbance values for each time-point: 24, 72, 120, and 168 hours. Furthermore, the statistical differences identified between the experimental groups at each time-point are shown in **Table 5**.

The analysis results demonstrated in all groups a normal cell proliferation and growth rate until 120 hours, followed by a pronounced decrease in cell viability at 168 hours. Although the scaffolds with PCL/HANP presented slightly higher cell viability rates when compared with the PCL group, only at 120 hours statistically significant differences were identified. Conversely, PEGDA scaffolds demonstrated significantly higher absorbance than the standard group, suggesting evidence of induction of cell adhesion and proliferation. The PCL/HANp/PEGDA scaffolds

presented overall a superior cytocompatibility performance, when in comparison with the gold standard PCL group.

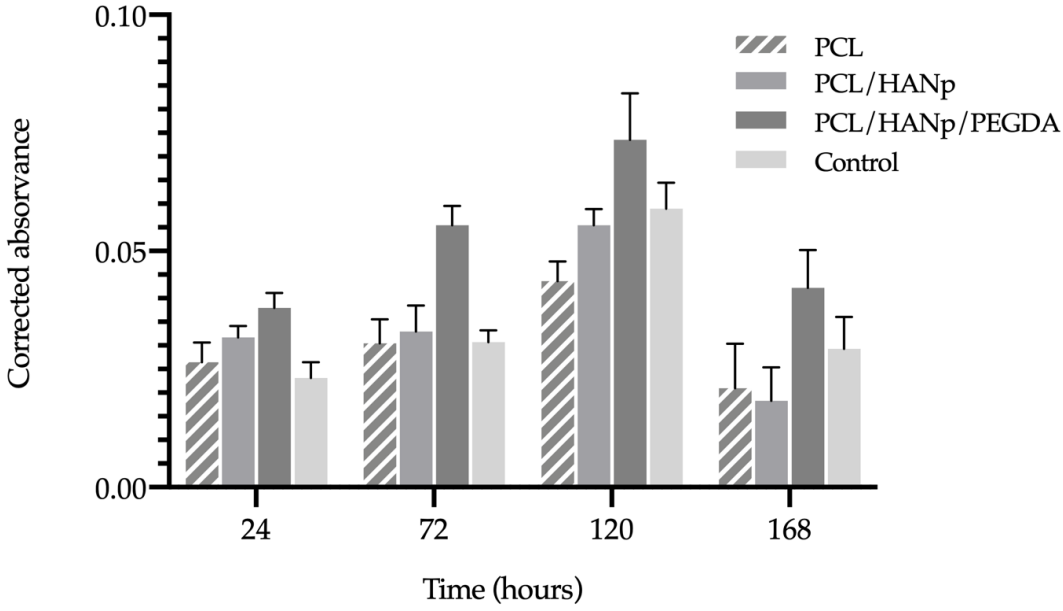


Figure 9. Corrected absorbance evaluated by PrestoBlue® viability assay for hDPSCs after 24, 72, 120 and 168 hours.

Table 4. Statistical significance of viability assay for hDPSCs after 24, 72, 120 and 168 hours (CT – control; ns - not significant). Results significances are presented through the symbol (*), according to the P value, with one, two, three or four symbols, corresponding to 0,01 < P ≤ 0,05; 0,001 < P 0,01; 0,0001 < P ≤ 0,001 and P ≤ 0,0001, respectively.

	24h				72h				120h				168h			
	PCL	PCL/ HANp	PCL/HANp/ PEGDA	CT	PCL	PCL/ HANp	PCL/HANp/ PEGDA	CT	PCL	PCL/ HANp	PCL/HANp/ PEGDA	CT	PCL	PCL/ HANP	PCL/HANp/ PEGDA	CT
PCL		ns	*	ns		ns	****	ns		*	****	**		ns	****	ns
PCL/HANp			ns	ns			****	ns			***	ns			****	*
PCL/HANp/PEGDA				**				****				**				*
CT																

Table 5. Corrected absorbance evaluated by PrestoBlue® viability assay for hDPSCs after 24, 72, 120 and 168 hours. Results presented in Mean ± SE.

	PCL	PCL/HANp	PCL/HANp/PEGDA	Control
24 h	0.027 ± 0.004	0.032 ± 0.002	0.038 ± 0.003	0.023 ± 0.003
72 h	0.031 ± 0.004	0.033 ± 0.005	0.056 ± 0.004	0.031 ± 0.002
120 h	0.044 ± 0.004	0.056 ± 0.003	0.074 ± 0.009	0.059 ± 0.005
168 h	0.021 ± 0.008	0.018 ± 0.006	0.042 ± 0.007	0.029 ± 0.006

The results of the percentage of viability inhibition, normalized to the PCL group (gold standard), are presented in **Figure 10** and **Table 6**. In accordance with Annex 3 of the ISO 10993-5:2009 guideline, inhibition of viability when superior to 30% is considered a cytotoxic effect (represented in Figure 10 by dashed lines).

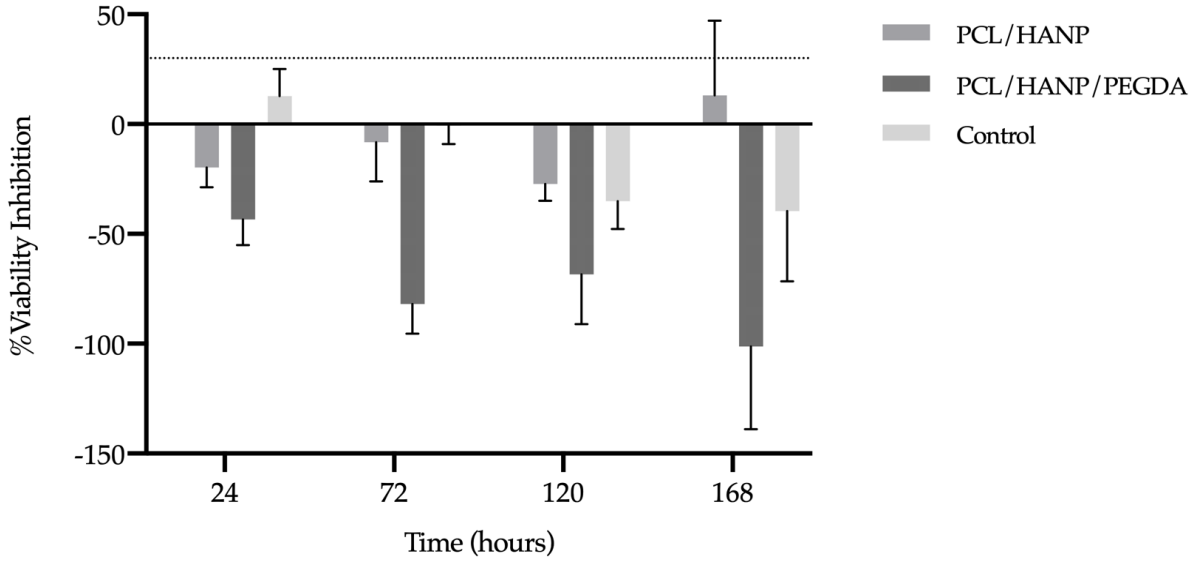


Figure 10. % Viability inhibition evaluated by PrestoBlue® viability assay for hDPSCs after 24, 72, 120 and 168 hours. Results are normalized to the PCL as 0%. The 30% threshold shown in the graph (dashed line) represents the inhibition above which the effect is considered cytotoxic (in accordance with ISO 10993-5:2009 guidelines).

Table 6. % Viability inhibition evaluated by PrestoBlue® viability assay for hDPSCs after 24, 72, 120 and 168 hours. Results presented in Mean ± SE.

	PCL/HANp	PCL/HANp/PEGDA	Control
24 h	-19.81 ± 7.72	-43.40 ± 10.16	12.72 ± 10.77
72 h	-8.20 ± 15.47	-81.97 ± 11.59	-0.82 ± 10.10
120 h	-27.22 ± 6.68	-68.48 ± 19.62	-35.13 ± 10.87
168 h	13.10 ± 29.43	-101.19 ± 32.71	-39.52 ± 27.76

The results of the percentage of viability inhibition suggest that PCL/HANP and PCL/HANP/PEGDA scaffolds can be classified as non-cytotoxic, since the percentage of viability inhibition did not exceed the pre-established limit of 30%, according to the previously mentioned guideline.

4. Discussion

Additive manufacturing has emerged as an innovative approach to scaffold fabrication for regeneration of critical bone defects [64]. The most widely used addictive manufacturing technique is extrusion printing as it prints a wide variety of biomaterials at a low cost and with good precision [65]. In the present study, this technique allowed the printing of porous, biodegradable, and reproducible scaffolds, based on PCL, HANp and PEGDA, as a potential substitute for the treatment of bone defects. There are several reasons for the choice of PCL as the main component of the developed scaffolds. This thermoplastic polymer is widely used due to its biocompatibility, biodegradability, ease of processing (with a melting point between 55 and 60˚C), with non-toxic degradation, and adjustable composition/structure [32-34,66-69]. Nevertheless, PCL presents some inconveniences such as low adhesion and cell proliferation and its slow degradation rate given the high degree of crystallinity and hydrophobicity [70,71]. These disadvantages can be overcome with the inclusion of specific compounds as inorganic bioactive materials, namely, calcium phosphates [72-74]. In this sense, hydroxyapatite nanoparticles were incorporated, thus improving the bioactivity, osteoconductivity, and hydrophilicity of the scaffold. Moreover, this inorganic component also tends to enhance the mechanical properties of the material [69,75]. The amount of HANp was set at 40% of the final weight of the composite, as higher proportions formed a mixture that was excessively thick, leading to

clogging of the nozzle and non-uniform printing of the filaments. The incorporation of HANp in the PCL matrix was performed by solvent casting technique. This technique was used because it is simple and allows the control of porosity, pore size and interconnectivity [76]. After the fabrication of the scaffolds using the extrusion-based technique, they were further submerged in a PEGDA solution to promote cell adhesion, proliferation, and migration of the composite [49]. Although there are already several notable works on PCL/HANp scaffolds [23-26,29,47,51,77-81] with promising results, in reviewing the literature, no data were found on the potential of the association of these materials with PEGDA hydrogel to be used in bone defects to improve and accelerate bone regeneration. Therefore, the purpose of this study was the production, optimization, characterisation, and *in vitro* evaluation of three different matrices: i) PCL scaffolds; ii) PCL scaffolds with added HANp; and iii) PCL/HANp scaffolds submerged in PEGDA solution. It is relevant to highlight that all scaffolds were produced successfully and demonstrated good reproducibility (**Figure 2**).

Regarding the FTIR spectroscopy analysis, it was possible to detect the functional groups in the respective samples (**Figure 3**). The spectra of the scaffold groups presented the respective characteristic absorption bands of PCL, HANp and PEGDA and are following the literature [60-63].

The wetting of the material was analysed by the contact angle of the samples for the different groups (**Figure 4**). The porous structure of the scaffolds did not allow a correct measurement of the angles. For this reason, flat segments of each composite were used for more precise measurement. Regarding the results of the contact angle measurement, it can be inferred that the PCL surface had a higher contact angle, supporting a hydrophobic nature [82,83]. Nevertheless, the addition of HANp to PCL slightly decreased the contact angle and therefore increased the wettability of the composite surface. These results are in agreement with the literature and are explained by the hydrophilic nature of hydroxyapatite [84,85]. Meanwhile, the PCL/HANp/PEGDA group demonstrated a significantly lower contact angle than the other groups. This is explained by the hydrophilic nature of the PEGDA hydrogel [49]. The addition of HANp and PEGDA may thus enhance cell activity, namely cell adhesion and proliferation, and therefore be a composite more suitable for bone tissue engineering.

To evaluate the internal and external morphology and porosity of the scaffolds, X-ray micro-computed tomography was performed (**Figure 5** and **Table 1**). According to the results, the three groups of scaffolds were correctly produced, presenting good geometry accuracy, filaments according to the pre-established pattern and interconnected channel networks. The porosity percentage of the scaffolds was also calculated, which is defined as the percentage of void space in a solid, which is considered a material-independent property [86]. The calculated porosities of the scaffolds were approximately 50%, which is recognized as a valid value considering the literature [47,86]. The pores of the scaffolds allow the formation of bone tissue as they facilitate the migration and proliferation of osteoblasts. These structures also allow for adequate vascularization in the scaffolds [86]. Furthermore, the porous surfaces enhance mechanical interlocking at the interface between the scaffold and the surrounding bone, providing higher mechanical stability. The addition of PEGDA slightly decreased the porosity of the scaffolds, however, there is no evidence of statistically significant differences between the different scaffolds. Thus, it appears that regardless of the material, all structures had similar porosity values. These results support the reliability of the biomanufacturing system used in the production of the samples.

SEM micrographs performed on the scaffolds revealed structures with a well-defined internal geometry with square and interconnected pores with regular dimensions and uniform distribution (**Figure 6**). The pores presented a size in the order of 380 μm. Studies have revealed that larger pores translate into higher mature bone formation and promote vascularization [87,88]. This phenomenon is explained by the formation of blood vessels that, by supplying oxygen and nutrients necessary for osteoblastic activity in the larger pores of the scaffolds, promote the formation of new bone mass [88,89]. The filaments also had a regular circular geometry approximately of 400μm in diameter, in agreement with the needle used (400μm). At high magnifications, a rough filament surface is visible on the PCL scaffold, in contrast to the PCL/HANp scaffold with a smoother surface, microporosities and homogeneously distributed hydroxyapatite nanoparticles. The addition of solvent (DMF) in the solvent casting method seems to promote microporosity and thus favour cell adhesion [26,90]. In turn, the PCL/HANp/PEGDA scaffold presents a uniform layer with small irregularities.

Concerning EDX (**Table 2**) quantification the presence of a considerable amount of Oxygen and Carbon atoms is noticeable in all samples, which was closely related to the composition of the PCL polymer matrix [91]. Moreover, the elemental composition analysis of the PCL/HANp and PCL/HANp/PEGDA groups also indicates significant amounts of Calcium and Phosphorus, which are the basic elements of the hydroxyapatite ceramic ($Ca_{10}(PO_4)_6(OH)_2$) [92]. In contrast, the PCL scaffold no longer shows concentrations of these chemical elements, as would be expected. EDX Ca/P determination was performed to the fabricated scaffolds, confirming the formation of CaP in the PCL/HANp and PCL/HANp/PEGDA scaffolds. The Ca/P molar ratio measured in these groups is similar to the stoichiometric value of HANp (1.67) [93]. As illustrated in the EDX Si mapping micrographs (Fig. 7), HANp (constituted by Calcium and Phosphorus) seems to be homogeneously distributed in the PCL matrix in the experimental groups of PCL/HANp and PCL/HANp/PEGDA. These data are following the SEM analysis results.

The values of the compressive modulus obtained for all scaffold groups are presented in Figure 8 and Table 3. The PCL/HANp group and the PCL/HANp/PEGDA group presented slightly higher and lower compression modulus, respectively, when compared to the PCL group. These results may be explained by the higher strength and stiffness properties associated with HANp [94,95]. In turn, PEGDA is considered a hydrogel and therefore when incorporated into the scaffold a decrease in compression modulus would be expected [42]. Notwithstanding, the average compression modulus of the three groups did not present statistically significant differences. The mechanical behaviour is mainly conditioned by structural features, such as porosity, pore size, and interconnectivity. Therefore, these results are in line with previously presented results on SEM micrographs and X-ray micro-computed tomography since the values of porosity/pore size/interconnectivity are very similar in all the produced scaffolds. Overall, the results of the mechanical behaviour demonstrated that the produced scaffolds fulfil the minimum compressive modulus required for bone graft substitutes, as it is superior to 0.5 MPa [42,96]. It should be noted that the compressive strength of the structures produced is within the range of values for human cancellous bone, from 5 to 50 MPa (depending on bone density) [97].

The cell viability and proliferation of hDPSCs in contact with the scaffolds was investigated by PrestoBlue™ (**Figure 9** and **Table 4**). This test was performed

according to ISO 10993-5:2009 "Biological evaluation of medical devices-Part 5-Test for *in vitro* cytotoxicity". The cells used in this assay were hDPSCs given their proven potential for osteogenic lineage and consequent suitability for bone tissue regeneration [1,98,99]. Moreover, in the literature there are other works that successfully assess the cytocompatibility of PCL and PCL/HANp scaffolds with this cell lineage [51,100-104]. The viability of the control group (without scaffolds) demonstrated a normal cell proliferation and growth rate, thus confirming the validity of this assay. According to Figure 9, the absorbance increased until the 5th day of cell culture, for all experimental conditions. However, on the 7th day of culture it is noticeable that all experimental groups presented a decreased cell viability. It can be hypothesised that cells on the 7th day are in the decline/apoptosis phase due to competitive inhibition resulting from the excess of cells in each well. During the cell death phase occurs the irreversible loss of cell division capacity (cell death) is triggered by the considerable increase in intracellular calcium concentration ($[Ca_{2}^{+}]_{i}$). At 24, 72 and 120 hours of incubation, the PCL/HANp group showed a higher viability value (only at 120 hours $p<0.05$) compared to the PCL scaffolds group. The fact that HANP is considered a bioactive, osteoconductive and hydrophilic material may contribute to these results [69,75]. In addition, the PrestoBlue™ viability assay demonstrated that the PCL/HANp/PEGDA scaffolds showed overall superior cytocompatibility performance compared with the gold standard PCL scaffold. The improved cytocompatibility results thus tend to be associated with the PEGDA hydrogel, as it has been supported by other groups working with this same material [42,105-107]. In sum, the results of the *in vitro* evaluation led to the assumption that the addition of PEGDA promoted cell migration and proliferation. According to Figure 10 and Table 6, all experimental groups can be classified as non-cytotoxic, as the % viability inhibition did not exceed the pre-established 30% limit throughout the test, according to the ISO 10993-5:2009 guideline.

5. Conclusions

This study describes the production, characterisation and *in vitro* performance of a scaffold based on PCL, HANp and PEGDA for bone application. Thus far, there is a wealth of literature proposing the use of PCL as a scaffold for bone pathologies. Nevertheless, to the best of our knowledge, this is the first study incorporating PCL, HANp and PEGDA in a scaffold for the healing of critical defects.

The characterisation revealed that scaffolds were successfully produced, with well-coordinated and positioned filaments, interconnected channels, and pores propitious to the migration and proliferation of osteoblasts and stem cells. Moreover, the scaffolds with PEGDA demonstrated to have hydrophilic properties that can also favour cellular activity, without compromising the mechanical properties of the composite. The results of the in *vitro* test are consistent with previously demonstrated results with a superior proliferation of hDPSCs in the PEGDA groups.

According to the results, PCL/HANp/PEGDA scaffolds are a very promising therapeutic system in critical fracture treatment, to accelerate and improve bone regeneration. The research on this system's performance in critical bone defects is an important step in its progression to clinical applications.

Author Contributions: Conceptualization, A.C.S., S.B, N.A. and A.C.M.; methodology, A.C.S., S.B., J.F.A.V. and M.F.; software, A.C.S., S.B., J.F.A.V. and M.F.; validation, A.C.S, S.B., R.A. M.B., B.L., P.S., J.F.A.V. and M.F.; formal analysis, A.C.S.; investigation, A.C.S., S.B., N.A. and A.C.M..; resources, N.A. and A.C.M; data curation, A.C.S.; writing—original draft preparation, A.C.S.; writing—review and editing, A.C.S.; visualization, A.C.S, S.B., R.A. M.B., B.L., P.S., J.F.A.V., M.F., L.A., J.D.S., N.A. and A.C.M.; supervision, L.A., J.D.S., N.A. and A.C.M; project administration, N.A. and A.C.M..; funding acquisition, N.A. and A.C.M. . All authors have read and agreed to the published version of the manuscript.

Funding: Mariana Vieira Branquinho (SFRH/BD/146172/2019), Ana Catarina Sousa (SFRH/BD/146689/2019), and Bruna Lopes (2021.05265.BD), acknowledge Fundação para a Ciência e Tecnologia (FCT), for financial support. Rui Damásio Alvites acknowledges the Animal Science Studies Centre (CECA), Agroenvironment, Technologies and Sciences Institute (ICETA), Porto University (UP), and FCT for the funding and availability of all technical, structural, and human resources necessary for the development of this work. This research was funded by Projects PEst-OE/AGR/UI0211/2011 from FCT, and COMPETE 2020, from ANI–Projetos ID&T Empresas em Copromoção, by the project "Print-on-Organs–Engineering bioinks and processes for direct printing on organs" with the reference POCI-01-0247-FEDER-033877, by the project "Bone2Move-Development of "in vivo" experimental

techniques and modelling methodologies for the evaluation of 4D scaffolds for bone defect in sheep model: an integrative research approach" with the reference POCI-01-0145-FEDER-031146. This work was also supported by the Fundação para a Ciência e a Tecnologia (FCT) and Centro2020 through the following Projects: UIDB/04044/2020, UIDP/04044/2020, and PAMI—ROTEIRO/0328/2013 (Nº 022158).

Institutional Review Board Statement: Not applicable.

Data Availability Statement: Further data on the reported results are available from the corresponding author on request.

Acknowledgments: Not applicable.

Conflicts of Interest: The authors declare no conflict of interest.

6. References

1. Campos, J.M.; Sousa, A.C.; Caseiro, A.R.; Pedrosa, S.S.; Pinto, P.O.; Branquinho, M.V.; Amorim, I.; Santos, J.D.; Pereira, T.; Mendonça, C.M.; et al. Dental pulp stem cells and Bonelike(®) for bone regeneration in ovine model. *Regen Biomater* **2019**, *6*, 49-59, doi:10.1093/rb/rby025.

2. Bohner, M. Resorbable biomaterials as bone graft substitutes. *Materials Today* **2010**, *13*, 24-30, doi:10.1016/S1369-7021(10)70014-6.

3. Forrestal, D.P.; Klein, T.J.; Woodruff, M.A. Challenges in engineering large customized bone constructs. *Biotechnology and bioengineering* **2017**, *114*, 1129-1139.

4. Bahraminasab, M. Challenges on optimization of 3D-printed bone scaffolds. *BioMedical Engineering OnLine* **2020**, *19*, 69, doi:10.1186/s12938-020-00810-2.

5. Lopes, B.; Sousa, P.; Alvites, R.; Branquinho, M.; Sousa, A.C.; Mendonça, C.; Atayde, L.M.; Luís, A.L.; Varejão, A.S.P.; Maurício, A.C. Peripheral Nerve Injury Treatments and Advances: One Health Perspective. *Int J Mol Sci* **2022**, *23*, doi:10.3390/ijms23020918.

6. Shang, F.; Yu, Y.; Liu, S.; Ming, L.; Zhang, Y.; Zhou, Z.; Zhao, J.; Jin, Y. Advancing application of mesenchymal stem cell-based bone tissue regeneration. *Bioactive Materials* **2021**, *6*, 666-683, doi:https://doi.org/10.1016/j.bioactmat.2020.08.014.

7. Visser, J.; Melchels, F.P.; Jeon, J.E.; Van Bussel, E.M.; Kimpton, L.S.; Byrne, H.M.; Dhert, W.J.; Dalton, P.D.; Hutmacher, D.W.; Malda, J. Reinforcement of hydrogels using three-dimensionally printed microfibres. *Nature communications* **2015**, *6*, 1-10.

8. Woodfield, T.; Lim, K.; Morouço, P.; Levato, R.; Malda, J.; Melchels, F. Biofabrication in tissue engineering. In *Comprehensive Biomaterials II*, Ducheyne P. ed.; Elsevier, A., Ed.; 2017; pp. 236–266.

9. Bahraminasab, M.; Edwards, K. Biocomposites for Hard Tissue Replacement and Repair. 2018; pp. 281-296.

10. Kohn, J. New approaches to biomaterials design. *Nature materials* **2004**, *3*, 745-747.

11. Zhang, L.; Yang, G.; Johnson, B.N.; Jia, X. Three-dimensional (3D) printed scaffold and material selection for bone repair. *Acta Biomaterialia* **2019**, *84*, 16-33, doi:https://doi.org/10.1016/j.actbio.2018.11.039.

12. Brown, B.N.; Valentin, J.E.; Stewart-Akers, A.M.; McCabe, G.P.; Badylak, S.F. Macrophage phenotype and remodeling outcomes in response to biologic scaffolds with and without a cellular component. *Biomaterials* **2009**, *30*, 1482-1491.

13. Porter, J.R.; Ruckh, T.T.; Popat, K.C. Bone tissue engineering: a review in bone biomimetics and drug delivery strategies. *Biotechnol Prog* **2009**, *25*, 1539-1560, doi:10.1002/btpr.246.

14. Ghassemi, T.; Shahroodi, A.; Ebrahimzadeh, M.H.; Mousavian, A.; Movaffagh, J.; Moradi, A. Current Concepts in Scaffolding for Bone Tissue Engineering. *Arch Bone Jt Surg* **2018**, *6*, 90-99.

15. Qu, H.; Fu, H.; Han, Z.; Sun, Y. Biomaterials for bone tissue engineering scaffolds: a review. *RSC Adv* **2019**, *9*, 26252-26262, doi:10.1039/c9ra05214c.

16. Langer, R.; Vacanti, J.P. Tissue engineering. *Science* **1993**, *260*, 920, doi:10.1126/science.8493529.

17. Dominici, M.; Le Blanc, K.; Mueller, I.; Slaper-Cortenbach, I.; Marini, F.C.; Krause, D.S.; Deans, R.J.; Keating, A.; Prockop, D.J.; Horwitz, E.M. Minimal criteria for defining multipotent mesenchymal stromal cells. The International Society for Cellular Therapy position statement. *Cytotherapy* **2006**, *8*, 315-317, doi:https://doi.org/10.1080/14653240600855905.

18. Lawson, A.C.; Czernuszka, J.T. Collagen-calcium phosphate composites. *Proceedings of the Institution of Mechanical Engineers, Part H: Journal of Engineering in Medicine* **1998**, *212*, 413-425, doi:10.1243/0954411981534187.

19. Jensen, S.S.; Broggini, N.; Hjørting-Hansen, E.; Schenk, R.; Buser, D. Bone healing and graft resorption of autograft, anorganic bovine bone and β-tricalcium phosphate. A histologic and histomorphometric study in the mandibles of minipigs. *Clinical Oral Implants Research* **2006**, *17*, 237-243, doi:https://doi.org/10.1111/j.1600-0501.2005.01257.x.

20. Jensen, S.S.; Yeo, A.; Dard, M.; Hunziker, E.; Schenk, R.; Buser, D. Evaluation of a novel biphasic calcium phosphate in standardized bone defects. A histologic and histomorphometric study in the mandibles of minipigs. *Clinical Oral Implants Research* **2007**, *18*, 752-760, doi:https://doi.org/10.1111/j.1600-0501.2007.01417.x.

21. Kattimani, V.S.; Kondaka, S.; Lingamaneni, K.P. Hydroxyapatite--Past, Present, and Future in Bone Regeneration. *Bone and Tissue Regeneration Insights* **2016**, *7*, BTRI.S36138, doi:10.4137/btri.S36138.

22. Song, H.H.; Yoo, M.K.; Moon, H.S.; Choi, Y.J.; Lee, H.C.; Cho, C.S. A novel polycaprolactone/hydroxyapatite scaffold for bone tissue engineering. In Proceedings of the Key Engineering Materials, 2007; pp. 265-268.

23. Zhao, J.; Guo, L.; Yang, X.; Weng, J. Preparation of bioactive porous HA/PCL composite scaffolds. *Applied Surface Science* **2008**, *255*, 2942-2946.

24. Park, S.A.; Lee, S.H.; Kim, W.D. Fabrication of porous polycaprolactone/hydroxyapatite (PCL/HA) blend scaffolds using a 3D plotting system for bone tissue engineering. *Bioprocess and biosystems engineering* **2011**, *34*, 505-513.

25. Zimmerling, A.; Yazdanpanah, Z.; Cooper, D.M.L.; Johnston, J.D.; Chen, X. 3D printing PCL/nHA bone scaffolds: exploring the influence of material synthesis techniques. *Biomaterials Research* **2021**, *25*, 3, doi:10.1186/s40824-021-00204-y.

26. Cestari, F.; Petretta, M.; Yang, Y.; Motta, A.; Grigolo, B.; Sglavo, V.M. 3D printing of PCL/nano-hydroxyapatite scaffolds derived from biogenic sources for bone tissue engineering. *Sustainable Materials and Technologies* **2021**, *29*, e00318, doi:https://doi.org/10.1016/j.susmat.2021.e00318.

27. Zhao, J.; Duan, K.; Zhang, J.W.; Lu, X.; Weng, J. The influence of polymer concentrations on the structure and mechanical properties of porous polycaprolactone-coated hydroxyapatite scaffolds. *Applied Surface Science* **2010**, *256*, 4586-4590, doi:https://doi.org/10.1016/j.apsusc.2010.02.053.

28. Jirkovec, R.; Holec, P.; Hauzerova, S.; Samkova, A.; Kalous, T.; Chvojka, J. Preparation of a Composite Scaffold from Polycaprolactone and Hydroxyapatite Particles by Means of Alternating Current Electrospinning. *ACS Omega* **2021**, *6*, 9234-9242, doi:10.1021/acsomega.1c00644.

29. Shor, L.; Güçeri, S.; Wen, X.; Gandhi, M.; Sun, W. Fabrication of three-dimensional polycaprolactone/hydroxyapatite tissue scaffolds and osteoblast-scaffold interactions in vitro. *Biomaterials* **2007**, *28*, 5291-5297.

30. Cho, Y.S.; Gwak, S.-J.; Cho, Y.-S. Fabrication of Polycaprolactone/Nano Hydroxyapatite (PCL/nHA) 3D Scaffold with Enhanced In Vitro Cell Response via Design for Additive Manufacturing (DfAM). *Polymers* **2021**, *13*, 1394.

31. Chuenjitkuntaworn, B.; Osathanon, T.; Nowwarote, N.; Supaphol, P.; Pavasant, P. The efficacy of polycaprolactone/hydroxyapatite scaffold in combination with mesenchymal stem cells for bone tissue engineering. *Journal of Biomedical Materials Research Part A* **2016**, *104*, 264-271, doi:https://doi.org/10.1002/jbm.a.35558.

32. Wang, S.; Gu, R.; Wang, F.; Zhao, X.; Yang, F.; Xu, Y.; Yan, F.; Zhu, Y.; Xia, D.; Liu, Y. 3D-Printed PCL/Zn scaffolds for bone regeneration with a dose-dependent effect on osteogenesis and osteoclastogenesis. *Materials Today Bio* **2022**, *13*, 100202, doi:https://doi.org/10.1016/j.mtbio.2021.100202.

33. Babilotte, J.; Guduric, V.; Le Nihouannen, D.; Naveau, A.; Fricain, J.-C.; Catros, S. 3D printed polymer–mineral composite biomaterials for bone tissue engineering: Fabrication and characterization. *Journal of Biomedical Materials Research Part B: Applied Biomaterials* **2019**, *107*, 2579-2595, doi:https://doi.org/10.1002/jbm.b.34348.

34. Kenry; Liu, B. Recent Advances in Biodegradable Conducting Polymers and Their Biomedical Applications. *Biomacromolecules* **2018**, *19*, 1783-1803, doi:10.1021/acs.biomac.8b00275.

35. Zhang, S.; Liu, C. Research progress in osteogenic differentiation of adipose-derived stem cells induced by bioscaffold materials. *Chinese Journal of Tissue Engineering Research* **2020**, *24*, 1107.

36. Patel, P.P.; Buckley, C.; Taylor, B.L.; Sahyoun, C.C.; Patel, S.D.; Mont, A.J.; Mai, L.; Patel, S.; Freeman, J.W. Mechanical and biological evaluation of a hydroxyapatite-reinforced scaffold for bone regeneration. *Journal of Biomedical Materials Research Part A* **2019**, *107*, 732-741, doi:https://doi.org/10.1002/jbm.a.36588.

37. Bal, Z.; Kaito, T.; Korkusuz, F.; Yoshikawa, H. Bone regeneration with hydroxyapatite-based biomaterials. *Emergent Materials* **2020**, *3*, 521-544, doi:10.1007/s42247-019-00063-3.

38. Wang, Y.; Cao, X.; Ma, M.; Lu, W.; Zhang, B.; Guo, Y. A GelMA-PEGDA-nHA Composite Hydrogel for Bone Tissue Engineering. *Materials (Basel)* **2020**, *13*, doi:10.3390/ma13173735.

39. Liu, W.; Jing, X.; Xu, Z.; Teng, C. PEGDA/HA mineralized hydrogel loaded with Exendin4 promotes bone regeneration in rat models with bone defects by inducing osteogenesis. *Journal of Biomaterials Applications* **2021**, *35*, 1337-1346, doi:10.1177/0885328220987046.

40. Martin, V.; Bettencourt, A. Bone regeneration: Biomaterials as local delivery systems with improved osteoinductive properties. *Materials Science and Engineering: C* **2018**, *82*, 363-371, doi:https://doi.org/10.1016/j.msec.2017.04.038.

41. Thrivikraman, G.; Athirasala, A.; Twohig, C.; Boda, S.K.; Bertassoni, L.E. Biomaterials for craniofacial bone regeneration. *Dental Clinics* **2017**, *61*, 835-856.

42. Kotturi, H.; Abuabed, A.; Zafar, H.; Sawyer, E.; Pallipparambil, B.; Jamadagni, H.; Khandaker, M. Evaluation of Polyethylene Glycol Diacrylate-Polycaprolactone Scaffolds for Tissue Engineering Applications. *J Funct Biomater* **2017**, *8*, doi:10.3390/jfb8030039.

43. Yang, F.; Williams, C.G.; Wang, D.A.; Lee, H.; Manson, P.N.; Elisseeff, J. The effect of incorporating RGD adhesive peptide in polyethylene glycol diacrylate hydrogel on osteogenesis of bone marrow stromal cells. *Biomaterials* **2005**, *26*, 5991-5998, doi:10.1016/j.biomaterials.2005.03.018.

44. Guarino, V.; Gloria, A.; Raucci, M.; Ambrosio, L. Hydrogel-Based Platforms for the Regeneration of Osteochondral Tissue and Intervertebral Disc. *Polymers* **2012**, *4*, 1590-1612, doi:10.3390/polym4031590.

45. Yang, Y.; Wang, G.; Liang, H.; Gao, C.; Peng, S.; Shen, L.; Shuai, C. Additive manufacturing of bone scaffolds. *Int J Bioprint* **2019**, *5*, 148, doi:10.18063/IJB.v5i1.148.

46. Sa, M.W.; Nguyen, B.B.; Moriarty, R.A.; Kamalitdinov, T.; Fisher, J.P.; Kim, J.Y. Fabrication and evaluation of 3D printed BCP scaffolds reinforced with ZrO(2) for bone tissue applications. *Biotechnol Bioeng* **2018**, *115*, 989-999, doi:10.1002/bit.26514.

47. Morouço, P.; Biscaia, S.; Viana, T.; Franco, M.; Malça, C.; Mateus, A.; Moura, C.; Ferreira, F.C.; Mitchell, G.; Alves, N.M. Fabrication of Poly(ε-caprolactone) Scaffolds Reinforced with Cellulose Nanofibers, with and without the Addition of Hydroxyapatite Nanoparticles. *Biomed Res Int* **2016**, *2016*, 1596157, doi:10.1155/2016/1596157.

48. Biscaia, S.; Dabrowska, E.; Tojeira, A.; Horta, J.; Carreira, P.; Morouço, P.; Mateus, A.; Alves, N. Development of heterogeneous structures with Polycaprolactone-Alginate using a new 3D printing system–BioMEDβeta: design and processing. *Procedia Manufacturing* **2017**, *12*, 113-119.

49. Francisco, L.; Moura, C.; Viana, T.; Ângelo, D.; Morouço, P.; Alves, N. Poly(ε-caprolactone) and Polyethylene Glycol Diacrylate-based Scaffolds for TMJ Bioengineered Disc Implants. *Procedia Manufacturing* **2017**, *12*, 291-297, doi:https://doi.org/10.1016/j.promfg.2017.08.032.

50. Moura, C.; Trindade, D.; Vieira, M.; Francisco, L.; Ângelo, D.F.; Alves, N. Multi-Material Implants for Temporomandibular Joint Disc Repair: Tailored Additive Manufacturing Production. *Front Bioeng Biotechnol* **2020**, *8*, 342, doi:10.3389/fbioe.2020.00342.

51. Biscaia, S.; Branquinho, M.V.; Alvites, R.D.; Fonseca, R.; Sousa, A.C.; Pedrosa, S.S.; Caseiro, A.R.; Guedes, F.; Patrício, T.; Viana, T.; et al. 3D Printed Poly(ε-caprolactone)/Hydroxyapatite Scaffolds for Bone Tissue Engineering: A Comparative Study on a Composite Preparation by Melt Blending or Solvent Casting Techniques and the Influence of Bioceramic Content on Scaffold Propertie. *Int J Mol Sci* **2022**, *23*, 2318.

52. Domingos, M.; Intranuovo, F.; Russo, T.; De Santis, R.; Gloria, A.; Ambrosio, L.; Ciurana, J.; Bartolo, P. The first systematic analysis of 3D rapid prototyped poly(ε-caprolactone) scaffolds manufactured through BioCell printing: the effect of pore size and geometry on compressive mechanical behaviour and in vitro hMSC viability. *Biofabrication* **2013**, *5*, 045004, doi:10.1088/1758-5082/5/4/045004.

53. Domingos, M.; Intranuovo, F.; Gloria, A.; Gristina, R.; Ambrosio, L.; Bártolo, P.J.; Favia, P. Improved osteoblast cell affinity on plasma-modified 3-D extruded PCL scaffolds. *Acta Biomaterialia* **2013**, *9*, 5997-6005, doi:https://doi.org/10.1016/j.actbio.2012.12.031.

54. Bartolo, P.; Domingos, M.; Gloria, A.; Ciurana, J. BioCell Printing: Integrated automated assembly system for tissue engineering constructs. *CIRP Annals* **2011**, *60*, 271-274, doi:https://doi.org/10.1016/j.cirp.2011.03.116.

55. Ângelo, D.F.; Morouço, P.; Monje Gil, F.; Mónico, L.; González-Gárcia, R.; Sousa, R.; Neto, L.; Caldeira, I.; Smith, M.; Smith, S.; et al. Preclinical randomized controlled trial of bilateral discectomy versus bilateral discopexy in Black Merino sheep temporomandibular joint: TEMPOJIMS – Phase 1- histologic, imaging and body weight results. *Journal of Cranio-Maxillofacial Surgery* **2018**, *46*, 688-696, doi:https://doi.org/10.1016/j.jcms.2018.01.006.

56. Viana, T.; Biscaia, S.; Dabrowska, E.; Franco, M.C.; Carreira, P.; Morouço, P.; Alves, N. A Novel Biomanufacturing System to Produce Multi-Material Scaffolds for Tissue Engineering: Concept and Preliminary Results. *Applied Mechanics and Materials* **2019**, *890*, 283-289, doi:10.4028/www.scientific.net/AMM.890.283.

57. Domingos, M.; Dinucci, D.; Cometa, S.; Alderighi, M.; Bártolo, P.J.; Chiellini, F. Polycaprolactone Scaffolds Fabricated via Bioextrusion for Tissue Engineering Applications. *International Journal of Biomaterials* **2009**, *2009*, 239643, doi:10.1155/2009/239643.

58. Morouço, P.; Ângelo, D.; Francisco, L.; Moura, C.; Alves, N. Tissue engineering for temporomandibular joint disc repair and regeneration: a methodological perspective. *Advances in Cellular and Molecular Otolaryngology* **2016**, *4*, 33709, doi:10.3402/acmo.v4.33709.

59. ThermoFisher. PrestoBlue™ Cell Viability Reagent. Available online: https://www.thermofisher.com/order/catalog/product/A13261 (accessed on

60. Lizarraga, K.; Flores-Morales, C.; Del Prado, M.; Álvarez-Pérez, M.; Pina-Barba, M.; Escobedo, C. Polycaprolactone- and polycaprolactone/ceramic-based 3D-bioplotted porous scaffolds for bone regeneration: A comparative study. *Materials Science and Engineering: C* **2017**, *79*, doi:10.1016/j.msec.2017.05.003.

61. Elzein, T.; Nasser-Eddine, M.; Delaite, C.; Bistac, S.; Dumas, P. FTIR study of polycaprolactone chain organization at interfaces. *Journal of Colloid and Interface Science* **2004**, *273*, 381-387, doi:https://doi.org/10.1016/j.jcis.2004.02.001.

62. Chang, M.C.; Tanaka, J. FT-IR study for hydroxyapatite/collagen nanocomposite cross-linked by glutaraldehyde. *Biomaterials* **2002**, *23*, 4811-4818, doi:10.1016/s0142-9612(02)00232-6.

63. Kianfar, P.; Vitale, A.; Dalle Vacche, S.; Bongiovanni, R. Enhancing properties and water resistance of PEO-based electrospun nanofibrous membranes by photo-crosslinking. *Journal of Materials Science* **2021**, *56*, 1-18, doi:10.1007/s10853-020-05346-3.

64. Do, A.V.; Khorsand, B.; Geary, S.M.; Salem, A.K. 3D Printing of Scaffolds for Tissue Regeneration Applications. *Adv Healthc Mater* **2015**, *4*, 1742-1762, doi:10.1002/adhm.201500168.

65. Garot, C.; Bettega, G.; Picart, C. Additive Manufacturing of Material Scaffolds for Bone Regeneration: Toward Application in the Clinics. *Advanced Functional Materials* **2021**, *31*, 2006967, doi:https://doi.org/10.1002/adfm.202006967.

66. Rohner, D.; Hutmacher, D.W.; Cheng, T.K.; Oberholzer, M.; Hammer, B. In vivo efficacy of bone-marrow-coated polycaprolactone scaffolds for the reconstruction of orbital defects in the pig. *J Biomed Mater Res B Appl Biomater* **2003**, *66*, 574-580, doi:10.1002/jbm.b.10037.

67. Williams, J.M.; Adewunmi, A.; Schek, R.M.; Flanagan, C.L.; Krebsbach, P.H.; Feinberg, S.E.; Hollister, S.J.; Das, S. Bone tissue engineering using polycaprolactone scaffolds fabricated via selective laser sintering. *Biomaterials* **2005**, *26*, 4817-4827, doi:10.1016/j.biomaterials.2004.11.057.

68. Ba Linh, N.T.; Min, Y.K.; Lee, B.T. Hybrid hydroxyapatite nanoparticles-loaded PCL/GE blend fibers for bone tissue engineering. *J Biomater Sci Polym Ed* **2013**, *24*, 520-538, doi:10.1080/09205063.2012.697696.

69. Keivani, F.; Shokrollahi, P.; Zandi, M.; Irani, S.; Shokrolahi, F.; Khorasani, S.C. Engineered electrospun poly(caprolactone)/polycaprolactone-g-hydroxyapatite nano-fibrous scaffold promotes human fibroblasts adhesion and proliferation. *Mater Sci Eng C Mater Biol Appl* **2016**, *68*, 78-88, doi:10.1016/j.msec.2016.05.098.

70. Lam, C.X.; Hutmacher, D.W.; Schantz, J.T.; Woodruff, M.A.; Teoh, S.H. Evaluation of polycaprolactone scaffold degradation for 6 months in vitro and in vivo. *J Biomed Mater Res A* **2009**, *90*, 906-919, doi:10.1002/jbm.a.32052.

71. Wutticharoenmongkol, P.; Pavasant, P.; Supaphol, P. Osteoblastic phenotype expression of MC3T3-E1 cultured on electrospun polycaprolactone fiber mats filled with hydroxyapatite nanoparticles. *Biomacromolecules* **2007**, *8*, 2602-2610, doi:10.1021/bm700451p.

72. Petretta, M.; Gambardella, A.; Boi, M.; Berni, M.; Cavallo, C.; Marchiori, G.; Maltarello, M.C.; Bellucci, D.; Fini, M.; Baldini, N.; et al. Composite Scaffolds for Bone Tissue Regeneration Based on PCL and Mg-Containing Bioactive Glasses. *Biology (Basel)* **2021**, *10*, doi:10.3390/biology10050398.

73. Hristov, V.; Radev, L.; Samuneva, B.; Apostolov, G. Organic / inorganic bioactive materials Part I: Synthesis, structure and in vitro assessment of collagen/silicocarnotite biocoatings. *Open Chemistry* **2009**, *7*, 702-710, doi:doi:10.2478/s11532-009-0067-2.

74. Rezwan, K.; Chen, Q.Z.; Blaker, J.J.; Boccaccini, A.R. Biodegradable and bioactive porous polymer/inorganic composite scaffolds for bone tissue engineering. *Biomaterials* **2006**, *27*, 3413-3431, doi:10.1016/j.biomaterials.2006.01.039.

75. Chen, Z.; Liu, Y.; Huang, J.; Wang, H.; Hao, M.; Hu, X.; Qian, X.; Fan, J.; Yang, H.; Yang, B. Enhanced In Vitro Biocompatible Polycaprolactone/Nano-Hydroxyapatite Scaffolds with Near-Field Direct-Writing Melt Electrospinning Technology. *Journal of Functional Biomaterials* **2022**, *13*, 161.

76. Sola, A.; Bertacchini, J.; D'Avella, D.; Anselmi, L.; Maraldi, T.; Marmiroli, S.; Messori, M. Development of solvent-casting particulate leaching (SCPL) polymer scaffolds as improved three-dimensional supports to mimic the bone marrow niche. *Materials Science and Engineering: C* **2019**, *96*, 153-165, doi:https://doi.org/10.1016/j.msec.2018.10.086.

77. Jiao, Z.; Luo, B.; Xiang, S.; Ma, H.; Yu, Y.; Yang, W. 3D printing of HA / PCL composite tissue engineering scaffolds. *Advanced Industrial and Engineering*

Polymer Research **2019**, *2*, 196-202, doi:https://doi.org/10.1016/j.aiepr.2019.09.003.

78. Roohani-Esfahani, S.-I.; Nouri-Khorasani, S.; Lu, Z.; Appleyard, R.; Zreiqat, H. The influence hydroxyapatite nanoparticle shape and size on the properties of biphasic calcium phosphate scaffolds coated with hydroxyapatite–PCL composites. *Biomaterials* **2010**, *31*, 5498-5509.

79. Cui, Z.; Nelson, B.; Peng, Y.; Li, K.; Pilla, S.; Li, W.-J.; Turng, L.-S.; Shen, C. Fabrication and characterization of injection molded poly (ε-caprolactone) and poly (ε-caprolactone)/hydroxyapatite scaffolds for tissue engineering. *Materials Science and Engineering: C* **2012**, *32*, 1674-1681.

80. Chuenjitkuntaworn, B.; Inrung, W.; Damrongsri, D.; Mekaapiruk, K.; Supaphol, P.; Pavasant, P. Polycaprolactone/hydroxyapatite composite scaffolds: preparation, characterization, and in vitro and in vivo biological responses of human primary bone cells. *Journal of Biomedical Materials Research Part A: An Official Journal of The Society for Biomaterials, The Japanese Society for Biomaterials, and The Australian Society for Biomaterials and the Korean Society for Biomaterials* **2010**, *94*, 241-251.

81. Gerdes, S.; Mostafavi, A.; Ramesh, S.; Memic, A.; Rivero, I.V.; Rao, P.; Tamayol, A. Process–structure–quality relationships of three-dimensional printed poly (caprolactone)-hydroxyapatite scaffolds. *Tissue Engineering Part A* **2020**, *26*, 279-291.

82. Janvikul, W.; Uppanan, P.; Thavornyutikarn, B.; Kosorn, W.; Kaewkong, P. Effects of surface topography, hydrophilicity and chemistry of surface-treated PCL scaffolds on chondrocyte infiltration and ECM production. *Procedia Engineering* **2013**, *59*, 158-165.

83. Ufere, S.K.J.; Sultana, N. Contact angle, conductivity and mechanical properties of polycaprolactone/hydroxyapatite/polypyrrole scaffolds using freeze-drying technique. *ARPN J. Eng. Appl. Sci* **2016**, *11*, 13686.

84. Jiang, W.; Shi, J.; Li, W.; Sun, K. Morphology, wettability, and mechanical properties of polycaprolactone/hydroxyapatite composite scaffolds with

interconnected pore structures fabricated by a mini-deposition system. *Polymer Engineering & Science* **2012**, *52*, 2396-2402.

85. Eosoly, S.; Lohfeld, S.; Brabazon, D. Effect of hydroxyapatite on biodegradable scaffolds fabricated by SLS. In Proceedings of the Key Engineering Materials, 2009; pp. 659-662.

86. Renghini, C.; Komlev, V.; Fiori, F.; Verné, E.; Baino, F.; Vitale-Brovarone, C. Micro-CT studies on 3-D bioactive glass–ceramic scaffolds for bone regeneration. *Acta Biomaterialia* **2009**, *5*, 1328-1337, doi:https://doi.org/10.1016/j.actbio.2008.10.017.

87. Abbasi, N.; Hamlet, S.; Love, R.M.; Nguyen, N.-T. Porous scaffolds for bone regeneration. *Journal of Science: Advanced Materials and Devices* **2020**, *5*, 1-9, doi:https://doi.org/10.1016/j.jsamd.2020.01.007.

88. Cheng, M.-q.; Wahafu, T.; Jiang, G.-f.; Liu, W.; Qiao, Y.-q.; Peng, X.-c.; Cheng, T.; Zhang, X.-l.; He, G.; Liu, X.-y. A novel open-porous magnesium scaffold with controllable microstructures and properties for bone regeneration. *Scientific reports* **2016**, *6*, 1-14.

89. Iviglia, G.; Kargozar, S.; Baino, F. Biomaterials, current strategies, and novel nano-technological approaches for periodontal regeneration. *Journal of functional biomaterials* **2019**, *10*, 3.

90. Aliotta, L.; Cinelli, P.; Coltelli, M.B.; Righetti, M.C.; Gazzano, M.; Lazzeri, A. Effect of nucleating agents on crystallinity and properties of poly (lactic acid) (PLA). *European Polymer Journal* **2017**, *93*, 822-832, doi:https://doi.org/10.1016/j.eurpolymj.2017.04.041.

91. Dziadek, M.; Menaszek, E.; Zagrajczuk, B.; Pawlik, J.; Cholewa-Kowalska, K. New generation poly(ε-caprolactone)/gel-derived bioactive glass composites for bone tissue engineering: Part I. Material properties. *Mater Sci Eng C Mater Biol Appl* **2015**, *56*, 9-21, doi:10.1016/j.msec.2015.06.020.

92. Abifarin, J.K.; Obada, D.O.; Dauda, E.T.; Dodoo-Arhin, D. Experimental data on the characterization of hydroxyapatite synthesized from biowastes. *Data in Brief* **2019**, *26*, 104485, doi:https://doi.org/10.1016/j.dib.2019.104485.

93. Eric, M.R.-M.o. Hydroxyapatite-Based Materials: Synthesis and Characterization. In *Biomedical Engineering*, Reza, F.-R., Ed.; IntechOpen: Rijeka, 2011; p. Ch. 4.

94. Du, J.; Zuo, Y.; Lin, L.; Huang, D.; Niu, L.; Wei, Y.; Wang, K.; Lin, Q.; Zou, Q.; Li, Y. Effect of hydroxyapatite fillers on the mechanical properties and osteogenesis capacity of bio-based polyurethane composite scaffolds. *Journal of the Mechanical Behavior of Biomedical Materials* **2018**, *88*, 150-159, doi:https://doi.org/10.1016/j.jmbbm.2018.08.028.

95. Osuchukwu, O.A.; Salihi, A.; Abdullahi, I.; Abdulkareem, B.; Nwannenna, C.S. Synthesis techniques, characterization and mechanical properties of natural derived hydroxyapatite scaffolds for bone implants: a review. *SN Applied Sciences* **2021**, *3*, 822, doi:10.1007/s42452-021-04795-y.

96. Kim, J.; Magno, M.H.; Waters, H.; Doll, B.A.; McBride, S.; Alvarez, P.; Darr, A.; Vasanji, A.; Kohn, J.; Hollinger, J.O. Bone regeneration in a rabbit critical-sized calvarial model using tyrosine-derived polycarbonate scaffolds. *Tissue Eng Part A* **2012**, *18*, 1132-1139, doi:10.1089/ten.TEA.2011.0582.

97. Nicoll, S. Materials for Bone Graft Substitutes and Osseous Tissue Regeneration. 2011; pp. 343-362.

98. Caseiro, A.; Alvites, R.; Pedrosa, S.; Miguel, J.; Reis, I.; Santos, J.; Mendonça, C.; Atayde, M.; Maurício, A. The potential clinical application of mesenchymal stem cells from the dental pulp (DPSCs) for bone regeneration. *Frontiers in Stem Cell and Regenerative Medicine Research* **2017**, *6*, 3-52.

99. Caseiro, A.R.; Santos Pedrosa, S.; Ivanova, G.; Vieira Branquinho, M.; Almeida, A.; Faria, F.; Amorim, I.; Pereira, T.; Maurício, A.C. Mesenchymal Stem/ Stromal Cells metabolomic and bioactive factors profiles: A comparative analysis on the umbilical cord and dental pulp derived Stem/ Stromal Cells secretome. *PLoS One* **2019**, *14*, e0221378, doi:10.1371/journal.pone.0221378.

100. Yang, X.; Yang, F.; Walboomers, X.F.; Bian, Z.; Fan, M.; Jansen, J.A. The performance of dental pulp stem cells on nanofibrous PCL/gelatin/nHA scaffolds. *J Biomed Mater Res A* **2010**, *93*, 247-257, doi:10.1002/jbm.a.32535.

101. Aghazadeh, M.; Samiei, M.; Hokmabad, V.R.; Alizadeh, E.; Jabbari, N.; Seifalian, A.; Salehi, R. The Effect of Melanocyte Stimulating Hormone and Hydroxyapatite on Osteogenesis in Pulp Stem Cells of Human Teeth Transferred into Polyester Scaffolds. *Fibers and Polymers* **2018**, *19*, 2245-2253, doi:10.1007/s12221-018-8309-6.

102. Park, S.; Kim, J.E.; Han, J.; Jeong, S.; Lim, J.W.; Lee, M.C.; Son, H.; Kim, H.B.; Choung, Y.-H.; Seonwoo, H.; et al. 3D-Printed Poly(ε-Caprolactone)/Hydroxyapatite Scaffolds Modified with Alkaline Hydrolysis Enhance Osteogenesis In Vitro. *Polymers* **2021**, *13*, 257.

103. Rosales-Ibáñez, R.; Cubo-Mateo, N.; Rodríguez-Navarrete, A.; González-González, A.M.; Villamar-Duque, T.E.; Flores-Sánchez, L.O.; Rodríguez-Lorenzo, L.M. Assessment of a PCL-3D Printing-Dental Pulp Stem Cells Triplet for Bone Engineering: An In Vitro Study. *Polymers* **2021**, *13*, 1154.

104. Jensen, J.; Kraft, D.C.; Lysdahl, H.; Foldager, C.B.; Chen, M.; Kristiansen, A.A.; Rölfing, J.H.; Bünger, C.E. Functionalization of polycaprolactone scaffolds with hyaluronic acid and β-TCP facilitates migration and osteogenic differentiation of human dental pulp stem cells in vitro. *Tissue Eng Part A* **2015**, *21*, 729-739, doi:10.1089/ten.TEA.2014.0177.

105. Soriente, A.; Amodio, S.P.; Fasolino, I.; Raucci, M.G.; Demitri, C.; Engel, E.; Ambrosio, L. Chitosan/PEGDA based scaffolds as bioinspired materials to control in vitro angiogenesis. *Materials Science and Engineering: C* **2021**, *118*, 111420, doi:https://doi.org/10.1016/j.msec.2020.111420.

106. Tang, A.; Li, J.; Li, J.; Zhao, S.; Liu, W.; Liu, T.; Wang, J.; Liu, Y. Nanocellulose/PEGDA aerogel scaffolds with tunable modulus prepared by stereolithography for three-dimensional cell culture. *Journal of Biomaterials Science, Polymer Edition* **2019**, *30*, 797-814, doi:10.1080/09205063.2019.1602904.

107. Zhang, X.; Yan, Z.; Guan, G.; Lu, Z.; Yan, S.; Du, A.; Wang, L.; Li, Q. Polyethylene glycol diacrylate scaffold filled with cell-laden methacrylamide gelatin/alginate hydrogels used for cartilage repair. *Journal of Biomaterials Applications* **2022**, *36*, 1019-1032, doi:10.1177/08853282211044853.

References

1. Dang, Y.; Zhang, Y.; Luo, G.; Li, D.; Ma, Y.; Xiao, Y.; Xiao, L.; Wang, X. The decisive early phase of biomaterial-induced bone regeneration. *Applied Materials Today* **2024**, *38*, 102236, doi:https://doi.org/10.1016/j.apmt.2024.102236.

2. Dimitriou, R.; Jones, E.; McGonagle, D.; Giannoudis, P.V. Bone regeneration: current concepts and future directions. *BMC Medicine* **2011**, *9*, 66, doi:10.1186/1741-7015-9-66.

3. Dimitriou, R.; Jones, E.; McGonagle, D.; Giannoudis, P.V. Bone regeneration: Current concepts and future directions. *BMC Medicine* **2011**, *9*, doi:10.1186/1741-7015-9-66.

4. Claes, L.; Recknagel, S.; Ignatius, A. Fracture healing under healthy and inflammatory conditions. *Nature Reviews Rheumatology* **2012**, *8*, 133-143, doi:10.1038/nrrheum.2012.1.

5. Shiu, H.T.; Leung, P.C.; Ko, C.H. The roles of cellular and molecular components of a hematoma at early stage of bone healing. *Journal of Tissue Engineering and Regenerative Medicine* **2018**, *12*, e1911-e1925, doi:https://doi.org/10.1002/term.2622.

6. Xiao, L.; Ma, Y.; Crawford, R.; Mendhi, J.; Zhang, Y.; Lu, H.; Zhao, Q.; Cao, J.; Wu, C.; Wang, X.; et al. The interplay between hemostasis and immune response in biomaterial development for osteogenesis. *Materials Today* **2022**, *54*, 202-224, doi:10.1016/j.mattod.2022.02.010.

7. Yang, J.; Zhou, Y.; Wei, F.; Xiao, Y. Blood clot formed on rough titanium surface induces early cell recruitment. *Clinical Oral Implants Research* **2016**, *27*, 1031-1038, doi:https://doi.org/10.1111/clr.12672.

8. Lu, Y.; Lekszycki, T. Modeling of an initial stage of bone fracture healing. *Continuum Mechanics and Thermodynamics* **2015**, *27*, 851-859, doi:10.1007/s00161-014-0380-7.

9. Song, J.; Li, L.; Fang, L.; Zhang, E.; Zhang, Y.; Zhang, Z.; Vangari, P.; Huang, Y.; Tian, F.; Zhao, Y. Advanced strategies of scaffolds design for bone regeneration. *BMEMat* **2023**, *1*, e12046.

10. Noori, A.; Ashrafi, S.J.; Vaez-Ghaemi, R.; Hatamian-Zaremi, A.; Webster, T. A review of fibrin and fibrin composites for bone tissue engineering. *International Journal of Nanomedicine* **2017**, *12*, 4937-4961, doi:10.2147/IJN.S124671.

11. Rodríguez-Merchán, E.C. Bone Healing Materials in the Treatment of Recalcitrant Nonunions and Bone Defects. *International Journal of Molecular Sciences* **2022**, *23*, doi:10.3390/ijms23063352.

CHAPTER IV

BIOINKS FOR OSTEOGENIC DIFFERENTIATION

[This page is intentionally left blank.]

Introductory Note

Three-dimensional (3D) bioprinting is a form of additive manufacturing (AD) that provides for the construction of structures similar to organs and tissues, using a combination of cells, growth factors, and biomaterials [1]. These biomaterials, commonly referred to as 'bioinks', are designed to replicate the characteristics of native tissues, thereby offering functionalities that are crucial for tissue regeneration [2,3]. Specifically, bioinks are defined as cell-laden hydrogels that possess the physicochemical properties necessary to support biofabrication processes, which are critical for extrusion-based 3D bioprinting [4]. A well-formulated bioink must accommodate cells in various forms and microenvironments, such as single cells or cells aggregates. Furthermore, bioinks can be enriched with bioactive molecules, including growth factors, DNA, and miRNA [2,5].

The main advantage of 3D bioprinting lies in its ability to precisely and spatially distribute cells within solid or semi-solid biomaterials, thus enhancing the efficiency of tissue regeneration [6]. This technology not only enables the reconstruction of bone defects with complex geometries but also allows the creation of patient-specific implants by converting computed tomography (CT) or microCT data into printable models of the defects [7-9]. An optimal scaffold for bone regeneration must closely resemble the three-dimensional structure and composition of human bone, have a resorption rate that allows the natural bone of the recipient site to replace it, and support the nutrition and vascularization of the graft cells. These characteristics are essential for graft success and contribute to superior bone healing outcomes compared to non-osteoinductive ceramics [10].

Hydrogels are extensively studied and employed as bioinks across various tissue engineering applications due to their favorable properties that promote cell attachment and metabolic activities [5,11]. An ideal bioink should presents biochemical and biophysical properties that closely mimic those of natural tissues while also demonstrating high printability. However, it is challenging for single-component hydrogels to meet all these stringent requirements simultaneously. They must support high cell viability and instructive capacities while maintaining print fidelity to preserve the intended shape of the printed construct [12]. To achieve the necessary shape retention and prevent construct collapse, bioinks often require a high crosslinking density or high viscosity. Nevertheless, these

conditions create a relatively rigid environment that can restrict cellular activities. Conversely, soft matrices, which are more conducive to cell viability, often lack structural stability and fail to maintain the desired printed form [13,14]. Moreover, even widely used natural biomaterials, known for their excellent biocompatibility, cannot singularly replicate the complexity of the natural extracellular matrix (ECM) [15,16]. Consequently, single-component hydrogel bioinks present a limited biofabrication window [17].

To address these limitations, multi-component hydrogel bioink systems are being developed and have gained substantial attention. These systems typically incorporate biomimetic elements, such as proteins, peptides, and growth factors, alongside a base polymer. Additionally, secondary polymers, such as, hyaluronic acid (HA) or nanoparticles, such as, nano-hydroxyapatite (nHA), are integrated to enhance both biofunctionality and printability [3,17-22].

In recent years, bone tissue engineering has been increasingly employed to develop 3D *in vitro* human bone models, particularly for drug testing applications. This approach aligns with the principles of reduction, refinement, and replacement (the 3Rs) in biomedical research, aiming to minimize the use of animal models [23,24]. For these 3D *in vitro* bone models to be effective, the engineered ECM must closely replicate the intricate structure of physiological human bone ECM. This structural mimicry is particularly crucial for models that aim to simulate bone pathologies where the process of remodeling is disrupted [25].

For instance, in osteogenesis imperfecta—a genetic disorder characterized by brittle bones—the collagen network within the bone ECM is more loosely woven, and the minerals present are smaller and disorganized, resulting in compromised bone strength [26]. Similarly, in the case of osteoporosis, studies using mouse models have shown that collagen fibrils in the bone are less aligned and only partially mineralized, contributing to bone fragility [27]. To accurately replicate these pathological ECM structures *in vitro*, it is first necessary to recreate the ECM structure of healthy bone. This serves as a baseline, enabling the differentiation between healthy and diseased states in the model [28].

The subsequent Chapter is dedicated to the development of a bioink formulation specifically designed for extrusion-based bioprinting. This formulation integrates alginate, nHA, and collagen (Col) with human bone marrow-derived

mesenchymal stem cells (hBMSCs). Notably, this study represents the first application of these specific biomaterials in conjunction with hBMSCs through biofabrication using a pressure-assisted extrusion technique. Consequently, this approach provides a bioprinted model that serves as an invaluable tool for studying osteogenesis and the early stages of tissue maturation *in vitro*. Additionally, the development of this bioink will serve as a preliminary study for the subsequent production of a hybrid scaffold, which will be the focus of the following chapter.

To achieve this aim, a comprehensive characterization of the bioprinted models was conducted, encompassing rheological, mechanical, and swelling analyses. These studies were essential to assess the physical properties and stability of the bioprinted constructs. In addition, *in vitro* evaluations were performed using LIVE/DEAD staining and the PrestoBlue™-based viability assay to assess cell viability and metabolic activity within the constructs. Finally, gene expression analysis was carried out to study the cellular responses and differentiation potential, providing deeper insights into the biological performance of the bioprinted models.

[This page is intentionally left blank.]

Innovative Ink-Based 3D Hydrogel Bioprinted Formulations for Tissue Engineering Applications

Ana Catarina Sousa, Grace Mcdermott, Fraser Shields, Rui Alvites, Bruna Lopes, Patrícia Sousa, Alícia Moreira, André Coelho, José Domingos Santos, Luís Atayde, Nuno Alves, Stephen Richardson, Marco Domingos and Ana Colette Maurício

In *Gels*

DOI: 10.3390/ gels10120831

[This page is intentionally left blank.]

Article

Innovative Ink-Based 3D Hydrogel Bioprinted Formulations for Tissue Engineering Applications

Ana Catarina Sousa [1,2,3], Grace Mcdermott [4], Fraser Shields [4], Rui Alvites [1,2,3,5], Bruna Lopes [1,2,3], Patrícia Sousa [1,2,3], Alícia Moreira [1,2,3], André Coelho [1,2,3], José Domingos Santos [6], Luís Atayde [1,2,3], Nuno Alves [7], Stephen Richardson [4], Marco Domingos [8] and Ana Colette Maurício [1,2,3*]

[1] Departamento de Clínicas Veterinárias, Instituto de Ciências Biomédicas de Abel Salazar (ICBAS), Universidade do Porto (UP), Rua de Jorge Viterbo Ferreira, nº 228, 4050-313 Porto, Portugal; anacatarinasoaressousa@hotmail.com (A.C.S.); ruialvites@hotmail.com (R.A.); brunisabel95@gmail.com (B.L.); pfrfs_10@hotmail.com (P.S.); alicia.moreira.1998@gmail.com (A.M.); andrefmc17@gmail.com (A.C.); ataydelm@gmail.com (L.A); ana.colette@hotmail.com or acmauricio@icbas.up.pt (A.C.M.).

[2] Centro de Estudos de Ciência Animal (CECA), Instituto de Ciências, Tecnologias e Agroambiente da Universidade do Porto (ICETA), Rua D. Manuel II, Apartado 55142, 4051-401, Porto, Portugal;

[3] Associate Laboratory for Animal and Veterinary Science (AL4AnimalS), Lisboa, Portugal.

[4] Department of Cell Matrix Biology & Regenerative Medicine, Faculty of Biology, Medicine & Health, The University of Manchester, Manchester M13 9PL, UK; grace.mcdermott@postgrad.manchester.ac.uk (G.M.); fraser.shields@postgrad.manchester.ac.uk (F.S.); s.richardson@manchester.ac.uk (S.R.).

[5] Instituto Universitário de Ciências da Saúde (CESPU), Avenida Central de Gandra 1317, Gandra, 4585-116 Paredes, Portugal.

[6] REQUIMTE-LAQV, Departamento de Engenharia Metalúrgica e Materiais, Faculdade de Engenharia, UP; jdsantos@fe.up.pt (J.D.S.).

[7] Centre for Rapid and Sustainable Product Development (CDRSP), Polytechnic Institute of Leiria, Portugal; nuno.alves@ipleiria.pt (N.A.).

[8] Department of Mechanical and Aerospace Engineering, School of Engineering, Faculty of Science and Engineering & Henry Royce Institute, The University of Manchester, Manchester M13 9PL, UK; e-mail@e-mail.com

* Correspondence: ana.colette@hotmail.com or acmauricio@icbas.up.pt (A.C.M.)

Abstract: Three-dimensional (3D) models with improved biomimicry are essential to reduce animal experimentation and drive innovation in tissue engineering. In this study, we investigate the use of alginate-based materials as polymeric inks for 3D bioprinting of osteogenic models using human bone marrow stem/stromal cells (hBMSCs). A composite bioink incorporating alginate, nano-hydroxyapatite (nHA), type I collagen (Col) and hBMSCs was developed and for extrusion-based printing. Rheological tests performed on crosslinked hydrogels confirm the formation of solid-like structures, consistently indicating a superior storage modulus in relation to the loss modulus. The swelling behavior analysis showed that the addition of Col and nHA into an alginate matrix can enhance the swelling rate of the resulting composite hydrogels, which maximizes cell proliferation within the structure. The LIVE/DEAD assay outcomes demonstrate that the inclusion of nHA and Col did not detrimentally affect the viability of hBMSCs over seven days post-printing. PrestoBlueTM revealed a higher hBMSCs viability in the alginate-nHA-Col hydrogel compared to the remaining groups. Gene expression analysis revealed that alginate-nHA-col bioink favored a higher expression of osteogenic markers, including secreted phosphoprotein-1 (SPP1) and collagen type 1 alpha 2 chain (COL1A2) in hBMSCs after 14 days, indicating the pro-osteogenic differentia-tion potential of the hydrogel. This study demonstrates that the incorporation of nHA and Col into alginate enhances osteogenic potential and therefore provides a bioprinted model to systematical-ly study osteogenesis and the early stages of tissue maturation in vitro.

Keywords: alginate; bioInk; bioprinting; bone regeneration; collagen; hydroxyapatite; human bone marrow stem/stromal cells.

---

1. Introduction

Bone diseases are an important global public health problem that have significant economic effects, particularly for people suffering from osteoporosis [1–3]. Research models that replicate the bone structure, its functions, and the cell–cell and cell–matrix interactions that occur in vivo have been developed to ensure the clinical translation of new treatments to more reliably treat these bone pathologies [4]. Considering the ever-increasing growth of bone tissue engineering and the challenge of bone's complexity, in the last decade, several three-dimensional (3D) models have been developed to mimic the bone

microenvironment, aiming to reduce or replace the dependence on animal experiments [5]. Nevertheless, these models are unable to fully replicate the complex structural and cellular composition of bone tissue [6].

Bioprinting has emerged as a transformative approach within regenerative medicine and tissue engineering, demonstrating significant potential for the generation of three-dimensional tissue constructs [7]. A noteworthy application of this technology is in the field of bone tissue regeneration, which has been increasingly emphasized. This is mainly due to the structural and biological complexities that define the nature of bone tissue [8]. The production of 3D models of bone tissue remains a major challenge to achieve, since the selection of materials and manufacturing processes and the establishment of optimal conditions to support multiple cell populations, as well as their osteodifferentiation, leads to the development of these models not being a trivial task [9]. The choice of biocompatible materials plays an important role not only in mimicking the physical properties of bone, but also in providing the biochemical pathways necessary to guide the behavior of stem cells. Various biomaterials, such as calcium phosphate ceramics, bioactive glass, and hydrogels (e.g., alginate), have been used in bioprinting to promote osteogenesis.

Alginate, an FDA-approved natural polysaccharide, is widely employed in bio-medical applications as a bioink [10,11]. This widespread use is attributed to its low cost [12], accessibility [13], and ease of preparation [14]. Consequently, alginate-based hydrogels emerge as a promising candidate capable of offering a three-dimensional (3D) microenvironment encompassing both organic and inorganic elements vital for osteoblast functionality. Nevertheless, alginate is an inert material and lacks osteoinductive signals necessary for promoting osteoblast differentiation and bone formation. To address these limitations, additional modifications are required to enhance its osteogenic potential. Combining alginate with collagen (Col), the primary structural component of the extracellular matrix (ECM), and bioactive ceramics, such as hydroxyapatite (HA), can significantly increase osteoconductivity [12,15,16]. These materials were selected due to bone's hierarchical structure, consisting of living cells immersed in a matrix primarily composed of Col and HA [17]. Researchers focus on mimicking the bone's composition to achieve a high degree of similarity between the 3D printed scaffold and bone tissue. Col represents nearly 80% of the organic material in bones [18,19]. It is a suitable biomaterial due to its outstanding biocompatibility, degradability,

adhesion characteristics, osteo-genic induction properties, and minimal immunogenicity [20]. Additionally, nano-HA (nHA) presents stability, biocompatibility, hydrophilicity, and degradability. This ceramic enhances the adhesion and proliferation of osteoblasts and possesses the capacity to establish chemical bonds with the surrounding bone tissue [21]. The combination of alginate, a biocompatible polymer capable of forming stable gels, nHA, an osteoconductive element, and Col, a primary organic component of natural bone, has been demonstrated to improve the biomineralization, promoting natural bone regeneration [22]. These biomaterials have been utilized in bone bioprinting applications to replicate the complex hierarchical structure of bone tissue, which is essential for its biological functions [23–26]. Hassani et al. developed cell-laden alginate-nHA-Col microcapsules for modular bone tissue, and the results suggest that this structure promotes mineralization and the osteogenesis signaling pathways of the encapsulated cells [27]. Despite their effectiveness in creating controlled microenvironments for osteogenesis, microcapsules present certain limitations. They are unable to fully replicate the complex hierarchical structure of native bone tissue, as cell–material interactions are restricted by the encapsulation process within the alginate matrix. This confinement limits the degree of cell–matrix interaction, potentially hindering cellular behaviors such as migration and differentiation. Addition-ally, microcapsules present challenges in reproducibility, as their size, composition, and cell distribution can differ. In contrast, bioprinting techniques using the same materials offer advantages in creating more structured, complex 3D environments that more closely mimic native bone architecture. These methods enable enhanced cell–matrix interactions, which can improve osteogenesis. Furthermore, the automation and standardization of biofabrication processes provides greater reproducibility of 3D tissue models.

In the field of regenerative medicine, the integration of biomaterials with mesenchymal stem/stromal cells (MSCs) has been prevalent, as this approach promotes the proliferation and differentiation of MSCs [28,29]. These cells can be isolated from several tissues, including bone marrow [30]. Human MSCs derived from bone marrow (hBMSCs) are considered multipotent stromal cells, and they possess the inherent capacity to differentiate into osteoblasts and form bone tissue, allowing their osteogenic differentiation to be studied directly in a 3D environment [31,32].

In light of these considerations, the present study aimed to develop a bioink formulation tailored for extrusion-based bioprinting, incorporating alginate, nHA, and Col, along with hBMSCs. This is the first study applying these biomaterials and hBMSCs, through biofabrication (using a pressure-assisted extrusion technique), seeking to address the fundamental challenge of replicating the composition of the native ECM in terms of materials (organic and inorganic) to study osteogenesis in 3D. Therefore, this technique ensures the spatial distribution and cell loading efficiency, facilitates the detailed study of cell–biomaterial interactions, and results in the creation of highly structured and functional tissue constructs. This approach provides a bioprinted model to study osteogenesis and the early stages of tissue maturation in vitro. Therefore, the current work highlights the production of a tailored bioink and underlines its significant contribution to the development of a 3D model for studying the osteogenic differentiation of MSCs. The methodology presented in this study can be readily adapted for broader applications in personalized medicine, including 5D bioprinting, which integrates 3D model construction with data on physiological activity, providing a powerful tool for personalized therapies, as demonstrated in previous studies [33,34]. Moreover, this alginate-based system holds potential for promising applications in toxicological testing using organoid models. This flexibility highlights the adaptability of our biofabrication approach, ex-tending its utility to the broader contexts of 5D personalized medicine and organoid-based toxicological screening.

2. Results and Discussion

The aim of the study was to explore the combination of alginate, nHA, and Col to create a composite ink for 3D bioprinting of constructs capable of replicating the com-position of native bone ECM, facilitating in vitro studies on osteogenesis and contributing to reducing animal experimentation in the field of tissue engineering.

Alginate was used due to its properties, namely, easy adjustability, low price, and accessibility [12,14]. Furthermore, the inclusion of nHA, a mineral, and Col, a protein, has been implemented due to their well-known capacity to enhance osteogenic potential and accelerate the regeneration of modular bone tissue [35]. While the inclusion of hydrox-yapatite in hydrogels can improve the osteogenic and rheological properties, Col can support high cell viability, proliferation, and

differentiation, providing an optimal mi-croenvironment conducive to cell survival and functional performance of the printed composite [19,36,37].

The concentrations of alginate, nHA, and Col used in this study (2%, 0.5%, and 0.5%, respectively) were selected based on findings from previous research [38]. A 2% alginate concentration was selected for its ideal balance of gel strength and printability, providing excellent gelling properties, structural integrity, and effective cell encapsulation and nutrient diffusion [38]. Additionally, the incorporation of 0.5% nHA and 0.5% Col is based on the research conducted by Hassani et al. [27], which demonstrated that these con-centrations contribute to an osteogenic microenvironment favorable to the development of bone tissue. These concentration ratios were chosen to leverage their synergistic effects, aiming to enhance the osteogenic differentiation and the overall structural integrity of the hydrogel [27]. The selected concentrations are consistent with those used in similar studies, but preliminary experiments were conducted to test a range of concentrations for each component. The final concentrations achieved the best balance of printability, structural stability, and biological functionality, as verified by our data.

The dual crosslinking methodology employed in this study follows a sequential process aimed at optimizing both the biological and mechanical properties of the hy-drogel. Initially, Col fibrillogenesis was induced by raising the temperature to 37 ˚C for 90 min, allowing the collagen component to self-assemble into fibrils that closely mimic the natural extracellular matrix. This step is key for promoting cell–matrix interactions, which support cellular adhesion and osteogenic differentiation. Afterwards, CaCl2 solution was introduced to initiate the ionic crosslinking of alginate. Despite the rapid gelation of al-ginate upon contact with Ca2+ ions, the solution was left to interact for an extended period of 40 min. This duration was selected to ensure comprehensive crosslinking throughout the hydrogel matrix, thereby enhancing its mechanical stability and functional integrity. The sequential approach of collagen self-assembly followed by alginate crosslinking is essential for creating a composite hydrogel that balances bioactivity with mechanical strength [39]. The dual crosslinking methodology employed presents notable benefits, but it also has limitations, including potential spatial heterogeneity and extended processing times. Future research should aim to address these issues by improving the distribution of crosslinking agents, investigating more efficient methods, and optimizing cell en-capsulation

techniques to enhance the methodology's applicability and performance in tissue engineering [39–42].

2.1. Rheological Characterization

To achieve optimal print fidelity, several material properties, including viscoelastic behavior, must be considered to ensure that the bioink flows smoothly through the nozzle, maintaining high cell viability during deposition [43]. The viscoelastic characteristics of the crosslinked hydrogels were assessed through oscillatory rheology using amplitude and frequency sweep tests (Figure 1). First, the upper limit of the linear viscoelastic region (LVR) was determined from the storage modulus (G') curve assuming a ±5% deviation between two consecutive measurements at 0.1% oscillation strain (Figure 1a).

Amplitude sweep tests (Figure 1a) also demonstrated that both formulations exhibited a gel-like or solid structure behavior in the LVR with a higher G' compared to the G'' (G' > G''). According to the literature, viscoelastic solids present a higher storage modulus than loss modulus, due to the strong internal chemical bonds and physicochemical reactions in the material [44]. Considering constant amplitude and frequency conditions (1% strain, 1 Hz frequency), the G' was about ten times higher than the G'', indicating a solid elastic behavior for both formulations. Furthermore, the addition of nHA and Col did not appear to significantly alter LVR ($p > 0.05$). Clearly from the results, nHA and Col did not seem to affect the initial characteristics of the hydrogel. The overall modulus of elasticity and loss values did not change between the gels.

Analysing Figure 1a also shows that the alginate-nHA-Col group presented a higher yield point (0.00974) compared to the alginate group (0.00864), suggesting that the addition of nHA and Col increased the material's resistance to initial deformation. Meanwhile, the flow point, indicating the transition to a viscous-dominated behavior, was lower in the alginate-nHA-Col group (0.0318) than in the alginate group (0.0685). These data suggest that although the composite hydrogel requires slightly more stress to begin yielding, it transitions to a flow state more readily, possibly due to the combination of the effects of the nHA reinforcement and the elastic behavior of the Col. To further evaluate the transition from the LVR to the flow state, the flow transition index (ratio of flow point to yield point) was calculated. The alginate group presented a higher index (3.26) compared to the

alginate-nHA-Col group (7.93), suggesting that the alginate-nHA-Col group has less tendency to brittle fracture [45].

Frequency sweeps were performed within the linear viscoelastic range (LVR) of both formulations at an oscillation strain of 0.1% (Figure 1b). The results demonstrated that both formulations exhibited viscoelastic gel-like properties, with no clear dependency of the G' or G" on frequency. Remarkably, a consistent difference of 8 kPa was observed between G' and G" across all tested frequencies for both formulations.

A non-dependence between these values and frequency suggests that the material's elastic and viscous properties were not influenced by the frequency of the applied stress. This is a characteristic of a gel that is stable and does not change its behavior significantly over a range of frequencies. This type of behavior is typical of gels that are well-formed, and it is often noted in materials that are used in applications where they need to maintain their structure and properties over time [46].

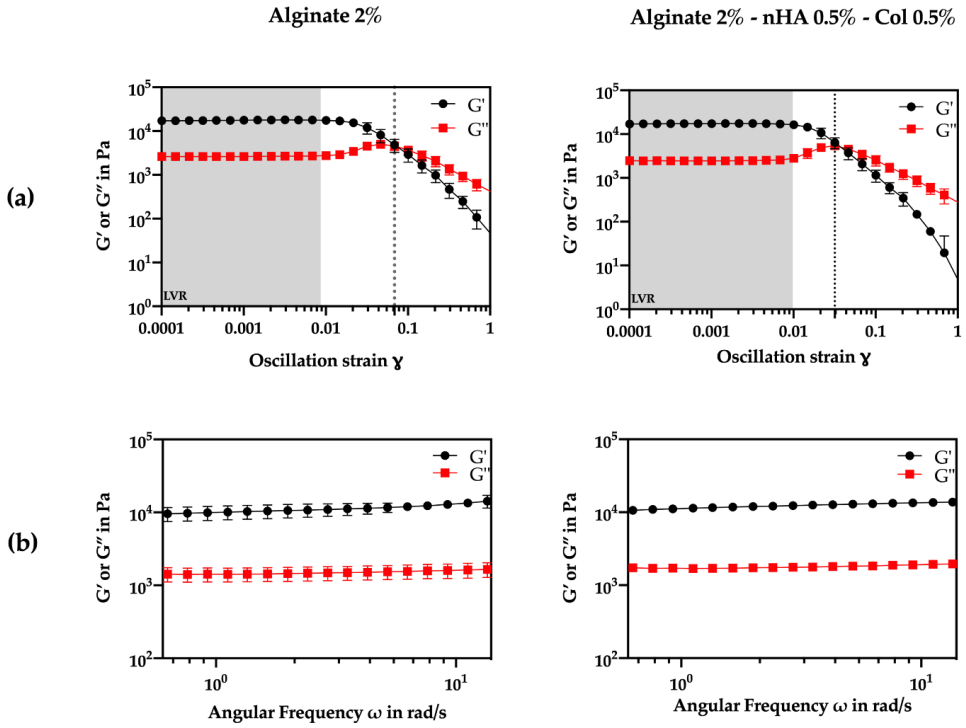


Figure 1. Rheological experiments with the storage moduli (G') (shown in black) and loss moduli (G") (shown in red) of crosslinked alginate and alginate-nHA-Col under a range of conditions. (a) Amplitude sweeps performed at a frequency of

1 Hz. (b) Frequency sweeps performed at an oscillation strain of 0.1%. The evaluations were performed in triplicate.

2.2. Mechanical Analysis

The success of a hydrogel is highly dependent on its mechanical properties, as these properties ensure the hydrogel's structural integrity under both in vitro and in vivo conditions [47]. Parameters such as porosity, pore size, composition, degree of crosslinking, and ionic strength of materials can significantly influence their mechanical strength [48]. In the present work, the mechanical properties of alginate-based gels were evaluated through compressive mechanical testing. Figure 2 illustrates the compressive strength-strain curve and Table 1 provides the Young's modulus measurements of the alginate-based hydrogels.

Based on the stress–strain curve (Figure 2), the alginate-only hydrogel presented a lower stress–strain behavior due to its brittle nature, whereas the composite hydrogel comprising nHA and Col revealed higher stress–strain behavior due to the combined effects of nHA's reinforcement and Col's elasticity. nHA contributed to the reinforcement of the hydrogel matrix, distributing stress more evenly and enhancing the material's toughness and resistance to deformation [48]. On the other hand, Col, being a fibrous protein, provided elasticity and improved the tensile strength of the hydrogel, providing a more flexible matrix that could stretch further before rupturing [49]. The combination seemed to make the hydrogel more durable and capable of withstanding higher stresses and strains.

Young's modulus was calculated at 10% strain and the addition of 0.5% (*w/v*) nHA and 0.5% (*w/v*) of Col 0.5 wt % to alginate decreased the Young's modulus of Alg hydrogel from 7.33 to 6.80 MPa (Table 1). Notwithstanding, no statistically significant differences were observed in the average Young's modulus between the two groups.

Based on these findings, the hydrogel composed of only alginate appeared to have a higher initial stiffness (higher Young's modulus) but a lower capacity to withstand large deformations (lower stress–strain behavior) due to its more fragile nature. Meanwhile, the hydrogel composed of alginate, nHA, and Col seemed to be more flexible initially (lower Young's modulus) and better able to withstand large

deformations (higher stress–strain behavior) due to the addition of Col, which increased elasticity, and nHA, which reinforced the matrix.

The combination of the different components in the hydrogel resulted in a material that can better absorb and dissipate stresses, resulting in greater deformation capacity and final strength, despite being initially more flexible.

The bioink formulation's rheological and mechanical properties were tailored to enhance the bioprinting process, allowing mimicry of the complex environment of the bone's ECM, which is crucial for supporting osteogenesis in vitro.

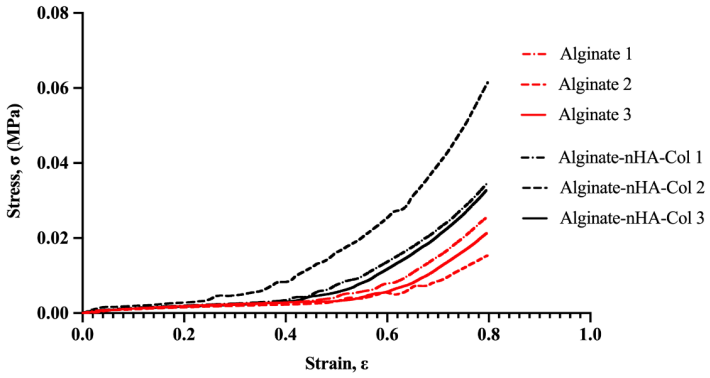


Figure 2. Stress–strain curves resulting from compression tests of alginate hydrogel (red) and alginate-nHA-Col hydrogel (black) (n = 3).

Table 1. Young's modulus measurement of alginate and alginate-nHA-Col hydrogels produced (mean ± sd values) (n = 3).

Parameter (MPa)	Alginate	Alginate-nHA-Col (w/v)	p Value
Young's Modulus	7.33 ± 1.21	6.80 ± 0.835	0.567

2.3. Hydrogel Swelling Behavior

The swelling properties play a fundamental role in facilitating the release of molecules, absorption of biofluids, and distribution of nutrients in the structure [35]. Swelling rates are an important feature of bioinks, with ideal formulations undergoing controlled degradation to facilitate new tissue growth [50–53]. Hydrogels intrinsically swell as solvent molecules infiltrate the spaces within the polymeric network. In 3D bioprinting, the extent of swelling is reflected in the dimensional alterations of bioprinted structures [54–56]. Moreover, the swelling ratio is essential in modulating the drug release dynamics from these polymeric

systems [56–58]. Hydrogel swelling behavior (pH = 7.4 at 37 ˚C) was evaluated at time intervals of 1, 2, 3, 4, 5, 24, 48, and 72 h. The absorption of DPBS by the hydrogels is shown in Figure 3. The hydrogels appeared to absorb a significant amount of DPBS at first, and then more gradually over time. The hydrogel appeared to reach swelling equilibrium in a relatively short time (3 h). The maximum swelling ratio was noted up to 24 h. The decrease in swelling rate noted after 24 h may result from the hydrogel reaching equilibrium, where osmotic forces balance the polymer network's elastic forces, leading to reduced swelling. Additionally, hydrolytic degradation of some alginate-based samples under the test conditions may have compromised structural integrity and water retention capacity [59].

Although the data were not significantly different, after 3 h in culture, the hydrogel with nHA and Col seemed to increase the swelling compared to the hydrogel with alginate only. The incorporation of Col and nHA to alginate can increase the swelling rate of the resulting composite material due to the enhanced stability and mechanical strength of the alginate hydrogel, leading to a more controlled degradation rate. The incorporation of Col and nHA into alginate matrices may potentially influence the swelling rate of the resulting composite hydrogels. Col, being a hydrophilic material, presents more hydrophilic bonds, which can result in water retention and consequently affect the swelling behavior [60]. Additionally, the hydrophilic nature of hydroxyapatite in the material composition can lead to overall water absorption and potentially enhance cell growth, proliferation, and viability within the material [21]. For bone mimicry, a high degree of swelling is particularly important, as it allows cell infiltration into the hydrogels and maximizes cell growth within the structure [61].

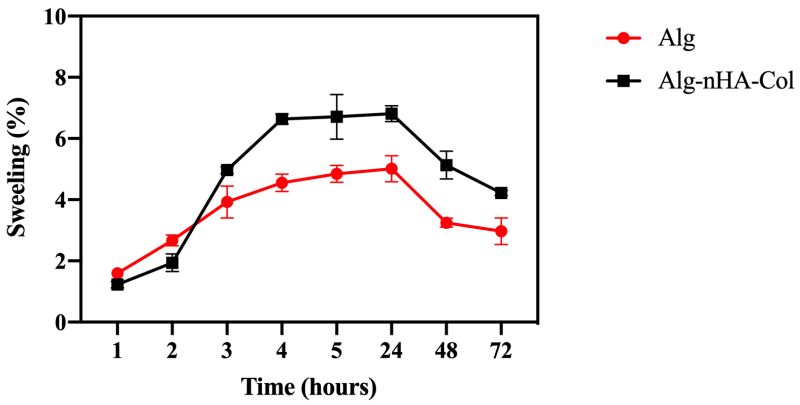


Figure 3. Hydrogel swelling rate from 1 to 72h. Alg: alginate (red); Alg-nHA-Col (black) (n = 3).

2.4. Bioprinting of Cell-Laden Hydrogels

This study integrated bioprinting and pressure-assisted extrusion technologies in the printing protocols for alginate-based bionks. The printing process was carried out using the RegenHU 3D Discovery Evolution system with 2% (*w/v*) alginate bioinks. This formulation was selected based on prior studies due to its low viscosity and shear-thinning properties, making it suitable for bioprinting cellular inks [38]. The bioprinting parameters, including needle diameter, pressure, feed speed, filament distance, and thickness, were properly adjusted to establish an optimum equilibrium between printing resolution, speed, and cell activity (Table 2). The printing parameters were adjusted to guarantee high cell viability during the printing process while ensuring the extrusion of accurate filaments, with the external filament diameter corresponding the internal diameter of the nozzle used. This precision is of paramount importance to ensure the fidelity of the structural form in the final constructs, thus achieving an accurate physical replication of the digital CAD model (Figure 4A–C).

Given the low viscosity of the ink formulations used, without compromising shape fidelity [38], suspension bioprinting strategies were employed. A 0.5% (*w/v*) agarose support bath was utilized to maintain the structure of the printed material in suspension (Figure 4D). Once the material had been deposited and crosslinked, the suspension bath was removed and the hydrogels with the cells could grow.

Table 2. Parameters used in the RegenHU 3D Discovery Evolution system. The values are shown in the respective units.

Parameters	Values (Unit)
Needle Diameter	600 µm
Pressure	0.02 MPa
Feed Rate	10 mm/s
Filament Distance	500 mm
Thickness	500 mm

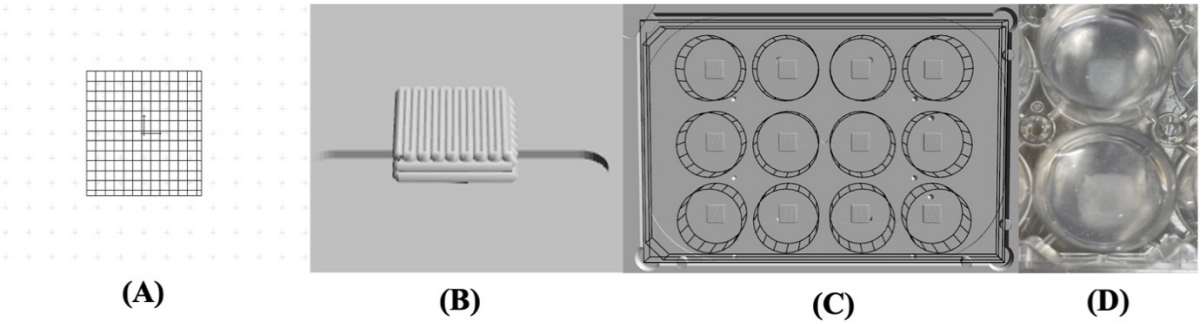


Figure 4. (A) CAD model designed in BioCAM™ software (*version* 2.0); (B) 3D generated model; (C) 3D generated model in a 12-well plate; (D) Cell-laden print in the agarose support bath.

2.5. Live/Dead Staining

Cell viability must be maintained both during and after the 3D tissue printing process. Therefore, an assessment of cell viability (hBMSCs) was performed using a Live/Dead analysis. This analysis was conducted after 1, 3, and 7 days in culture (Figure 5A,B).

The staining demonstrated high levels of cell viability in both alginate and alginate-nHA-Col hydrogels throughout all time points (Figure 5A).

The hBMSCs viability and distribution did not appear to depend on the inclusion of nHA and Col to the gel, and the cells seemed to be homogeneously distributed in both hydrogels. In fact, some cell death was observed throughout the experiment, although this was to be expected due to exposure to significant shear stress during the printing process, which can cause cell damage and death [62]. Nevertheless, the results of the alginate-nHA-Col group indicated that live cell portions remained above 80% one week after processing (Figure 5B). It is important to note that alginate-nHA-Col group presented slightly higher values of cell viability, but with no significant differences when compared to the alginate group throughout the experiment.

In addition, data showed that a spherical cell morphology was preserved throughout the culture in both conditions. Maintaining a spherical cell morphology within bioinks is advantageous for preserving cell viability and functionality throughout the bioprinting process. This preservation of native cell structure is essential for ensuring proper differentiation into specific cell lineages, which is critical for effective tissue engineering applications [53].

These findings suggest that alginate-nHA-Col hydrogels were non-cytotoxic and provided a supportive matrix conducive to high cell viability of hBMSCs. The results confirmed the hydrogels' ability to sustain hBMSC culture, suggesting that the pressure-assisted extrusion process did not adversely affect cell viability.

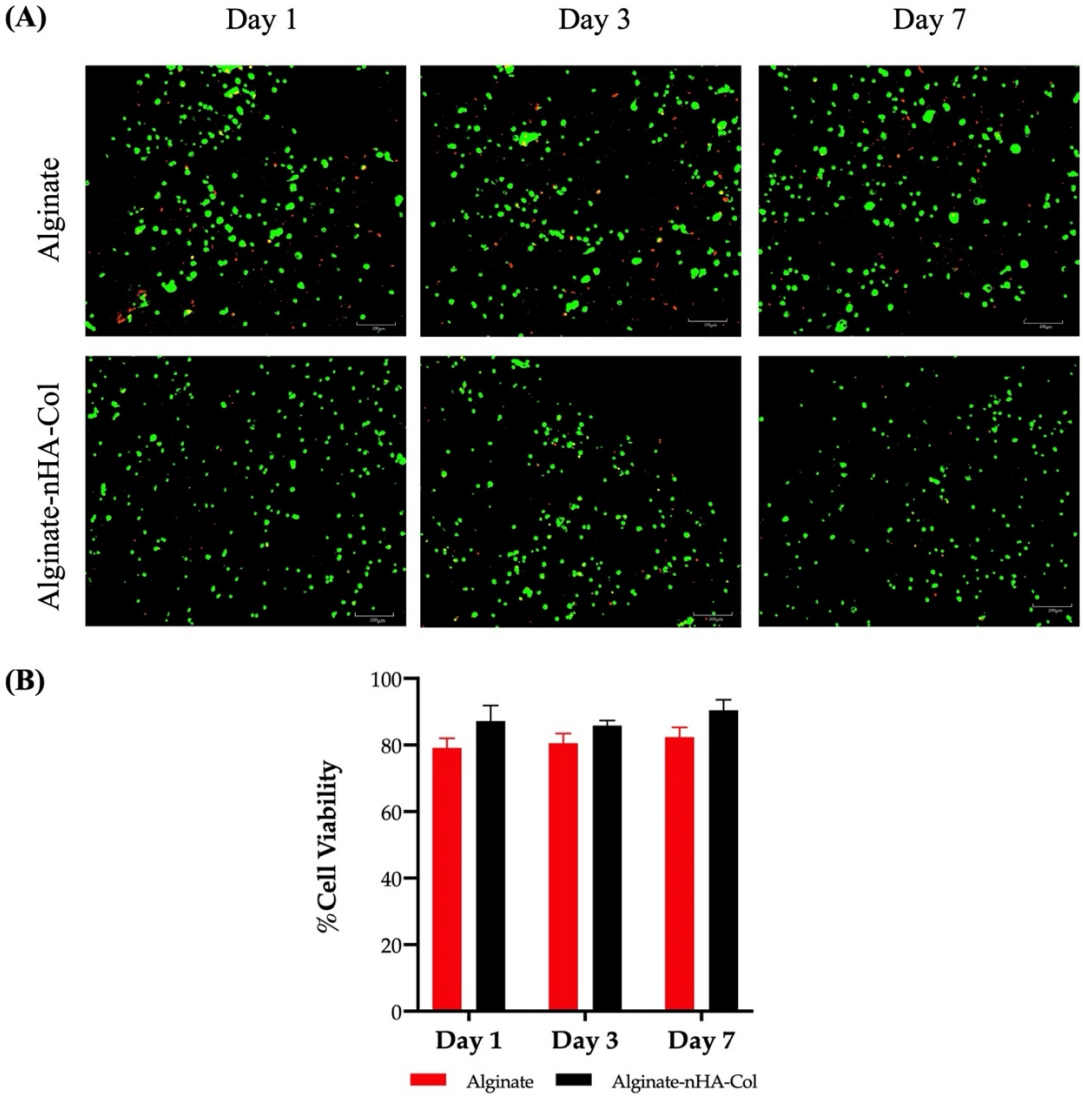


Figure 5. (A) Live/dead staining images of printed hBMSCs in alginate and alginate-nHA-Col after 1, 3, and 7 days in culture. Live cells are stained green and dead cells are stained red. (B) The percentage of cell viability of bioprinted hBMSCs cultured in 2% alginate and 2% alginate-0.5% nHA-0.5% Col for 1, 3, and 7 days (n = 3).

2.6. Cell Viability Assay

In accordance with the ISO 10993-5:2009 guidelines, the assessment of cellular viability was determined using PrestoBlue™ (*Thermo Fisher Scientific, Waltham, MA, USA*) on both alginate and alginate-nHA-Col hydrogels in the presence of hBMSCs. The control group, devoid of hydrogels, was also included for reference. Figure 6A represents the corrected absorbance values for the designated time points (1, 3, 5, and 7 days). The data showed cell proliferation in all groups up to day 5. While the hydrogels containing alginate, nHA, and Col exhibited slightly higher cell viability rates compared to the other groups, statistically significant differences were only observed on day 3. In contrast, alginate-nHA-Col hydrogels showed significantly greater absorbance than the control group, suggesting enhanced cell adhesion and proliferation. These findings are consistent with previous studies, indicating that the alginate-nHA-Col hydrogels demonstrated superior cytocompatibility overall when compared to the control group [27].

Figure 6B displays the viability inhibition percentages, normalized to the control group. According to the ISO 10993-5:2009 guideline, a cytotoxic effect is considered when an inhibition of viability larger than 30% is identified (outlined in Figure 6B by dashed lines). These findings suggest that both alginate and alginate-nHA-Col can be classified as non-cytotoxic.

In agreement with the results presented in the Live/Dead analysis, the viability results confirmed that, on one hand, the hydrogels are supportive of hBMSCs encapsulation and function and that, on the other, the printing process does not negatively impact cell survival, which remained viable for up to seven days post-encapsulation.

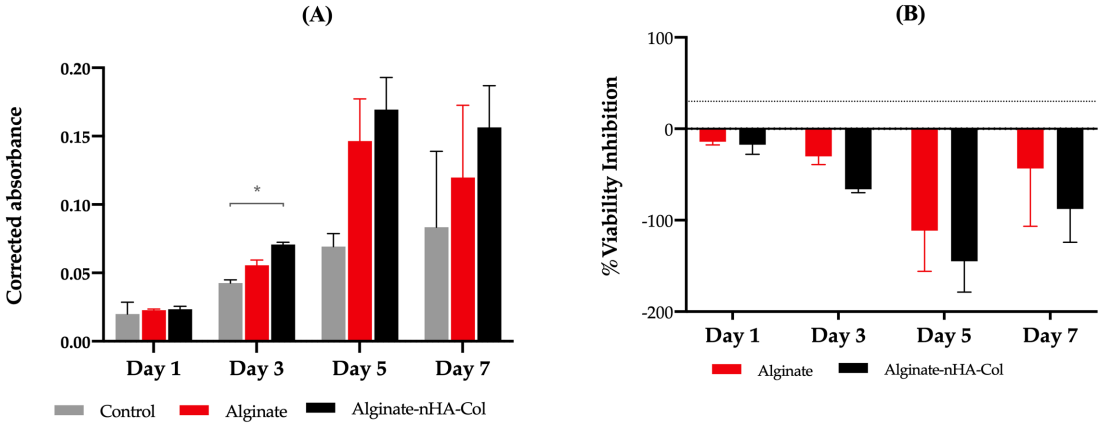


Figure 6. (A) Corrected absorbance evaluated by Presto Blue® viability assay for hBMSCs (n = 3). Result significances are presented through the symbol (*), according to the p value, with * $p < 0.05$. (B) Percent viability inhibition assay. The results were normalized in relation to the control. The 30% threshold shown (dashed line) represents the inhibition above which the effect is considered cytotoxic (under ISO 10993-5:2009 guidelines).

2.7. Gene Expression

Osteogenesis of hBMSCs cultured in alginate and alginate-nHA-Col for 7 and 14 days was evaluated using qPCR for a panel of key differentiation marker genes (Figure 7). This gene expression analysis provided insights into the biofunctionality and osteoinductive potential of the inks for bone tissue regeneration.

After 14 days of culture, gene expression analysis revealed a higher expression of osteogenic markers (Figure 7) in all experimental groups compared to the same groups after 7 days. At both time points, the expression of RUNX2 in the alginate-nHA-Col group was slightly higher than the alginate group at both time points (Figure 7A). RUNX2 is a gene expressed during early bone differentiation, and its increased expression from 7 to 14 days is consistent with expected osteogenic progression. Similarly, in the study by Im et al., bioinks composed of alginate, tempo-oxidized cellulose nanofibrils, and polydopamine nanoparticles demonstrated an increase in RUNX2 gene expression over the same time period, further supporting these findings [8]. This gene plays a crucial role in regulating the osteogenic differentiation of hBMSCs and presence of this gene leads to the formation of mature osteoblasts and complete bone formation [63]. ALPL is associated with the biological process of endochondral ossification/osteoblast differentiation [64] and showed a minimal increase from day 7 to day 14 (Figure 7B). Gene expression of IBSP demonstrated an increase in both groups from 7 to

14 days (Figure 7C). IBSP expression has been shown to increase the expression of key osteogenic and angiogenic markers, indicating its beneficial role in promoting the formation and vascularization of bone tissue [65,66]. Furthermore, IBSP encodes bone sialoprotein, a protein involved in matrix production by promoting the nucleation of hydroxyapatite crystals during the mineralization process [67]. This trend was similarly observed in the study by Van der Heide et al., where IBSP expression increased over time, confirming its role in bone mineralization [68].

Although not statistically significant, the expression of SPP1 in the alginate group was higher than in the alginate-nHA-Col group (Figure 7D). SPP1 is a crucial component of the organic matrix of bone and serves as a binding protein for osteoclasts, the cells responsible for bone remodeling [69].

COL1A2 was not expressed in any of the groups after 7 days (Figure 7E). However, after 14 days, the alginate-nHA-Col group showed an up-regulation of COL1A2 expression compared to the alginate group. The observed increase in COL1A2 gene expression aligns with findings reported in the literature [70]. Col is a major ECM protein synthesized by osteoblasts and significantly contributes to bone strength [71]. The observed increased expression of these osteoblastic genes in 3D hBMSCs constructs after 14 days suggests that the incorporation of alginate, nHA, and Col elements in the bioink is important for enhancing osteogenic differentiation.

The presence of bone-related gene expression in alginate-nHa-Col at day 14 also suggests a positive and sustained long-term osteogenic effect in hBMSCs. Nevertheless, osteogenic differentiation is a complex process that involves the sequential expression of several genetic markers at different times. For instance, early markers such as RUNX2 and osterix are expressed during the initial phases of differentiation, while later markers such as SPP1 and osteocalcin are associated with mature osteoblasts and mineralization [72]. As future research, it is important to evaluate genetic markers over an extended period, such as 21 days. In addition, further studies, such as staining with ALP and Alizarin Red, would be pertinent in providing better validation of the support's functionality and osteogenic differentiation.

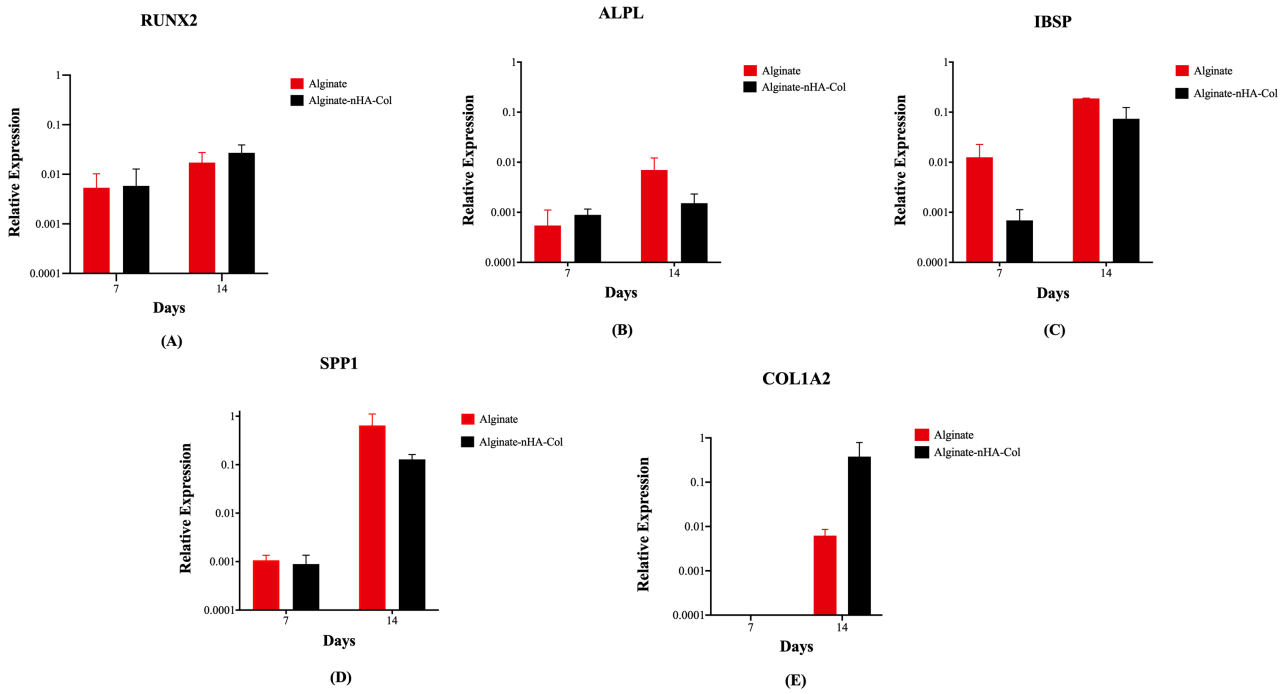


Figure 7. Gene expression levels of printed hBMSCs in alginate and alginate-nHA-Col bioinks after 7 and 14 days under osteogenic differentiation: runt-related transcription factor 2 (RUNX2) (A), alkaline phosphatase (ALPL) (B), integrin-binding sialoprotein (IBSP) (C), secreted phosphoprotein-1 (SPP1) (D), and collagen type 1 alpha 2 chain (COL1A2) (E).

3. Conclusions

The current work developed a composite hydrogel bioink to replicate native tissue composition for 3D osteogenesis studies, enabling efficient cell distribution, tissue structuring, and MSC differentiation analysis.

Rheological tests revealed that adding nHA and Col maintains viscoelastic properties, forming solid-like structures with a G' about ten times higher than the G'', confirming solid elastic behavior. Mechanical tests suggest that the incorporation of Col and nHA enhances the hydrogel's mechanical performance under compressive stresses. Additionally, swelling behavior analysis indicates that the inclusion of Col and nHA into the alginate matrix increases the swelling rate of the composite hydrogels, thereby promoting optimal cell proliferation within the structure.

The LIVE/DEAD™ results of the alginate-nHA-Col group showed that live cell portions remained above 80% one week after processing. Corroborating this, PrestoBlue results also confirm the ability of developed materials to support the

encapsulation and printing of hBMSCs without significant loss cell viability one-week post-printing. PCR analysis demonstrated that the alginate-nHA-Col enhanced the expression of osteogenic markers, such as SPP1 and COL1A2, in hBMSCs, suggesting the hydrogel's pro-osteogenic differentiation potential.

Future studies should include measurements of final Young's modulus, porosity, and structural analysis via Scanning Electron Microscopy (SEM) analysis, along with the characterization of chemical composition and crystalline structure using X-ray diffraction (XRD) analysis, in order to optimize 3D bioprinted models for accurately mimicking bone tissue properties and enhancing their functional relevance in regenerative medicine applications.

The incorporation of nHA and Col into alginate appears to form a bioink with optimum physical and biological properties, providing a promising 3D bioprinted model to mimic bone tissue. This study represents a significant step forward in the development of bioinks for this field, offering a viable and ethical solution for studying osteogenesis and early tissue maturation in vitro.

4. Materials and Methods

4.1. Materials

Sodium alginate (#180947-100G), nHA (particle size < 200 nm; #677418-25G) and Col type I (#5074-35ML) were purchased from Sigma-Aldrich (Saint Louis, Missouri (MO), United States of America (USA)). The hydrogel formulations were prepared using an agarose (#A6013-100G) fluid gel bath also obtained from Sigma-Aldrich (Saint Louis, MO, USA). Subsequently to their production, the hydrogels were cross-linked using calcium chloride dihydrate ($CaCl_2.2H_2O$; #22317.230-250G), from VWR Chemicals (Bridgeport, PA, USA).

4.2. Preparation of Alginate-Based Solutions

The alginate solution was prepared by dissolving sodium alginate (4% (*w/v*)) in Milli-Q water with continuous magnetic stirring overnight. Following this, the 4% alginate solution underwent sterilization via autoclaving and was subsequently subjected to a 1:1 dilution with Milli-Q water, resulting in the formulation of a 2% alginate solution. For the preparation of the alginate-nHA-Col solution, the alginate solution was combined with nHA (0.5% (*w/v*) and Col (0.5% (*w/v*)) (Figure 8). Table 3 provides an overview of the compositions of the alginate-based solutions.

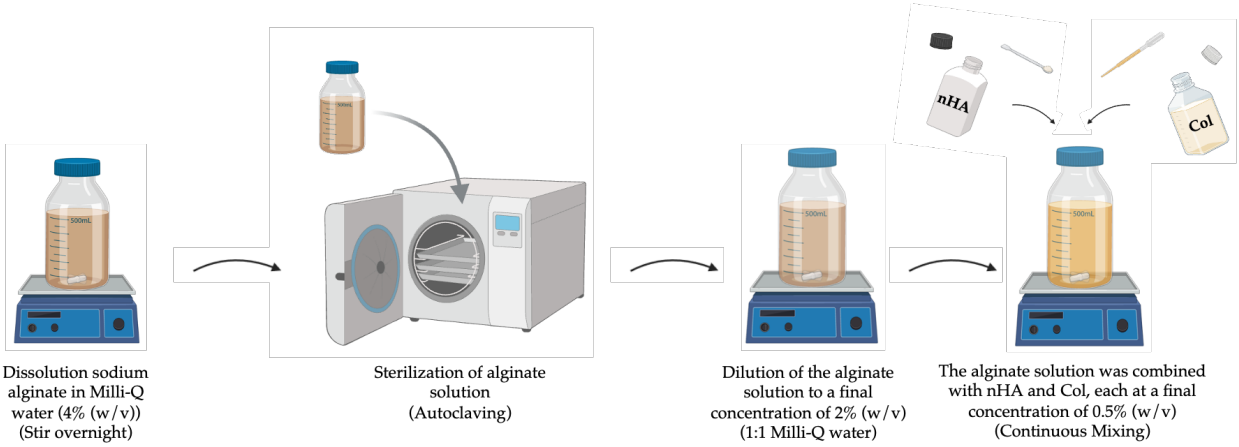


Figure 8. Graphical representation of the preparation of alginate and alginate-nHA-Col-based solutions.

Table 3. Composition of alginate-based solutions.

Solutions	Sodium Alginate (*w/v*)	nHA (*w/v*)	Col (*w/v*)
Alginate	2	-	-
Alginate-nHA-Col	2	0.5	0.5

4.3. Cell Culture and Maintenance

All experiments followed the relevant guidelines and were conducted with approvals from the NHS Health Research Authority National Research Ethics Service (21/NS/0056) and the University of Manchester, as well as written informed donor consent. The cells used in this study were previously isolated from bone marrow collected from a 49-year-old female donor after hip replacement surgery. The Strassburg et al. protocol was used to isolate the cells [73]. The hBMSCs were cultured under standard conditions in αMEM media (Sigma-Aldrich, # M4526, Saint Louis, MO, USA) enriched with 10% (*v/v*) fetal bovine serum (FBS) (Gibco, *Thermo Fisher Scientific, Waltham, MA, USA,* #A3160802) 110 mg L^{-1} sodium pyruvate, 1000 mg L^{-1} glucose, 100 U mL^{-1} penicillin, 100 µg mL^{-1} streptomycin (Gibco, #15140122) 0.25 µg mL^{-1} amphotericin (Gibco, #15290026) and 2 mM GlutaMAX (Gibco, #35050061). The hBMSCs were then maintained at 37 ˚C in an 80% humidified atmosphere with 5% CO_2.

4.4. Oscillatory Rheological Measurements

The Anton Paar RheoCompass™ rheometer (MCR92, Anton Paar, Graz, Austria) operated with Anton Paar RheoCompass v1.30.1164 software was used to

evaluate the rheological properties of the samples. Measurements were conducted using a PP12.5 measuring plate, featuring a diameter of 12.5 mm and a 1 mm gap. Alginate-based hydrogels with different compositions (as detailed in Table 4) were prepared following the transwell methodology. Briefly, 400 μL of the solution was pipetted onto 12-well plate transwell inserts. The alginate-nHA-Col hydrogels gelation was achieved through a dual-crosslinking procedure. Initially, Col crosslinking was induced by incubating at 37 ˚C for 90 min. Subsequently, the alginate was gelled using 150 μM calcium chloride ($CaCl_2$) solution in Milli-Q water for 40 min, as the process used for alginate-only hydrogels. Finally, the hydrogels were removed from the inserts and washed with DPBS.

Table 4. Name, accession number, forward/reverse sequences, and concentrations of the primers used to assess osteogenic differentation.

Primer	Accession Number	Forward Primer Sequence 5′-3′	Reverse Primer Sequence 5′-3′	Concentration (nM)
glyceraldehyde-3-phosphate dehydrogenase (GAPDH)	NM_001256799	CTCCTCTGACTTCAACAG	CGTTGTCATACCAGGAAA	600
runt-related transcription factor 2 (RUNX2)	NM_001024630	CGCTGCAACAAGACC	CGCCATGACAGTAACC	900
alkaline phosphatase (ALPL)	NM_000478	ACGTCTTCACATTTGGTG	GGTAGTTGTTGTGAGCATA	450
integrin-binding sialoprotein (IBSP)	NM_004967	GACTGCTTTAATTTTGCTCAG	GTCACTACTGCCCTGAAC	600
secreted phosphoprotein-1 (SPP1)	NM_001040058	CTGACATCCAGTACCCTG	CAGCTGACTCGTTTCATA	600
collagen type 1 alpha 2 chain (COL1A2)	NM_000089	TGAAGCTGGTCCCCAAGGA	AATACCAGGAGCGCGCCGTTG	300

The measurement conditions were as follows: Amplitude Sweep: Temperature = 25 °C, Frequency = 1 Hz, Oscillation Strain = 0.01–100%; Frequency Sweep: Temperature = 25 °C, Frequency = 0.1–10 Hz, Oscillation Strain = 0.1%. The data were measured in triplicate and the results were shown as mean ± standard deviation.

4.5. Hydrogel Swelling Behavior

Hydrogel swelling behavior was assessed under physiological conditions (pH = 7.4 at 37 °C). Initially, the weight of the hydrogels (prepared as outlined in Section 4.3) was measured post-crosslinking using precision scales (GR-300-EC, A&D Instruments, Abingdon, UK). Subsequently, these hydrogels were immersed in DPBS at 37 °C within a 12-well plate, and the weight of the swollen hydrogels was recorded. At specific time intervals (1, 2, 3, 4, 24, 48, and 72 h), the hydrogels were reweighed after blotting off excess water with tissue paper. The swelling behavior was quantified as a percentage of the swelling ratio, computed using Equation (1).

$$\text{Swelling ratio (\%)} = (Wf - Wi)/Wi \times 100, \quad (1)$$

Wf and Wi are the final and initial weights of the hydrogel (in g), respectively.

4.6. Mechanical Analysis

The compressive strength and Young's modulus (expressed in kPa) of the hydrogels were assessed using the ElectroForce 5500® Test instrument (TA Instruments, New Castle, DE, USA) equipped with a 5 N load cell. Alginate and alginate-nHA-Col hydrogels (prepared as outlined in Section 4.4 of the Section 4) were tested in triplicate, each sample having a height of 3 mm and a diameter of 12 mm. A compression test was conducted employing a flat probe with a diameter of 10 mm and a cross-head displacement rate of 2.0 mm/min. Compression was continued until 80% strain was reached. The compressive (Young's) modulus was determined by calculating the slope of the linear portion of the stress–strain curve at 10% strain. The settings for the loading procedure were programmed using the WinTest® Software (*WinTest 8.0*) (TA instruments). The real-time monitoring of the applied load was performed using the WinTest® Software.

4.7. Bioprinting of Cell-Laden Hydrogels

A pressure-assisted extrusion printer (3D Discovery, RegenHU, Villaz-St-Pierre, Switzerland) with an enclosed biosafety cabinet was employed in the fabrication of cell-laden constructs (Figure 9A). Alginate-based inks loaded with hBMSCs at a density of 2×10^6 cells/mL were prepared as described in Sections 4.2 and 4.3 and printed inside a suspension bath of agarose particles (Figure 9B) [74], using a set of process parameters previously optimized in our lab. The suspension bath was prepared based on a protocol originally reported by Moxon et al. [75].

Square-based scaffolds (6 × 6 mm) were designed using BioCAD™ software (version 2.0) (RegenHU, Villaz-St-Pierre, Switzerland) and printed in 12-well plates under sterile conditions and at room temperature. Following bioprinting, crosslinking was performed in a two-step process. Initially, Col fibrils were allowed to self-assemble for 90 min at 37 ˚C. Subsequently, a $CaCl_2$ solution was added to the wells and incubated for 40 min at 37 ˚C to induce the crosslinking of alginate. The cell-laden hydrogels were then rinsed with DPBS and cultured in αMEM medium at 37 ˚C under 5% CO_2 and 80% humidity.

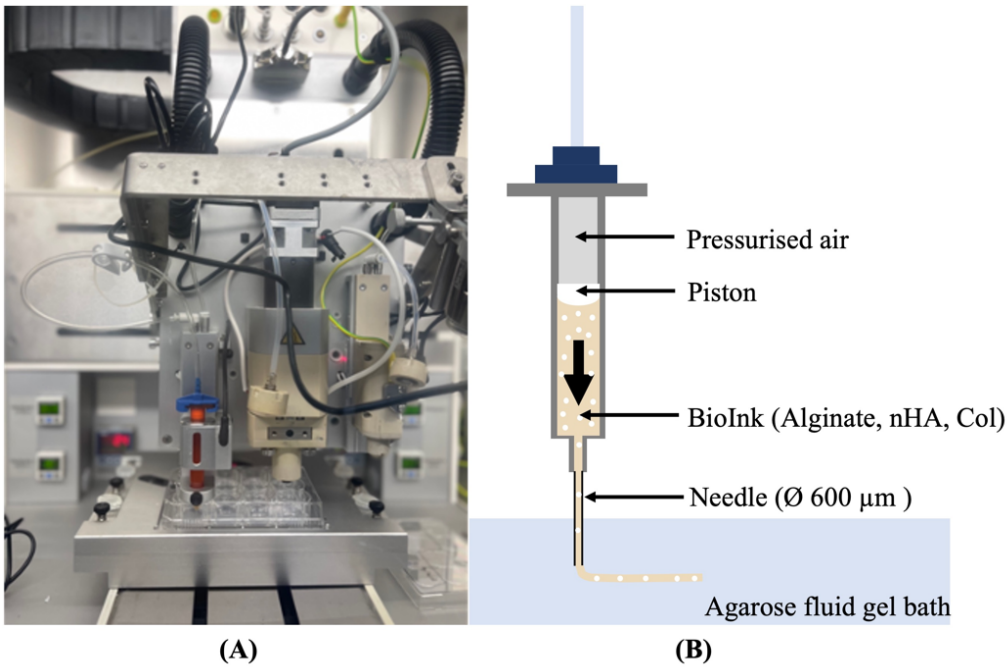


Figure 9. (**A**) 3D Discovery Evolution bioprinter; (**B**) Schematic representation of the pressure-assisted extrusion process, in which pressurized air drives the bioink from the bioprinter cartridge through a needle into a well plate containing a suspension bath.

4.8. Live/Dead Staining

A Live/Dead assay kit (Invitrogen™, *Thermo Fisher Scientific, Waltham, MA, USA,* #L3224) was used to evaluate the viability of hBMSCs cultured on alginate and alginate-nHA-Col hydrogels. According to the manufacturer's protocol, 600 µL of assay solution containing 4 µM ethidium homodimer-1 (EthD-1) and 2 µM calcein AM were added to the cell-hydrogel constructs. After a 20 min incubation, the cells were washed with DPBS and imaged using the CellVoyager™ CQ1 Benchtop High-Content Analysis System (Yokogawa, Tokyo, Japan) with an excitation wavelength of 495 nm. Cell imaging was conducted at one, three, and seven days post-culture, with three images acquired per time point. The acquired images were systematically analyzed, and subsequently, the number of cells quantified using ImageJ2 software (version: 2.3.0/1.53q). Cell viability was assessed by calculating the ratio of live cells to the total cell count. To ensure reproducibility, all measurements were conducted in triplicate at each time point.

4.9. Cell Viability Assay

To evaluate the cellular viability of hBMSCs within alginate-based hydrogels, the PrestoBlue™ (Invitrogen™ #A13261) assay was performed at one, three, five, and seven days. The evaluation was performed as previously described [21]. In brief, at each timepoint, the culture media was aspirated and substituted with fresh complete media supplemented with 10% (*v/v*) of the PrestoBlue™ reagent.

After a one-hour incubation at 37 ˚C in a controlled environment with 80% humidity and 5% CO_2, the supernatant media were transferred to a 96-well plate. Absorbance measurements were taken at 570 nm and 595 nm using a SPARK® multimode microplate reader (TECAN, Männedorf, Switzerland). Cell viability was quantified through absorbance spectroscopy by calculating the corrected absorbance, determined by subtracting the absorbance at 595 nm (used for normalization) from that at 570 nm (reflecting the experimental outcome). The resulting values were further adjusted by subtracting the average absorbance of control wells from that of the experimental wells. Residual substances were removed by gently washing the cells with DPBS, and fresh culture medium was added to each well. All measurements were conducted in triplicate at each time point.

4.10. Gene Expression

To quantify gene expression levels, RNA extraction and complementary DNA (cDNA) synthesis were performed following established protocols [76,77]. Quantitative real-time polymerase chain reactions (qPCRs) were carried out on a StepOnePlus system (Applied Biosystems, Massachusetts, EUA), utilizing pre-designed intron-spanning primers (Sigma-Aldrich, Saint Louis, MO, USA) (Table 4). In brief, a total of 10 ng cDNA was added to each reaction in addition to 5 μL of Fast SYBR Green Reagent, 1 μL of forward primer, 1 μL of reverse primer, and 2.5 μL of molecular biology grade water.

cDNA synthesized in-house from Total Human RNA (Clontech) served as the positive control in this study. The levels of osteogenic genes were standardized by normalization against the pre-validated reference gene GAPDH [78].

4.11. Statistical Analysis

To ensure experimental reproducibility, all experiments were performed in biological triplicates to capture variability between samples, and each assay was conducted in technical triplicates to account for within-experiment variability.

Statistical tests were carried out using GraphPad Prism® (version 10.3.1 for mac OS, La Jolla, California (CA), USA). Results were presented as mean ± standard error of the mean (SE). Comparisons between groups were made using one-way ANOVA, followed by Tukey's multiple comparisons test. Exclusively for the comparison of gene expression, a Mann–Whitney U test was used. Statistical significance was acknowledged solely when $p \leq 0.05$. Significance levels were denoted by asterisks (*), with * $p < 0.05$, ** $p < 0.01$, *** $p < 0.001$, and **** $p < 0.0001$.

Author Contributions: Conceptualization, A.C.S., M.D. and A.C.M.; methodology, A.C.S., G.M. and F.S.; validation, A.C.S., G.M. and F.S.; formal analysis, A.C.S., G.M., F.S. and M.D.; investigation, A.C.S., G.M., F.S., R.A., B.L., P.S., A.M. and A.C.; resources, J.D.S., L.A., N.A., S.M.R., M.D. and A.C.M.; data curation, A.C.S., G.M. and F.S.; writing—original draft preparation, A.C.S.; writing—review and editing, R.A., J.D.S., L.A., N.A. and A.C.M.; visualization, A.C.S., G.M., F.S., R.A., B.L., P.S., A.M., A.C., J.D.S., L.A., N.A., S.M.R., M.D. and A.C.M.; supervision, J.D.S., L.A., N.A., S.M.R., M.D. and A.C.M.; project administration, M.D. and A.C.M.; funding

acquisition, S.M.R., M.D. and A.C.M. All authors have read and agreed to the published version of the manuscript.

Funding: Ana Catarina Sousa (SFRH/BD/146689/2019), Bruna Lopes (2021.05265.BD), Patrícia Sousa (2023.00246.BD), André Coelho (2023.00428.BD), and Alícia Moreira (2023.00544.BD) acknowledge Fundação para a Ciência e Tecnologia (FCT) for financial support. Rui Alvites acknowledges the CECA, UP, and FCT for the funding and accessibility of all technical, structural, and human resources necessary for the development of this work. The work was supported through the project UIDB/00211/2020 funded by FCT/MCTES, national funds. This research was funded by Projects PEst-OE/AGR/UI0211/2011 from FCT, and COMPETE 2020, from ANI–Projetos ID&T Empresas em Copromoção, by the project "InnovaBIOMAS—Optimized Additive Biofabrication System for the Production of Hierarchical Multi-Tissue Scaffolds Applied in the Treatment of Joint Diseases" with the reference 2022.10564.PTDC, by the project "Bone2Move-Development of "in vivo" experimental techniques and modelling methodologies for the evaluation of 4D scaffolds for bone defect in sheep model: an integrative research approach" with the reference POCI-01-0145-FEDER-031146. Marco Domingos would like to thank the Henry Royce Institute EPSRC grants EP/R00661X/1, EP/S019367/1, EP/P025021/1 and EP/P025498/1. Stephen Richardson would also like to thank the EPSRC Centre for Doctoral Training in Advanced Biomedical Materials (EP/S022201/1) for PhD studentships funding Grace McDermott and Fraser Shields.

Institutional Review Board Statement: Not applicable.

Informed Consent Statement: The study was conducted in accordance with the Declaration of Helsinki and approved by the NHS Health Research Authority National Research Ethics Service (number: 21/NS/0056) and the University of Manchester.

Data Availability Statement: Data are contained within the article.

Conflicts of Interest: The authors declare no conflicts of interest.

List of Abbreviations

3D	three-dimensional
ALPL	alkaline phosphatase
$CaCl_2$	calcium chloride
Col	collagen
COL1A2	collagen type 1 alpha 2 chain
DPBS	Dulbecco's phosphate-buffered saline
ECM	extracellular matrix
FBS	fetal bovine serum
G'	storage modulus
G''	loss modulus
IBSP	integrin-binding sialoprotein
hBMSC	human bone marrow stem/stromal cell
HA	hydroxyapatite
LVR	linear viscoelastic region
MSC	mesenchymal stem/stromal cell
nHA	nano-hydroxyapatite
qPCR	quantitative real-time polymerase chain reaction
RUNX2	runt-related transcription factor 2
SPP1	secreted phosphoprotein-1
SE	standard error of the mean

References

1. Wu, A.-M.; Bisignano, C.; James, S.L.; Abady, G.G.; Abedi, A.; Abu-Gharbieh, E.; Alhassan, R.K.; Alipour, V.; Arabloo, J.; Asaad, M.; et al. Global, regional, and national burden of bone fractures in 204 countries and territories, 1990–2019: A systematic analysis from the Global Burden of Disease Study 2019. *Lancet Healthy Longev.* **2021**, *2*, e580–e592. https://doi.org/10.1016/S2666-7568(21)00172-0.
2. Polinder, S.; Haagsma, J.; Panneman, M.; Scholten, A.; Brugmans, M.; Van Beeck, E. The economic burden of injury: Health care and productivity costs of injuries in the Netherlands. *Accid. Anal. Prev.* **2016**, *93*, 92–100. https://doi.org/10.1016/j.aap.2016.04.003.
3. Borgström, F.; Karlsson, L.; Ortsäter, G.; Norton, N.; Halbout, P.; Cooper, C.; Lorentzon, M.; McCloskey, E.V.; Harvey, N.C.; Javaid, M.K.; et al. Fragility fractures in Europe: Burden, management and opportunities. *Arch. Osteoporos.* **2020**, *15*, 59. https://doi.org/10.1007/s11657-020-0706-y.
4. Caddeo, S.; Boffito, M.; Sartori, S. Tissue Engineering Approaches in the Design of Healthy and Pathological In Vitro Tissue Models. *Front. Bioeng. Biotechnol.* **2017**, *5*, 40. https://doi.org/10.3389/fbioe.2017.00040.
5. Owen, R.; Reilly, G.C. In vitro Models of Bone Remodelling and Associated Disorders. *Front. Bioeng. Biotechnol.* **2018**, *6*, 134. https://doi.org/10.3389/fbioe.2018.00134.
6. Kwakwa, K.A.; Vanderburgh, J.P.; Guelcher, S.A.; Sterling, J.A. Engineering 3D Models of Tumors and Bone to Understand Tumor-Induced Bone Disease and Improve Treatments. *Curr. Osteoporos. Rep.* **2017**, *15*, 247–254. https://doi.org/10.1007/s11914-017-0385-9.
7. Tripathi, S.; Mandal, S.S.; Bauri, S.; Maiti, P. 3D bioprinting and its innovative approach for biomedical applications. *MedComm* **2023**, *4*, e194. https://doi.org/10.1002/mco2.194.
8. Im, S.; Choe, G.; Seok, J.M.; Yeo, S.J.; Lee, J.H.; Kim, W.D.; Lee, J.Y.; Park, S.A. An osteogenic bioink composed of alginate, cellulose nanofibrils, and polydopamine nanoparticles for 3D bioprinting and bone tissue engineering. *Int. J. Biol. Macromol.* **2022**, *205*, 520–529. https://doi.org/10.1016/j.ijbiomac.2022.02.012.
9. Vanderburgh, J.P.; Guelcher, S.A.; Sterling, J.A. 3D bone models to study the complex physical and cellular interactions between tumor and the bone

microenvironment. *J. Cell. Biochem.* **2018**, *119*, 5053–5059. https://doi.org/10.1002/jcb.26774.

10. Gonzalez-Fernandez, T.; Sikorski, P.; Leach, J.K. Bio-instructive materials for musculoskeletal regeneration. *Acta Biomater.* **2019**, *96*, 20–34. https://doi.org/10.1016/j.actbio.2019.07.014.
11. Gonzalez-Fernandez, T.; Tenorio, A.J.; Campbell, K.T.; Silva, E.A.; Leach, J.K. Alginate-Based Bioinks for 3D Bioprinting and Fabrication of Anatomically Accurate Bone Grafts. *Tissue Eng. Part A* **2021**, *27*, 1168–1181. https://doi.org/10.1089/ten.TEA.2020.0305.
12. Datta, S. Advantage of Alginate Bioinks in Biofabrication for Various Tissue Engineering Applications. *Int. J. Polym. Sci.* **2023**, *2023*, 6661452. https://doi.org/10.1155/2023/6661452.
13. Mahmud, R.U.; Rahman, M.Z. 13.13—Synthesis and characterization of nanocomposites for tissue engineering. In *Comprehensive Materials Processing*, 2nd ed.; Hashmi, S., Ed.; Elsevier: Oxford, UK, 2024; pp. 241–269.
14. Hariyadi, D.M.; Islam, N. Current Status of Alginate in Drug Delivery. *Adv. Pharmacol. Pharm. Sci.* **2020**, *2020*, 8886095. https://doi.org/10.1155/2020/8886095.
15. Shams, E.; Barzad, M.S.; Mohamadnia, S.; Tavakoli, O.; Mehrdadfar, A. A review on alginate-based bioinks, combination with other natural biomaterials and characteristics. *J. Biomater. Appl.* **2022**, *37*, 355–372. https://doi.org/10.1177/08853282221085690.
16. Sudipto, D.; Ranjit, B.; Jonali, D. Importance of Alginate Bioink for 3D Bioprinting in Tissue Engineering and Regenerative Medicine. In *Alginates*; Leonel, P., Ed.; IntechOpen: Rijeka, Croatia, 2019; Chapter 7. https://www.intechopen.com/chapters/70389
17. Ma, C.; Du, T.; Niu, X.; Fan, Y. Biomechanics and mechanobiology of the bone matrix. *Bone Res.* **2022**, *10*, 59. https://doi.org/10.1038/s41413-022-00223-y.
18. Bielajew, B.J.; Hu, J.C.; Athanasiou, K.A. Collagen: Quantification, biomechanics and role of minor subtypes in cartilage. *Nat. Rev. Mater.* **2020**, *5*, 730–747. https://doi.org/10.1038/s41578-020-0213-1.
19. Li, Z.; Ruan, C.; Niu, X. Collagen-based bioinks for regenerative medicine: Fabrication, application and prospective. *Med. Nov. Technol. Devices* **2023**, *17*, 100211. https://doi.org/10.1016/j.medntd.2023.100211.

20. Li, Y.; Liu, Y.; Li, R.; Bai, H.; Zhu, Z.; Zhu, L.; Zhu, C.; Che, Z.; Liu, H.; Wang, J.; et al. Collagen-based biomaterials for bone tissue engineering. *Mater. Des.* **2021**, *210*, 110049. https://doi.org/10.1016/j.matdes.2021.110049.
21. Sousa, A.C.; Biscaia, S.; Alvites, R.; Branquinho, M.; Lopes, B.; Sousa, P.; Valente, J.; Franco, M.; Santos, J.D.; Mendonça, C.; et al. Assessment of 3D-Printed Polycaprolactone, Hydroxyapatite Nanoparticles and Diacrylate Poly(ethylene glycol) Scaffolds for Bone Regeneration. *Pharmaceutics* **2022**, *14*, 2643. https://doi.org/10.3390/pharmaceutics14122643.
22. Sancilio, S.; Gallorini, M.; Di Nisio, C.; Marsich, E.; Di Pietro, R.; Schweikl, H.; Cataldi, A. Alginate/Hydroxyapatite-Based Nanocomposite Scaffolds for Bone Tissue Engineering Improve Dental Pulp Biomineralization and Differentiation. *Stem Cells Int.* **2018**, *2018*, 9643721. https://doi.org/10.1155/2018/9643721.
23. Quinlan, E.; López-Noriega, A.; Thompson, E.; Kelly, H.M.; Cryan, S.A.; O'Brien, F.J. Development of collagen-hydroxyapatite scaffolds incorporating PLGA and alginate microparticles for the controlled delivery of rhBMP-2 for bone tissue engineering. *J. Control. Release* **2015**, *198*, 71–79. https://doi.org/10.1016/j.jconrel.2014.11.021.
24. Soleymani, S.; Naghib, S.M. 3D and 4D printing hydroxyapatite-based scaffolds for bone tissue engineering and regeneration. *Heliyon* **2023**, *9*, e19363. https://doi.org/10.1016/j.heliyon.2023.e19363.
25. Melo, P.; Montalbano, G.; Fiorilli, S.; Vitale-Brovarone, C. 3D Printing in Alginic Acid Bath of In-Situ Crosslinked Collagen Composite Scaffolds. *Materials* **2021**, *14*, 6720. https://doi.org/10.3390/ma14216720.
26. Chen, Y.; Zhou, Y.; Wang, C. Investigation of Collagen-Incorporated Sodium Alginate Bioprinting Hydrogel for Tissue Engineering. *J. Compos. Sci.* **2022**, *6*, 227.
27. Hassani, A.; Khoshfetrat, A.B.; Rahbarghazi, R.; Sakai, S. Collagen and nano-hydroxyapatite interactions in alginate-based microcapsule provide an appropriate osteogenic microenvironment for modular bone tissue formation. *Carbohydr. Polym.* **2022**, *277*, 118807. https://doi.org/10.1016/j.carbpol.2021.118807.
28. Campos, J.M.; Sousa, A.C.; Caseiro, A.R.; Pedrosa, S.S.; Pinto, P.O.; Branquinho, M.V.; Amorim, I.; Santos, J.D.; Pereira, T.; Mendonça, C.M.; et al. Dental pulp stem cells and Bonelike(®) for bone regeneration in ovine model. *Regen. Biomater.* **2019**, *6*, 49–59. https://doi.org/10.1093/rb/rby025.

29. Merimi, M.; El Majzoub, R.; Lagneaux, L.; Agha, D.; Fatima, B.; Meuleman, N.; Fahmi, H.; Lewalle, P.; Mohammad, F.-K.; Najar, M. The Therapeutic Potential of Mesenchymal Stromal Cells for Regenerative Medicine: Current Knowledge and Future Understandings. *Front. Cell Dev. Biol.* **2021**, *9*, 661532. https://doi.org/10.3389/fcell.2021.661532.
30. Aleynik, D.; Charykova, I.; Rubtsova, Y.; Linkova, D.; Farafontova, E.; Egorikhina, M. Specific Features of the Functional Activity of Human Adipose Stromal Cells in the Structure of a Partial Skin-Equivalent. *Int. J. Mol. Sci.* **2024**, *25*, 6290. https://doi.org/10.3390/ijms25126290.
31. Sai, B.; Dai, Y.; Fan, S.; Wang, F.; Wang, L.; Li, Z.; Tang, J.; Wang, L.; Zhang, X.; Zheng, L.; et al. Cancer-educated mesenchymal stem cells promote the survival of cancer cells at primary and distant metastatic sites via the expansion of bone marrow-derived-PMN-MDSCs. *Cell Death Dis.* **2019**, *10*, 941. https://doi.org/10.1038/s41419-019-2149-1.
32. Kemp, K.C.; Hows, J.; Donaldson, C. Bone marrow-derived mesenchymal stem cells. *Leuk. Lymphoma* **2005**, *46*, 1531–1544. https://doi.org/10.1080/10428190500215076.
33. Foresti, R.; Rossi, S.; Pinelli, S.; Alinovi, R.; Sciancalepore, C.; Delmonte, N.; Selleri, S.; Caffarra, C.; Raposio, E.; Macaluso, G.; et al. In-vivo vascular application via ultra-fast bioprinting for future 5D personalised nanomedicine. *Sci. Rep.* **2020**, *10*, 3205. https://doi.org/10.1038/s41598-020-60196-y.
34. Lai, J.; Wang, M. Developments of additive manufacturing and 5D printing in tissue engineering. *J. Mater. Res.* **2023**, *38*, 4692–4725.
35. Hassani, A.; Avci, Ç.B.; Kerdar, S.N.; Amini, H.; Amini, M.; Ahmadi, M.; Sakai, S.; Bagca, B.G.; Ozates, N.P.; Rahbarghazi, R.; et al. Interaction of alginate with nano-hydroxyapatite-collagen using strontium provides suitable osteogenic platform. *J. Nanobiotechnol.* **2022**, *20*, 310. https://doi.org/10.1186/s12951-022-01511-9.
36. Ojeda, E.; García-Barrientos, Á.; Martínez de Cestafe, N.; Alonso, J.M.; Pérez-González, R.; Sáez-Martínez, V. Nanometric Hydroxyapatite Particles as Active Ingredient for Bioinks: A Review. *Macromol* **2022**, *2*, 20–29. https://doi.org/10.3390/macromol2010002.
37. Li, N.; Guo, R.; Zhang, Z.J. Bioink Formulations for Bone Tissue Regeneration. *Front. Bioeng. Biotechnol.* **2021**, *9*, 630488. https://doi.org/10.3389/fbioe.2021.630488.

38. Ferreira, M.J.S.L.M. Integrating 3D Bioprinting and Pluripotent Stem Cell Technologies for Articular Cartilage Tissue Engineering. Ph.D. Thesis, The University of Manchester, Manchester, UK, 2022.
39. Chen, Z.-Y.; Gao, S.; Zhou, R.-B.; Wang, R.-D.; Zhou, F. Dual-crosslinked networks of superior stretchability and toughness polyacrylamide-carboxymethylcellulose hydrogel for delivery of alendronate. *Mater. Des.* **2022**, *217*, 110627. https://doi.org/10.1016/j.matdes.2022.110627.
40. Kajave, N.S.; Schmitt, T.; Nguyen, T.U.; Kishore, V. Dual crosslinking strategy to generate mechanically viable cell-laden printable constructs using methacrylated collagen bioinks. *Mater. Sci. Eng. C Mater. Biol. Appl.* **2020**, *107*, 110290. https://doi.org/10.1016/j.msec.2019.110290.
41. Shehzad, A.; Mukasheva, F.; Moazzam, M.; Sultanova, D.; Abdikhan, B.; Trifonov, A.; Akilbekova, D. Dual-Crosslinking of Gelatin-Based Hydrogels: Promising Compositions for a 3D Printed Organotypic Bone Model. *Bioengineering* **2023**, *10*, 704.
42. Naranjo-Alcazar, R.; Bendix, S.; Groth, T.; Gallego Ferrer, G. Research Progress in Enzymatically Cross-Linked Hydrogels as Injectable Systems for Bioprinting and Tissue Engineering. *Gels* **2023**, *9*, 230. https://doi.org/10.3390/gels9030230.
43. Bercea, M. Rheology as a Tool for Fine-Tuning the Properties of Printable Bioinspired Gels. *Molecules* **2023**, *28*, 2766. https://doi.org/10.3390/molecules28062766.
44. Kostenko, A.; Connon, C.J.; Swioklo, S. Storable Cell-Laden Alginate Based Bioinks for 3D Biofabrication. *Bioengineering* **2022**, *10*, 23. https://doi.org/10.3390/bioengineering10010023.
45. Paar, A. Amplitude Sweeps. Available online: https://wiki.anton-paar.com/uk-en/amplitude-sweeps/#:~:text=The%20limit%20of%20the%20linear,with%20the%20lowest%20strain%20values (accessed on 1 December 2024).
46. Kocen, R.; Gasik, M.; Gantar, A.; Novak, S. Viscoelastic behaviour of hydrogel-based composites for tissue engineering under mechanical load. *Biomed. Mater.* **2017**, *12*, 025004. https://doi.org/10.1088/1748-605X/aa5b00.
47. Shaabani, A.; Sedghi, R.; Motasadizadeh, H.; Dinarvand, R. Self-healable conductive polyurethane with the body temperature-responsive shape memory for bone tissue engineering. *Chem. Eng. J.* **2021**, *411*, 128449. https://doi.org/10.1016/j.cej.2021.128449.

48. Martinez, A.W.; Caves, J.M.; Ravi, S.; Li, W.; Chaikof, E.L. Effects of crosslinking on the mechanical properties, drug release and cytocompatibility of protein polymers. *Acta Biomater.* **2014**, *10*, 26–33. https://doi.org/10.1016/j.actbio.2013.08.029.
49. Yi, B.; Xu, Q.; Liu, W. An overview of substrate stiffness guided cellular response and its applications in tissue regeneration. *Bioact. Mater.* **2022**, *15*, 82–102. https://doi.org/10.1016/j.bioactmat.2021.12.005.
50. Sharma, R.; Kirsch, R.; Valente, K.P.; Perez, M.R.; Willerth, S.M. Physical and Mechanical Characterization of Fibrin-Based Bioprinted Constructs Containing Drug-Releasing Microspheres for Neural Tissue Engineering Applications. *Processes* **2021**, *9*, 1205. https://doi.org/10.3390/pr9071205.
51. Moeinzadeh, S.; Jabbari, E. Gelation characteristics, physico-mechanical properties and degradation kinetics of micellar hydrogels. *Eur. Polym. J.* **2015**, *72*, 566–576. https://doi.org/10.1016/j.eurpolymj.2015.04.028.
52. Rizwan, M.; Chan, S.W.; Comeau, P.A.; Willett, T.L.; Yim, E.K.F. Effect of sterilization treatment on mechanical properties, biodegradation, bioactivity and printability of GelMA hydrogels. *Biomed. Mater.* **2020**, *15*, 065017. https://doi.org/10.1088/1748-605X/aba40c.
53. Wu, Z.; Su, X.; Xu, Y.; Kong, B.; Sun, W.; Mi, S. Bioprinting three-dimensional cell-laden tissue constructs with controllable degradation. *Sci. Rep.* **2016**, *6*, 24474. https://doi.org/10.1038/srep24474.
54. Wei, L.; Li, Z.; Li, J.; Zhang, Y.; Yao, B.; Liu, Y.; Song, W.; Fu, X.; Wu, X.; Huang, S. An approach for mechanical property optimization of cell-laden alginate-gelatin composite bioink with bioactive glass nanoparticles. *J. Mater. Sci. Mater. Med.* **2020**, *31*, 103. https://doi.org/10.1007/s10856-020-06440-3.
55. Mao, Q.; Wang, Y.; Li, Y.; Juengpanich, S.; Li, W.; Chen, M.; Yin, J.; Fu, J.; Cai, X. Fabrication of liver microtissue with liver decellularized extracellular matrix (dECM) bioink by digital light processing (DLP) bioprinting. *Mater. Sci. Eng. C* **2020**, *109*, 110625.
56. Liu, W.; Borrell, M.A.; Venerus, D.C.; Mieler, W.F.; Kang-Mieler, J.J. Characterization of biodegradable microsphere-hydrogel ocular drug delivery system for controlled and extended release of ranibizumab. *Transl. Vis. Sci. Technol.* **2019**, *8*, 12.
57. Li, Z.; Huang, S.; Liu, Y.; Yao, B.; Hu, T.; Shi, H.; Xie, J.; Fu, X. Tuning Alginate-Gelatin Bioink Properties by Varying Solvent and Their Impact on Stem Cell

Behavior. *Sci. Rep.* **2018**, *8*, 8020. https://doi.org/10.1038/s41598-018-26407-3.

58. Noh, I.; Kim, N.; Tran, H.N.; Lee, J.; Lee, C. 3D printable hyaluronic acid-based hydrogel for its potential application as a bioink in tissue engineering. *Biomater. Res.* **2019**, *23*, 3.
59. Malektaj, H.; Drozdov, A.D.; deClaville Christiansen, J. Swelling of Homogeneous Alginate Gels with Multi-Stimuli Sensitivity. *Int. J. Mol. Sci.* **2023**, *24*, 5064. https://doi.org/10.3390/ijms24065064.
60. Naomi, R.; Ridzuan, P.M.; Bahari, H. Current Insights into Collagen Type I. *Polymers* **2021**, *13*, 2642. https://doi.org/10.3390/polym13162642.
61. Iviglia, G.; Cassinelli, C.; Torre, E.; Baino, F.; Morra, M.; Vitale-Brovarone, C. Novel bioceramic-reinforced hydrogel for alveolar bone regeneration. *Acta Biomater.* **2016**, *44*, 97–109. https://doi.org/10.1016/j.actbio.2016.08.012.
62. Fischer, L.; Nosratlo, M.; Hast, K.; Karakaya, E.; Ströhlein, N.; Esser, T.U.; Gerum, R.; Richter, S.; Engel, F.B.; Detsch, R.; et al. Calcium supplementation of bioinks reduces shear stress-induced cell damage during bioprinting. *Biofabrication* **2022**, *14*, 045005. https://doi.org/10.1088/1758-5090/ac84af.
63. Du, L.; Qin, C.; Zhang, H.; Han, F.; Xue, J.; Wang, Y.; Wu, J.; Xiao, Y.; Huan, Z.; Wu, C. Multicellular Bioprinting of Biomimetic Inks for Tendon-to-Bone Regeneration. *Adv. Sci.* **2023**, *10*, 2301309. https://doi.org/10.1002/advs.202301309.
64. Fideles, S.O.M.; Ortiz, A.C.; Assis, A.F.; Duarte, M.J.; Oliveira, F.S.; Passos, G.A.; Beloti, M.M.; Rosa, A.L. Effect of cell source and osteoblast differentiation on gene expression profiles of mesenchymal stem cells derived from bone marrow or adipose tissue. *J. Cell. Biochem.* **2019**, *120*, 11842–11852. https://doi.org/10.1002/jcb.28463.
65. Kriegel, A.; Schlosser, C.; Habeck, T.; Dahmen, C.; Götz, H.; Clauder, F.; Armbruster, F.P.; Baranowski, A.; Drees, P.; Rommens, P.M.; et al. Bone Sialoprotein Immobilized in Collagen Type I Enhances Bone Regeneration In Vitro and In Vivo. *Int. J. Bioprint.* **2022**, *8*, 591. https://doi.org/10.18063/ijb.v8i3.591.
66. Kriegel, A.; Langendorf, E.; Kottmann, V.; Kämmerer, P.W.; Armbruster, F.P.; Wiesmann-Imilowski, N.; Baranowski, A.; Gercek, E.; Drees, P.; Rommens, P.M.; et al. Bone Sialoprotein Immobilized in Collagen Type I Enhances Angiogenesis In Vitro and In Ovo. *Polymers* **2023**, *15*, 1007.

67. Ogata, Y. Bone sialoprotein and its transcriptional regulatory mechanism. *J. Periodontal Res.* **2008**, *43*, 127–135. https://doi.org/10.1111/j.1600-0765.2007.01014.x.
68. Van der Heide, D.; Hatt, L.P.; Della Bella, E.; Hangartner, A.; Lackington, W.A.; Yuan, H.; De Groot-Barrère, F.; Stoddart, M.J.; D'Este, M. Characterization and biological evaluation of 3D printed composite ink consisting of collagen, hyaluronic acid and calcium phosphate for bone regeneration. *Carbohydr. Polym. Technol. Appl.* **2024**, *7*, 100518. https://doi.org/10.1016/j.carpta.2024.100518.
69. Singh, A.; Gill, G.; Kaur, H.; Amhmed, M.; Jakhu, H. Role of osteopontin in bone remodeling and orthodontic tooth movement: A review. *Prog. Orthod.* **2018**, *19*, 18. https://doi.org/10.1186/s40510-018-0216-2.
70. Liu, B.; Li, J.; Lei, X.; Cheng, P.; Song, Y.; Gao, Y.; Hu, J.; Wang, C.; Zhang, S.; Li, D.; et al. 3D-bioprinted functional and biomimetic hydrogel scaffolds incorporated with nanosilicates to promote bone healing in rat calvarial defect model. *Mater. Sci. Eng. C* **2020**, *112*, 110905. https://doi.org/10.1016/j.msec.2020.110905.
71. Viguet-Carrin, S.; Garnero, P.; Delmas, P.D. The role of collagen in bone strength. *Osteoporos. Int.* **2006**, *17*, 319–336. https://doi.org/10.1007/s00198-005-2035-9.
72. Gromolak, S.; Krawczenko, A.; Antończyk, A.; Buczak, K.; Kiełbowicz, Z.; Klimczak, A. Biological Characteristics and Osteogenic Differentiation of Ovine Bone Marrow Derived Mesenchymal Stem Cells Stimulated with FGF-2 and BMP-2. *Int. J. Mol. Sci.* **2020**, *21*, 9726. https://doi.org/10.3390/ijms21249726.
73. Strassburg, S.; Richardson, S.M.; Freemont, A.J.; Hoyland, J.A. Co-culture induces mesenchymal stem cell differentiation and modulation of the degenerate human nucleus pulposus cell phenotype. *Regen. Med.* **2010**, *5*, 701–711. https://doi.org/10.2217/rme.10.59.
74. Senior, J.J.; Cooke, M.E.; Grover, L.M.; Smith, A.M. Fabrication of Complex Hydrogel Structures Using Suspended Layer Additive Manufacturing (SLAM). *Adv. Funct. Mater.* **2019**, *29*, 1904845. https://doi.org/10.1002/adfm.201904845.
75. Moxon, S.R.; Cooke, M.E.; Cox, S.C.; Snow, M.; Jeys, L.; Jones, S.W.; Smith, A.M.; Grover, L.M. Suspended Manufacture of Biological Structures. *Adv. Mater.* **2017**, *29*, 1605594. https://doi.org/10.1002/adma.201605594.

76. Minogue, B.M.; Richardson, S.M.; Zeef, L.A.; Freemont, A.J.; Hoyland, J.A. Characterization of the human nucleus pulposus cell phenotype and evaluation of novel marker gene expression to define adult stem cell differentiation. *Arthritis Rheum.* **2010**, *62*, 3695–3705. https://doi.org/10.1002/art.27710.
77. Minogue, B.M.; Richardson, S.M.; Zeef, L.A.; Freemont, A.J.; Hoyland, J.A. Transcriptional profiling of bovine intervertebral disc cells: Implications for identification of normal and degenerate human intervertebral disc cell phenotypes. *Arthritis Res. Ther.* **2010**, *12*, R22. https://doi.org/10.1186/ar2929.
78. Livak, K.J.; Schmittgen, T.D. Analysis of Relative Gene Expression Data Using Real-Time Quantitative PCR and the $2^{-\Delta\Delta CT}$ Method. *Methods* **2001**, *25*, 402–408. https://doi.org/10.1006/meth.2001.1262.

Disclaimer/Publisher's Note: The statements, opinions and data contained in all publications are solely those of the individual author(s) and contributor(s) and not of MDPI and/or the editor(s). MDPI and/or the editor(s) disclaim responsibility for any injury to people or property resulting from any ideas, methods, instructions or products referred to in the content.

5. References

1. Kim, J.; Choi, Y.J.; Gal, C.W.; Sung, A.; Park, H.; Yun, H.S. 142Development of an alginate-gelatin bioink enhancing osteogenic differentiation by gelatin release. *Int J Bioprint* **2023**, *9*, 660, doi:10.18063/ijb.v9i2.660.

2. Santoni, S.; Gugliandolo, S.G.; Sponchioni, M.; Moscatelli, D.; Colosimo, B.M. 3D bioprinting: current status and trends—a guide to the literature and industrial practice. *Bio-Design and Manufacturing* **2022**, *5*, 14-42.

3. Ahadian, S.; Khademhosseini, A. A Perspective on 3D Bioprinting in Tissue Regeneration. *Biodes Manuf* **2018**, *1*, 157-160, doi:10.1007/s42242-018-0020-3.

4. Groll, J.; Burdick, J.A.; Cho, D.-W.; Derby, B.; Gelinsky, M.; Heilshorn, S.C.; Juengst, T.; Malda, J.; Mironov, V.A.; Nakayama, K. A definition of bioinks and their distinction from biomaterial inks. *Biofabrication* **2018**, *11*, 013001.

5. Groll, J.; Burdick, J.A.; Cho, D.W.; Derby, B.; Gelinsky, M.; Heilshorn, S.C.; Jüngst, T.; Malda, J.; Mironov, V.A.; Nakayama, K.; et al. A definition of bioinks and their distinction from biomaterial inks. *Biofabrication* **2018**, *11*, 013001, doi:10.1088/1758-5090/aaec52.

6. Gao, G.; Cui, X. Three-dimensional bioprinting in tissue engineering and regenerative medicine. *Biotechnol Lett* **2016**, *38*, 203-211, doi:10.1007/s10529-015-1975-1.

7. Li, L.; Yu, F.; Shi, J.; Shen, S.; Teng, H.; Yang, J.; Wang, X.; Jiang, Q. In situ repair of bone and cartilage defects using 3D scanning and 3D printing. *Sci Rep* **2017**, *7*, 9416, doi:10.1038/s41598-017-10060-3.

8. Costa, J.B.; Silva-Correia, J.; Ribeiro, V.P.; da Silva Morais, A.; Oliveira, J.M.; Reis, R.L. Engineering patient-specific bioprinted constructs for treatment of degenerated intervertebral disc. *Materials Today Communications* **2019**, *19*, 506-512.

9. Datta, P.; Ozbolat, V.; Ayan, B.; Dhawan, A.; Ozbolat, I.T. Bone tissue bioprinting for craniofacial reconstruction. *Biotechnol Bioeng* **2017**, *114*, 2424-2431, doi:10.1002/bit.26349.

10. Habibovic, P.; Yuan, H.; van den Doel, M.; Sees, T.M.; van Blitterswijk, C.A.; de Groot, K. Relevance of osteoinductive biomaterials in critical-sized orthotopic defect. *J Orthop Res* **2006**, *24*, 867-876, doi:10.1002/jor.20115.

11. Bian, L. Functional hydrogel bioink, a key challenge of 3D cellular bioprinting. *APL Bioeng* **2020**, *4*, 030401, doi:10.1063/5.0018548.

12. Cui, X.; Li, J.; Hartanto, Y.; Durham, M.; Tang, J.; Zhang, H.; Hooper, G.; Lim, K.; Woodfield, T. Advances in Extrusion 3D Bioprinting: A Focus on Multicomponent Hydrogel-Based Bioinks. *Adv Healthc Mater* **2020**, *9*, e1901648, doi:10.1002/adhm.201901648.

13. Kyle, S.; Jessop, Z.M.; Al-Sabah, A.; Whitaker, I.S. 'Printability' of Candidate Biomaterials for Extrusion Based 3D Printing: State-of-the-Art. *Adv Healthc Mater* **2017**, *6*, doi:10.1002/adhm.201700264.

14. Bell, J.H.; Haycock, J.W. Next generation nerve guides: materials, fabrication, growth factors, and cell delivery. *Tissue Eng Part B Rev* **2012**, *18*, 116-128, doi:10.1089/ten.TEB.2011.0498.

15. Sellaro, T.L.; Ranade, A.; Faulk, D.M.; McCabe, G.P.; Dorko, K.; Badylak, S.F.; Strom, S.C. Maintenance of human hepatocyte function in vitro by liver-derived extracellular matrix gels. *Tissue Eng Part A* **2010**, *16*, 1075-1082, doi:10.1089/ten.TEA.2008.0587.

16. Pati, F.; Jang, J.; Ha, D.H.; Won Kim, S.; Rhie, J.W.; Shim, J.H.; Kim, D.H.; Cho, D.W. Printing three-dimensional tissue analogues with decellularized extracellular matrix bioink. *Nat Commun* **2014**, *5*, 3935, doi:10.1038/ncomms4935.

17. Malda, J.; Visser, J.; Melchels, F.P.; Jüngst, T.; Hennink, W.E.; Dhert, W.J.; Groll, J.; Hutmacher, D.W. 25th anniversary article: Engineering hydrogels for biofabrication. *Adv Mater* **2013**, *25*, 5011-5028, doi:10.1002/adma.201302042.

18. Ramiah, P.; Du Toit, L.C.; Choonara, Y.E.; Kondiah, P.P.; Pillay, V. Hydrogel-based bioinks for 3D bioprinting in tissue regeneration. *Frontiers in Materials* **2020**, *7*, 76.

19. Fatimi, A.; Okoro, O.V.; Podstawczyk, D.; Siminska-Stanny, J.; Shavandi, A. Natural Hydrogel-Based Bio-Inks for 3D Bioprinting in Tissue Engineering: A Review. *Gels* **2022**, *8*, doi:10.3390/gels8030179.

20. Gopinathan, J.; Noh, I. Recent trends in bioinks for 3D printing. *Biomater Res* **2018**, *22*, 11, doi:10.1186/s40824-018-0122-1.

21. Kim, D.; Kim, M.; Lee, J.; Jang, J. Review on Multicomponent Hydrogel Bioinks Based on Natural Biomaterials for Bioprinting 3D Liver Tissues. *Front Bioeng Biotechnol* **2022**, *10*, 764682, doi:10.3389/fbioe.2022.764682.

22. Hassani, A.; Khoshfetrat, A.B.; Rahbarghazi, R.; Sakai, S. Collagen and nano-hydroxyapatite interactions in alginate-based microcapsule provide an appropriate osteogenic microenvironment for modular bone tissue formation. *Carbohydr Polym* **2022**, *277*, 118807, doi:10.1016/j.carbpol.2021.118807.

23. Holmes, A.; Brown, R.; Shakesheff, K. Engineering tissue alternatives to animals: Applying tissue engineering to basic research and safety testing. *Regenerative Medicine* **2009**, *4*, 579-592, doi:10.2217/rme.09.26.

24. Owen, R.; Reilly, G.C. In vitro models of bone remodelling and associated disorders. *Frontiers in bioengineering and biotechnology* **2018**, *6*, 134.

25. Bala, Y.; Seeman, E. Bone's Material Constituents and their Contribution to Bone Strength in Health, Disease, and Treatment. *Calcified Tissue International* **2015**, *97*, 308-326, doi:10.1007/s00223-015-9971-y.

26. Bishop, N. Bone Material Properties in Osteogenesis Imperfecta. *Journal of Bone and Mineral Research* **2016**, *31*, 699-708, doi:10.1002/jbmr.2835.

27. Karunaratne, A.; Xi, L.; Bentley, L.; Sykes, D.; Boyde, A.; Esapa, C.T.; Terrill, N.J.; Brown, S.D.M.; Cox, R.D.; Thakker, R.V.; et al. Multiscale alterations in bone matrix quality increased fragility in steroid induced osteoporosis. *Bone* **2016**, *84*, 15-24, doi:10.1016/j.bone.2015.11.019.

28. de Wildt, B.W.M.; Ansari, S.; Sommerdijk, N.A.J.M.; Ito, K.; Akiva, A.; Hofmann, S. From bone regeneration to three-dimensional in vitro models: tissue engineering of organized bone extracellular matrix. *Current Opinion in Biomedical Engineering* **2019**, *10*, 107-115, doi:https://doi.org/10.1016/j.cobme.2019.05.005.

CHAPTER V

HYBRID SCAFFOLD FOR BONE TISSUE ENGINEERING

[This page is intentionally left blank.]

Introductory Note

As mentioned in the previous chapter, cell-laden hydrogels have emerged as a promising approach for effective cell delivery in bone tissue engineering applications [1,2]. Natural polymers are often preferred over synthetic alternatives for hydrogel preparation due to their closer resemblance to the physical and chemical properties of the native extracellular matrix (ECM). A notable example is the hydrogel composed of alginate and gelatin, which integrates the osteoinductive properties of gelatin with the low toxicity and efficient gelation characteristics of alginate [3]. This combination makes them particularly suitable as cell carriers in bone tissue engineering [4].

However, despite their advantages, cell-laden hydrogels face significant challenges, including inadequate mechanical strength and low durability. These limitations are primarily due to their highly swollen state and rapid degradation rate. To address these issues, researchers have explored the integration of polymeric scaffolds with hydrogels. This can be achieved either by printing the hydrogels alongside scaffolds or by directly injecting them into porous scaffold spaces [5,6]. The resulting hybrid constructs maintain the mechanical stiffness imparted by the scaffolds while offering an expanded surface area that promotes cell proliferation. This combination effectively enhances the structural integrity and functional longevity of the engineered tissue constructs.

In the subsequent chapter, hybrid scaffolds composed of 3D-printed constructs and cell-laden hydrogels were developed. The fabrication process began with the production of porous 3D scaffolds using polycaprolactone (PCL) and hydroxyapatite nanoparticles (nHA), employing optimized polymer composites via extrusion techniques. These scaffolds were then integrated with bioactive hydrogels containing human dental pulp stem/stromal cells (hDPSCs), alginate, nHA, and collagen (Col) to enhance the biological efficacy of the printed constructs. The biofabricated constructs underwent extensive characterization, including cytocompatibility tests to ensure the viability and proliferation of embedded cells, assessment of osteogenic differentiation to evaluate their potential in bone tissue regeneration, and biocompatibility evaluations using a rat model to confirm their safety and effectiveness *in vivo*. This comprehensive analysis aimed to optimize the hybrid scaffolds for future applications in bone tissue engineering and Regenerative Medicine.

[This page is intentionally left blank.]

Hybrid Scaffolds for Bone Tissue Engineering: Integration of Composites and Bioactive Hydrogels Loaded with hDPSCs

Ana Catarina Sousa, Rui Alvites, Bruna Lopes, Patrícia Sousa, Alícia Moreira, André Coelho, Alexandra Rêma, Sara Biscaia, Rachel Cordeiro, Fátima Faria, Gabriela Fernandes da Silva, Irina Amorim, José Domingos Santos, Luís Atayde, Nuno Alves, Marco Domingos, and Ana Colette Maurício

In *Biomaterials Advances*

DOI: 10.1016/j.bioadv.2024.214042

[This page is intentionally left black.]

Research Article

Hybrid Scaffolds for Bone Tissue Engineering: Integration of Composites and Bioactive Hydrogels Loaded with hDPSCs

Ana Catarina Sousa [1,2,3], Rui Alvites [1,2,3,4], Bruna Lopes [1,2,3], Patrícia Sousa [1,2,3], Alícia Moreira [1,2,3], André Coelho [1,2,3], Alexandra Rêma [1,2,3], Sara Biscaia [1,5], Rachel Cordeiro [1,5], Fátima Faria [6], Gabriela Fernandes da Silva [6], Irina Amorim [6,7,8], José Domingos Santos [9], Luís Atayde [1,2,3], Nuno Alves [5], Marco Domingos[10,†,*] and Ana Colette Maurício[1,2,3,†,*]

1 Departamento de Clínicas Veterinárias, Instituto de Ciências Biomédicas de Abel Salazar (ICBAS), Universidade do Porto (UP), Rua de Jorge Viterbo Ferreira, nº 228, 4050-313 Porto, Portugal; anacatarinasoaressousa@hotmail.com (A.C.S.); ruialvites@hotmail.com (R.A.); brunisabel95@gmail.com (B.L.); pfrfs_10@hotmail.com (P.S.); alicia.moreira.1998@gmail.com (A.M.); andrefmc17@gmail.com (A.C.); alexandrarema@gmail.com (A.R.) ataydelm@gmail.com (L.A); ana.colette@hotmail.com or acmauricio@icbas.up.pt (A.C.M.).

2 Centro de Estudos de Ciência Animal (CECA), Instituto de Ciências, Tecnologias e Agroambiente da Universidade do Porto (ICETA), Rua D. Manuel II, Apartado 55142, 4051-401, Porto, Portugal.

3 Associate Laboratory for Animal and Veterinary Science (AL4AnimalS), Lisboa, Portugal.

4 Instituto Universitário de Ciências da Saúde (CESPU), Avenida Central de Gandra 1317, Gandra, 4585-116 Paredes, Portugal.

5 Centre for Rapid and Sustainable Product Development (CDRSP), Polytechnic Institute of Leiria, Portugal; sara.biscaia@ipleiria.pt (S.B.); rachel.s.cordeiro@ipleiria.pt (R.C.); nuno.alves@ipleiria.pt (N.A.).

6 Departamento de Patologia e Imunologia Molecular Instituto de Ciências Biomédicas de Abel Salazar (ICBAS), Universidade do Porto, Rua de Jorge

Viterbo Ferreira 228, 4050-313 Porto, Portugal; fatimafaria10@yahoo.com.br (F.F.); gafernandessilva@gmail.com (G.F.S.).

[7] Institute for Research and Innovation in Health (i3S), Universidade do Porto, Rua Alfredo Allen, 208, 4200-14 135 Porto, Portugal.

[8] Institute of Molecular Pathology and Immunology, University of Porto (IPATIMUP), Rua Júlio Amaral de 16 Carvalho, 45, 4200-135 Porto, Portugal; iamorim@ipatimup.pt (I.A.).

[9] REQUIMTE-LAQV, Departamento de Engenharia Metalúrgica e Materiais, Faculdade de Engenharia, UP, Rua Dr. Roberto Frias, 4200-465, Porto, Portugal; jdsantos@fe.up.pt (J.D.S.).

[10] Department of Solids and Structures, School of Engineering, Faculty of Science and Engineering & Henry Royce Institute, The University of Manchester, Manchester M13 9PL, UK; marco.domingos@manchester.ac.uk (M.D.).

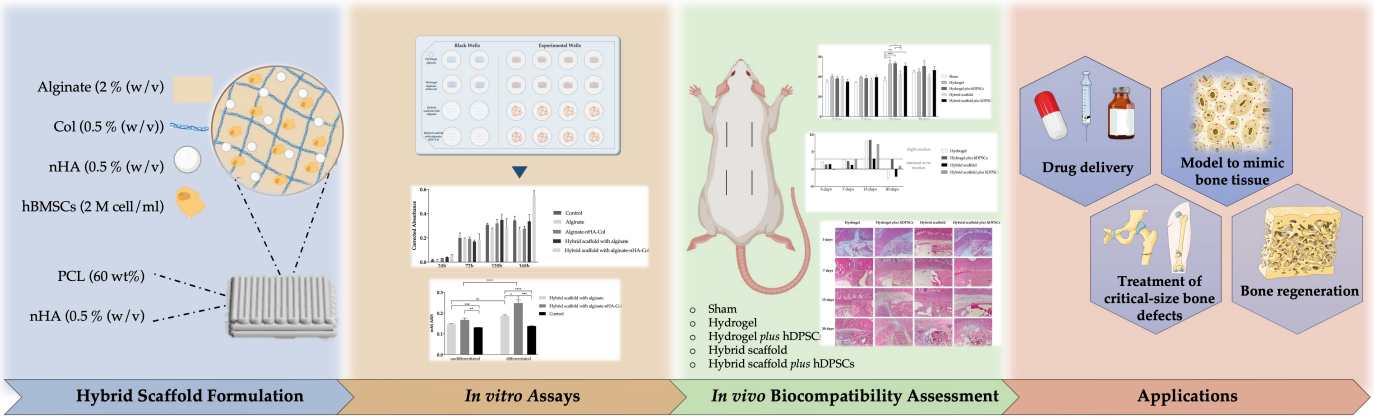
†. These authors contributed equally as last authors.

* Correspondence: marco.domingos@manchester.ac.uk (M.D.) and ana.colette@hotmail.com or acmauricio@icbas.up.pt (A.C.M.)

Abstract: Bone tissue regeneration remains a significant challenge in clinical settings due to the complexity of replicating the mechanical and biological properties of bone environment**.** This study addresses this challenge by proposing a hybrid scaffold designed to enhance both bioactivity and physical stability for bone tissue regeneration. This research is the fisrt to develop a rigid 3D structure composed of polycaprolactone (PCL) and hydroxyapatite nanoparticles (nHA) integrated with a bioink containing human dental pulp stem/stromal cells (hDPSCs), alginate, nHA and collagen (Col). The biofabricated constructs were extensively characterized through cytocompatibility tests, osteogenic differentiation assessment, and biocompatibility evaluation in a rat model. *In vitro* results demontrated that the hybrid scaffolds presented significantly higher cell viability after 168 hours compared to the control group. Furthermore, the hybrid scaffolds showed increased osteogenic differentiation relative to other groups. *In vivo* evaluation indicated good biocompatibility, characterized by minimal inflammatory response and successful tissue integration. These findings highlight the scaffold's potential to support bone tissue regeneration by combining the mechanical strength of PCL and nHA with the biological activity of the alginate-nHA-Col and hDPSCs bioink. The current study provides a promising foundation

for the development of biomaterials aimed at improving clinical outcomes in bone repair and regeneration, particulary for the treatment of critical-size bone defects, targeted drug administration, and three-dimensional models for bone tissue engineering.

Keywords: Alginate; Bioink; Bone regeneration; Collagen; Hybrid scaffold; Human Dental Pulp Stem/ Stromal Cells; Hydroxyapatite; Rat model



1. Introduction

Bone tissue engineering (BTE) has made considerable advances and has emerged as a rapidly evolving field within Regenerative Medicine. This area has focus on scaffolds, efficiently integrated cellular components and bioactive growth factors aiming to facilitate the process of bone repair and regeneration [1]. Recent studies suggest that cell-based therapies using mesenchymal stem cells (MSCs) with osteoconductive biomaterials could potentially provide treatments for several conditions related to bone fractures. This approach results in a synergy between MSCs - which have proliferation and differentiation capacities - and the support properties of biomaterials [2,3]. In accordance with the Mesenchymal and Tissue Stem Cell Committee of the International Society for Cellular Therapy (ISCT), human MSCs (hMSCs) are defined as being adherent to plastic in standard conditions, capable of tridifferentiation (osteoblasts, adipocytes and chondroblasts), expressing specific surface markers and lacking expression of hematopoietic markers [4]. hMSCs are considered multipotent stem cells, and they have the capacity to differentiate into various cell types beyond the three classical differentiation pathways. The isolation process is relatively easy, allowing large-scale cultivation, with genomic stability and minimal ethical concerns [5-7]. These

cells can be isolated from various human tissues niches, such as bone marrow, adipose tissue, umbilical cord, placenta and dental pulp [8]. Dental pulp, a soft and highly vascularized tissue located within the protective layers of enamel and dentin, has been highlighted as a valuable source of hMSCs [9-11]. Human Dental Pulp Stem Cells (hDPSCs) are derived from dental pulp tissue and present properties, such as their accessibility, availability throughout life, high proliferation and differentiation capabilities, especially towards the osteogenic lineage. Also, as reported in the literature, these cells promote the mineral deposition both *in vitro* and *in vivo* [3,12-18].

In the field of BTE, scaffolds have been used to promote and guide the regeneration of damaged tissues that cannot heal naturally. Therefore, these scaffolds ensure a three-dimensional network that replicates the extracellular matrix (ECM), sustaining the cell viability, growth and migration, while maintaining the structure of the regenerated tissue [19,20]. When it comes to bone regeneration, the scaffold must fulfill certain properties, such as: biocompatibility, facilitating the adhesion and proliferation of bone-forming cells; high mechanical properties; suitable pore interconnectivity and dimensions, allowing efficient transport of nutrients and oxygen, and controlled biodegradation/ bioresorbability [21-23]. Sousa *et al.* developed a biodegradable 3D-printed scaffold composed of polycaprolactone (PCL), nano-hydroxyapatite (nHA) and diacrylate poly (ethylene glycol) (PEGDA). Whilst PCL/nHA provides mechanical support, osteoconductivity and interconnectivity between the pores for cell migration, the PEGDA coating provides more hydrophilicity and improves properties for cell adhesion. The results suggest that these 3D structures have increased cell adhesion and proliferation compared to the control group [22]. Currently, cell-laden hydrogels have emerged as a promising approach to cell delivery [24,25]. Hydrogels based on natural polymers, such as alginate and gelatin, are commonly employed due to their chemical and physical properties, that closely resemble those of the natural ECM [26-28]. Chloe *et al.* produced bioinks composed of bone morphogenetic protein-2 (BMP-2) - loaded poly (lactic-co-glycolic acid) (PLGA) nanoparticles and alginate, designed for MSC printing and to promote osteogenic differentiation [29].

One of the biggest challenges in the engineering of bone substitutes is the integration of the mechanical and biological properties of the bone tissue matrix while simultaneously promoting the vascularization of large tissue constructs [21]. To address these limitations, synthetic rigid porous scaffolds have been integrated

with hydrogels, either through 3D printing alongside scaffolds or by direct injection into porous spaces [30,31]. This synergy of hydrogels and porous supports increases the rigidity of the hybrid constructions while offering a greater surface area for cell proliferation [26]. Wu *et al.* developed an innovative microsphere-scaffold hybrid system by integrating chitosan/hydroxyapatite (HA) microspheres loaded with alendronate (AL) into a poly (L-lactic acid)/nanohydroxyapatite (PLLA/nHA) matrix. The study demonstrated that the microspheres-scaffold hybrid system provided more sustained drug release and maintained mechanical properties comparable to the control. They significantly enhanced the osteogenic differentiation of adipose-derived stem cells and achieved complete repair of large bone defects within 8 weeks *in vivo* [32].

In a previous study conducted by our group, bioinks comprising alginate, nHA and collagen (Col) were also produced by extrusion bioprinting, along with human bone marrow stem/stromal cells (hBMSCs). These studies have shown that these structures induce osteogenic potential and provide a 3D structure suitable for bone tissue engineering. The current paper aims to develop a hybrid scaffold comprising 3D-printed constructs and cell-laden hydrogels with enhanced bioactivity and physical stability for bone tissue regeneration. In the scope of this work, porous 3D scaffolds were manufactured with optimized composites through extrusion, which was followed by the integration of bioactive hydrogels loaded with stem cells to improve the performance of the printed constructs. The base structure is composed of PCL and nHA scaffold, leveraging the mechanical strength of PCL and the osteoconductive properties of nHA. Meanwhile, the bioactive hydrogel is comprised of alginate, nHA, Col and hDPSCs.

The innovation of this approach lies in the combination of these biomaterials to provide a scaffold that not only supports cellular attachment and proliferation, but also promotes osteogenic differentiation and vascularization. The biofabricated constructs were further characterized *in vitro*, assessing their cytocompatibility and differentiation properties, and *in vivo*, by subcutaneous implantation on a rat animal model, following ISO 10993-6:2016 guidelines. The *in vivo* study aimed to assess the devices' biocompatibility and to demonstrate their potential for clinical applications in treating critical and non-critical bone defects.

This study centres on the development of a bone substitute with potential applications in the biomedical field, namely in the treatment of critical-size bone defects, targeted drug delivery, and as a three-dimensional model for bone tissue. These applications are highly relevant to advancements in bone tissue regeneration, promising significant enhancement of clinical outcomes and contributing to Regenerative Medicine.

2. Materials and Methods

2.1. Materials

PCL (CAPA® 6500, Perstorp Caprolactones, Cheshire, United Kingdom) (Mw: 50 kDa) and nHA (particle size < 200 nm) (Sigma-Aldrich, Saint Louis, USA) were used to formulate the scaffolds. The formulations were produced by solvent casting using N,N-Dimethylformamide (DMF) (CHEM-LAB, Belgium).

Regarding the production of the hydrogel, sodium alginate (#180947), nHA (particle size < 200 nm) and type I Col (#5074) (all from Sigma-Aldrich, Saint Louis, USA) were used. After production, the hydrogels were cross-linked with calcium chloride dihydrate ($CaCl_2.2H_2O$; #22317.230, VWR Chemicals, Pennsylvania, USA).

2.2. Preparation of Scaffolds

The scaffold production (diameter: 10 mm, height: 3 mm, nozzle needle: 0.4 mm, pore size: 380 μm) was prepared as detailed in a previous study [22]. Briefly: PCL (60 wt%) and nHa (40 wt%) were dissolved in DMF (2 mL of DMF for each 0.5 g) at 80 ºC with constant stirring and dried in a controlled environment for 96 hours. The membranes were cut into pieces and subsequently placed in the biomanufacturing system developed by the CDRSP-IPLeiria [33].

2.3. Encapsulation of the Cells in Hydrogel and Injection Into the Scaffolds

The alginate and alginate-nHA-Col solutions were prepared as described in the following section: to prepare the alginate solution, 4% (w/v) sodium alginate was dissolved in Milli-Q water and diluted 1:1 with Milli-Q water, resulting in a 2% alginate solution. To prepare the alginate-nHA-Col solution, the 2% (w/v) alginate solution was added to 0.5% (w/v) nHA and 0.5% (w/v) Col. The methodologies and concentrations of alginate, nHA and Col used in this study were determined based on findings of previous research [34,35].

A cell suspension (2 x 10^6 cells/mL) was prepared and added to the previously prepared solutions. Subsequently, these gel-cell suspensions were injected into the scaffolds prepared in subsection 2.2.

These hybrid scaffolds were then crosslinked. Collagen crosslinking was induced by incubation at 37 ˚C for 90 minutes. Subsequently, the alginate was gelled using a 150 μM $CaCl_2$ solution in Milli-Q water for 40 minutes, just like the process used for alginate-only hydrogels. Lastly, the hydrogels were rinsed with Dulbecco's phosphate-buffered saline solution (DPBS, Gibco, 14190169).

2.4. In Vitro Assays

2.4.1. Cell Culture and Maintenance

The hDPSCs from AllCells, LLC, Alameda, CA, USA (Cat. DP0037F, Lot no. DPSC090411-01) were cultured in αMEM, GlutaMAX™ Supplement, no nucleosides (Gibco, 32561029), which was supplemented with 10% (v/v) fetal bovine serum (FBS) (Gibco, A3160802), 100 IU/mL penicillin, 0.1 mg/mL streptomycin (Gibco, 15140122), 2.05 μg/mL amphotericin B (Gibco, 15290026), and 10 mM HEPES solution (Gibco, 15630122), Thermo Fisher Scientific, Waltham, MA USA. These cells were incubated at 37 ºC, in an 80% humidified atmosphere and a 5% CO_2 environment. The hDPSCs characterization was described by Campos *et al*. [3].

2.4.2. Cytocompatibility Assessment

The cytocompatibility of this system was evaluated by the Presto Blue™ viability assay. The Presto Blue™ (Invitrogen, A13262, Thermo Fisher Scientific, Waltham, USA) is a ready-to-use preparation and allows a live-cell test. Viable cells reduce this compound to resazurin, causing a color change (from blue to reddish) and alterations in the fluorescence of the solution. Consequently, absorbance measurements of the solution reflect cell viability and allow a quantitative assessment of cell proliferation. Therefore, changes in cell viability and proliferation were monitored through corresponding changes in absorbance measurements.

All the groups were incubated overnight at 37 ˚C in a humidified atmosphere (80%) with 5% CO_2. For the control group, an adherent 24-well plate was used without materials. For the Presto Blue™ assay, at each time point (24, 72, 120, and 168 hours), the culture medium was replaced with fresh complete medium

containing 10% (v/v) Presto Blue™ cell viability reagent. Cells were incubated for 60 minutes at 37 ˚C in a 5% CO_2 and 80% humidified atmosphere. The supernatant was transferred to a 96-well plate, and absorbance was read at 570 and 595 nm. Wells were washed with DPBS to remove Presto Blue™ residues, and fresh culture medium was added.

For this experiment, four groups were included for testing (hydrogel with alginate, hydrogel with alginate-nHA-Col, hybrid scaffold with alginate, and hybrid scaffold with alginate-nHA-Col) and a control group, with blank wells used as a reference, as shown in **Figure 1**. The excitation wavelength for Presto Blue™ is 570 nm, and the emission wavelength is 595 nm. For each well, the value at 595 nm was subtracted from the value at 570 nm to obtain a normalized value. The corrected absorbance for each experimental well (considering only seeded materials) was calculated by subtracting the average absorbance of the blank wells from the normalized values of the respective sample group. Absorbance values were measured in triplicates using a Multiskan™ FC Microplate Photometer (Thermo Scientific™, 51119000, Thermo Fisher Scientific, USA). Data were further processed, normalized to the mean of the control group and presented as a percentage of viability inhibition compared to the control group.

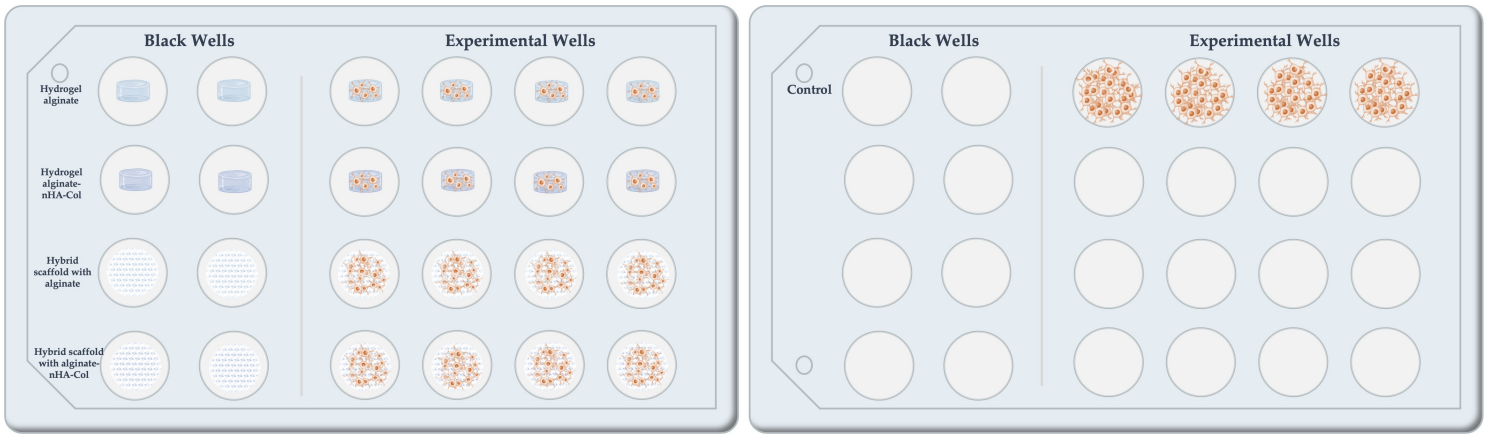


Figure 1. Schematic representation of the experimental set-up for the *in vitro* cytocompatibility evaluation.

2.4.3. Osteogenic Differentiation Assay

The osteogenic differentiation test was conducted on the following groups: control (scaffold without hydrogel), hybrid scaffold with alginate hydrogel, and hybrid scaffold with alginate-nHA-Col groups. All the groups contained encapsulated hDPSCs in the hydrogel. This assay was performed as described in

previous works [3,36]. In short, after a period of incubation, the hybrid scaffolds were transferred to specifically formulated osteogenesis media (StemPro™ Osteogenesis Differentiation Kit, Gibco A1007201, Thermo Fisher Scientific, Waltham, USA). Control wells (undifferentiated) were placed in culture media without osteogenic supplements. The media were replaced every 3 days. After 21 days, osteogenic differentiation was semi-quantitatively assessed using the Alizarin Red S assay (TMS-008-C, Merck KGaA, Darmstadt, Germany). Hybrid scaffolds were fixed in 4% formaldehyde (Merck KGaA, Darmstadt, Germany, 100496), stained with a 40 mM ARS solution and incubated under agitation for 30 minutes. After removing the supernatant, hybrid scaffolds were washed with diH_2O.

For the assay, a 10% acetic acid solution (ARK2183, Sigma-Aldrich, St. Louis, USA) was added to the hybrid scaffolds, which were then scraped to collect cells and mineral deposits. Each sample was subjected to a 10-minute incubation in an 85 ˚C water bath, followed by 5 minutes on ice, and then centrifuged. Absorbance at 405 nm was measured in triplicate using a Thermo Scientific™ Multiskan™ FC Microplate Photometer.

2.4.4. Scanning Electronic Microscopy (SEM)

After the cytocompatibility assessment, seeded and unseeded hybrid scaffolds from each group were prepared for SEM, following the Utah State University Biological Sample Fixation for SEM. Briefly, scaffolds were washed three times with 0.1 M HEPES buffer and then fixed with 2% glutaraldehyde (Merc-KGaA, Darmstadt, Germany, G5882) buffered solution overnight. Subsequently, the samples were rinsed three times with 0.1M HEPES buffer, for 5 minutes each and under gentle agitation. The samples then underwent a graded ethanol dehydration series (50%, 70%, 95% and 99%), with each concentration applied 2-3 times for 10-15 minutes. Lastly, the samples were infiltrated with a graded series of hexamethyldisilazane (HMDS)-ethanol solutions (1:2; 1:1; 2:1), culminating in immersion in a 98% HMDS solution (Alfa Aesar, A15139, Thermo Fisher Scientific, Waltham, MA, USA) for three 15-minute intervals. The HMDS was removed, and the samples were left to dry overnight in an air flow chamber.

SEM analysis and Energy Dispersive X-ray Spectroscopy (EDX) were performed using a high-resolution (Schottky) Environmental Scanning Electron Microscope equipped with X-ray Microanalysis and Electron Backscatter Diffraction

capabilities (FEI Quanta 400 FEG ESEM/EDAX Genesis X4M, ThermoFisher Scientific, Waltham, USA). The microscope operated in high vacuum mode at an accelerating voltage of 15 kV. The scaffolds were coated with gold/palladium for 80 seconds using a 15mA current. Depending on the nature of the samples and where required, electron backscatter diffraction images were obtained.

2.5. *In Vivo* Biocompatibility Assessment of Hydrogel/ Hybrid Scaffolds in Subcutaneous Tissue

To evaluate the biocompatibility of the hybrid system, thus complementing the *in vitro* characterization and cytocompatibility studies, 16 male Sasco Sprague-Dawley rats (Charles River, Barcelona, Spain), with 250-300g, were used, according to ISO Standard 10993-6: 2016 – "Biological evaluation of medical devices - Part 6: Tests for local effects after implantation". Animal testing procedures were in conformity with the Directive 2010/63/EU of the European Parliament and the Portuguese DL 113/2013. All the procedures were approved by the ICBAS-UP Animal Welfare Organism of the Ethics Committee (ORBEA) (Project 288/2018) and by the Veterinary Authorities of Portugal (DGAV). Humane end points were followed in agreement with the OECD Guidelines (2000).

Animals were housed with controlled temperature and humidity and 12–12 h light/dark cycles. Animals were fed with standard chow and water *ad libitum*. The surgical procedure implies intraperitoneally administration of anesthesia Xylazine/Ketamin (Rompun®, Bayer AG, Leverkusen, Germany/Clorketam 1000®, Vétoquinol, Lure, France; 1.25/9 mg per 100 g b.w.), and aseptic skin preparation (**Figure 2-A**). Furthermore, a subcutaneous injection containing 5 mL of serum and metoclopramide hydrochloride was also administered (Vomend®, Dechra, Northwich, England) (1 mg per 100g b.w) to prevent dehydration and with antiemetic effects, respectively. Four 15–20 mm long linear incisions were made paired along the dorsum (**Figure 2-B)**. Five groups (n=3) were considered for each timepoint: 1) Sham (surgical access to the site, but no device implantation); 2) hydrogel; 3) hydrogel *plus* hDPSCs; 4) hybrid scaffold and 5) hybrid scaffold *plus* hDPSCs. Biomaterials were implanted subcutaneously (**Figure 2-C**), skin and subcutaneous tissues were sutured (**Figure 2-D**), and animals recovered and returned to their housing groups. At 3, 7, 15 and 30 days after surgery, animals were subjected to deep anesthesia according to the protocol described above, and subsequently euthanized by lethal intra-cardiac injection (Eutasil® 200 mg/mL,

CEVA Sante Animale, Libourne, France, 200 mg/kg b.w.). Collection of skin and subcutaneous tissues from the implant area was performed and samples were fixed in 4% formaldehyde (Merck®, Germany, 100496). Simultaneously, a macroscopic inspection of the lesion site was carried out in search of signs of local reactivity such as neovascularization, adhesions or the presence of purulent material. To assess the systemic biological response, a detailed necropsy examination was performed, and several organs, including lungs, kidneys, spleen and heart, underwent further histological analysis.

For the histopathological analysis, fixed samples were processed following routine procedures and stained with Hematoxylin-Eosin (H&E). The sections were evaluated using a Nikon microscope (Nikon, Amstelveen, Netherlands, Eclipse E600) and a photo camera (Nikon, Netherlands, Digital Sight DS-5M). Samples were assessed for inflammatory infiltration, angiogenesis, fibrosis, and necrosis surrounding the material, in accordance with the ISO-10993-6:2016 guidelines, Annex E. This evaluation was conducted by a veterinary pathologist with recognized expertise in the field. Each sample received scores based on the classification of individual parameters as outlined by the ISO system. This enabled a semi-quantitative classification of the biomaterials into categories: “minimal or no reaction” (score 0.0 to 2.9), “slight reaction” (score 3.0 to 8.9), “moderate reaction” (score 9.0 to 15.0), or “severe reaction” (score > 15).

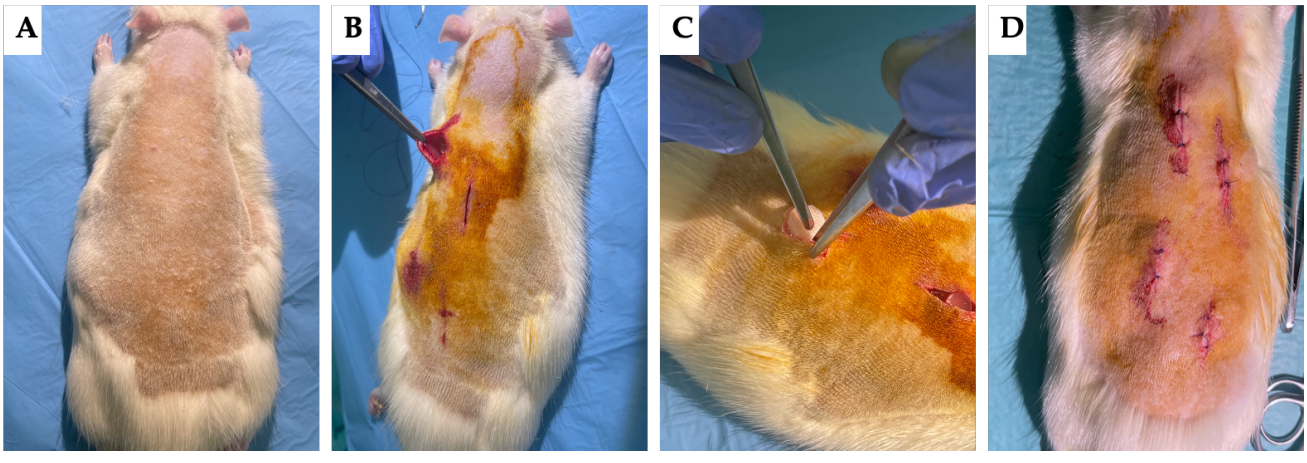


Figure 2. A: Trichotomy of the region to be intervened; B: After aseptic skin preparation, four linear incisions are made, paired along the dorsum; C: Biomaterials are implanted subcutaneously; D: The skin and subcutaneous tissues are sutured.

2.6. Statistical Analysis

For statistical analysis, GraphPad Prism version 6.00 for Mac OS x, GraphPad Software (La Jolla, CA, USA) was used. The trials were executed in quadruplicates, and the results were expressed as mean ± standard error of the mean (SE). Statistical analysis was performed using One-Way ANOVA analysis followed by Tukey multi-comparison test. Statistical significance was considered at $p < 0.05$. The significance levels are represented by asterisks (*), with one, two, three, or four asterisks indicating $0.01 \leq p < 0.05$; $0.001 \leq p < 0.01$; $0.0001 \leq p < 0.001$; and $p < 0.0001$, respectively.

3. Results

3.1. Cytocompatibility Assessment

In accordance with ISO 10993-5:2009 guidelines, the cell viability was assessed using PrestoBlue™ on samples of alginate hydrogels, alginate-nHA-Col hydrogels, scaffolds with embedded alginate hydrogels and scaffolds with embedded alginate-nHA-Col hydrogels. All the hydrogels contained hDPSCs. Moreover, cell-absent controls were performed for each of these groups. An additional group of cells seeded with no biomaterials was considered as a control of the cells, to assess their normal behavior and proliferation in culture. **Figure 3** presents the corrected absorbance values for each time-point: 24, 72, 120, and 168 hours. Additionally, the statistical differences identified between the experimental groups at each time-point are shown in **Table 1**.

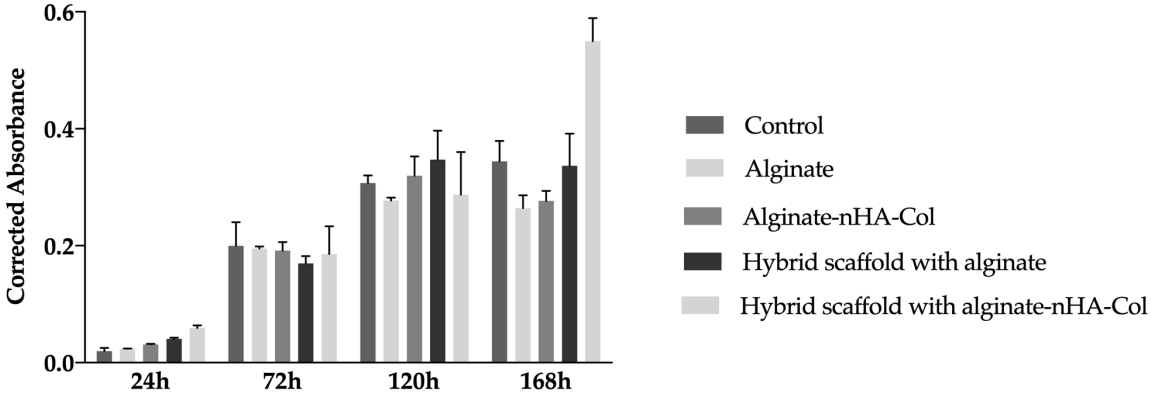


Figure 3. Cytocompatibility tested by PrestoBlue™ viability assay for hDPSCs. Results presented in mean ± SE (standard error of the mean).

Table 1. Differences were considered statistically significant at $p \leq 0.05$. Results significances are presented through the symbol (*), according to the p-value, with one, two, three or four symbols, corresponding to $0.01 < p \leq 0.05$; $0.001 < p \leq 0.01$; $0.0001 < p \leq 0.001$ and $p \leq 0.0001$, respectively. A – Control; B - Alginate; C - Alginate-nHA-Col; D – Hybrid scaffold with alginate; E – Hybrid scaffold with alginate-nHA-Col.

	24 h					72 h					120					168 h				
	A	**B**	**C**	**D**	**E**	**A**	**B**	**C**	**D**	**E**	**A**	**B**	**C**	**D**	**E**	**A**	**B**	**C**	**D**	**E**
A		ns	*	****	****		ns	ns	ns	ns		*	ns	ns	ns		*	ns	ns	****
B			****	****	****			ns	ns	ns			ns	ns	ns			ns	ns	****
C				**	****				ns	ns				ns	ns				ns	****
D					****					ns					ns					*
E																				

The findings presented in **Figure 3** indicate a normal cell proliferation rate and growth across all experimental groups up to 120 hours. Notably, a slight decrease in cell viability compared to previous time-points was observed at 168 hours in the groups comprising the alginate hydrogel, alginate-nHA-Col hydrogel, and the hybrid scaffold with alginate. Despite this decrease, the hybrid scaffold with alginate-nHA-Col presented significantly higher cell viability rates than the control group at 24 and 168 hours. This observation was further supported by the significantly higher absorbance values recorded for the hybrid scaffolds compared to the standard group, suggesting enhanced cell adhesion and proliferation induced by the hybrid scaffolds. These results underscore the potential of the hybrid scaffold alginate-nHA-Col in promoting cellular viability and proliferation, thereby highlighting its suitability for applications in bone tissue engineering and regeneration.

Furthermore, the percentage of viability inhibition, normalised to the control group, was also assessed and is shown in **Figure 4**. According to Annex 3 of the ISO 10993-5:2009 guideline, viability inhibition when superior to 30 per cent is defined as a cytotoxic reaction (shown in **Figure 4** by dashed lines).

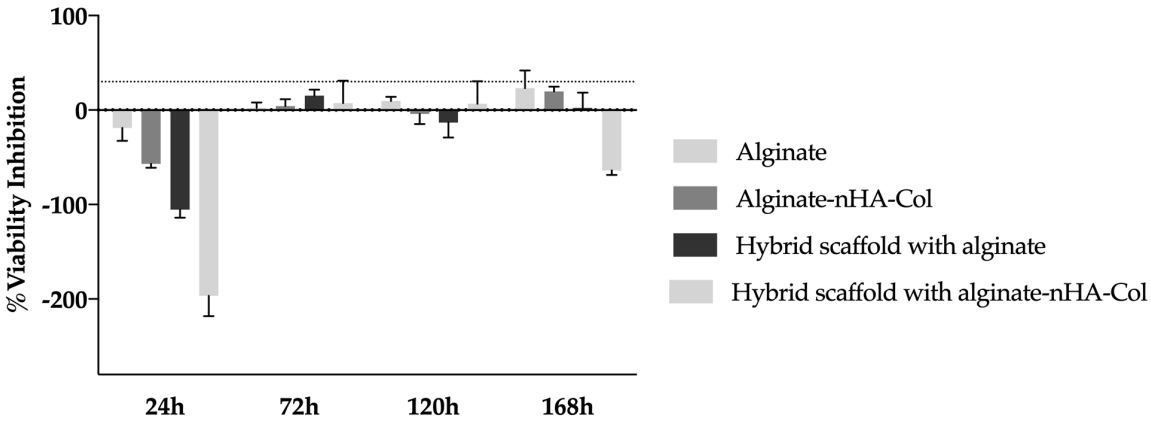


Figure 4. % of viability inhibition assessed by PrestoBlue® viability assay after 24, 72, 120 and 168 h. The results were normalized to the control group as 0%. The 30 per cent threshold presented in the graph (dashed line) indicates the inhibition above which the effect is considered cytotoxic (in conformity with ISO 10993-5:2009 guidelines).

The results of the viability inhibition assays suggest that these biomaterials, across all experimental groups, can be classified as non-cytotoxic. This classification is based on the fact that the percentage of viability inhibition did not exceed the pre-established threshold of 30%, as outlined in the referenced guidelines.

3.2. Osteogenic Differentiation Assay

The osteogenic potential of the hybrid scaffolds was assessed using ARS protocol, following a 21 days incubation period. The analysis was performed through the detection of mineral deposition, as outlined in previous studies [37,38]. ARS was extracted and subsequently quantified at 405 nm. The results are shown in **Figures 5** and **6**. These results suggest that the incorporation of nHA and Col into alginate promoted the osteogenic differentiation of hDPSCs.

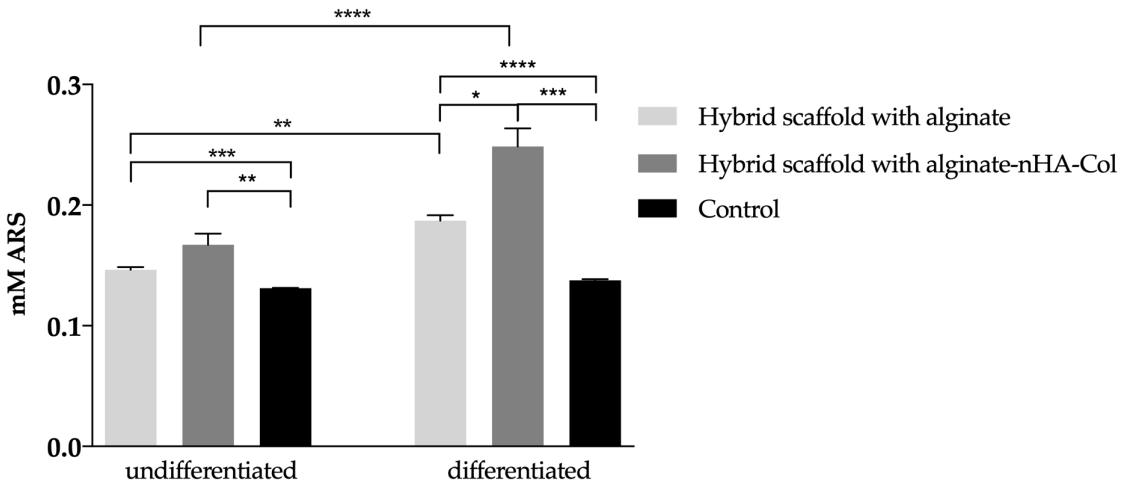


Figure 5. ARS Semi-Quantification in mM between groups. Results presented in Mean ± SE. Differences were considered statistically significant at $p \leq 0.05$. Results significance are presented through the symbol (*), according to the p value, with one, two, three or four symbols, corresponding to $0.01 < p \leq 0.05$; $0.001 < p \leq 0.01$; $0.0001 < p \leq 0.001$ and $p \leq 0.0001$, respectively.

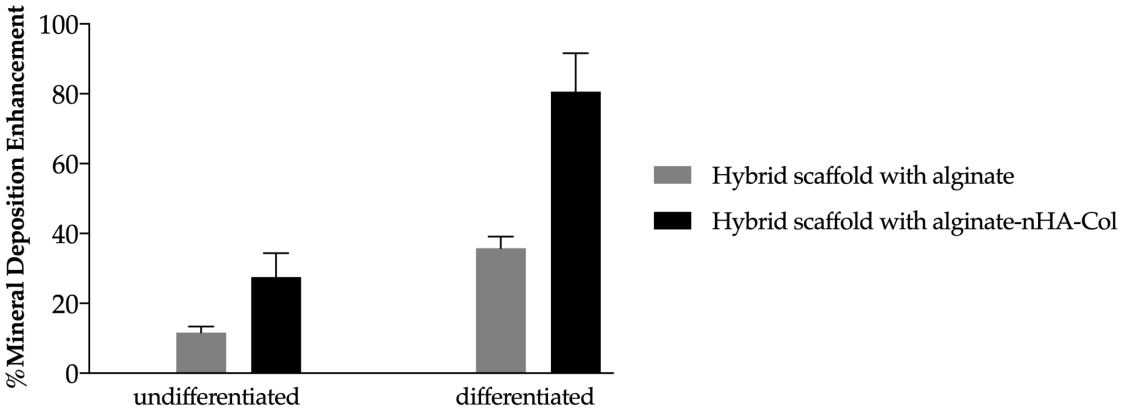


Figure 6. ARS Semi-Quantification in mM between groups. Results of % mineral deposition enhancement are presented in mean ± SE, normalized to the control group as 100%.

The findings presented in Figure 5 indicate that scaffolds incorporating the alginate-nHA-Col hydrogel exhibit significantly increased mineral deposition in the group supplemented with osteodifferentiation media, compared to scaffolds lacking both nHA and Col, as well as to the control group. This suggests that the presence of nHA and Col in the hydrogel promotes osteodifferentiation. Furthermore, in the undifferentiated group, the hydrogels containing nHA and Col

demonstrated superior mineral deposition, indicating that these components induce spontaneous osteodifferentiation. This observation supports the hypothesis that nHA and Col possess inherent osteoinductive properties.

3.3. Scanning Electronic Microscopy (SEM)

Following the cytocompatibility and osteogenic differentiation assessment, the samples were processed for analysis by SEM and EDX. Hydrogels are highly hydrated materials, and the SEM operates in high vacuum mode, which can lead to dehydration and collapse of the structures. Given the nature of the hydrogels, only the following groups were analysed: control (scaffold without cells), hybrid scaffold with alginate hydrogel *plus* hDPSCs, and hybrid scaffold with alginate, nHA and Col *plus* hDPSCs. The results are presented in **Figures 7**, **8**, **9, 10, 11**. The analysis suggests that the hDPSCs were fixed and proliferated on the hybrid scaffolds, exhibiting a normal structure and morphology, revealing the permissible nature of the materials.

The results (**Figure 7**) demonstrated a heterogeneous and arbitrary distribution of the hydrogel within the 3D structure. This suggests that the hydrogel is unevenly dispersed throughout the scaffold matrix, seeming to indicate variability in the incorporation process. Furthermore, it was not possible to quantitatively evaluate the cells between the experimental groups. However, qualitatively, all groups showed positive results in terms of 3D cell attachment, cell adhesion and morphological structure. These results suggest that, despite the random distribution of the hydrogel, the structure allows favorable cell interactions and maintains an environment conducive to cell migration and structural development.

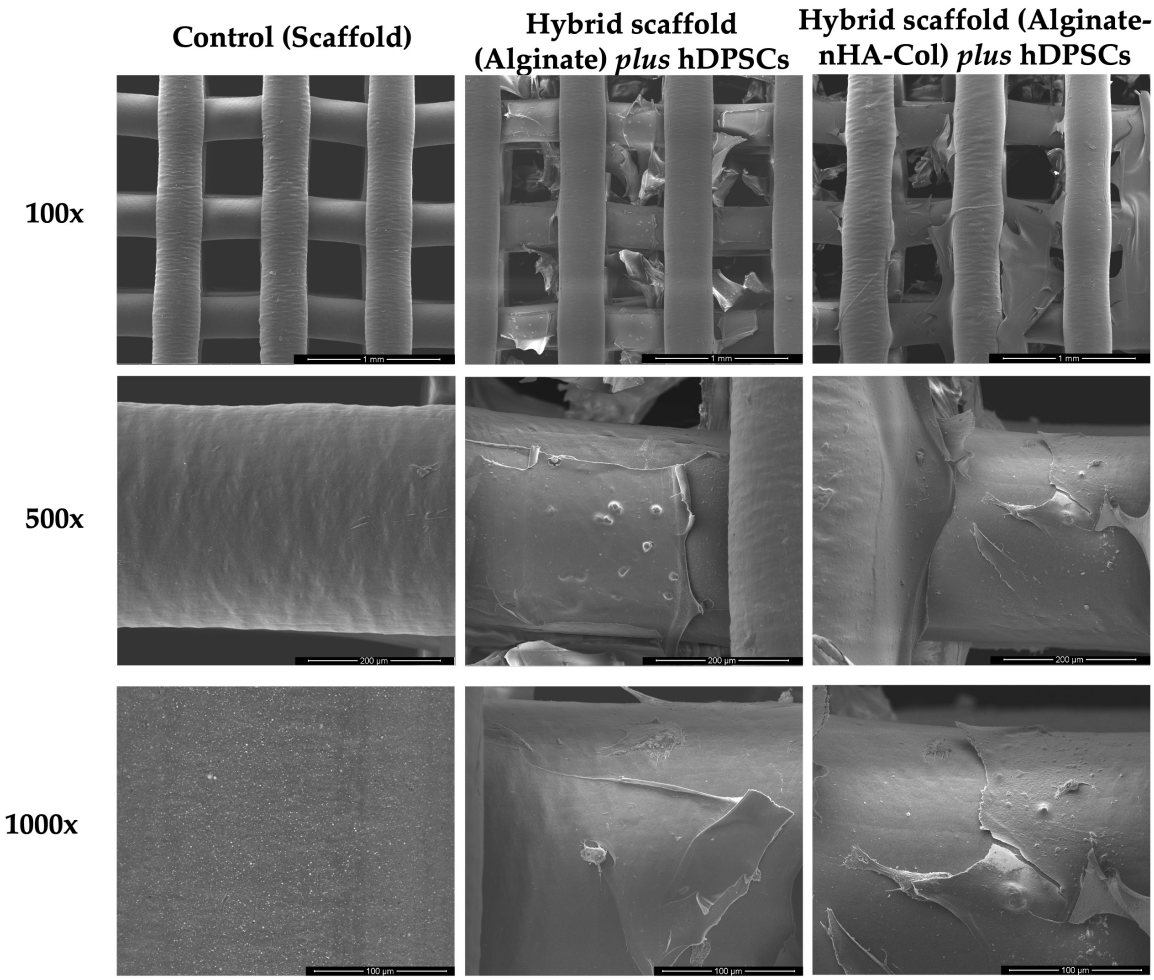


Figure 7. SEM images for the control, hybrid scaffold with alginate hydrogel *plus* hDPSCs, and hybrid scaffold with alginate-nHA-Col *plus* hDPSCs groups. Upper panel 100x magnification, middle panel 500x magnification and lower panel 1000x magnification. First column: control; middle column: hybrid scaffold with alginate *plus* hDPSCs; third column: hybrid scaffold with alginate-nHA-Col *plus* hDPSCs.

In **Figure 8**, individualized cell clusters are visible within the hybrid scaffold with alginate-nHA-Col seeded with hDPSCs. The micrographs depict distinct (fibroblast-like), normal morphology, and well-defined cell aggregates, indicating adequate cellular adhesion and proliferation within the support matrix.

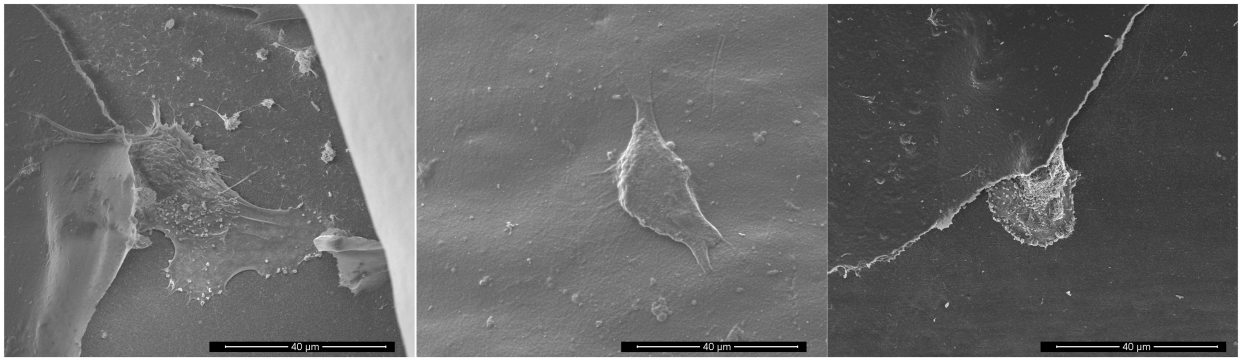


Figure 8. SEM images for the hybrid scaffold with alginate-nHA-Col *plus* hDPSCs (2500x magnification).

The EDX analysis (**Figures S1, S2** and **S3**), displaying the spectrum of energies detected, revealed the composition of the elements on the surface of all the materials. The EDX analysis of the control group (**Figure S1**), comprising a scaffold of PCL and nHA, revealed the presence of the elements carbon (C), phosphorus (P), oxygen (O) and calcium (Ca). This elemental composition is in line with the expected materials used in the scaffold structure. For the hybrid scaffold with alginate and the hybrid scaffold with alginate-nHA-Col (both with hDPSCs) groups, EDX detected the same elements (C, O, P, and Ca) in the scaffold areas. Meanwhile, in the hydrogel regions (identified as Z1 in **Figure S2** and Z1 and Z3 in **Figure S3**), the same elements were present but with noticeably lower calcium content. This finding is consistent with the material composition, in which the scaffold comprises 40 wt% nHA, while the hydrogel contains only 0.5% (w/v) of nHA. The EDX results thus validate the appropriate distribution and integration of the hydrogel with the scaffold, ensuring that the composite material retains its intended structural and compositional characteristics.

3.4. In Vivo Biocompatibility Assessment of Hydrogel/ Hybrid Scaffolds in Subcutaneous Tissue

Following the *in vitro* evaluation, a biocompatibility assessment of the samples was performed in accordance with the ISO 10993-6:2016 standards. The following groups were considered: sham, hydrogel (based on alginate, nHA and Col), hydrogel *plus* hDPSCs, hybrid scaffold, and hybrid scaffold *plus* hDPSCs. The assessment protocol involved a comprehensive histological scoring for each sample, accompanied by an intricate histopathological analysis of the biological tissue's response. This encompassed quantifying fibrosis levels, identifying tissue morphology alterations and inflammatory cell types, assessing necrosis presence

and extent, evaluating neovascularization, and considering other pertinent parameters as outlined in the guidelines. The results are presented in **Table 2**, **Figures 9**, **10 and 11**.

Table 2. Global histological scores presented as mean ± SE following ISO-10993-6 guidelines for the sham, hydrogel, hydrogel *plus* hDPSCs, hybrid scaffold, and hybrid scaffold *plus* hDPSCs groups, at 3, 7, 15 and 30 days after implantation. ISO SCORE: "minimal or no reaction" (score 0.0 to 2.9), "slight reaction" (score 3.0 to 8.9), "moderate reaction" (score 9.0 to 15.0), or "severe reaction" (score > 15).

	Sham		**Hydrogel**		**Hydrogel *plus* hDPSCs**		**Hybrid scaffold**		**Hybrid scaffold *plus* hDPSCs**	
	Mean	**SE**	**Mean**	**SE**	**Mean**	**SE**	**Mean**	**SE**	**Mean**	**SE**
3 days	17.80	1.270	20.00	0.913	19.11	1.020	19.22	0.760	17.56	1.094
ISO SCORE	-		**2.200**		**1.311**		**1.422**		**-0.244**	
7 days	16.89	0.564	19.70	0.597	19.17	1.537	18.11	0.949	19.78	1.103
ISO SCORE	-		**2.811**		**2.278**		**1.222**		**2.889**	
15 days	18.22	1.544	26.44	1.757	26.67	0.782	21.25	1.556	25.44	1.435
ISO SCORE	-		**8.222**		**8.444**		**3.028**		**7.222**	
30 days	22.33	0.760	22.44	1.510	25.25	2.750	20.11	1.033	23.33	1.732
ISO SCORE	-		**-2.806**		**2.917**		**-2.222**		**1.000**	

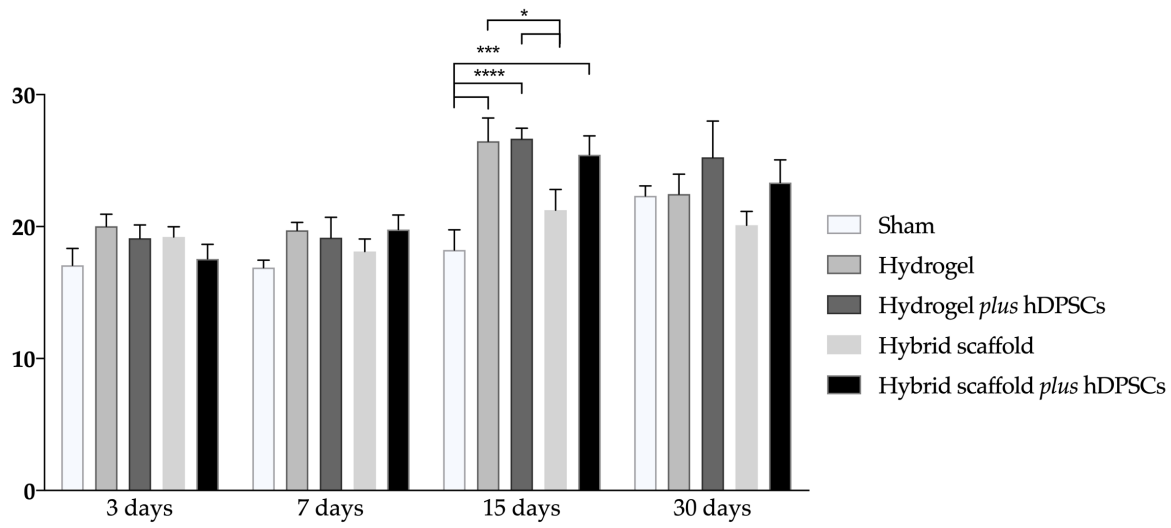


Figure 9. Global histological score, according to ISO-10993-6 guidelines for the sham, hydrogel, hydrogel *plus* hDPSCs, hybrid scaffold, and hybrid scaffold *plus* hDPSCs groups, at 3, 7, 15 and 30 days after implantation. Results presented in mean ± SEM. Differences were considered statistically significant at $p \leq 0.05$.

Results significance are presented through the symbol (*), according to the p value, with one, two, three or four symbols, corresponding to $0.01 < p \leq 0.05$; $0.001 < p \leq 0.01$; $0.0001 < p \leq 0.001$ and $p \leq 0.0001$, respectively.

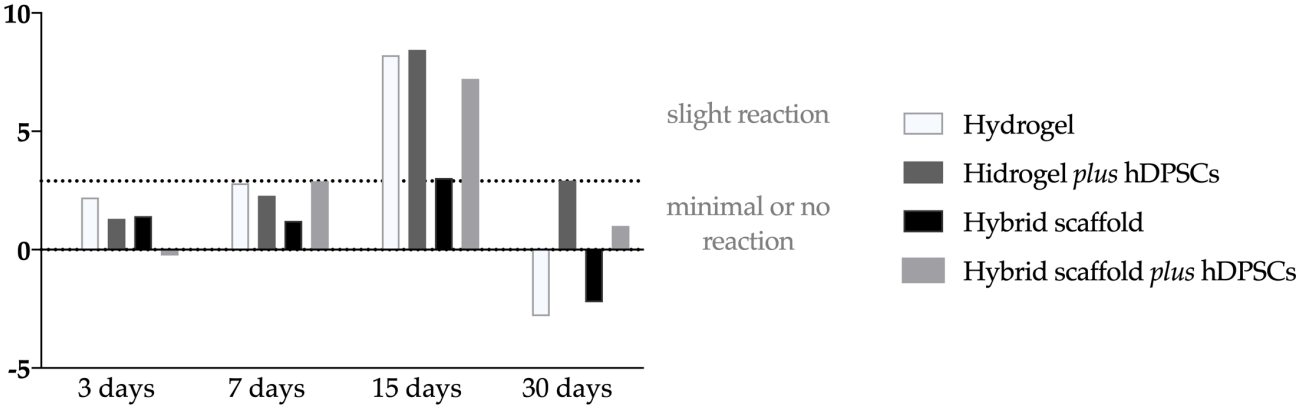


Figure 10. Calculated score, according to ISO-10993-6 guidelines, for the hydrogel, hydrogel *plus* hDPSCs, hybrid scaffold, and hybrid scaffold *plus* hDPSCs groups, at 3, 7, 15 and 30 days after implantation.

The histological scoring system was determined by subtracting the global histological score of each experimental group from the score of the corresponding sham group at each time-point (**Figure 10**).

Microscopically, all samples exhibited minimal fibrosis and a wide array of capillaries with supporting structures at every time-point. Polymorphonuclear (PMN) cells, characteristic of an acute inflammatory response, were observed in all samples at all time-points. Nevertheless, their presence decreased as the recovery period progressed, suggesting a recovery from the initial acute inflammatory phase. Necrosis and giant cells were rarely observed.

Mononuclear inflammatory cells, mainly macrophages and lymphocytes, were detected in higher quantities compared to PMN cells in all groups and time-points.

According to the ISO 10993-6 scoring system, the scaffold materials were classified as eliciting a "slight reaction" at the 15-day post-implantation time. At 3, 7 and 30-day post-implantation, the reactions were reduced to "minimal to no reaction" compared to the sham group, indicating a favorable integration of the materials over time.

Importantly, no significant alterations were observed in the microscopic evaluation of the different organs, suggesting that the materials tested did not induce systemic toxicity or adverse effects beyond the local implantation site.

According to the macroscopic and microscopic evaluations, considering the aforementioned guidelines, the biomaterials tested, specifically the alginate-nHA-Col hybrid structure, can be classified as biocompatible.

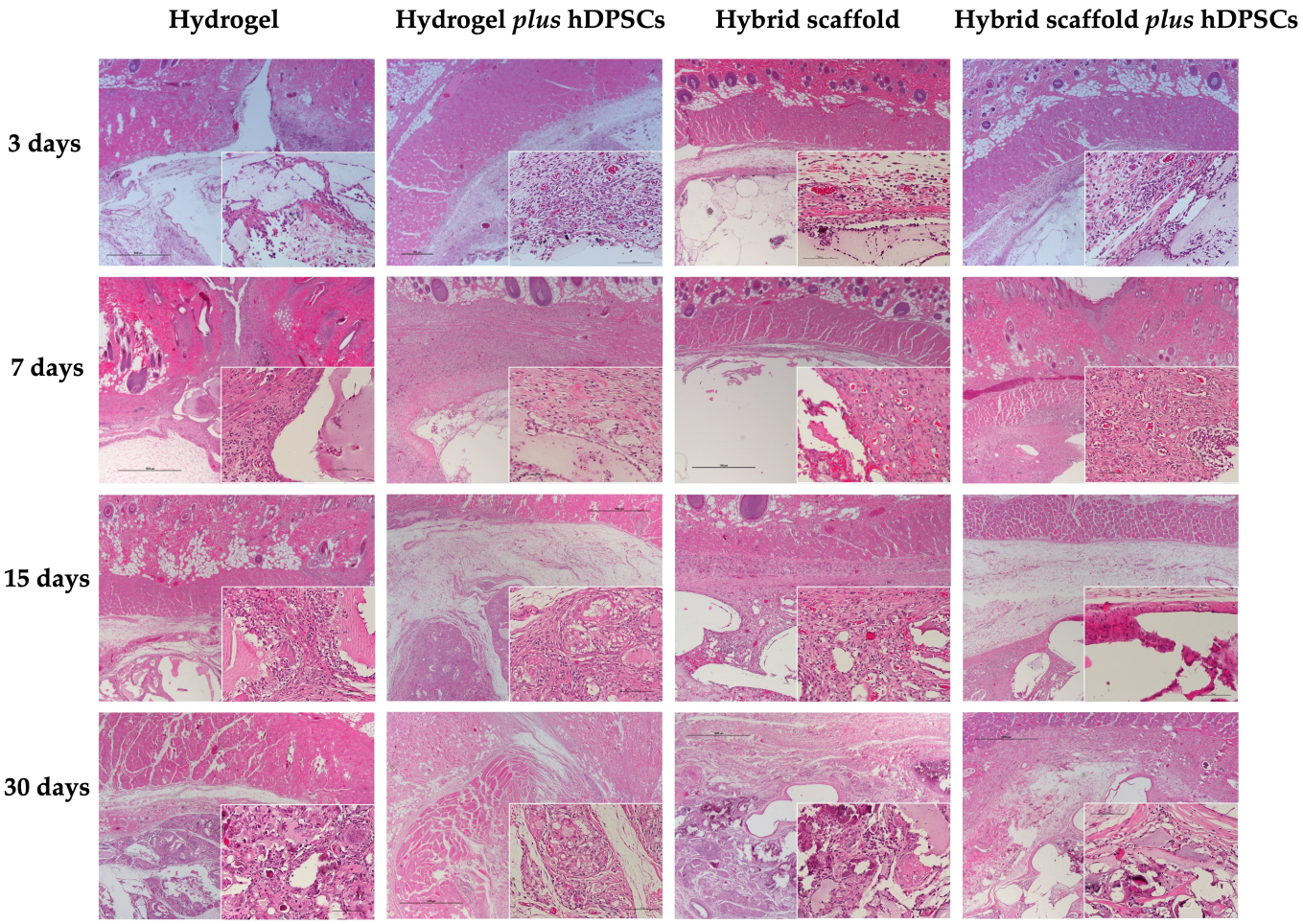


Figure 11. Histological evaluation following H&E staining for hydrogel, hydrogel *plus* hDPSCs, hybrid scaffold, and hybrid scaffold *plus* hDPSCs groups. The sections were assessed using a Nikon microscope (Nikon Eclipse E600) coupled to a photo camera (Nikon Digital Sight DS-5M). For each panel, the main image corresponds to a magnification of 20x and the inset image to a magnification of 200x.

4. Discussion

The current research aimed to develop and evaluate, *in vitro* and *in vivo*, a hybrid structure comprising 3D printed constructs (using PCL and nHA) and hydrogels (using alginate, nHA and Col) loaded with hDPSCs. The purpose was to improve physical stability and bioactivity for bone tissue regeneration applications. PCL and nHA were selected for scaffold support due to their proven efficacy in bone regeneration, as established by previous research from our group [22]. PCL is a thermoplastic polymer extensively used in biomedical applications due to its biocompatibility, biodegradability, facility of processing, non-toxic degradation, and tunable composition and structure [39,40]. Notwithstanding these advantages, PCL has limitations, such as slow cell adhesion and proliferation and a slow degradation rate owing to its high crystallinity and hydrophobic nature [41]. To overcome the challenges arising from these limitations, scaffolds can incorporate inorganic bioactive materials such as calcium phosphates [42]. Therefore, in the present study, nHA was integrated to improve the structure's bioactivity, osteoconductivity and hydrophilicity, thereby enhancing its mechanical properties and improving tissue integration [22,43,44]. Regarding hydrogel production, alginate was selected as the hydrogel component due to its biocompatibility, ease of gelation and ability to form hydrogels under mild conditions. Nevertheless, alginate hydrogels are usually mechanically weak and lack cell-interactive molecules, which limits their suitability for load-bearing and cell proliferation applications. To address these limitations, various materials, including nanomaterials, such as nHA, have been incorporated into alginate, to enhance the hydrogel's printability, mechanical strength and biological activity. Nanomaterials such as nHA interact effectively with the polymer filaments in hydrogels due to their large surface areas and inherent bioactivity, improving the overall performance of composite hydrogels [45-47]. Besides nHA, Col, a natural component of the ECM renowned for its biocompatibility and ability to support bone formation and remodeling, was also incorporated into the hydrogel. Col is an excellent structural support and favors the cellular activities, which are so crucial for tissue regeneration [21]. Furthermore, to improve the hydrogel's bioactivity, hDPSCs were also incorporated to harness their osteogenic potential. Several studies have demonstrated that these cells promote mineral deposition and osteodifferentiation in [3,8,16,17,48]. hDPSCs are a highly valuable cell source for BTE due to their capacity to proliferate rapidly, secrete bioactive factors, and be easily isolated from dental pulp - a minimally invasive procedure. Additionally,

hDPSCs can be cryopreserved whilst maintaining their regenerative capabilities, thereby making them a practical and scalable option for clinical applications [8,16,48]. An ideal implant for bone regeneration has yet to be definitively established, as each material exhibits unique advantages and limitations. In light of this, the authors proposed the hypothesis that combining the mechanical properties of the PCL and nHA scaffold with the biocompatible characteristics of the hydrogel with hDPSCs could enhance the efficacy of the devices in stabilizing large bone defects. This synergistic approach is anticipated to address the limitations of each material when used alone, potentially leading to a more effective solution for the treatment of critical and non-united fractures.

Firstly, different implants were developed to systematically compare the properties of the various components. The study categorized the implants into the following groups: hydrogel with alginate, hydrogel with alginate-nHA-Col, hybrid scaffold with alginate, and hybrid scaffold with alginate-nHA-Col. For each group, tests were conducet both with and without cells. The production of these biomaterials strictly followed the protocols established in subsections 2.2 and 2.3 of the Materials and Methods section. This ensured consistency and reproducibility across all samples.

After the production process, the implants underwent a thorough evaluation to assess their cytocompatibility and osteogenic differentiation capabilities. Regarding the cytocompatibility test, all the implants revealed non-cytotoxic effects on cell viability and proliferation, in line with the criteria of the ISO 10993-5:2009 standards. The findings obtained through PrestoBlue™ analysis show that the hybrid scaffolds with alginate-nHA-Col presented superior viability results, thus suggesting that the addition of alginate, nHA and Col-based hydrogels to the rigid scaffold tends to improve cell proliferation and viability.

Moreover, the osteogenic differentiation test showed that the incorporation of nHA and Col into alginate hydrogels appears to increase their ability to promote mineral deposition and osteodifferentiation, both under induced and spontaneous conditions. nHA is known for its osteoconductive properties, providing a favorable surface for the attachment and proliferation of bone cells, which improves the mineralization process [49]. On the other hand, Col, a primary component of the natural ECM, provides structural support and biochemical pathways that are essential for cell differentiation and tissue formation [50]. The synergistic effect of

these two compounds in the alginate hydrogel matrix seems to result in an optimal microenvironment that facilitates both the recruitment and differentiation of osteoprogenitor cells. As future research, it is important to evaluate osteogenic gene expression, as it would provide a better validation of the scaffold's functionality and its capacity to promote osteogenic differentiation.

Afterwards, a qualitative morphological assessment of the samples (SEM) was performed. The outcomes suggest that the composition of the hybrid scaffold provides a favorable microenvironment for the attachment and growth of hDPSCs, promoting the formation of cell clusters. The presence of these clusters highlights the potential of the alginate-nHA-Col structure to support tissue regeneration by facilitating the organization and interaction of cells within the three-dimensional structure. These findings corroborate the results of the cytocompatibility tests, which demonstrated significant cell proliferation and high cell viability in all the samples tested. The cell proliferation observed indicates that the hybrid scaffolds provide a favorable environment for cell growth, supporting the cellular activities essential for tissue regeneration.

Furthermore, the EDX findings confirm the efficient incorporation of the hydrogel into the PCL/nHA matrix. The reduction in calcium content in the hydrogel regions is expected, due to the significantly lower concentration of hydroxyapatite in the hydrogel compared to the scaffold. The EDX results validated the proper distribution and integration of the hydrogel with the scaffold, ensuring that the composite material maintains the desired structural and compositional characteristics.

Considering the assessment of biocompatibility in the rat model, the hybrid scaffold devices presented minimal or no reaction, except in the 15-day post-implantation period (slight reaction). The results indicate a significant difference after these 15 days of implantation, particularly when comparing the control group to the experimental groups - hydrogel, hydrogel *plus* hDPSCs and hybrid scaffold *plus* hDPSCs. Differences at this time point are probably due to the different tissue/biomaterials interactions that, particularly in the case of hydrogels, can be related with the calcium ions release that will lead to a persistence of inflammatory response and to a potential enhancement of cellular activity. According to Chan and Mooney, the *in vivo* application of calcium alginate gels triggers the release of inflammatory cytokines from the surrounding tissues [51]. Nevertheless, after 30 days, these differences were no longer statistically significant and the histological results are compatible with tissue adaptation to the implanted materials. Presumably, over time, the inflammation decreases as the

immune system adapts to the foreign material or as the structure degrades. Overall, the macroscopic and microscopic evaluations, combined with the ISO 10993-6 scoring standards, confirm the biocompatibility of the hybrid scaffold with alginate-nHA-Col structure. The structure supports tissue integration with minimal adverse reactions, promoting angiogenesis and undergoing predictable inflammatory resolution, thus demonstrating its potential suitability for biomedical applications.

After evaluating biocompatibility *in vivo*, the following step involves implementing a scale-up animal model of bone defects *in vivo*, namely using the ovine model. The forthcoming research will address non-critical and critical bone defects, targeting the femur and iliac crest respectively, according to bone injury models already established in our group [3,52]. The authors believe that the *in vivo* study in an ovine model will provide crucial insights into the efficacy of the hybrid's scaffolds developed, evaluating their regenerative characteristics towards bone lesion stabilization and support, and allowing scalability of therapeutic options developed, so that they can be used in human medicine, and in species of clinical interest in veterinary medicine, following the assumptions of the "one health" concept.

5. Conclusions

This study developed a hybrid scaffold comprising PCL, nHA, and a bioink composed of alginate, nHA, Col and hDPSCs.

The *in vitro* evaluation revealed that the hybrid scaffold with alginate-nHA-Col presented superior cell attachment, proliferation and osteogenic differentiation, compared to control groups. The inclusion of nHA and Col in the bioink significantly enhanced mineral deposition and spontaneous osteodifferentiation, suggesting their osteoinductive properties.

The *in vivo* assessments in a rat model, with minimal inflammatory responses, confirmed the biocompatibility of the scaffold. The transient slight reaction at 15 days post-implantation, followed by the absence of any reaction at 30 days, aligns with the expected inflammatory response and subsequent resolution phases associated with biomaterial implantation. This response highlights the scaffold's ability to effectively integrate with host tissues.

Overall, the hybrid scaffold presents good potential for clinical applications in bone repair and regeneration. Its combination of mechanical strength and

biological activity addresses the critical needs of bone tissue engineering, offering a feasible treatment for critical-size bone defects and non-united fractures. Future research should focus on conducting long-term studies to evaluate its performance in more complex and clinically relevant models.

Author Contributions: Conceptualization, Ana Catarina Sousa, Nuno Alves, Marco Domingos and Ana Colette Maurício; methodology, Ana Catarina Sousa, Rui Alvites, Bruna Lopes, Patrícia Sousa, Alícia Moreira, André Coelho, Alexandra Rema, Sara Biscaia, Rachel Cordeiro, Fátima Faria, Gabriela Fernandes da Silva and Irina Amorim; software, José Domingos Santos and Luís Atayde; validation, José Domingos Santos, Luís Atayde, Nuno Alves, Marco Domingos and Ana Colette Maurício; formal analysis, Ana Catarina Sousa; investigation, Ana Catarina Sousa; resources, José Domingos Santos, Luís Atayde, Nuno Alves, Marco Domingos and Ana Colette Maurício; data curation, Ana Catarina Sousa; writing—original draft preparation, Ana Catarina Sousa; writing—review and editing, Ana Catarina Sousa, Rui Alvites, Bruna Lopes, Patrícia Sousa Alícia Moreira, André Coelho, Alexandra Rema, Sara Biscaia, Rachel Cordeiro, Fátima Faria, Gabriela Fernandes da Silva, Irina Amorim, José Domingos Santos, Luís Atayde, Nuno Alves, Marco Domingos and Ana Colette Maurício; visualization, Marco Domingos and Ana Colette Maurício; supervision, Marco Domingos and Ana Colette Maurício; project administration, Marco Domingos and Ana Colette Maurício; funding acquisition, José Domingos Santos, Luís Atayde, Nuno Alves, Marco Domingos and Ana Colette Maurício. All authors have read and agreed to the published version of the manuscript.

Funding: Ana Catarina Sousa (SFRH/BD/146689/2019), Bruna Lopes (2021.05265.BD), Patrícia Sousa (2023.00246.BD), André Coelho (2023.00428.BD), Alícia Moreira (2023.00544.BD) and acknowledge Fundação para a Ciência e Tecnologia (FCT), for financial support. Rui Alvites acknowledges the CECA, UP, and FCT for the funding and accessibility of all technical, structural, and human resources necessary for the development of this work. The work was supported through the project UIDB/00211/2020 funded by FCT/MCTES, national funds. This research was funded by Projects PEst-OE/AGR/UI0211/2011 from FCT, and COM-PETE 2020, from ANI–Projetos ID&T Empresas em Copromoção, by the project "InnovaBIOMAS - Optimized Additive Biofabrication System for the Production of Hierarchical Multi-Tissue Scaffolds Applied in the Treatment of Joint Diseases" with the reference 2022.10564.PTDC, by the project "Bone2Move-

Development of "*in vivo*" experimental techniques and modelling methodologies for the evaluation of 4D scaffolds for bone defect in sheep model: an integrative research approach" with the reference POCI-01-0145-FEDER-031146. Marco Domingos would would like to thank the Engineering and Physical Sciences Research Council (EPSRC) and Medical Research Council (MRC) Centre for Doctoral Training in Regenerative Medicine (EP/L014904/1) and the Henry Royce Institute EPSRC grants EP/R00661X/1, EP/S019367/1, EP/P025021/1 and EP/P025498/1.

Institutional Review Board Statement: The study was conducted with the guidelines of the Directive 2010/63/EU of the European Parliament and Portuguese DL 113/2013. All the procedures were approved by the ICBAS-UP Animal Welfare Organism of the Ethics Committee (ORBEA) (Project 288/2018) and by the Veterinary Authorities of Portugal (DGAV). Humane end points were followed in agreement to the OECD Guidelines (2000).

Data Availability Statement: The data that support the findings of this study are available from the
corresponding author on request.

Acknowledgments: The authors of this paper acknowledge Daniela Silva from the Scanning Electronic Microscopy Laboratory of the Materials Centre at the University of Porto.

Conflicts of Interest: The authors declare no conflict of interest.

6. Abbreviations

3D	Three-dimensional
Al	Alendronate
ARS	Alizarin Red S
BMP-2	Bone Morphogenetic Protein-2
BTE	Bone tissue engineering
$CaCl_2$	Calcium chloride
CECA	Centro de Estudos de Ciência Animal

CDRSP	Centre for Rapid and Sustainable Product Development
Col	Collagen
DGAV	Veterinary Authorities of Portugal
DMF	N,N-Dimethylformamide
DPBS	Dulbecco's phosphate-buffered saline
EDX	Energy Dispersive X-ray Spectroscopy
ECM	Extracellular Matrix
FBS	Fetal Bovine Serum
H&E	Hematoxylin-Eosin
HA	Hydroxyapatite
hBMSC	Human Bone Marrow Stem/Stromal Cell
hDPSC	Human Dental Pulp Stem/Stromal Cell
HMDS	Hexamethyldisilazane
hMSC	Human Mesenchymal Stem/Stromal Cell
i3S	Institute for Research and Innovation in Health
IPATIMUP	Institute of Molecular Pathology and Immunology, University of Porto
ISCT	International Society for Cellular Therapy
MSC	Mesenchymal Stem/Stromal Cell
nHA	Nano-Hydroxyapatite
ORBEA	Animal Welfare Organism of the Ethics Committee
PCL	Polycaprolactone

PEGDA	Diacrylate Poly(Ethylene Glycol)
PLGA	Poly (Lactic-co-Glycolic Acid)
PLLA	Poly (L-lactic acid)
PMN	Polymorphonuclear
SE	Standard Deviation of the mean
SEM	Scanning Electronic Microscopy

7. References

1. Xue, N.; Ding, X.; Huang, R.; Jiang, R.; Huang, H.; Pan, X.; Min, W.; Chen, J.; Duan, J.A.; Liu, P.; et al. Bone Tissue Engineering in the Treatment of Bone Defects. *Pharmaceuticals (Basel)* **2022**, *15*, doi:10.3390/ph15070879.

2. Grayson, W.L.; Bunnell, B.A.; Martin, E.; Frazier, T.; Hung, B.P.; Gimble, J.M. Stromal cells and stem cells in clinical bone regeneration. *Nature Reviews Endocrinology* **2015**, *11*, 140-150.

3. Campos, J.M.; Sousa, A.C.; Caseiro, A.R.; Pedrosa, S.S.; Pinto, P.O.; Branquinho, M.V.; Amorim, I.; Santos, J.D.; Pereira, T.; Mendonça, C.M.; et al. Dental pulp stem cells and Bonelike(®) for bone regeneration in ovine model. *Regenerative Biomaterials* **2019**, *6*, 49-59, doi:10.1093/rb/rby025.

4. Dominici, M.; Le Blanc, K.; Mueller, I.; Slaper-Cortenbach, I.; Marini, F.; Krause, D.; Deans, R.; Keating, A.; Prockop, D.; Horwitz, E. Minimal criteria for defining multipotent mesenchymal stromal cells. The International Society for Cellular Therapy position statement. *Cytotherapy* **2006**, *8*, 315-317, doi:10.1080/14653240600855905.

5. Bakopoulou, A.; About, I. Stem Cells of Dental Origin: Current Research Trends and Key Milestones towards Clinical Application. *Stem Cells International* **2016**, *2016*, 4209891, doi:https://doi.org/10.1155/2016/4209891.

6. Najar, M.; Melki, R.; Khalife, F.; Lagneaux, L.; Bouhtit, F.; Moussa Agha, D.; Fahmi, H.; Lewalle, P.; Fayyad-Kazan, M.; Merimi, M. Therapeutic Mesenchymal Stem/Stromal Cells: Value, Challenges and Optimization. *Frontiers in Cell and Developmental Biology* **2022**, *9*, doi:10.3389/fcell.2021.716853.

7. Theodosaki, A.M.; Tzemi, M.; Galanis, N.; Bakopoulou, A.; Kotsiomiti, E.; Aggelidou, E.; Kritis, A. Bone Regeneration with Mesenchymal Stem Cells in Scaffolds: Systematic Review of Human Clinical Trials. *Stem Cell Reviews and Reports* **2024**, *20*, 938-966, doi:10.1007/s12015-024-10696-5.

8. Yoshida, S.; Tomokiyo, A.; Hasegawa, D.; Hamano, S.; Sugii, H.; Maeda, H. Insight into the Role of Dental Pulp Stem Cells in Regenerative Therapy. *Biology* **2020**, *9*, 160.

9. Gronthos, S.; Mankani, M.; Brahim, J.; Robey, P.G.; Shi, S. Postnatal human dental pulp stem cells (DPSCs) in vitro and in vivo. *Proceedings of the National Academy of Sciences* **2000**, *97*, 13625-13630.

10. Papaccio, G.; Graziano, A.; d'Aquino, R.; Graziano, M.F.; Pirozzi, G.; Menditti, D.; De Rosa, A.; Carinci, F.; Laino, G. Long-term cryopreservation of dental pulp stem cells (SBP-DPSCs) and their differentiated osteoblasts: a cell source for tissue repair. *J Cell Physiol* **2006**, *208*, 319-325, doi:10.1002/jcp.20667.

11. Kawashima, N. Characterisation of dental pulp stem cells: a new horizon for tissue regeneration? *Archives of oral biology* **2012**, *57*, 1439-1458.

12. Gronthos, S.; Brahim, J.; Li, W.; Fisher, L.W.; Cherman, N.; Boyde, A.; DenBesten, P.; Robey, P.G.; Shi, S. Stem cell properties of human dental pulp stem cells. *J Dent Res* **2002**, *81*, 531-535, doi:10.1177/154405910208100806.

13. Caseiro, A.; Pereira, T.; Bártolo, P.; Santos, J.; Luís, A.; Maurício, A. Mesenchymal stem cells and biomaterials systems–perspectives for skeletal muscle tissue repair and regeneration. *Procedia engineering* **2015**, *110*, 90-97.

14. Gärtner, A.; Pereira, T.; Armada-da-Silva, P.; Amado, S.; Veloso, A.; Amorim, I.; Ribeiro, J.; Santos, J.; Bárcia, R.; Cruz, P. Effects of umbilical cord tissue

mesenchymal stem cells (UCX®) on rat sciatic nerve regeneration after neurotmesis injuries. *Journal of stem cells & regenerative medicine* **2014**, *10*, 14.

15. Pereira, T.; Ivanova, G.; Caseiro, A.R.; Barbosa, P.; Bártolo, P.J.; Santos, J.D.; Luís, A.L.; Maurício, A.C. MSCs Conditioned Media and Umbilical Cord Blood Plasma Metabolomics and Composition. *PLOS ONE* **2014**, *9*, e113769, doi:10.1371/journal.pone.0113769.

16. Caseiro, A.; Alvites, R.; Pedrosa, S.; Miguel, J.; Reis, I.; Santos, J.; Mendonça, C.; Atayde, M.; Maurício, A. The potential clinical application of mesenchymal stem cells from the dental pulp (DPSCs) for bone regeneration. *Frontiers in Stem Cell and Regenerative Medicine Research* **2017**, *6*, 3-52, doi:10.2174/9781681084770117060004.

17. Caseiro, A.R.; Santos Pedrosa, S.; Ivanova, G.; Vieira Branquinho, M.; Almeida, A.; Faria, F.; Amorim, I.; Pereira, T.; Maurício, A.C. Mesenchymal Stem/ Stromal Cells metabolomic and bioactive factors profiles: A comparative analysis on the umbilical cord and dental pulp derived Stem/ Stromal Cells secretome. *PLOS ONE* **2019**, *14*, e0221378, doi:10.1371/journal.pone.0221378.

18. Shahi, S.; Dehghani, F.; Abdolahinia, E.D.; Sharifi, S.; Ahmadian, E.; Gajdács, M.; Kárpáti, K.; Dizaj, S.M.; Eftekhari, A.; Kavetskyy, T. Effect of gelatinous spongy scaffold containing nano-hydroxyapatite on the induction of odontogenic activity of dental pulp stem cells. *Journal of King Saud University - Science* **2022**, *34*, 102340, doi:https://doi.org/10.1016/j.jksus.2022.102340.

19. Abbasi, N.; Hamlet, S.; Love, R.M.; Nguyen, N.-T. Porous scaffolds for bone regeneration. *Journal of Science: Advanced Materials and Devices* **2020**, *5*, 1-9, doi:https://doi.org/10.1016/j.jsamd.2020.01.007.

20. Xiao, L.; Liu, H.; Huang, H.; Wu, S.; Xue, L.; Geng, Z.; Cai, L.; Yan, F. 3D nanofiber scaffolds from 2D electrospun membranes boost cell penetration and positive host response for regenerative medicine. *J Nanobiotechnology* **2024**, *22*, 322, doi:10.1186/s12951-024-02578-2.

21. Tang, G.; Liu, Z.; Liu, Y.; Yu, J.; Wang, X.; Tan, Z.; Ye, X. Recent Trends in the Development of Bone Regenerative Biomaterials. *Frontiers in Cell and Developmental Biology* **2021**, *9*, doi:10.3389/fcell.2021.665813.

22. Sousa, A.C.; Biscaia, S.; Alvites, R.; Branquinho, M.; Lopes, B.; Sousa, P.; Valente, J.; Franco, M.; Santos, J.D.; Mendonça, C.; et al. Assessment of 3D-Printed Polycaprolactone, Hydroxyapatite Nanoparticles and Diacrylate Poly(ethylene glycol) Scaffolds for Bone Regeneration. *Pharmaceutics* **2022**, *14*, doi:10.3390/pharmaceutics14122643.

23. Lee, S.S.; Du, X.; Kim, I.; Ferguson, S.J. Scaffolds for bone-tissue engineering. *Matter* **2022**, *5*, 2722-2759, doi:https://doi.org/10.1016/j.matt.2022.06.003.

24. Hull, S.M.; Brunel, L.G.; Heilshorn, S.C. 3D Bioprinting of Cell-Laden Hydrogels for Improved Biological Functionality. *Advanced Materials* **2022**, *34*, 2103691, doi:https://doi.org/10.1002/adma.202103691.

25. Kim, W.; Kim, G.H. Highly bioactive cell-laden hydrogel constructs bioprinted using an emulsion bioink for tissue engineering applications. *Biofabrication* **2022**, *14*, 045018, doi:10.1088/1758-5090/ac8fb8.

26. Chen, Y.-T.; Chuang, Y.-H.; Chen, C.-M.; Wang, J.-Y.; Wang, J. Development of hybrid scaffolds with biodegradable polymer composites and bioactive hydrogels for bone tissue engineering. *Biomaterials Advances* **2023**, *153*, 213562, doi:https://doi.org/10.1016/j.bioadv.2023.213562.

27. Ghorbani, F.; Li, D.; Zhong, Z.; Sahranavard, M.; Qian, Z.; Ni, S.; Zhang, Z.; Zamanian, A.; Yu, B. Bioprinting a cell-laden matrix for bone regeneration: A focused review. *Journal of Applied Polymer Science* **2021**, *138*, 49888, doi:https://doi.org/10.1002/app.49888.

28. Luo, Y.; Li, Y.; Qin, X.; Wa, Q. 3D printing of concentrated alginate/gelatin scaffolds with homogeneous nano apatite coating for bone tissue engineering. *Materials and Design* **2018**, *146*, 12-19, doi:10.1016/j.matdes.2018.03.002.

29. Choe, G.; Lee, M.; Oh, S.; Seok, J.M.; Kim, J.; Im, S.; Park, S.A.; Lee, J.Y. Three-dimensional bioprinting of mesenchymal stem cells using an osteoinductive

bioink containing alginate and BMP-2-loaded PLGA nanoparticles for bone tissue engineering. *Biomaterials Advances* **2022**, *136*, 212789, doi:https://doi.org/10.1016/j.bioadv.2022.212789.

30. Hamid, O.A.; Eltaher, H.M.; Sottile, V.; Yang, J. 3D bioprinting of a stem cell-laden, multi-material tubular composite: An approach for spinal cord repair. *Materials Science and Engineering: C* **2021**, *120*, 111707, doi:https://doi.org/10.1016/j.msec.2020.111707.

31. Dong, L.; Wang, S.-J.; Zhao, X.-R.; Zhu, Y.-F.; Yu, J.-K. 3D- Printed Poly(ε-caprolactone) Scaffold Integrated with Cell-laden Chitosan Hydrogels for Bone Tissue Engineering. *Scientific Reports* **2017**, *7*, 13412, doi:10.1038/s41598-017-13838-7.

32. Wu, H.; Lei, P.; Liu, G.; Shrike Zhang, Y.; Yang, J.; Zhang, L.; Xie, J.; Niu, W.; Liu, H.; Ruan, J.; et al. Reconstruction of Large-scale Defects with a Novel Hybrid Scaffold Made from Poly(L-lactic acid)/Nanohydroxyapatite/Alendronate-loaded Chitosan Microsphere: in vitro and in vivo Studies. *Scientific Reports* **2017**, *7*, 359, doi:10.1038/s41598-017-00506-z.

33. Viana, T.; Biscaia, S.; Dabrowska, E.; Franco, M.C.; Carreira, P.; Morouço, P.; Alves, N. A Novel Biomanufacturing System to Produce Multi-Material Scaffolds for Tissue Engineering: Concept and Preliminary Results. *Applied Mechanics and Materials* **2019**, *890*, 283-289, doi:10.4028/www.scientific.net/AMM.890.283.

34. Ferreira, M.J.S.L.M. Integrating 3D Bioprinting and Pluripotent Stem Cell Technologies for Articular Cartilage Tissue Engineering. The University of Manchester, 2022.

35. Hassani, A.; Khoshfetrat, A.B.; Rahbarghazi, R.; Sakai, S. Collagen and nano-hydroxyapatite interactions in alginate-based microcapsule provide an appropriate osteogenic microenvironment for modular bone tissue formation. *Carbohydrate Polymers* **2022**, *277*, 118807, doi:https://doi.org/10.1016/j.carbpol.2021.118807.

36. Branquinho, M.V.; Ferreira, S.O.; Alvites, R.D.; Magueta, A.F.; Ivanov, M.; Sousa, A.C.; Amorim, I.; Faria, F.; Fernandes, M.H.V.; Vilarinho, P.M.; et al. In Vitro and In Vivo Characterization of PLLA-316L Stainless Steel Electromechanical Devices for Bone Tissue Engineering—A Preliminary Study. *International Journal of Molecular Sciences* **2021**, *22*, doi:10.3390/ijms22147655.

37. Alvites, R.D.; Branquinho, V.M.; Caseiro, A.R.; Amorim, I.; Santos Pedrosa, S.; Rêma, A.; Faria, F.; Porto, B.; Oliveira, C.; Teixeira, P.; et al. Rat Olfactory Mucosa Mesenchymal Stem/Stromal Cells (OM-MSCs): A Characterization Study. *International Journal of Cell Biology* **2020**, *2020*, doi:10.1155/2020/2938258.

38. Caseiro, A.R.; Ivanova, G.; Pedrosa, S.S.; Branquinho, V.M.; Georgieva, P.; Barbosa, P.P.; Santos, J.D.; Magalhães, R.; Teixeira, P.; Pereira, T.; et al. Human umbilical cord blood plasma as an alternative to animal sera for mesenchymal stromal cells in vitro expansion - A multicomponent metabolomic analysis. *PLoS ONE* **2018**, *13*, 1-35, doi:10.1371/journal.pone.0203936.

39. Wang, S.; Gu, R.; Wang, F.; Zhao, X.; Yang, F.; Xu, Y.; Yan, F.; Zhu, Y.; Xia, D.; Liu, Y. 3D-Printed PCL/Zn scaffolds for bone regeneration with a dose-dependent effect on osteogenesis and osteoclastogenesis. *Mater Today Bio* **2022**, *13*, 100202, doi:10.1016/j.mtbio.2021.100202.

40. Babilotte, J.; Guduric, V.; Le Nihouannen, D.; Naveau, A.; Fricain, J.C.; Catros, S. 3D printed polymer-mineral composite biomaterials for bone tissue engineering: Fabrication and characterization. *J Biomed Mater Res B Appl Biomater* **2019**, *107*, 2579-2595, doi:10.1002/jbm.b.34348.

41. Lam, C.X.; Hutmacher, D.W.; Schantz, J.T.; Woodruff, M.A.; Teoh, S.H. Evaluation of polycaprolactone scaffold degradation for 6 months in vitro and in vivo. *J Biomed Mater Res A* **2009**, *90*, 906-919, doi:10.1002/jbm.a.32052.

42. Petretta, M.; Gambardella, A.; Boi, M.; Berni, M.; Cavallo, C.; Marchiori, G.; Maltarello, M.C.; Bellucci, D.; Fini, M.; Baldini, N.; et al. Composite Scaffolds

for Bone Tissue Regeneration Based on PCL and Mg-Containing Bioactive Glasses. *Biology (Basel)* **2021**, *10*, doi:10.3390/biology10050398.

43. Keivani, F.; Shokrollahi, P.; Zandi, M.; Irani, S.; Shokrolahi, F.; Khorasani, S.C. Engineered electrospun poly(caprolactone)/polycaprolactone-g-hydroxyapatite nano-fibrous scaffold promotes human fibroblasts adhesion and proliferation. *Mater Sci Eng C Mater Biol Appl* **2016**, *68*, 78-88, doi:10.1016/j.msec.2016.05.098.

44. Geng, Z.; Sang, S.; Wang, S.; Meng, F.; Li, Z.; Zhu, S.; Cui, Z.; Jing, Y.; Wang, C.; Su, J. Optimizing the strontium content to achieve an ideal osseointegration through balancing apatite-forming ability and osteogenic activity. *Biomaterials Advances* **2022**, *133*, 112647, doi:https://doi.org/10.1016/j.msec.2022.112647.

45. Bendtsen, S.T.; Quinnell, S.P.; Wei, M. Development of a novel alginate-polyvinyl alcohol-hydroxyapatite hydrogel for 3D bioprinting bone tissue engineered scaffolds. *J Biomed Mater Res A* **2017**, *105*, 1457-1468, doi:10.1002/jbm.a.36036.

46. Im, S.; Choe, G.; Seok, J.M.; Yeo, S.J.; Lee, J.H.; Kim, W.D.; Lee, J.Y.; Park, S.A. An osteogenic bioink composed of alginate, cellulose nanofibrils, and polydopamine nanoparticles for 3D bioprinting and bone tissue engineering. *International Journal of Biological Macromolecules* **2022**, *205*, 520-529, doi:https://doi.org/10.1016/j.ijbiomac.2022.02.012.

47. Choe, G.; Oh, S.; Seok, J.M.; Park, S.; Lee, J. Graphene oxide/alginate composites as novel bioinks for three-dimensional mesenchymal stem cell printing and bone regeneration applications. *Nanoscale* **2019**, *11*, doi:10.1039/C9NR07643C.

48. Tsutsui, T.W. Dental pulp stem cells: advances to applications. *Stem cells and cloning: advances and applications* **2020**, *13*, 33, doi:10.2147/SCCAA.S166759.

49. Pokhrel, S. Hydroxyapatite: Preparation, Properties and Its Biomedical Applications. *Advances in Chemical Engineering and Science* **2018**, *08*, 225-240, doi:10.4236/aces.2018.84016.

50. Li, Y.; Liu, Y.; Li, R.; Bai, H.; Zhu, Z.; Zhu, L.; Zhu, C.; Che, Z.; Liu, H.; Wang, J.; et al. Collagen-based biomaterials for bone tissue engineering. *Materials & Design* **2021**, *210*, 110049, doi:https://doi.org/10.1016/j.matdes.2021.110049.

51. Chan, G.; Mooney, D.J. Ca(2+) released from calcium alginate gels can promote inflammatory responses in vitro and in vivo. *Acta Biomater* **2013**, *9*, 9281-9291, doi:10.1016/j.actbio.2013.08.002.

52. Pinto, P.; Branquinho, M.; Caseiro, A.; Sousa, A.; Brandão, A.; Pedrosa, S.; Alvites, R.; Campos, J.; Santos, F.; Santos, J. The application of bonelike® Poro as a synthetic bone substitute for the management of critical-sized bone defects-a comparative approach to the autograft technique-a preliminary study. *Bone Reports* **2021**, 101064.

8. Supporting Material

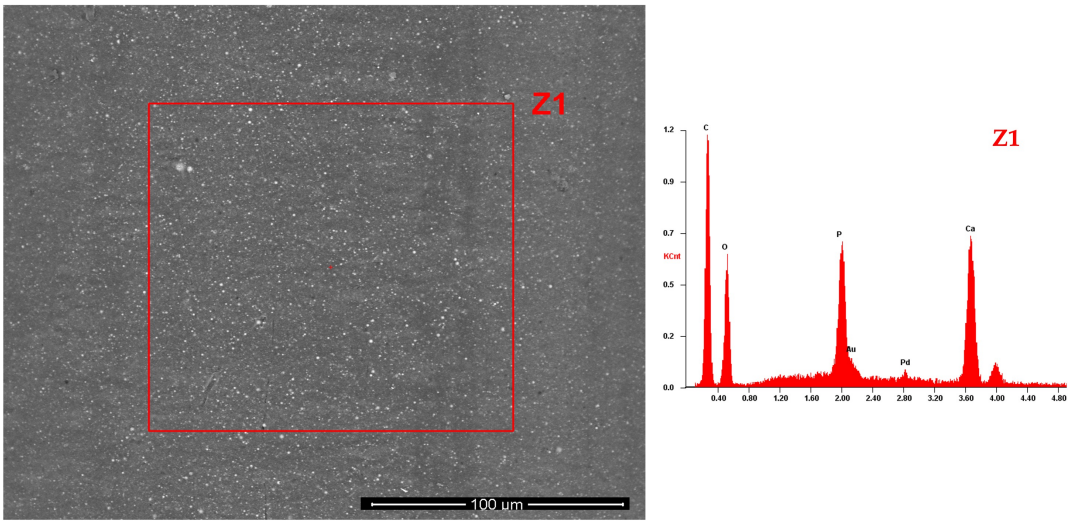


Figure S1. SEM image (1000x magnification) and corresponding EDX analysis of the control group.

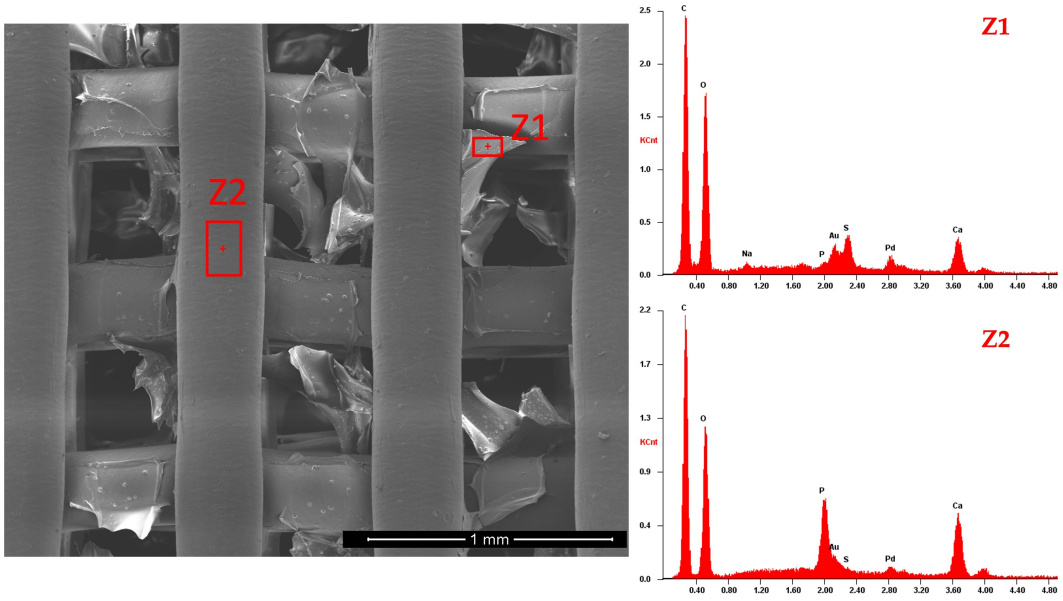


Figure S2. SEM image (100x magnification) and corresponding EDX analysis of the hybrid scaffold with alginate *plus* hDPSCs group.

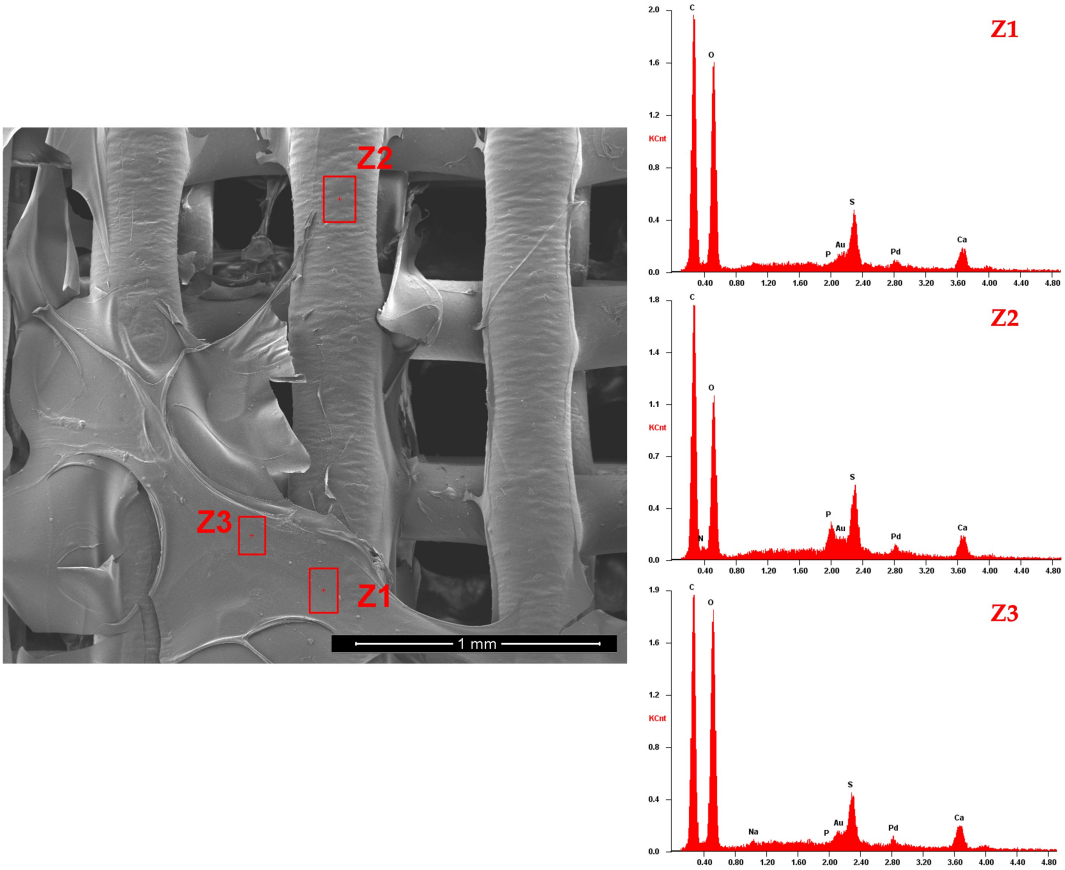


Figure S3. SEM image (100x magnification) and corresponding EDX analysis of the hybrid scaffold with alginate-nHA-Col *plus* hDPSCs group.

References

1. Kim, J.; Choi, Y.J.; Gal, C.W.; Sung, A.; Park, H.; Yun, H.S. 142Development of an alginate-gelatin bioink enhancing osteogenic differentiation by gelatin release. *Int J Bioprint* **2023**, *9*, 660, doi:10.18063/ijb.v9i2.660.

2. Santoni, S.; Gugliandolo, S.G.; Sponchioni, M.; Moscatelli, D.; Colosimo, B.M. 3D bioprinting: current status and trends—a guide to the literature and industrial practice. *Bio-Design and Manufacturing* **2022**, *5*, 14-42.

3. Ahadian, S.; Khademhosseini, A. A Perspective on 3D Bioprinting in Tissue Regeneration. *Biodes Manuf* **2018**, *1*, 157-160, doi:10.1007/s42242-018-0020-3.

4. Groll, J.; Burdick, J.A.; Cho, D.-W.; Derby, B.; Gelinsky, M.; Heilshorn, S.C.; Juengst, T.; Malda, J.; Mironov, V.A.; Nakayama, K. A definition of bioinks and their distinction from biomaterial inks. *Biofabrication* **2018**, *11*, 013001.

5. Groll, J.; Burdick, J.A.; Cho, D.W.; Derby, B.; Gelinsky, M.; Heilshorn, S.C.; Jüngst, T.; Malda, J.; Mironov, V.A.; Nakayama, K.; et al. A definition of bioinks and their distinction from biomaterial inks. *Biofabrication* **2018**, *11*, 013001, doi:10.1088/1758-5090/aaec52.

6. Gao, G.; Cui, X. Three-dimensional bioprinting in tissue engineering and regenerative medicine. *Biotechnol Lett* **2016**, *38*, 203-211, doi:10.1007/s10529-015-1975-1.

7. Li, L.; Yu, F.; Shi, J.; Shen, S.; Teng, H.; Yang, J.; Wang, X.; Jiang, Q. In situ repair of bone and cartilage defects using 3D scanning and 3D printing. *Sci Rep* **2017**, *7*, 9416, doi:10.1038/s41598-017-10060-3.

8. Costa, J.B.; Silva-Correia, J.; Ribeiro, V.P.; da Silva Morais, A.; Oliveira, J.M.; Reis, R.L. Engineering patient-specific bioprinted constructs for treatment of degenerated intervertebral disc. *Materials Today Communications* **2019**, *19*, 506-512.

9. Datta, P.; Ozbolat, V.; Ayan, B.; Dhawan, A.; Ozbolat, I.T. Bone tissue bioprinting for craniofacial reconstruction. *Biotechnol Bioeng* **2017**, *114*, 2424-2431, doi:10.1002/bit.26349.

10. Habibovic, P.; Yuan, H.; van den Doel, M.; Sees, T.M.; van Blitterswijk, C.A.; de Groot, K. Relevance of osteoinductive biomaterials in critical-sized orthotopic defect. *J Orthop Res* **2006**, *24*, 867-876, doi:10.1002/jor.20115.

11. Bian, L. Functional hydrogel bioink, a key challenge of 3D cellular bioprinting. *APL Bioeng* **2020**, *4*, 030401, doi:10.1063/5.0018548.

12. Cui, X.; Li, J.; Hartanto, Y.; Durham, M.; Tang, J.; Zhang, H.; Hooper, G.; Lim, K.; Woodfield, T. Advances in Extrusion 3D Bioprinting: A Focus on Multicomponent Hydrogel-Based Bioinks. *Adv Healthc Mater* **2020**, *9*, e1901648, doi:10.1002/adhm.201901648.

13. Kyle, S.; Jessop, Z.M.; Al-Sabah, A.; Whitaker, I.S. 'Printability' of Candidate Biomaterials for Extrusion Based 3D Printing: State-of-the-Art. *Adv Healthc Mater* **2017**, *6*, doi:10.1002/adhm.201700264.

14. Bell, J.H.; Haycock, J.W. Next generation nerve guides: materials, fabrication, growth factors, and cell delivery. *Tissue Eng Part B Rev* **2012**, *18*, 116-128, doi:10.1089/ten.TEB.2011.0498.

15. Sellaro, T.L.; Ranade, A.; Faulk, D.M.; McCabe, G.P.; Dorko, K.; Badylak, S.F.; Strom, S.C. Maintenance of human hepatocyte function in vitro by liver-derived extracellular matrix gels. *Tissue Eng Part A* **2010**, *16*, 1075-1082, doi:10.1089/ten.TEA.2008.0587.

16. Pati, F.; Jang, J.; Ha, D.H.; Won Kim, S.; Rhie, J.W.; Shim, J.H.; Kim, D.H.; Cho, D.W. Printing three-dimensional tissue analogues with decellularized extracellular matrix bioink. *Nat Commun* **2014**, *5*, 3935, doi:10.1038/ncomms4935.

17. Malda, J.; Visser, J.; Melchels, F.P.; Jüngst, T.; Hennink, W.E.; Dhert, W.J.; Groll, J.; Hutmacher, D.W. 25th anniversary article: Engineering hydrogels for biofabrication. *Adv Mater* **2013**, *25*, 5011-5028, doi:10.1002/adma.201302042.

18. Ramiah, P.; Du Toit, L.C.; Choonara, Y.E.; Kondiah, P.P.; Pillay, V. Hydrogel-based bioinks for 3D bioprinting in tissue regeneration. *Frontiers in Materials* **2020**, *7*, 76.

19. Fatimi, A.; Okoro, O.V.; Podstawczyk, D.; Siminska-Stanny, J.; Shavandi, A. Natural Hydrogel-Based Bio-Inks for 3D Bioprinting in Tissue Engineering: A Review. *Gels* **2022**, *8*, doi:10.3390/gels8030179.

20. Gopinathan, J.; Noh, I. Recent trends in bioinks for 3D printing. *Biomater Res* **2018**, *22*, 11, doi:10.1186/s40824-018-0122-1.

21. Kim, D.; Kim, M.; Lee, J.; Jang, J. Review on Multicomponent Hydrogel Bioinks Based on Natural Biomaterials for Bioprinting 3D Liver Tissues. *Front Bioeng Biotechnol* **2022**, *10*, 764682, doi:10.3389/fbioe.2022.764682.

22. Hassani, A.; Khoshfetrat, A.B.; Rahbarghazi, R.; Sakai, S. Collagen and nano-hydroxyapatite interactions in alginate-based microcapsule provide an appropriate osteogenic microenvironment for modular bone tissue formation. *Carbohydr Polym* **2022**, *277*, 118807, doi:10.1016/j.carbpol.2021.118807.

23. Holmes, A.; Brown, R.; Shakesheff, K. Engineering tissue alternatives to animals: Applying tissue engineering to basic research and safety testing. *Regenerative Medicine* **2009**, *4*, 579-592, doi:10.2217/rme.09.26.

24. Owen, R.; Reilly, G.C. In vitro models of bone remodelling and associated disorders. *Frontiers in bioengineering and biotechnology* **2018**, *6*, 134.

25. Bala, Y.; Seeman, E. Bone's Material Constituents and their Contribution to Bone Strength in Health, Disease, and Treatment. *Calcified Tissue International* **2015**, *97*, 308-326, doi:10.1007/s00223-015-9971-y.

26. Bishop, N. Bone Material Properties in Osteogenesis Imperfecta. *Journal of Bone and Mineral Research* **2016**, *31*, 699-708, doi:10.1002/jbmr.2835.

27. Karunaratne, A.; Xi, L.; Bentley, L.; Sykes, D.; Boyde, A.; Esapa, C.T.; Terrill, N.J.; Brown, S.D.M.; Cox, R.D.; Thakker, R.V.; et al. Multiscale alterations in bone matrix quality increased fragility in steroid induced osteoporosis. *Bone* **2016**, *84*, 15-24, doi:10.1016/j.bone.2015.11.019.

28. de Wildt, B.W.M.; Ansari, S.; Sommerdijk, N.A.J.M.; Ito, K.; Akiva, A.; Hofmann, S. From bone regeneration to three-dimensional in vitro models: tissue engineering of organized bone extracellular matrix. *Current Opinion in Biomedical Engineering* **2019**, *10*, 107-115, doi:https://doi.org/10.1016/j.cobme.2019.05.005.

CHAPTER VI

APPLICATION OF BIOMATERIALS AND CELLULAR THERAPIES FOR THE *IN VIVO* TREATMENT OF CRITICAL-SIZED BONE DEFECTS

[This page is intentionally left blank.]

Introductory Note

Before biomaterials can be applied in clinical settings, it is imperative to conduct extensive and detailed studies to evaluate their safety, biocompatibility, osteoconduction, osteointegration and osteoinduction capacity, and cell adhesion properties [1,2]. The initial phase of studying any novel approach involves assessing the acute toxicity/ cytocompatibility of specific biomaterials, cell therapies or drugs, an assessment that is crucial for minimizing the unnecessary use of animals in early research stages. Once cytocompatibility is confirmed, subsequent *in vivo* assays are necessary to evaluate not only the efficacy of the therapy in promoting bone regeneration but also to observe biocompatibility and other critical phenomena, such as material degradation, bone regeneration, osteoconductivity and immune response.

Experimental animal models are widely utilized in biomedical research because *in vitro* models cannot fully replicate the complexity of the human body [3]. These models provide essential foundational knowledge useful for both pre-clinical and clinical studies [4]. The selection of an appropriate animal model is crucial for ensuring relevance to human conditions, minimizing the use of animals, and avoiding unnecessary expenditure of time, effort, and resources [5]. The range of animal models used in bone regeneration research has expanded, including rodents, companion animals, pigs, small ruminants, lagomorphs, and even primates. Each model offers unique advantages and limitations, mimicking specific processes and phases of human bone regeneration. Therefore, it is crucial to a particular therapeutic approach to be tested in a series of animal models, progressing in complexity, before advancing to clinical trials in human patients [6]. Among various options for pre-clinical studies, ovine has become a favored *in vivo* experimental model, particularly in orthopedic and dental research. This preference is due to their similarities with humans, including comparable body weight, the presence of long bones, and a bone regeneration timeline akin to that of humans. These characteristics enable researchers to accurately assess orthopedic and dental implants designed for human use, thereby allowing for the credible extrapolation of results to human clinical applications [7].

The subsequent chapter focused on evaluating the performance of a novel scaffold composed of poly (ε-caprolactone) (PCL) - extensively utilized throughout

this thesis for its mechanical properties and versatility - combined with Bonelike® (BL), a commercially available synthetic graft based on calcium phosphates. This scaffold was tested in conjunction with conditioned medium derived from human dental pulp stem cells (hDPSCs-CM). This cellular therapy was utilized for treating bone defects because it enhances osteogenic differentiation, reduces inflammation, and promotes angiogenesis. Additionally, it provides a non-invasive and ethical alternative to standard cell-based therapies, while minimizing the risk of immune rejection [8-10].

Initially, BL was characterized using scanning electron microscopy (SEM) and energy-dispersive X-ray spectroscopy (EDX), followed by *in vitro* assessments of its cytocompatibility and osteodifferentiation potential. The study then progressed to an *in vivo* analysis involving an ovine model, where a critical bone defect was surgically induced in the iliac crest. Various therapeutic approaches were applied, including untreated controls, PCL scaffolds with hDPSCs-CM, PCL/ nanohydroxyapatite (nHA) scaffolds with hDPSCs-CM, and PCL/BL scaffolds with hDPSCs-CM. Preliminary outcomes were evaluated through radiographic imaging to assess bone regeneration.

The Application of Bonelike® and hDPSCs Conditioned Medium for the Management of Critical-Sized Bone Defects

[This page is intentionally left blank.]

1. Introduction

Bone defects, often caused by trauma, pathological fractures or tumor resections, present significant clinical challenges, particularly in individuals over 55, where around 37 million fragility fractures occur annually [11]. Traditional treatment options, such as autografts and allografts, have limitations, and this fact leads to the exploration of alternative strategies, including bone tissue engineering. These therapeutic strategies are crucial in both human and veterinary medicine, particularly in situations involving traumatic injuries, tumor resections with substantial and irregular bone loss, corrective osteotomies, spinal fusion, arthrodesis or arthroplasties, and non-union or delayed bone union treatments [2-4]. Additionally, bone regeneration is particularly challenging in patients with metabolic diseases and other local or systemic conditions, especially those related to aging, where intrinsic biological restoration mechanisms are insufficient [12-15].

These clinical scenarios often result in poor outcomes and present significant challenges to orthopedic surgeons [12,14-18]. Critical-sized bone defects - defined as the smallest bone defect that cannot heal spontaneously without intervention during the individual's lifetime - are particularly problematic, with the size of the defect varying based on the bone and species involved [19-21]. In humans, Court-Brown defined a critical-sized defect as one involving 50% of the cortical diameter with a minimum length of 1 cm [22]. If bone union does not occur within one year, it is unlikely to occur at all, resulting in permanent non-union and the formation of fibrous scar tissue between the bone edges, without restoration of bone continuity and function [19].

Recent advancements emphasize the use of composite scaffolds in treating large bone defects. These scaffolds combine osteoconductive matrices, growth factors, and cellular systems with osteogenic potential, offering promising solutions. An ideal bone substitute should be biocompatible, resorbable, mechanically robust, and supportive of bone healing without adverse reactions [23]. This approach is gaining traction as it enhances bone regeneration and offers a viable alternative to traditional methods [18,24].

BL is a glass-reinforced hydroxyapatite (HA) composite, characterized by a P_2O_5-CaO glass-based system within a HA matrix, presenting osteoconductive proprieties. This biomaterial is designed for use as a synthetic bone graft and has

demonstrated significant advantages in various clinical applications, including dental, maxillofacial and orthopedic surgeries [13,25-28]. BL is composed of spherical granules with diameters ranging from 250 to 500 μm, a structural characteristic that enhances its clinical utility. Atayde *et al.* have identified several key advantages of this material: BL can be easily extruded through a syringe, facilitating its application in surgical procedures. Furthermore, its spherical shape and the presence of pores within the granules contribute to improved osteointegration, osteoconduction and controlled degradation [29].

Recent advances in Regenerative Medicine have increasingly focused on cell-free therapies to mitigate the risks associated with the use of stem cells *per se* [30-36]. Research indicate that the regenerative effects attributed to mesenchymal stem cells (MSCs) extend beyond the cells themselves, encompassing their paracrine activity, or secretome, which is crucial for tissue repair even in the absence of the cells [37]. The conditioned medium (CM), consisting of a secretome produced under specific culture conditions, comprises a complex array of cytokines, proteins, exosomes, growth factors and other bioactive soluble molecules secreted by MSCs into their extracellular environment. Since these bioactive molecules are present in the CM and not inside the cells, the medium retains the therapeutic bioactivity of the MSCs [38].

Recent studies have demonstrated the effectiveness of MSC-CM in various therapeutic contexts, including cardiac regeneration, bone repair, nerve regeneration, and in the treatment of lung injuries and other diseases [39-42]. Notably, the secretome from dental stem cells, including dental pulp mesenchymal stem/stromal cells (hDPSCs), has shown significant regenerative potential and utility in treating a range of conditions, such as spinal cord injury, peripheral nerve injury, Alzheimer's disease, Parkinson's disease, and damage to bone and cartilage tissues [10,43-46].

The scientific literature contains numerous experimental reports documenting the therapeutic potential of CM and extracellular vesicles derived from hDPSCs [47,48]. This approach not only enhances biocompatibility but also allows for the customization of MSCs to produce a secretome optimized for specific therapeutic applications [49]. Buss *et al.* demonstrated that CM from hDPSCs cultures significantly promoted the healing of critical-size defects in the calvaria of

rats. The application of this CM resulted in a marked enhancement of the regenerative process, particularly in bone formation and vascularization within the defect site. These findings underscore the potential of hDPSCs-CM as a promising therapeutic strategy for treating critical-size bone defects, offering a viable alternative to traditional regenerative approaches.

One of the challenges in the application of cell therapies is maintaining these at the site of injury/delivery. To ensure the retention of hDPSCs-CM at the target site, various types of membranes have been utilized [50]. Currently, the market offers a diverse range of membrane products, with natural membranes often consisting of variants of porcine collagen, such as Bio-Gide® (Geistlich, Wolhusen, Switzerland). These natural collagen membranes are well known for their non-inflammatory nature and their robust load-bearing capacity, which withstands the compressive forces exerted by surrounding soft tissues and provides a suitable environment for tissue regeneration [51-53]. In the case of injectable solutions, including hDPSCs-CM, these membranes are particularly advantageous due to their ease of use, the rapid formation of a solid membrane after injection and the ability to fill complex defects [52,54,55]. The natural collagen matrix of Bio-Gide® facilitates swift and uniform vascularization, promoting optimal tissue integration and stabilization of the wound [56]. Its smooth side prevents the encroachment of soft tissue into the defect area and supports fibroblast attachment, while the rough, open-pore surface acts as a scaffold for the ingrowth of bone cells and blood vessels [56-60].

In the present study, we assessed the efficacy of the PCL/BL scaffold combined with hDPSCs-CM for potential clinical application in both human and veterinary orthopedics [61]. The BL component was initially characterized using SEM and EDX to analyze its surface morphology and elemental composition. Subsequently, the cytocompatibility of the PCL/BL scaffold was investigated through *in vitro* assays, including tests for cellular viability and osteodifferentiation. Furthermore, the performance of the PCL/BL scaffold combined with hDPSCs-CM, with and without a collagen membrane, was assessed *in vivo*. An ovine model of critical-sized bone defects in the iliac crest was chosen for these studies due to its advantages, including minimal morbidity, a relatively low risk of complications, ease of reproducibility and the ability to create two

defects per animal, thereby reducing the overall number of animals required for the study.

2. Materials and Methods

2.1. Biomaterials

2.1.1. Materials

PCL (CAPA® 6500, Mw: 50 kDa) from Perstorp Caprolactones (Cheshire, United Kingdom) and nHA (particle size < 200 nm; #677418-25G, Sigma-Aldrich, Saint Louis, Missouri, United States of America) were utilized in this study. The formulations were prepared using N,N-dimethylformamide (DMF) obtained from CHEM-LAB (Belgium) and were fabricated using the solvent casting technique.

The preparation of BL was conducted as described in the study by Campos *et al.* [29]. In summary, HA and P_2O_5-CaO-based glass were synthesized separately and then combined. The HA was produced via a precipitation method involving the reaction of calcium hydroxide ($Ca(OH)_2$) (Prolabo, Paris, France) with orthophosphoric acid (H_3PO_4) (Merk, Darmstadt, Germany). The P_2O_5-CaO-based glass, with a composition of $65P_2O_5$-5CaO-$10CaF_2$-$10Na_2O$ (in mol %), was synthesized from reagent-grade chemicals using a platinum crucible heated to 1450ºC. The BL material was formulated by adding 2.5 wt% of glass to the HA, followed by mixing with a pore-forming agent. This mixture was then extruded, spheronized, and the resulting pellets were sintered. Standard sieving techniques were applied to obtain particles within the 250-500 µm size range. The resulting biomaterial has been thoroughly characterized in several studies [62-64].

Additionally, a resorbable collagen membrane (Geistlich Bio-Gide® 25 x 25 mm, Geistlich Pharma AG, Wolhusen, Switzerland) was acquired for later use.

2.1.2. Sample Design

To develop the scaffolds, protocols were established based on a thorough review of existing literature [65-68]. The biomanufacturing system employed in this study was the Biomate Project, developed by CDRSP-IPLeiria [65,68-76]. This system integrates three biomanufacturing techniques: micro-extrusion, multi-head dispensing, and electrospinning [66]. Using this system, three distinct types of

matrices were produced: (i) PCL scaffolds (PCL); (ii) PCL scaffolds incorporating nHA (PCL/nHA); (iii) PCL scaffolds incorporating BL (PCL/BL).

The methodologies for scaffold production were as follows:

i) **PCL scaffolds**: PCL was dissolved in DMF at 80°C and then dried in a controlled environment for 96 hours. The resulting membranes were cut into pieces and prepared for bioextrusion;
ii) **PCL/nHA scaffolds**: PCL (40 wt%) and nHA (60 wt%) were mixed separately in DMF and subsequently dried in a controlled environment. After complete drying, the membranes were cut into pieces for subsequent use in the bioextrusion process;
iii) **PCL/BL scaffolds**: PCL (40 wt%) and BL (60 wt%) were dissolved separately in DMF and dried in a controlled environment. The fully dried membranes were then cut into pieces and prepared for bioextrusion.

Prior to the assay, the scaffolds were sterilized by exposure to ultraviolet radiation, applied in 20-minute cycles on each surface of the biomaterials.

2.2 Scanning electron microscopy (SEM) and energy-dispersive X-ray spectroscopy (EDX)

SEM and EDX analysis were performed on the BL using a high-resolution Schottky field emission environmental scanning electron microscope, specifically the Quanta 400 FEG ESEM, equipped with X-ray microanalysis and electron backscatter diffraction (EBSD) capabilities. The SEM analyses were conducted under high vacuum conditions, utilizing an accelerating voltage of 15 kV to ensure optimal resolution. Prior to imaging, the samples were coated with a gold/palladium alloy for 120 seconds at a current of 15 mA to enhance conductivity and image quality. When necessary, EBSD imaging was utilized to assess the crystallographic orientation of the samples, providing detailed insights into their microstructural properties.

2.3. Conditioned Medium (CM)

2.3.1. Cell culture and maintenance

The hDPSCs were sourced from Lonza (Cat. PT-5025, Lot No. 20TL365542, Basel, Switzerland). The ells were thawed and expanded *in vitro* following standard protocols as previously described [77-89]. The hPDSCs were cultured in αMEM containing GlutaMAX™, without nucleosides (32561029, Gibco®). This medium was supplemented with 10% (v/v) fetal bovine serum (FBS, A31608-02, Gibco®), 100 IU/mL penicillin, 0.1 mg/mL streptomycin (15140122, Gibco®), 2.05 µg/mL amphotericin B (15290026, Gibco®) and 10 mM HEPES buffer solution (15630122, Gibco®). The cells were maintained at 37º C in a humidified atmosphere with 5% CO_2.

2.3.2. Conditioned medium (CM) preparation

The hDPSCs at passage 5 were cultured until they reached 70-80% confluence. Once this level of confluence was achieved, the culture medium was removed, and the cells were washed three times with Dulbecco's Phosphate-Buffered Saline (DPBS). Following this, a basal culture medium free of FBS and other supplements was added, and the cells were incubated for 48 hours to stimulate the secretion of paracrine factors, resulting in the production of CM. After the incubation period, the CM was collected, centrifuged, and filtered using a 0.2 µm syringe filter (Filtropur S, PES, Sarstedt®, Nümbrecht, Germany). The filtered CM was then concentrated fivefold using a Pierce™ Protein Concentrator with a 3k MWCO, 5-20 mL capacity (88525, Thermo Scientific®, Waltham, Massachusetts, United States of America) following the manufacturer's instructions, and sterilized. The concentrated CM was stored at -80º C until further use.

2.4. Cytocompatibility Assessment

The cytocompatibility evaluation was assessed using the Presto Blue™-based viability assay (Invitrogen, A13262, Thermo Fisher Scientific, Waltham, United States of America). In this test, a resazurin-based solution, to which cells are permeable, is used as an indicator of cell viability. The assay is based on the reduction of resazurin by metabolically active cells, thereby providing a quantitative measure of cell proliferation. After addition to the cells, the Presto Blue™ reagent is reduced at the mitochondrial level, leading to a color change from

blue to red and to an increase in fluorescence. This color change can be detected through fluorescence or absorbance measurements, which directly correlate with cell viability. Therefore, changes in cell viability and proliferation were monitored through corresponding alterations in absorbance measurements of the solution.

All the groups were incubated overnight at 37 ºC in a humidified atmosphere (80%) with 5% CO_2. For the control group, an adherent 24-well plate was used without materials. For the Presto Blue™ assay, at each time point (24, 72, 120 and 168 hours), the culture medium was replaced with fresh complete medium containing 10% (v/v) Presto Blue™ cell viability reagent. Cells were incubated for 60 minutes at 37 ˚C in a 5% CO_2 and 80% humidified atmosphere. Subsequently, the supernatant was moved to a 96-well plate, and absorbance was read at 570 and 595 nm. Wells were washed with DPBS to remove Presto Blue™ residues, and fresh culture medium was added.

In this experiment, four experimental groups were tested: PCL scaffold, PCL/nHA scaffold, and PCL/BL scaffold, along with a control group consisting of blank wells used as a reference. The Presto Blue™ assay was employed, with an excitation wavelength of 570 nm and an emission wavelength of 595 nm. For each well, the absorbance value at 595 nm was subtracted from the value at 570 nm to obtain a normalized absorbance. The corrected absorbance for each experimental well, which accounted only for the seeded materials, was determined by subtracting the average absorbance of the blank wells from the normalized absorbance values of the respective sample groups. Absorbance measurements were conducted in triplicate using a Multiskan™ FC Microplate Photometer (Thermo Scientific™, 51119000, Thermo Fisher Scientific, United States of America). The data were then processed and normalized with the blank of each group.

2.5. Osteogenic Differentiation Assay

The osteogenic differentiation test was conducted across four groups: control, PCL scaffold, PCL/nHA scaffold, and PCL/BL scaffold. All groups were seeded with hDPSCs on the top of the support. The experimental procedure followed methodologies established in prior studies [62,90]. Briefly: after an incubation period, the scaffolds were transferred to the osteogenic differentiation medium, StemPro™ Osteogenesis Differentiation Kit (Gibco A1007201, Thermo Fisher Scientific, Waltham, MA, United States of America). Control samples

(undifferentiated) were maintained in culture medium lacking osteogenic differentiation medium. Media were replaced every three days.

After 21 days, osteogenic differentiation was evaluated semi-quantitatively using the Alizarin Red S (ARS) assay (TMS-008-C, Merck KGaA, Darmstadt, Germany). Scaffolds were fixed in 4% formaldehyde (Merck KGaA, Darmstadt, Germany, 100496), stained with a 40 mM ARS solution, and incubated with agitation for 30 minutes. Following staining, the supernatant was discarded, and the scaffolds were rinsed with deionized water (diH_2O).

To quantify the mineralization, a 10% acetic acid solution (ARK2183, Sigma-Aldrich, St. Louis, Missouri, United States of America) was added to each well to dissolve the mineral deposits and cellular material. Samples were then subjected to a 10-minute incubation in an 85 ˚C water bath, followed by 5 minutes on ice, and were subsequently centrifuged. The absorbance of the solution at 405 nm was measured in triplicate using a Thermo Scientific™ Multiskan™ FC Microplate Photometer.

2.6. In vivo bone regeneration assessment

2.6.1. Animals and Ethical Issues

A comprehensive dossier detailing all planned activities for the ovine model was submitted to the Animal Welfare Body (ORBEA) of the School of Medicine and Biomedical Sciences - University of Porto (ICBAS-UP). This submission included a thorough description of the procedures, justifications for their necessity, and measures to minimize animal use, discomfort, and suffering. Approval for the project (project no. 192/2017/ORBEA) enabled the execution of the planned *in vivo* studies.

All procedures were conducted in accordance with European Union (EU) Directive 2010/63/EU, which has been transposed into Portuguese law as DL 113/2013 and DL 1/2019. The ICBAS-UP Animal Welfare Organization, the Ethics Committee and the Portuguese Veterinary Authorities approved all animal procedures. In compliance with The Organization for Economic Cooperation and Development (OECD) guidelines on humane endpoints [Guidance Document on the Recognition, Assessment and Use of Clinical Signs as Humane Endpoints for

Experimental Animals Used in Safety Evaluation (2000)], protocols were followed to minimize animal suffering and distress.

The study employed ten non-pregnant adult female Merino sheep (*Ovis aries*), each weighing between 30-40 kg and aged 7 to 8 years (**Figure 1**). These animals were sourced from a certified breeder, approved by the host institution, and were confirmed to be free from brucellosis (B3 or B4 status). Prior to movement, the animals underwent testing for infectious diseases and were vaccinated against bluetongue. Upon arrival, they were quarantined and acclimatized for two weeks, during which they received a prophylactic protocol including hoof trimming, shearing, internal deworming, and vaccination against enterotoxemia.



Figure 1. Merino sheep (*Ovis aries*).

Before surgery and throughout the study, the animals underwent general physical examinations. They were housed in communal groups to facilitate natural social behavior, provided with hay and concentrate to meet their nutritional requirements, and had continuous access to fresh water. The animals underwent a 12-hour fasting period prior to the surgical interventions.

2.6.2. Surgical Procedure

1) Pre-surgical procedure:

Premedication included the intramuscular administration of xylazine (Rompun® 20 mg/mL, Bayer, 0.1 mg/kg) and butorphanol (Dolorex® 10 mg/mL, MSD, 0.05 mg/kg) to facilitate sedation and prepare for the trichotomy of both hind

limbs. The surgical field was prepared using 10% iodopovidone (Betadine®) and 70% ethanol for antisepsis.

During the procedure, intravenous fluids (0.9% NaCl, B Braun®) were administered at a maintenance rate. General anesthesia was induced with intravenous tiletamine-zolazepam (Zoletil®, 100 mg/mL, Virbac, 3 mg/kg). Anesthesia was continuously monitored by assessing cardiorespiratory parameters, and additional boluses of tiletamine-zolazepam were administered as necessary.

Loco-regional anesthesia was administered using lidocaine hydrochloride (Anestesin® 2%, 20 mg/mL, Medinfar-Sorológico) via an epidural spinal catheter placed between the L6 and S1 vertebrae.

2) Surgical technique:

The surgical technique was conducted following the protocol described by Lansdowne *et al.* [61]. The animal was positioned in sternal recumbency with the hind limbs extended cranially. A curved ventro-dorsal incision was made in the skin at the cranial region of the iliac crest. Subcutaneous tissue was dissected until periosteum was exposed.

A precise incision was made in the *gluteus medius* muscle, approximately 1 cm proximal to its insertion at the iliac crest, exposing the gluteal surface of the *iliac ala*. On the medial side, a fascial incision was made 5 mm distal and parallel to the iliac crest insertion. The *iliocostalis* and *longissimus lumborum* muscles were then retracted to provide access and explosion of the sacropelvic surface of the *iliac ala*.

The procedure was performed bilaterally. Circular bone defects, each with a diameter of 17 mm, were created in the mid-portion of the *ileum*, using a custom-made trephine drill. Continuous cooling of the surgical area was maintained with a saline solution (NaCl 0.9%, B Braun®) to prevent thermal damage to the bone edges.

3) Biomaterial and conditioned medium (CM) application:

This study included four experimental groups: a control group with untreated defects, a PCL scaffold *plus* hDPSCs-CM group, a PCL/nHA scaffold *plus* hDPSCs-CM group, and a PCL/BL *plus* hDPSCs-CM group. Regarding the defects

treated with CM, 0.5 mL of CM, obtained through *in vitro* culture as previously described, were uniformly applied to each defect. Following the assignment of each defect to a specific study group and the application of the designated therapeutic approach, one group per time point received an additional treatment with a resorbable bilayer collagen membrane (Geistlich Bio-Gide®, 25 x 25 mm). After treatment, the surrounding soft tissue was sutured, and the surgical site was closed uniformly across all groups.

To summarize, a total of 10 animals were included in this study, yielding 20 defects (n=20). The distribution of defects was as follows: n=2 for the control group, n=6 for the PCL *plus* hDPSCs-CM group, n=6 for the PCL/nHA *plus* hDPSCs-CM group, and n=6 for the PCL/BL *plus* hDPSCs-CM group (**Figure 2**).

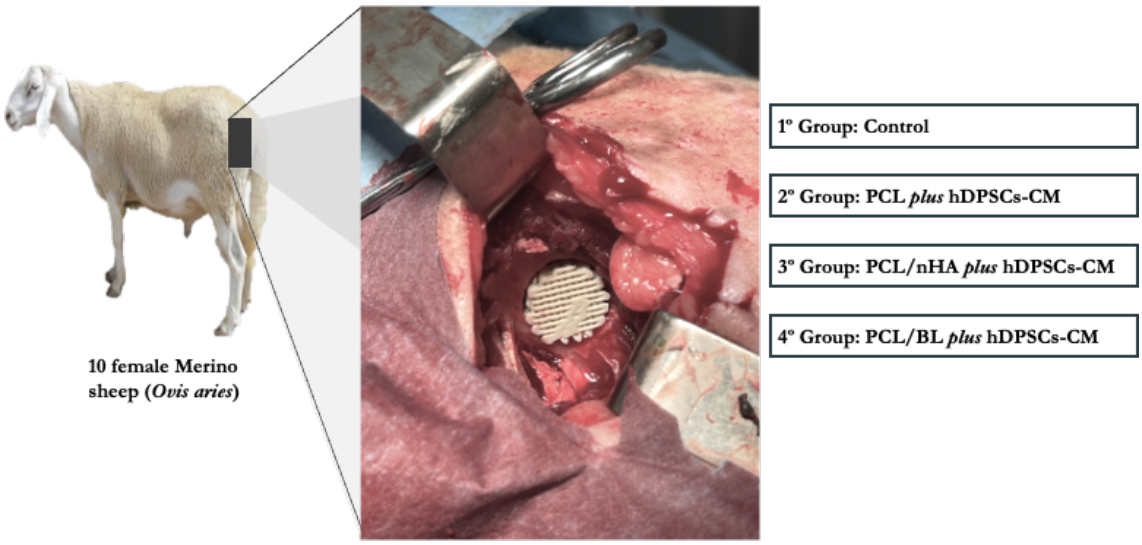


Figure 2. Experimental design of 10 Merino sheep, with bone defects divided into four groups (control, PCL *plus* hDPSCs-CM, PCL/nHA *plus* hDPSCs-CM, and PCL/BL *plus* hDPSCs-CM). The image of the surgical field represents the scaffolds PCL/BL *plus* hDPSCs-CM after application in the critical defect created in the *iliac ala*.

4) Post-surgical procedures:

Post-operative radiographs were taken to evaluate the defect sites, with the animals positioned in sternal recumbency for a craniomedial to caudolateral oblique view. This imaging approach was utilized to assess the stability and retention of biomaterials at the application sites and to confirm the location of the

defects. Following complete recovery from anesthesia, the animals were housed in groups of 4/5 in a straw yard. Prophylactic treatment included antibiotic therapy with ampicillin (Albipen LA®, 100 mg/mL, MSD, 20 mg/kg) administered every 48 hours for 6 days, along with a non-steroidal anti-inflammatory drug, meloxicam (Meloxidyl®, 20 mg/mL, Ceva, 0.5 mg/kg), also given every 48 hours for 6 days.

To evaluate the *in loco* bone regeneration phenomena, animals were sacrificed at different timepoints as described below. This procedure was carried out in a controlled, quiet and isolated environment to ensure minimal stress and discomfort to the animals. Euthanasia was performed humanely through the administration of an overdose of intravenous sodium pentobarbital (Euthasol®, 400 mg/mL, Ecuphar, 140 mg/kg).

The animals were euthanized after recovery periods of 90- and 150-days post-surgery to analyze bone healing. The 90-day period was selected to observe the initial phase of bone healing, while the 150-day period allowed for the examination of more advanced stages of bone healing, as well as for the absorption and degradation of the biomaterial.

Post-mortem, the *ilea* were dissected, and all soft tissues were removed from the bone. A cranial to caudal tabletop X-ray imaging with a caudal-to-cranial tabletop incidence at 55 kV and 0.8 mAs was performed on all samples to ensure accurate visualization of the defect and surrounding structures and to qualitative evaluation of bone regeneration. Isolated sample sections were individually preserved and maintained in 4% paraformaldehyde (252931.13.15, AppliChem, Panreac®).

2.7. Statistical Analysis

Statistical analyses were conducted using GraphPad Prism (version 9.00 for Mac OS X, GraphPad Software, La Jolla, California, United States of America). Data are presented as the mean ± standard error of the mean (mean ± SEM). Group comparisons were performed using a two-tailed unpaired t-test, with a 95% confidence interval (CI 95%). Differences were considered statistically significant at $p \leq 0.05$. Statistical significance between groups is denoted by the symbol (*), with varying levels of significance indicated by one, two, three or four (*),

corresponding, respectively, to the p-value ranges: $0.01 < p \leq 0.05$ (*), $0.001 < p \leq 0.01$ (**), $0.0001 < p \leq 0.001$ (***), and $p \leq 0.0001$ (****).

3. Results

3.1. Scanning electron microscopy (SEM) and energy-dispersive X-ray spectroscopy (EDX)

SEM was utilized to analyze the prepared BL granules, providing detailed insights into their morphology and topography (**Figure 3**). In **Figure 3-A**, the spherical structure of BL is clearly observed. At higher magnification, variations in surface roughness are evident (**Figure 3-B**), along with the presence of microporosity, which is homogeneously distributed across the entire sphere (**Figure 3-C**). The SEM analysis showed micropores between values close to 1.0 μm and 1.5 μm (**Figure 3-C**), approximately.

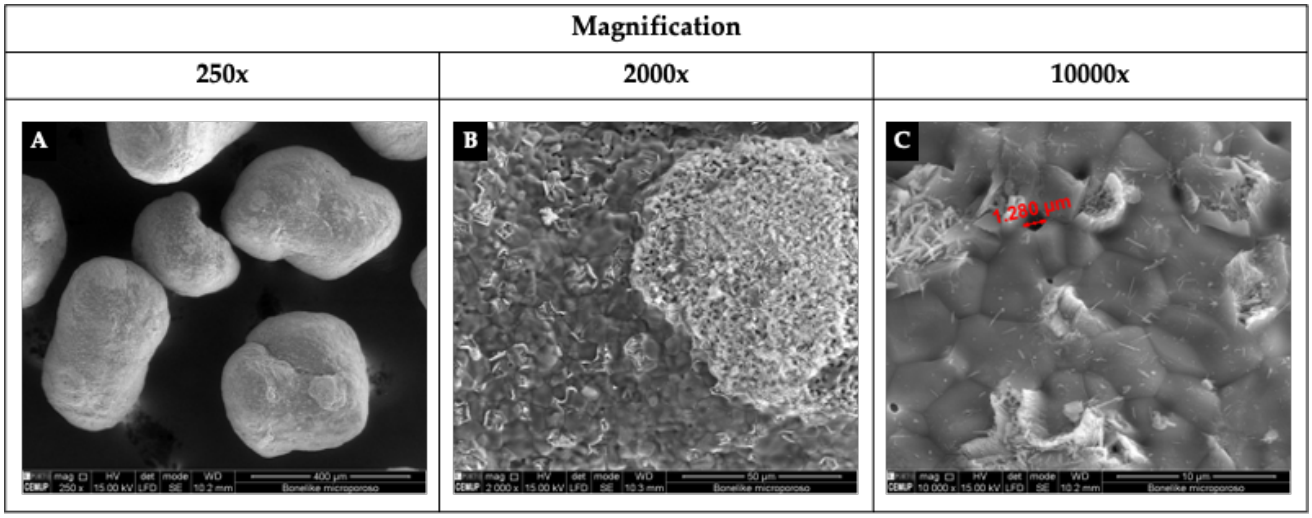


Figure 3. SEM images of Bonelike® granules (total magnification: (A) 250x, (B) 2000x and (C) 10000x). Figure C illustrates the measurement of microporosity, highlighted in red.

The qualitative chemical composition of the elements present in the BL material is presented in **Figure 4**. EDX analysis of BL reveals well-defined peaks corresponding to oxygen (O), phosphorus (P), and calcium (Ca). Additionally, smaller peaks of carbon (C), gold (Au), and palladium (Pd) are also detected. The presence of O, P, and Ca is consistent with the expected composition of BL, as it is

a modified calcium phosphate material. The detection of C, Au, and Pd is attributed to the coating applied to make the sample conductive for analysis.

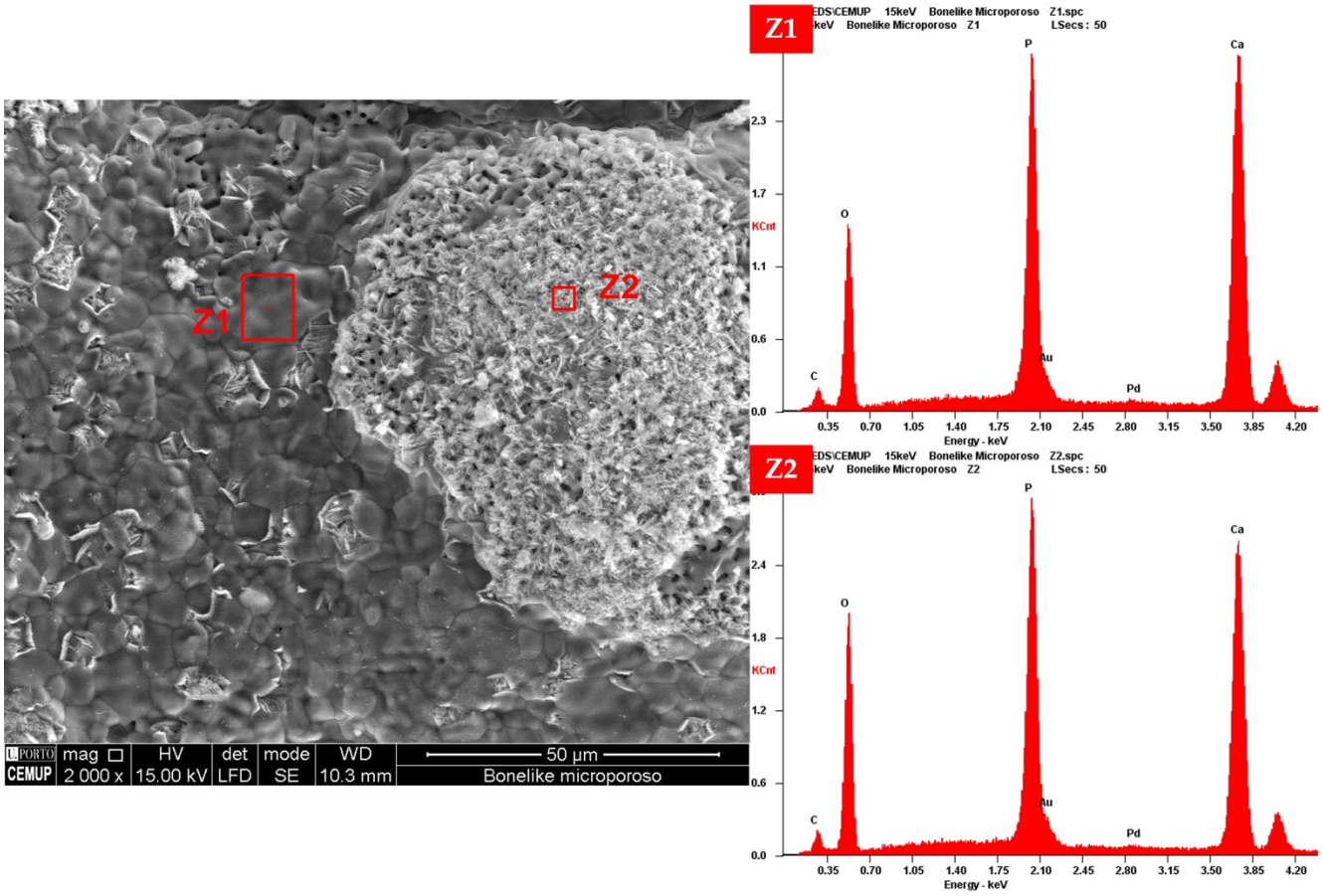


Figure 4. SEM image (2000x magnification) and corresponding EDX analysis of the Bonelike®(BL).

3.2. Cytocompatibility Assessment

In accordance with the ISO 10993-5:2009 standards, the cell viability was evaluated using PrestoBlue™ reagent across the different experimental groups: PCL, PCL/nHA, and PCL/BL. An additional group of cells seeded with no biomaterials was considered as a control of the cells, to assess their normal behavior and proliferation in the standard culture medium. **Figure 5** illustrates the corrected absorbance values and the corresponding statistical comparisons at each time point: 24, 72, 120 and 168 hours.

The viability assessment (**Figure 5** and **Table 1**) confirmed the assay's reliability, as the cell population exhibited normal growth and proliferation comparable to the control group. Results were interpreted following ISO 10993-

5:2009 "Biological evaluation of medical devices" - Part 5 - "Test for *in vitro* cytotoxicity" guidelines. The absorbance values increased steadily over time for all groups, revealing an increase in cell proliferation with maintenance of cell viability. The experimental results suggest that PCL/nHA and PCL/BL groups consistently demonstrated higher cell viability compared to the PCL group most of the time points measured. However, it is important to note that these observed differences did not reach statistical significance. In contrast, the control group exhibited statistically significant differences in cell viability when compared to the PCL group, which is regarded as the gold standard in this study.

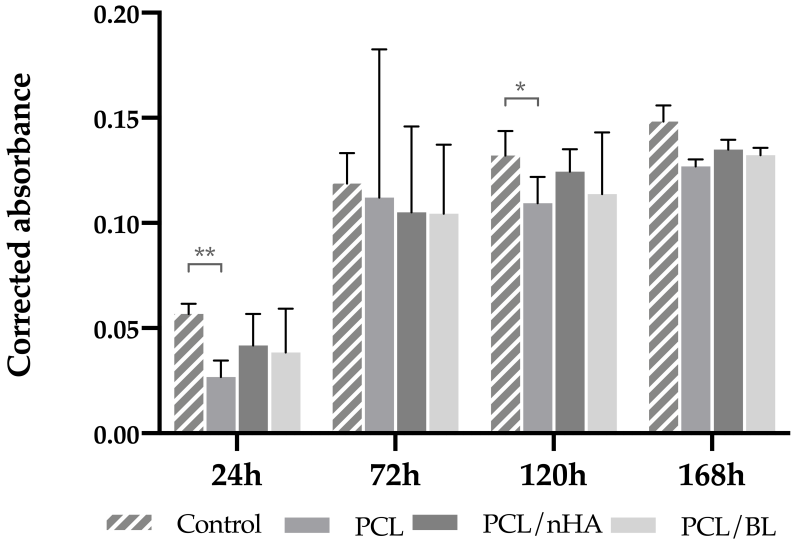


Figure 5. Cytocompatibility tested by PrestoBlue™-based viability assay for hDPSCs. Results presented in Mean ± SEM (standard error of the mean).

Table 1. Corrected absorbance evaluated by PrestoBlue®-based viability assay for hDPSCs after 24, 72, 120 and 168 hours. Results presented in Mean ± SE.

	Control	PCL	PCL/nHA	PCL/BL
24 h	0.057 ± 0.005	0.027 ± 0.008	0.042 ± 0.015	0.038 ± 0.021
72 h	0.119 ± 0.014	0.112 ± 0.070	0.105 ± 0.041	0.104 ± 0.033
120 h	0.132 ± 0.012	0.109 ± 0.012	0.124 ± 0.011	0.114 ± 0.029
168 h	0.148 ± 0.008	0.127 ± 0.003	0.135 ± 0.005	0.132 ± 0.004

The results for the percentage inhibition of cell viability, normalized to the control group, are presented in **Figure 6** and **Table 2**. According to Annex 3 of the

ISO 10993-5:2009 guideline, a viability inhibition exceeding 30% is considered indicative of cytotoxic effects, as denoted by the dashed lines in **Figure 6**. The data suggest that the studied biomaterials generally exhibit cytocompatibility with hDPSCs. However, it is noteworthy that, during the initial 24 hours, some groups exhibit viability inhibition percentages that exceed or approach the 30% threshold, which classifies them as cytotoxic. This early cytotoxicity appears to be transient and probably related to a period of cellular adaptation to the presence of the biomaterial, as subsequent measurements indicate a reduction in cytotoxic effects and an enhancement in cell proliferation. For instance, both the PCL and PCL/BL groups displayed borderline or slightly cytotoxic values at 24 hours, but, in subsequent time points, showed a significant reduction in cytotoxicity, and promoted cell proliferation.

Despite these early instances of cytotoxicity, the overall levels of viability inhibition remained relatively low. Even in cases where cytotoxic effects were observed, the values were close to the threshold rather than markedly high. Most of the tested groups did not exhibit significant cytotoxicity and, in many cases, were associated with enhanced cell adhesion and proliferation, which reinforces their potential biocompatibility and suitability for further application.

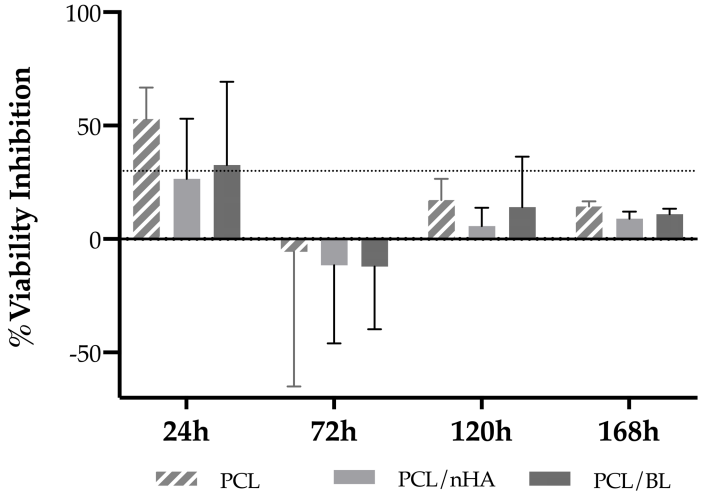


Figure 6. % of viability inhibition assessed by PrestoBlue® viability assay after 24, 72, 120 and 168 h. The results were normalized to the control group as 0%. The 30 % threshold presented in the graph (dashed line) indicates the inhibition above which the effect is considered cytotoxic (in conformity with ISO 10993-5:2009 guidelines).

Table 2. % Viability inhibition evaluated by PrestoBlue®-based viability assay for hDPSCs after 24, 72, 120 and 168 hours. Results presented in Mean ± SE.

	PCL	PCL/nHA	PCL/BL
24 h	52.96 ± 13.80	26.59 ± 26.45	32.67 ± 36.72
72 h	-5.564 ± 59.38	-11.53 ± 34.40	-12.16 ± 27.60
120 h	17.15 ± 9.409	5.755 ± 8.062	14.06 ± 22.21
168 h	14.37 ± 2.247	8.972 ± 3.166	10.90 ± 2.414

3.3. Osteogenic Differentiation Assay

The osteogenic potential of the samples was assessed using ARS protocol, following a 21 days incubation period. The analysis was performed through the detection of mineral deposition, as outlined in previous studies [93,94]. ARS was extracted and subsequently quantified at 405 nm. The results are shown in **Figure 7** and **Table 3**. These results demonstrated that the PCL, PCL/nHA, and PCL/BL groups exhibited significantly enhanced osteogenic differentiation when compared to the control group. Moreover, the data suggest that the incorporation of HA in the PCL/nHA and in the PCL/BL groups may further promote osteogenic differentiation of hDPSCs compared to the PCL group. However, while the trend toward increased differentiation in the HA-containing groups was observed, this enhancement did not reach statistical significance.

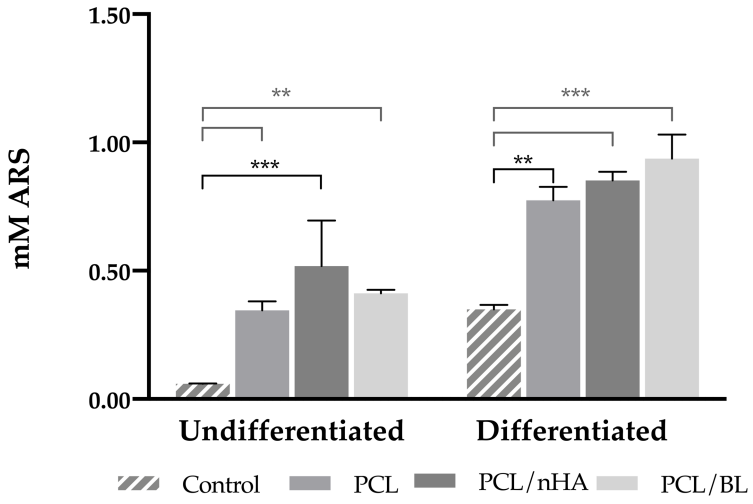


Figure 7. ARS Semi-Quantification in mM between groups. Results presented in mean ± SEM. Differences were considered statistically significant at $p \leq 0.05$.

Results significances are presented through the symbol (*), according to the p value, with two or three (*) corresponding to $0.001 < p \leq 0.01$ and $0.0001 < p \leq 0.001$, respectively.

Table 3. ARS Semi-Quantification in mM between groups. Results presented in mean ± SEM.

	Control	PCL	PCL/HA	PCL/BL
Undifferentiated	0.059 ± 0.002	0.346 ± 0.035	0.518 ± 0.179	0.412 ± 0.013
Differentiated	0.349 ± 0.018	0.774 ± 0.052	0.852 ± 0.035	0.937 ± 0.094

3.4. In vivo bone regeneration assessment

All animals successfully recovered from anesthesia without significant complications and remained under observation for the entire duration of the study. At the designated time points, the animals were sacrificed, and their *ilia* were harvested for subsequent analysis.

3.4.1 Macroscopic Analysis

After the soft tissue was removed, the defect areas were examined. The treated defects exhibited substantial filling with tissue of a hard consistency, indicative of satisfactory macroscopic bone healing. In contrast, the control defects displayed a soft consistency, attributed to incomplete ossification and to the presence of fibrous tissue within the defect site.

3.4.2 Radiographic Analysis

Qualitative analysis of the *ex vivo post-mortem* radiographic images confirmed the presence of the intended bone defects across all experimental groups, as illustrated in **Figure 8**. The radiographic assessment also revealed the presence of neoformed bone within the defects across all samples. Notably, there was a significant increase in new bone formation between the 90-day and the 150-day time points, indicating progressive bone healing over time.

In the PCL *plus* hDPSCs-CM group, the bone defects appeared more radiolucent, which is consistent with the material's low density and its limited ability to obstruct X-ray radiation, resulting in defects that appear as dark areas on

the radiographs. In contrast, defects treated with PCL/nHA exhibited increased radiopacity, suggesting a higher density and more effective blockage of X-rays due to the incorporation of HA. The PCL/BL *plus* hDPSCs-CM group demonstrated an even more pronounced radiopaque signal at the lesion site, reflecting the higher density of the BL component compared to the other groups.

Control defects, which were untreated, showed minimal bone deposition primarily at the periphery and incomplete bone healing, thereby validating the critical nature of the bone defect model. These control defects were characterized by a thin grey line at the edges and a radiolucent center, indicative of the presence of fibrous tissue rather than new bone formation.

Defects treated with PCL *plus* hDPSCs-CM, PCL/nHA *plus* hDPSCs-CM, and PCL/BL *plus* hDPSCs-CM showed reduced radiolucency line compared to the control group, indicating improved mineralization in these groups. Remarkably, the PCL/BL *plus* hDPSCs-CM - treated group continued to exhibit a pronounced radiopaque signal at the lesion site, even after 150 days, suggesting ongoing mineralization and effective integration of the material. The continuity between the PCL/BL scaffolds and the newly formed bone was more apparent, with a less distinct defect line compared to the PCL *plus* hDPSCs-CM and PCL/nHA *plus* hDPSCs-CM groups, indicating superior integration of the BL scaffolds into the newly-formed bone matrix.

Conversely, the PCL *plus* hDPSCs-CM and PCL/nHA *plus* hDPSCs-CM groups displayed more radiolucent line defect, suggesting less effective bone matrix formation. Overall, the radiographic results suggest that BL treatment leads to superior integration and mineralization within the defect compared to both the control and other treatment groups. This enhanced bone healing process in the PCL/BL *plus* hDPSCs-CM group may be attributed to the higher density and osteoconductive properties of the BL component, which supports more effective bone regeneration.

Furthermore, in the analysis of the *ex vivo post-mortem* X-rays, no macroscopic differences were observed between the groups with and without membranes (**Figure 9**). Despite this initial observation, it is essential to conduct further assessments, such as histomorphometry and histological analyses, to provide more detailed and conclusive evidence regarding the potential differences

in tissue response and integration between the membrane-treated and non-treated groups.

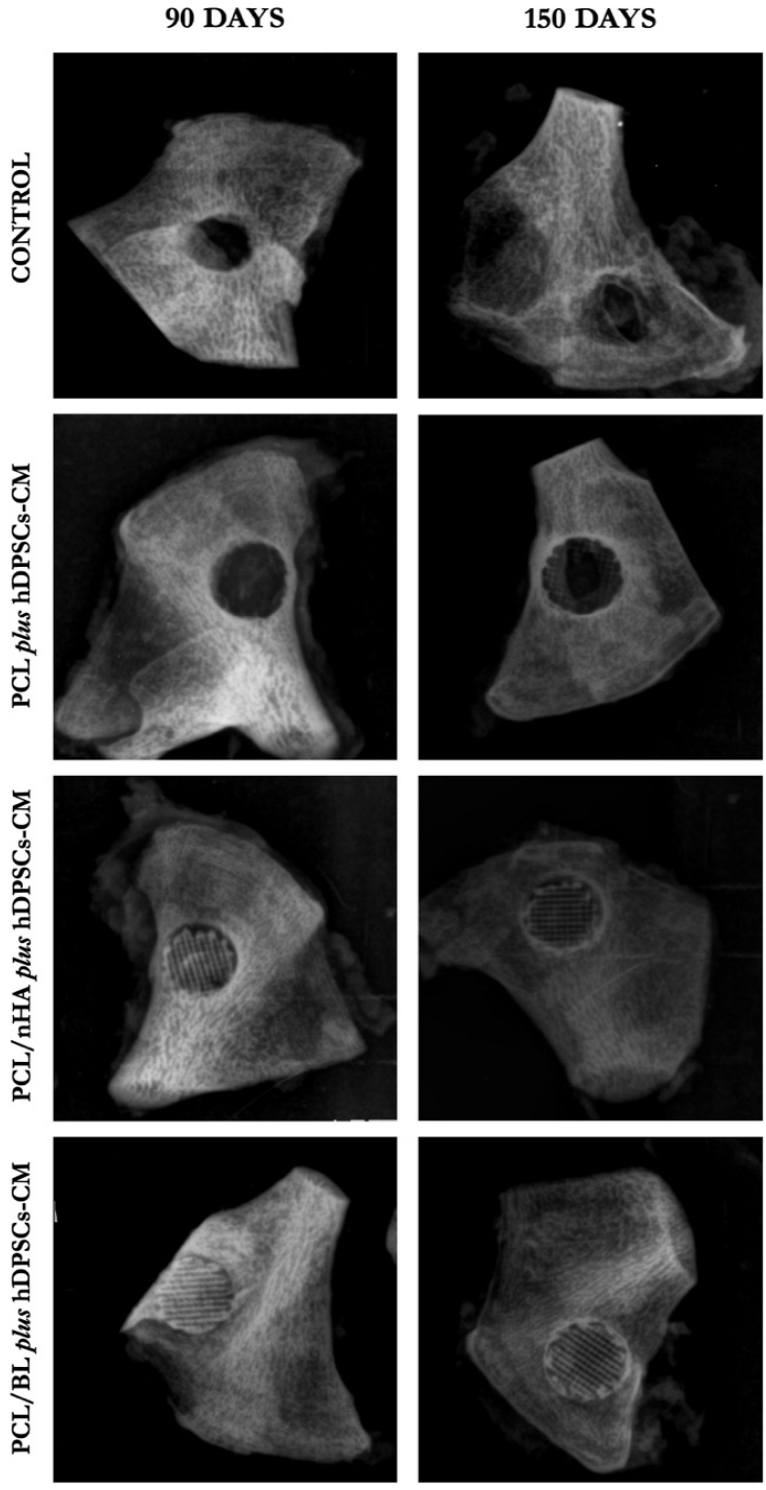


Figure 8. *Post-mortem ex vivo* representative X-Ray images for control, PCL *plus* hDPSCs-CM, PCL/nHA *plus* hDPSCs-CM, and PCL/BL *plus* hDPSCs-CM groups after 90 and 150 days.

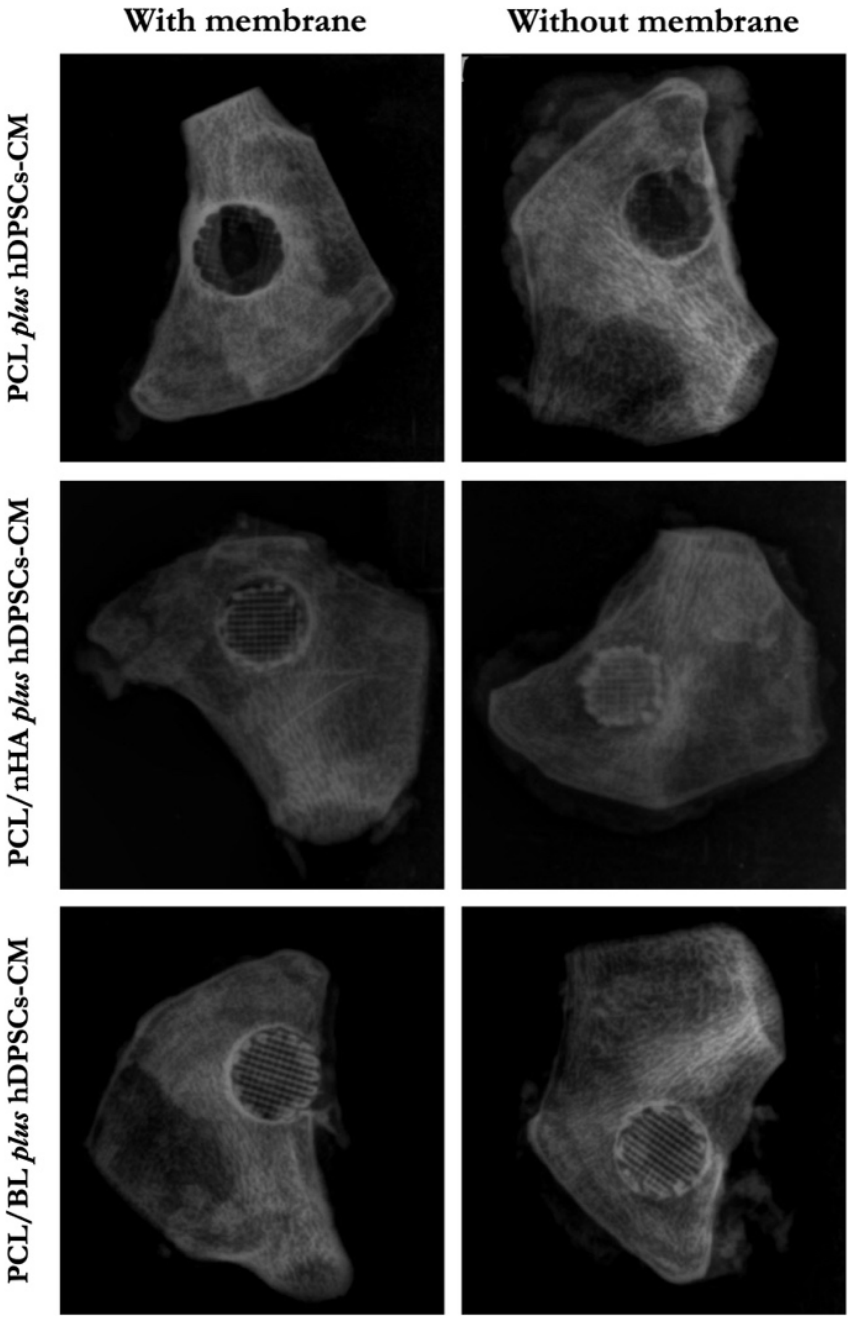


Figure 9. Representative *ex vivo post-mortem* X-ray images with and without membrane for the PCL *plus* hDPSCs-CM, PCL/nHA *plus* hDPSCs-CM, and PCL/BL *plus* hDPSCs-CM groups after 150 days.

4. Discussion

The treatment of non-unions and critical-sized bone defects remains a significant challenge for orthopedic surgeons. Current surgical approaches lack consensus and often result in suboptimal outcomes [95-97]. This study suggests the use of an innovative PCL/BL scaffold, combined with the CM from hDPSCs, as a

bioactive matrix to promote bone regeneration. This approach offers a potential alternative to the commonly employed autologous grafting technique.

In the current study, the work developed by Atayde *et al.* [29] and Campos *et al.* [62] was complemented. That study demonstrated the osteointegration, osteoconduction and degradation dynamics of the synthetic bone substitute BL, by adding a material with mechanical strength, PCL, to improve the regenerative system, potentially leading to more durable and effective outcomes in bone repair, particularly in the context of critical-sized defects where both biological and mechanical factors play essential roles in successful healing. PCL was selected for this study due to its ease of processing via 3D printing, its biocompatibility, its tunable composition and structure and its favorable mechanical properties [98,99]. By integrating PCL into the BL matrix, the study seeks to address the limitations of previous materials and to offer a novel solution for bone regeneration, not only promoting the initial osteoconductive and osteointegrative properties but also ensuring that the repaired tissue can withstand physiological loads over time. This approach could represent a significant advancement in the development of composite biomaterials for orthopedic applications, especially in complex cases requiring long-term durability and stabilization.

The biomaterial BL was thoroughly analyzed using SEM and EDX spectroscopy, to validate its structural and chemical properties. The results obtained are consistent with previous findings reported in the literature [29,62,100]. SEM imaging revealed that BL presents a characteristic spherical morphology, with visible microporosities, which aligns with the expectations for this material. Furthermore, EDX analysis confirmed the presence of O, P, and Ca as the primary elements, which are indicative of BL's composition as a modified calcium phosphate.

In the cytocompatibility assessments, hDPSCs were selected due to their well-documented regenerative potential, particularly their propensity for differentiation along the osteogenic lineage, which is essential for bone tissue regeneration [62,101-103]. The experimental outcomes demonstrated a normal rate of cell proliferation and growth, indicating that the biological potential of the scaffolds under investigation was effectively evaluated. After a 72-hour period, the PCL/BL devices demonstrated non-cytotoxic effects on cell viability and

proliferation, in accordance with the ISO 10993-5:2009 standard. The results indicated that the scaffolds composed of both PCL and BL showed cell viability outcomes that were comparable to those observed in the control group, with no statistically significant differences detected. This finding suggests that the PCL/BL scaffold supports cellular proliferation and viability, reinforcing its potential as a biocompatible material for applications in bone tissue engineering.

Osteogenic differentiation was evaluated through Alizarin Red S staining, which revealed that the PCL/nHA and the PCL/BL scaffolds showed significantly higher mineral deposition compared to the control group. This enhanced mineralization was also observed in the undifferentiated cell groups, suggesting that the HA component within these scaffolds increased the inherent osteoinductive properties, facilitating the differentiation of progenitor cells into the osteogenic lineage. These findings align with previous research, where BL demonstrated both osteoconductive and osteoinductive properties *in vitro* [104].

There is growing interest and research focus on CM in Regenerative Medicine [105]. To enhance bone regeneration, the current study proposes combining scaffolds with CM derived from hDPSCs, and this combination promotes osteogenic differentiation, due to its content of growth factors and extracellular vesicles [48,105-107]. This CM presents several advantages over direct stem cell applications: it is readily manufacturable, and easily sterilized, packaged, stored and transported, allowing an off-the-shelf approach [10]. Additionally, by being cell-free, it circumvents the need for donor-recipient compatibility assessments, thereby reducing the risk of immune rejection [106]. This approach provides a viable alternative to stem cell transplantation, which is often limited by issues such as suboptimal efficacy and potential carcinogenicity post-grafting.

Additionally, the collagen membrane Geistlich Bio-Gide® was evaluated to prevent soft tissue invasion into the bone defect and to ensure the localized retention of CM from hDPSCs at the lesion/delivery site. This membrane works as a barrier membrane, designed to restrict the growth of non-bone tissue into the defect while providing a stable environment for the CM. According to Schwarz *et al*. and Rothamel *et al*., this membrane facilitates effective bone regeneration and promotes optimal integration with the surrounding tissue, thereby enhancing the overall efficacy of the regenerative process [56,57,108].

To assess the regenerative potential of the PCL/BL scaffolds in combination with hDPSCs-CM and the collagen membrane, a standardized critical pre-clinical bone defect model was used. Selecting an appropriate animal model is essential for assessing the osteoconductive, osteointegrative, and mechanical properties of bone substitute biomaterials, as well as their biocompatibility, degradation, resorption, and interactions with host tissues [91,109-111]. The ovine model was selected due to its phylogenetic proximity to humans, which includes characteristics such as similarity in musculoskeletal size and biomechanics. Additionally, ovine bone tissue exhibits histological similarities to human bone, including the presence and organization of Haversian systems and the mechanisms of cortical bone remodeling [4]. In line with previous research [100], defects were created in a non-weight-bearing bone, ileum, reducing the risk of post-surgical fractures and allowing for the establishment of two defects per animal, reducing the total number of animals needed for the study. This model demonstrated high reproducibility, enabling the generation of defects with consistent size and biological behavior, thereby minimizing inter-individual variability [100].

Bone regeneration and remodeling in both untreated and treated defects were assessed after 90 and 150 days. Macroscopic observations suggested that PCL *plus* hDPSCs-CM, PCL/nHA *plus* hDPSCs-CM, and PCL/BL *plus* hDPSCs-CM treated groups exhibited high-quality defect filling tissue. These observations are anticipated to be corroborated by subsequent microstructural analyses. Efficient bone bridging was observed in the treated groups, whereas untreated defects failed to achieve healing and were characterized by non-union, with connective tissue formation. This outcome confirms the critical nature of the selected defect model.

Radiographic imaging of the control defects revealed soft tissue within the lesion, appearing grey to black at the center (radiolucent), with minimal new bone proliferation at the defect edges, and indicated the presence of fibrous tissue due to insufficient bone healing. In contrast, the treated groups displayed filling tissue that was denser and more radiopaque, closely resembling native bone. Specifically, defects filled with BL granules were visible as small radiopaque structures with increased density, attributed to the chemical composition of the biomaterial (calcium phosphate content). The continuity between the PCL/BL scaffolds and the newly formed bone was more pronounced, exhibiting a less defined defect boundary compared to the PCL *plus* hDPSCs-CM and the PCL/nHA *plus* hDPSCs-CM

groups. This observation suggests that the BL scaffolds demonstrated superior integration into the newly formed bone matrix, facilitating more effective bone bridging and integration. These findings support the potential of BL as an effective bone substitute in treating critical-sized defects, offering improved integration and bone regeneration compared to traditional methods. Furthermore, no significant macroscopic differences were observed between the experimental groups with membrane application and those without. This lack of observable variation suggests that the presence or absence of the collagen membrane did not significantly influence the overall appearance or outcomes of the bone defects at the macroscopic level.

Despite these promising results, further research is needed to validate and extend these findings. Current efforts include the systematic processing of samples for advanced histological and histomorphometric analyses. These analyses will provide detailed insights into the microstructural characteristics of the newly formed bone and the integration of the scaffolds. Histological examination will assess the cellular and tissue organization, while histomorphometric analysis will quantify unmineralized *voids*, neoformed bone, unfilled area (connective tissue), biomaterial, and bone bridge thickness. These comprehensive evaluations are essential to fully understand the efficacy and mechanisms of the scaffold materials in bone regeneration, and to confirm the observed benefits before translating these findings into clinical practice.

5. Conclusions

This study investigates the development and performance of a scaffold composed of PCL and BL for bone regeneration applications, evaluating its efficacy both *in vitro* and *in vivo*.

The *in vitro* analysis confirmed that the PCL/BL scaffold supports cellular proliferation and viability, underscoring its potential as a biocompatible material for bone tissue engineering. Additionally, the scaffold demonstrated both osteoconductive and osteoinductive properties *in vitro*.

The *in vivo* performance was assessed using an ovine model of critical bone defects, with evaluations conducted at 90- and 150-days post-implantation. The results indicated that the PCL/BL scaffold, when combined with hDPSCs-CM,

constitutes a highly promising therapeutic system for bone regeneration. Post-mortem radiographic analysis revealed that defects treated with PCL/BL *plus* hDPSCs-CM showed significantly enhanced new bone formation compared to controls.

To further validate these findings and support clinical translation, additional studies are necessary. These should include comprehensive histological and histomorphometric analyses to assess the detailed interactions between the scaffold *plus* hDPSCs-CM and the regenerating bone tissue.

References

1. Pinto, P.O.; Atayde, L.; Campos, J.M.; Caseiro, A.; Pereira, T.; Mendonça, C.; Santos, J.D.; Maurxhtício, A.C. Therapeutic Strategies for Bone Regeneration: The Importance of Biomaterials Testing in Adequate Animal Models. 2016; pp. 275-319.
2. Pearce, A.I.; Richards, R.G.; Milz, S.; Schneider, E.; Pearce, S.G. Animal models for implant biomaterial research in bone: a review. *Eur Cell Mater* **2007**, *13*, 1-10, doi:10.22203/ecm.v013a01.
3. Calasans-Maia, M.D.; Monteiro, M.L.; Ascoli, F.O.; Granjeiro, J.M. The rabbit as an animal model for experimental surgery. *Acta Cir Bras* **2009**, *24*, 325-328, doi:10.1590/s0102-86502009000400014.
4. Martini, L.; Fini, M.; Giavaresi, G.; Giardino, R. Sheep model in orthopedic research: a literature review. *Comp Med* **2001**, *51*, 292-299.
5. Sartoretto, S.C.; Uzeda, M.J.; Miguel, F.B.; Nascimento, J.R.; Ascoli, F.; Calasans-Maia, M.D. SHEEP AS AN EXPERIMENTAL MODEL FOR BIOMATERIAL IMPLANT EVALUATION. *Acta Ortop Bras* **2016**, *24*, 262-266, doi:10.1590/1413-785220162405161949.
6. Huang, W.; Percie du Sert, N.; Vollert, J.; Rice, A.S.C. General Principles of Preclinical Study Design. *Handb Exp Pharmacol* **2020**, *257*, 55-69, doi:10.1007/164_2019_277.
7. Cipitria, A.; Reichert, J.C.; Epari, D.R.; Saifzadeh, S.; Berner, A.; Schell, H.; Mehta, M.; Schuetz, M.A.; Duda, G.N.; Hutmacher, D.W. Polycaprolactone scaffold and reduced rhBMP-7 dose for the regeneration of critical-sized defects in sheep tibiae. *Biomaterials* **2013**, *34*, 9960-9968, doi:10.1016/j.biomaterials.2013.09.011.
8. Koh, B.; Ab Rahman, F.H.; Matlan, N.A.; Rajan, M.; Musta'ain, A.Y.; Mohd Jeffry Lee, M.R.; Ramli, R.; Mohd Yunus, S.S.; Binti Hj Idrus, R.; Yazid, M.D. Potential role of dental pulp stem cells conditioned medium for odontoblastic differentiation. *Biological Research* **2022**, *55*, 11, doi:10.1186/s40659-022-00380-8.
9. Yamaguchi, S.; Shibata, R.; Yamamoto, N.; Nishikawa, M.; Hibi, H.; Tanigawa, T.; Ueda, M.; Murohara, T.; Yamamoto, A. Dental pulp-derived stem cell conditioned medium reduces cardiac injury following ischemia-reperfusion. *Scientific Reports* **2015**, *5*, 16295, doi:10.1038/srep16295.

10. El Moshy, S.; Radwan, I.A.; Rady, D.; Abbass, M.M.S.; El-Rashidy, A.A.; Sadek, K.M.; Dörfer, C.E.; Fawzy El-Sayed, K.M. Dental Stem Cell-Derived Secretome/Conditioned Medium: The Future for Regenerative Therapeutic Applications. *Stem Cells International* **2020**, *2020*, 7593402, doi:https://doi.org/10.1155/2020/7593402.
11. Shi, W.; Jiang, Y.; Wu, T.; Zhang, Y.; Li, T. Advancements in drug-loaded hydrogel systems for bone defect repair. *Regenerative Therapy* **2024**, *25*, 174-185, doi:https://doi.org/10.1016/j.reth.2023.12.010.
12. Calori, G.; Mazza, E.; Colombo, M.; Ripamonti, C. The use of bone-graft substitutes in large bone defects: any specific needs? *Injury* **2011**, *42*, S56-S63.
13. Gutierres, M.; Dias, A.; Lopes, M.; Hussain, N.S.; Cabral, A.; Almeida, L.; Santos, J. Opening wedge high tibial osteotomy using 3D biomodelling Bonelike® macroporous structures: case report. *Journal of Materials Science: Materials in Medicine* **2007**, *18*, 2377-2382.
14. Innes, J. Bone grafting in small animal orthopaedic surgery. *In Practice* **2014**, *36*, 173-181.
15. Vertenten, G.; Gasthuys, F.; Cornelissen, M.; Schacht, E.; Vlaminck, L. Enhancing bone healing and regeneration: present and future perspectives in veterinary orthopaedics. *Veterinary and Comparative Orthopaedics and Traumatology* **2010**, *23*, 153-162.
16. Cross, A.; Tobias, K.; Johnston, S. Fracture biology and biomechanics. *Veterinary surgery: small animal* **2012**, *1*, 565-571.
17. Johnson, A.L.; Houlton, J.E.; Vannini, R. *AO principles of fracture management in the dog and cat*; Georg Thieme Verlag: 2005.
18. Campana, V.; Milano, G.; Pagano, E.; Barba, M.; Cicione, C.; Salonna, G.; Lattanzi, W.; Logroscino, G. Bone substitutes in orthopaedic surgery: from basic science to clinical practice. *J Mater Sci Mater Med* **2014**, *25*, 2445-2461, doi:10.1007/s10856-014-5240-2.
19. Hollinger, J.O.; Kleinschmidt, J.C. The critical size defect as an experimental model to test bone repair materials. *The Journal of craniofacial surgery* **1990**, *1*, 60-68.
20. Bezstarosti, H.; Metsemakers, W.J.; van Lieshout, E.M.M.; Voskamp, L.W.; Kortram, K.; McNally, M.A.; Marais, L.C.; Verhofstad, M.H.J. Management of critical-sized bone defects in the treatment of fracture-related infection: a

systematic review and pooled analysis. *Arch Orthop Trauma Surg* **2021**, *141*, 1215-1230, doi:10.1007/s00402-020-03525-0.

21. Gosain, A.K.; Song, L.; Yu, P.; Mehrara, B.J.; Maeda, C.Y.; Gold, L.I.; Longaker, M.T. Osteogenesis in cranial defects: reassessment of the concept of critical size and the expression of TGF-beta isoforms. *Plast Reconstr Surg* **2000**, *106*, 360-371; discussion 372, doi:10.1097/00006534-200008000-00018.
22. Court-Brown, C. External casting of diaphyseal fractures of the tibia and fibula. *Current Orthopaedics* **1998**, *12*, 262-272.
23. Berner, A.; Reichert, J.C.; Muller, M.B.; Zellner, J.; Pfeifer, C.; Dienstknecht, T.; Nerlich, M.; Sommerville, S.; Dickinson, I.C.; Schutz, M.A.; et al. Treatment of long bone defects and non-unions: from research to clinical practice. *Cell Tissue Res* **2012**, *347*, 501-519, doi:10.1007/s00441-011-1184-8.
24. Blokhuis, T.J.; Termaat, M.F.; den Boer, F.C.; Patka, P.; Bakker, F.C.; Henk, J.T.M. Properties of calcium phosphate ceramics in relation to their in vivo behavior. *Journal of trauma and acute care surgery* **2000**, *48*, 179.
25. Gutierres, M.; Hussain, N.S.; Lopes, M.; Afonso, A.; Cabral, A.; Almeida, L.; Santos, J. Histological and scanning electron microscopy analyses of bone/implant interface using the novel Bonelike® synthetic bone graft. *Journal of orthopaedic research* **2006**, *24*, 953-958.
26. Gutierres, M.; Sooraj Hussain, N.; Afonso, A.; Almeida, L.; Cabral, T.; Lopes, M.; Santos, J.D. Biological behaviour of bonelike® graft implanted in the tibia of humans. In Proceedings of the Key Engineering Materials, 2005; pp. 1041-1044.
27. Pavan Kumar, G.; Vijayakumar, R.; Naga Sowmya, B.; Nandyala, S.H.; Lopes, M.; Santos, J.D. Treatment of a Large Cystic Lesion in Anterior Maxilla Using Glass Reinforced Hydroxyapatite–A Case Report. In Proceedings of the Solid State Phenomena, 2014; pp. 97-108.
28. Torres, J.; Gutierres, M.; Lopes, M.A.; Santos, J.D.; Cabral, A.; Pinto, R.; Van Eck, C. Bone marrow stem cells added to a hydroxyapatite scaffold result in better outcomes after surgical treatment of intertrochanteric hip fractures. *BioMed research international* **2014**, *2014*.
29. Atayde, L.; Cortez, P.; Afonso, A.; Santos, M.; Maurício, A.; Santos, J. Morphology effect of bioglass-reinforced hydroxyapatite (Bonelike®) on

osteoregeneration. *Journal of Biomedical Materials Research Part B: Applied Biomaterials* **2015**, *103*, 292-304.

30. Grawish, M.E.; Saeed, M.A.; Sultan, N.; Scheven, B.A. Therapeutic applications of dental pulp stem cells in regenerating dental, periodontal and oral-related structures. *World Journal of Meta-Analysis* **2021**, *9*, 176-192.
31. Harrell, C.R.; Fellabaum, C.; Jovicic, N.; Djonov, V.; Arsenijevic, N.; Volarevic, V. Molecular Mechanisms Responsible for Therapeutic Potential of Mesenchymal Stem Cell-Derived Secretome. *Cells* **2019**, *8*, doi:10.3390/cells8050467.
32. Gwam, C.; Mohammed, N.; Ma, X. Stem cell secretome, regeneration, and clinical translation: a narrative review. *Ann Transl Med* **2021**, *9*, 70, doi:10.21037/atm-20-5030.
33. El Moshy, S.; Radwan, I.A.; Rady, D.; Abbass, M.M.S.; El-Rashidy, A.A.; Sadek, K.M.; Dörfer, C.E.; Fawzy El-Sayed, K.M. Dental Stem Cell-Derived Secretome/Conditioned Medium: The Future for Regenerative Therapeutic Applications. *Stem Cells Int* **2020**, *2020*, 7593402, doi:10.1155/2020/7593402.
34. Xiao, Z.; Lei, T.; Liu, Y.; Yang, Y.; Bi, W.; Du, H. The potential therapy with dental tissue-derived mesenchymal stem cells in Parkinson's disease. *Stem Cell Res Ther* **2021**, *12*, 5, doi:10.1186/s13287-020-01957-4.
35. Ahangar, P.; Mills, S.J.; Cowin, A.J. Mesenchymal Stem Cell Secretome as an Emerging Cell-Free Alternative for Improving Wound Repair. *Int J Mol Sci* **2020**, *21*, doi:10.3390/ijms21197038.
36. Meiliana, A.; Dewi, N.M.; Wijaya, A. Mesenchymal stem cell secretome: Cell-free therapeutic strategy in regenerative medicine. *The Indonesian Biomedical Journal* **2019**, *11*, 113-124.
37. Bogatcheva, N.V.; Coleman, M.E. Conditioned Medium of Mesenchymal Stromal Cells: A New Class of Therapeutics. *Biochemistry (Mosc)* **2019**, *84*, 1375-1389, doi:10.1134/S0006297919110129.
38. Xia, J.; Minamino, S.; Kuwabara, K.; Arai, S. Stem cell secretome as a new booster for regenerative medicine. *Biosci Trends* **2019**, *13*, 299-307, doi:10.5582/bst.2019.01226.
39. Sadat, S.; Gehmert, S.; Song, Y.H.; Yen, Y.; Bai, X.; Gaiser, S.; Klein, H.; Alt, E. The cardioprotective effect of mesenchymal stem cells is mediated by IGF-I

and VEGF. *Biochem Biophys Res Commun* **2007**, *363*, 674-679, doi:10.1016/j.bbrc.2007.09.058.

40. Lee, K.; Kim, H.; Kim, J.M.; Kim, J.R.; Kim, K.J.; Kim, Y.J.; Park, S.I.; Jeong, J.H.; Moon, Y.M.; Lim, H.S.; et al. Systemic transplantation of human adipose-derived stem cells stimulates bone repair by promoting osteoblast and osteoclast function. *J Cell Mol Med* **2011**, *15*, 2082-2094, doi:10.1111/j.1582-4934.2010.01230.x.
41. Badyra, B.; Sulkowski, M.; Milczarek, O.; Majka, M. Mesenchymal stem cells as a multimodal treatment for nervous system diseases. *Stem Cells Transl Med* **2020**, *9*, 1174-1189, doi:10.1002/sctm.19-0430.
42. Monsel, A.; Zhu, Y.G.; Gudapati, V.; Lim, H.; Lee, J.W. Mesenchymal stem cell derived secretome and extracellular vesicles for acute lung injury and other inflammatory lung diseases. *Expert Opin Biol Ther* **2016**, *16*, 859-871, doi:10.1517/14712598.2016.1170804.
43. Sultan, N.; Amin, L.E.; Zaher, A.R.; Scheven, B.A.; Grawish, M.E. Dental pulp stem cells: Novel cell-based and cell-free therapy for peripheral nerve repair. *World Journal of Stomatology* **2019**, *7*, 1-19.
44. Luzuriaga, J.; Polo, Y.; Pastor-Alonso, O.; Pardo-Rodríguez, B.; Larrañaga, A.; Unda, F.; Sarasua, J.R.; Pineda, J.R.; Ibarretxe, G. Advances and Perspectives in Dental Pulp Stem Cell Based Neuroregeneration Therapies. *Int J Mol Sci* **2021**, *22*, doi:10.3390/ijms22073546.
45. Ueda, T.; Inden, M.; Ito, T.; Kurita, H.; Hozumi, I. Characteristics and Therapeutic Potential of Dental Pulp Stem Cells on Neurodegenerative Diseases. *Front Neurosci* **2020**, *14*, 407, doi:10.3389/fnins.2020.00407.
46. Ahmed Nel, M.; Murakami, M.; Hirose, Y.; Nakashima, M. Therapeutic Potential of Dental Pulp Stem Cell Secretome for Alzheimer's Disease Treatment: An In Vitro Study. *Stem Cells Int* **2016**, *2016*, 8102478, doi:10.1155/2016/8102478.
47. Mita, T.; Furukawa-Hibi, Y.; Takeuchi, H.; Hattori, H.; Yamada, K.; Hibi, H.; Ueda, M.; Yamamoto, A. Conditioned medium from the stem cells of human dental pulp improves cognitive function in a mouse model of Alzheimer's disease. *Behav Brain Res* **2015**, *293*, 189-197, doi:10.1016/j.bbr.2015.07.043.
48. Buss, L.F.; de Martin, G.S.; Martinez, E.F.; Filgueiras, I.A.d.A.A.P.; Magnabosco, J.L.; Alves, B.F.; de Macedo Almeida, B.; Kotaka, T.; Teixeira,

M.L.; Ferreira, J.R.M.; et al. Conditioned Media from Human Pulp Stem Cell Cultures Improve Bone Regeneration in Rat Calvarial Critical-Size Defects. *Journal of Functional Biomaterials* **2023**, *14*, 396.

49. Ferreira, J.R.; Teixeira, G.Q.; Santos, S.G.; Barbosa, M.A.; Almeida-Porada, G.; Goncalves, R.M. Mesenchymal Stromal Cell Secretome: Influencing Therapeutic Potential by Cellular Pre-conditioning. *Front Immunol* **2018**, *9*, 2837, doi:10.3389/fimmu.2018.02837.
50. Chichiricco, P.M.; Matricardi, P.; Colaço, B.; Gomes, P.; Jérôme, C.; Lesoeur, J.; Veziers, J.; Réthoré, G.; Weiss, P.; Struillou, X.; et al. Injectable Hydrogel Membrane for Guided Bone Regeneration. *Bioengineering* **2023**, *10*, 94.
51. Elgali, I.; Omar, O.; Dahlin, C.; Thomsen, P. Guided bone regeneration: materials and biological mechanisms revisited. *European Journal of Oral Sciences* **2017**, *125*, 315-337, doi:https://doi.org/10.1111/eos.12364.
52. Milella, E.; Ramires, P.A.; Brescia, E.; La Sala, G.; Di Paola, L.; Bruno, V. Physicochemical, mechanical, and biological properties of commercial membranes for GTR. *Journal of Biomedical Materials Research* **2001**, *58*, 427-435, doi:https://doi.org/10.1002/jbm.1038.
53. Bottino, M.C.; Thomas, V.; Schmidt, G.; Vohra, Y.K.; Chu, T.-M.G.; Kowolik, M.J.; Janowski, G.M. Recent advances in the development of GTR/GBR membranes for periodontal regeneration—A materials perspective. *Dental Materials* **2012**, *28*, 703-721, doi:https://doi.org/10.1016/j.dental.2012.04.022.
54. Dimitriou, R.; Mataliotakis, G.I.; Calori, G.M.; Giannoudis, P.V. The role of barrier membranes for guided bone regeneration and restoration of large bone defects: current experimental and clinical evidence. *BMC Medicine* **2012**, *10*, 81, doi:10.1186/1741-7015-10-81.
55. Jung, R.E.; Hälg, G.A.; Thoma, D.S.; Hämmerle, C.H.F. A randomized, controlled clinical trial to evaluate a new membrane for guided bone regeneration around dental implants. *Clinical Oral Implants Research* **2009**, *20*, 162-168, doi:https://doi.org/10.1111/j.1600-0501.2008.01634.x.
56. Rothamel, D.; Schwarz, F.; Sager, M.; Herten, M.; Sculean, A.; Becker, J. Biodegradation of differently cross-linked collagen membranes: an experimental study in the rat. *Clin Oral Implants Res* **2005**, *16*, 369-378, doi:10.1111/j.1600-0501.2005.01108.x.

57. Schwarz, F.; Rothamel, D.; Herten, M.; Sager, M.; Becker, J. Angiogenesis pattern of native and cross-linked collagen membranes: an immunohistochemical study in the rat. *Clin Oral Implants Res* **2006**, *17*, 403-409, doi:10.1111/j.1600-0501.2005.01225.x.
58. Tal, H.; Kozlovsky, A.; Artzi, Z.; Nemcovsky, C.E.; Moses, O. Long-term bio-degradation of cross-linked and non-cross-linked collagen barriers in human guided bone regeneration. *Clin Oral Implants Res* **2008**, *19*, 295-302, doi:10.1111/j.1600-0501.2007.01424.x.
59. Zitzmann, N.U.; Naef, R.; Schärer, P. Resorbable versus nonresorbable membranes in combination with Bio-Oss for guided bone regeneration. *Int J Oral Maxillofac Implants* **1997**, *12*, 844-852.
60. Rothamel, D.; Schwarz, F.; Sculean, A.; Herten, M.; Scherbaum, W.; Becker, J. Biocompatibility of various collagen membranes in cultures of human PDL fibroblasts and human osteoblast-like cells. *Clin Oral Implants Res* **2004**, *15*, 443-449, doi:10.1111/j.1600-0501.2004.01039.x.
61. Lansdowne, J.L.; Devine, D.; Eberli, U.; Emans, P.; Welting, T.J.; Odekerken, J.C.; Schiuma, D.; Thalhauser, M.; Bouré, L.; Zeiter, S. Characterization of an ovine bilateral critical sized bone defect iliac wing model to examine treatment modalities based on bone tissue engineering. *BioMed research international* **2014**, *2014*.
62. Campos, J.M.; Sousa, A.C.; Caseiro, A.R.; Pedrosa, S.S.; Pinto, P.O.; Branquinho, M.V.; Amorim, I.; Santos, J.D.; Pereira, T.; Mendonça, C.M.; et al. Dental pulp stem cells and Bonelike(®) for bone regeneration in ovine model. *Regenerative Biomaterials* **2019**, *6*, 49-59, doi:10.1093/rb/rby025.
63. Jha, L.J.; Santos, J.D.; Knowles, J.C. Characterization of apatite layer formation on P2O5-CaO, P2O5-CaO-Na2O, and P2O5-CaO-Na2O-Al2O3 glass hydroxyapatite composites. *J Biomed Mater Res* **1996**, *31*, 481-486, doi:10.1002/(sici)1097-4636(199608)31:4<481::Aid-jbm7>3.0.Co;2-h.
64. Santos, J.D.; Jha, L.J.; Monteiro, F.J. In vitro calcium phosphate formation on SiO2-Na2O-CaO-P2O5 glass reinforced hydroxyapatite composite: a study by XPS analysis. *Journal of Materials Science: Materials in Medicine* **1996**, *7*, 181-185, doi:10.1007/BF00121258.
65. Morouço, P.; Biscaia, S.; Viana, T.; Franco, M.; Malça, C.; Mateus, A.; Moura, C.; Ferreira, F.C.; Mitchell, G.; Alves, N.M. Fabrication of Poly(ε-caprolactone) Scaffolds Reinforced with Cellulose Nanofibers, with and without the

Addition of Hydroxyapatite Nanoparticles. *Biomed Res Int* **2016**, *2016*, 1596157, doi:10.1155/2016/1596157.

66. Biscaia, S.; Dabrowska, E.; Tojeira, A.; Horta, J.; Carreira, P.; Morouço, P.; Mateus, A.; Alves, N. Development of heterogeneous structures with Polycaprolactone-Alginate using a new 3D printing system–BioMEDβeta: design and processing. *Procedia Manufacturing* **2017**, *12*, 113-119.
67. Francisco, L.; Moura, C.; Viana, T.; Ângelo, D.; Morouço, P.; Alves, N. Poly(ε-caprolactone) and Polyethylene Glycol Diacrylate-based Scaffolds for TMJ Bioengineered Disc Implants. *Procedia Manufacturing* **2017**, *12*, 291-297, doi:https://doi.org/10.1016/j.promfg.2017.08.032.
68. Moura, C.; Trindade, D.; Vieira, M.; Francisco, L.; Ângelo, D.F.; Alves, N. Multi-Material Implants for Temporomandibular Joint Disc Repair: Tailored Additive Manufacturing Production. *Front Bioeng Biotechnol* **2020**, *8*, 342, doi:10.3389/fbioe.2020.00342.
69. Biscaia, S.; Branquinho, M.V.; Alvites, R.D.; Fonseca, R.; Sousa, A.C.; Pedrosa, S.S.; Caseiro, A.R.; Guedes, F.; Patrício, T.; Viana, T.; et al. 3D Printed Poly(ε-caprolactone)/Hydroxyapatite Scaffolds for Bone Tissue Engineering: A Comparative Study on a Composite Preparation by Melt Blending or Solvent Casting Techniques and the Influence of Bioceramic Content on Scaffold Propertie. *Int J Mol Sci* **2022**, *23*, 2318.
70. Domingos, M.; Intranuovo, F.; Russo, T.; De Santis, R.; Gloria, A.; Ambrosio, L.; Ciurana, J.; Bartolo, P. The first systematic analysis of 3D rapid prototyped poly(ε-caprolactone) scaffolds manufactured through BioCell printing: the effect of pore size and geometry on compressive mechanical behaviour and in vitro hMSC viability. *Biofabrication* **2013**, *5*, 045004, doi:10.1088/1758-5082/5/4/045004.
71. Domingos, M.; Intranuovo, F.; Gloria, A.; Gristina, R.; Ambrosio, L.; Bártolo, P.J.; Favia, P. Improved osteoblast cell affinity on plasma-modified 3-D extruded PCL scaffolds. *Acta Biomaterialia* **2013**, *9*, 5997-6005, doi:https://doi.org/10.1016/j.actbio.2012.12.031.
72. Bartolo, P.; Domingos, M.; Gloria, A.; Ciurana, J. BioCell Printing: Integrated automated assembly system for tissue engineering constructs. *CIRP Annals* **2011**, *60*, 271-274, doi:https://doi.org/10.1016/j.cirp.2011.03.116.
73. Ângelo, D.F.; Morouço, P.; Monje Gil, F.; Mónico, L.; González-Gárcia, R.; Sousa, R.; Neto, L.; Caldeira, I.; Smith, M.; Smith, S.; et al. Preclinical

randomized controlled trial of bilateral discectomy versus bilateral discopexy in Black Merino sheep temporomandibular joint: TEMPOJIMS – Phase 1- histologic, imaging and body weight results. *Journal of Cranio-Maxillofacial Surgery* **2018**, *46*, 688-696, doi:https://doi.org/10.1016/j.jcms.2018.01.006.

74. Viana, T.; Biscaia, S.; Dabrowska, E.; Franco, M.C.; Carreira, P.; Morouço, P.; Alves, N. A Novel Biomanufacturing System to Produce Multi-Material Scaffolds for Tissue Engineering: Concept and Preliminary Results. *Applied Mechanics and Materials* **2019**, *890*, 283-289, doi:10.4028/www.scientific.net/AMM.890.283.
75. Domingos, M.; Dinucci, D.; Cometa, S.; Alderighi, M.; Bártolo, P.J.; Chiellini, F. Polycaprolactone Scaffolds Fabricated via Bioextrusion for Tissue Engineering Applications. *International Journal of Biomaterials* **2009**, *2009*, 239643, doi:10.1155/2009/239643.
76. Morouço, P.; Ângelo, D.; Francisco, L.; Moura, C.; Alves, N. Tissue engineering for temporomandibular joint disc repair and regeneration: a methodological perspective. *Advances in Cellular and Molecular Otolaryngology* **2016**, *4*, 33709, doi:10.3402/acmo.v4.33709.
77. Alexandre, N.; Amorim, I.; Caseiro, A.R.; Pereira, T.; Alvites, R.; Rema, A.; Goncalves, A.; Valadares, G.; Costa, E.; Santos-Silva, A.; et al. Long term performance evaluation of small-diameter vascular grafts based on polyvinyl alcohol hydrogel and dextran and MSCs-based therapies using the ovine pre-clinical animal model. *Int J Pharm* **2017**, doi:10.1016/j.ijpharm.2017.02.043.
78. Alexandre, N.; Costa, E.; Coimbra, S.; Silva, A.; Lopes, A.; Rodrigues, M.; Santos, M.; Mauricio, A.C.; Santos, J.D.; Luis, A.L. In vitro and in vivo evaluation of blood coagulation activation of polyvinyl alcohol hydrogel plus dextran-based vascular grafts. *J Biomed Mater Res A* **2015**, *103*, 1366-1379, doi:10.1002/jbm.a.35275.
79. Alexandre, N.; Ribeiro, J.; Gartner, A.; Pereira, T.; Amorim, I.; Fragoso, J.; Lopes, A.; Fernandes, J.; Costa, E.; Santos-Silva, A.; et al. Biocompatibility and hemocompatibility of polyvinyl alcohol hydrogel used for vascular grafting--In vitro and in vivo studies. *J Biomed Mater Res A* **2014**, *102*, 4262-4275, doi:10.1002/jbm.a.35098.

80. Caseiro, A.R.; Pereira, T.; Ivanova, G.; Luis, A.L.; Mauricio, A.C. Neuromuscular Regeneration: Perspective on the Application of Mesenchymal Stem Cells and Their Secretion Products. *Stem Cells Int* **2016**, *2016*, 9756973, doi:10.1155/2016/9756973.
81. Gartner, A.; Pereira, T.; Alves, M.G.; Armada-da-Silva, P.A.; Amorim, I.; Gomes, R.; Ribeiro, J.; Franca, M.L.; Lopes, C.; Carvalho, R.A.; et al. Use of poly(DL-lactide-epsilon-caprolactone) membranes and mesenchymal stem cells from the Wharton's jelly of the umbilical cord for promoting nerve regeneration in axonotmesis: in vitro and in vivo analysis. *Differentiation* **2012**, *84*, 355-365, doi:10.1016/j.diff.2012.10.001.
82. Gartner, A.; Pereira, T.; Simoes, M.J.; Armada-da-Silva, P.A.; Franca, M.L.; Sousa, R.; Bompasso, S.; Raimondo, S.; Shirosaki, Y.; Nakamura, Y.; et al. Use of hybrid chitosan membranes and human mesenchymal stem cells from the Wharton jelly of umbilical cord for promoting nerve regeneration in an axonotmesis rat model. *Neural Regen Res* **2012**, *7*, 2247-2258, doi:10.3969/j.issn.1673-5374.2012.29.002.
83. Pereira, T.; Armada-da Silva, P.A.; Amorim, I.; Rema, A.; Caseiro, A.R.; Gartner, A.; Rodrigues, M.; Lopes, M.A.; Bartolo, P.J.; Santos, J.D.; et al. Effects of Human Mesenchymal Stem Cells Isolated from Wharton's Jelly of the Umbilical Cord and Conditioned Media on Skeletal Muscle Regeneration Using a Myectomy Model. *Stem Cells Int* **2014**, *2014*, 376918, doi:10.1155/2014/376918.
84. Pereira, T.; Gartner, A.; Amorim, I.; Almeida, A.; Caseiro, A.R.; Armada-da-Silva, P.A.; Amado, S.; Fregnan, F.; Varejao, A.S.; Santos, J.D.; et al. Promoting nerve regeneration in a neurotmesis rat model using poly(DL-lactide-epsilon-caprolactone) membranes and mesenchymal stem cells from the Wharton's jelly: in vitro and in vivo analysis. *Biomed Res Int* **2014**, *2014*, 302659, doi:10.1155/2014/302659.
85. Pereira, T.; Ivanova, G.; Caseiro, A.R.; Barbosa, P.; Bartolo, P.J.; Santos, J.D.; Luis, A.L.; Mauricio, A.C. MSCs Conditioned Media and Umbilical Cord Blood Plasma Metabolomics and Composition. *PloS one* **2014**, *9*, e113769, doi:10.1371/journal.pone.0113769.
86. Ribeiro, J.; Gartner, A.; Pereira, T.; Gomes, R.; Lopes, M.A.; Goncalves, C.; Varejao, A.; Luis, A.L.; Mauricio, A.C. Perspectives of employing mesenchymal stem cells from the Wharton's jelly of the umbilical cord for

peripheral nerve repair. *Int Rev Neurobiol* **2013**, *108*, 79-120, doi:10.1016/B978-0-12-410499-0.00004-6.

87. Ribeiro, J.; Pereira, T.; Amorim, I.; Caseiro, A.R.; Lopes, M.A.; Lima, J.; Gartner, A.; Santos, J.D.; Bartolo, P.J.; Rodrigues, J.M.; et al. Cell therapy with human MSCs isolated from the umbilical cord Wharton jelly associated to a PVA membrane in the treatment of chronic skin wounds. *Int J Med Sci* **2014**, *11*, 979-987, doi:10.7150/ijms.9139.
88. Ribeiro, J.; Pereira, T.; Caseiro, A.R.; Armada-da-Silva, P.; Pires, I.; Prada, J.; Amorim, I.; Amado, S.; Franca, M.; Goncalves, C.; et al. Evaluation of biodegradable electric conductive tube-guides and mesenchymal stem cells. *World J Stem Cells* **2015**, *7*, 956-975, doi:10.4252/wjsc.v7.i6.956.
89. Silva, D.M.; Caseiro, A.R.; Amorim, I.; Pereira, I.; Faria, F.; Pereira, T.; Santos, J.D.; Gama, F.M.; Mauricio, A.C. Inflammatory response to dextrin-based hydrogel associated with human mesenchymal stem cells, urinary bladder matrix and Bonelike(R) granules in rat subcutaneous implants. *Biomed Mater* **2016**, *11*, 065004, doi:10.1088/1748-6041/11/6/065004.
90. Branquinho, M.V.; Ferreira, S.O.; Alvites, R.D.; Magueta, A.F.; Ivanov, M.; Sousa, A.C.; Amorim, I.; Faria, F.; Fernandes, M.H.V.; Vilarinho, P.M.; et al. In Vitro and In Vivo Characterization of PLLA-316L Stainless Steel Electromechanical Devices for Bone Tissue Engineering—A Preliminary Study. *International Journal of Molecular Sciences* **2021**, *22*, doi:10.3390/ijms22147655.
91. Atayde, L.; Cortez, P.; Pereira, T.; Armada-da-Silva, P.; Afonso, A.; Lopes, M.; Santos, J.; Maurício, A. A new sheep model with automatized analysis of biomaterial-induced bone tissue regeneration. *Journal of Materials Science: Materials in Medicine* **2014**, *25*, 1885-1901.
92. Campos, J.; Sousa, A.; Caseiro, A.; Pedrosa, S.; Pinto, P.; Branquinho, M.; Amorim, I.; Santos, J.; Pereira, T.; Mendonça, C. Dental pulp stem cells and Bonelike® for bone regeneration in ovine model. *Regenerative biomaterials* **2018**, *6*, 49-59.
93. Alvites, R.D.; Branquinho, V.M.; Caseiro, A.R.; Amorim, I.; Santos Pedrosa, S.; Rêma, A.; Faria, F.; Porto, B.; Oliveira, C.; Teixeira, P.; et al. Rat Olfactory Mucosa Mesenchymal Stem/Stromal Cells (OM-MSCs): A Characterization Study. *International Journal of Cell Biology* **2020**, *2020*, doi:10.1155/2020/2938258.

94. Caseiro, A.R.; Ivanova, G.; Pedrosa, S.S.; Branquinho, V.M.; Georgieva, P.; Barbosa, P.P.; Santos, J.D.; Magalhães, R.; Teixeira, P.; Pereira, T.; et al. Human umbilical cord blood plasma as an alternative to animal sera for mesenchymal stromal cells in vitro expansion - A multicomponent metabolomic analysis. *PloS one* **2018**, *13*, 1-35, doi:10.1371/journal.pone.0203936.
95. Calori, G.M.; Mazza, E.; Colombo, M.; Ripamonti, C. The use of bone-graft substitutes in large bone defects: Any specific needs? *Injury* **2011**, *42*, S56-S63, doi:https://doi.org/10.1016/j.injury.2011.06.011.
96. Toogood, P.; Miclau, T. Critical-Sized Bone Defects: Sequence and Planning. *Journal of Orthopaedic Trauma* **2017**, *31*, S23-S26, doi:10.1097/BOT.0000000000000980.
97. Roddy, E.; DeBaun, M.R.; Daoud-Gray, A.; Yang, Y.P.; Gardner, M.J. Treatment of critical-sized bone defects: clinical and tissue engineering perspectives. *European Journal of Orthopaedic Surgery & Traumatology* **2018**, *28*, 351-362, doi:10.1007/s00590-017-2063-0.
98. Sousa, A.C.; Biscaia, S.; Alvites, R.; Branquinho, M.; Lopes, B.; Sousa, P.; Valente, J.; Franco, M.; Santos, J.D.; Mendonça, C.; et al. Assessment of 3D-Printed Polycaprolactone, Hydroxyapatite Nanoparticles and Diacrylate Poly(ethylene glycol) Scaffolds for Bone Regeneration. *Pharmaceutics* **2022**, *14*, doi:10.3390/pharmaceutics14122643.
99. Hou, Y.; Wang, W.; Bartolo, P. Investigation of polycaprolactone for bone tissue engineering scaffolds: In vitro degradation and biological studies. *Materials & Design* **2022**, *216*, 110582, doi:https://doi.org/10.1016/j.matdes.2022.110582.
100. Pinto, P.O.; Branquinho, M.V.; Caseiro, A.R.; Sousa, A.C.; Brandão, A.; Pedrosa, S.S.; Alvites, R.D.; Campos, J.M.; Santos, F.L.; Santos, J.D.; et al. The application of Bonelike® Poro as a synthetic bone substitute for the management of critical-sized bone defects - A comparative approach to the autograft technique - A preliminary study. *Bone Reports* **2021**, *14*, 101064, doi:https://doi.org/10.1016/j.bonr.2021.101064.
101. Caseiro, A.; Damásio Alvites, R.; Pedrosa, S.; Campos, J.M.; Reis, I.; Santos, J.D.; Mendonça, C.; Atayde, L.; Mauricio, A.C. The potential clinical application of mesenchymal stem cells from the dental pulp (DPSCs) for bone regeneration. 2017.

102. Laino, G.; Graziano, A.; d'Aquino, R.; Pirozzi, G.; Lanza, V.; Valiante, S.; De Rosa, A.; Naro, F.; Vivarelli, E.; Papaccio, G. An approachable human adult stem cell source for hard-tissue engineering. *J Cell Physiol* **2006**, *206*, 693-701, doi:10.1002/jcp.20526.
103. Papaccio, G.; Graziano, A.; d'Aquino, R.; Graziano, M.F.; Pirozzi, G.; Menditti, D.; De Rosa, A.; Carinci, F.; Laino, G. Long-term cryopreservation of dental pulp stem cells (SBP-DPSCs) and their differentiated osteoblasts: a cell source for tissue repair. *J Cell Physiol* **2006**, *208*, 319-325, doi:10.1002/jcp.20667.
104. Sousa, A.C. Avaliação e ensaios pré-clínicos de Bonelike® para regeneração óssea em defeitos não-críticos. Faculty of Engineering - University of Porto, 2018.
105. Kichenbrand, C.; Velot, E.; Menu, P.; Moby, V. Dental Pulp Stem Cell-Derived Conditioned Medium: An Attractive Alternative for Regenerative Therapy. *Tissue Engineering Part B: Reviews* **2019**, *25*, 78-88, doi:10.1089/ten.teb.2018.0168.
106. Liu, Y. Application of dental pulp stem cells for bone regeneration. *Frontiers in Medicine* **2024**, *11*, doi:10.3389/fmed.2024.1339573.
107. Katagiri, W.; Watanabe, J.; Toyama, N.; Osugi, M.; Sakaguchi, K.; Hibi, H. Clinical Study of Bone Regeneration by Conditioned Medium From Mesenchymal Stem Cells After Maxillary Sinus Floor Elevation. *Implant Dent* **2017**, *26*, 607-612, doi:10.1097/id.0000000000000618.
108. Schwarz, F.; Hegewald, A.; Sahm, N.; Becker, J. Long-term follow-up of simultaneous guided bone regeneration using native and cross-linked collagen membranes over 6 years. *Clin Oral Implants Res* **2014**, *25*, 1010-1015, doi:10.1111/clr.12220.
109. Hollinger, J.O.; Kleinschmidt, J.C. The Critical Size Defect as an Experimental Model To Test Bone Repair Materials. *Journal of Craniofacial Surgery* **1990**, *1*.
110. Li, Y.; Chen, S.-K.; Li, L.; Qin, L.; Wang, X.-L.; Lai, Y.-X. Bone defect animal models for testing efficacy of bone substitute biomaterials. *Journal of Orthopaedic Translation* **2015**, *3*, 95-104, doi:https://doi.org/10.1016/j.jot.2015.05.002.
111. Pinto, P.O.; Pinto, P.O.; Atayde, L.M.; Atayde, L.M.; Campos, J.M.; Campos, J.M.; Caseiro, A.R.; Caseiro, A.R.; Caseiro, A.R.; Pereira, T.; et al. Therapeutic Strategies for Bone Regeneration: The Importance of Biomaterials Testing in

Adequate Animal Models. In *Advanced Composite Materials*; 2016; pp. 275-319.

CHAPTER VII

GENERAL DISCUSSION, CONCLUSIONS AND FUTURE PERSPECTIVES

[This page is intentionally left blank.]

General Discussion and Conclusions

[This page is intentionally left blank.]

The field of Regenerative Medicine has made significant progress with the advancement of three-dimensional (3D) printing technology, which has emerged as a valuable technique for creating patient-specific medical devices, such as tissue scaffolds [1]. A key development in this field is the synergistic integration of 3D-printed scaffolds with cell-based therapies, particularly mesenchymal stem/stromal cells (MSCs). MSCs, due to their multipotency and immunomodulatory properties, play a crucial role in enhancing the regenerative process when combined with biocompatible scaffolds [2]. This combination not only facilitates the structural support required for tissue regeneration but also accelerates healing by promoting cellular differentiation, reducing inflammation, and enhancing angiogenesis. Among the numerous applications of this approach, bone regeneration has been highlighted due to the high prevalence of bone-related diseases. Bone is one of the most frequently transplanted tissues, with approximately 1 million procedures performed annually throughout Europe [3]. The demand for bone transplantation arises from various conditions, including traumatic injuries (e.g., non-union fractures), degenerative conditions (e.g., osteonecrosis of the femoral head), congenital deformities (e.g., cleft palates), and age-related bone loss (e.g., mandibular resorption) [4].

Currently, autologous bone grafting remains the gold standard in orthopedic and maxillofacial surgeries for the repair and regeneration of skeletal defects [5]. This technique involves harvesting bone from the patient, typically from sites such as the iliac crest, to repair or reconstruct damaged bone. While autologous grafting is advantageous due to its inherent biocompatibility and osteogenic potential, it is not without limitations. The quantity of bone available for harvesting is limited, and the procedure is often associated with significant donor site morbidity, including pain, infection, and longer recovery times [6].

To address these challenges, recent research, including the current thesis, has focused on the development of alternative strategies for bone regeneration. A promising approach involves the use of mesenchymal/stromal stem cells (MSCs) in combination with advanced biomaterials fabricated through 3D printing techniques. The current thesis aims to address the limitations of traditional bone grafting by leveraging the capabilities of 3D printing to create customized, patient-specific scaffolds. These scaffolds, combined with MSCs, provide a conducive environment for bone regeneration, mimicking the natural extracellular matrix and supporting the growth and differentiation of cells. The

research conducted in this thesis explores the design, fabrication, and characterization of these scaffolds, with a focus on optimizing their mechanical properties, biocompatibility, and osteoinductive potential.

The development of a functional scaffold for regenerative medicine applications indeed requires a comprehensive multi-step approach, involving extensive preclinical testing (**Figure 1**). The initial phase involves the production and detailed physicochemical characterization of the scaffold, ensuring it meets predefined criteria such as porosity, mechanical integrity, biodegradability, and biomaterial composition. Advanced characterization techniques, including rheological, mechanical, and morphological assessments, are employed to ascertain the scaffold's suitability for tissue engineering applications. Subsequently, *in vitro* studies are essential to evaluate the scaffold's biological performance, including cellular adhesion, proliferation, differentiation, and extracellular matrix deposition. These evaluations typically involve a combination of quantitative assays, gene expression profiling, and microscopic imaging to comprehensively assess cell behavior in response to the scaffold. Following successful *in vitro* validation, *in vivo* studies are imperative to further assess the scaffold's biocompatibility, integration, and capacity to promote tissue regeneration within a living organism. This phase includes evaluating the scaffold's immunogenicity, biodegradation kinetics, vascularization, and functional integration with host tissue. The data obtained from these *in vivo* models provide invaluable insights into the scaffold's translational potential, offering a critical foundation for future clinical applications [7-10].

This thesis systematically investigated the integration of 3D printing technologies with cellular therapies, demonstrating the potential for developing advanced tissue-engineered constructs. The thesis begins with a thorough review of the literature on 3D printing, bioprinting, and cell-based therapies, highlighting their respective strengths and limitations in various tissue engineering applications, including bone, skin, cardiovascular, neural, and liver tissue regeneration. By identifying the challenges in merging these approaches this chapter sets the stage for the subsequent experimental studies that aim to overcome these hurdles. The characterization of human dental pulp stem cells (hDPSCs), performed in the second chapter, provides essential insight into the potential of these cells for regenerative therapies. Through detailed biological analyses, including trilineage differentiation capacity and gene expression

profiling, the study confirms the suitability of hDPSCs for use in osteogenic applications. The selection of hDPSCs, based on their robust regenerative potential and ease of acquisition, underscores their importance as a promising cell source for tissue engineering. The development of 3D-printed synthetic bone grafts, as explored in the **Chapter III**, marked a critical advancement in the production of biomimetic scaffolds capable of mimicking the complex structure and function of natural bone. Using a combination of polycaprolactone (PCL), hydroxyapatite nanoparticles (nHA), and polyethylene glycol diacrylate (PEGDA), the extrusion-based additive manufacturing technique enabled the production of scaffolds with enhanced mechanical properties and biocompatibility. The study's focus on surface chemistry, morphological properties, and cytocompatibility ensures that the scaffolds combine the physical and biological criteria necessary for bone tissue regeneration. These scaffolds' mechanical strength and cytocompatibility were key factors contributing to their potential for clinical application in treating critical-sized bone defects. This thesis further explores the bioprinting of complex tissue constructs, as detailed in **Chapter IV**. A bioink formulation tailored for extrusion-based bioprinting was developed, consisting of alginate, nHA, and type I collagen (Col), integrated with human bone marrow-derived mesenchymal stem cells (hBMSCs). The bioprinted constructs underwent extensive characterization, including rheological, mechanical, and swelling behavior assessments, ensuring their structural integrity and stability under physiological conditions. Biological evaluations, including cell viability, metabolic activity assays, and gene expression analyses, provided critical insights into the bioactivity of the constructs, highlighting significant osteogenic differentiation. This approach provides a bioprinted model that constitutes a valuable platform for the *in vitro* investigation of osteogenesis and the early phases of tissue maturation. Moreover, the formulation of this bioink laid the groundwork for the subsequent development of a hybrid scaffold, as detailed in the following chapter. **Chapter V** integrates 3D-printed scaffolds composed of PCL and nHA (described in **Chapter III**) with bioactive hydrogels comprising alginate, nHA, and Col embedded with hDPSCs (described in **Chapter IV**), emphasizing the synergistic effects of these components in enhancing biological outcomes. The incorporation of bioactive hydrogels into mechanically robust scaffolds resulted in a substantial improvement in the biological performance of the hybrid structures. The extensive *in vitro* and *in vivo* evaluations confirmed that the hybrid scaffolds

supported cell viability, proliferation, and osteogenic differentiation. The use of a rat model demonstrated the biocompatibility and effectiveness of the scaffolds, confirming their safety for future clinical translation. Finally, in the **Chapter VI**, the performance of a novel scaffold combining PCL with Bonelike® (BL), a commercially available synthetic graft, was tested. This scaffold, in conjunction with a conditioned medium derived from hDPSCs (hDPSCs-CM), was evaluated both *in vitro* and *in vivo* using an ovine model. Preliminary results, obtained through radiographic imaging, showed promising bone regeneration, particularly in defects treated with PCL/BL scaffolds in combination with the hDPSCs-CM.

In summary, this thesis has successfully demonstrated that the integration of 3D printing technologies and cellular therapies offers a promising strategy to address key challenges in Regenerative Medicine. The studies presented underscore the critical role of scaffold architecture, biomaterial selection, and the incorporation of cell-based therapies in promoting tissue regeneration. Nevertheless, significant challenges remain, particularly regarding the scalability of these constructs for clinical translation and the variability in cellular responses *in vivo*.

The key findings and significant results from each chapter are succinctly outlined and analyzed in the following sections.

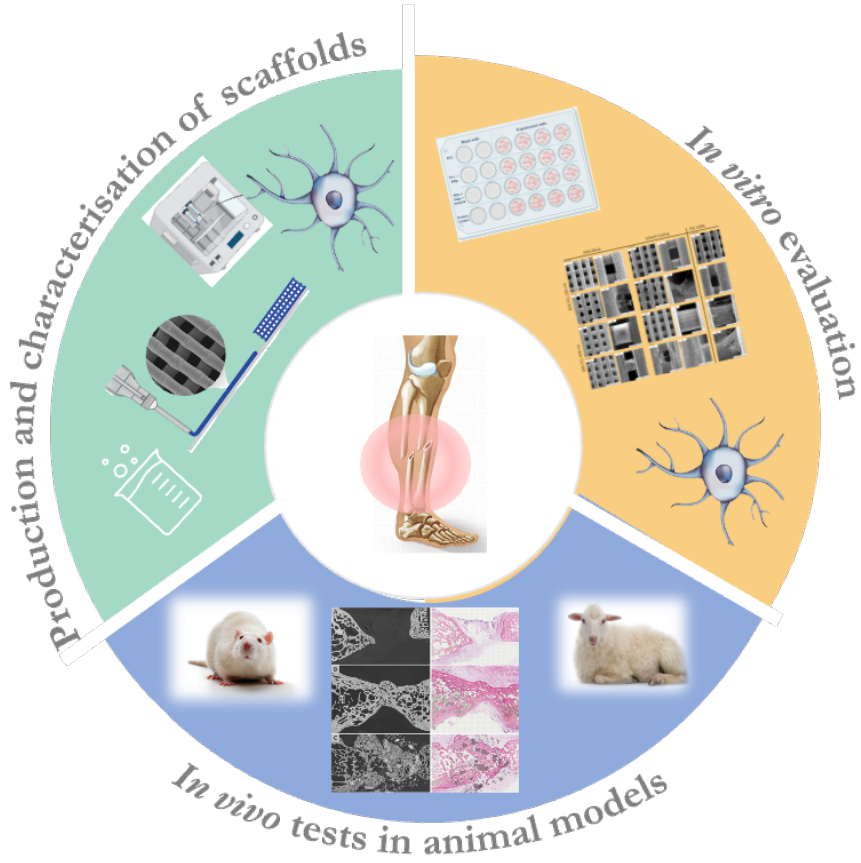


Figure 1. Stages of preclinical trials in scaffold development for bone regeneration.

State of the Art

A profound knowledge of the fundamental principles underlying 3D printing technologies and cellular therapies is crucial for guiding the strategic development of advanced regenerative medicine approaches. Therefore, an extensive review is presented in **Chapter I - State of Art**, which includes the article titled "Three-Dimensional Printing/Bioprinting and Cellular Therapies for Regenerative Medicine: Current Advances".

A global life expectancy continues to rise, accompanied by increasing expectations for effective therapeutic solutions, 3D printing technology represents a revolutionary advancement in the field of medicine. This innovative method facilitates the precise fabrication of patient-specific medical devices, implants, and tissue constructs, thereby revolutionizing treatment paradigms.

The capacity for customization inherent in 3D printing allows for the development of highly individualized therapeutic interventions, which are meticulously tailored to meet the distinct anatomical and physiological characteristics of each patient. This approach enhances the efficacy of medical treatments by optimizing fit and functionality, thus potentially improving clinical outcomes and patient satisfaction. Furthermore, the integration of 3D printing within the broader context of personalized medicine underscores a paradigm shift towards more nuanced and dynamic healthcare delivery models. By enabling healthcare practitioners to provide tailored treatment plans and meticulous follow-up care, 3D printing not only advances the precision of medical interventions but also aligns with the overarching objective of fostering a more holistic understanding of patient health. Consequently, the incorporation of 3D printing technology into clinical practice holds the promise of significantly eleve the standard of care, ultimately transforming the landscape of regenerative medicine and personalized therapies. Bioprinting has opened a whole new era in tissue regeneration allowing the production of patient-specific autologous organs and tissues [11-15]. This allows for the development of tissue and organ models that closely resemble the human body with high reproducibility [16-18]. By simultaneously printing multiple cell types and biomaterials, bioprinting can replicate the structural and biochemical complexity of living tissues, creating a heterogeneous microenvironment at specified locations [19-21].

Despite the extensive research conducted and the progress achieved in the field, there remains significant opportunity for further improvement and advancement [1,22]. There are several critical barriers that need to be addressed, such as the development of functional vascular networks, regulatory and ethical issues, and the advancement of suitable biomaterials [23-28].

Characterization of Mesenchymal Stem/Stromal Cells

The burgeoning evidence suggesting that MSCs contribute to bone regeneration, has prompted the investigation of various stem cell types in numerous preclinical trials, over the years. A plethora of published studies has explored diverse sources of MSCs, encompassing bone marrow, umbilical cord, adipose tissue, umbilical cord blood, placenta, Wharton's jelly, muscle, amniotic fluid, and dental tissue [29]. Among these, MSC-like populations have been identified in several dental tissues. Notably, the seminal work by Gronthos et *al.*

led to the isolation of hDPSCs from human dental pulp tissue [30]. These cells present several remarkable attributes, including accessibility, lifelong availability, significant proliferative potential, multipotency, and the ability to differentiate into a variety of cell types and tissues [31]. Furthermore, the application of hDPSCs provides advantages, including the modulation of immune and inflammatory responses, intrinsic mobilization of progenitor cells to injury sites through various paracrine signaling mechanisms, and a substantial presence of growth factors that promote tissue regeneration [32-35]. The hDPSCs are recognized as a promising source for bone tissue engineering, with the osteogenic differentiation capacity of hDPSCs demonstrated in both *in vitro* and *in vivo* studies. By harnessing their osteogenic potential, hDPSCs have been effectively combined with 3D polymeric scaffolds to generate bone-like hard tissues, thereby underscoring their utility in tissue engineering and Regenerative Medicine [36-38]. Considering these attributes, hDPSCs were selected for use in this thesis.

The initial step to embody the knowledge and application of this MSCs as a "regenerative tool" involved their isolation, culture, and characterization in accordance with the minimal criteria for MSC identification, as outlined by the International Society for Cellular Therapy (ISCT) [34,39]. The protocols employed were developed following an extensive review of the literature, encompassing key research on various aspects of hDPSC handling, including isolation techniques, expansion media, supplementation, and cryopreservation methods [40-46]. The MSCs were isolated from human dental pulp using the explant method, as described in **Chapter II - Characterization of Mesenchymal Stem/Stromal Cells**. According to the literature, this method, when compared to enzymatic digestion, offers several advantages, including higher cell yield and viability, reduced cellular stress, lower cost, and decreased risk of biological contamination [47-50]. Additionally, it has been shown to better preserve the biological characteristics of MSCs and is frequently described as simpler to perform than enzymatic digestion techniques. However, this method also presents certain drawbacks, such as a longer time required to obtain the initial cell population compared to enzymatic approaches, and the need for further optimization of growth conditions for explant-derived MSCs [47,50-52]. In this approach proved to be highly effective, yielding the desired quantity of cells within two weeks of dental pulp culture. The method facilitated the successful

isolation of targeted cell lines, which were subsequently utilized for further characterization and analysis.

The isolated cells were confirmed to be MSCs according to the criteria established by the International Society for Cellular Therapy (ISCT) [39]. These cells demonstrated adherence to plastic surfaces and maintained strong attachment to the culture substrate, even when subjected to mechanical stress from DPBS washing and trypsin-induced detachment. Additionally, the cells showed a characteristic "fibroblast-like" morphology when cultured in tissue culture flasks, further supporting their identification as MSCs. The biological characterization demonstrated that these cells exhibit normal proliferative activity and the ability to form colonies, a critical indicator of their self-renewal capacity. Additionally, hDPSCs displayed trilineage differentiation potential, successfully differentiating into adipogenic, chondrogenic, and osteogenic lineages. The expression of key MSC-specific genes, including CD105, CD73 and CD90, along with the absence of CD19, CD45 and CD34 markers further confirmed their stemness properties. The expression of genes related to the different paths of differentiation also confirms the potential of these cells to follow these same differentiations. These findings underscore the potential of hDPSCs for therapeutic applications in Regenerative Medicine, reinforcing their suitability for future clinical interventions. Moreover, in the context of this thesis, they provide a solid foundation for their use in the subsequent experimental chapters.

Fabrication and Characterization of a 3D Scaffold for Regenerative Medicine

Notwithstanding significant advances in synthetic bone substitutes over recent decades, the creation of biodegradable 3D scaffolds with optimal mechanical and biological properties remains an unmet challenge [53]. This chapter focuses on the development of synthetic bone grafts that closely mimic the complex architecture of natural bone, with a specific emphasis on the healing of critical-sized defects.

In this novel study (article: "**Assessment of 3D-Printed Polycaprolactone, Hydroxyapatite Nanoparticles and Diacrylate Poly (ethylene glycol) Scaffolds for Bone Regeneration**"), scaffolds were fabricated for the first time using a combination of PCL, nHA and PEGDA, through an

extrusion-based additive manufacturing technique. PCL was chosen as the primary component due to its biocompatible, biodegradable, easy of processing, non-toxic degradation and adjustable composition and structure [54-60]. However, PCL has limitations, such as poor cell adhesion, reduced proliferation rates and a slow degradation process due to its high crystallinity and hydrophobicity [61,62]. These drawbacks can be mitigated by incorporating bioactive inorganic materials, such as calcium phosphates [63-65]. In this context, nHA nanoparticles were integrated into the PCL matrix to improve the scaffold's bioactivity, osteoconductivity, and hydrophilicity, while also enhancing its mechanical properties [60,66].

The proportion of nHA was optimized at 40% of the final composite weight, as higher concentrations resulted in excessive thickness, leading to nozzle clogging and uneven filament deposition during the printing process. The nHA incorporation was achieved using the solvent casting technique, which offers simplicity and control over porosity, pore size, and interconnectivity [67]. After extrusion-based scaffold fabrication, the constructs were submerged in a PEGDA solution to further promote cell adhesion, proliferation, and migration [68].

While previous studies have shown promising results with PCL/nHA scaffolds [69-80], no prior research has explored the potential of combining these materials with PEGDA hydrogel to enhance bone defect repair and accelerate bone regeneration. Therefore, this study aimed to produce, optimize, characterize, and evaluate *in vitro* PCL/nHA scaffolds immersed in PEGDA solution.

The characterization of the scaffolds confirmed their successful fabrication, displaying well-aligned and positioned filaments with interconnected channels and pores, conducive to osteoblast and stem cell migration and proliferation. Furthermore, scaffolds treated with PEGDA exhibited hydrophilic properties, which can enhance cellular activity without compromising the mechanical integrity of the composite. The *in vitro* results align with previous studies, showing superior proliferation of hDPSCs in PEGDA-treated groups.

Based on the findings, the PCL/nHA/PEGDA scaffolds represent a promising therapeutic system for treating critical bone fractures, accelerating and enhancing bone regeneration. Investigating the performance of this system in critical bone defects is a crucial step toward advancing its application in clinical settings.

Bioinks for Osteogenic Differentiation

The fourth chapter ("**Chapter IV - Bioinks for Osteogenic Differentiation"**) presents the experimental development of a bioprinted structure that served as a model for investigating osteogenesis and the early BMPs stages of tissue maturation *in vitro*. Such research models, designed to replicate the structure and function of bone, as well as the cell-cell and cell-matrix interactions that occur *in vivo*, are essential for the clinical translation of novel therapeutic approaches for bone-related pathologies [81]. Given the inherent complexity of bone tissue, over the past decade there has been increasing interest over the past decade in the development of 3D models that closely mimic the bone microenvironment. These models also aim to reduce or replace the reliance on animal experiments in bone research [82].

This study utilizes a biofabrication approach involving alginate, nHA, Col, and hBMSCs through a pressure-assisted extrusion technique. This method ensures precise spatial distribution of cells, enhances cell loading efficiency, and allows for a detailed investigation of cell-biomaterial interactions, ultimately leading to the creation of well-structured and functional tissue constructs. The hBMSCs were selected for this study due to their accessibility and their recognized multipotency. As stromal cells with the capacity to differentiate into osteoblasts and generate bone tissue, hBMSCs are considered ideal for investigating osteogenic differentiation within a 3D environment [83,84].

The development of this cell-laden hydrogel also served as a preliminary investigation for the subsequent fabrication of a hybrid scaffold, which is discussed in the following chapter (**Chapter V - Hybrid Scaffold for Bone Tissue Engineering**). Cell-laden hydrogels have gained attention as a promising strategy for bone tissue engineering, primarily due to their capacity to facilitate efficient cell delivery and support bone regeneration. These hydrogels closely mimic the native extracellular matrix (ECM) of bone, providing an optimal

microenvironment for cell proliferation and differentiation. The preservation of a 3D cell distribution within the hydrogel enhances the replication of the natural tissue architecture. Additionally, these systems can be engineered for the controlled release of growth factors and bioactive molecules, further promoting osteogenesis [85-88]. One of the main advantages of cell-laden hydrogels is their highly customizable properties, such as adjustable porosity, stiffness, and degradation rates, which can be tailored to meet the specific demands of bone regeneration. These hydrogels also offer protection to encapsulated cells from mechanical stress during and after implantation, enhancing cell viability and function. In bone tissue engineering, hydrogels have been employed to deliver MSCs to bone defect sites, facilitating osteogenic differentiation and bone formation. Furthermore, they can be engineered for the controlled release of bone morphogenetic proteins (BMPs) and other osteogenic factors, as well as angiogenic molecules that promote vascularization, a critical factor in successful bone regeneration [85,86,89].

The findings of this study (article: "**3D Bioprinting of Alginate-Based Hydrogels to Investigate Osteogenic Differentiation of hBMSCS *in vitro***") indicate that the incorporation of nHA and Col into alginate significantly enhances the physicochemical and biological properties of the resulting bioink, thereby creating a promising 3D bioprinted model that closely mimics bone tissue architecture. Rheological assessments confirmed that the viscoelastic properties of the bioink are preserved upon the addition of nHA and Col. Mechanical testing further demonstrated that these modifications improve the hydrogel's performance under compressive loading conditions. Additionally, LIVE/DEAD™ assays and PrestoBlue™ viability assays provided compelling evidence that the developed bioinks successfully support the encapsulation and printing of hBMSCs without a significant loss in cell viability, even seven days post-printing. Polymerase chain reaction (PCR) analysis revealed that the alginate-nHA-Col composite notably upregulates the expression of key osteogenic markers in hBMSCs, indicating the hydrogel's potential to promote osteogenic differentiation. This study marks a significant advancement in bioink development for bone tissue engineering, offering a viable and ethical method for exploring osteogenesis and early tissue maturation *in vitro*. The proposed approach is expected to enhance therapeutic strategies for bone-related pathologies.

Hybrid Scaffold for Bone Tissue Engineering

As previously mentioned, cell-laden hydrogels are considered a promising approach for efficient cell delivery in bone tissue engineering applications [90,91]. However, despite their advantages, these hydrogels encounter significant challenges, including insufficient mechanical strength and low durability. These limitations are primarily attributed to their highly swollen state and rapid degradation rates. These limitations are primarily due to their highly swollen state and rapid degradation rate. To overcome these challenges, researchers have investigated the integration of polymeric scaffolds with hydrogels. This integration can be accomplished either by co-printing the hydrogels alongside scaffolds or by directly injecting hydrogels into the porous spaces of the scaffolds [92,93]. The resulting hybrid constructs effectively retain the mechanical stiffness conferred by the scaffolds while providing an increased surface area that facilitates cell proliferation. This synergistic combination significantly enhances the structural integrity and functional longevity of the engineered tissue constructs, thereby improving their efficacy in bone tissue regeneration applications.

In this chapter (**Chapter V - Hybrid Scaffold for Bone Tissue Engineering**), hybrid scaffolds that combine 3D-printed constructs with cell-laden hydrogels were developed. The fabrication process commenced with the production of porous 3D scaffolds using PCL and nHA, employing optimized polymer composites through extrusion techniques, as detailed in Chapter III ("**Chapter III - Fabrication and Characterization of a 3D Scaffold for Regenerative Medicine**"). Subsequently, these scaffolds were integrated with bioactive hydrogels containing hDPSCs, alginate, nHA and Col ("**Chapter IV - Bioinks for Osteogenic Differentiation**"). This integration aimed to enhance the biological efficacy of the printed constructs.

The biofabricated hybrid constructs underwent comprehensive characterization to evaluate their potential for bone tissue engineering applications (article: "**Hybrid Scaffolds for Bone Tissue Engineering: Integration of Composites and Bioactive Hydrogels Loaded with hDPSCs**". *In vitro* analysis revealed that the hybrid scaffold incorporating alginate, nHA, and Col presented superior cell attachment, proliferation, and osteogenic differentiation compared to control groups. The inclusion of nHA and Col in the

bioink significantly enhanced mineral deposition and spontaneous osteodifferentiation, indicating their osteoinductive properties. To further assess the constructs' biocompatibility, evaluations were conducted in a rat model. These *in vivo* assessments demonstrated minimal inflammatory responses, confirming the safety and effectiveness of the hybrid scaffolds. A transient, slight inflammatory reaction was observed at 15 days post-implantation, which resolved by 30 days. This aligns with expected inflammatory responses and the subsequent resolution phases typically associated with biomaterial implantation, highlighting the scaffold's ability to integrate effectively with host tissues.

Overall, the hybrid scaffold presents significant promise for clinical applications in bone repair and regeneration. Its combination of mechanical strength and biological activity addresses critical needs in bone tissue engineering, providing a viable treatment option for critical-sized bone defects and non-union fractures. Future research should prioritize long-term studies to further evaluate the performance of these constructs in more complex and clinically relevant models.

Application of Biomaterials and Cellular Therapies for the *In Vivo* Treatment of Critical-Sized Bone Defect

Before biomaterials can be applied in clinical settings, it is imperative to conduct extensive and detailed studies to evaluate their safety, biocompatibility, osteoconduction, osteointegration, osteoinduction and cell adhesion properties [94,95]. Once cytocompatibility is confirmed, subsequent *in vivo* assays are necessary to evaluate not only the efficacy of the therapy in promoting bone regeneration but also to observe biocompatibility and other critical phenomena, such as material degradation, bone regeneration, osteoconductivity and immune response.

Despite the advancements achieved through the *in vitro* model developed in Chapter IV ("**Chapter - Bioinks for Osteogenic Differentiation**"), it is important to acknowledge that such models cannot fully replicate the intricate complexity of the human body. Consequently, experimental animal models remain indispensable in biomedical research [96]. While *in vitro* models serve as valuable tools for preliminary investigations, the complexity of biological

systems necessitates the continued use of experimental animal models in the field of biomedical research to ensure comprehensive evaluation and validation of therapeutic strategies [97]. It is crucial for a particular therapeutic approach be tested in a series of animal models, progressing in complexity, before advancing to clinical trials in human patients [10]. The selection of an appropriate animal model is essential for ensuring the relevance of research to human conditions, minimizing animal use, and optimizing the allocation of time, effort and resources [98]. A variety of animal models are employed in bone regeneration research, including rodents, companion animals, pigs, small ruminants, lagomorphs, and primates, each offering distinct advantages and limitations that replicate specific processes and phases of human bone regeneration. Among various options for pre-clinical studies, ovine has become a favored *in vivo* experimental model, particularly in orthopedic and dental research. This preference stems from their similarities to humans, including comparable body weight, the presence of long bones, and a bone regeneration timeline that closely resembles that of humans [99].

The current chapter, titled "**Application of Biomaterials and Cellular Therapies for the *In Vivo* Treatment of Critical-Sized Bone Defect**", focused on evaluating the performance of a novel scaffold composed of PCL, a material chosen for its mechanical strength and versatility, extensively employed throughout the thesis, combined with Bonelike® (BL), a synthetic graft composed of calcium phosphates that is commercially available. The scaffold was tested alongside conditioned medium derived from human dental pulp stem cells (hDPSCs-CM), which was employed in the treatment of bone defects due to its ability to enhance osteogenic differentiation, reduce inflammatory responses, and promote angiogenesis. Furthermore, the use of this cell-based therapy offers a non-invasive, ethically sound alternative that minimizes the potential for immune rejection [100-102]. Following comprehensive *in vitro* and *in vivo* evaluations, the results confirmed that the PCL/BL scaffold supports cellular proliferation and viability, demonstrating its biocompatibility and potential use in bone tissue engineering. The *in vitro* analysis further revealed that the scaffold exhibits both osteoconductive and osteoinductive properties, indicating its capacity to support and promote bone formation. The scaffold's *in vivo* performance was tested using an ovine model of critical-sized bone defects, with assessments carried out at 90- and 150-days post-implantation. The findings

indicated that the combination of the PCL/BL scaffold *plus* hDPSCs-CM represents a promising therapeutic approach for bone regeneration. Radiographic analysis *post-mortem* showed significantly enhanced new bone formation in the defects treated with the PCL/BL scaffold *plus* hDPSCs-CM, compared to the control group. To further substantiate these findings and facilitate clinical translation, additional studies are required. These should include comprehensive histological and histomorphometric analyses to provide a detailed assessment of the interactions between the PCL/BL scaffold combined with hDPSCs-CM and the regenerating bone tissue.

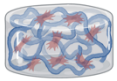
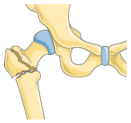
Therefore, this thesis has achieved the following milestones:

- Development and characterization of a protocol for the isolation, processing, and cryopreservation of hDPSCs, ensuring compliance with the minimal criteria for MSC acceptance as recommended by the ISCT;
- Fabrication, characterization, and *in vitro* evaluation of scaffolds composed of PCL, nHA and PEGDA, aimed at enhancing the acceleration and effectiveness of bone regeneration;
- Development and evaluation of a bioprinted model using alginate, nHA, and Col in conjunction with hBMSCs, facilitating a systematic study of osteogenesis and the early stages of tissue maturation *in vitro*;
- Production and comprehensive evaluation (both *in vitro* and *in vivo*) of a hybrid scaffold designed to enhance bioactivity and physical stability for bone tissue regeneration, with a particular focus on the treatment of critical-sized bone defects;
- Application and analysis of PCL/BL scaffolds combined with hDPSCs-CM for the *in vivo* treatment of critical-sized bone defects.

Overall, this work significantly contributes to the growing knowledge in the field of Regenerative Medicine. It advances our understanding of how 3D printing technologies and cellular therapies can be combined to develop functional, clinically relevant tissue-engineered constructs. The medical devices developed throughout this thesis are systematically summarized in **Table 1.** The findings suggest that this approach has immense potential for future applications in bone regeneration and beyond, offering new possibilities for personalized and effective treatments in Regenerative Medicine.

[This page is intentionally left blank.]

Table 1. Bone-tissue engineering applications of the different scaffolds studied in this thesis.

Chapter	Printing technology	Biomaterials	Cellular Therapies	Application in bone tissue engineering
III	Extrusion printing	PCL, nHA and PEGDA	-	 Treatment of critical bone defects
IV	3D bioprinting	Alginate, nHA and Col	hBMSCs	Bioprinted model to study osteogenesis and the early stages of tissue maturation 
V	Extrusion printing + 3D bioprinting	PCL, nHA, alginate and Col	hDPSCs	Treatment of critical and non-critical bone defects 
VI	Extrusion printing	Bonelike®, PCL and Bio-Gide® membranes	hDPSCs-CM	Treatment of non-unions and critical-sized bone defects 

[This page is intentionally left blank.]

Future Perspectives

[This page is intentionally left blank.]

Is **Bioprinting** the future of **Regenerative Medicine**?

The application of bioprinting in regenerative medicine, particularly in bone regeneration, represents an undoubtedly significant advancement toward the development of personalized therapeutic solutions for patients, with promising prospects for future advancements. Despite the achievements documented in numerous studies, there remains substantial potential for further improvement [103]. Currently, bioprinting technologies that employ 3D printing are hindered by the absence of standardized guidelines that establish clear and precise protocols for the fabrication of these constructs, limiting their clinical applicability. Moreover, the fabrication of complex structures, particularly those designed to incorporate specialized vascular systems, necessitates a greater degree of manufacturing complexity than that required for non-vascularized bone tissue, thereby presenting notable challenges and obstacles to successful implementation.

Regarding the objectives of this thesis, the following areas are particularly important for further development:

(1) *In vivo* assessments of hybrid scaffolds to evaluate their efficacy in promoting bone tissue regeneration in an ovine model.

Concerning **Chapter V - Hybrid Scaffold for Bone Tissue Engineering**, building upon the knowledge gained from the ovine model, the subsequent phase will focus on conducting *in vivo* analyses utilizing this animal model. The ovine model has demonstrated its value due to its anatomical and physiological similarities to human bone healing processes, in addition to the established expertise in surgical techniques. Although *in vivo* experiments have been performed with a rat model, this study was designed to evaluate the biocompatibility of the scaffolds. By advancing this research with larger animal models, the study aims to more accurately replicate human clinical conditions more accurately, thereby enhancing the translatability of the findings. This progression is essential for validating the efficacy of the therapeutic strategies being investigated and for preparing for potential clinical applications.

(2) Progression of *In Vivo* analysis of PCL/BL scaffold *plus* hDPSCs-CM.

A critical subsequent step involves completing the ongoing analysis of the *in vivo* tests conducted on the samples described in **Chapter VI**, titled "**Application of Biomaterials and Cell Therapies for the *In Vivo* Treatment of Critical-Sized Bone Defects**." This phase will encompass comprehensive histomorphometric and histological evaluations, which are essential for both quantitative and qualitative assessments of bone regeneration, tissue integration, and the overall biocompatibility of the biomaterials employed. The data generated from these analyses will be pivotal in elucidating the therapeutic efficacy of the tested biomaterials, enabling a thorough understanding of their performance in promoting bone regeneration. Furthermore, the findings will inform potential avenues for optimizing the biomaterials and their application in regenerative medicine. Ultimately, this comprehensive evaluation aims to enhance the effectiveness of strategies employed in the treatment of critical-sized bone defects.

(3) Collaborations with industry or clinical trials that translate research into practical applications.

Collaborations with industry and the initiation of clinical trials are essential for translating research findings into practical applications. These partnerships can facilitate the development and commercialization of innovative biomaterials and therapies, ensuring that scientific advancements effectively address real-world challenges in Regenerative Medicine. Through strategic partnerships with industry stakeholders, researchers can leverage essential resources, specialized knowledge, and comprehensive market analysis to enhance the translational potential of laboratory findings into clinical applications. Moreover, conducting clinical trials is indispensable for validating the safety and efficacy of new treatments, providing an important bridge between experimental research and patient care.

(4) One Health approach

From a One Health perspective, the investigation of the therapeutic effects of the hybrid scaffold developed in **Chapter V**, as well as the PCL/BL *plus* hDPSCs-CM described in **Chapter VI**, is essential in pre-clinical studies. Once these treatments are thoroughly evaluated, they can be translated into practical applications within clinical settings for both human and veterinary medicine. This integrative approach aims to provide patients with bone injuries - human or animal

- with access to novel and innovative cell-based therapies that could significantly enhance their healing process. The advancement of these therapies is key to broadening treatment modalities and improving outcomes for patients with bone defects.

[This page is intentionally left blank.]

References

1. Saini, G.; Segaran, N.; Mayer, J.L.; Saini, A.; Albadawi, H.; Oklu, R. Applications of 3D Bioprinting in Tissue Engineering and Regenerative Medicine. *J Clin Med* **2021**, *10*, doi:10.3390/jcm10214966.
2. Stamnitz, S.; Klimczak, A. Mesenchymal Stem Cells, Bioactive Factors, and Scaffolds in Bone Repair: From Research Perspectives to Clinical Practice. *Cells* **2021**, *10*, doi:10.3390/cells10081925.
3. Ghayor, C.; Weber, F.E. Osteoconductive Microarchitecture of Bone Substitutes for Bone Regeneration Revisited. *Front Physiol* **2018**, *9*, 960, doi:10.3389/fphys.2018.00960.
4. Bowles-Welch, A.C.; Jimenez, A.C.; Stevens, H.Y.; Frey Rubio, D.A.; Kippner, L.E.; Yeago, C.; Roy, K. Mesenchymal stromal cells for bone trauma, defects, and disease: Considerations for manufacturing, clinical translation, and effective treatments. *Bone Rep* **2023**, *18*, 101656, doi:10.1016/j.bonr.2023.101656.
5. Robinson, P.G.; Abrams, G.D.; Sherman, S.L.; Safran, M.R.; Murray, I.R. Autologous Bone Grafting. *Operative Techniques in Sports Medicine* **2020**, *28*, 150780, doi:https://doi.org/10.1016/j.otsm.2020.150780.
6. Weibull, L.; Widmark, G.; Ivanoff, C.-J.; Borg, E.; Rasmusson, L. Morbidity after Chin Bone Harvesting - A Retrospective Long-Term Follow-Up Study. *Clinical implant dentistry and related research* **2009**, *11*, 149-157, doi:10.1111/j.1708-8208.2008.00102.x.
7. Kim, Y.-H.; Vijayavenkataraman, S.; Cidonio, G. Biomaterials and scaffolds for tissue engineering and regenerative medicine. *BMC Methods* **2024**, *1*, 2, doi:10.1186/s44330-024-00002-7.
8. Hosseinkhani, M.; Mehrabani, D.; Karimfar, M.H.; Bakhtiyari, S.; Manafi, A.; Shirazi, R. Tissue engineered scaffolds in regenerative medicine. *World J Plast Surg* **2014**, *3*, 3-7.
9. Muzzio, N.; Moya, S.; Romero, G. Multifunctional Scaffolds and Synergistic Strategies in Tissue Engineering and Regenerative Medicine. *Pharmaceutics* **2021**, *13*, doi:10.3390/pharmaceutics13060792.
10. Huang, W.; Percie du Sert, N.; Vollert, J.; Rice, A.S.C. General Principles of Preclinical Study Design. *Handb Exp Pharmacol* **2020**, *257*, 55-69, doi:10.1007/164_2019_277.

11. Yilmaz, B.; Al Rashid, A.; Mou, Y.A.; Evis, Z.; Koç, M. Bioprinting: A review of processes, materials and applications. *Bioprinting* **2021**, *23*, e00148, doi:https://doi.org/10.1016/j.bprint.2021.e00148.
12. Koons, G.L.; Mikos, A.G. Progress in three-dimensional printing with growth factors. *J Control Release* **2019**, *295*, 50-59, doi:10.1016/j.jconrel.2018.12.035.
13. Zhang, Y.S.; Haghiashtiani, G.; Hübscher, T.; Kelly, D.J.; Lee, J.M.; Lutolf, M.; McAlpine, M.C.; Yeong, W.Y.; Zenobi-Wong, M.; Malda, J. 3D extrusion bioprinting. *Nature Reviews Methods Primers* **2021**, *1*, 75, doi:10.1038/s43586-021-00073-8.
14. Ng, W.L.; Lee, J.M.; Zhou, M.; Chen, Y.W.; Lee, K.A.; Yeong, W.Y.; Shen, Y.F. Vat polymerization-based bioprinting-process, materials, applications and regulatory challenges. *Biofabrication* **2020**, *12*, 022001, doi:10.1088/1758-5090/ab6034.
15. Abbadessa, A.; Ronca, A.; Salerno, A. Integrating bioprinting, cell therapies and drug delivery towards in vivo regeneration of cartilage, bone and osteochondral tissue. *Drug Deliv Transl Res* **2024**, *14*, 858-894, doi:10.1007/s13346-023-01437-1.
16. Reddy, V.S.; Tian, Y.; Zhang, C.; Ye, Z.; Roy, K.; Chinnappan, A.; Ramakrishna, S.; Liu, W.; Ghosh, R. A review on electrospun nanofibers based advanced applications: From health care to energy devices. *Polymers* **2021**, *13*, 3746.
17. Bejoy, A.M.; Makkithaya, K.N.; Hunakunti, B.B.; Hegde, A.; Krishnamurthy, K.; Sarkar, A.; Lobo, C.F.; Keshav, D.; Dharshini, G.; Mascarenhas, S. An insight on advances and applications of 3d bioprinting: A review. *Bioprinting* **2021**, *24*, e00176.
18. Ozbolat, I.T.; Peng, W.; Ozbolat, V. Application areas of 3D bioprinting. *Drug discovery today* **2016**, *21*, 1257-1271.
19. Gungor-Ozkerim, P.S.; Inci, I.; Zhang, Y.S.; Khademhosseini, A.; Dokmeci, M.R. Bioinks for 3D bioprinting: an overview. *Biomaterials science* **2018**, *6*, 915-946.
20. De Santis, M.M.; Alsafadi, H.N.; Tas, S.; Bölükbas, D.A.; Prithiviraj, S.; Da Silva, I.A.; Mittendorfer, M.; Ota, C.; Stegmayr, J.; Daoud, F. Extracellular-matrix-reinforced bioinks for 3D bioprinting human tissue. *Advanced materials* **2021**, *33*, 2005476.

21. Reddy, V.S.; Ramasubramanian, B.; Telrandhe, V.M.; Ramakrishna, S. Contemporary standpoint and future of 3D bioprinting in tissue/organs printing. *Current Opinion in Biomedical Engineering* **2023**, *27*, 100461, doi:https://doi.org/10.1016/j.cobme.2023.100461.
22. Ramadan, Q.; Zourob, M. 3D Bioprinting at the Frontier of Regenerative Medicine, Pharmaceutical, and Food Industries. *Front Med Technol* **2020**, *2*, 607648, doi:10.3389/fmedt.2020.607648.
23. Jafarkhani, M.; Salehi, Z.; Aidun, A.; Shokrgozar, M.A. Bioprinting in Vascularization Strategies. *Iran Biomed J* **2019**, *23*, 9-20, doi:10.29252/.23.1.9.
24. Jain, R.K.; Au, P.; Tam, J.; Duda, D.G.; Fukumura, D. Engineering vascularized tissue. *Nat Biotechnol* **2005**, *23*, 821-823, doi:10.1038/nbt0705-821.
25. Zheng, K.; Chai, M.; Luo, B.; Cheng, K.; Wang, Z.; Li, N.; Shi, X. Recent progress of 3D printed vascularized tissues and organs. *Smart Materials in Medicine* **2024**, *5*, 183-195, doi:https://doi.org/10.1016/j.smaim.2024.01.001.
26. Persaud, A.; Maus, A.; Strait, L.; Zhu, D. 3D Bioprinting with Live Cells. *Engineered Regeneration* **2022**, *3*, 292-309, doi:https://doi.org/10.1016/j.engreg.2022.07.002.
27. Bishop, E.S.; Mostafa, S.; Pakvasa, M.; Luu, H.H.; Lee, M.J.; Wolf, J.M.; Ameer, G.A.; He, T.-C.; Reid, R.R. 3-D bioprinting technologies in tissue engineering and regenerative medicine: Current and future trends. *Genes & Diseases* **2017**, *4*, 185-195, doi:https://doi.org/10.1016/j.gendis.2017.10.002.
28. Liang, K. Tissue Bioprinting: Promise and Challenges. *Bioengineering (Basel)* **2023**, *10*, doi:10.3390/bioengineering10121400.
29. Kangari, P.; Talaei-Khozani, T.; Razeghian-Jahromi, I.; Razmkhah, M. Mesenchymal stem cells: amazing remedies for bone and cartilage defects. *Stem Cell Research & Therapy* **2020**, *11*, 492, doi:10.1186/s13287-020-02001-1.
30. Gronthos, S.; Mankani, M.; Brahim, J.; Robey, P.G.; Shi, S. Postnatal human dental pulp stem cells (DPSCs) in vitro and in vivo. *Proc Natl Acad Sci U S A* **2000**, *97*, 13625-13630, doi:10.1073/pnas.240309797.
31. La Noce, M.; Paino, F.; Spina, A.; Naddeo, P.; Montella, R.; Desiderio, V.; De Rosa, A.; Papaccio, G.; Tirino, V.; Laino, L. Dental pulp stem cells: State of the art and suggestions for a true translation of research into therapy.

Journal of Dentistry **2014**, *42*, 761-768, doi:https://doi.org/10.1016/j.jdent.2014.02.018.

32. Gronthos, S.; Brahim, J.; Li, W.; Fisher, L.W.; Cherman, N.; Boyde, A.; DenBesten, P.; Robey, P.G.; Shi, S. Stem cell properties of human dental pulp stem cells. *J Dent Res* **2002**, *81*, 531-535, doi:10.1177/154405910208100806.
33. Caseiro, A.; Pereira, T.; Bártolo, P.; Santos, J.; Luís, A.; Maurício, A. Mesenchymal stem cells and biomaterials systems–perspectives for skeletal muscle tissue repair and regeneration. *Procedia engineering* **2015**, *110*, 90-97.
34. Gärtner, A.; Pereira, T.; Armada-da-Silva, P.; Amado, S.; Veloso, A.; Amorim, I.; Ribeiro, J.; Santos, J.; Bárcia, R.; Cruz, P. Effects of umbilical cord tissue mesenchymal stem cells (UCX®) on rat sciatic nerve regeneration after neurotmesis injuries. *Journal of stem cells & regenerative medicine* **2014**, *10*, 14.
35. Pereira, T.; Ivanova, G.; Caseiro, A.R.; Barbosa, P.; Bártolo, P.J.; Santos, J.D.; Luís, A.L.; Maurício, A.C. MSCs Conditioned Media and Umbilical Cord Blood Plasma Metabolomics and Composition. *PLOS ONE* **2014**, *9*, e113769, doi:10.1371/journal.pone.0113769.
36. Hao, X.; Li, D.; Zhang, D.; Jia, L. Microarray analysis of long non-coding RNAs related to osteogenic differentiation of human dental pulp stem cells. *Journal of Dental Sciences* **2022**, *17*, 733-743, doi:https://doi.org/10.1016/j.jds.2021.10.014.
37. Xie, H.; Lin, Y.; Fang, F. Glycogen synthase kinase-3β inhibitor promotes the migration and osteogenic differentiation of rat dental pulp stem cells via the β-catenin/PI3K/Akt signaling pathway. *Journal of Dental Sciences* **2022**, *17*, 802-810, doi:https://doi.org/10.1016/j.jds.2021.09.035.
38. Pinto, P.O.; Branquinho, M.V.; Caseiro, A.R.; Sousa, A.C.; Brandão, A.; Pedrosa, S.S.; Alvites, R.D.; Campos, J.M.; Santos, F.L.; Santos, J.D.; et al. The application of Bonelike® Poro as a synthetic bone substitute for the management of critical-sized bone defects - A comparative approach to the autograft technique - A preliminary study. *Bone Reports* **2021**, *14*, 101064, doi:https://doi.org/10.1016/j.bonr.2021.101064.
39. Dominici, M.; Le Blanc, K.; Mueller, I.; Slaper-Cortenbach, I.; Marini, F.C.; Krause, D.S.; Deans, R.J.; Keating, A.; Prockop, D.J.; Horwitz, E.M. Minimal criteria for defining multipotent mesenchymal stromal cells. The

International Society for Cellular Therapy position statement. *Cytotherapy* **2006**, *8*, 315-317, doi:https://doi.org/10.1080/14653240600855905.

40. Yasui, T.; Mabuchi, Y.; Morikawa, S.; Onizawa, K.; Akazawa, C.; Nakagawa, T.; Okano, H.; Matsuzaki, Y. Isolation of dental pulp stem cells with high osteogenic potential. *Inflammation and Regeneration* **2017**, *37*, 8, doi:10.1186/s41232-017-0039-4.
41. Suchánek, J.; Soukup, T.; Ivancaková, R.; Karbanová, J.; Hubková, V.; Pytlík, R.; Kucerová, L. Human dental pulp stem cells--isolation and long term cultivation. *Acta Medica (Hradec Kralove)* **2007**, *50*, 195-201.
42. Naz, S.; Khan, F.R.; Zohra, R.R.; Lakhundi, S.S.; Khan, M.S.; Mohammed, N.; Ahmad, T. Isolation and culture of dental pulp stem cells from permanent and deciduous teeth. *Pak J Med Sci* **2019**, *35*, 997-1002, doi:10.12669/pjms.35.4.540.
43. Pisciotta, A.; Carnevale, G.; Meloni, S.; Riccio, M.; Biasi, S.; Gibellini, L.; Ferrari, A.; Bruzzesi, G.; Pol, A. Human Dental pulp stem cells (hDPSCs): Isolation, enrichment and comparative differentiation of two sub-populations Integrative control of development. *BMC Developmental Biology* **2015**, *15*, doi:10.1186/s12861-015-0065-x.
44. Rodas-Junco, B.A.; Villicaña, C. Dental Pulp Stem Cells: Current Advances in Isolation, Expansion and Preservation. *Tissue Engineering and Regenerative Medicine* **2017**, *14*, 333-347, doi:10.1007/s13770-017-0036-3.
45. Ferro, F.; Spelat, R.; Baheney, C.S. Dental pulp stem cell (DPSC) isolation, characterization, and differentiation. In *Stem Cells and Tissue Repair*; Springer: 2014; pp. 91-115.
46. Machado, C.d.V.; Carvalho, C.M.; Campos, T.M.C.; Passos, S.T.; Telles, P.D.d.S. Isolation and culture of stem cells derived from dental pulp of permanent teeth: a successful method. *RFO UPF* **2015**, *20*, 159-163.
47. Yoon, J.H.; Roh, E.Y.; Shin, S.; Jung, N.H.; Song, E.Y.; Chang, J.Y.; Kim, B.J.; Jeon, H.W. Comparison of Explant-Derived and Enzymatic Digestion-Derived MSCs and the Growth Factors from Wharton's Jelly. *BioMed Research International* **2013**, *2013*, 428726, doi:https://doi.org/10.1155/2013/428726.
48. Varaa, N.; Azandeh, S.; Khodabandeh, Z.; Gharravi, A.M. Wharton's Jelly Mesenchymal Stem Cell: Various Protocols for Isolation and Differentiation of Hepatocyte-Like Cells; Narrative Review. *Iran J Med Sci* **2019**, *44*, 437-448, doi:10.30476/ijms.2019.44952.

49. Huang, Q.; Yang, Y.; Luo, C.; Wen, Y.; Liu, R.; Li, S.; Chen, T.; Sun, H.; Tang, L. An efficient protocol to generate placental chorionic plate-derived mesenchymal stem cells with superior proliferative and immunomodulatory properties. *Stem Cell Research & Therapy* **2019**, *10*, 301, doi:10.1186/s13287-019-1405-8.
50. Hassan, G.; Kasem, I.; Antaki, R.; Mohammad, M.B.; AlKadry, R.; Aljamali, M. Isolation of umbilical cord mesenchymal stem cells using human blood derivatives accompanied with explant method. *Stem Cell Investigation* **2019**, *6*.
51. Yoon, J.H.; Roh, E.Y.; Shin, S.; Jung, N.H.; Song, E.Y.; Chang, J.Y.; Kim, B.J.; Jeon, H.W. Comparison of explant-derived and enzymatic digestion-derived MSCs and the growth factors from Wharton's jelly. *Biomed Res Int* **2013**, *2013*, 428726, doi:10.1155/2013/428726.
52. Varaa, N.; Azandeh, S.; Khodabandeh, Z.; Gharravi, A.M. Wharton's Jelly Mesenchymal Stem Cell: Various Protocols for Isolation and Differentiation of Hepatocyte-Like Cells; Narrative Review. *Iranian Journal of Medical Sciences* **2019**, *44*, 437-448, doi:10.30476/ijms.2019.44952.
53. Sousa, A.C.; Biscaia, S.; Alvites, R.; Branquinho, M.; Lopes, B.; Sousa, P.; Valente, J.; Franco, M.; Santos, J.D.; Mendonça, C.; et al. Assessment of 3D-Printed Polycaprolactone, Hydroxyapatite Nanoparticles and Diacrylate Poly(ethylene glycol) Scaffolds for Bone Regeneration. *Pharmaceutics* **2022**, *14*, 2643.
54. Wang, S.; Gu, R.; Wang, F.; Zhao, X.; Yang, F.; Xu, Y.; Yan, F.; Zhu, Y.; Xia, D.; Liu, Y. 3D-Printed PCL/Zn scaffolds for bone regeneration with a dose-dependent effect on osteogenesis and osteoclastogenesis. *Materials Today Bio* **2022**, *13*, 100202, doi:https://doi.org/10.1016/j.mtbio.2021.100202.
55. Babilotte, J.; Guduric, V.; Le Nihouannen, D.; Naveau, A.; Fricain, J.-C.; Catros, S. 3D printed polymer–mineral composite biomaterials for bone tissue engineering: Fabrication and characterization. *Journal of Biomedical Materials Research Part B: Applied Biomaterials* **2019**, *107*, 2579-2595, doi:https://doi.org/10.1002/jbm.b.34348.
56. Kenry; Liu, B. Recent Advances in Biodegradable Conducting Polymers and Their Biomedical Applications. *Biomacromolecules* **2018**, *19*, 1783-1803, doi:10.1021/acs.biomac.8b00275.
57. Rohner, D.; Hutmacher, D.W.; Cheng, T.K.; Oberholzer, M.; Hammer, B. In vivo efficacy of bone-marrow-coated polycaprolactone scaffolds for the

reconstruction of orbital defects in the pig. *J Biomed Mater Res B Appl Biomater* **2003**, *66*, 574-580, doi:10.1002/jbm.b.10037.

58. Williams, J.M.; Adewunmi, A.; Schek, R.M.; Flanagan, C.L.; Krebsbach, P.H.; Feinberg, S.E.; Hollister, S.J.; Das, S. Bone tissue engineering using polycaprolactone scaffolds fabricated via selective laser sintering. *Biomaterials* **2005**, *26*, 4817-4827, doi:10.1016/j.biomaterials.2004.11.057.
59. Ba Linh, N.T.; Min, Y.K.; Lee, B.T. Hybrid hydroxyapatite nanoparticles-loaded PCL/GE blend fibers for bone tissue engineering. *J Biomater Sci Polym Ed* **2013**, *24*, 520-538, doi:10.1080/09205063.2012.697696.
60. Keivani, F.; Shokrollahi, P.; Zandi, M.; Irani, S.; Shokrolahi, F.; Khorasani, S.C. Engineered electrospun poly(caprolactone)/polycaprolactone-g-hydroxyapatite nano-fibrous scaffold promotes human fibroblasts adhesion and proliferation. *Mater Sci Eng C Mater Biol Appl* **2016**, *68*, 78-88, doi:10.1016/j.msec.2016.05.098.
61. Lam, C.X.; Hutmacher, D.W.; Schantz, J.T.; Woodruff, M.A.; Teoh, S.H. Evaluation of polycaprolactone scaffold degradation for 6 months in vitro and in vivo. *J Biomed Mater Res A* **2009**, *90*, 906-919, doi:10.1002/jbm.a.32052.
62. Wutticharoenmongkol, P.; Pavasant, P.; Supaphol, P. Osteoblastic phenotype expression of MC3T3-E1 cultured on electrospun polycaprolactone fiber mats filled with hydroxyapatite nanoparticles. *Biomacromolecules* **2007**, *8*, 2602-2610, doi:10.1021/bm700451p.
63. Petretta, M.; Gambardella, A.; Boi, M.; Berni, M.; Cavallo, C.; Marchiori, G.; Maltarello, M.C.; Bellucci, D.; Fini, M.; Baldini, N.; et al. Composite Scaffolds for Bone Tissue Regeneration Based on PCL and Mg-Containing Bioactive Glasses. *Biology (Basel)* **2021**, *10*, doi:10.3390/biology10050398.
64. Hristov, V.; Radev, L.; Samuneva, B.; Apostolov, G. Organic / inorganic bioactive materials Part I: Synthesis, structure and in vitro assessment of collagen/silicocarnotite biocoatings. *Open Chemistry* **2009**, *7*, 702-710, doi:doi:10.2478/s11532-009-0067-2.
65. Rezwan, K.; Chen, Q.Z.; Blaker, J.J.; Boccaccini, A.R. Biodegradable and bioactive porous polymer/inorganic composite scaffolds for bone tissue engineering. *Biomaterials* **2006**, *27*, 3413-3431, doi:10.1016/j.biomaterials.2006.01.039.

66. Chen, Z.; Liu, Y.; Huang, J.; Wang, H.; Hao, M.; Hu, X.; Qian, X.; Fan, J.; Yang, H.; Yang, B. Enhanced In Vitro Biocompatible Polycaprolactone/Nano-Hydroxyapatite Scaffolds with Near-Field Direct-Writing Melt Electrospinning Technology. *Journal of Functional Biomaterials* **2022**, *13*, 161.
67. Sola, A.; Bertacchini, J.; D'Avella, D.; Anselmi, L.; Maraldi, T.; Marmiroli, S.; Messori, M. Development of solvent-casting particulate leaching (SCPL) polymer scaffolds as improved three-dimensional supports to mimic the bone marrow niche. *Materials Science and Engineering: C* **2019**, *96*, 153-165, doi:https://doi.org/10.1016/j.msec.2018.10.086.
68. Francisco, L.; Moura, C.; Viana, T.; Ângelo, D.; Morouço, P.; Alves, N. Poly(ε-caprolactone) and Polyethylene Glycol Diacrylate-based Scaffolds for TMJ Bioengineered Disc Implants. *Procedia Manufacturing* **2017**, *12*, 291-297, doi:https://doi.org/10.1016/j.promfg.2017.08.032.
69. Cestari, F.; Petretta, M.; Yang, Y.; Motta, A.; Grigolo, B.; Sglavo, V.M. 3D printing of PCL/nano-hydroxyapatite scaffolds derived from biogenic sources for bone tissue engineering. *Sustainable Materials and Technologies* **2021**, *29*, e00318, doi:https://doi.org/10.1016/j.susmat.2021.e00318.
70. Jiao, Z.; Luo, B.; Xiang, S.; Ma, H.; Yu, Y.; Yang, W. 3D printing of HA / PCL composite tissue engineering scaffolds. *Advanced Industrial and Engineering Polymer Research* **2019**, *2*, 196-202, doi:https://doi.org/10.1016/j.aiepr.2019.09.003.
71. Zimmerling, A.; Yazdanpanah, Z.; Cooper, D.M.L.; Johnston, J.D.; Chen, X. 3D printing PCL/nHA bone scaffolds: exploring the influence of material synthesis techniques. *Biomaterials Research* **2021**, *25*, 3, doi:10.1186/s40824-021-00204-y.
72. Morouço, P.; Biscaia, S.; Viana, T.; Franco, M.; Malça, C.; Mateus, A.; Moura, C.; Ferreira, F.C.; Mitchell, G.; Alves, N.M. Fabrication of Poly(ε-caprolactone) Scaffolds Reinforced with Cellulose Nanofibers, with and without the Addition of Hydroxyapatite Nanoparticles. *Biomed Res Int* **2016**, *2016*, 1596157, doi:10.1155/2016/1596157.
73. Zhao, J.; Guo, L.; Yang, X.; Weng, J. Preparation of bioactive porous HA/PCL composite scaffolds. *Applied Surface Science* **2008**, *255*, 2942-2946.
74. Roohani-Esfahani, S.-I.; Nouri-Khorasani, S.; Lu, Z.; Appleyard, R.; Zreiqat, H. The influence hydroxyapatite nanoparticle shape and size on the properties of biphasic calcium phosphate scaffolds coated with hydroxyapatite–PCL composites. *Biomaterials* **2010**, *31*, 5498-5509.

75. Park, S.A.; Lee, S.H.; Kim, W.D. Fabrication of porous polycaprolactone/hydroxyapatite (PCL/HA) blend scaffolds using a 3D plotting system for bone tissue engineering. *Bioprocess and biosystems engineering* **2011**, *34*, 505-513.
76. Cui, Z.; Nelson, B.; Peng, Y.; Li, K.; Pilla, S.; Li, W.-J.; Turng, L.-S.; Shen, C. Fabrication and characterization of injection molded poly (ε-caprolactone) and poly (ε-caprolactone)/hydroxyapatite scaffolds for tissue engineering. *Materials Science and Engineering: C* **2012**, *32*, 1674-1681.
77. Shor, L.; Güçeri, S.; Wen, X.; Gandhi, M.; Sun, W. Fabrication of three-dimensional polycaprolactone/hydroxyapatite tissue scaffolds and osteoblast-scaffold interactions in vitro. *Biomaterials* **2007**, *28*, 5291-5297.
78. Chuenjitkuntaworn, B.; Inrung, W.; Damrongsri, D.; Mekaapiruk, K.; Supaphol, P.; Pavasant, P. Polycaprolactone/hydroxyapatite composite scaffolds: preparation, characterization, and in vitro and in vivo biological responses of human primary bone cells. *Journal of Biomedical Materials Research Part A: An Official Journal of The Society for Biomaterials, The Japanese Society for Biomaterials, and The Australian Society for Biomaterials and the Korean Society for Biomaterials* **2010**, *94*, 241-251.
79. Gerdes, S.; Mostafavi, A.; Ramesh, S.; Memic, A.; Rivero, I.V.; Rao, P.; Tamayol, A. Process–structure–quality relationships of three-dimensional printed poly (caprolactone)-hydroxyapatite scaffolds. *Tissue Engineering Part A* **2020**, *26*, 279-291.
80. Biscaia, S.; Branquinho, M.V.; Alvites, R.D.; Fonseca, R.; Sousa, A.C.; Pedrosa, S.S.; Caseiro, A.R.; Guedes, F.; Patrício, T.; Viana, T.; et al. 3D Printed Poly(ε-caprolactone)/Hydroxyapatite Scaffolds for Bone Tissue Engineering: A Comparative Study on a Composite Preparation by Melt Blending or Solvent Casting Techniques and the Influence of Bioceramic Content on Scaffold Propertie. *Int J Mol Sci* **2022**, *23*, 2318.
81. Caddeo, S.; Boffito, M.; Sartori, S. Tissue Engineering Approaches in the Design of Healthy and Pathological In Vitro Tissue Models. *Front Bioeng Biotechnol* **2017**, *5*, 40, doi:10.3389/fbioe.2017.00040.
82. Owen, R.; Reilly, G.C. In vitro Models of Bone Remodelling and Associated Disorders. *Frontiers in Bioengineering and Biotechnology* **2018**, *6*, doi:10.3389/fbioe.2018.00134.
83. Sai, B.; Dai, Y.; Fan, S.; Wang, F.; Wang, L.; Li, Z.; Tang, J.; Wang, L.; Zhang, X.; Zheng, L.; et al. Cancer-educated mesenchymal stem cells promote the

survival of cancer cells at primary and distant metastatic sites via the expansion of bone marrow-derived-PMN-MDSCs. *Cell Death & Disease* **2019**, *10*, 941, doi:10.1038/s41419-019-2149-1.

84. Kemp, K.C.; Hows, J.; Donaldson, C. Bone marrow-derived mesenchymal stem cells. *Leuk Lymphoma* **2005**, *46*, 1531-1544, doi:10.1080/10428190500215076.
85. Amini, A.R.; Laurencin, C.T.; Nukavarapu, S.P. Bone tissue engineering: recent advances and challenges. *Crit Rev Biomed Eng* **2012**, *40*, 363-408, doi:10.1615/critrevbiomedeng.v40.i5.10.
86. Dang, M.; Saunders, L.; Niu, X.; Fan, Y.; Ma, P.X. Biomimetic delivery of signals for bone tissue engineering. *Bone Research* **2018**, *6*, 25, doi:10.1038/s41413-018-0025-8.
87. V. K., A.D.; Ray, S.; Arora, U.; Mitra, S.; Sionkowska, A.; Jaiswal, A.K. Dual drug delivery platforms for bone tissue engineering. *Frontiers in Bioengineering and Biotechnology* **2022**, *10*, doi:10.3389/fbioe.2022.969843.
88. Percival, K.M.; Paul, V.; Husseini, G.A. Recent Advancements in Bone Tissue Engineering: Integrating Smart Scaffold Technologies and Bio-Responsive Systems for Enhanced Regeneration. *International Journal of Molecular Sciences* **2024**, *25*, 6012.
89. Zhang, X.; Jiang, W.; Xie, C.; Wu, X.; Ren, Q.; Wang, F.; Shen, X.; Hong, Y.; Wu, H.; Liao, Y.; et al. Msx1+ stem cells recruited by bioactive tissue engineering graft for bone regeneration. *Nature Communications* **2022**, *13*, 5211, doi:10.1038/s41467-022-32868-y.
90. Hwang, C.M.; Sant, S.; Masaeli, M.; Kachouie, N.N.; Zamanian, B.; Lee, S.-H.; Khademhosseini, A. Fabrication of three-dimensional porous cell-laden hydrogel for tissue engineering. *Biofabrication* **2010**, *2*, 035003.
91. Kim, W.; Kim, G.H. Highly bioactive cell-laden hydrogel constructs bioprinted using an emulsion bioink for tissue engineering applications. *Biofabrication* **2022**, *14*, 045018.
92. Hamid, O.A.; Eltaher, H.M.; Sottile, V.; Yang, J. 3D bioprinting of a stem cell-laden, multi-material tubular composite: An approach for spinal cord repair. *Materials Science and Engineering: C* **2021**, *120*, 111707.
93. Dong, L.; Wang, S.-J.; Zhao, X.-R.; Zhu, Y.-F.; Yu, J.-K. 3D-printed poly (ε-caprolactone) scaffold integrated with cell-laden chitosan hydrogels for bone tissue engineering. *Scientific reports* **2017**, *7*, 13412.

94. Pinto, P.O.; Atayde, L.; Campos, J.M.; Caseiro, A.; Pereira, T.; Mendonça, C.; Santos, J.D.; Maurxhtício, A.C. Therapeutic Strategies for Bone Regeneration: The Importance of Biomaterials Testing in Adequate Animal Models. 2016; pp. 275-319.
95. Pearce, A.I.; Richards, R.G.; Milz, S.; Schneider, E.; Pearce, S.G. Animal models for implant biomaterial research in bone: a review. *Eur Cell Mater* **2007**, *13*, 1-10, doi:10.22203/ecm.v013a01.
96. Calasans-Maia, M.D.; Monteiro, M.L.; Ascoli, F.O.; Granjeiro, J.M. The rabbit as an animal model for experimental surgery. *Acta Cir Bras* **2009**, *24*, 325-328, doi:10.1590/s0102-86502009000400014.
97. Martini, L.; Fini, M.; Giavaresi, G.; Giardino, R. Sheep model in orthopedic research: a literature review. *Comp Med* **2001**, *51*, 292-299.
98. Sartoretto, S.C.; Uzeda, M.J.; Miguel, F.B.; Nascimento, J.R.; Ascoli, F.; Calasans-Maia, M.D. SHEEP AS AN EXPERIMENTAL MODEL FOR BIOMATERIAL IMPLANT EVALUATION. *Acta Ortop Bras* **2016**, *24*, 262-266, doi:10.1590/1413-785220162405161949.
99. Cipitria, A.; Reichert, J.C.; Epari, D.R.; Saifzadeh, S.; Berner, A.; Schell, H.; Mehta, M.; Schuetz, M.A.; Duda, G.N.; Hutmacher, D.W. Polycaprolactone scaffold and reduced rhBMP-7 dose for the regeneration of critical-sized defects in sheep tibiae. *Biomaterials* **2013**, *34*, 9960-9968, doi:10.1016/j.biomaterials.2013.09.011.
100. Koh, B.; Ab Rahman, F.H.; Matlan, N.A.; Rajan, M.; Musta'ain, A.Y.; Mohd Jeffry Lee, M.R.; Ramli, R.; Mohd Yunus, S.S.; Binti Hj Idrus, R.; Yazid, M.D. Potential role of dental pulp stem cells conditioned medium for odontoblastic differentiation. *Biological Research* **2022**, *55*, 11, doi:10.1186/s40659-022-00380-8.
101. Yamaguchi, S.; Shibata, R.; Yamamoto, N.; Nishikawa, M.; Hibi, H.; Tanigawa, T.; Ueda, M.; Murohara, T.; Yamamoto, A. Dental pulp-derived stem cell conditioned medium reduces cardiac injury following ischemia-reperfusion. *Scientific Reports* **2015**, *5*, 16295, doi:10.1038/srep16295.
102. El Moshy, S.; Radwan, I.A.; Rady, D.; Abbass, M.M.S.; El-Rashidy, A.A.; Sadek, K.M.; Dörfer, C.E.; Fawzy El-Sayed, K.M. Dental Stem Cell-Derived Secretome/Conditioned Medium: The Future for Regenerative Therapeutic Applications. *Stem Cells International* **2020**, *2020*, 7593402, doi:https://doi.org/10.1155/2020/7593402.

103. Xing, F.; Xiang, Z.; Rommens, P.M.; Ritz, U. 3D Bioprinting for Vascularized Tissue-Engineered Bone Fabrication. *Materials (Basel)* **2020**, *13*, doi:10.3390/ma13102278.